

UNIVERSITÀ DEGLI STUDI DI PADOVA
AND
AARHUS UNIVERSITY

DEPARTMENT OF INDUSTRIAL ENGINEERING
AND
DEPARTMENT OF CIVIL AND ARCHITECTURAL ENGINEERING
MASTER DEGREE IN MECHANICAL ENGINEERING

**Fatigue design of welded joints in
as-welded and HFMI treated conditions**

Supervisor:
PROF. GIOVANNI MENEGHETTI

Candidate:
MARCO SOLIGO
1233975

Co-Supervisor:
PROF. HALID CAN YILDIRIM
PROF. ALBERTO CAMPAGNOLO

Academic Year 2021-2022

Marco Soligo:
Fatigue design of welded joints in as-welded and HFMI treated conditions
Master Degree in Mechanical Engineering, ©4th March 2022

*Dedicated to my family
for their support and love.*

Abstract(English)

In the design of the welded joints, the fatigue endurance is evaluated with the application of the global approach of nominal stress, based on recommended S-N curves, available in different codes and guidelines [1]. However, this approach presents some disadvantages: indeed, there is the necessity to define several fatigue classes to account for different geometries and sizes. Furthermore, in some cases, the detection of the nominal stress is very tough due to the complexity of the geometry of welded joint. Along with this, the experimental reality shows that the failure predominantly originate from the region with material discontinuity, as the welds themselves. Thus, the fatigue strength reveals to be a local phenomenon.

To consider the size and shape effect of the different welded joints, the local approach can be used that they are developed thanks to the increasing use of the Finite Element analysis software in the industry. In this work, the extrapolation of hot-spot stress and the Effective Notch Stress method [1] [2], both available in the IIW guideline, are cited. Despite the great reliability offered by these methods, some of them are not able to consider some important effects that can decrease the fatigue strength of the welded joint, such as the size effect. To overcome this problem, the concepts of the Linear Elastic Fracture Mechanics has been non-conventionally extended to structural design of welded joints, with the definition of the V-notch concept (i.e. weld toe, root). To define and quantify the linear elastic distribution occurring in the V-notch region, the Notch Stress Intensity Factors (NSIFs) approach has been proposed by Lazzarin and Tovo [6] at the University of Padua, aiming to build a correlation between the asymptotic local stress field at the V-notch and the crack initiation. Recently, other two Finite Elements approaches have been introduced, capable of defining reliable results in terms of fatigue life with a decreasing of the computational and modelling time: the Strain Energy Density (SED), proposed by Lazzarin and Zambardi in 2001 [25] [26], and the Peak Stress Method (PSM) defined by Meneghetti and Lazzarin in 2007 [5]. There are several advantages of these approaches: first of all, these methods require a coarse meshes, so this characteristic makes these approaches easily applicable to the industry; furthermore, these methods are characterized by only one fatigue design curve, independently of the geometry of the welded joint. Over the years, these approaches have been calibrated and extended for 2D and 3D, for several Finite Elements software and for different element typologies. Furthermore, these methods have been recently used, beyond in the case of traction residual stress state post-welded (as-welded) or in stress relieved condition, also for joints that are characterized by a compression residual stress state due to a post-welded treatment, such as High Frequency Mechanical Impact (HFMI) [33]. This treatment is a post-welded technique for the fatigue strength enhancement of welded joints thanks to a plastic deformation at the weld toe, consequently inducing beneficial compressive residual stress near to the treated areas and at the same time improving the local geometry.

The fatigue behavior of the structures characterized by the presence of welded joints is complex because it can be influenced by several intrinsic factor due to the nature of the welded joint. Indeed, the fatigue strength of some welded joints can be reduced by the presence of welding defects, such as slag inclusion, gas pores, undercut at the weld toe or misalignment. These defects can increase the degree of stress and strain concentration at the geometrical profile of the joint.

In this thesis, the effects that will be analyzed is the misalignment effect inside the welded joints. The misalignment of the welded joints is a result of the thermal-input during welding and also its mechanical restraints. In many cases, the misalignment effect can not be completely avoided during the fatigue test because they have a influence on the fatigue life of the welded joints due to the introduction of additional tensile stress due to the presence of a secondary bending.

Chapter 1 aims to introduce the reader to the basis and principles of the local approaches which are going to be employed in this thesis. Two methods have been extracted from the IIW guideline, while the remaining three have been developed in the University of Padua, as describe before. For each methods the advantage and disadvantage are reported.

Chapter 2 is the description of the training for the thesis student for the application of NSIFs method, SED and PSM approaches for the fatigue assessment of 2D and 3D welded joints. The data are collected to do a statistical analysis and comparison with the reference design fatigue curves proposed in the literature.

Chapter 3 describes the fatigue assessment of specific geometry in as-welded condition in term s of nominal stress, hot-spot stress, equivalent peak stress (PSM) and strain energy density (SED). As in the chapter 2, the data are inserted in their respective design fatigue curve obtained from the literature, in order to define the grade

of effectiveness and conservativeness provided by each method.

Initially, Chapter 4 introduces the reader to the basis, the principles and the benefits of the post-welded treatment HFMI on welded joints. Subsequently, the fatigue assessment of HFMI treatment welded joints are described, applying the hot-spot method and the PSM combined with the SET for blunt notches [ref]. The re-elaborated data are inserted in their respective design curves in order to define the grade of effectiveness and conservativeness provided by each method.

Chapter 5, after a briefly introduction about the misalignment effect on the welded joints, describes the procedure to define the factor k_{mis} to consider the misalignment effect on the fatigue life of the welded joints. Furthermore, in this chapter the misalignment effect is studied on the joints subjected to CAL and VAL condition. A new fatigue design curve is proposed for the welded joints characterized by the presence of axial and angular misalignment.

Chapter 6 describes the experimental procedure used for the detection of the membrane stress value and mostly, the bending stress due to the misalignment of the welded joint. In this chapter, the procedure for the calculation of the k_{mis} factor through the experimental data, the formulas obtained from Chapter 5 and the formula from IIW guideline [1], are described.

Chapter 7 defined the conclusion of this work, describing also the future improvement.

Abstract(Italiano)

Nella progettazione strutturale delle giunzioni saldate, la resistenza a fatica viene valutata mediante l'approccio globale delle tensioni nominali, basato sulle curve di progettazione a fatica S-N, reperibili nei codici o in normativa. Tale approccio però, presenta diversi svantaggi: vi è infatti la necessità di definire diverse classi di fatica che tengano conto delle diverse geometrie e dimensioni dei giunti. Inoltre, in alcuni casi, il rilevamento e il calcolo della tensione nominale risulta difficoltoso poiché la geometria dei giunti è particolarmente complessa. In parallelo a quanto esposto precedentemente, la realtà sperimentale evidenzia che la rottura mediante l'innesco di una cricca, avviene prevalentemente nelle regioni in cui è presente una discontinuità di materiale, ovvero in corrispondenza della saldatura. La vita a fatica quindi, si rivela essere un fenomeno locale.

Per tener in considerazione l'effetto delle dimensioni e delle forme dei diversi giunti saldati, si possono utilizzare gli approcci locali, sviluppati grazie all'impiego sempre maggiore di software di analisi agli elementi finiti. All'interno del suddetto elaborato, vengono citati l'estrapolazione della tensione di hot-spot, reperibile nella guida IIW, e l'Effective Notch Stress method, anch'esso reperibile nella guida IIW. Nonostante la grande affidabilità di tali approcci, alcuni di essi non considerano importanti parametri ed effetti che abbattano la resistenza a fatica dei componenti saldati, per esempio l'effetto scala. Per ovviare tale problema, i concetti della Meccanica della Frattura Lineare Elastica sono stati estesi per lo studio a fatica delle giunzioni saldate, con la definizione del concetto di V-notch (piede cordone, radice). Per definire e quantificare la distribuzione del campo tensione che si sviluppa in corrispondenza del V-notch, è stato proposto da Lazzarin e Tovo presso l'Università degli Studi di Padova, il metodo chiamato Notch Stress Intensity Factor, che prevede di instaurare una correlazione tra il campo di tensione locale asintotico e l'innesco della cricca. Recentemente, sono stati introdotti altri due metodi agli Elementi Finiti, in grado di definire risultati affidabili in termini di vita a fatica con una riduzione dei tempi di simulazione e modellazione: lo Strain Energy Density (SED), proposto da Lazzarin e Zambardi nel 2001, e il Peak Stress Method, definito da Meneghetti e Lazzarin nel 2007. I vantaggi di questi approcci sono molteplici: innanzitutto richiedono delle mesh grossolane, quindi è possibile applicarli anche in ambito industriale; inoltre, a differenza dell'approccio globale con le tensioni nominali, prevedono l'utilizzo di un'unica curva a fatica indipendentemente dalla geometria del giunto analizzato. Negli ultimi anni tali approcci sono stati calibrati ed estesi per geometrie 2D e 3D, per diversi software agli elementi finiti e per tipologie di elementi differenti. Inoltre, questi approcci sono stati utilizzati recentemente, oltre che nei casi di tensioni residue post-saldatura di forte trazione (as-welded) o nulle (stress-relieved), anche per i giunti soggetti ad uno stato di tensione di forte compressione dovuto a trattamenti post-saldatura come High Frequency Mechanical Impact (HFMI). Tale trattamento prevede un incremento della vita a fatica dei giunti as-welded mediante una deformazione plastica del materiale saldato, eseguita tramite l'utilizzo di appositi indentatori. Tale deformazione porta ad avere delle elevate tensioni residue di compressione in corrispondenza del piede cordone della saldatura, migliorando inoltre la geometria locale.

Il comportamento a fatica delle strutture caratterizzate da giunti saldati è complicato poiché influenzato da diversi fattori intrinseci dovuti alla natura del giunto saldato. Infatti, difetti come porosità, undercuts a piede cordone o disallineamenti portano a un aumento della concentrazione di tensione in corrispondenza del profilo geometrico. L'effetto che si considererà all'interno di questo elaborato è quello dei disallineamenti che possono essere presenti nei giunti. Tali difetti sono dovuti inevitabilmente alla lavorazione e deformazione che avviene durante il processo di saldatura. In molti casi i disallineamenti non possono essere ignorati nelle verifiche a fatica poiché inducono un momento flettente aggiuntivo che può avere un importante effetto nella vita a fatica.

Il Capitolo 1 ha lo scopo di introdurre il lettore alle basi e principi degli approcci locali che sono stati utilizzati in questa tesi. Due metodi sono stati estratti dalla normativa IIW, mentre i restanti tre sono stati sviluppati presso l'Università degli Studi di Padova, come descritto precedentemente. Per ciascun metodo sono riportati anche i vantaggi e svantaggi.

Il Capitolo 2 è la descrizione dell'addestramento per il testista per l'applicazione dei metodi NSIFs, SED e PSM per la verifica a fatica di strutture 2D e 3D. I dati ottenuti vengono successivamente raccolti per eseguire una nuova analisi statistica e comparare i risultati ottenuti con le curve proposte nella letteratura di riferimento.

Il Capitolo 3 descrive la verifica a fatica di specifiche geometrie di giunti as-welded in termini di tensione nominale, tensione di hot-spot, tensione equivalente di picco (PSM) e densità di energia di deformazione (SED). Come nel Capitolo 2, i dati vengono inseriti nelle curve di riferimento ricavate dalla letteratura per poter effettuare una comparazione in termini di numero di cicli per poter capire il grado di efficacia e sicurezza di

ciascun metodo applicato.

Il Capitolo 4 inizialmente introduce il lettore alle basi, ai principi e ai benefici del trattamento post-saldature HFMI sui giunti saldati. Successivamente, si descrive la verifica a fatica di specifiche geometrie di giunti trattati HFMI, applicando l'hot-spot method e il PSM combinato al SED per intagli smussati. Anche in questo caso i dati vengono inseriti nelle curve di riferimento per poter capire il grado di efficacia e sicurezza di ciascun metodo applicato.

Il Capitolo 5, dopo una breve introduzione degli effetti dovuti ai disallineamenti nei giunti saldati, descrive la metodologia utilizzata per poter definire il fattore k_{mis} che tiene conto degli effetti che i disallineamenti hanno sulla vita a fatica dei giunti saldati. In questo capitolo si studia l'effetto dei disallineamenti nei giunti saldati sia in condizioni CAL che VAL e si propone una nuova curva per il design a fatica dei giunti saldati con disallineamenti sia assiali che angolari.

Il Capitolo 6 descrive la procedura sperimentale che è stata seguita per poter ottenere il valore delle tensioni membranali e soprattutto di flessione dovuti ai disallineamenti. In questo capitolo si descrive la procedura di calcolo eseguita per poter ricavare il fattore k_{mis} attraverso i dati ottenuti sperimentalmente, le formule ricavate dal Capitolo 5 e le formula prese da normativa.

Il Capitolo 7 definisce le conclusioni di questo lavoro descrivendo anche i futuri miglioramenti da poter eseguire.

Acknowledgements

It's not easy to express my gratitude to who gave me the support and the courage to reach this important achievement of my life.

Firstly, I would like to sincerely thank Professor Giovanni Meneghetti, from University of Padua, and Professor Halid Can Yildirim, from Aarhus University, whose gave me the opportunity of doing my thesis abroad, allowing me to live in a foreign country for the first time. This period in Aarhus has been very important for my personal growth and it allowed me to draw relevant guidance for my future career. Furthermore, I would also like to thank for your patience, for your support and, above all, for helping me in this period with your advice and with your strong passion in your job. Thanks to Professor Alberto Campagnolo, who has been always available, and your guidance helped me in all the time of research and writing of this thesis.

Thanks to my parents, who always believed in me and in my abilities. Both of you taught me that the passion and determination are the keys to reach my goals. To my mum that, despite some misunderstandings, you have always believed in me and you have taught me the values of the life. To my dad that, despite you don't speak a lot, I'm sure that you are proud of me. To my sister Martina, my reference point and idol: thanks for your support despite the distance.

Thanks to all my friends for supporting me, for sharing successes and fails with me and for the moments of leisure. To my fellow students for their feedback, cooperation and of course friendship.

Thanks to my grandfathers, who even if you are not here with us, I know that you would be proud of me and of my journey. I also dedicate to you this important achievement of my career.

Ringraziamenti

Non è mai facile esprimere gratitudine verso coloro che mi hanno sostenuto e dato la forza e il coraggio per raggiungere questo importante traguardo della mia vita.

Prima di tutto, vorrei ringraziare il Professor Giovanni Meneghetti dell'Università degli Studi di Padova e il Professor Halid Can Yildirim dell'Università di Aarhus, che mi hanno dato l'opportunità di eseguire il lavoro di tesi all'estero e mi hanno permesso di vivere in un altro paese per la prima volta. Questo periodo speso ad Aarhus è stato molto importante per la mia crescita personale e mi ha permesso di definire un percorso chiaro per la mia futura carriera lavorativa. Inoltre, li ringrazio per la loro pazienza, per il loro supporto e soprattutto per avermi aiutato in questo mio percorso con i loro consigli e con la loro passione per il proprio lavoro. Un grazie al Professor Alberto Campagnolo che si è reso sempre disponibile nei miei confronti e mi ha sempre aiutato a trovare una soluzione ai dubbi più spinosi e grazie ai consigli che mi ha dato: sono stati fondamentali per la buona riuscita di questa tesi.

Un grazie ai miei genitori che hanno sempre avuto fiducia in me e nelle mie capacità anche nei momenti più difficili. Entrambi mi avete insegnato che con la passione e determinazione si possono raggiungere gli obiettivi prefissati. A mia mamma che, nonostante i litigi, ha sempre creduto in me e mi ha insegnato i veri valori della vita. A mio papà che, nonostante non sia di molte parole, so per certo che è fiero e orgoglioso di me. A mia sorella Martina, da sempre fonte di ispirazione e mio idolo da seguire: hai sempre avuto una parola di sostegno nei miei confronti nonostante la distanza e hai sempre creduto in me.

Un grazie a tutti i miei amici, con cui ho condiviso le delusioni e successi di questo percorso e soprattutto momenti di svago. Un riconoscimento va anche ai miei compagni di corso, con cui ho condiviso opinioni e idee.

Un grazie anche ai miei nonni, Guido e Danilo, che anche se non siete qui presenti, so che sareste fieri di me e del mio percorso intrapreso. Dedico anche a voi questo traguardo importante della mia carriera.

Contents

1	Description of global and local approaches for fatigue assessment of welded joints	1
1.1	Global approaches of the IIW guideline	1
1.2	Local approaches of the IIW guideline	3
1.2.1	SHSS (Structural Hot Spot Stress) approach	3
1.2.2	Effective Notch Stress (ESN) approach	7
1.3	Local approaches of University of Padua	9
1.3.1	NSIFs (Notch Stress Intensity Factors) approach	10
1.3.2	Strain Energy Density (SED) approach	12
1.3.3	Peak Stress Method (PSM)	14
1.3.4	Attentions on the PSM	20
2	Numerical analysis of experimental data to detect the NSIFs, SED and PSM parameters	21
2.1	Description of transverse attachments geometries	21
2.1.1	Maddox 1987, 1st specimen	22
2.1.2	Gurney 1991, 2nd specimen	24
2.1.3	Gurney 1991, 3rd specimen	25
2.1.4	Gurney 1991, 4th specimen	27
2.2	NSIFs (Notch Stress Intensity Factors) approach	28
2.2.1	Calculation of NSIFs in Ansys®APDL	29
2.2.2	NSIFs K_1 and K_2 results	39
2.3	Nominal Stress approach	41
2.3.1	Results of Nominal Stress approach	41
2.4	SED (Strain Energy Density) approach	42
2.4.1	Calculation of SED in Ansys®APDL	42
2.4.2	SED results	46
2.5	PSM (Peak Stress Method) approach	48
2.5.1	Calculation of Equivalent Peak Stress in Ansys®APDL	49
2.5.2	PSM results	53
2.5.3	Comparison between Analytical and PSM-estimated K_1	55
2.6	Geometry description of square chord with circular brace joint: Gandhi (1998)	56
2.7	PSM approach with Submodeling technique	58
2.7.1	PSM with Submodeling technique: results	65
2.8	PSM approach with four-node Tetra element (Tetra 285)	67
2.8.1	PSM with Tetra 4 elements: results	68
2.9	PSM approach with ten-node Tetra element (Tetra 187)	70
2.9.1	PSM with Tetra 10 elements: results	71
2.10	Comparison of the results and data entry in the PSM curve	74
3	Numerical analysis of experimental data and fatigue assessment of As-welded joint by local approaches	77
3.1	Marquis 2010, longitudinal attachment FAT 71	77
3.1.1	PSM approach with Submodeling technique	81
3.1.2	PSM approach with Submodeling technique: results	86
3.1.3	PSM approach with Tetra 187	89
3.1.4	PSM approach with Tetra 187: results	90
3.1.5	Data results for PSM curve	92
3.1.6	SED (Strain Energy Density) approach	93

CONTENTS

3.1.7	SED (Strain Energy Density) approach: results	94
3.1.8	Data results for SED curve	95
3.1.9	SHSS (Structural Hot Spot Stress) approach	96
3.1.10	Data results for IIW curve	98
3.2	Vanrostenberghe 2015, longitudinal attachment FAT 63	100
3.2.1	PSM approach with Submodeling technique	104
3.2.2	PSM approach with Submodeling technique: results	108
3.2.3	PSM approach Tetra 187	113
3.2.4	PSM approach with Tetra 187: results	114
3.2.5	Data results for PSM curve	117
3.2.6	SED (Strain Energy Density) approach	118
3.2.7	SED (Strain Energy Density) approach: results	120
3.2.8	Data results for SED curve	121
3.2.9	SHSS (Structural Hot Spot Stress) approach	122
3.2.10	Data results for IIW curve	126
3.3	Yildirim 2020, transverse attachment FAT 80	128
3.3.1	PSM approach Plane 182	131
3.3.2	PSM approach with Plane 182: results	132
3.3.3	Data results for PSM curve	133
3.3.4	SHSS (Structural Hot Spot Stress) approach	134
3.3.5	Data results for IIW curve	136
3.4	Okawa 2013, transverse attachment FAT 80	137
3.4.1	PSM approach Plane 182	140
3.4.2	PSM approach with Plane 182: results	141
3.4.3	Data results for PSM curve	142
3.4.4	SHSS (Structural Hot Spot Stress) approach	143
3.4.5	Data results for IIW curve	145
3.5	Kuhlmann-Gunther 2009, transverse attachment FAT 80	146
3.5.1	PSM approach Plane 182	149
3.5.2	PSM approach with Plane 182: results	150
3.5.3	Data results for PSM curve	151
3.5.4	SHSS (Structural Hot Spot Stress) approach	152
3.5.5	Data results for IIW curve	154
3.6	Kuhlmann 2006, transverse attachment FAT 80	156
3.6.1	SHSS (Structural Hot Spot Stress) approach	158
3.7	Summary of the results	161
4	Numerical analysis of experimental data and fatigue assessment of HFMI-treated joint by local approaches	165
4.1	Principles of HFMI post-weld treatments on welded joints to improve the weld toe	165
4.1.1	Description of HFMI treatment	166
4.1.2	Fatigue assessment of HFMI-treated joints (IIW recommendations)	169
4.1.3	Fatigue assessment of HFMI-treated joints: University of Padua approach	176
4.2	Marquis 2010, longitudinal attachment FAT 71	178
4.2.1	PSM combined with SED for blunt notches	179
4.2.2	Data results for SED curve	184
4.2.3	SHSS(Structural Hot Spot Stress) approach	185
4.3	Vanrostenberghe 2015, longitudinal attachment FAT 63	186
4.3.1	PSM combined with SED for blunt notches	189
4.3.2	Data results for SED curve	195
4.3.3	SHSS(Structural Hot Spot Stress) approach	197
4.4	Yildirim 2020, transverse attachment FAT 80	197
4.4.1	PSM combined with SED for blunt notches	199
4.4.2	Data results for SED curve	203
4.4.3	SHSS(Structural Hot Spot Stress) approach	204
4.5	Okawa 2013, transverse attachment FAT 80	205
4.5.1	PSM combined with SED for blunt notches	206
4.5.2	Data results for SED curve	209

CONTENTS

4.5.3	SHSS(Structural Hot Spot Stress) approach	211
4.6	Kuhlmann-Gunther 2009, transverse attachment FAT 80	212
4.6.1	PSM combined with SED for blunt notches	213
4.6.2	Data results for SED curve	219
4.6.3	SHSS(Structural Hot Spot Stress) approach	220
4.7	Kuhlmann 2006, transverse attachment FAT 80	221
4.7.1	PSM combined with SED for blunt notches	223
4.7.2	Data results for SED curve	226
4.7.3	SHSS(Structural Hot Spot Stress) approach	227
4.8	Summary of the results	228
5	Assessment of misalignment effect of cruciform joints in HFMI condition	235
5.1	Definition of angular and linear misalignment	235
5.2	Procedure for the detection of misalignment effect	236
5.2.1	Definition of sample's geometry	236
5.2.2	Preliminary analysis of the samples	239
5.2.3	Ideal model and application of local approaches	242
5.2.4	Ideal model with Misalignment and application of local approaches	254
5.2.5	Definition of several ratio to understand the misalignment effect	265
5.2.6	Definition of k_{mis} factor for the detection of misalignment effect	268
5.2.7	Definition of k_{mis} factor for the detection of misalignment effect for joint subjected to CAL condition	283
5.2.8	Definition of k_{mis} factor for the detection of misalignment effect in CAL condition	290
6	Testing program and comparison of results	307
6.1	Experimental instrumentation	307
6.1.1	Geometry of the tested specimens	307
6.1.2	Strain gauge E.R.M.	308
6.1.3	Strain gauge control unit IMC	311
6.1.4	Connectors	312
6.1.5	Multimeter	313
6.1.6	Schenck Hydropuls®PSA machine	313
6.2	Misalignment measurement method	314
6.2.1	Description of measurement method	315
6.3	Experimental procedure	319
6.3.1	Verification of the functioning of the strain gauge cables with multimeter	320
6.3.2	Connection between strain gauges, connectors and strain gauge control unit IMC	320
6.3.3	Configuration of the software <i>IMC Devices</i>	322
6.3.4	Mounting of the specimen in the machine	323
6.3.5	Manual application of the static load	325
6.3.6	Elaboration of the results	325
6.4	Detection of the misalignment effect	330
6.4.1	Calculation of k_{mis} with obtained formula in paragraph 5.2.8	330
6.4.2	Calculation of k_{mis} with formula from IIW guideline [1]	332
6.4.3	Calculation of k_{mis} from experimental data	333
7	Conclusions	337
7.1	Future improvements	344
	APPENDICES	344
A	Nodal stress $\Delta\sigma_{yy}$ and $\Delta\sigma_{11}$ and relative comparison	345
A.1	Brace side	345
A.2	Chord side	346
B	Nodal stress $\Delta\sigma_{11}$ and average peak stress value	347
B.1	Marquis 2010, longitudinal attachment FAT 71	347
B.2	Vanrostenbergh 2010, longitudinal attachment FAT 63	348

C	Experimental results in As- welded condition	351
C.1	Marquis 2010, longitudinal stiffener FAT 71	351
C.2	Vanrostenberghe 2015, longitudinal stiffener FAT 63	351
C.3	Yildirim 2020, transverse attachment FAT 80	352
C.4	Okawa 2013, transverse attachment FAT 80	352
C.5	Kuhulmann-Gunther 2009, transverse attachment FAT 80	353
D	Experimental results in HFMI-treated condition	355
D.1	Marquis 2010, longitudinal stiffener FAT 71	355
D.2	Vanrostenberghe, longitudinal stiffener FAT 63	356
D.3	Yildirim 2020, transverse attachment FAT 80	357
D.4	Okawa 2013, transverse attachment FAT 80	358
D.5	Kuhlmann-Gunther 2009, transverse attachment FAT 80	358
D.6	Kuhlmann 2006, transverse attachment FAT 80	359
E	Matlab codes	361
E.1	MatLab code to build the model inside Ansys®APDL with the sampling	361
E.2	MatLab code for the application of local approaches for ideal model	364
E.2.1	Code for application of ENS	364
E.2.2	Code for application of SHSS	366
E.2.3	Code for application of PSM (Sharp V-notch)	368
E.2.4	Code for application of PSM (No sharp V-notch)	370
E.3	MatLab code for the application of local approaches for ideal model with misalignment	375
E.3.1	Code for application of ENS	375
E.3.2	Code for application of SHSS	378
E.3.3	Code for application of PSM (Sharp V-notch)	382
E.3.4	Code for application of PSM (No sharp V-notch)	385
E.4	MatLab code for the statistical analysis for the detection of misalignment factor	390
E.4.1	Free slope	390
E.4.2	Fixed slope m=5	392
F	Results of misalignment analysis	395
F.1	Dimension of HFMI groove	395
F.2	Results of ideal model	396
F.3	Results of ideal model with misalignment	398
G	Results of analysis of joint in CAL condition	401
G.1	Results and Experimental data from [49]	401
G.2	Results and Experimental data from [50]	402
G.3	Results and Experimental data from [51]	403
G.4	Results and Experimental data from [52]	404
G.5	Results and Experimental data from [53]	405
G.6	Results and Experimental data from [54]	407
G.7	Results and Experimental data from [55]	407
G.8	Results and Experimental data from [56]	408
G.9	Results and Experimental data from [57]	409
G.10	Results and Experimental data from [58]	410
G.11	Results and Experimental data from [59]	411
G.12	Results and Experimental data from [60]	412
G.13	Results and Experimental data from [61]	412
G.14	Results and Experimental data from [62]	413
G.15	Results and Experimental data from [63]	414
G.16	Results and Experimental data from [64]	415

H	Experimental and elaboration results	417
H.1	Cruciform joint	417
H.1.1	Experimental data	417
H.1.2	Elaboration results	420
H.2	T-joint	423
H.2.1	Experimental data	423
H.2.2	Elaboration results	426
	Bibliography	429

Chapter 1

Description of global and local approaches for fatigue assessment of welded joints

The objective of this elaborate is to execute fatigue assessment on welded joint in as-welded and HFMI-treated conditions and evaluated the effect of misalignment (axial and angular) on the joints' fatigue life. The assessment are performed with the application of global and local approaches through the use of the finite element software *Ansys* ®*Mechanical APDL* with the license of the University of Padua. The aim of this first chapter is to present the principles, methodologies, advantages and disadvantages of each method used. All approaches assume the linear elastic behaviour of the material.

1.1 Global approaches of the IIW guideline

The most common method for the fatigue assessment of welded joints is the nominal stress approach. This method is based on the calculation of the nominal stress range in a sectional area under consideration disregarding the local stress raising effects of welded joint, but at the same time including the effects of the macro-geometric shape near to the joints.

The nominal approach is called *Global* because it proceeds directly from the external load, with the hypothesis of linear or constants stress distribution through the area considered.

The fatigue strength of the welded joints is defined in terms of a several double logarithmic design curves called *S-N curves* where:

- S is the applied nominal stress range $\Delta\sigma_{nom}$ defined in *MPa*;
- N or N_f is the number of cycles to failure of the component under investigation. There are different definition of N: Hobbacher [1] defined the fatigue life as:

The number of stress cycles of a particular magnitude required to cause fatigue failure of the component.

Hobbacher adds also that small welded specimen failures refer to complete fracture, instead of for the large structural details, N is related to the observation of a through-the-thickness crack.

The IIW recommendations describe the S-N curves with the following equation:

$$N = \frac{C}{\Delta\sigma^m} \quad (1.1)$$

where:

- m is the inverse slope of the curve and may adopt different values over the range of possible fatigue lives, from the low cycles to the high cycles regime;
- C is a constant.

Generally, the S-N curves are referred to joint in as-welded condition and their fatigue life is principally dependent on the external applied stress range $\Delta\sigma$ and these joints are independent on the stress ratio $R = \frac{\sigma_{min}}{\sigma_{max}}$ and material yield strength. For this reason, from each specimens, the maximum principal stress range $\Delta\sigma_{11}$ is extracted from the section where the crack is more likely to develop. Of course, if the structure is characterised by a maximum shear stress range $\Delta\tau_{11}$, different S-N curves are available. One example of S-N curves are available in *Figure 1.1* and *Figure 1.2*. This curves represent the fatigue resistance in terms of nominal stress $\Delta\sigma_{nom}$, subjected to CAL (Constant Amplitude Loading) for steel and aluminium alloys.

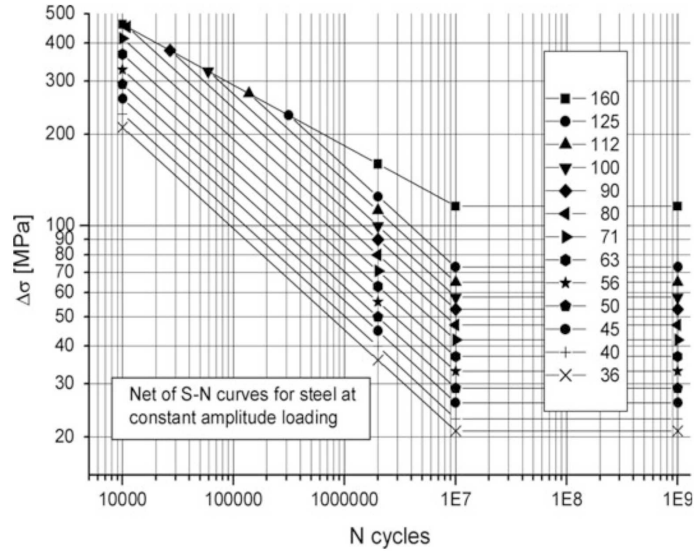


Figure 1.1: Fatigue resistance S-N curves for steel, normal stress, CAL [1]

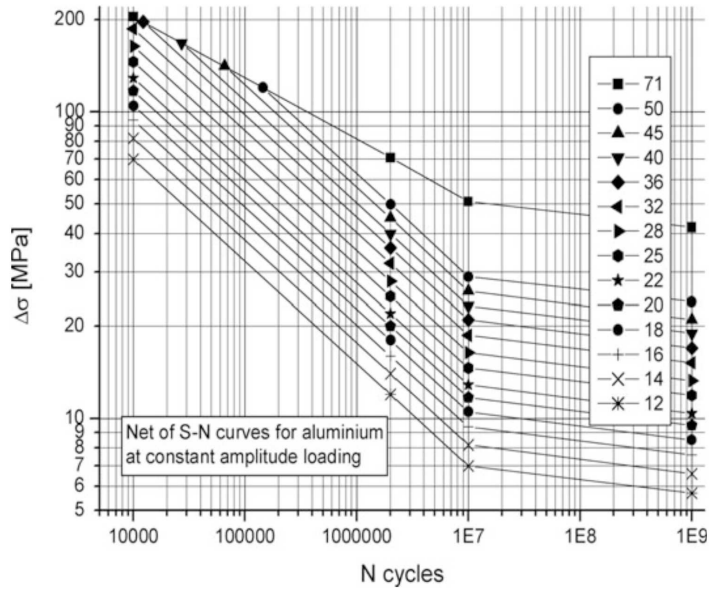


Figure 1.2: Fatigue resistance S-N curves for aluminium alloys, normal stress, CAL [1]

This curves are defined thanks to experimental investigations and so include the effects of:

- Structural hot spot stress concentration due to the detail shown;
- Local stress due to the weld geometry;
- Weld imperfection consistent with normal fabrication standards;
- Direction of loading;
- High residual stresses;
- Metallurgical conditions;
- Welding process (fusion welding, unless otherwise stated);
- Inspection procedure (NDT), if specified;
- Post weld treatment, if specified.

Each S-N curve are identified by the characteristic fatigue strength of the component in MPa at 2 million cycles. This value is called the *Fatigue Class (FAT)*.

The slope of the fatigue strength S-N curves in terms of $\Delta\sigma_{nom}$ is equal to $m = 3$, while in terms of $\Delta\tau_{nom}$ is equal to $m = 5$. The constant amplitude knee point is placed for $N = 10^7$ cycles for normal stresses, while for shear stresses is place for $N = 10^8$. The knee point is called *Constant Amplitude Fatigue Limit CAFL* and below it, the fatigue life is assumed infinite. Indeed, from the CAFL the curve should be horizontally.

However, some recently studies defined that the CAFL does not exist and for this reason, the slope after the knee point could be equal to $m = 22$.

As above-mentioned, this method is the most common approach but nevertheless, it is characterised by several disadvantages:

- The fatigue assessment in terms of nominal stress approach does not include the effects of the shape and the size, that they have a strong impact on the service life. For this reason, there are different fatigue design curves S-N in based on the geometry of the components.
- In some cases, the detection of the nominal stress $\Delta\sigma_{nom}$ is very complex, indeed there is the need to satisfy the engineering state of art in those areas related to VAL (Variable Amplitude Loading) or where the nominal stress is not immediately obtainable.

1.2 Local approaches of the IIW guideline

Local fatigue assessment methods like *Structural Hot Spot Stress* and *Effective Notch Stress* as defined by the *International Institute of Welding* are widely used by design engineers and researchers to assess the fatigue strength of welded components.

The objective of the local approaches is to focus on the stress growth due to the geometric changes and the weld profile itself.

The IIW recommendations [1] proposes two different local method that are applied in this thesis: the first one is the *Structural Hot Spot Stress*, the second is the *Effective Notch Stress*. These two approaches are characterized that in FE environment and linear elastic hypothesis, the stress increment due to the presence of weld profile is dependent on the mesh size. The idea is to consider only the raise stress effects due to the joint geometry, so the element size is considered as a secondary effect.

1.2.1 SHSS (Structural Hot Spot Stress) approach

The structural stress σ_{hs} at the hot spot considers all stress raising effects of structural detail but it does not include the non-linear peak stress due to the local notch, i.e. the weld toe is excluded from the structural stress. The Structural Hot Spot Stress value depends on the global dimension of the joint and on the loading parameters in proximity of the welded joint. This value is defined on the surface at the hot spot of the joint which is to be assessed.

The SHSS approach is suitable for the structures that are characterized by structural discontinuities and geometric complexity. Indeed, in this case is tough to detect a nominal stress comparable to a classified structural details.

The SHSS approach is applied on the exterior surface, where the non-linear peak is deleted by the linearization of the stress through the plate's thickness or also by extrapolation of stresses at reference points, place on the weld toe's surface.

The system to calculate the SHSS value is described in IIW recommendations [1]. The first step is to establish the reference points and after to define the structural hot spot stress by extrapolation of the stresses from those reference points. The number of the points depends on the employed hot spot typology; indeed two types of hot spots are define according to their orientation in respect to weld toe like *Figure 1.3* and *Table 1.1* shows.

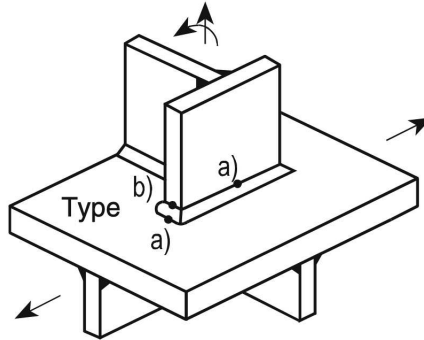


Figure 1.3: Types of hot spots [1]

Types	Description	Determination
a	Weld toe on plate surface	FEA or measurement and extrapolation
b	Weld toe on plate edge	FEA or measurement and extrapolation

Table 1.1: Types of hot spots [1]

As above-mentioned, the number of reference points depends on the typology of hot spot as shows the following figure:

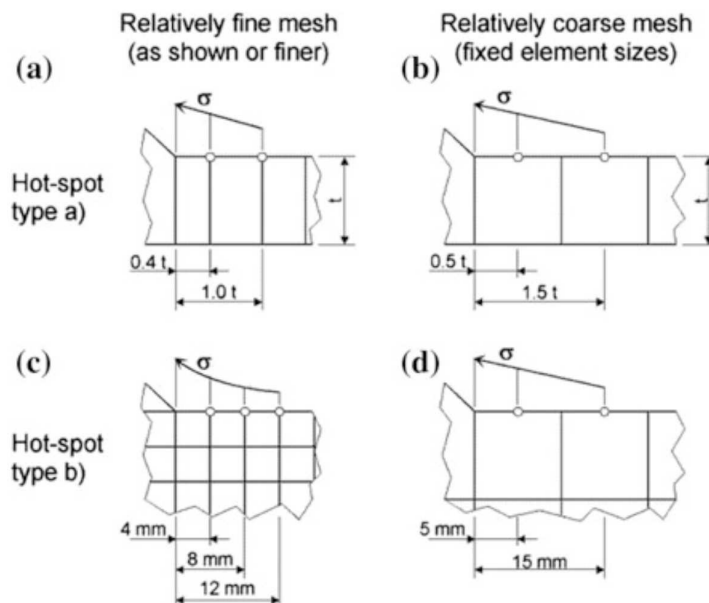


Figure 1.4: Reference points at different types of meshing [1]

The reference point closest to weld toe must be chosen to avoid any non-linear effect due to the weld profile itself. For this reason, the minimum distance recommended from weld toe is equal to $0.4 \cdot t$, where t is the main thickness of the plate. Once the stresses at the reference points are obtained, a linear extrapolation with two reference points, or quadratic one with three points is applied to define the *Hot Spot Stress* value at the weld toe (Figure 1.5).

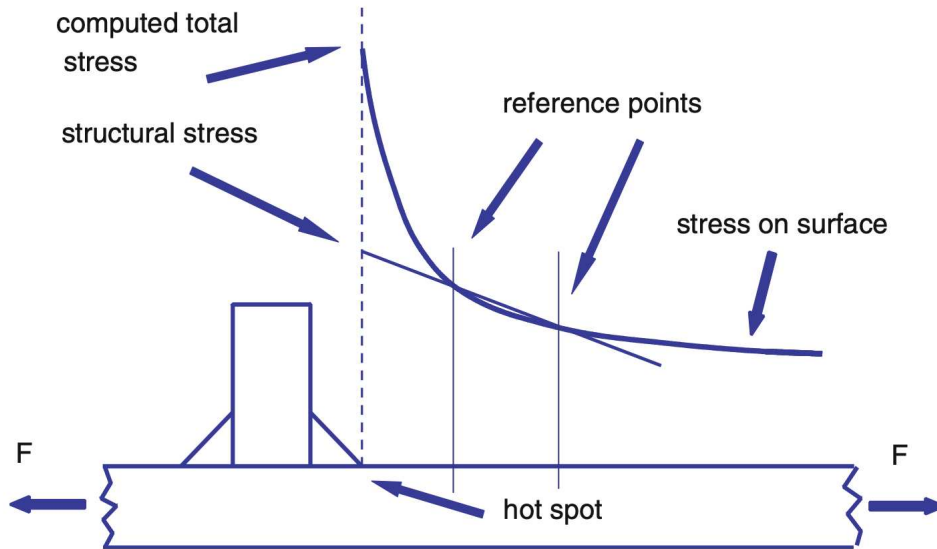


Figure 1.5: Definition of structural hot spot stress at weld toe [1]

The Hot Spot method can be limited to the assessment of the weld toe crack, some examples are illustrated in the Figure 1.6:

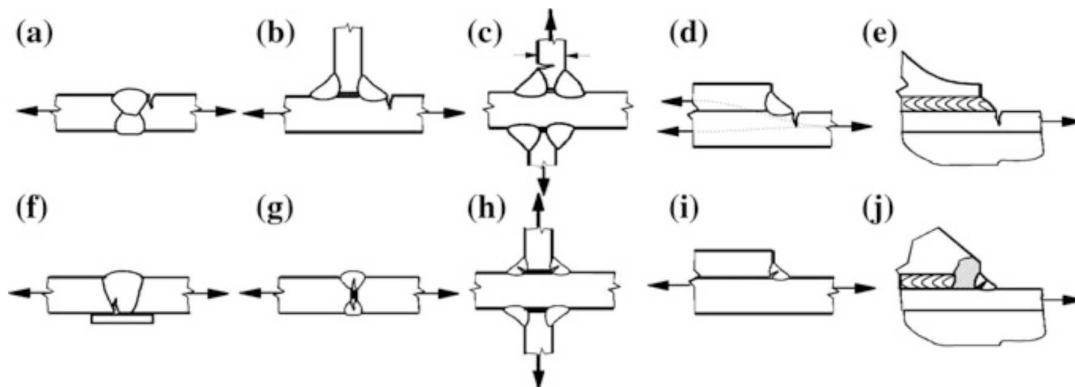


Figure 1.6: Different locations of crack propagation in welded joints: **a-e** represents weld toe cracks, where SHSS approach can be applied; **f-i** represents weld root cracks, where SHSS approach can not be applied [1]

According to Figure 1.4, for hot spot type a, two different extrapolation formulae are possible:

1. Linear extrapolation with two reference points:

$$\sigma_{hs} = 1,67 \cdot \sigma_{0,4-t} - 0,67 \cdot \sigma_{1,0-t} \quad (1.2)$$

2. Quadratic extrapolation with three reference points in cases of important non-linear stress effect on the hot spot:

$$\sigma_{hs} = 2,52 \cdot \sigma_{0,4-t} - 2,24 \cdot \sigma_{0,9-t} + 0,72 \cdot \sigma_{1,4-t} \quad (1.3)$$

For the Hot Spot method, the different nominal FAT classes are collapsed in only two FAT classes, as *Figure 1.7* shows: FAT 90 and FAT 100. These curve present the following characteristics:

- The curve are referred to as-welded condition unless stated otherwise;
- The effects of high tensile residual stress are included;
- Only small effects of misalignment are included. In the presence of a consistent misalignment, a stress magnification factor K_m , defined by IIW guideline [1], must be included;
- The design value of the structural hot spot stress range $\Delta\sigma_{hs}$ must be minor to $2 \cdot f_y$ to avoid plastic yielding.

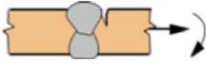
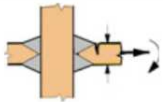
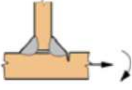
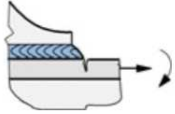
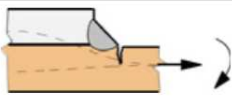
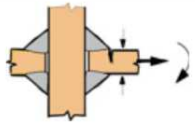
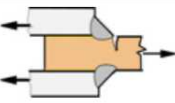
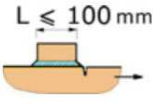
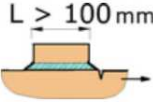
No.	Structural detail	Description	Requirements	FAT Steel	FAT Alu.
1		Butt joint	As welded, NDT	100	40
2		Cruciform or T-joint with full penetration K-butt welds	K-butt welds, no lamellar tearing	100	40
3		Non load-carrying fillet welds	Transverse non-load carrying attachment, not thicker than main plate, as welded	100	40
4		Bracket ends, ends of longitudinal stiffeners	Fillet welds welded around or not, as welded	100	40
5		Cover plate ends and similar joints	As welded	100	40
6		Cruciform joints with load-carrying fillet welds	Fillet welds, as welded	90	36
7		Lap joint with load carrying fillet welds	Fillet welds, as welded	90	36
8		Type "b" joint with short attachment	Fillet or full penetration weld, as welded	100	40
9		Type "b" joint with long attachment	Fillet or full penetration weld, as welded	90	36

Figure 1.7: SHSS FAT classes [1]

The thickness correction factor, used for nominal approach and defined in IIW recommendations [1], can be accounted for SHSS method because this method does not include and predict the effect of the thickness.

In the article of 2004 [36], Potiainen, Tanskanen and Marquis give some advises for the modelling:

- The extrapolation of the hot spot stress value can be executed with the using of both fine and coarse meshes;
- The first principal stress and the stress along x-axis can be detected in the reference points;
- For 2D models, the *mapped-mesh* algorithm can be used to create the mesh with four-node linear plane elements (PLANE 182 in ANSYS®);
- For 3D structures, eight-node or twenty-node linear hexahedral elements can be adopted for the mesh (SOLID185 and SOLID 186 in ANSYS®). In the case of 8-node element, several elements layers are allowed along the main plate thickness; instead for the 20-node hexahedral elements, only one elements is allowed to avoid any influence of the singularity.

1.2.2 Effective Notch Stress (ESN) approach

In 2008, the IIW approved the guideline concerning fatigue design of welded components based on the Effective notch stress (ESN) approach to fatigue assessment [1].

Effective notch stress is the total stress at the root of a notch and in this method the maximum principal stress or von Mises stress at the notch, e.g. weld toe or root, can be idealized by considering a linear-elastic material behaviour through the finite element analysis.

To consider the non-linear material behaviour at the notch root and also to include shape effects of the weld, the weld profile at weld toe or root is replaced by a fictitious notch radius as *Figure 1.8* shows. This method is applicable for plates that are characterized by a thickness $t \geq 5$ and for these welds, it is proposed that:

$$\rho_f = \rho + 1\text{mm} \quad (1.4)$$

where:

- ρ is the actual radius of the weld toe;
- ρ_f is the effective radius which is implemented to the finite element model. For the worst case and practical applications, the actual radius ρ is assumed equal to zero. Thus, the ENS approach for fatigue assessment is reduced to $\rho_f = 1\text{mm}$ at weld toe or root.

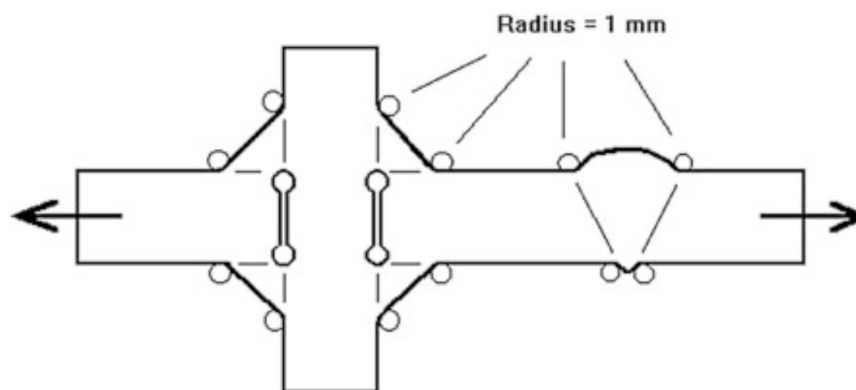


Figure 1.8: Fictitious rounding of weld toes and roots [1]

The ENS approach is suitable to assessment of welded joints characterized by potential crack initiation from weld toe or root (Figure 1.9). Furthermore, the fatigue assessment has to additionally executed at weld toe for parent material with SHSS and the related fatigue class FAT for the base material.

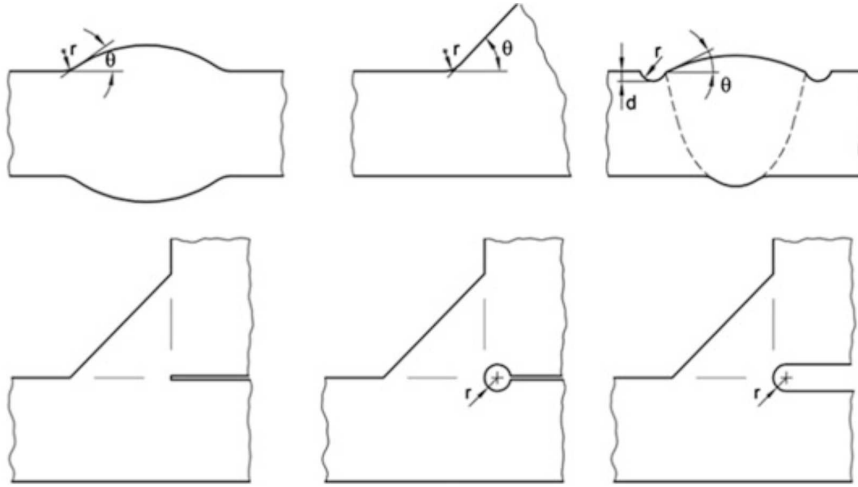


Figure 1.9: Recommended rounding of weld toes and roots [1]

This approach is restricted to assessment of as-welded weld toe and roots. Effective notch stresses or stress concentration factors can be obtained by parametric formulae, diagrams or finite element model. In this case the IIW recommendations gives some rules for the global element size and mesh pattern as Figure 1.10. The rules for size are expressed in Table 1.2 and have to be observed in the curved part and straight part of the notch surfaces in normal and tangential direction.

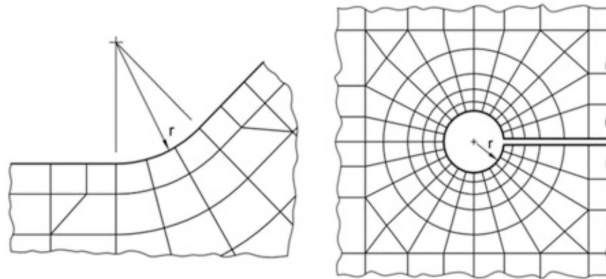


Figure 1.10: Recommended meshing at weld toes and roots [1]

Element type	Relative size	Absolute size [mm]	No. of elements in 45° arc	No. of elements in 360° arc
Quadratic with mid-side nodes	$\leq r/4$	≤ 0.25	≥ 3	≥ 24
Linear	$\leq r/6$	≤ 0.15	≥ 5	≥ 40

Table 1.2: Recommended size of elements on surface [1]

For the Effective Notch Stress Method, the different nominal FAT classes for the steel are collapsed in only one FAT classes, as Table 1.3 shows: FAT 225. These curve present the following characteristics:

- The curve are referred to as-welded condition;
- The effects of high tensile residual stress are included;
- The effect of possible misalignment is not included;

- The fatigue resistance of weld toe is additionally limited by fatigue resistance of the parent material that is determined by the use of SHSS approach and the FAT classes of non-welded parent material.

No.	Quality of weld notch	Description	FAT
1	Effective notch radius equal to 1mm replacing weld toe and weld root	Notch as-welded, normal welding quality m=3	225

Table 1.3: Effective Notch fatigue resistance for steel [1]

1.3 Local approaches of University of Padua

In the classical mechanics, during a verification of structural resistance, the resistance of the structure under analysis is determined by a point value approach. This type of analysis is characterised by a comparison between the stress calculated at the most stress point of the structure and a reference value, the yield strength f_y is generally used. This approach can not be used for the cracks or sharp notches because a linear elastic analysis would show that the stress value at the tip of the defect tends to infinite.

On the other hand, the experimental reality illustrates that, due to the local material yielding near to the tip of the crack, this event is avoided. Thanks to the development of the linear elastic fracture mechanics (LEFM) theory, the structural resistance is determined by a field approach rather than a point value criterion.

The LEFM theory was extended also for the fatigue study of welded joints. This extension is called *non-conventional extension of the linear elastic fracture mechanics*. Indeed, the case of a V-notch with fillet radius different from zero ($\rho \neq 0$) is characterised by the same behaviour of a sharp notch with fillet radius equal to zero ($\rho = 0$), as evidenced by Smith and Miller (1978). In conclusion the notch that has a fillet radius $0 \leq \rho \leq 4 \cdot a_0$ can be consider like a sharp notch.

Thanks to the LEFM extension, the fatigue assessment of the welded joints is treated like a notch effect problem: the theory of the notch stress intensity factors NSIFs, elaborated by Gross and Mendelson (1972) [21]. Indeed, the weld toe profile is considered as a sharp V-notch having a tip radius equal to zero ($\rho = 0$) and the weld root is considered like a pre-crack in the welded structure.

The V-notch can be solicited in three different modes, like the *Figure 1.11* shows:

1. Mode I: tensile opening;
2. Mode II: in-plane shear;
3. Mode III: out-of-plane shear.

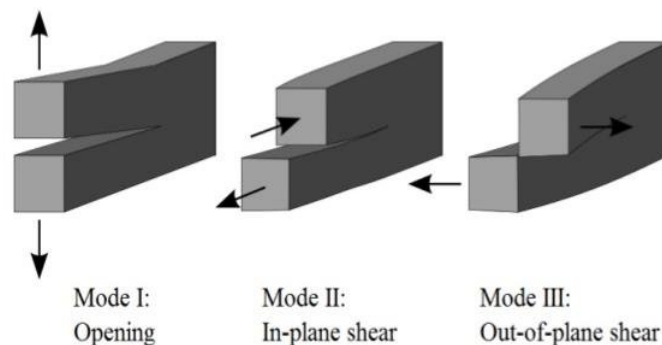


Figure 1.11: Description of the three solicitation mode for a V-notch [22]

1.3.1 NSIFs (Notch Stress Intensity Factors) approach

In plane problems, a V-notch is considered and it is subjected to only mode I and mode II of solicitation; the expression of the stress field for mode I and II is described by the equation (1.5):

$$\begin{Bmatrix} \sigma_{\theta\theta} \\ \sigma_{rr} \\ \tau_{r\theta} \end{Bmatrix} = \frac{K_1}{r^{1-\lambda_1}} \cdot \begin{Bmatrix} \tilde{\sigma}_{\theta\theta}(\theta) \\ \tilde{\sigma}_{rr}(\theta) \\ \tilde{\sigma}_{r\theta}(\theta) \end{Bmatrix}_I + \frac{K_2}{r^{1-\lambda_2}} \cdot \begin{Bmatrix} \tilde{\sigma}_{\theta\theta}(\theta) \\ \tilde{\sigma}_{rr}(\theta) \\ \tilde{\sigma}_{r\theta}(\theta) \end{Bmatrix}_{II} \quad (1.5)$$

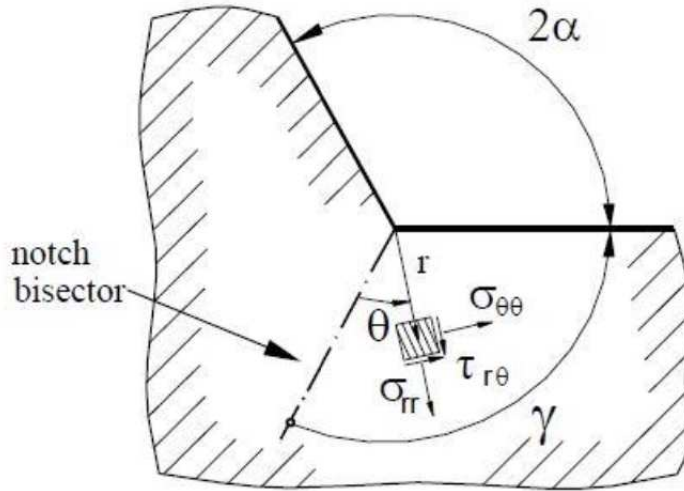


Figure 1.12: V-notch with a cylindrical local reference system [23]

where:

- $\sigma_{\theta\theta}, \sigma_{rr}, \tau_{r\theta}$ are the plane stress that are described in the cylindrical local reference system as shows in *Figure 1.12*;
- $\tilde{\sigma}_{\theta\theta}(\theta), \tilde{\sigma}_{rr}(\theta), \tilde{\sigma}_{r\theta}(\theta)$ are the trigonometric functions that depend on θ and also on the mode of solicitation
- λ_1, λ_2 are the Williams' eigenvalues that depend on the opening angle 2α of the V-notch. They express the grade of singularity of the stress field. The *Table 1.4* shows the typical values of λ_1, λ_2 in function of the opening angle 2α and also the *Figure 1.13* shows the trend of them:

2α [°]	λ_1 (Mode I)	λ_2 (Mode II)
0	0.5	0.5
30	0.501	0.598
45	0.505	0.660
60	0.512	0.731
90	0.544	0.909
120	0.616	1.149
135	0.674	1.302
150	0.752	1.486

Table 1.4: Value of λ_1 and λ_2 in function of the opening angle 2α

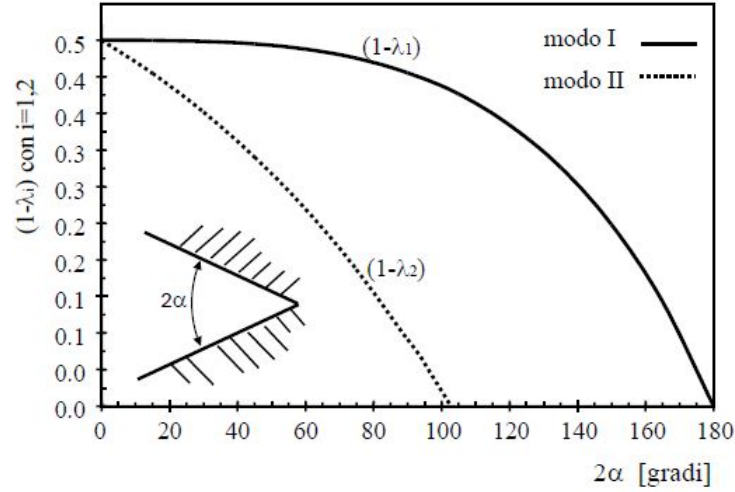


Figure 1.13: Trend of Williams' eigenvalues for Mode I and II in function of opening angle 2α . For $2\alpha > 102.5^\circ$ mode II is not singular [23]

- K_1 and K_2 are the Notch Stress Intensity Factors (NSIFs) associated to Mode I and II. These factors described the intensity of the local stress field components in the V-notch region.

Williams studied two-dimensional notch problems under mode I and II; subsequently, Qian and Hasebe studied the notch problem under mode III loading and defined K_3 and λ_3 for asymmetric structures. The three different NSIFs are defined in equation (1.6)-(1.8) with reference to *Figure 1.14a* and *Figure 1.14b* for the coordinates system:

$$K_1 = \sqrt{2\pi} \lim_{r \rightarrow 0^+} r^{1-\lambda_1} \cdot \sigma_{\theta\theta}(r, \theta=0) \quad (1.6)$$

$$K_2 = \sqrt{2\pi} \lim_{r \rightarrow 0^+} r^{1-\lambda_2} \cdot \tau_{r\theta}(r, \theta=0) \quad (1.7)$$

$$K_3 = \sqrt{2\pi} \lim_{r \rightarrow 0^+} r^{1-\lambda_3} \cdot \tau_{\theta z}(r, \theta=0) \quad (1.8)$$

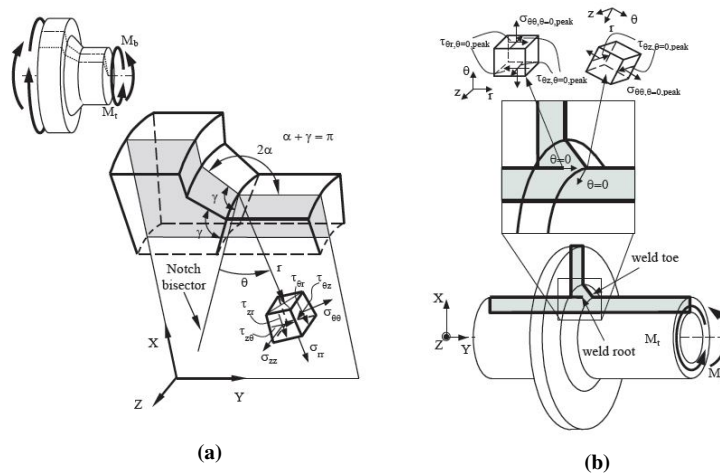


Figure 1.14: Different example of polar reference system centred at weld toe and definition of stress components [24].

Thanks to the work of Lazzarin and Tovo in 1998 [6], the NSIFs approach allows the fatigue assessment of sharp notched components with the using of only one fatigue design curve, in contrast to the nominal stress approach. This curve expresses the fatigue strength in terms of NSIF K_1 for mode I of loading. As show in Figure 1.15, due to the large variation of the geometrical parameters, the scatter band of nominal stress approach is larger than NSIFs approach. Indeed, for the nominal stress approach is necessary to adopt different design curve in based on the geometry of the joint because the fatigue is a local phenomenon which concentrate on the initiation and propagation of a crack near to the V-notch region. The NSIFs approach propose a unique fatigue design curve K_1-N_f for different joint's geometries because the shape and size effects are accounted inside the tensional parameter K_1 .

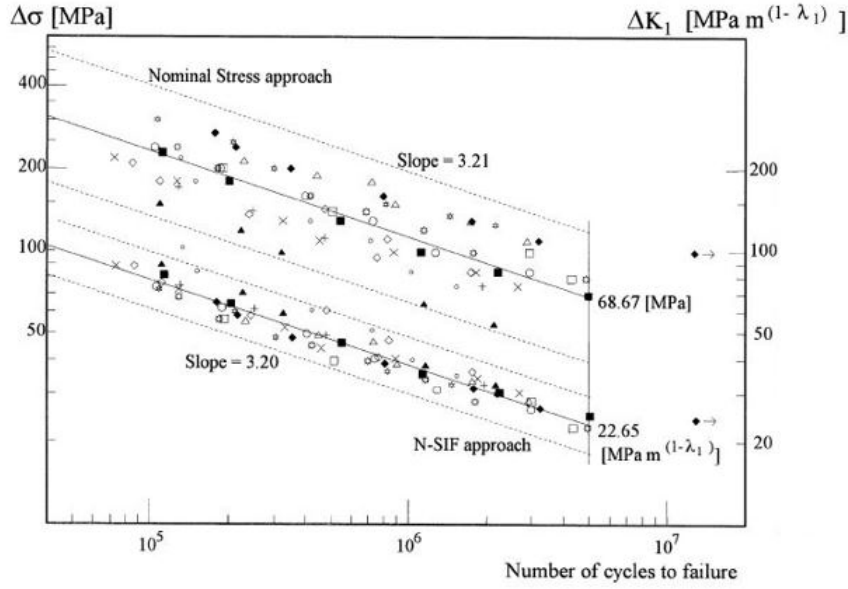


Figure 1.15: Fatigue strength in terms of nominal stress and NSIF ranges [6]

On the other hand, the NSIFs approach presents three relevant disadvantages in engineering applications as written by Campagnolo in [24]:

1. Very refine meshes are required (element size has to be roughly 10^{-5}) to calculate the NSIFs and so the computational time increases;
2. A large number of *stress distance* values are required to calculate K_i and so the post-process operation, that are necessary, can be complex and can require a lot of time;
3. The unit of measurement of $K_{i,i=1,2,3}$ are expressed in $[\text{MPa} \cdot \text{m}^{1-\lambda_{i,i=1,2,3}}]$, so it changes with the singularity of the stress distribution that depends on the opening angle 2α . Due to this, the comparison of stress field between V-notch with different opening angle is not possible.

1.3.2 Strain Energy Density (SED) approach

The energetic criterion has been proposed by Lazzarin and Zambardi [25] in 2001 to overcome the limits of NSIFs approach.

The proposal of SED considers as critical parameter to evaluate the structural resistance, the averaged strain energy density inside a circular sector of radius R_0 , that is a property of the material.

This approach is based on the structural volume, derived from Neuber's theory. Indeed the materials are sensitive to the average stress state inside a structural volume, characterized by the fact that the dimension is a material's property.

The typical values of R_0 are 0.28mm for steel structures and 0.12mm for aluminium alloys.

Initially, the method had been calibrated only for Mode I loading [25], but subsequently it was extended also for Mode II and III.

Under plane strain hypothesis, the averaged strain energy density inside a structural volume of radius R_c is expressed in function of NSIFs for Mode I and II for a V-notch, characterised by a opening angle 2α (1.9):

$$\bar{W} = \frac{1}{E} \cdot \left(c_{w1} \cdot e_1 \cdot \frac{K_1^2}{R_0^{1-\lambda_1}} + c_{w2} \cdot e_2 \cdot \frac{K_2^2}{R_0^{1-\lambda_2}} + c_{w3} \cdot e_3 \cdot \frac{K_3^2}{R_0^{1-\lambda_3}} \right) \quad (1.9)$$

where:

- $K_{i,i=1,2,3}$ are the Notch Stress Intensity Factors (NSIFs) for mode I, II and II of loading;
- R_0 is the radius of structural volume;
- E is the Young modulus;
- $c_{wi,i=1,2,3}$ are the coefficient that they depend on the stress ratio $R = \frac{\sigma_{min}}{\sigma_{max}}$ and are defined by the equation (1.10) when stress relived SR joints [26]:

$$c_w(R) = \begin{cases} \frac{1+R^2}{(1-R)^2} \text{ for } -1 \leq R < 0 \\ \frac{1-R^2}{(1-R)^2} \text{ for } 0 \leq R \leq 1 \end{cases} \quad (1.10)$$

- $e_{i,i=1,2,3}$ are the parameters to consider the dependence on the opening angle 2α of V-notch and also on the Poisson's ratio ν . The value of $e_{i,i=1,2,3}$ are defined in *Table 1.5* in function of the opening angle and for $\nu = 0.3$ (steel):

2α [°]	e_1	e_2 [31]	e_3 [32]
0	0.133	0.341	0.414
30	0.147	0.273	0.379
45	0.150	0.243	0.362
60	0.151	0.215	0.345
90	0.145	0.168	0.310
120	0.129	0.128	0.276
135	0.117	0.111	0.259
150	0.104	0.096	0.241

Table 1.5: Value of e_1, e_2 and e_3 in function of the opening angle 2α

To calculate the SED in FE software, the averaged strain energy density can be obtained by the summation of the energy that is contained inside each element, divided by the structural volume(1.11). This approach is called "direct approach":

$$\Delta \bar{W}_{FEM} = \frac{\sum_{V(R_0)} W_{FEM,i}}{V(R_0)} \quad (1.11)$$

The unit of measure is $\left[\frac{MJ}{m^3} \right]$ or $\left[\frac{J}{mm^3} \right]$.

The SED approach is characterized by several advantages:

- The comparison of stress field between V-notch with different opening angle is possible because the fatigue resistance is expressed in terms of energy, so the unit of measure remain constant;
- As the NSIFs approach, the design fatigue curve is unique and it is showed in *Figure 1.16*, which express the fatigue strength in terms of Strain Energy;
- If SED is calculated by FE software, the required mesh doesn't have to be fine.

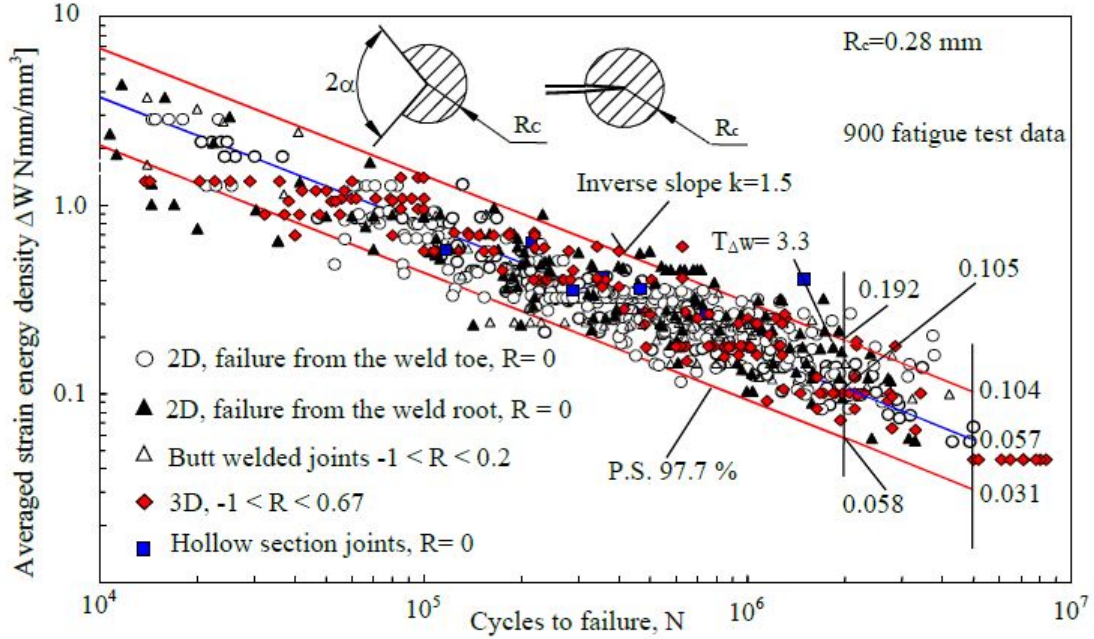


Figure 1.16: Fatigue design curve for SED approach [25]

1.3.3 Peak Stress Method (PSM)

The Peak Stress Method is an approach that allows to detect rapidly the value of NSIFs for the fatigue strength assessment of welded joints. This approach is based on finite element analysis with coarse mesh and it doesn't require a refined mesh in correspondence of the V-notch.

As the SED approach, The PSM wants to overcome the limits of NSIFs' approach. The method is applicable to steel structures and aluminium alloys.

The PSM gives the correlation between the mode I,II and III NSIFs and the corresponding peak stress components (see equations (1.12)-(1.14)):

$$K_1 \cong K_{FE}^* \cdot \sigma_{\theta\theta, \theta=0, peak} \cdot d^{1-\lambda_1} \quad (1.12)$$

$$K_2 \cong K_{FE}^{**} \cdot \tau_{r\theta, \theta=0, peak} \cdot d^{1-\lambda_2} \quad (1.13)$$

$$K_3 \cong K_{FE}^{***} \cdot \tau_{\theta z, \theta=0, peak} \cdot d^{1-\lambda_3} \quad (1.14)$$

where:

- $K_{FE}^*, K_{FE}^{**}, K_{FE}^{***}$ are the calibration constants related to mode I,II,II and depend on the element type, the software type, the mesh conformation and the nodal stress evaluation method;
- $\sigma_{\theta\theta, \theta=0, peak}, \tau_{r\theta, \theta=0, peak}, \tau_{\theta z, \theta=0, peak}$ are the peak nodal stresses detected at the V-notch profiles (see Figure 1.14a);
- d is the global element size;
- $\lambda_1, \lambda_2, \lambda_3$ are the Williams' eigenvalues.

Under plane strain hypothesis, the averaged Strain Energy Density (SED) defined by equation (1.9), can be rewritten in function of the peak stresses $\sigma_{\theta\theta, \theta=0, peak}, \tau_{r\theta, \theta=0, peak}, \tau_{\theta z, \theta=0, peak}$ thanks to the using of the equations (1.12)-(1.14) and the imposing of the following relation:

$$\bar{W} = (1 - \nu^2) \cdot \frac{\sigma_{eq, peak}^2}{2E} \quad (1.15)$$

where the $\sigma_{eq, peak}$ is defined in function of the peak stresses as follows:

$$\sigma_{eq,peak} = \sqrt{f_{w1}^2 \cdot \sigma_{\theta\theta,\theta=0,peak}^2 + f_{w2}^2 \cdot \tau_{r\theta,\theta=0,peak}^2 + f_{w3}^2 \cdot \tau_{z\theta,\theta=0,peak}^2} \quad (1.16)$$

where:

- $f_{wi,i=1,2,3}$ are the peak stresses corrective factors and are defined like follows:

$$f_{wi} = K_{FE}^j \cdot \sqrt{\frac{2e_i}{1-\nu^2}} \cdot \left(\frac{d}{R_0}\right)^{1-\lambda_i} \Big|_{\substack{i=1,2,3 \\ j=**,***}} \quad (1.17)$$

where:

- $e_{i,i=1,2,3}$ are the parameters to consider the dependence on the opening angle 2α of V-notch and also on the Poisson's ratio ν . The value of $e_{i,i=1,2,3}$ are defined in *Table 1.5* in function of the opening angle and for $\nu = 0.3$ (steel);
- R_0 is the radius of structural volume;
- K_{FE}^j are the calibration constants related to mode I,II and III for PSM approach;
- d is the global element size of the mesh
- λ_i are the Williams' eigenvalues.

The Peak Stress Method presents several advantages:

- The comparison of stress field between V-notch with different opening angle is possible because the fatigue resistance is expressed in terms of equivalent peak stress, so the unit of measure remain constant;
- As the NSIFs approach, the design fatigue curve is unique;
- The post-process analysis require only one nodal peak stress instead of a large number of stress distance values as in NSIFs approach;
- FE analysis require a coarser mesh than the NSIFs and SED approaches. Indeed the global element size d can be higher than the control radius R_0 , unlike the "direct approach" to calculate the SED where is necessary to have $d < R_0$;
- The modeling of the control volume to calculate the averaged SED is not necessary.

PSM for 2D geometries: linear plane elements

Initially, the PSM approach was proposed to 2D geometries subjected to mode I loading by Meneghetti and Lazzarin [5]. Subsequently, this method was extended also for 2D geometries subjected to mode II and III by Meneghetti in 2012 [28] and 2013 [29].

Another important thing is that the PSM calibration constants K_{FE}^j depend on different factors:

- The FE software used: the original one is *Ansys @Mechanical APDL* but recently, a new calibration has been developed for others commercial software like *Abaqus, Straus* and other four software [7].
- typology of the element: in *Ansys@* the four-node linear plane element is used with *Simple Enhanced Strain* and *Plane Strain* as Key Options;
- Pattern of mesh: the mesh is generated automatically by the *free-mesh* algorithm, additionally for V-notches that are characterised by a opening angle $2\alpha \leq 90^\circ$, four elements have to share the node at the V-notch tip; instead for V-notches with a opening angle $2\alpha > 90^\circ$, two elements must share the node at V-notch tip as explained in *Figure 1.17*.

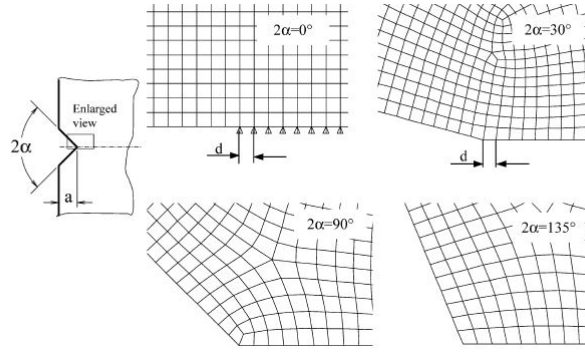


Figure 1.17: Mesh patterns that have to adopt during a numerical analysis [5]

The global element size must respect a ratio with a component's reference dimension. The value of this ratio depends on the opening angle 2α and the mode of loading (see Table 1.6):

2α [°]	Mode I	Mode II	Mode III
	a/d_{min}	a/d_{min}	a/d_{min}
$0^\circ < 2\alpha < 135^\circ$	3	14	/
0° (root)	/	/	12 (root)
135° (weld toe)	/	/	3 (weld toe)

Table 1.6: Value of the ratio a/d_{min} in function of the opening angle 2α that must be respected

The PSM calibration constants assume the values reported in Table 1.7:

K_{FE}^*	K_{FE}^{**}	K_{FE}^{***}
$1.38 \pm 3\%$	$3.38 \pm 3\%$	$1.93 \pm 3\%$

Table 1.7: Value of calibration constant for PSM

As above-mentioned, the PSM is characterised by unique fatigue design curve that expresses the fatigue strength of welded joints in terms of equivalent peak stress $\Delta\sigma_{eq,peak}$ but also in terms of NSIF K_1 , when the welded joints is subjected predominantly to mode I.

The curves that are represented in Figure 1.18 and Figure 1.19, are valid for the joints with the following characteristics:

- As-welded joints
- $360 < f_y < 670MPa$ where f_y is the yield strength
- The main plate thickness is ranged between 6 and 100mm
- V-notch opening angle 2α is range from 0° to 135°
- Stress ratio $R = \frac{\sigma_{min}}{\sigma_{max}} \cong 0$

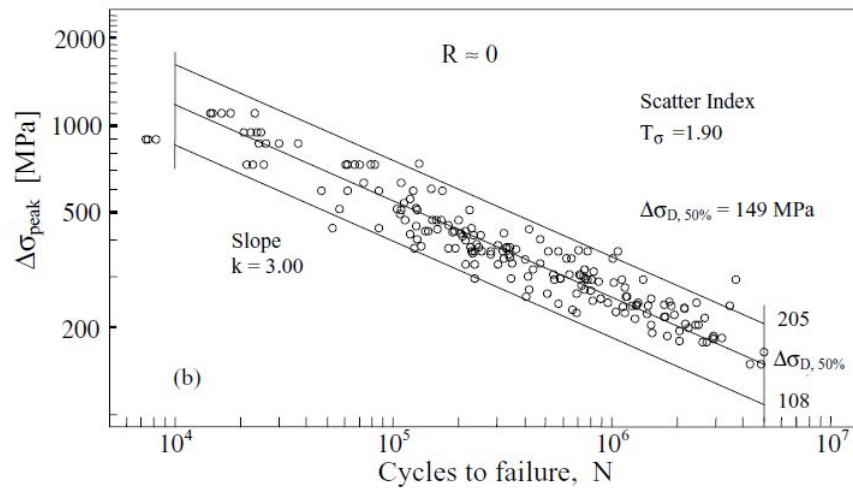


Figure 1.18: PSM Fatigue design curve in terms of equivalent peak stress, steel structures, weld toe and root failures [5]

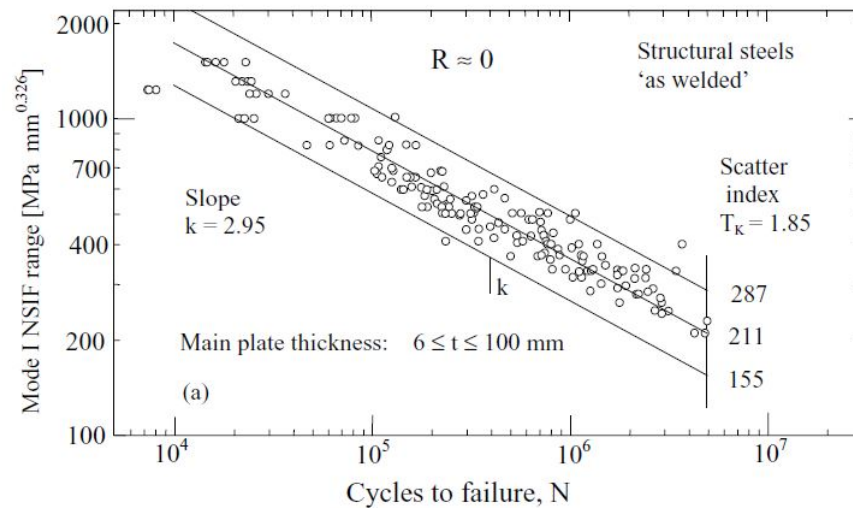


Figure 1.19: PSM Fatigue design curve in terms of NSIF K_I mode I obtained from peak stress, steel structures, weld toe and root failures [5]

PSM for 3D geometries: linear hexahedral elements

In 2014, the Peak Stress Method was extended to 3D model, that can be characterized by a complex geometry and both by toe and root cracking [10]. For this type of analysis, a linear hexahedral elements has been chosen and is necessary to adopt the *Submodeling technique*.

This method is characterised by different step:

1. The Main model of the structure is created;
2. The main model is meshed with ten-node quadratic elements (SOLID 187 in ANSYS ®);
3. The cut boundary is defined with a convergence analysis and the sub model is extracted from the main model;
4. The nodal displacements belonging to the cut boundary are extracted from the main model and inserted in the sub model as boundary condition;
5. The sub model is meshed with eight-node linear elements (SOLID 185 in ANSYS ®).

The advantage of this technique is that allows to extract accurate results in a restricted region like the fracture area.

As in 2D PSM analysis, the 3D PSM calibration constants depend on different factors:

- The FE software used: the original one is *Ansys* ®*Mechanical APDL*;
- typology of the element: in *Ansys*®the eight-node linear hexahedral element is used with *Simple Enhanced Strain* as Key Options 1;
- Pattern of mesh: same rule of 2D geometries.

So, the PSM calibration constants assume the values reported in *Table 1.8*:

K_{FE}^*	K_{FE}^{**}
$1.38 \pm 3\%$	$3.38 \pm 3\%$

Table 1.8: Value of calibration constant for PSM (3D)

Meneghetti, Atzori and Guzzella proposed a fatigue design curve in terms of $\Delta\sigma_{eq, peak}$ for 3D structures. The curve that is represented in *Figure 1.20*, is valid for the joints with the following characteristics:

- As-welded joints
- $360 < f_y < 670MPa$ where f_y is the yield strength
- The main plate thickness is ranged between 6 and 100mm
- V-notch opening angle 2α is range from 0° to 135°
- Stress ratio $R = \frac{\sigma_{min}}{\sigma_{max}}$ is ranged between -0.36 and 0.7, for weld toe and root failures.

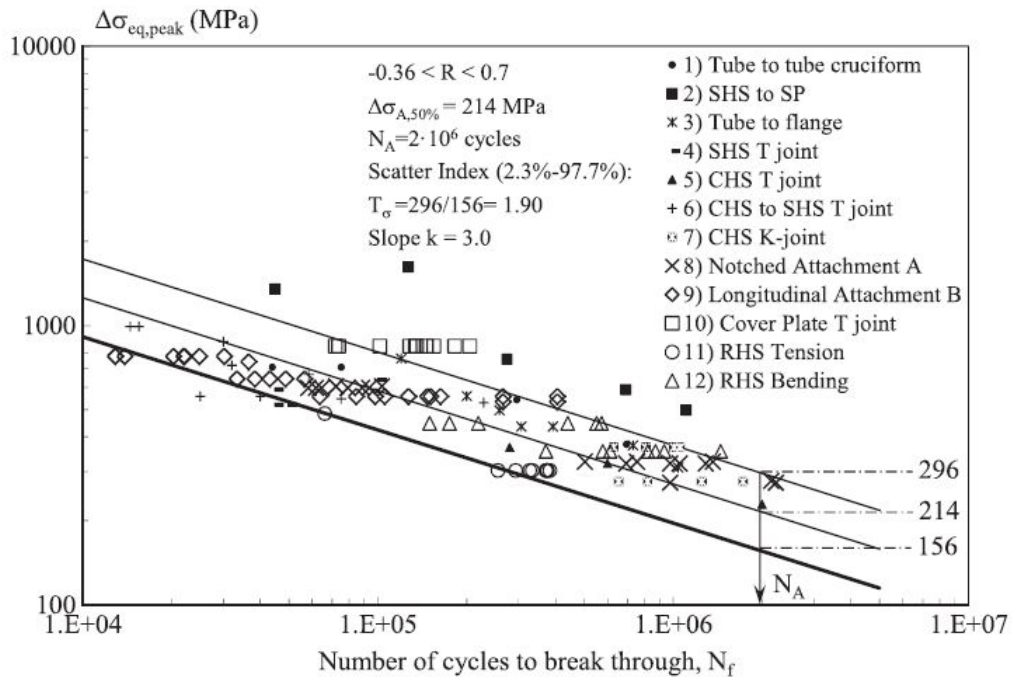


Figure 1.20: PSM Fatigue design curve in terms of equivalent peak stress, steel structures, weld toe and root failures [10]

PSM for 3D geometries: quadratic tetrahedral elements

The PSM was extended to the ten-node tetra elements (SOLID 187 in ANSYS®) by Meneghetti and Campagnolo in 2018 [24], with the aim of reducing the modelling and computational time for the simulation. Subsequently, the calibration constants for ten-node tetra elements has been improved in 2019 [30]. As in 2D PSM analysis, the 3D PSM calibration constants depend on different factors:

- The FE software used: the original one is *Ansys*®*Mechanical APDL*;
- typology of the element: in *Ansys*®(SOLID 187) the ten-node quadratic tetrahedral element is used with *Pure Displacement* as Key Options 1;
- Pattern of mesh: the mesh is generate automatically by the *free-mesh* algorithm and it is intrinsically irregular, that is the node of the notch tip could be shared by different elements having a important different shape and size. For this reason, the peak stress could vary along the notch tip profile even in the case of a constant applied NSIF. This problem can be solved by introducing an average peak stress value, which has been defined as the moving average on three adjacent vertex nodes, starting from the generic node $n=k$:

$$\bar{\sigma}_{i,j,peak,n=k} = \frac{\sigma_{i,j,peak,n=k-1} + \sigma_{i,j,peak,n=k} + \sigma_{i,j,peak,n=k+1}}{3} \Big|_{n=node} \quad (1.18)$$

Another important thing related to equation (1.18) is that only peak stresses calculated at vertex nodes of tetra elements have be introduced in this equation, thus the stresses at mid-side nodes must be neglected [30].

The PSM calibration constants assume the values reported in *Figure 1.21*:

2α [°]	Mode I				Mode II				Mode III			
	Tetra 4		Tetra 10		Tetra 4		Tetra 10		Tetra 4		Tetra 10	
	K* _{FE}	(a/d) _{min}	K* _{FE}	(a/d) _{min}	K** _{FE}	(a/d) _{min}	K** _{FE}	(a/d) _{min}	K*** _{FE}	(a/d) _{min}	K*** _{FE}	(a/d) _{min}
0	1.75 ± 22%	3	1.05 ± 15%	3	2.65 ± 15%	3	1.63 ± 20%	1	2.50 ± 15%	5	1.37 ± 15%	3
90					-	-	-	-				
120											1.70 ± 10%	3
135			1.21 ± 10%	1								

Figure 1.21: Summary of calibration constants K_{FE}^* , K_{FE}^{**} and K_{FE}^{***} for tetra elements of *Ansys*®*element library* [30]

The advantages of the PSM with ten-node tetrahedral elements respect to eight-node are:

- The calibration constants are valid for mode I, II and III;
- This method allows the analysis of complex 3D structures without the submodeling technique;
- The mesh is generate automatically by *free-mesh* algorithm;
- The FE meshes are coarse and the calculation of peak stresses is relatively rapid and simple

On the other hand, this method presents also some disadvantages as:

- The PSM calibration constants for ten-node are more dependent on the V-notch opening angle 2α than the eight-node;
- The error of the calibration constants are $\pm 10 - 15\%$, higher than the eight-node's error ($\pm 3\%$).

1.3.4 Attentions on the PSM

Concerning the PSM, is important to underline some precautions:

- The PSM calibration constants are not calibrated for V-notch opening angle higher than 135° , but recently for ten-node tetra elements the PSM constants has been calibrated up to 180° ;
- The PSM is validate for stress ratio R between -0.36 and 0.7 but in as-welded condition the influence of R does not affect the fatigue life of the structures, so the PSM can be extended up to stress ratio equals to -1;
- An important consideration is relative to the weld toe radius ρ :
 - $\rho < 1.5 - 1.8mm$, the weld toe radius can be considered equal to $0mm$, so to have the worst possible case: V-notch;
 - $1.8 < \rho < 4mm$, this is the case of blunt notch, so the PSM is applied in combination with SED approach;
 - $\rho > 4mm$, the classical mechanical point criterion is used for fatigue assessment
- If the Peak Stress method detects a crack initiation in a singularity region which is different from the experimental one, the $\Delta\sigma_{eq,peak}$ related to effective area must be calculated.

Chapter 2

Numerical analysis of experimental data to detect the NSIFs, SED and PSM parameters

The objective of this chapter is to perform a fatigue assessment of four different experimental data of welded joint in terms of nominal stress, Notch Stress Intensity Factor K_1 for mode I of loading, averaged Strain Energy Density SED and Equivalent Peak Stress. The aim of this re-elaboration is to re-plot the experimental data in a double logarithm graph, where on the abscissa is placed the fatigue life N_f and the ordinate is expressed in terms of:

- Nominal Stress $\Delta\sigma$ [MPa];
- ΔK_1 [MPa · mm^{1- λ_1}];
- ΔW (SED) [MJ/m³];
- $\Delta\sigma_{eq,peak}$ [MPa].

Subsequently, the results are collected together to be compared in terms of statistical scatter band with respect to the design fatigue curve defined in literature.

The analysed data consist in four transverse attachments that Maddox in 1987 [37] and Gurney in 1991 [38] modelled in 2D. In this chapter, another transverse attachments is studied: a square chord with circular brace that was elaborated by Gandhi in 1998 [39] in 3D.

The assessment are performed with the application of global and local approaches above-mentioned through the use of the finite element software *Ansys®Mechanical APDL* with the license of the University of Padua. For the modelling and study of 2D geometries, the four-node linear element PLANE 182 is adopted with *Simple Enhanced Strain* as Key Options 1 and *Plane Strain* as Key Options 3; on the other hand, in the case of 3D structure, the eight-node linear element SOLID 185 (also called Brick 185) is used with *Simple Enhanced Strain* as Key Options 1, the four-node linear elements SOLID 285 (also called Tetra 285) and also the ten-node quadratic element SOLID 187 (also called Tetra 187) is adopted with *Pure displacement* as Key Options 1.

All geometries are created directly in Ansys®, thanks to the use of the Ansys®CAD environment.

All the following joints are studied in as-welded conditions. According to the non-conventional LEFM extension to welded joints, the weld toe profile is considered as a V-notch with tip radius equal to zero (worst case) and the root is assumed as pre-crack in the structure.

2.1 Description of transverse attachments geometries

The first four typology of welded joint that are studied, are transverse stiffeners characterized by a fatigue class FAT 80 and tested by Maddox in 1987 [37] and Gurney in 1991 [38] under constant amplitude loading CAL. The principal informations and the mechanical properties about these four welded joints are summarized in the *Table 2.1* and *Table 2.2*:

Weld condition	Fracture location	Load application	V-notch opening angle 2α
As-welded, non-load carrying (NLC), full penetration	Weld toe	Main plate, parent material	135°

Table 2.1: Information about the specimens

Material model	Yield strength f_y [MPa]	Young modulus [MPa]	Poisson's ratio ν
Linear elastic, isotropic	360-672	206000	0.3

Table 2.2: Information about mechanical properties

The transverse attachments are defined with a transverse NLC geometry as *Figure 2.1* shows for cruciform joints and *Figure 2.2* for T-shape profile.

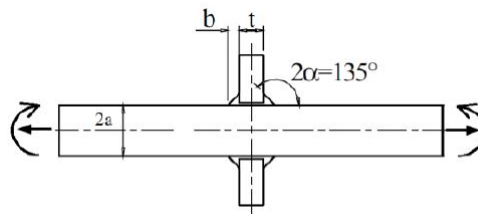


Figure 2.1: General scheme of a transverse NLC joint, subjected to axial and bending load [40]

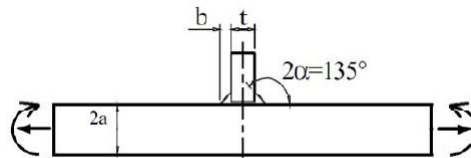


Figure 2.2: General scheme of a transverse T-joint, subjected to axial and bending load [40]

where:

- $2a$ is the main plate thickness;
- t is the stiffener thickness;
- b is the weld leg;
- 2α is the V-notch opening angle.

The sketches of the joints' geometry don't give any informations about the main plate and also about the attachment length. Indeed, they has to be sufficiently long and distant from weld toe to guarantee that they represent the stress flowing from the "infinite".

2.1.1 Maddox 1987, 1st specimen

The first joint analysed is a transverse NLC joint and initially studied by Maddox in 1987. The dimensions of it are defined in the following table and figure:

2a [mm]	t [mm]	b [mm]
13	10	8

Table 2.3: Dimension of the 1st joint

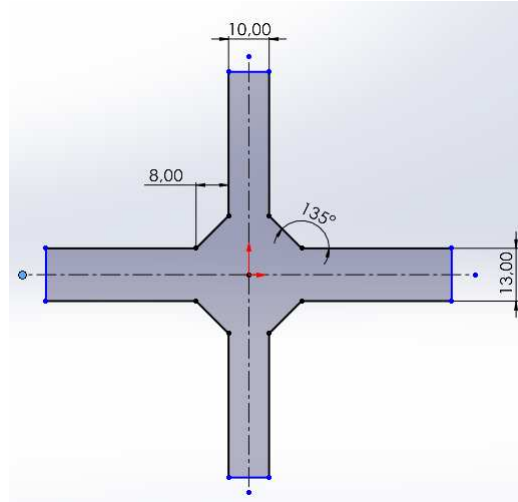


Figure 2.3: Maddox 1st joint, the quotes are expressed in [mm].

The experimental data are defined in the following table in terms of nominal stress $\Delta\sigma_{nom}$:

Stress Ratio R	$\Delta\sigma_{nom}$ [MPa]	N_f [cycles]
0	200	192 000
	140	507 000
	100	2 937 000
	80	4 297 000

Table 2.4: Experimental data of the 1st joint

The modelling procedure in Ansys®APDL is briefly described:

- Thanks to the double symmetry of the transverse NLC joint, only 1/4 of the joint is created to reduce the computational time;
- A root has been created and it is characterized by a initial opening length equal to 0.1mm;
- The first specimen is subjected to an axial load and it is applied on the main plate as a constant pressure equal to $p = -\Delta\sigma_{nom}$ on Line 2 (Figure 2.4);
- Symmetry boundary conditions are applied on Line 7, 10 and 1 (Figure 2.4).

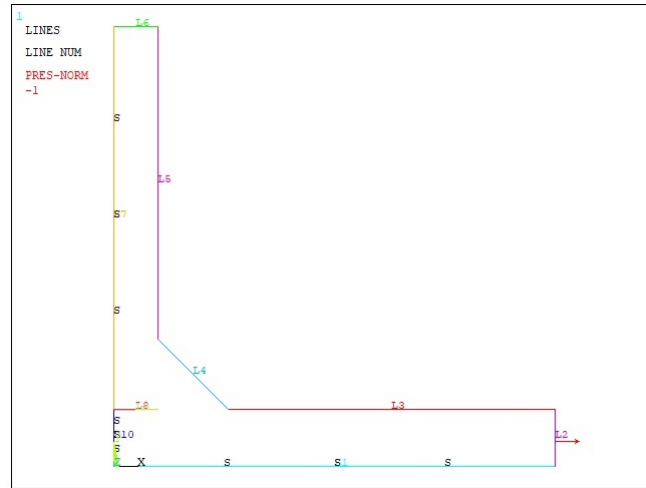


Figure 2.4: Maddox 1st joint inside Ansys®APDL environment. S indicate the symmetry boundary condition, while the red arrow represents the external pressure

2.1.2 Gurney 1991, 2nd specimen

The second joint analysed is a transverse NLC joint and initially studied by Gurney in 1991. The dimensions of it are defined in the following table and figure:

2a [mm]	t [mm]	b [mm]
100	220	15

Table 2.5: Dimension of the 2nd joint

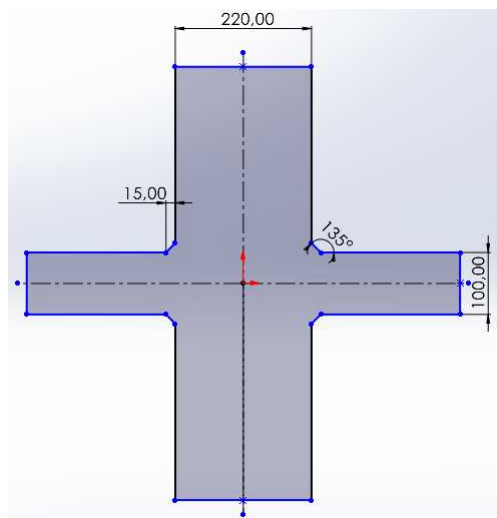


Figure 2.5: Gurney 2nd joint, the quotes are expressed in [mm].

The experimental data are defined in the following table in terms of nominal stress $\Delta\sigma_{nom}$:

Stress Ratio R	$\Delta\sigma_{nom}$ [MPa]	N_f [cycles]
0	150	109 000
	120	224 000
	100	322 000
	65	1 153 000
	55	2 147 000

Table 2.6: Experimental data of the 2nd joint

The modelling procedure in Ansys®APDL is briefly described:

- Thanks to the double symmetry of the transverse NLC joint, only 1/4 of the joint is created to reduce the computational time;
- A root has been created and it is characterized by a initial opening length equal to 0.5mm;
- The second specimen is subjected to an axial load and it is applied on the main plate as a constant pressure equal to $p = -\Delta\sigma_{nom}$ on Line 2 (Figure 2.6);
- Symmetry boundary conditions are applied on Line 7, 10 and 1 (Figure 2.6).

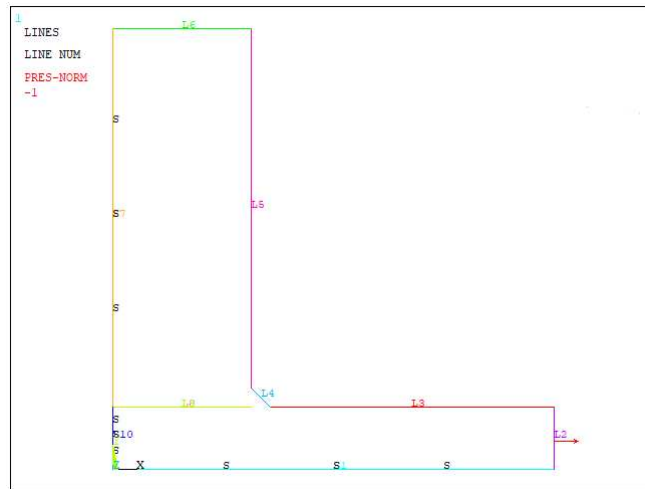


Figure 2.6: Gurney 2nd joint inside Ansys®APDL environment. S indicate the symmetry boundary condition, while the red arrow represents the external pressure

2.1.3 Gurney 1991, 3rd specimen

The third joint analysed is a transverse NLC joint and initially studied by Gurney in 1991. The dimensions of it are defined in the following table and figure:

2a [mm]	t [mm]	b [mm]
100	13	8

Table 2.7: Dimension of the 3rd joint

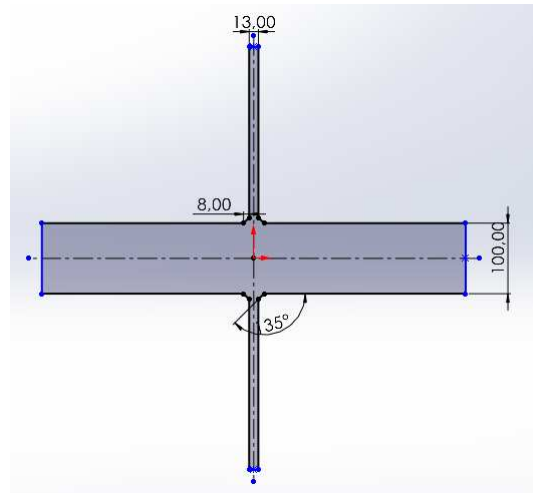


Figure 2.7: Gurney 3rd joint, the quotes are expressed in [mm].

The experimental data are defined in the following table in terms of nominal stress $\Delta\sigma_{nom}$:

Stress Ratio R	$\Delta\sigma_{nom}$ [MPa]	N_f [cycles]
0	260	120 000
	220	200 000
	180	302 000
	140	744 000
	120	1 180 000
	110	2 158 000

Table 2.8: Experimental data of the 3rd joint

The modelling procedure in Ansys®APDL is briefly described:

- Thanks to the double symmetry of the transverse NLC joint, only 1/4 of the joint is created to reduce the computational time;
- A root has been created and it is characterized by a initial opening length equal to 0.1mm;
- The third specimen is subjected to a bending load and it is applied on the main plate as a linear pressure. The bending solicitation follows the Navier's linear stress distribution and so the value of the nominal stress inside the *Table 2.8* represents the maximum stress reached at the top of the main plate. Due to the double symmetry of the joint, only one half of Navier's distribution is defined, so the pressure p are equal to zero on the bottom Keypoint of the line 2 and equal to $-\Delta\sigma_{nom}$ on the top Keypoint of the Line 2 (*Figure 2.8*);
- Due to the antisymmetric loading, a symmetry boundary condition is applied only on the Line 7 and 10, while an antisymmetry boundary condition is applied on the Line 1 (*Figure 2.8*). To eliminate any type of lability, a keypoint belonging to one of the two symmetry axes has to be constrained along the y-direction ($u_y = 0$).

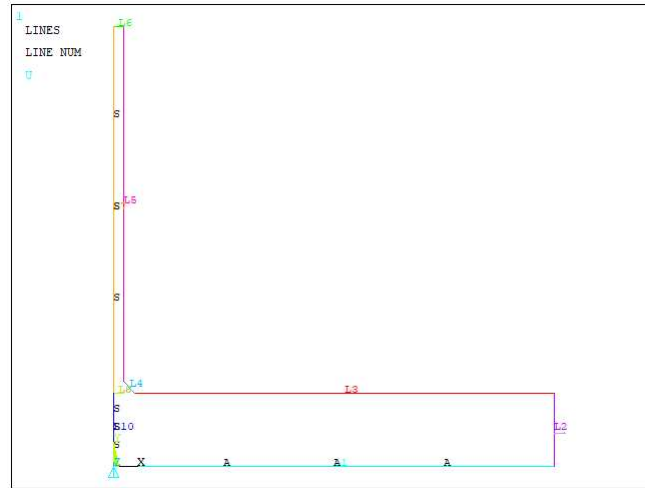


Figure 2.8: Gurney 3rd joint inside Ansys®APDL environment. S indicate the symmetry boundary condition and A the antisymmetric boundary condition, while the red arrow represents the external pressure

2.1.4 Gurney 1991, 4th specimen

The fourth joint analysed is a T-shape joint and initially studied by Gurney in 1991. The dimensions of it are defined in the following table and figure:

2a [mm]	t [mm]	b [mm]
6	6	6

Table 2.9: Dimension of the 4th joint

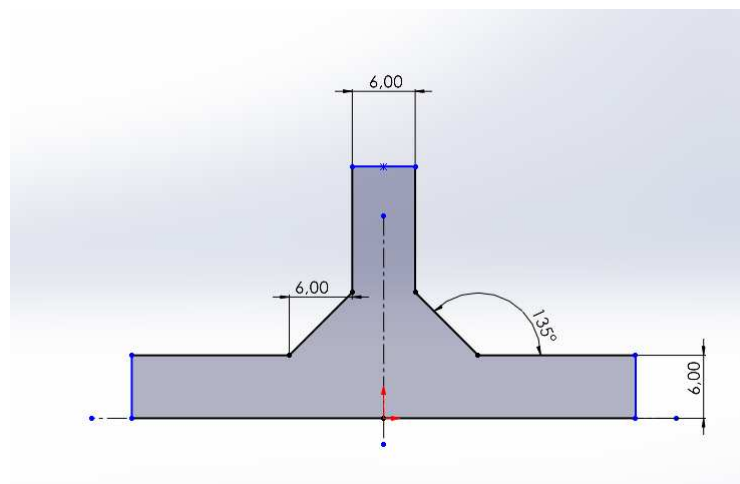


Figure 2.9: Gurney 4th joint, the quotes are expressed in [mm].

The experimental data are defined in the following table in terms of nominal stress $\Delta\sigma_{nom}$:

Stress Ratio R	$\Delta\sigma_{nom}$ [MPa]	N_f [cycles]
0	300	135 000
	260	237 000
	200	407 000
	190	573 000
	180	665 000
	160	1 525 000
	150	1 534 000
	140	2 601 000

Table 2.10: Experimental data of the 4th joint

The modelling procedure in Ansys®APDL is briefly described:

- Thanks to the symmetry of the transverse NLC joint, only 1/2 of the joint is created to reduce the computational time;
- A root has been created and it is characterized by an initial opening length equal to 0.1mm;
- The third specimen is subjected to a bending load and it is applied on the main plate as a linear pressure. The bending solicitation follows the Navier’s linear stress distribution and so the value of the nominal stress inside the *Table 2.8* represents the maximum stress reached at the top of the main plate. Due to the symmetry of the joint, the Navier’s distribution is defined as following: the pressure p are equal to $\Delta\sigma_{nom}$ on the bottom Keypoint of the line 2 and equal to $-\Delta\sigma_{nom}$ on the top Keypoint of the Line 2 (*Figure 2.10*);
- A symmetry boundary condition is applied only on the Line 7 and 10 (*Figure 2.10*). To eliminate any type of lability, a keypoint belonging to the axes of symmetry has to be constrained along the y-direction ($u_y = 0$).

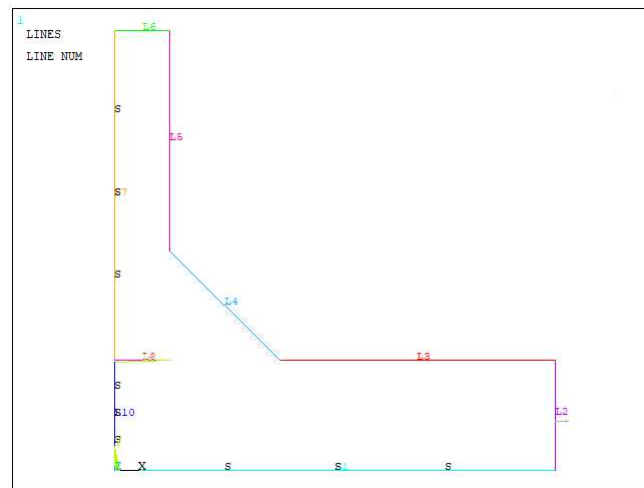


Figure 2.10: Gurney 4th joint inside Ansys®APDL environment. S indicate the symmetry boundary condition, while the red arrow represents the external pressure

2.2 NSIFs (Notch Stress Intensity Factors) approach

According to the non-conventional LEFM extension to sharp V-notches, the V-notch area is subjected to a non-linear stress concentration due to the structural geometry change and weld profile itself. The intensity of the asymptotic local stress field is expressed by the notch stress intensity factors NSIFs under fracture modes I, II and III (*Figure 1.11*). Thanks to the knowledge of the NSIFs value, the fatigue life of the welded joint

characterized by a sharp V-notches, can be estimate.

The weld toe of each specimens is subjected to pure mode I because it is characterised by a V-notch opening angle 2α equal to 135° . Indeed, referring to graph of the Williams eigenvalues trend in *Figure 1.13*, mode II is not singular for V-notch opening angle greater than 102.5° , so $\lambda_2 = 0$. Due to the absence of out-plane shear stresses, mode III is null.

On the other hand, the root of each specimens is characterised by a V-notch opening angle 2α equal to 0° , so it is subjected to mode I and also mode II, indeed on the root is applied a shear stress and the value of λ_2 is different from zero due to the V-notch opening angle lower than 102.5° . For the same consideration of the weld toe, mode III is null.

According to Gross and Mendelson definition [21] and *Figure 2.11*, the NSIFs are defined by the following equations:

$$K_1 = \sqrt{2\pi} \lim_{r \rightarrow 0^+} r^{1-\lambda_1} \cdot \sigma_{\theta\theta}(r, \theta=0) \quad (2.1)$$

$$K_2 = \sqrt{2\pi} \lim_{r \rightarrow 0^+} r^{1-\lambda_2} \cdot \tau_{r\theta}(r, \theta=0) \quad (2.2)$$

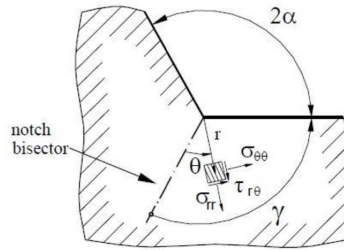


Figure 2.11: V-notch with a cylindrical local reference system [23]

where:

- r is the radial distance from the V-notch tip;
- $\sigma_{\theta\theta}(r, \theta=0)$, $\tau_{r\theta}(r, \theta=0)$ are the stress values for $\theta = 0^\circ$ (along the V-notch bisector), r tending to 0 mm;
- λ_1, λ_2 are the Williams' eigenvalues that depend on the opening angle 2α of the V-notch. They express the grade of singularity of the stress field.

Each specimen is characterised by a V-notch opening angle 2α equal to 135° and so the corresponding eigenvalues λ_1 and λ_2 are reported in the following table:

2α [°]	λ_1 (Mode I)	λ_2 (Mode II)
135	0.674	1.302

Table 2.11: Value of λ_1 and λ_2 in function of the opening angle 2α

2.2.1 Calculation of NSIFs in Ansys®APDL

The following procedure refers to the 1st specimen (Maddox 1991) but it can be similarly extended for the other joints.

The four-node linear element PLANE 182 is chosen inside Ansys®APDL, with *Simple Enhanced Strain* as Key Options 1 and *Plane Strain* as Key Options 3.

To calculate the NSIFs K_1 and K_2 , the local stress distributions along the V-notch and root bisector are needed. Due to the non-linear stress increase at V-notch area and root area, the dimension of the finite element has to be very small (*Global Element Size* $\cong 10^{-5}mm$) to perceive the local stress. For this reason, an right mesh must be laid on the model with small transition towards notch-tip and root.

To reach this objective, the following procedure is applied:

1. Three circular areas is created with the center at the weld toe and root tip, with respective diameters $\Phi_1 = 0.0002mm$, $\Phi_2 = 0.56mm$ and $\Phi_3 = 1.4mm$, as indicated in Figure 2.12 and Figure 2.13. This choice of the diameters allows a smooth element transition and the second one will be useful for SED approach

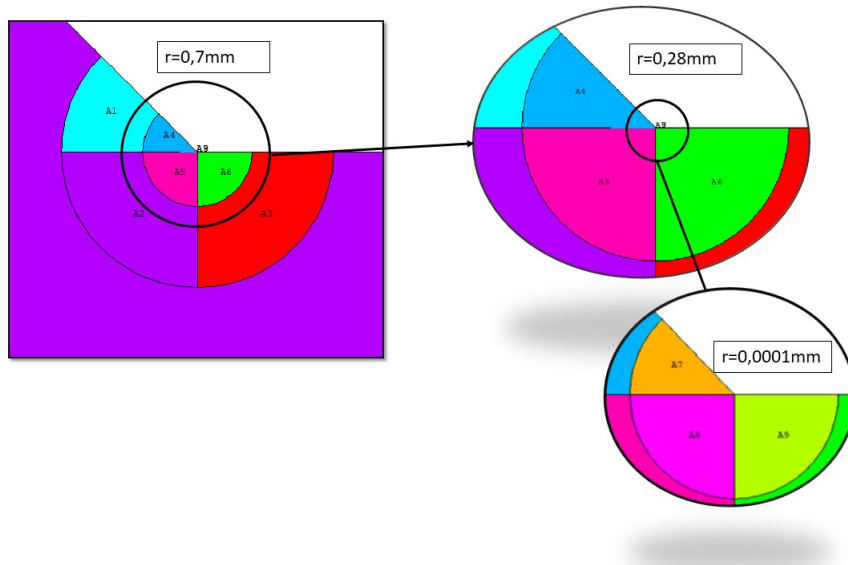


Figure 2.12: Three circular areas with the center on the weld tip

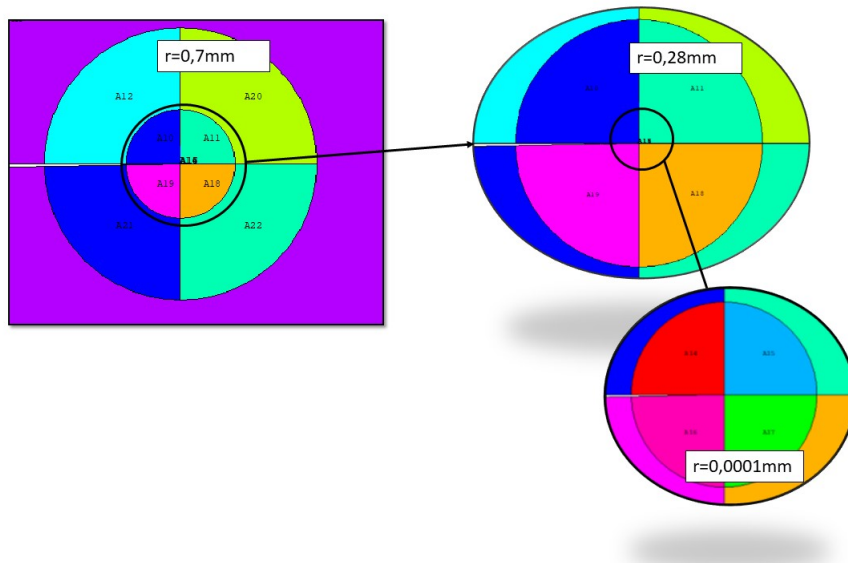


Figure 2.13: Three circular areas with the center on the root tip

2. For the mesh of the first circle:
 - (a) The radial line are divided in five parts, with spacing equal to 1;
 - (b) The arc of 45° is divided in four parts, with spacing equal to 1 (only for the weld toe);
 - (c) The arcs of 90° are divided in 8 parts, with unitary spacing ratio. The all arcs of the root are divided with these options;
 - (d) To guide the mesh during its creation, a concentration keypoint is created at the weld toe and root tip:

Meshing → *SizeCNTRLs* → *ConcentratKPS* → *Create*

with the following options:

- NPT is the keypoint located at weld toe or root tip;
- $DELR=0.00002$;
- $RRat=1$, $NTHET=4$ for 45° arc or 8 for 90° arc

Subsequently, the mesh can be created with *free-mesh* algorithm;

3. For the mesh of the second circle:

- The radial line are divided in fifty parts, with spacing equal to 2000;
- The arc of 45° is divided in four parts, with spacing equal to 1 (only for the weld toe);
- The arcs of 90° are divided in 8 parts, with unitary spacing ratio. The all arcs of the root are divided with these options;
- The mesh can be created with *mapped-mesh* algorithm;

4. For the mesh of the third circle:

- The radial line are divided in five parts, with spacing equal to 2;
- The arc of 45° is divided in four parts, with spacing equal to 1 (only for the weld toe);
- The arcs of 90° are divided in 8 parts, with unitary spacing ratio. The all arcs of the root are divided with these options;
- The mesh can be created with *mapped-mesh* algorithm;

5. A mesh obtained by *mapped-mesh* algorithm is laid on the remaining area with a global element size changing according to the welded joint into account.

After this procedure, the size of the element inside the smaller circular sector is equal to 0.00005mm at weld toe and root as shown *Figure 2.14* and *Figure 2.15*.

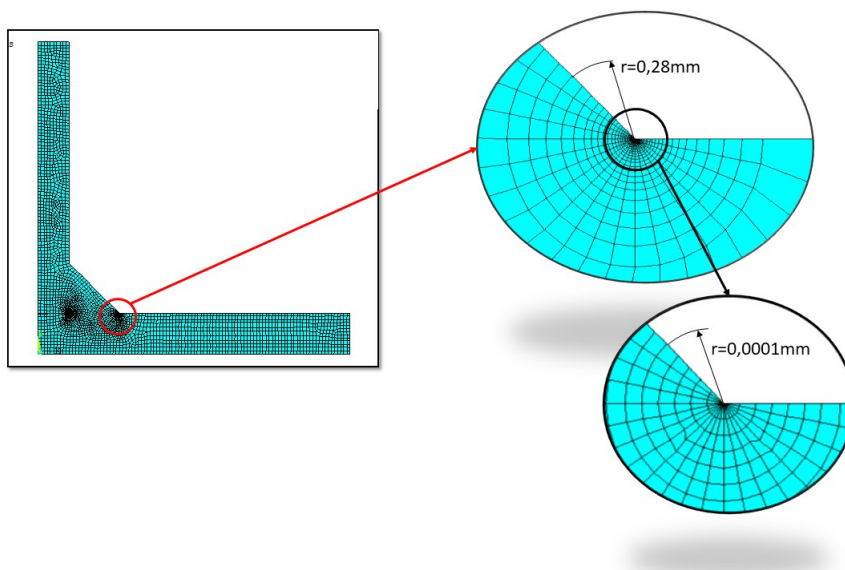


Figure 2.14: Mesh pattern for the 1st specimen at the weld toe

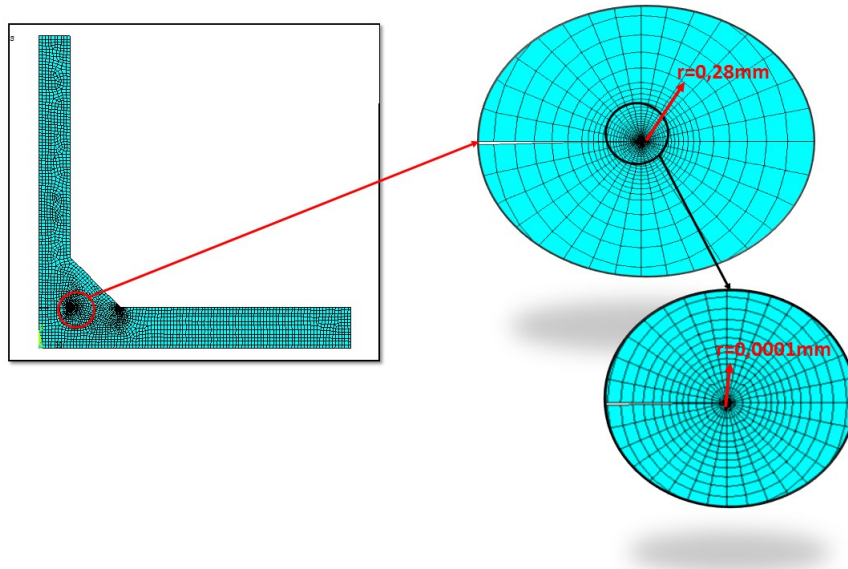


Figure 2.15: Mesh pattern for the 1st specimen at the root

After the creation of the mesh, the system can be solved:

Solution → *Solve* → *Current LS*

To obtain the singular stress field along the V-notch bisector at the weld toe and root, a local reference coordinate system X-Y-Z is created as shown *Figure 2.11*. To create it, the following procedure has to be adopted:

1. The WorkPlane is displayed and placed through a offset at the weld toe Keypoint with the following commands:

Utility Menu → *Offset WorkPlane to* → *Keypoint*

2. The WorkPlane is rotated by an angle equal to 112.5° clockwise about the z-axis, as shown *Figure 2.16*. With this rotation, the x-axis is aligned with the V-notch bisector and represents r in the equation (2.1) and σ_{yy} replaces $\sigma_{\theta\theta, \theta=0}$. The commands to rotate the WorkPlane are:

Utility Menu → *Offset WP by Increments* → *Degrees*

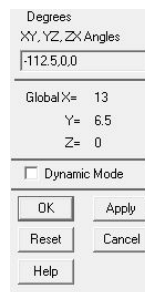


Figure 2.16: Rotation of WorkPlane by 112.5° clockwise about the z-axis

3. Subsequently, the local reference coordinate system is created in the WorkPlane origin with the following commands:

Utility Menu → *Local Coordinate System* → *Created Local CS* → *At WP origin*

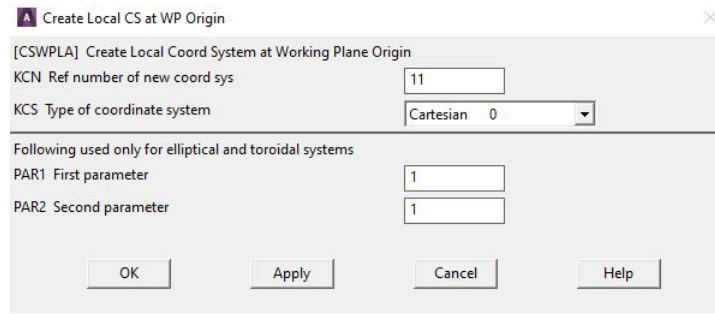


Figure 2.17: Creation of a local coordinate system at WP origin. As KCN option, a number greater than 10 must be chosen; so 11 is defined.

4. To plot the results in the new coordinate system, the following commands are executed:

General Postproc → Option for Outp

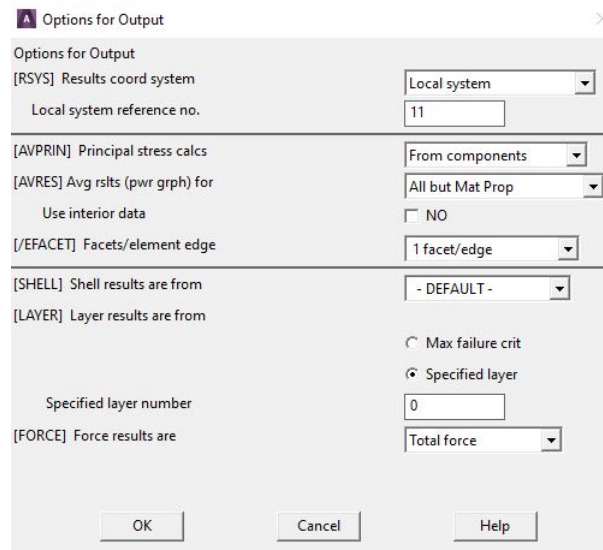


Figure 2.18: Option for Output window.

5. The node belonging the V-notch bisector are used to create a path as shown *Figure 2.19*. The commands to create the path are:

General Postproc → Path Operations → Define Path → By Nodes

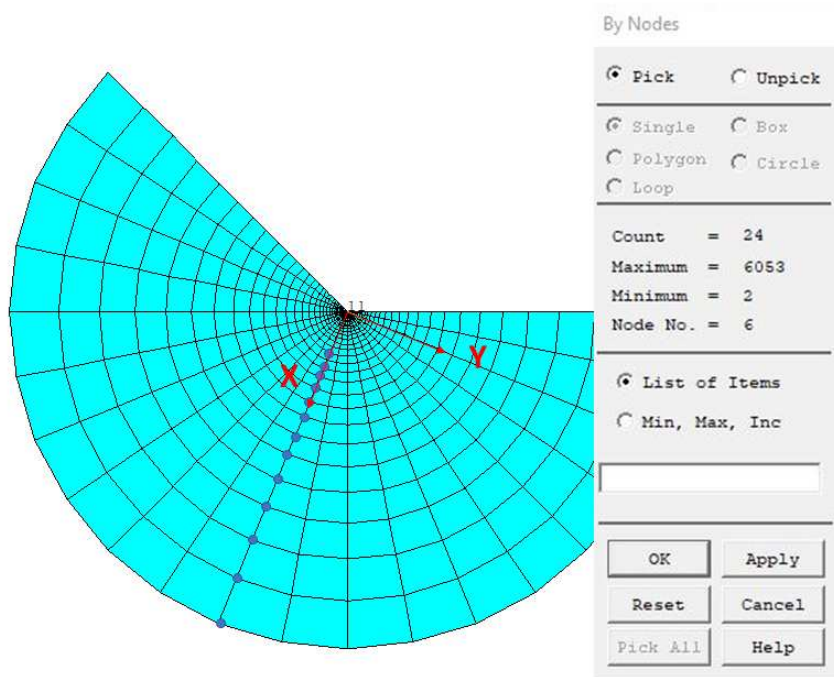


Figure 2.19: Selection of the nodes along the x-axis of the local reference system, from 0 to 0.28 mm.

- The $\Delta\sigma_{yy}$ and x are plotted along the x-axis of the local reference system. In Ansys®, the $\Delta\sigma_{yy}$ and x are defined as SY and S:

General Postproc → Path Operations → Define Path → Map onto Path → S/SY

The results are reported in in a double logarithmic graph with in abscissa the x values and in ordinate the $\Delta\sigma_{yy}$ values (Figure 2.20) for an external applied pressure $\Delta\sigma_{nom} = 1\text{MPa}$.

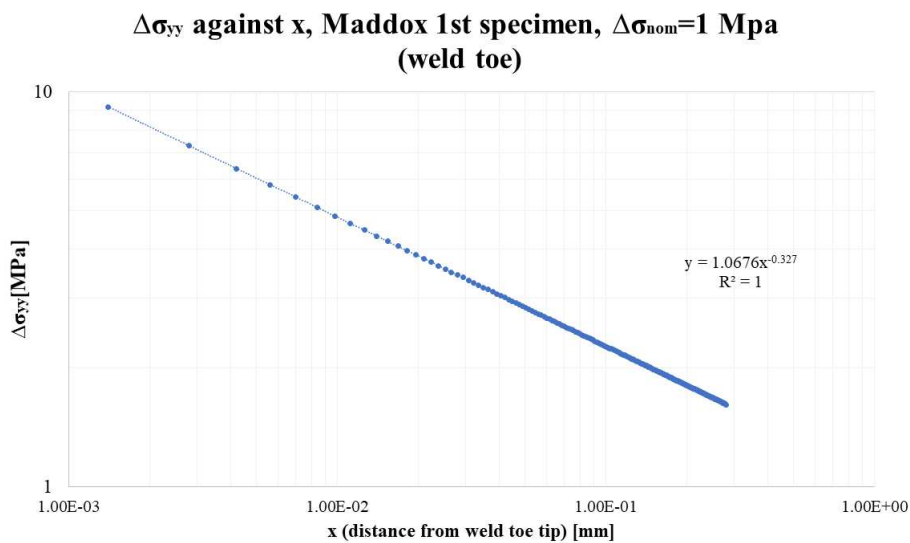


Figure 2.20: Singular stress field along the V-notch bisector at the weld toe, in case of Maddox 1st specimen and 1 MPa as nominal stress.

As Figure 2.20 shows, the inverse slope of the asymptotic stress field k is equal to 0.327 and it is in good agreement with the theoretical value $k = 1 - \lambda_1 = 0.326$.

Subsequently, the K_1 value is detected by the averaging of the all points K_1 along the path from $x = 1.40 \cdot 10^{-4} \text{mm}$ to $x = 0.28 \text{mm}$, excluded the value for $x = 0$ because the graph is double logarithmic. To calculate the K_1 , the equation (2.1) is used and the results are reported in the following graph:

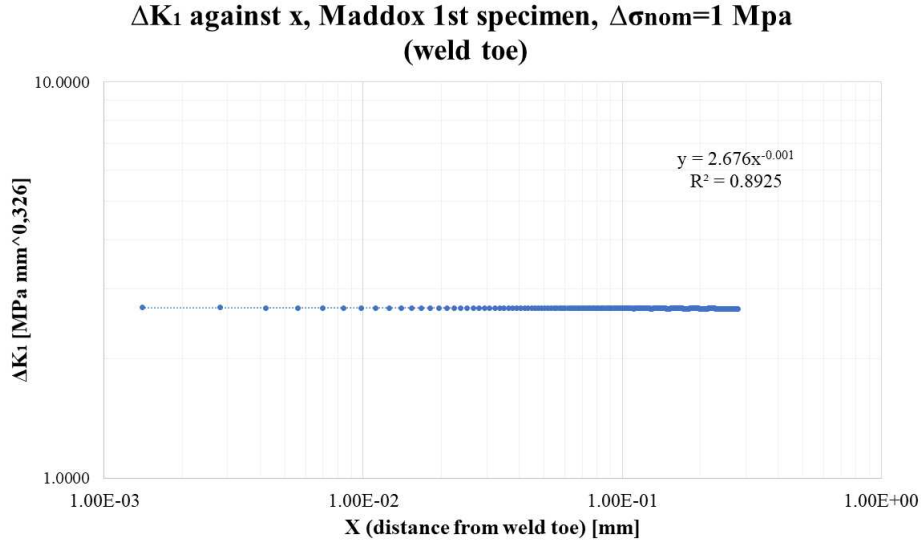


Figure 2.21: K_1 constancy in case of Maddox 1st specimen and 1 MPa as nominal stress.

The analytical result of the NSIF K_1 for the weld toe when the specimen is subjected to a nominal stress of 1 MPa is:

$$K_1 = 2.684 \text{MPa} \cdot \text{mm}^{0.326} \quad (2.3)$$

This result is in good agreement with the line intercept in Figure 2.21 and with the value found by Maddox in 1987 [37]:

$$K_{1,graph} = 2.676 \text{MPa} \cdot \text{mm}^{0.326} \quad (2.4)$$

$$K_{1,Maddox} = 2.633 \text{MPa} \cdot \text{mm}^{0.326} \quad (2.5)$$

Thus, the relative error expresses in percentage between the analytical NSIF K_1 and the K_1 calculated by Maddox is:

$$\Delta\% = \frac{K_{1,analytical} - K_{1,Maddox}}{K_{1,Maddox}} \cdot 100 = 1.93\% \quad (2.6)$$

The same procedure is executed for the calculation of NSIFs K_1 and K_2 at the root with the following differences:

1. The local coordinate system is placed at the root tip and the WorkPlane is rotated by 180° clockwise about the z-axis. The result can be shown in the following figure:

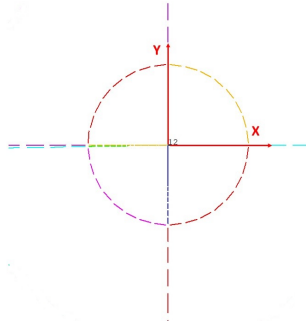


Figure 2.22: Local reference system with the center at root tip

2. The number of the local reference system is 12:

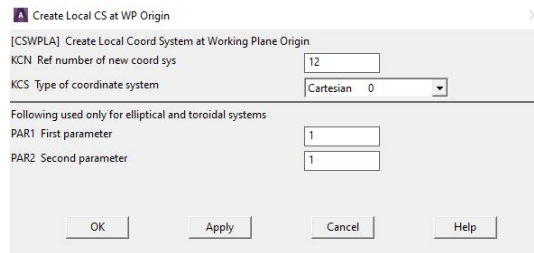


Figure 2.23: Creation of a local coordinate system at WP origin. As KCN option, a number greater than 10 must be chosen; so 12 is defined.

3. The node belonging the V-notch bisector are used to create a path as shown *Figure 2.24*:

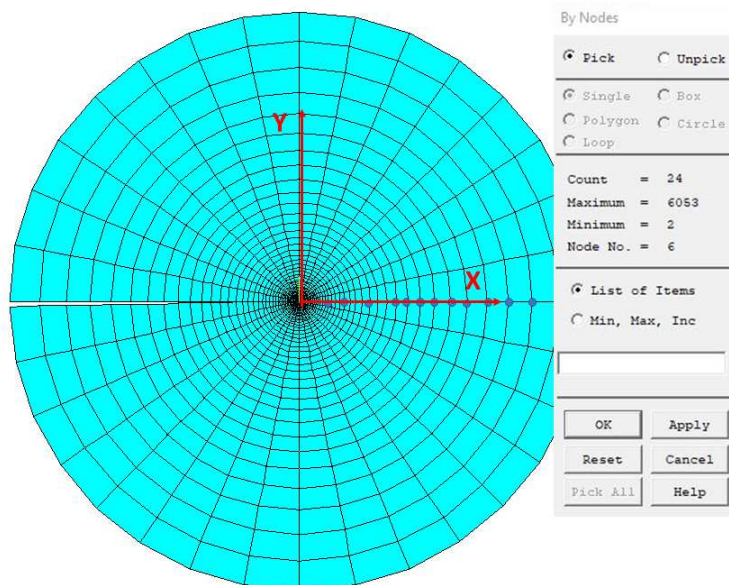


Figure 2.24: Selection of the nodes along the x-axis of the local reference system, from 0 to 0.28 mm.

4. The $\Delta\sigma_{yy}, \Delta\tau_{xy}$ (to calculate K_2) and x are plotted along the x -axis of the local reference system. In Ansys®, the $\Delta\sigma_{yy}, \Delta\tau_{xy}$ and x are defined as SY, SXY and S:

General Postproc → Path Operations → Define Path → Map onto Path → S/SY/SXY

The results are reported in a double logarithmic graph with in abscissa the x values and in ordinate the $\Delta\sigma_{yy}/\Delta\tau_{xy}$ values (Figure 2.20) for an external applied pressure $\Delta\sigma_{nom} = 1\text{MPa}$.

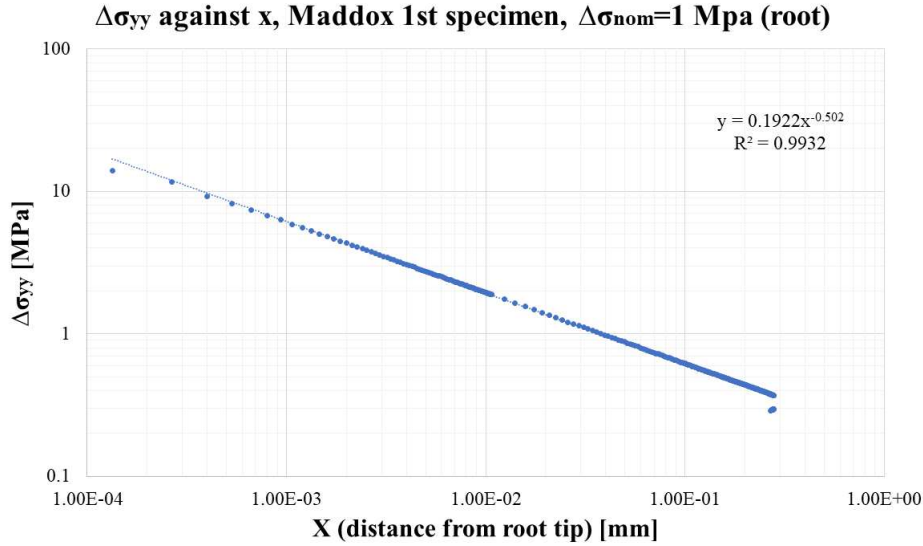


Figure 2.25: Singular stress field ($\Delta\sigma_{yy}$) along the V-notch bisector at the weld root, in case of Maddox 1st specimen and 1 MPa as nominal stress.

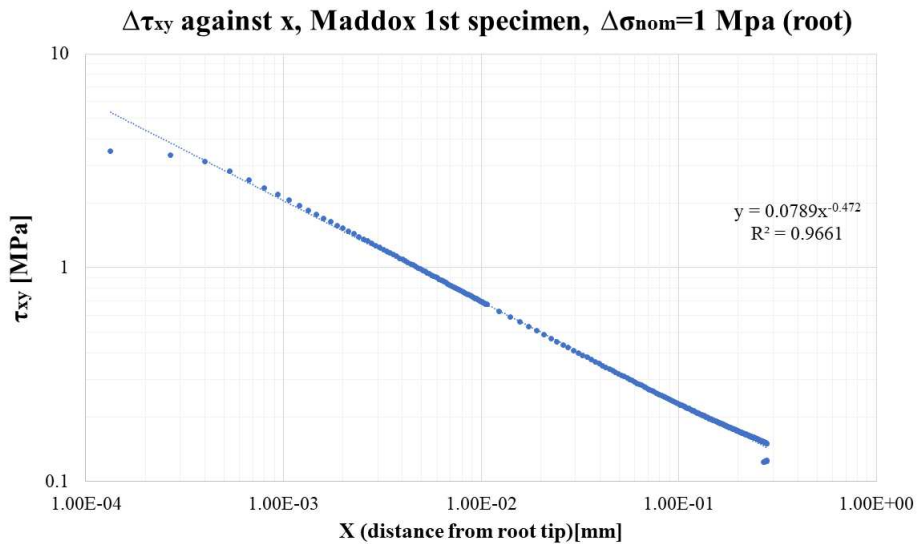


Figure 2.26: Singular stress field ($\Delta\tau_{xy}$) along the V-notch bisector at the weld root, in case of Maddox 1st specimen and 1 MPa as nominal stress.

As Figure 2.25 and Figure 2.26 show, the inverse slope of the asymptotic stress field k is equal to 0.502 for $\Delta\sigma_{yy}$ and 0.472 for $\Delta\tau_{xy}$. These values are in good agreement with the theoretical value $k = 1 - \lambda_1 = 0.5$ and $k = 1 - \lambda_2 = 0.5$.

Subsequently, the K_1 and K_2 values are detected by the averaging of the all points K_1 and K_2 along the path from $x = 1.40 \cdot 10^{-4}\text{mm}$ to $x = 0.28\text{mm}$, excluded the value for $x = 0$ because the graph is double logarithmic. To calculate the K_1 and K_2 , the equations (2.1)-(2.2) are used and the results are reported in the following graphs:

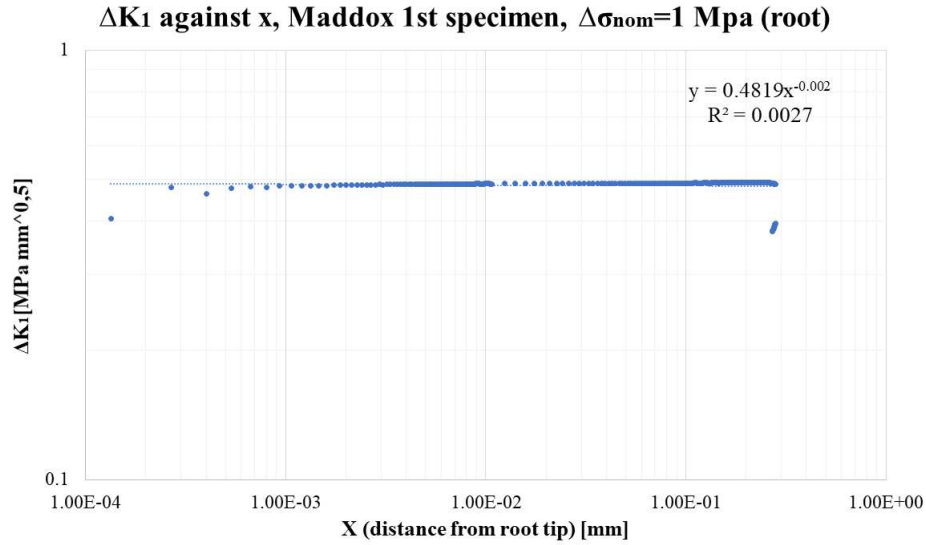


Figure 2.27: K_1 constancy in case of Maddox 1st specimen and 1 MPa as nominal stress.

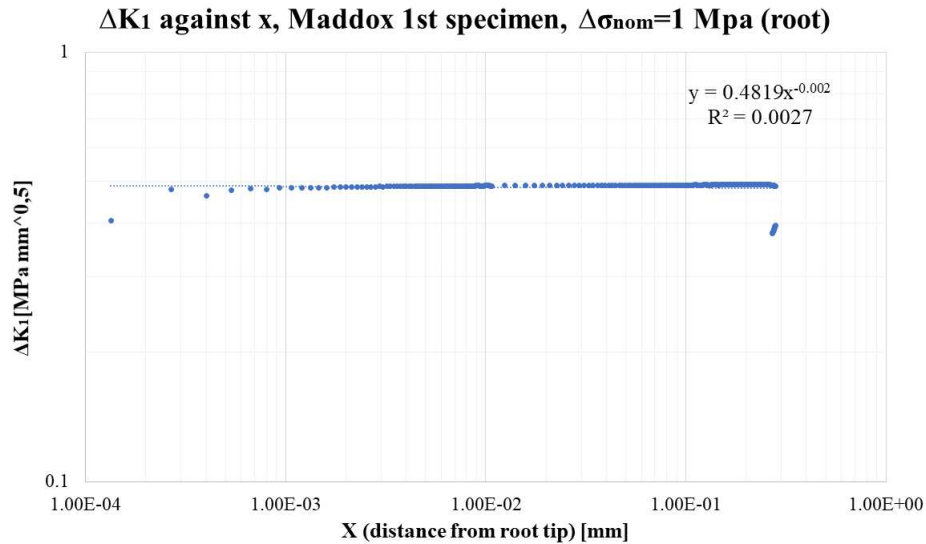


Figure 2.28: K_2 constancy in case of Maddox 1st specimen and 1 MPa as nominal stress.

The analytical results of the NSIFs K_1 and K_2 for the weld root when the specimen is subjected to a nominal stress of 1 MPa are:

$$K_1 = 0.485 \text{ MPa} \cdot \text{mm}^{0.5} \quad (2.7)$$

$$K_2 = 0.181 \text{ MPa} \cdot \text{mm}^{0.5} \quad (2.8)$$

This results are in good agreement with the line intercept in *Figure 2.27* and *Figure 2.28*:

$$K_1 = 0.482 \text{ MPa} \cdot \text{mm}^{0.5} \quad (2.9)$$

$$K_2 = 0.198 \text{ MPa} \cdot \text{mm}^{0.5} \quad (2.10)$$

The values of K_1 and K_2 at the root were not calculated by Maddox in 1987; indeed he did not consider the influence of the weld root.

For this reason the comparison with the literature is not possible.

2.2.2 NSIFs K_1 and K_2 results

Thanks to the linear elasticity hypothesis, the K_1 and K_2 values can be defined for different loading conditions with the following expression:

$$K_{1/2,gen} = \frac{\Delta\sigma_{gen}}{\Delta\sigma_{ref}} \cdot K_{1/2,ref} \quad (2.11)$$

where:

- $K_{1/2,gen}$ is a generic value of K_1 or K_2 for a generic loading condition that has to be detected;
- $\Delta\sigma_{gen}$ is the respective applied nominal stress;
- $K_{1/2,ref}$ is the reference value of NSIFs that are already detected;
- $\Delta\sigma_{ref}$ is the reference nominal stress.

The results obtained by the re-elaboration of each set of experimental data are displayed on the following tables in terms of NSIFs K_1 and K_2 for the root and weld toe.

Specimen type and load	$\Delta\sigma_{nom}$ [MPa]	$K_{1,weld-toe}$ [MPa·mm ^{0.326}]	N_f [cycles]
Maddox 1st specimen Transverse NLC/axial	200	536.75	192 000
	140	375.73	507 000
	100	268.38	2 937 000
	80	214.70	4 297 000
Gurney 2nd specimen Transverse NLC/axial	150	913.63	109 000
	120	730.91	224 000
	100	609.09	322 000
	65	395.91	1 153 000
	55	335.00	2 147 000
Gurney 3rd specimen Transverse NLC/bending	260	778.93	120 000
	220	659.10	200 000
	180	539.26	302 000
	140	419.42	744 000
	120	359.51	1 180 000
	110	329.55	2 158 000
Gurney 4th specimen T-shape joint/bending	300	578.07	135 000
	260	500.99	237 000
	200	385.38	407 000
	190	366.11	573 000
	180	346.84	665 000
	160	308.30	1 525 000
	150	289.03	1 534 000
	140	269.76	2 601 000

Table 2.12: Results of K_1 at the weld toe

Specimen type and load	$\Delta\sigma_{nom}$ [MPa]	$K_{1,root}$ [MPa \cdot mm ^{0.5}]	$K_{2,root}$ [MPa \cdot mm ^{0.5}]	N_f [cycles]
Maddox 1st specimen Transverse NLC/axial	200	97.01	36.29	192 000
	140	67.91	25.40	507 000
	100	48.50	18.14	2 937 000
	80	38.80	14.51	4 297 000
Gurney 2nd specimen Transverse NLC/axial	150	399.03	352.42	109 000
	120	319.22	281.93	224 000
	100	266.02	234.94	322 000
	65	172.91	152.71	1 153 000
	55	146.31	129.22	2 147 000
Gurney 3rd specimen Transverse NLC/bending	260	144.43	53.96	120 000
	220	122.21	45.66	200 000
	180	99.99	37.36	302 000
	140	77.77	29.06	744 000
	120	66.66	24.91	1 180 000
	110	61.10	22.83	2 158 000
Gurney 4th specimen T-shape joint/bending	300	99.12	0.81	135 000
	260	85.91	0.70	237 000
	200	66.08	0.54	407 000
	190	62.78	0.51	573 000
	180	59.47	0.49	665 000
	160	52.87	0.43	1 525 000
	150	49.56	0.40	1 534 000
	140	46.26	0.38	2 601 000

Table 2.13: Results of K_1 at the root

As the tables show, the weld toe area is characterised by NSIF K_1 greater than the root region. Since the V-notch opening angle 2α at the weld toe is the same for each specimens (135°), the grade of singularity is the same, so the comparison in terms of NSIF K_1 is possible. Indeed the all re-elaborated data are collected together and subjected to a statistical analysis: the results are reported in the Figure 2.29, where the inverse slope is set to $k = 3$, in agreement with the literature and the red line represents the design curve obtained by statistical analysis with the re-elaborated data. The graph represented in Figure 2.29 is also characterized by the presence of the K_1 design curve proposed by Lazzarin and Tovo [6] (Black lines).

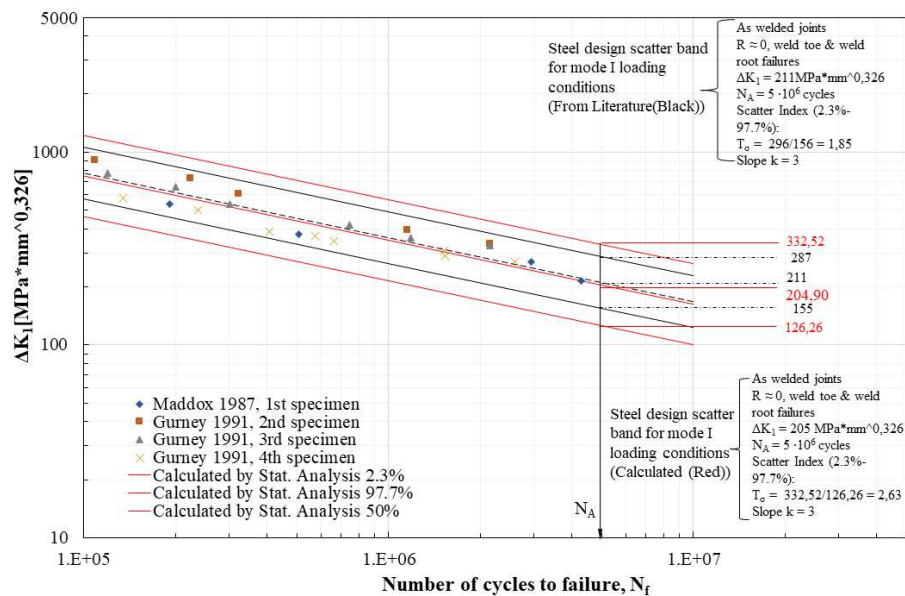


Figure 2.29: Fatigue strength in terms of K_1 , calculated at the weld toe.

The following conclusions can be defined:

1. The NSIFs approach has correctly defined that the crack initiation point is the weld toe, according to the experimental results;
2. The all experimental data fall above the lines that represents the 97.7% of probability of survival. Thus, the NSIF K_1 design curve has demonstrated to be effective and conservative
3. The theoretical scatter band amplitude T_K is equal to 1.85 and it is lower than the re-elaborated T_K that is 2.63. This is due to that during the re-elaboration only 23 data have been employed.

2.3 Nominal Stress approach

As described in the paragraph 1.1, the Nominal Stress approach is the most common method for the fatigue assessment of welded joints. According to the IIW recommendations written by Hobbacher [1], the nominal stress approach evaluate the maximum principal stress in the section where crack is more likely to develop and propagate.

2.3.1 Results of Nominal Stress approach

The results of the re-elaboration of each set of data are reported in terms of maximum nominal stress calculated in the main plate of each specimen. The results are displayed on the following table only for the weld toe region:

Specimen type and load	$\Delta\sigma_{nom}$ [MPa]	N_f [cycles]
Maddox 1st specimen Transverse NLC/axial	200	192 000
	140	507 000
	100	2 937 000
	80	4 297 000
Gurney 2nd specimen Transverse NLC/axial	150	109 000
	120.3	224 000
	100	322 000
	65.1	1 153 000
	55	2 147 000
Gurney 3rd specimen Transverse NLC/bending	260	120 000
	220	200 000
	180	302 000
	140	744 000
	120	1 180 000
	110	2 158 000
Gurney 4th specimen T-shape joint/bending	300	135 000
	260	237 000
	200	407 000
	190	573 000
	180	665 000
	160	1 525 000
	150	1 534 000
	140	2 601 000

Table 2.14: Results in terms of nominal stress at the weld toe

The results are reported in the *Figure 2.30*, where the inverse slope is set to $k = 3$, in agreement with the literature and the black line represents the design curve obtained by statistical analysis with the re-elaborated data.

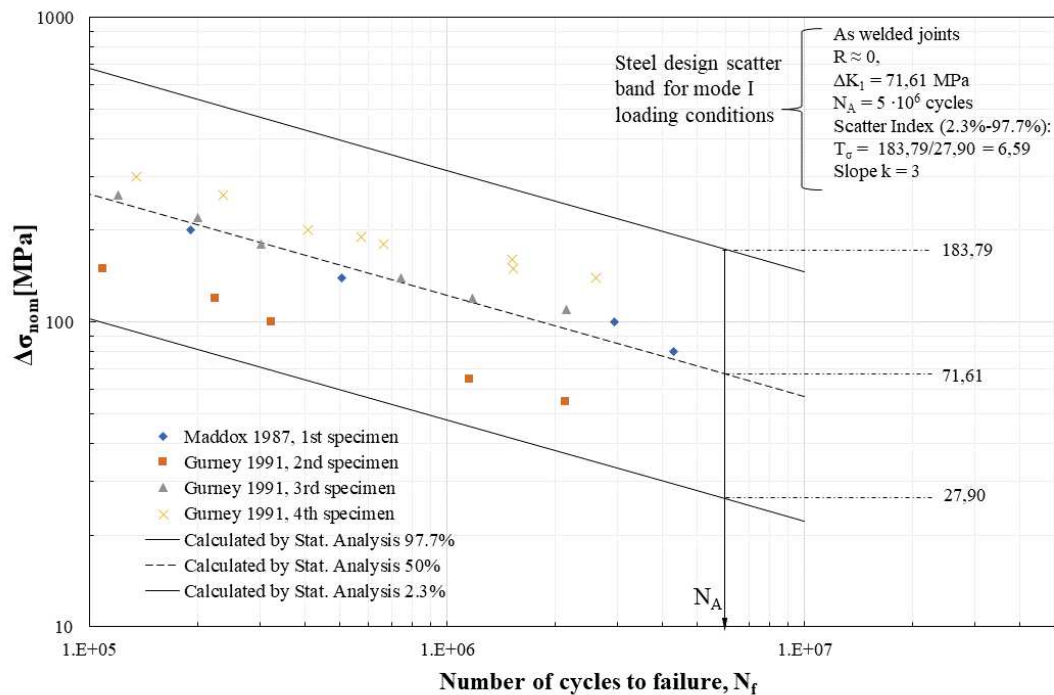


Figure 2.30: Fatigue strength in terms of nominal stress range, calculated at the weld toe.

The following conclusions can be defined:

1. The all experimental data fall above the lines that represents the 97.7% of probability of survival.
2. The scatter band amplitude T_{σ} is equal to 6.59 and it is very large, due to that during the re-elaboration, only 23 data have been employed. Furthermore, the fatigue is a local phenomenon, which focuses on the crack initiation and development in the V-notch area.
3. If each data set is subjected by a singular statistical analysis, the inverse slope k is ranged from 2.9 to 3.73. This is another fact that justifies the large scatter band.

2.4 SED (Strain Energy Density) approach

As described in the paragraph 1.3.2, the SED approach is an energetic criterion, proposed by Lazzarin and Zambardi [25] in 2001 to overcome the limits of NSIFs approach. This method derives from the Neuber's idea of structural volume. Indeed, the Averaged Strain Energy Density (SED) inside a circular sector of radius R_0 with the center in the V-notch tip, is the critical parameter to evaluate the fatigue strength of welded components. The typical values of R_0 are 0.28mm for steel structures and 0.12mm for aluminium alloys.

2.4.1 Calculation of SED in Ansys®APDL

The following procedure refers to the 1st specimen (Maddox 1991) but it can be similarly extended for the other joints.

The four-node linear element PLANE 182 is chosen inside Ansys®APDL, with *Simple Enhanced Strain* as Key Option 1 and *Plane Strain* as Key Option 3.

First of all, the circular sector of radius $R_0 = 0.28\text{mm}$ is created with the center respectively at the weld toe tip and root tip as *Figure 2.31a-2.31b* shows:

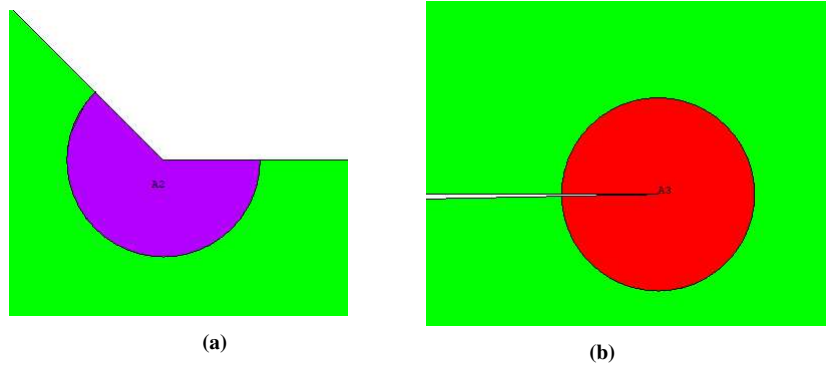


Figure 2.31: Modelling of the structural volume around the weld toe and root tip.

To create the mesh of the model, the following procedure are executed:

1. The element inside the structural volume are characterised by a *global element size* equal to 0.05mm:

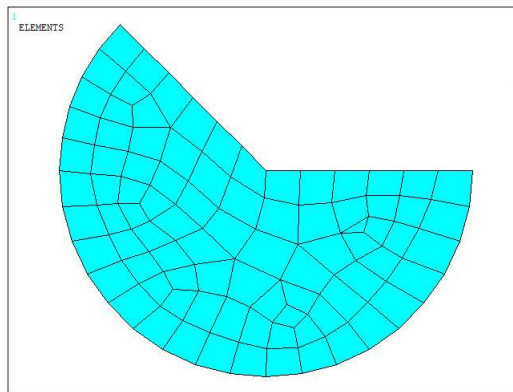


Figure 2.32: Mesh of the structural volume at the weld toe with global element size of 0.05mm

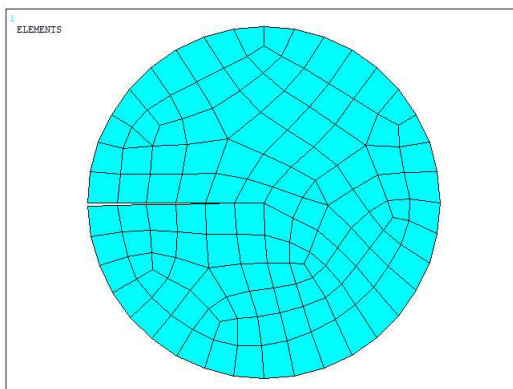


Figure 2.33: Mesh of the structural volume at the root with global element size of 0.05mm

2. Two circular sectors with a radius equal to 0.7 mm, are created around the structural volume, as *Figure 2.34* shows, to guarantee a smooth element transition towards the circular sector.

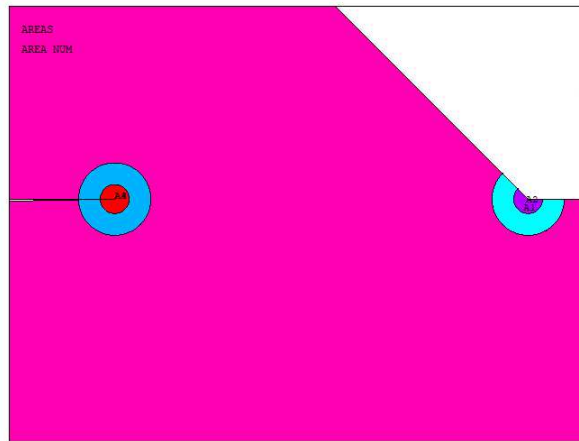


Figure 2.34: The Circular sector to guarantee a smooth element transition are coloured in blue

3. The element inside circular sector with a radius of 0.7mm, are characterised by a *global element size* equal to 0.1mm.

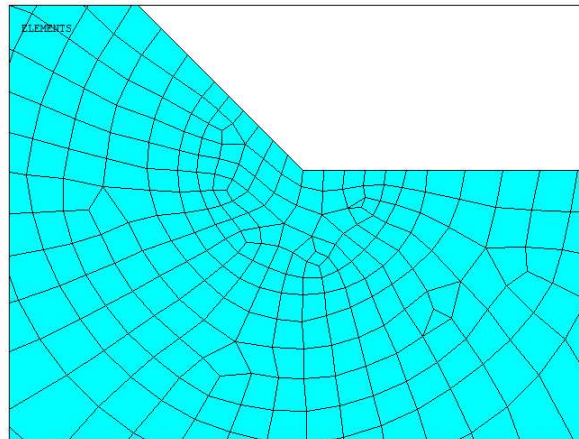


Figure 2.35: Smooth transition towards circular sectors

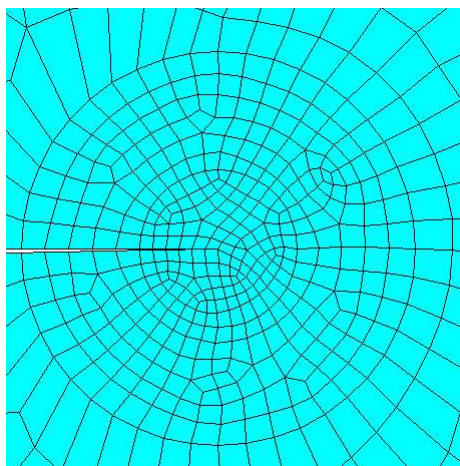


Figure 2.36: Smooth transition towards circular sectors

4. A mesh obtained by *free-mesh* algorithm is laid on the remaining area with a global element size changing according to the welded joint into account.

After the creation of the mesh, the system can be solved:

Solution → *Solve* → *Current LS*

The averaged Strain Energy Density is defined as the energy contained inside the structural volume. To define this value, the element belonging to the structural volume have to be selected with the following commands:

Utility Menu → *Select* → *Entities* → *Areas* → *By Num/Pick* → *From Full*

Utility Menu → *Select* → *Entities* → *Elements* → *Attached to* → *Areas*

Subsequently, two *Element Table* are created :

1. The first one to define the energy inside each element selected. This Element Table is called *SENE*;
2. The second one to define the volume of each element selected. This Element Table is called *VOLU*;

The commands to create the Element Table are:

General Postproc → *Element Table* → *Define Element Table* → *SENE/VOLU*

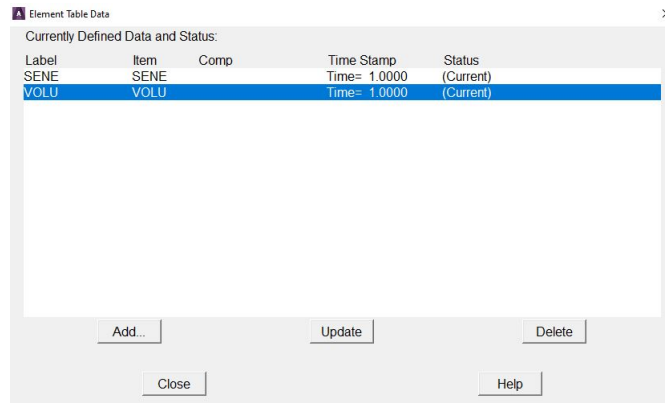


Figure 2.37: *Element Table in Ansys®APDL*

After the creation of the Element Tables, each single element *SENE* and *VOLU* values must be summed with the following commands:

General Postproc → *Element Table* → *Sum of Each Item*

Finally, the averaged Strain Energy Density value can be calculated with the following expression:

$$\Delta \bar{W}_{FEM} = \frac{\sum_{V(R_0)} W_{FEM,i}}{V(R_0)} = \frac{SENE}{VOLU} \quad (2.12)$$

The result of SED for the weld toe when the specimen is subjected to a nominal stress of 1 MPa is:

$$SENE = 1.44 \cdot 10^{-6} MJ \quad (2.13)$$

$$VOLU = 0.153187 mm^3 \quad (2.14)$$

$$SED = \frac{SENE}{VOLU} = \frac{1.44 \cdot 10^{-6}}{0.153187} = 9.39 \cdot 10^{-6} \frac{MJ}{m^3} \quad (2.15)$$

The result of SED for the root when the specimen is subjected to a nominal stress of 1 MPa is:

$$SENE = 3.43 \cdot 10^{-7} MJ \quad (2.16)$$

$$VOLU = 0.244280 mm^3 \quad (2.17)$$

$$SED = \frac{SENE}{VOLU} = \frac{3.43 \cdot 10^{-7}}{0.24428} = 1.40 \cdot 10^{-6} \frac{MJ}{m^3} \quad (2.18)$$

2.4.2 SED results

Thanks to the linear elasticity hypothesis, the SED value can be defined for different loading conditions with the following expression:

$$SED_{gen} = \left(\frac{\Delta\sigma_{gen}}{\Delta\sigma_{ref}} \right)^2 \cdot SED_{ref} \quad (2.19)$$

where:

- SED_{gen} is a generic value of the SED for a generic loading condition that has to be detected;
- $\Delta\sigma_{gen}$ is the respective applied nominal stress;
- SED_{ref} is the reference value of SED that are already detected;
- $\Delta\sigma_{ref}$ is the reference nominal stress

One important thing to underline is that the comparison of stress field between V-notch with different opening angle is possible because the fatigue resistance is expressed in terms of energy (SED), so the unit of measure remain constant.

The results obtained by the re-elaboration of each set of experimental data are displayed on the following tables in terms of SED for the root and weld toe.

Specimen type and load	$\Delta\sigma_{nom}$ [MPa]	SED [MJ/m^3]	N_f [cycles]
Maddox 1st specimen Transverse NLC/axial	200	0.38	192 000
	140	0.18	507 000
	100	0.09	2 937 000
	80	0.06	4 297 000
Gurney 2nd specimen Transverse NLC/axial	150	1.09	109 000
	120	0.70	224 000
	100	0.49	322 000
	65	0.21	1 153 000
	55	0.15	2 147 000
Gurney 3rd specimen Transverse NLC/bending	260	0.80	120 000
	220	0.57	200 000
	180	0.39	302 000
	140	0.23	744 000
	120	0.17	1 180 000
	110	0.14	2 158 000
Gurney 4th specimen T-shape joint/bending	300	0.42	135 000
	260	0.32	237 000
	200	0.19	407 000
	190	0.17	573 000
	180	0.15	665 000
	160	0.12	1 525 000
	150	0.11	1 534 000
	140	0.09	2 601 000

Table 2.15: Results of SED at the Weld toe

Specimen type and load	$\Delta\sigma_{nom}$ [MPa]	SED_{root} [MJ/m ³]	N_f [cycles]
Maddox 1st specimen Transverse NLC/axial	200	0.056	192 000
	140	0.027	507 000
	100	0.014	2 937 000
	80	0.009	4 297 000
Gurney 2nd specimen Transverse NLC/axial	150	1.16	109 000
	120	0.74	224 000
	100	0.52	322 000
	65	0.22	1 153 000
	55	0.16	2 147 000
Gurney 3rd specimen Transverse NLC/bending	260	0.111	120 000
	220	0.079	200 000
	180	0.053	302 000
	140	0.032	744 000
	120	0.024	1 180 000
	110	0.020	2 158 000
Gurney 4th specimen T-shape joint/bending	300	0.028	135 000
	260	0.021	237 000
	200	0.012	407 000
	190	0.011	573 000
	180	0.010	665 000
	160	0.008	1 525 000
	150	0.007	1 534 000
	140	0.006	2 601 000

Table 2.16: Results of SED at the root

As the tables show, the weld toe area is characterised by a SED value greater than the root region with the exception of the 2nd specimen Gurney, where SED value of the root are major than the weld toe. The all re-elaborated data are collected together and subjected to a statistical analysis: the results are reported in the Figure 2.38, where the inverse slope is set to $k = 1.5$, in agreement with the literature and the red line represents the design curve obtained by statistical analysis with the re-elaborated data. The graph represented in Figure 2.38 is also characterized by the presence of the SED design curve proposed by Lazzarin and Zambardi [25] (Black lines).

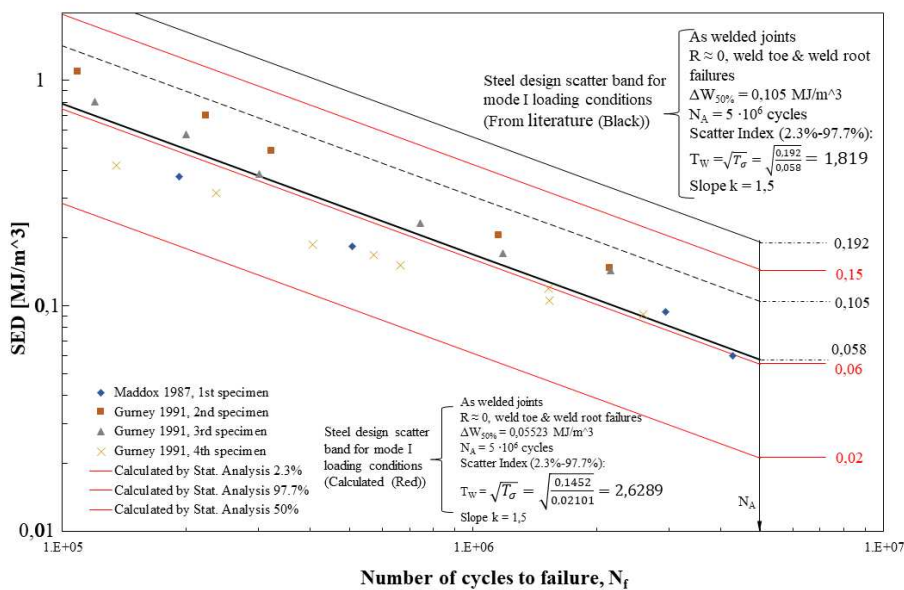


Figure 2.38: Fatigue strength in terms of SED, calculated at the weld toe.

The following conclusions can be defined:

1. The SED approach has correctly defined that the crack initiation point is the weld toe, according to the experimental results for 3 joints with only one exception: the 2nd specimen, where the value of the root is higher than the weld toe;
2. The all experimental data fall above the lines that represents the 97.7% of probability of survival. Thus, the SED design curve has demonstrated to be effective and conservative
3. The theoretical scatter band amplitude T_W is equal to 1.819 and it is lower than the re-elaborated T_W that is 2.74. This is due to that during the re-elaboration only 23 data have been employed against the 900 experimental data available to Lazzarin and Zambardi [25].

2.5 PSM (Peak Stress Method) approach

As described in the paragraph 1.3.3, the objective of the Peak Stress method is to detect rapidly the value of NSIFs for fatigue assessment of welded joints. Indeed, the NSIFs approach shows a major drawback in engineering application, due to the very refined finite elements size at the V-notch tip ($size = 10^{-5}$), causing an increase of computational time.

The PSM wants to overcome the limits of NSIF's approach and the peak stress method is characterized by two principal advantages:

1. FE analysis require a coarser mesh than the NSIFs and SED approaches. Indeed the global element size d can be higher than the control radius R_0 , unlike the "direct approach" to calculate the SED where is necessary to have $d < R_0$;
2. The post-process analysis require only one nodal peak stress instead of a large number of stress distance values as in NSIFs approach;

As defined in the *Chapter 1*, the PSM gives the correlation between the mode I,II and III NSIFs and the corresponding peak stress component, as defined by the following equations:

$$K_1 \cong K_{FE}^* \cdot \sigma_{\theta\theta, \theta=0, peak} \cdot d^{1-\lambda_1} \quad (2.20)$$

$$K_2 \cong K_{FE}^{**} \cdot \tau_{r\theta, \theta=0, peak} \cdot d^{1-\lambda_2} \quad (2.21)$$

$$K_3 \cong K_{FE}^{***} \cdot \tau_{\theta z, \theta=0, peak} \cdot d^{1-\lambda_3} \quad (2.22)$$

where:

- $K_{FE}^*, K_{FE}^{**}, K_{FE}^{***}$ are the calibration constants related to mode I,II,II and depend on the element type, the software type, the mesh conformation and the nodal stress evaluation method;
- $\sigma_{\theta\theta, \theta=0, peak}, \tau_{r\theta, \theta=0, peak}, \tau_{\theta z, \theta=0, peak}$ are the peak nodal stresses detected at the V-notch profiles (see *Figure 1.14a*);
- d is the global element size;
- $\lambda_1, \lambda_2, \lambda_3$ are the Williams' eigenvalues.

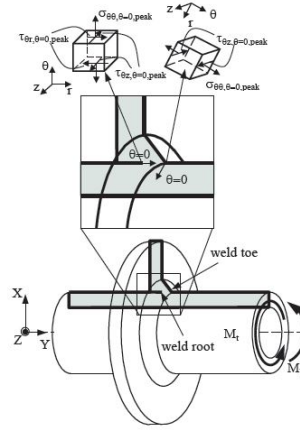


Figure 2.39: Nodal stresses at the V-notch [24]

The equivalent stress peak is define in the equation (2.23):

$$\sigma_{eq, peak} = \sqrt{f_{w1}^2 \cdot \sigma_{\theta\theta, \theta=0, peak}^2 + f_{w2}^2 \cdot \tau_{r\theta, \theta=0, peak}^2 + f_{w3}^2 \cdot \tau_{z\theta, \theta=0, peak}^2} \quad (2.23)$$

where:

- $f_{wi, i=1,2,3}$ are the peak stresses corrective factors and are defined like follows as the equation (1.17):

$$f_{wi} = K_{FE}^j \cdot \sqrt{\frac{2e_i}{1-\nu^2}} \cdot \left(\frac{d}{R_0}\right)^{1-\lambda_i} \Big|_{\substack{i=1,2,3 \\ j=*,**,***}} \quad (2.24)$$

- $\sigma_{\theta\theta, \theta=0, peak}$, $\tau_{r\theta, \theta=0, peak}$, $\tau_{z\theta, \theta=0, peak}^2$ are the nodal peak stresses defined in the paragraph 1.3.3.

2.5.1 Calculation of Equivalent Peak Stress in Ansys®APDL

The following procedure refers to the 1st specimen (Maddox 1991) but it can be similarly extended for the other joints.

The four-node linear element PLANE 182 is chosen inside Ansys®APDL, with *Simple Enhanced Strain* as Key Options 1 and *Plane Strain* as Key Options 3.

As defined during in the paragraph 2.2, the weld toe is subjected to pure mode I because it is characterised by a V-notch opening angle 2α equal to 135° .

On the other hand, the root is characterised by a V-notch opening angle equal to 0° , so it is subjected to mode I and also mode II.

Under mode I and mode II, the PSM requirements are defined in the following table:

Element type	Mesh algorithm	$(a/d)_{min}$	2α	Mode I	
				Mesh Pattern $2\alpha < 90^\circ$	Mesh Pattern $2\alpha > 90^\circ$
Plane 182 KeyOpt:Simple Enhanced Strain + Plane Strain	Free	3	$0^\circ < 2\alpha < 135^\circ$	Four adjacent elements share the same node	Two adjacent elements share the same node
Mode II					
Plane 182 KeyOpt:Simple Enhanced Strain + Plane Strain	Free	14	$0^\circ < 2\alpha < 135^\circ$	Four adjacent elements share the same node	Four adjacent elements share the same node up to $2\alpha = 102.5^\circ$

Table 2.17: Requirements for PSM.

The mode I PSM calibration constant is equal to $K_{FE}^* = 1.38 \pm 3\%$, instead for mode II the calibration constant is equal to $K_{FE}^{**} = 3.38 \pm 3\%$.

The size of the element is obtained with the following procedure:

1. From literature the ratio $(a/d)_{min}$ is determined. In this case there are 2 ratio: the first one for mode I and the second for mode II. The highest ratio is chosen;
2. The value of a is the reference dimension for selecting the maximal FE sizes d for PSM application and is defined as the minimum value between:
 - (a) Half joint main plate thickness that for the 1st specimen is equal to $a = 13/2 = 6.5$
 - (b) The minimum value between z and l , where z is the weld leg (8mm in this case) and l is the depth of root face (5mm in this case) as the figure below shows

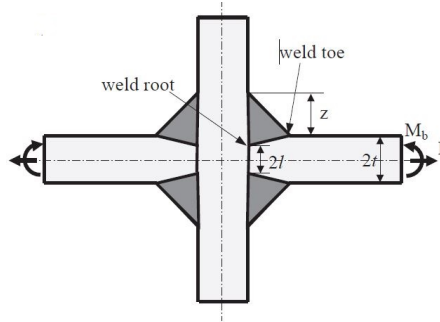


Figure 2.40: Indication for z and l [11]

so the minimum is l , the depth of the root face;

3. Subsequently, the minimum element size is defined as follow:

$$d_{min} = \frac{a}{14} = \frac{5}{14} = 0.357mm \quad (2.25)$$

4. The chosen dimension of elements is 0.3mm

The $\lambda_1, e_1, \lambda_2$ and e_2 values are depended on the V-notch opening angle 2α , that is 135° for the weld toe and 0° for the root:

2α [°]	λ_1 (Mode I)	e_1 (Mode I)	λ_2 (Mode II)	e_2 (Mode II)
135°	0.674	0.117	/	/
0°	0.5	0.133	0.5	0.341

Table 2.18: Value of $\lambda_1, e_1, \lambda_2$ and e_2 in function of the opening angle 2α

The corrective stress factors for mode I and II are calculated with the equation (2.24) for the weld toe and root. The results are reported in the *Table 2.19*

2α [°]	f_{w1}	f_{w2}
135°	0.716	/
0°	0.775	3.029

Table 2.19: Values of the corrective stress factors f_{w1} and f_{w2} in function of the opening angle 2α

Finally, the mesh can be laid on the model and the results is displayed on the *Figure 2.41*:

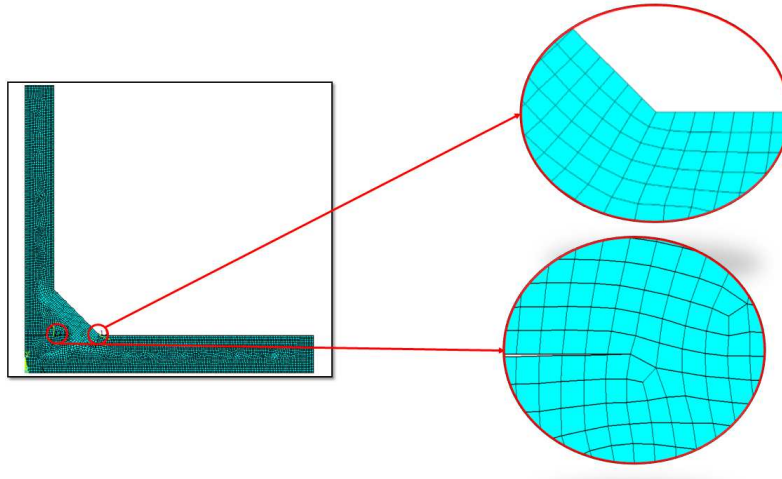


Figure 2.41: Mesh conformation with global element size $d = 0.3\text{mm}$

After the application of load and constraint in according to the paragraph 2.1.1 , the system can be solved:

Solution → *Solve* → *Current LS*

The results of the first principal stress is plotted with the following commands in the *Figure 2.42*:

General Postproc → *Plot Results* → *Contour Plot* → *Nodal Solution* → *Stress* → *1st Principal Stress*

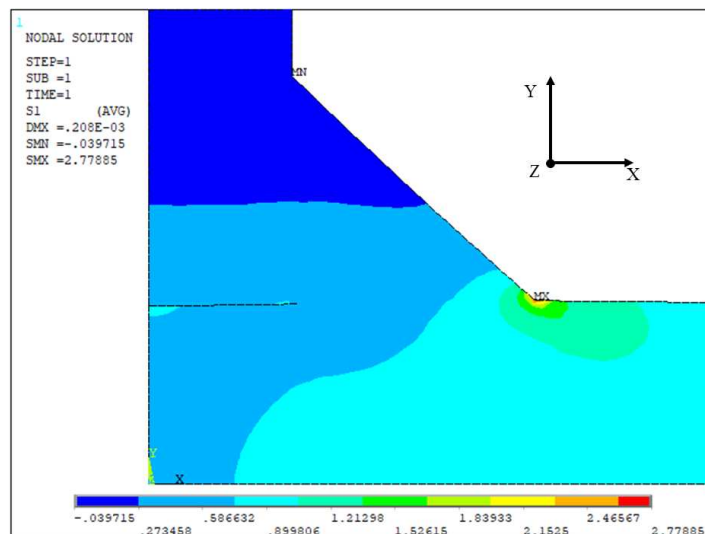


Figure 2.42: Plot of 1st principal stress in Maddox 1987 1st specimen, for an external applied nominal stress range of 1MPa. In black the global coordinate system.

In reference to Figure 2.42, the peak stress $\Delta\sigma_{\theta\theta,\theta=0,peak}$ must be evaluated in the most solicited point of the model, for example the weld toe tip. To obtain a very accurate results of the peak stress $\Delta\sigma_{\theta\theta,\theta=0,peak}$, the rigorous procedure is to create a local coordinate system as the one adopted for the detection of K_1 . If the structure is subjected to pure mode I loading, the 1st principal stress can be approximated equal to the local stress $\Delta\sigma_{yy}$. Due to the presence of the root, this approximation can not be done because the root is subjected to mode I and II.

Thus, a local coordinate systems are created at the weld toe and root to detect the stress $\Delta\sigma_{yy}$. The procedure for local system creation is the same describe in the paragraph 2.2.1 for the NSIFS detection.

For an external applied nominal stress range $\Delta\sigma_{nom} = 1MPa$, the maximum $\Delta\sigma_{yy}$ is located at the weld toe tip for three specimens with only one exception: Gurney 1991 2nd specimen, where the peak stress is placed at the weld root.

In the case of Maddox 1987 1st specimen the results at the weld toe and root are:

$$\Delta\sigma_{yy,weld-toe} = \Delta\sigma_{\theta\theta,\theta=0,peak} = 2.78MPa \quad (2.26)$$

$$\Delta\sigma_{yy,root} = \Delta\sigma_{\theta\theta,\theta=0,peak} = -0.64MPa \quad (2.27)$$

$$\Delta\tau_{xy,root} = \Delta\tau_{r\theta,\theta=0,peak} = -0.13MPa \quad (2.28)$$

$$(2.29)$$

Defined the peak stresses, K_1, K_2 and $\Delta\sigma_{eq,peak}$ can be calculated with the formulae (2.20)-(2.21) and (2.23):

$$\Delta K_{1,weld-toe} \cong K_{FE}^* \cdot \sigma_{\theta\theta,\theta=0,peak} \cdot d^{1-\lambda_1} = 1.38 \cdot 2.78 \cdot d^{1-0.674} = 2.59MPamm^{0.326} \quad (2.30)$$

$$\Delta K_{1,root} \cong K_{FE}^* \cdot \sigma_{\theta\theta,\theta=0,peak} \cdot d^{1-\lambda_1} = 1.38 \cdot |0.64| \cdot d^{1-0.5} = 0.48MPamm^{0.5} \quad (2.31)$$

$$\Delta K_{2,root} \cong K_{FE}^{**} \cdot \tau_{r\theta,\theta=0,peak} \cdot d^{1-\lambda_2} = 3.38 \cdot |0.13| \cdot d^{1-0.5} = 0.25MPamm^{0.5} \quad (2.32)$$

$$\Delta\sigma_{eq,peak,weld-toe} = \Delta\sigma_{\theta\theta,\theta=0,peak} \cdot f_{w1} = 2.78 \cdot 0.716 = 1.987MPa \quad (2.33)$$

$$\begin{aligned} \Delta\sigma_{eq,peak,root} &= \sqrt{f_{w1}^2 \cdot \sigma_{\theta\theta,\theta=0,peak}^2 + f_{w2}^2 \cdot \tau_{r\theta,\theta=0,peak}^2} \\ &= \sqrt{0.775^2 \cdot (-0.64)^2 + 3.029^2 \cdot (-0.13)^2} = 0.64MPa \end{aligned} \quad (2.34)$$

This result is in good agreement with the value found by Maddox in 1987 [37]:

$$\Delta\sigma_{eq,peak,Maddox} = 1.87MPa \quad (2.35)$$

Thus, the relative error expresses in percentage between the calculated $\Delta\sigma_{eq,peak}$ and the $\Delta\sigma_{eq,peak,Maddox}$ calculated by Maddox is:

$$\Delta\% = \frac{\Delta\sigma_{eq,peak,calculated} - \Delta\sigma_{eq,peak,Maddox}}{\Delta\sigma_{eq,peak,Maddox}} \cdot 100 = 6.25\% \quad (2.36)$$

2.5.2 PSM results

Thanks to the linear elasticity hypothesis, the equivalent peak stress can be defined for different loading conditions with the following expression:

$$\Delta\sigma_{eq,peak,gen} = \frac{\Delta\sigma_{gen}}{\Delta\sigma_{ref}} \cdot \Delta\sigma_{eq,peak,ref} \quad (2.37)$$

where:

- $\Delta\sigma_{eq,peak,gen}$ is a generic value of the equivalent peak stress for a generic loading condition that has to be detected;
- $\Delta\sigma_{gen}$ is the respective applied nominal stress;
- $\Delta\sigma_{eq,peak,ref}$ is the reference value of equivalent peak stress that are already detected;
- $\Delta\sigma_{ref}$ is the reference nominal stress.

One important thing to underline is that the comparison of stress field between V-notch with different opening angle is possible because the fatigue resistance is expressed in terms of equivalent peak stress, so the unit of measure remain constant.

The results obtained by the re-elaboration of each set of experimental data are displayed on the following tables in terms of $\Delta\sigma_{eq,peak}$ and $K_1/2$ for the root and weld toe. Furthermore, inside the table is reported the dimension of the element for each geometry.

Specimen type,load and element dimension	$\Delta\sigma_{nom}$ [MPa]	$\Delta\sigma_{eq,peak,weld-toe}$ [MPa]	$K_{1,weld-toe}$ [MPa·mm ^{0.326}]	N_f [cycles]
Maddox 1st specimen Transverse NLC/axial, d=0.3mm	200	397.38	517.48	192 000
	140	278.17	362.24	507 000
	100	198.69	258.74	2 937 000
	80	158.95	206.99	4 297 000
Gurney 2nd specimen Transverse NLC/axial, d=1mm	150	692.06	901.22	109 000
	120	553.65	720.97	224 000
	100	461.37	600.81	322 000
	65	299.89	390.53	1 153 000
Gurney 3rd specimen Transverse NLC/bending, d=0.4mm	55	253.76	330.45	2 147 000
	260	577.35	751.84	120 000
	220	488.53	636.17	200 000
	180	399.70	520.50	302 000
	140	310.88	404.84	744 000
Gurney 4th specimen T-shape joint/bending, d=0.2mm	120	266.47	347.00	1 180 000
	110	244.26	318.09	2 158 000
	300	429.77	559.66	135 000
	260	372.47	485.04	237 000
	200	286.52	373.11	407 000
	190	272.19	354.45	573 000
	180	257.86	335.80	665 000
	160	229.21	298.47	1 525 000
150	214.89	279.83	1 534 000	
140	200.56	261.18	2 601 000	

Table 2.20: Results of PSM approach at the weld toe

Specimen type,load and element dimension	$\Delta\sigma_{nom}$ [MPa]	$\Delta\sigma_{eq,peak,root}$ [MPa]	$K_{1,root}$ [MPa·mm ^{0.5}]	$K_{2,root}$ [MPa·mm ^{0.5}]	N_f [cycles]
Maddox 1st specimen Transverse NLC/axial, d=0.3mm	200	128.00	96.87	49.33	192 000
	140	89.60	67.81	34.53	507 000
	100	64.00	48.43	24.67	2 937 000
	80	51.20	38.75	19.73	4 297 000
Gurney 2nd specimen Transverse NLC/axial, d=1mm	150	706.31	387.22	357.54	109 000
	120	565.05	309.78	286.03	224 000
	100	470.87	258.15	238.36	322 000
	65	306.07	167.80	154.93	1 153 000
Gurney 3rd specimen Transverse NLC/bending, d=0.4mm	55	258.98	141.98	131.10	2 147 000
	260	182.8 1	144.39	65.52	120 000
	220	154.68	122.18	55.44	200 000
	180	126.56	99.97	45.36	302 000
	140	98.44	77.75	35.28	744 000
Gurney 4th specimen T-shape joint/bending, d=0.2mm	120	84.37	66.64	30.24	1 180 000
	110	77.34	61.09	27.72	2 158 000
	300	429.77	95.70	6.17	135 000
	260	372.47	82.94	5.35	237 000
	200	286.52	63.80	4.12	407 000
	190	272.19	60.61	3.91	573 000
Gurney 4th specimen T-shape joint/bending, d=0.2mm	180	257.86	57.42	3.70	665 000
	160	229.21	51.04	3.29	1 525 000
	150	214.89	47.85	3.07	1 534 000
	140	200.56	44.66	2.89	2 601 000

Table 2.21: Results of PSM approach at the weld root

As the tables show, the weld toe area is characterised by a equivalent peak stress value greater than the root region with the exception of the 2nd specimen Gurney, where the peak stress value of the root are major than the weld toe.

The all re-elaborated data are collected together and subjected to a statistical analysis: the results are reported in the Figure 2.43, where the inverse slope is set to $k = 3$, in agreement with the literature and the red line represents the design curve obtained by statistical analysis with the re-elaborated data. The graph represented in Figure 2.43 is also characterized by the presence of the PSM design curve proposed by Meneghetti and Lazzarin [5] (Black lines).

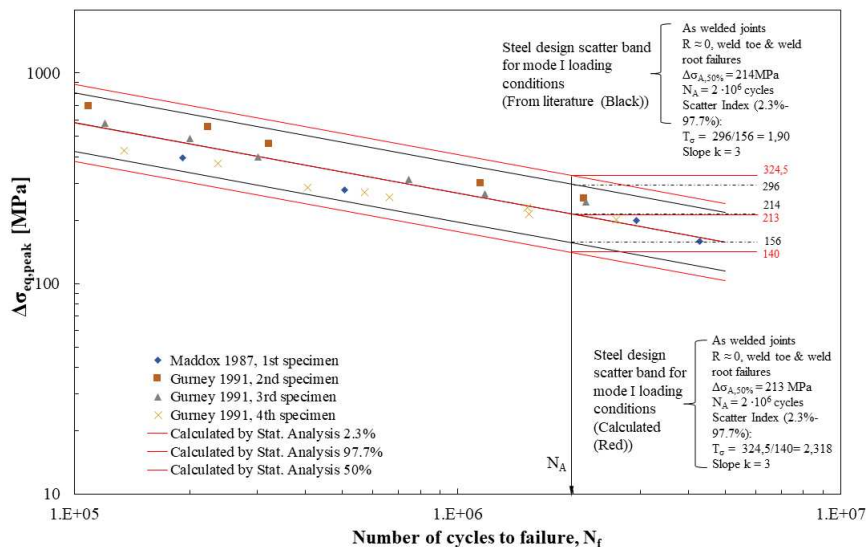


Figure 2.43: Fatigue strength in terms of equivalent peak stress, calculated at the weld toe.

The following conclusions can be defined:

1. The PSM approach has correctly defined that the crack initiation point is the weld toe, according to the experimental results for 3 joints with only one exception: the 2nd specimen, where the value of the t ;
2. The all experimental data fall above the lines that represents the 97.7% of probability of survival. Thus, the PSM design curve has demonstrated to be effective and conservative
3. The theoretical scatter band amplitude T_W is equal to 1.90 and it is lower than the re-elaborated T_W that is 2.74. This is due to that during the re-elaboration only 23 data have been employed.

2.5.3 Comparison between Analytical and PSM-estimated K_1

One of the most important advantages of the PSM approach is the possibility to detect rapidly the value of NSIFs for fatigue assessment. For this reason, a comparison between the PSM-estimated and analytical K_1 values at the weld toe and root is performed:

Specimen type and load	$K_{1,weld-toe,PSM}$ [MPa·mm ^{0.326}]	$K_{1,weld-toe,analytical}$ [MPa·mm ^{0.326}]	Rel. error [%]
Maddox 1st specimen Transverse NLC/axial	517.48	536.75	≈ 3.72%
	362.24	375.73	
	258.74	268.38	
	206.99	214.70	
Gurney 2nd specimen Transverse NLC/axial	901.22	913.63	≈ 1.38%
	720.97	730.91	
	600.81	609.09	
	390.53	395.91	
Gurney 3rd specimen Transverse NLC/bending	751.84	778.93	≈ 3.60%
	636.17	659.10	
	520.50	539.26	
	404.84	419.42	
	347.00	359.51	
Gurney 4th specimen T-shape joint/bending	318.09	329.55	≈ 3.29%
	559.66	578.07	
	485.04	500.99	
	373.11	385.38	
	354.45	366.11	
	335.80	346.84	
	298.47	308.30	
279.83	289.03		
261.18	269.76		

Table 2.22: Comparison between the PSM-estimated and the analytical K_1 at the weld toe

Specimen type and load	$K_{1,root,PSM}$ [MPa·mm ^{0.5}]	$K_{1,root,analytical}$ [MPa·mm ^{0.5}]	Rel. error [%]
Maddox 1st specimen Transverse NLC/axial	96.87	97.01	≈ 0.14%
	67.81	67.91	
	48.43	48.50	
	38.75	38.80	
Gurney 2nd specimen Transverse NLC/axial	387.22	399.03	≈ 3.05%
	309.78	319.22	
	258.15	266.02	
	167.80	172.91	
	141.98	146.31	
Gurney 3rd specimen Transverse NLC/bending	144.43	144.39	≈ 0.02%
	122.18	122.21	
	99.97	99.99	
	77.75	77.77	
	66.64	66.66	
Gurney 4th specimen T-shape joint/bending	61.09	61.10	≈ 3.58%
	95.70	99.12	
	82.94	85.91	
	63.80	66.08	
	60.61	62.78	
	57.42	59.47	
	51.04	52.87	
47.85	49.56		
44.66	46.26		

Table 2.23: Comparison between the PSM-estimated and the analytical K_1 at the weld root

As the tables show and in agreement with the theory, the totality of relative error falls below $\pm 4\%$.

2.6 Geometry description of square chord with circular brace joint: Gandhi (1998)

The fifth joint analysed is a tube-to-beam structure, studied by Gandhi in 1998 [39] under CAL (Constant Amplitude Loading). The structure is characterised by a circular hollow section tube (CHS or Brace side) welded on the top of a rectangular hollow section double cantilever beam (SHS or Chord side).

The principal information and mechanical properties about this typology of the joint are summarized in the *Table 2.24* and *Table 2.25*:

Weld condition	Fracture location	Load application
As-welded, non-load carrying (NLC), full penetration	Weld toe, SHS and CHS sides, depending on the geometry	Axial, main plate, parent material °

Table 2.24: Information about the specimens

Material model	Yield strength f_y [MPa]	Young modulus [MPa]	Poisson's ratio ν
API2H, Linear elastic, isotropic	355	206000	0.3

Table 2.25: Information about mechanical properties

The geometry of this type of joint is defined in the Figure 2.44 and there are seven different type of structure as Figure 2.45 shows.

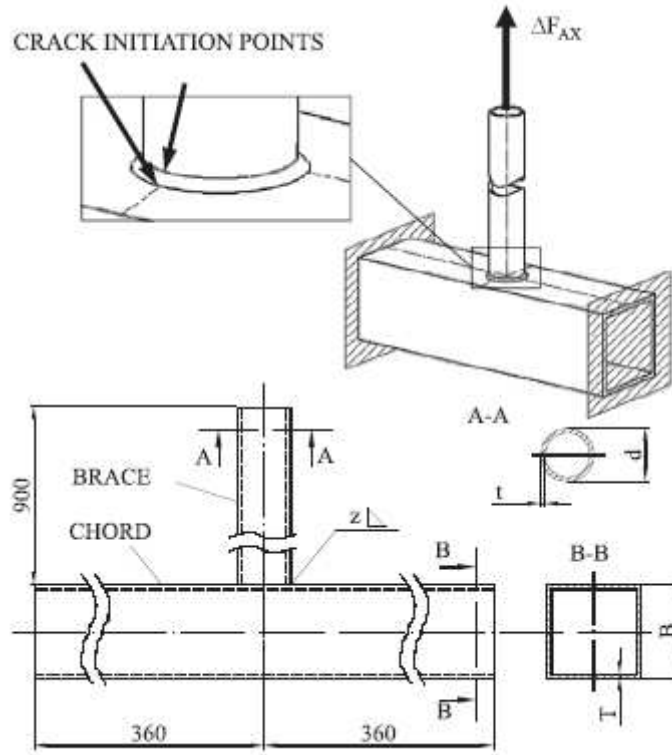


Figure 2.44: Geometry of Gandhi structure. The quotes are defined in [mm] [39].

N ^o	B (mm)	T (mm)	d (mm)	t (mm)	z (mm)
1	200	10	51	6.3	6.3
2	200	10	82.5	6.3	6.3
3	200	10	159	6.3	6.3
4	200	10	76	4.5	4.5
5	200	10	82.5	8.8	8.8
6	300	12.5	127	8	8
7	200	6.3	88.9	4	4

Figure 2.45: Seven different type of geometries for the same specimen [39].

The parameters of the weld profile for the Gandhi's geometry number 4, are defined in the following table:

ρ weld toe tip [mm]	Weld leg [mm]	Weld flack angle [°]	2 α
$\cong 0$	6.3	45	SHS: 135° CHS: 135°

Table 2.26: Information about the weld profile

The experimental data for the Gandhi N^o4 are defined in the table below in terms of nominal stress $\Delta\sigma_{nom}$:

Stress ratio R	$\Delta\sigma_{nom}$ [MPa]	N_f [cycles]
-0.36	49.58	201 000 (complete fracture)
		269 000 (through-the-thickness crack)

Table 2.27: Experimental data for Gandhi N^o4

The modeling procedure in Ansys®APDL is briefly described:

- Thanks to the double symmetry of the structure, only 1/4 of the joint is created to reduce the computational time;
- The structure is subjected to an axial load and it is applied to the CHS top sectional area as a constant pressure equal to $p = -\Delta\sigma_{nom}$;
- Symmetry boundary conditions are applied on the highlighted area in the *Figure 2.46-2.47*.

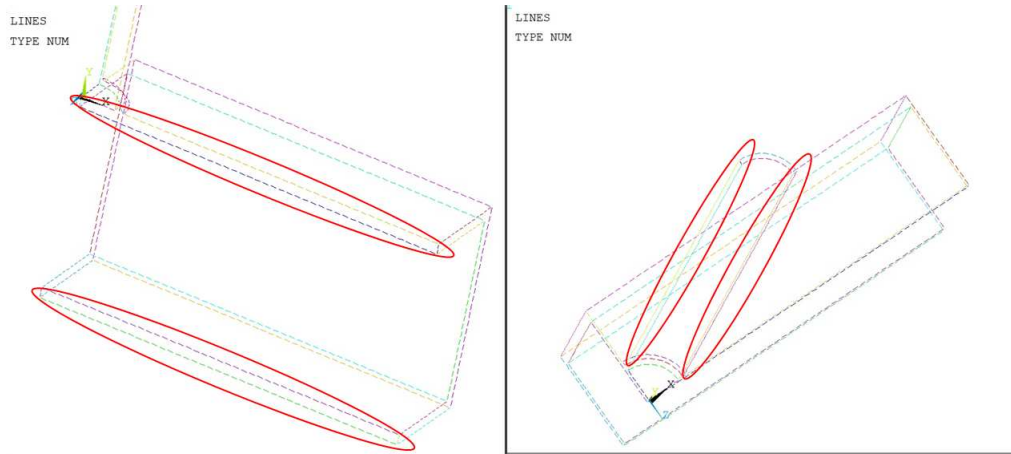


Figure 2.46: Gandhi N°4 inside Ansys®APDL where the red circle highlights the area where the symmetry condition is applied.

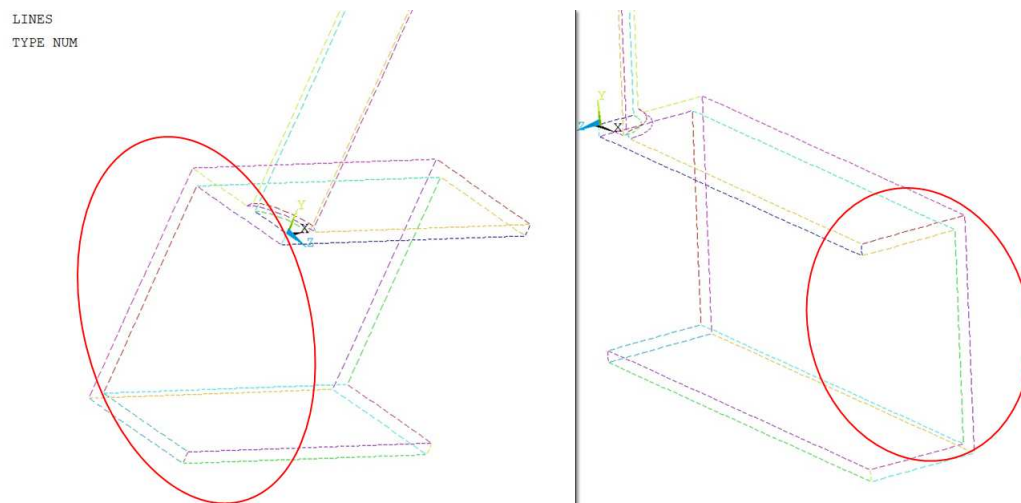


Figure 2.47: Gandhi N°4 inside Ansys®APDL where the red circle highlights the area where the symmetry condition is applied.

2.7 PSM approach with Submodeling technique

The fatigue assessment for the structure Gandhi N°4 is performed by the application of Peak Stress Method for 3D structures with the adoption of eight-node linear elements. As describe in the paragraph 1.3.3, the submodelling technique is request.

Main Model

First of all, is necessary to study the main model and the ten-node quadratic element SOLID 187 is chosen in Ansys®APDL with *Pure Displacement* Key Options 1, which means that the nodal forces are only dependent

on the displacements.

The main model is displayed on the *Figure 2.48*. The cut boundary is defined by a stress convergence analysis, indeed four different meshes, with global element size respectively equal to 8, 5, 4 and 3 mm, are laid on the main model.

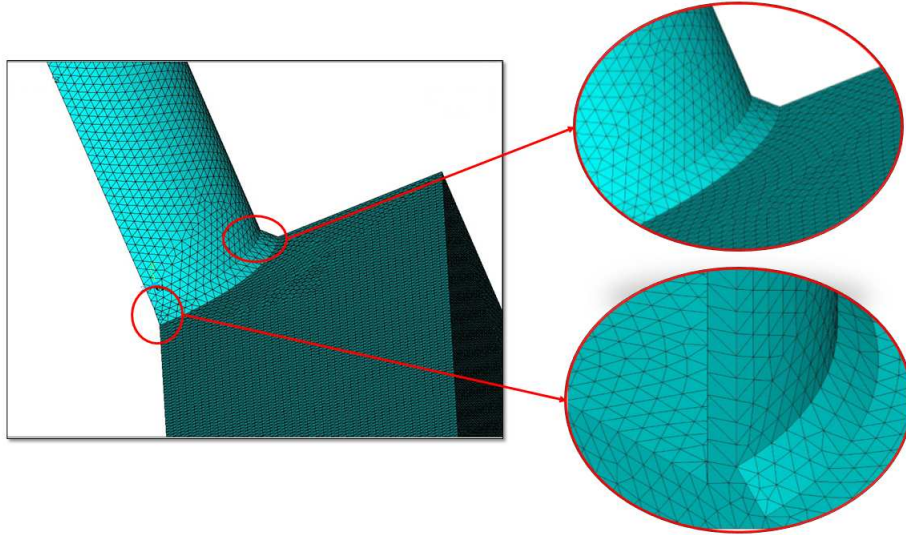


Figure 2.48: Example of mesh with global element size equal to 3mm.

The parameter to complete the convergence analysis is the first principal stress range $\Delta\sigma_{11}$, obtained along the x-axis that starts from the weld toe tip SHS side, as *Figure 2.49* shows:

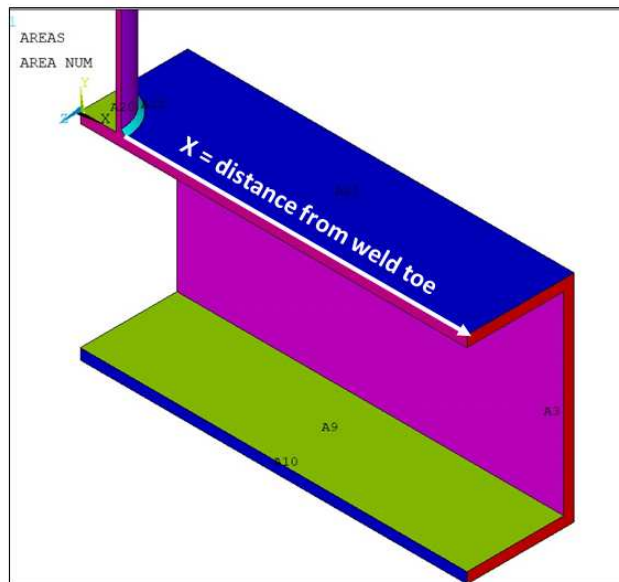


Figure 2.49: Direction of x-axis and path along which $\Delta\sigma_{11}$ is defined.

The results of the convergence stress analysis are reported in the following graph:

Cut Boundary Gandhi 4

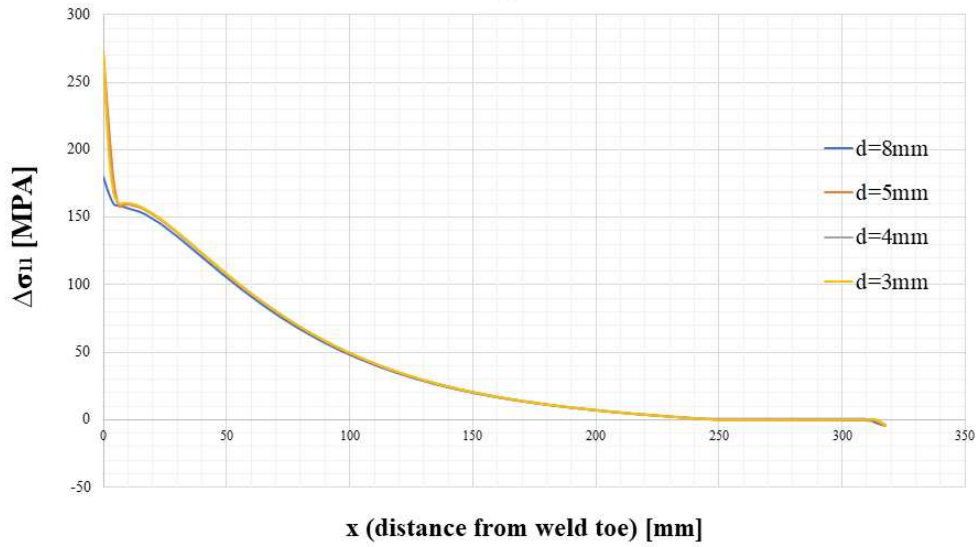


Figure 2.50: Results of convergence stress analysis.

As Figure 2.50 shows, the cut boundary is placed at $x = 50.8mm$ from the weld toe (chord side), where the compatibility between the results is achieved.

Submodel

The next step is to create and study the sub model. The eight-node linear element SOLID 185 is chosen in Ansys®APDL with *Simple Enhanced Strain* as Key Option 1.

When the Submodelling technique is employed, the reference system of the submodel must coincide with that of the mainmodel because the submodel’s boundary conditions are interpolated in the cut boundary with respect to the main model reference system.

The weld toe is prevailing subjected to mode I because it is characterised by a opening angle 2α equal to 135° . Indeed, referring to graph of the Williams eigenvalues trend in Figure 1.13, mode II is not singular for V-notch opening angle greater than 102.5° , so $\lambda_2 = 0$ and the mode III can be neglected. For this reason the equation (2.20) is used.

Under mode I, the PSM, with Brick elements SOLID 185, requirements are define in the following table:

Element type	Mesh algorithm	Mode I			
		$(a/d)_{min}$	2α	Mesh Pattern $2\alpha < 90^\circ$	Mesh Pattern $2\alpha > 90^\circ$
Solid 185 KeyOpt:Pure Displacement	Free	3	$0^\circ < 2\alpha < 135^\circ$	Four adjacent elements share the same node	Two adjacent elements share the same node

Table 2.28: Requirements for PSM with Brick elements SOLID185.

The mode I PSM calibration constant is equal to $K_{FE}^* = 1.38 \pm 3\%$. To define the global element size of the model, the size of the element is obtained with the following procedure:

1. From literature the ratio $(a/d)_{min}$ is determined. In this case the ratio for pure mode I is chosen and it is equal to 3;
2. The value of a is the reference dimension for selecting the maximal FE sizes d for PSM application and is defined as lower thickness of the structure, so in this case is equal to 4.5mm;
3. Subsequently, the minimum element size is defined as follow:

$$d_{min} = \frac{a}{3} = \frac{4.5}{3} = 1.5mm \tag{2.38}$$

4. The chosen dimension of elements is 1 mm

The λ_1 and e_1 values are depended on the opening angle 2α , that is 135° for the weld toe at CHS and SHS sides:

2α [°]	λ_1 (Mode I)	e_1 (Mode I)
135°	0.674	0.117

Table 2.29: Value of λ_1 and e_1 in function of the opening angle 2α

The corrective stress factors for mode I is calculated with the equation (2.24). The result is reported in the *Table 2.30*

2α [°]	f_{w1}
135°	1.04

Table 2.30: Value of the corrective stress factors f_{w1} in function of the opening angle 2α

To create the submodel, the one possible procedure is the revolution by 90° about the global reference system y-axis of the sectional area reported in *Figure 2.52*, which is pre-meshed with the same requirements above-mentioned with elements PLANE 182 with *Simple Enhanced Strain* as Key Options 1 and *Plane Strain* as Key Options 3. These elements after the extrusion, will be SOLID 185.

The number of extruded elements must be chosen to have cubic elements. For this reason two different submodels is created with different *Extrude Options* to obtain along the chord and the brace brick elements with cubic shape:

1. The first submodel is used for the Brace's tension analysis and the number of element division is obtained with the following formula:

$$n^{\circ} of division = \frac{\pi \cdot \phi}{4d} = \frac{\pi \cdot 76}{4 \cdot 1} = 59.69 \quad (2.39)$$

where ϕ is the diameter of the Brace (76mm) and d is the dimension of the elements (1mm in this case);

2. The second submodel is used for the Chord's tension analysis and the number of element division is obtained with the following formula:

$$n^{\circ} of division = \frac{\pi \cdot \phi}{4d} = \frac{\pi \cdot 85}{4 \cdot 1} = 66.76 \quad (2.40)$$

where ϕ is the diameter of the Chord (85mm) and d is the dimension of the elements (1mm in this case);

To obtain a correct extrusion in Ansys®APDL, the following commands are used:

Preprocessor→*Modelling*→*Operate*→*Extrude*→*Elem Ext Opts*

SOLID 185 is selected as Element type number and as the number of element extrusion depend on which submodel is created (see equation (2.39)-(2.40)). The *Figure 2.51* shows the correct options for the extrusion.

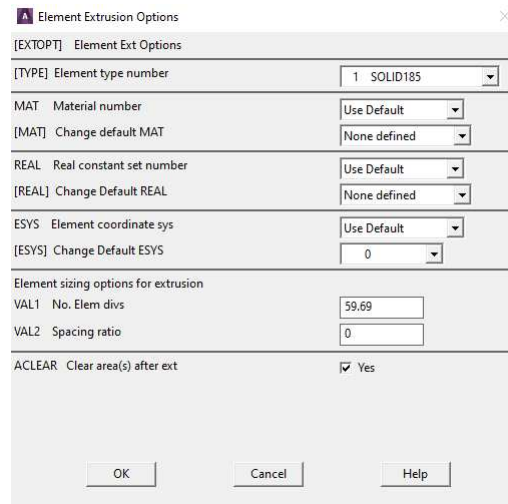


Figure 2.51: The element extrusion options.

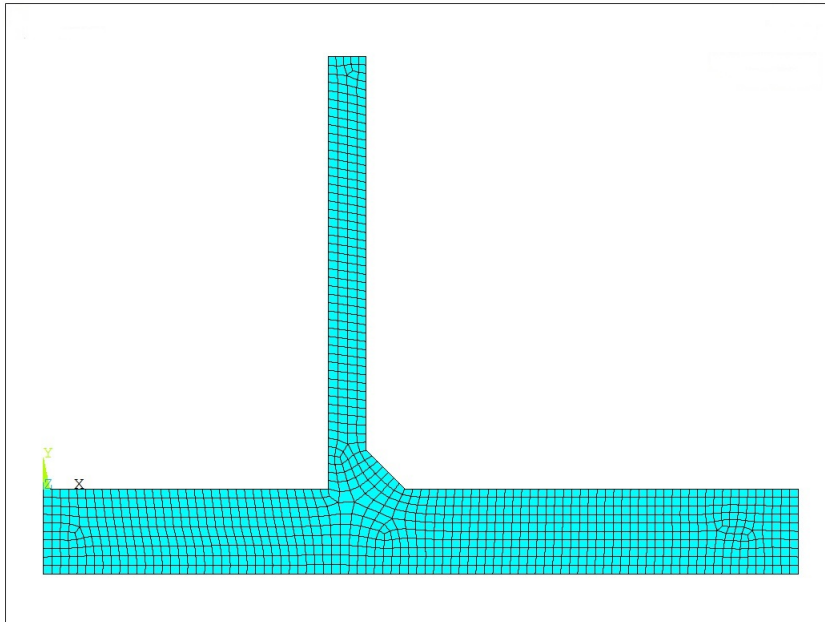


Figure 2.52: The sectional area that has to be extruded.

After that, the area can be extruded with the commands below:

Preprocessor→*Modelling*→*Operate*→*Extrude*→*Area*→*About Axis*

The result is reported in the *Figure 2.53*:

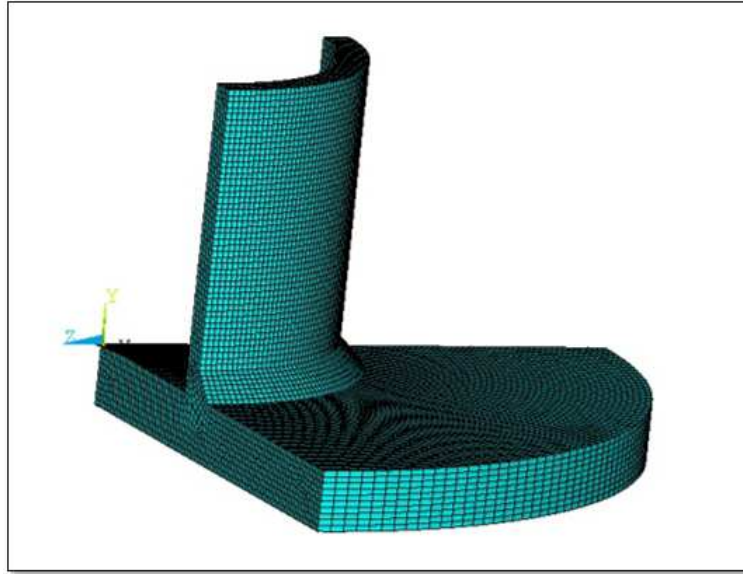


Figure 2.53: *Submodel geometry.*

The submodel is characterized by symmetry boundary conditions that are applied to the highlighted areas in the *Figure 2.54* with the following commands:

Preprocessor→*Loads*→*Define Loads* → *Apply*→*Displacements*→*Symmetry B.C.*→ *on Areas*

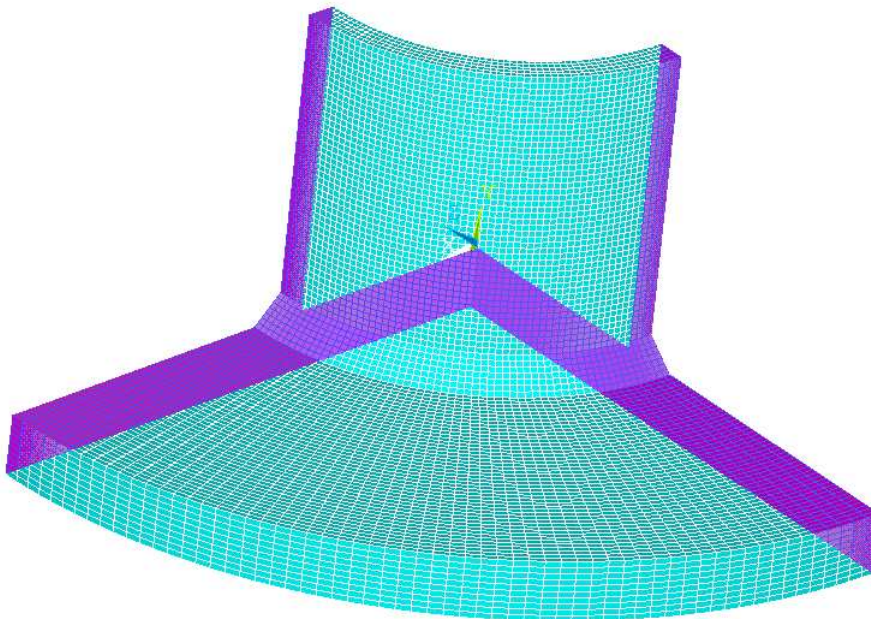


Figure 2.54: *Selected area for the symmetry boundary condition.*

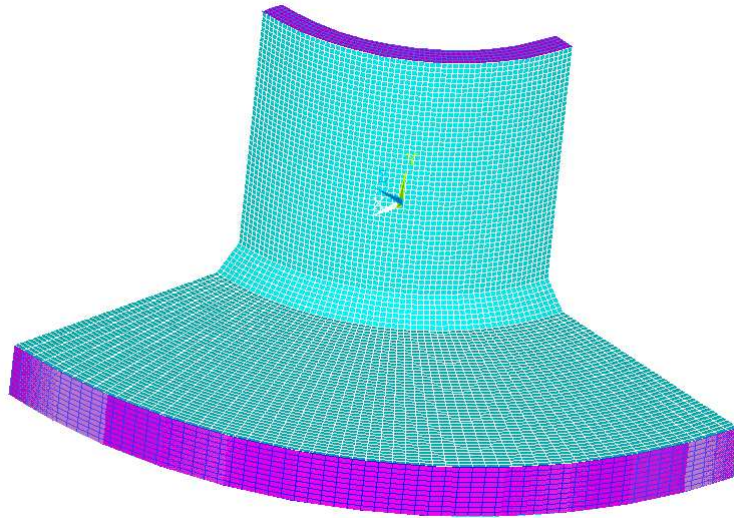


Figure 2.55: Selected area for the cut boundary condition.

To apply the nodal displacements to the nodes belonging to the cut boundary (*Figure 2.55* represents the area of it), the following procedure is applied:

1. First of all, the nodes attached to the cut boundary are selected with the following commands:

Select→*Entities*→*Areas*→*From Full*→ *Selection of the Cur boundary areas*

Select→*Entities*→*Node*→*Attached to*→*Areas All*

2. Subsequently, a file containing the coordinates of the cut boundary nodes is created:

Preprocessor→*Modelling*→*Create*→*Nodes*→*Write Node File*

where the file is saved with the extension *name-file.node*;

3. After that, the main model is opened again and solved. The displacements are interpolated in the cut boundary nodal coordinates and the file with these information is saved with *.cbdo* extension as the *Figure 2.56* shows and with the following commands:

General Postproc→*Submodelling*→*Interpolate DOF*

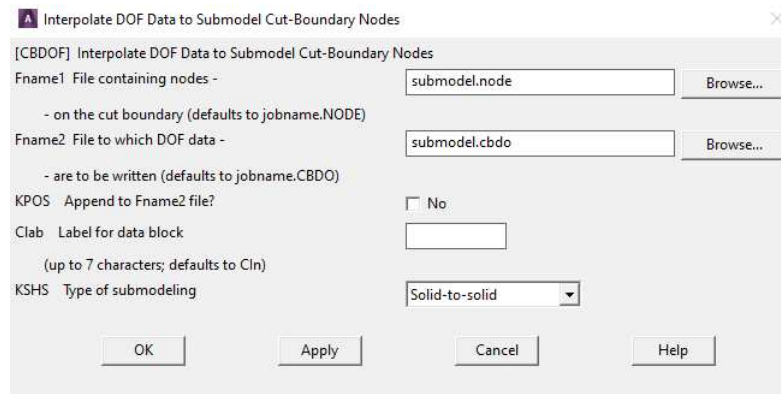


Figure 2.56: Window for configuration for Interpolate DOF.

4. The submodel is opened again and the nodal displacements are defined on the cut boundary with these commands:

File → *Read Input from* → *submodel.cbdo*

5. The system can be solved;

Solution → *Solve* → *Current LS*

2.7.1 PSM with Submodeling technique: results

Before the post-processing of the data, it is advised to disable the *PowerGraphics* option in Ansys®APDL toolbar as *Figure 2.57* shows, otherwise the output results are given by the average of only the superficial nodal stresses, without considering the inner ones.

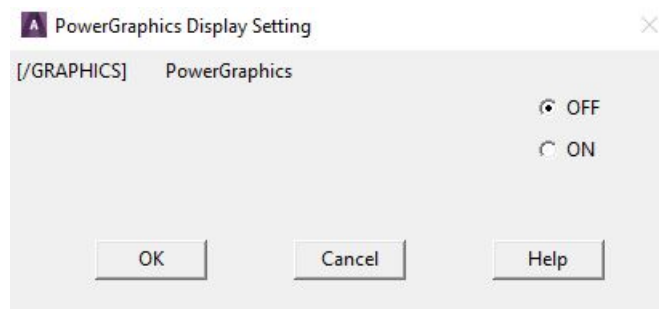


Figure 2.57: PowerGraphics disabled.

The structure is subjected to pure mode I loading, so in this situation it can be demonstrated that, in the case that the stress flow is aligned with the external pressure direction, the first principal stress range $\Delta\sigma_{11}$ can be approximated equal to local stress $\Delta\sigma_{yy}$, evaluated with a local reference system with the origin placed on the V-notch. To reduce the post-processing time, the first principal stress is replaced by $\Delta\sigma_{yy}$, and the results can be observed in the *Figure 2.58*, for an external applied pressure equal to 49.58 MPa:

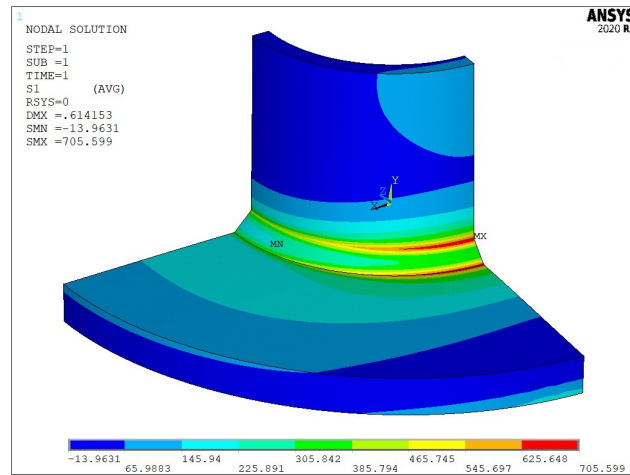


Figure 2.58: Plot of the first principal stress on the sub model.

To obtain the trend of the nodal stress at the V-notch, brace and chord side, the nodes attached to the respective lines are selected with the following commands:

Select→Entities→Lines→From full

Select→Entities→Nodes→Attached to→Lines all

The selection of the nodes belonging to the chord and brace lines must be done separately. The results are plotted in function of the angular coordinate θ , that is range from 0° to 90° and it is defined in Figure 2.59. The results are illustrated on the graph in Figure 2.60:

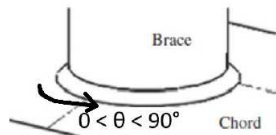


Figure 2.59: The angular coordinate θ .

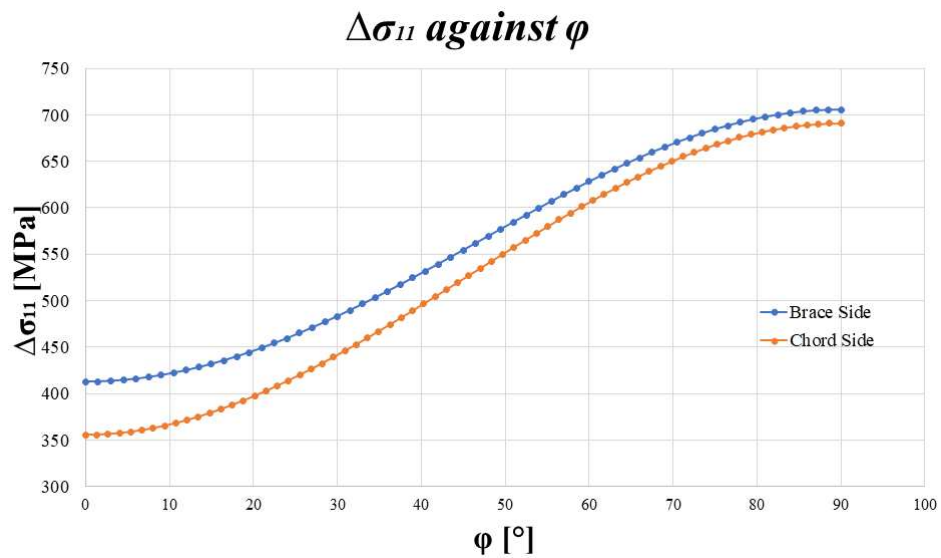


Figure 2.60: Trend of the first principal stress respect with the angular coordinate θ along the chord and brace side.

For an external applied pressure $\Delta\sigma_{nom} = 49.58MPa$, the maximum value is located at $\theta = 90^\circ$ for both sides:

$$\Delta\sigma_{11, chordside} = 690.93MPa \quad (2.41)$$

$$\Delta\sigma_{11, braceside} = 705.60MPa \quad (2.42)$$

The Notch stress intensity factor ΔK_1 and the equivalent peak stress are calculated by the formulae (2.20) and (2.23):

$$K_{1, chord-side} \cong K_{FE}^* \cdot \sigma_{\theta\theta, \theta=0, peak} \cdot d^{1-\lambda_1} = 1.38 \cdot 690.93 \cdot 1^{1-0.674} = 953.48MPamm^{0.326} \quad (2.43)$$

$$\Delta\sigma_{eq, peak, chord-side} = \sigma_{\theta\theta, \theta=0, peak} \cdot f_{w1} = 690.93 \cdot 1.06 = 732.20MPa \quad (2.44)$$

$$K_{1, brace-side} \cong K_{FE}^* \cdot \sigma_{\theta\theta, \theta=0, peak} \cdot d^{1-\lambda_1} = 1.38 \cdot 705.60 \cdot 1^{1-0.674} = 973.73MPamm^{0.326} \quad (2.45)$$

$$\Delta\sigma_{eq, peak, brace-side} = \sigma_{\theta\theta, \theta=0, peak} \cdot f_{w1} = 705.60 \cdot 1.06 = 747.74MPa \quad (2.46)$$

The PSM with Brick 185 defined that the brace is more solicited than the chord side. The experimental fracture for Gandhi N°4 is located at the weld toe, CHS, so the PSM detects the crack initiation in the correct location.

2.8 PSM approach with four-node Tetra element (Tetra 285)

The fatigue assessment for the structure Gandhi N°4 is performed by the application of Peak Stress Method for 3D structures with the adoption of four-node linear elements.

The element SOLID 285 is chosen from the Ansys®APDL library and this elements is characterised that it has not Key option in its definition.

As defined in the paragraph 2.7, the model is prevailing subjected to mode I. Under mode I, the PSM requirements, with Tetra elements SOLID 285, are define in the following table:

Element type	Mesh algorithm	Mode I		
		$(a/d)_{min}$	2α	Mesh Pattern
Solid 285 KeyOpt:none	Free	3	135°	No particular indications

Table 2.31: Requirements for PSM with Brick elements SOLID 285.

The mode I PSM calibration constant is equal to $K_{FE}^* = 1.75 \pm 22\%$. The size of the element is obtained with the following procedure:

1. From literature the ratio $(a/d)_{min}$ is determined. In this case the ratio for pure mode I is chosen and it is equal to 3;
2. The value of a is the reference dimension for selecting the maximal FE sizes d for PSM application and is defined as lower thickness of the structure, so in this case is equal to 4.5mm;
3. Subsequently, the minimum element size is defined as follow:

$$d_{min} = \frac{a}{3} = \frac{4.5}{3} = 1.5mm \quad (2.47)$$

4. The chosen dimension of elements is 1.5 mm

The λ_1 and e_1 values are depended on the opening angle 2α , that is 135° for the weld toe at CHS and SHS sides:

2α [°]	λ_1 (Mode I)	e_1 (Mode I)
135°	0.674	0.117

Table 2.32: Value of λ_1 and e_1 in function of the opening angle 2α

The corrective stress factors for mode I is calculated with the equation (2.24). The result is reported in the Table 2.33

2α [°]	f_{w1}
135°	1.51

Table 2.33: Value of the corrective stress factors f_{w1} in function of the opening angle 2α

2.8.1 PSM with Tetra 4 elements: results

Before the post-processing of the data, it is advised to disable the *PowerGraphics* option in Ansys®APDL toolbar as Figure 2.57 shows, otherwise the output results are given by the average of only the superficial nodal stresses, without considering the inner ones.

To obtain the correct value of the equivalent peak stress with the application of PSM Tetra 285, three considerations must be done:

1. The mesh is generate automatically by the *free-mesh* algorithm and it is intrinsically irregular, that is the node of the notch tip could be shared by different elements having a important different shape and size. For this reason, the peak stress could vary along the notch tip profile even in the case of a constant applied NSIF [24]. This problem can be solved by introducing an average peak stress value, which has been defined as the moving average on three adjacent vertex nodes, starting from the generic node $n=k$:

$$\bar{\sigma}_{i,j,peak,n=k} = \frac{\sigma_{i,j,peak,n=k-1} + \sigma_{i,j,peak,n=k} + \sigma_{i,j,peak,n=k+1}}{3} \Big|_{n=node} \quad (2.48)$$

2. Another important thing related to equation (2.48) is that only peak stresses calculated at vertex nodes of tetra elements have be introduced in this equation, thus the stresses at mid-side nodes must be neglected [30].
3. The V-notch profile edge nodes must be excluded from the average because they are affected by the nodal values in the adjacent areas.

In the analysis with Tetra 285 elements, the structure is subjected to pure mode I loading, so in this situation it can be demonstrated that, in the case that the stress flow is aligned with the external pressure direction, the first principal stress range $\Delta\sigma_{11}$ can be approximated equal to local stress $\Delta\sigma_{yy}$, evaluated with a local reference system with the origin placed on the V-notch. To reduce the post-processing time, the first principal stress is replaced by $\Delta\sigma_{yy}$ and the results can be observed in the Figure 2.61, for an external applied pressure equal to 49.58 MPa:

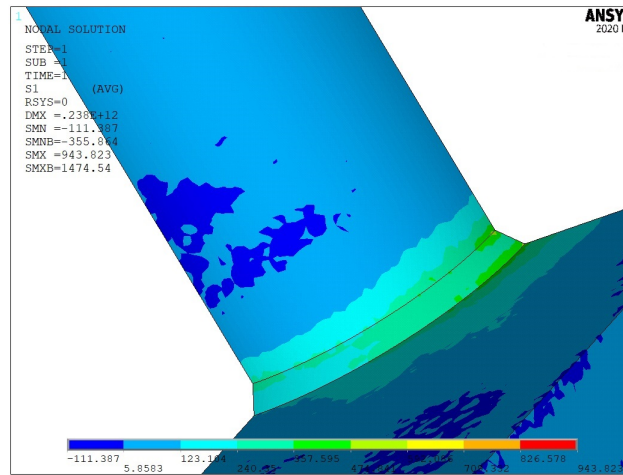


Figure 2.61: Plot of the first principal stress.

To obtain the trend of the nodal stress at the V-notch, brace and chord side, the nodes attached to the respective lines are selected with the following commands:

Select→Entities→Lines→From full

Select→Entities→Nodes→Attached to→Lines all

The selection of the nodes belonging to the chord and brace lines must be done separately. The averaged and the non-averaged nodal $\Delta\sigma_{11}$ values are plotted in the following graph, respect to the angular coordinate θ , that is range from 0° to 90° and it is defined in Figure 2.59. The results are illustrated on the graph in Figure 2.62:

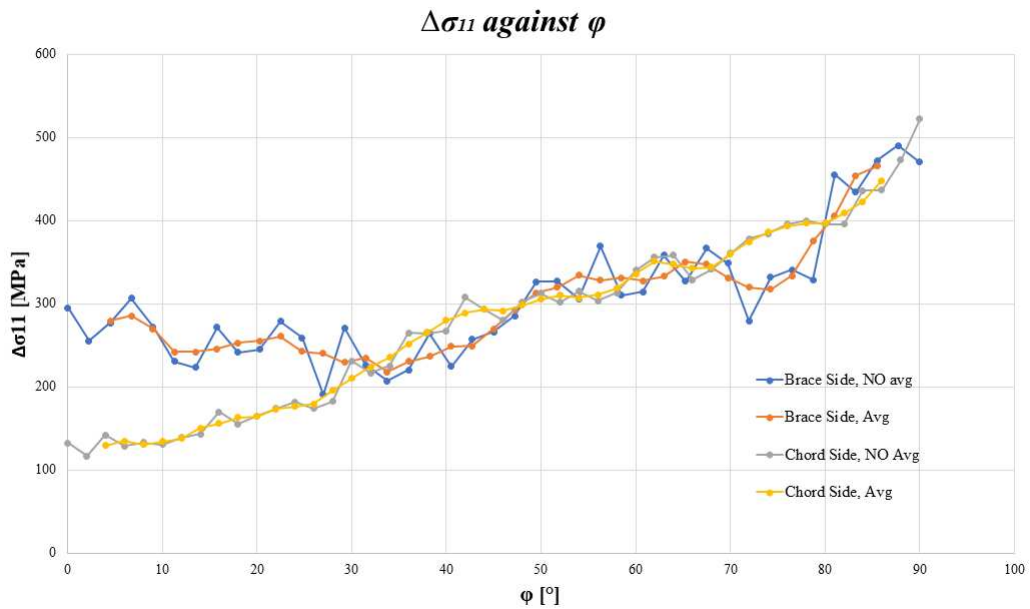


Figure 2.62: Trend of the first principal stress respect with the angular coordinate θ along the chord and brace side.

For an external applied pressure $\Delta\sigma_{nom} = 49.58MPa$, the maximum value is located at $\theta = 85^\circ$ for both sides:

$$\overline{\Delta\sigma}_{11, chordside} = 448.56MPa \quad (2.49)$$

$$\overline{\Delta\sigma}_{11, braceside} = 465.77MPa \quad (2.50)$$

The Notch stress intensity factor ΔK_1 and the equivalent peak stress are calculated by the formulae (2.20) and (2.23):

$$K_{1, \text{chord-side}} \cong K_{FE}^* \cdot \overline{\Delta \sigma_{\theta\theta, \theta=0, \text{peak}}} \cdot d^{1-\lambda_1} = 1.75 \cdot 448.56 \cdot 1^{1-0.674} = 895.91 \text{MPamm}^{0.326} \quad (2.51)$$

$$\Delta \sigma_{eq, \text{peak, chord-side}} = \overline{\Delta \sigma_{\theta\theta, \theta=0, \text{peak}}} \cdot f_{w1} = 448.56 \cdot 1.51 = 676.12 \text{MPa} \quad (2.52)$$

$$K_{1, \text{brace-side}} \cong K_{FE}^* \cdot \overline{\Delta \sigma_{\theta\theta, \theta=0, \text{peak}}} \cdot d^{1-\lambda_1} = 1.75 \cdot 465.77 \cdot 1^{1-0.674} = 930.29 \text{MPamm}^{0.326} \quad (2.53)$$

$$\Delta \sigma_{eq, \text{peak, brace-side}} = \overline{\Delta \sigma_{\theta\theta, \theta=0, \text{peak}}} \cdot f_{w1} = 465.77 \cdot 1.51 = 702.07 \text{MPa} \quad (2.54)$$

The PSM with Tetra 285 defined that the brace is more solicited than the chord side. The experimental fracture for Gandhi N°4 is located at the weld toe, CHS, so the PSM detects the crack initiation in the correct location.

2.9 PSM approach with ten-node Tetra element (Tetra 187)

The fatigue assessment for the structure Gandhi N°4 is performed by the application of Peak Stress Method for 3D structures with the adoption of ten-node quadratic elements.

The element SOLID 187 is chosen from the Ansys®APDL library with *Pure Displacement* as Key Option 1, which means that the nodal forces are only dependent on the displacements.

As defined in the paragraph 2.7, the model is prevailing subjected to mode I. Under mode I, the PSM requirements, with Tetra elements SOLID 187, are define in the following table:

Element type	Mesh algorithm	Mode I		
		$(a/d)_{min}$	2α	Mesh Pattern
Solid 187 KeyOpt:Pure Displacement	Free	1	135°	No particular indications

Table 2.34: Requirements for PSM with Brick elements SOLID 187.

The mode I PSM calibration constant is equal to $K_{FE}^* = 1.21 \pm 10\%$. The size of the element is obtained with the following procedure:

1. From literature the ratio $(a/d)_{min}$ is determined. In this case the ratio for pure mode I is chosen and it is equal to 1;
2. The value of a is the reference dimension for selecting the maximal FE sizes d for PSM application and is defined as lower thickness of the structure, so in this case is equal to 4.5mm;
3. Subsequently, the minimum element size is defined as follow:

$$d_{min} = \frac{a}{1} = \frac{4.5}{1} = 4.5 \text{mm} \quad (2.55)$$

4. The chosen dimension of elements is 3 mm

The λ_1 and e_1 values are depended on the opening angle 2α , that is 135° for the weld toe at CHS and SHS sides:

2α [°]	λ_1 (Mode I)	e_1 (Mode I)
135°	0.674	0.117

Table 2.35: Value of λ_1 and e_1 in function of the opening angle 2α

The corrective stress factors for mode I is calculated with the equation (2.24). The result is reported in the Table 2.36

2α [°]	f_{w1}
135°	1.31

Table 2.36: Value of the corrective stress factors f_{w1} in function of the opening angle 2α

2.9.1 PSM with Tetra 10 elements: results

Before the post-processing of the data, it is advised to disable the *PowerGraphics* option in Ansys®APDL toolbar as *Figure 2.57* shows, otherwise the output results are given by the average of only the superficial nodal stresses, without considering the inner ones.

To obtain the correct value of the equivalent peak stress with the application of PSM Tetra 187, the same consideration of PSM Tetra 285 must be done.

In the analysis with Tetra 187 elements, a series of local systems are created on each nodes along the brace and chord side. To create these local systems, the following procedure has to be adopted:

1. The WorkPlane is displayed and the nodes along the chord side are selected with the following commands:

Select→*Entities*→*Lies*→*From full*→*click on the chord line*

Select→*Entities*→*Nodes*→*Attached to*→*Lines all*

To eliminate the intermediate nodes, the following APDL command is applied:

NSLE,R,CORNER

this command select only the corner nodes;

2. Subsequently, the WorkPlane is placed through a offset at one node of chord side with the following commands:

Utility Menu→*Offset WorkPlane to*→*Node*

3. The WorkPlane is subjected to two rotation to obtain the correct orientation of the local system:

- (a) The first rotation is characterised by an angle ϕ equal to 3.91° clockwise about the x-axis that is obtained with the following equation:

$$\phi_{chord-side} = \frac{90}{n^{\circ}nodes - 1} = \frac{90}{24 - 1} = 3.91^\circ \quad (2.56)$$

With this rotation, the z-axis is tangent to the profile of the chord side.

- (b) The second rotation is characterised by an angle equal to 112.5° clockwise about the z-axis. With this rotation, the x-axis is aligned with the V-notch bisector and represents r in the equation (2.1) and σ_{yy} replaces $\sigma_{\theta\theta, \theta=0}$. The commands to rotate the WorkPlane are:

Utility Menu→*Offset WP by Increments* →*Degrees*

4. Subsequently, the local reference coordinate system is created in the WorkPlane origin with the following commands:

Utility Menu→*Local Coordinate System*→*Created Local CS*→*At WP origin*

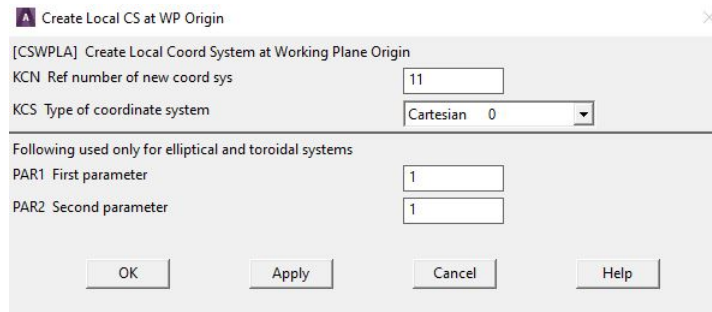


Figure 2.63: Creation of a local coordinate system at WP origin. As KCN option, a number greater than 10 must be chosen; so 11 is defined.

5. To plot the results in the new coordinate system, the following commands are executed:

General Postproc → Option for Outp

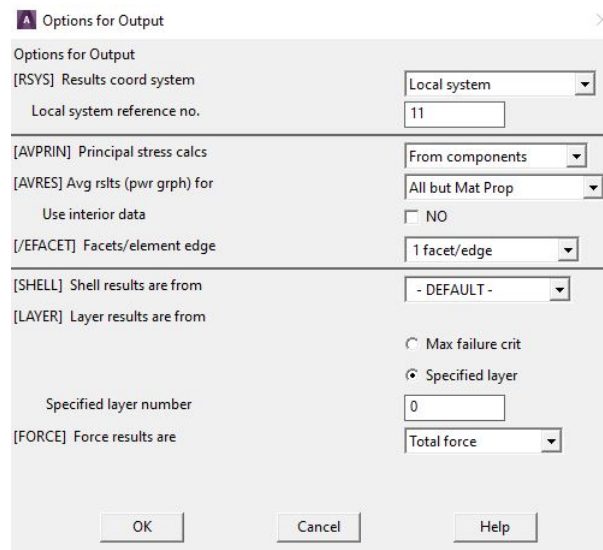


Figure 2.64: Option for Output window.

6. Before the creation of the another local reference system on the next node, is needed that the WorkPlane is aligned to the global reference system to avoid mistakes. The commands to execute this operation are:

Utility Menu → Align WP with → Global Cartesian

The same procedure is executed for the brace side but with the first rotation angle defined as follows:

$$\phi_{\text{Brace-side}} = \frac{90}{n^{\circ} \text{nodes} - 1} = \frac{90}{21 - 1} = 4.50^{\circ} \quad (2.57)$$

The local reference system created are displayed on the *Figure 2.65-2.66*:

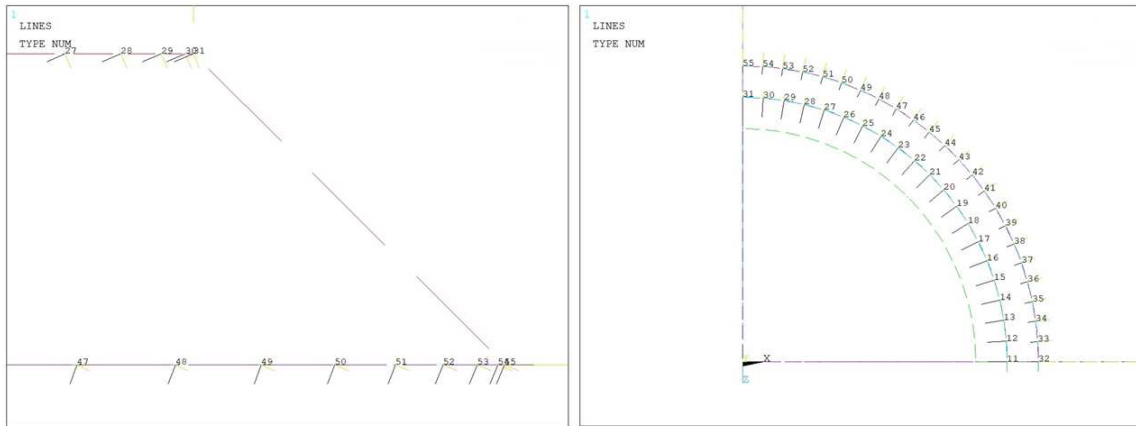


Figure 2.65: Local reference system along the chord and brace side.

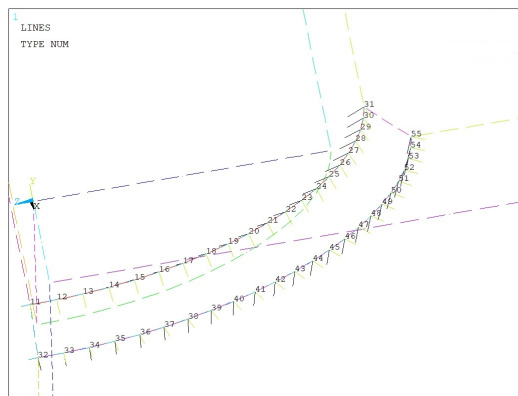


Figure 2.66: Local reference system along the chord and brace side.

During the analysis of the results, the first principal stress is evaluated and compared with $\Delta\sigma_{yy}$. The results of the first principal stress can be observed in the Figure 2.67, for an external applied pressure equal to 49.58 MPa:

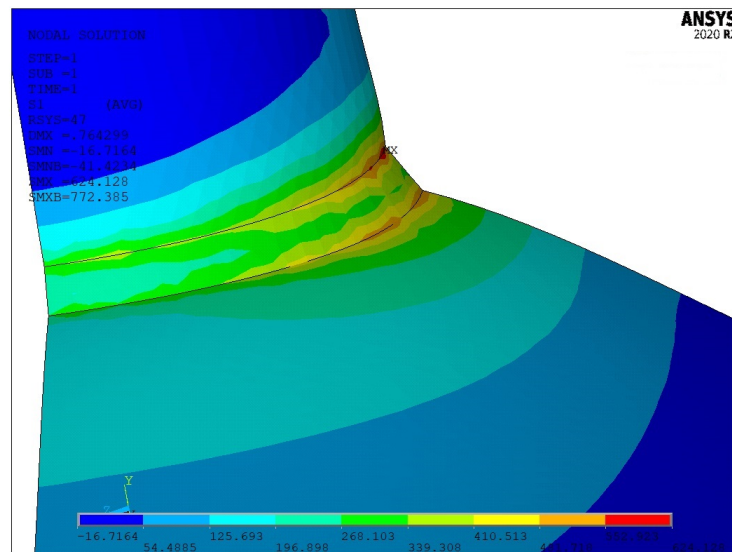


Figure 2.67: Plot of the first principal stress.

The results of the nodal tension $\Delta\sigma_{yy}$ and $\Delta\sigma_{11}$ along the chord and the brace and the relative comparison, are reported in the Appendix A.

The averaged and the non-averaged nodal $\Delta\sigma_{yy}$ values are plotted in the following graph, respect to the angular coordinate θ :

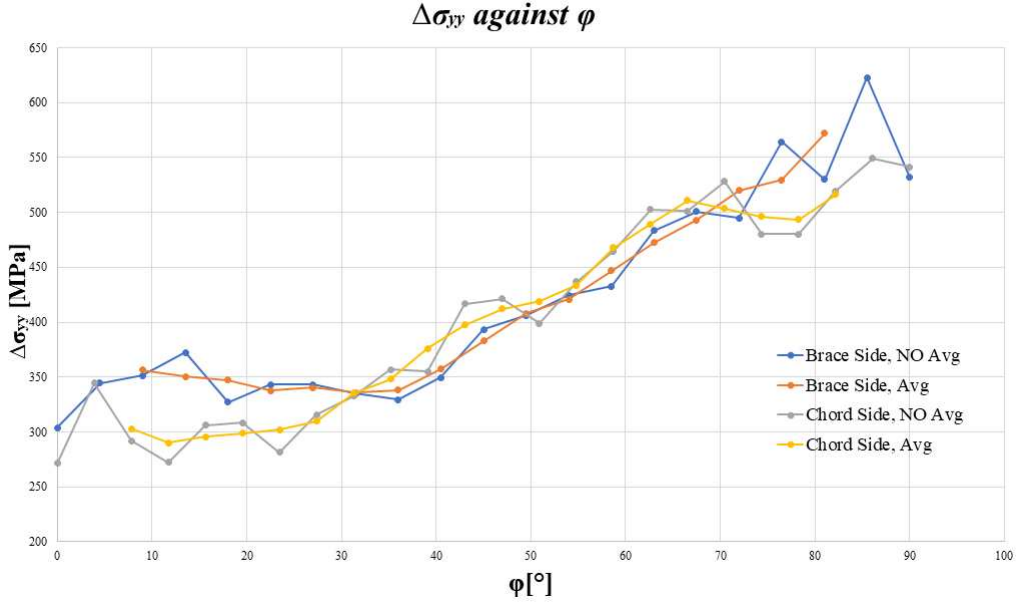


Figure 2.68: $\Delta\sigma_{yy}$ stress averaged and non-averaged, in function of angular coordinate θ along chord and brace side.

For an external applied pressure $\Delta\sigma_{nom} = 49.58MPa$, the maximum value is located at $\theta = 81^\circ$ for both sides:

$$\Delta\sigma_{yy,chordside} = 516.28MPa \quad (2.58)$$

$$\Delta\sigma_{11,chordside} = 519.76MPa \quad (2.59)$$

$$\Delta\sigma_{yy,braceside} = 572.29MPa \quad (2.60)$$

$$\Delta\sigma_{11,braceside} = 574.93MPa \quad (2.61)$$

The Notch stress intensity factor ΔK_1 and the equivalent peak stress are calculated by the formulae (2.20) and (2.23):

$$K_{1,chord-side} \cong K_{FE}^* \cdot \overline{\Delta\sigma_{\theta\theta,\theta=0,peak}} \cdot d^{1-\lambda_1} = 1.21 \cdot 516.28 \cdot 1^{1-0.674} = 893.75MPamm^{0.326} \quad (2.62)$$

$$\Delta\sigma_{eq,peak,chord-side} = \overline{\Delta\sigma_{\theta\theta,\theta=0,peak}} \cdot f_{w1} = 516.28 \cdot 1.31 = 674.49MPa \quad (2.63)$$

$$K_{1,brace-side} \cong K_{FE}^* \cdot \overline{\Delta\sigma_{\theta\theta,\theta=0,peak}} \cdot d^{1-\lambda_1} = 1.21 \cdot 572.29 \cdot 1^{1-0.674} = 990.69MPamm^{0.326} \quad (2.64)$$

$$\Delta\sigma_{eq,peak,brace-side} = \overline{\Delta\sigma_{\theta\theta,\theta=0,peak}} \cdot f_{w1} = 572.29 \cdot 1.31 = 747.65MPa \quad (2.65)$$

The PSM with Tetra187 defined that the brace is more solicited than the chord side. The experimental fracture for Gandhi N^o4 is located at the weld toe, CHS, so the PSM detects the crack initiation in the correct location.

2.10 Comparison of the results and data entry in the PSM curve

The relative errors between the $\Delta\sigma_{eq,peak}$ detected with the PSM brick 185, PSM Tetra 285 and PSM Tetra 187, are reported in the following table:

<i>Brace side</i>		
Type of Analysis	$\Delta\sigma_{eq,peak}$ [MPa]	ΔK_1 [MPamm ^{0.326}]
<i>Brick 185</i>	734.85	973.73
<i>Tetra 285</i>	702.07	930.29
<i>Tetra 187</i>	747.65	990.69
Rel. error %:185-285		4.67%
Rel. error %:285-187		6.49%
Rel. error %:185-187		1.74%

Table 2.37: Comparison of the results.

In the following graphs, a comparison between the trends of the nodal stress along the brace and chord side obtained by the three method is done and the results are represented in the figures below:

Brace Side- Comparison between different element

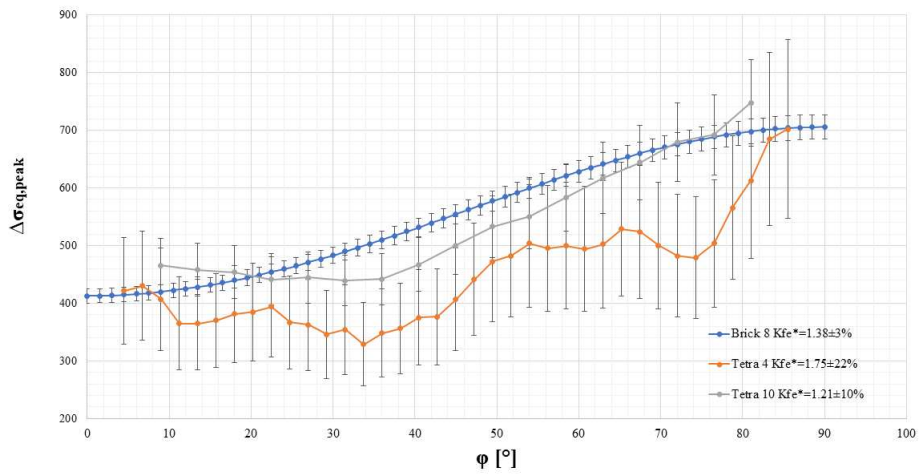


Figure 2.69: Comparison of the nodal stress trend between the three different approach.

Chord Side- Comparison between different element

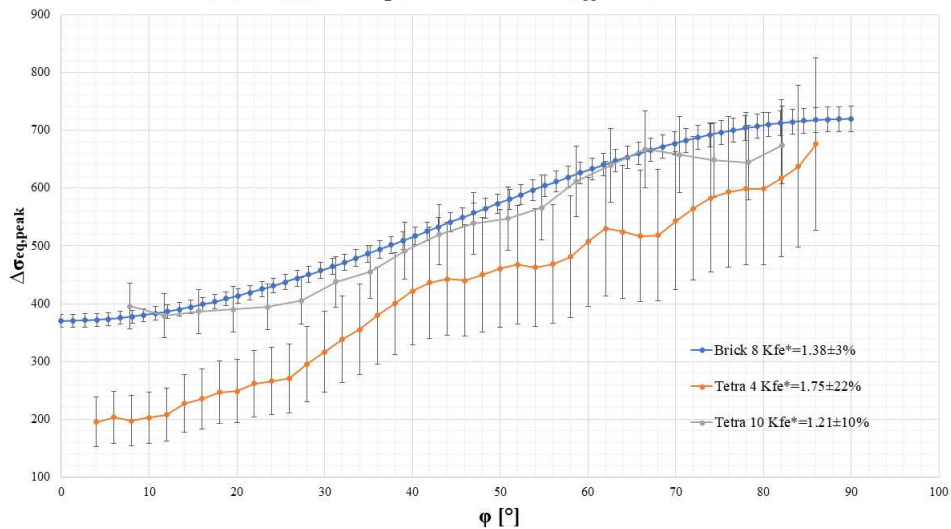


Figure 2.70: Comparison of the nodal stress trend between the three different approach.

The single available experimental data is inserted inside the PSM design curve proposed by Meneghetti,

Guzzella and Atzori in the 2014 [10] for structures prevailing subjected to mode I. The geometry Gandhi N°4 is characterized by:

- $N_2 = 32000$ cycles is the number of cycles to first visible cracking by visual examination;
- $N_3 = 201000$ cycles is the number of cycles to through thickness cracking;
- $N_4 = 269000$ cycles is the number of cycles to complete failure of the specimen;

The following graph represents the life of the specimens subjected to a constant load and evaluated for different number of cycles.

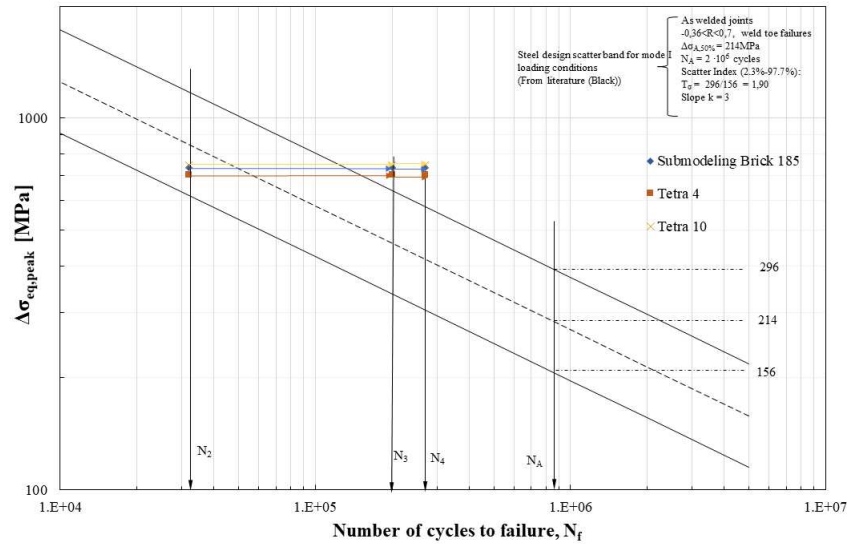


Figure 2.71: Data inside the PSM design curve.

The following conclusions can be defined:

1. The PSM approach has correctly defined that the crack initiation point is the weld toe, according to the experimental results;
2. The all experimental data fall above the lines that represents the 97.7% of probability of survival. Thus, the PSM design curve has demonstrated to be effective and conservative

Chapter 3

Numerical analysis of experimental data and fatigue assessment of As-welded joint by local approaches

The objective of this chapter is to perform a fatigue assessment on various as-welded joint in terms of nominal stress, averaged Strain Energy Density SED, Equivalent Peak Stress and Structural Hot-Spot stress. The re-elaborated data are collected together and entered inside their respective design curve, available in the literature. Subsequently, a fatigue life N_f comparison with the experimental data, is elaborated to identify the grade of conservatives defined by each method.

The analysed joint are:

1. One longitudinal stiffeners FAT 71 analysed by Marquis and Yildirim in 2010 [41];
2. Other two longitudinal stiffeners but characterized by FAT 63 class and analysed by Yildirim in 2013 [42] and subsequently by Vanrostenberghe in 2015;
3. Four transverse attachments FAT 80, analysed by Yildirim in 2020, Okawa in 2013 [43], Kuhlmann in 2006 and by Kuhlmann and Gunther in 2009 [44].

The assessment are performed with the application of local approaches above-mentioned through the use of the finite element software Ansys®Mechanical APDL with the license of the University of Padua. For the modelling and study of 2D geometries, the four-node linear element PLANE 182 is adopted with *Simple Enhanced Strain* as Key Options 1 and *Plane Strain* as Key Options 3; on the other hand, in the case of 3D structure, the eight-node linear element SOLID 185 (also called Brick 185) is used with *Simple Enhanced Strain* as Key Options 1 and also the ten-node quadratic element SOLID 187 (also called Tetra 187) is adopted with *Pure displacement* as Key Options 1.

The all specimens have been modelled inside *SOLIDWORKS 2020* and after they have been imported inside Ansys®APDL with *.IGS* extension. All the following joints are studied in as-welded conditions. According to the non-conventional LEFM extension to welded joints, the weld toe profile is considered as a V-notch with tip radius equal to zero (worst case) and the root is assumed as pre-crack in the structure.

3.1 Marquis 2010, longitudinal attachment FAT 71

The first joint analysed is a longitudinal stiffener characterised by a fatigue class FAT 71, studied by Marquis and Yildirim in 2010 [41] under CAL (Constant Amplitude Loading).

The principal information and mechanical properties about this typology of the joint are summarized in the *Table 3.1* and *Table 3.2*:

Weld condition	Fracture location	Load application	Main plate/gusset thickness
As-welded, non-load carrying (NLC), full penetration	Weld toe	Axial, main plate, parent material	Main plate: 8mm Gusset: 8mm

Table 3.1: Information about the specimens

Material model	Yield strength f_y [MPa]	Young modulus [MPa]	Poisson's ratio ν
S700, HSS, Linear elastic, isotropic	700	206000	0.3

Table 3.2: Information about mechanical properties

The dimensions of this joint are defined in the following table and figure:

t [mm]	b [mm]	w [mm]	L [mm]	h [mm]	2α [°]	z [mm]
8	150	100	350	40	150	10.40

Table 3.3: Dimension of the longitudinal attachment FAT 71

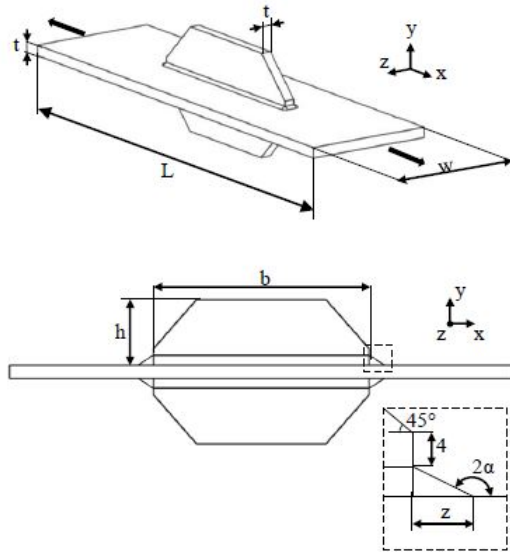
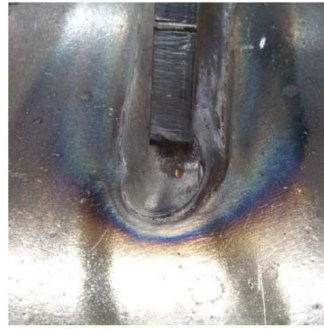


Figure 3.1: Marquis 2010, longitudinal attachment FAT 71 [33].

The parameters of the weld profile is described in the following table and figure:

ρ weld toe tip [mm]	Weld leg [mm]	Weld flack angle [°]	2α
0.4-1.32	5.20	30	Weld toe: 150° Gusset: 120°

Table 3.4: Information about the weld profile



$\rho = 0.40 - 1.32$ mm
Alnes [13]
 $K_t = 3.85 - 2.69$
Pedersen et al. [16]

Figure 3.2: As-welded profile, local geometry [45].

The radius ρ of the weld toe is lower than 1.5mm, so the assumption of a sharp V-notch ($\rho = 0$ mm) at the weld toe is acceptable with the non conventional LEFM extension to welded joints. As described in the IIW recommendations [1], the effect of misalignment can be neglected in continuous welds longitudinally loaded. The first analysed joint is characterised by an angular distortion lower than 1° , so the misalignment is neglected.

The experimental data are defined in the following table in terms of nominal stress $\Delta\sigma_{nom}$:

Stress Ratio R	$\Delta\sigma_{nom}$ [MPa]	N_f [cycles]
-1	159.7	229 600
	158.9	265 500
	158.5	679 800
	149.5	402 100
	136.7	2 808 000
	116.8	564 900
	104.5	844 100
	100.5	6 403 000

Table 3.5: Experimental data of the 1st joint, Marquis 2010. The number barred represents the run-outs

FAT 71 is modelled in *SOLIDWORKS 2020* and subsequently, is imported inside Ansys®APDL with *.IGS* extension. The results is reported in the figure below:

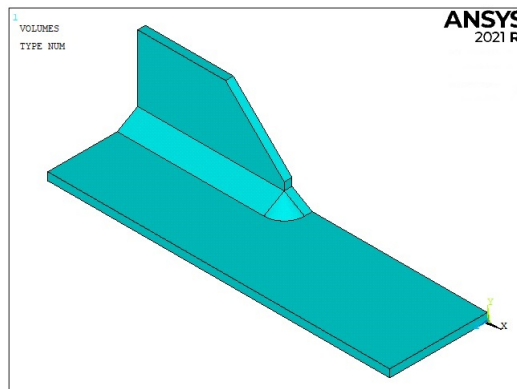


Figure 3.3: Model of longitudinal attachment FAT 71 .

The modelling procedure in Ansys®APDL is briefly described:

- Thanks to the triple symmetry of the longitudinal stiffener, only 1/8 of the geometry is modelled to reduce the computational time;
- The first joint is subjected to an axial load and it is applied on the main plait as a constant pressure equal to $p = \Delta\sigma_{nom}$, on the Area A30 as *Figure 3.4* shows;
- Symmetry boundary conditions are applied on A20, A21 and A23(*Figure 3.5*).

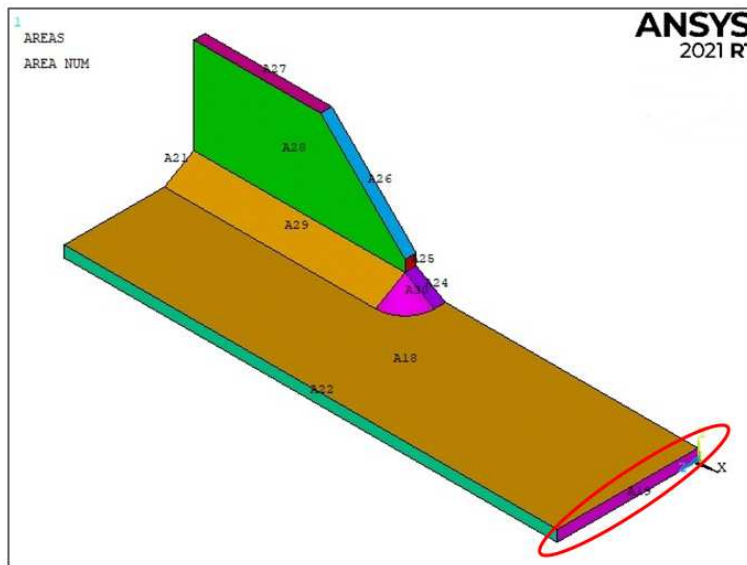


Figure 3.4: Model of longitudinal attachment FAT 71 .

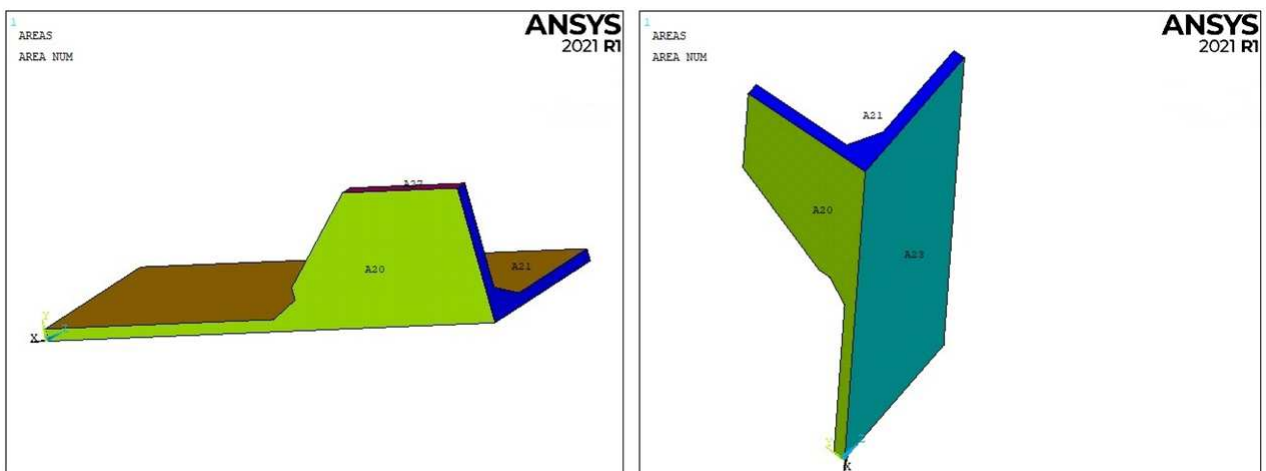


Figure 3.5: Model of longitudinal attachment FAT 71 .

In the following figure, there are the all boundary conditions applied:

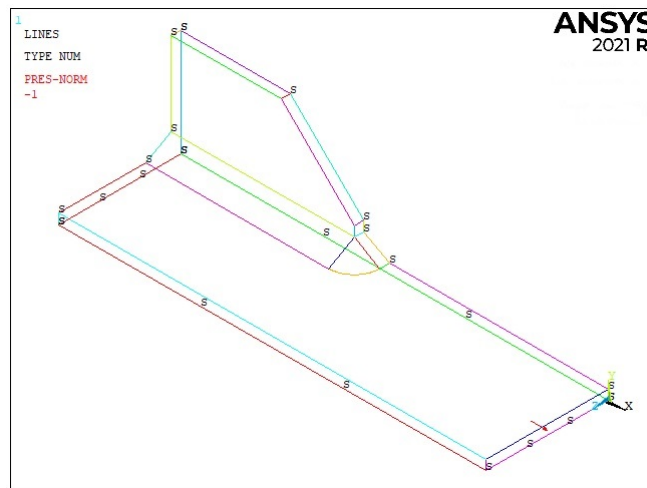


Figure 3.6: Boundary conditions of the model. *S* indicate the symmetry boundary condition, while the red arrow represents the external pressure.

3.1.1 PSM approach with Submodeling technique

The fatigue assessment for the first joint (Marquis 2010) is initially performed by the application of Peak Stress Method for 3D structures with the adoption of eight-node linear elements. As describe in the paragraph 1.3.3, the submodelling technique is request.

The structure is prevailing subjected to mode I at the attachment edge with a opening angle 2α equal to 150° . Indeed, referring to the graph of the Williams eigenvalues trend in *Figure 1.13*, mode II is not singular for V-notch opening angle greater than 102.5° , so $\lambda_2 = 0$. The mode III becomes singular in the junction part of the longitudinal stiffener, but its contribute is practically null, so it can be neglected.

Another important observation is that the V-notch opening angle 2α is equal to 150° and the PSM with the submodeling technique is not calibrated for V-notch opening angle higher than 135° . For this reason, the available calibration constants for $2\alpha = 135^\circ$ is extended for this case.

Main Model

First of all, is necessary to study the main model and the ten-node quadratic element SOLID 187 is chosen in Ansys®APDL with *Pure Displacement* Key Options 1, which means that the nodal forces are only dependent on the displacements.

The main model is displayed on the *Figure 3.7*. The cut boundary is defined by a stress convergence analysis, indeed four different meshes, with global element size respectively equal to 5, 4, 3, 2 and 1 mm, are laid on the main model.

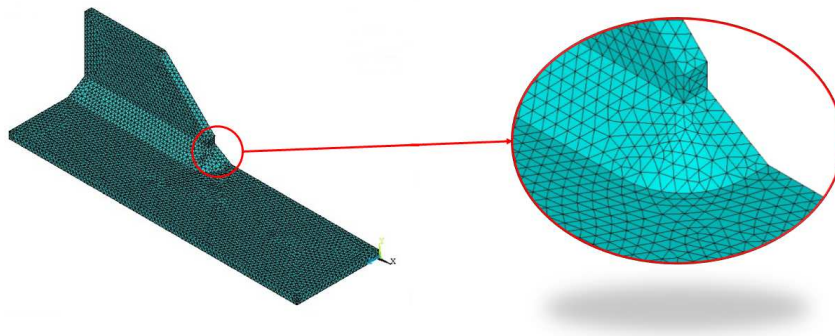


Figure 3.7: Example of main model with global element size equal to 2 mm.

The parameter to complete the convergence analysis is the first principal stress range $\Delta\sigma_{11}$, obtained along the x-axis that starts from the weld toe along the longitudinal direction, as Figure 3.8 shows:

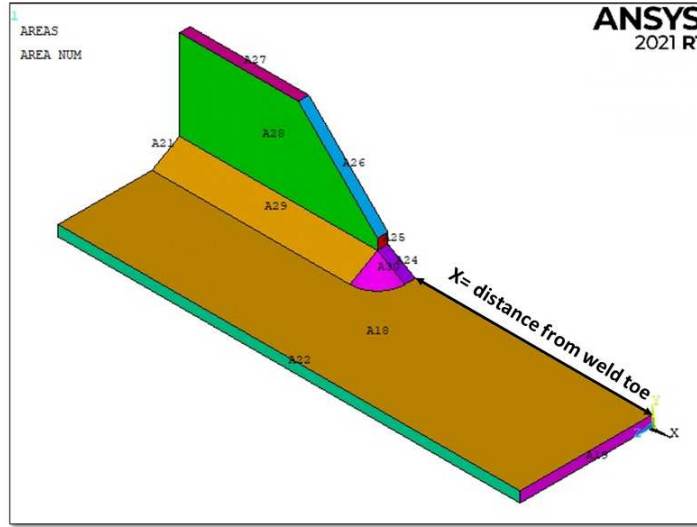


Figure 3.8: Direction of x-axis and path along which $\Delta\sigma_{11}$ is defined.

The results of the convergence stress analysis are reported in the following graph:

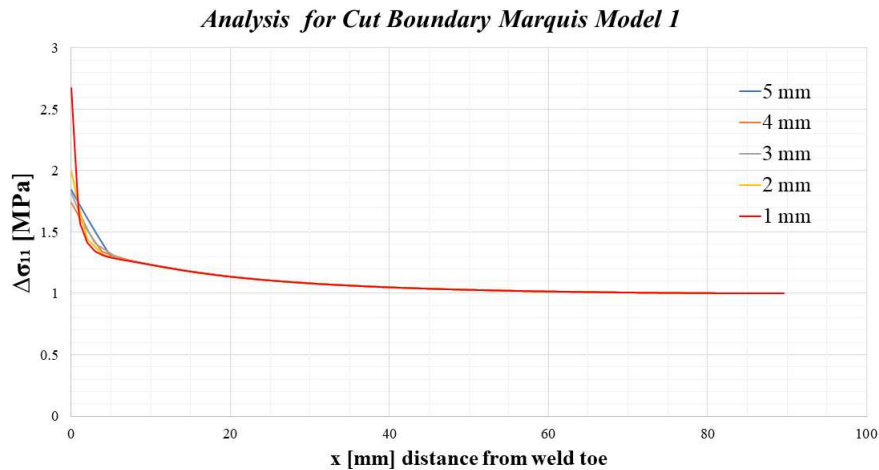


Figure 3.9: Results of convergence stress analysis.

As Figure 3.9 shows, the cut boundary is placed at $x = 15.0\text{mm}$ from the weld toe, where the compatibility between the results is achieved.

Submodel

The next step is to create and study the submodel. The eight-node linear element SOLID 185 is chosen in Ansys®APDL with *Simple Enhanced Strain* as Key Option 1.

As described in the paragraph 2.7, the reference system of the submodel must coincide with that of the main model because the submodel's boundary conditions are interpolated in the cut boundary with respect to the main model reference system.

Due to the same consideration of the main model, the weld toe is prevailing subjected to mode I because the opening angle 2α is equal to 150° , so mode II is null and mode III can be neglected due to its little contribute. Under mode I, the PSM, with Brick elements SOLID 185, requirements are define in the following table:

<i>Location: weld toe $2\alpha = 150^\circ$</i>				<i>Mode I</i>	
Element type	Mesh algorithm	$(a/d)_{min}$	2α	Mesh Pattern $2\alpha < 90^\circ$	Mesh Pattern $2\alpha > 90^\circ$
Solid 185 KeyOpt:Simple Enhanced Strain	Free	3	135° extended to 150°	Four adjacent elements share the same node	Two adjacent elements share the same node
<i>Location: gusset $2\alpha = 120^\circ$</i>				<i>Mode I</i>	
Element type	Mesh algorithm	$(a/d)_{min}$	2α	Mesh Pattern $2\alpha < 90^\circ$	Mesh Pattern $2\alpha > 90^\circ$
Solid 185 KeyOpt:Simple Enhanced Strain	Free	3	$0^\circ <$ $2\alpha < 135^\circ$	Four adjacent elements share the same node	Two adjacent elements share the same node

Table 3.6: Requirements for PSM with Brick elements SOLID 185.

The mode I PSM calibration constant is extended at the weld toe where $2\alpha = 150^\circ$ and it is equal to $K_{FE}^* = 1.38 \pm 3\%$; at the gusset, where $2\alpha = 120^\circ$, the PSM calibration constant for mode I is again equal to $K_{FE}^* = 1.38 \pm 3\%$.

The size of the element is obtained with the following procedure:

1. From literature the ratio $(a/d)_{min}$ is determined according to the *Table 3.6*. In this case the ratio for pure mode I is chosen and it is equal to 3;
2. The value of a is the reference dimension for selecting the maximal FE sizes d for PSM application and is defined as the half of the thickness t , so in this case is equal to 4 mm;
3. Subsequently, the minimum element size is defined as follow:

$$d_{min} = \frac{a}{3} = \frac{4}{3} = 1.33mm \quad (3.1)$$

4. The chosen dimension of elements is 1 mm

The λ_1 and e_1 values are depended on the opening angle 2α , that is 150° for the weld toe and 120° for the gusset:

2α [°]	λ_1 (Mode I)	e_1 (Mode I)
120°	0.616	0.130
150°	0.752	0.103

Table 3.7: Value of λ_1 and e_1 in function of the opening angle 2α

The corrective stress factors for mode I is calculated with the equation (2.24). The result is reported in the *Table 3.8*

2α [°]	f_{w1}
120°	1.203
150°	0.900

Table 3.8: Value of the corrective stress factors f_{w1} in function of the opening angle 2α

The submodel is created by the extrusion by 4mm along the global z-axis of the sectional area, reported in *Figure 3.11*, which is pre-meshed with the same requirements above-mentioned with elements PLANE 182 with *Simple Enhanced Strain* as Key Options 1 and *Plane Strain* as Key Options 3. These elements after the extrusion, will be SOLID 185.

To obtain a correct extrusion in Ansys®APDL, the following commands are used:

Preprocessor→*Modelling*→*Operate*→*Extrude*→*Elem Ext Opts*

SOLID 185 is selected as Element type number and as the number of element extrusion is equal to 4 to obtain element with cube shape. The *Figure 2.51* shows the correct options for the extrusion.

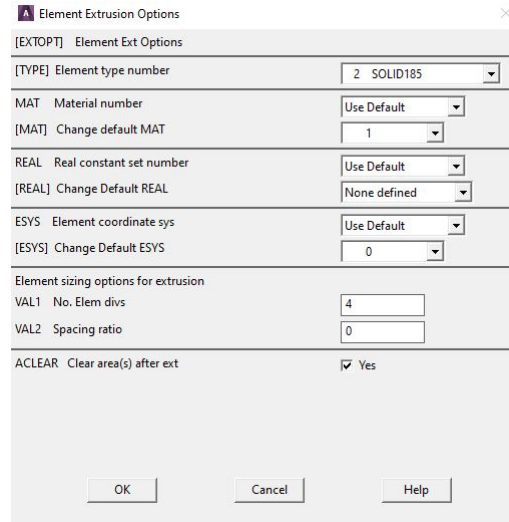


Figure 3.10: *The element extrusion options.*

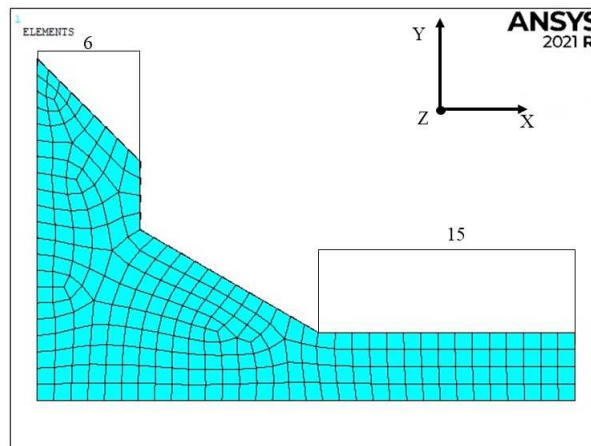


Figure 3.11: *The sectional area that has to be extruded.*

After that, the area can be extruded with the commands below:

Preprocessor→*Modelling*→*Operate*→*Extrude*→*Area*→*About Axis*

The submodel is characterized by symmetry boundary conditions that are applied to the highlighted areas in the *Figure 3.12* with the following commands:

Preprocessor→*Loads*→*Define Loads* → *Apply*→*Displacements*→*Symmetry B.C.*→ *on Areas*

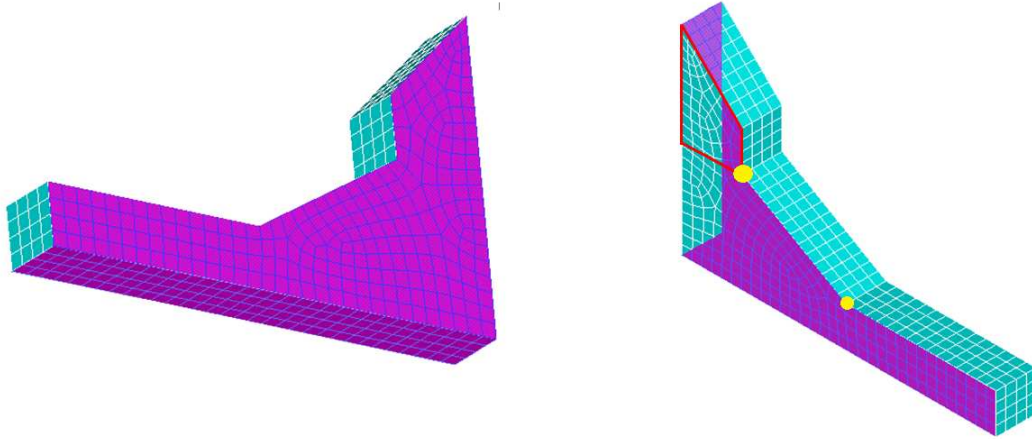


Figure 3.12: Selected area for the cut boundary condition on the right; on the left the selected areas for symmetry boundary conditions.

To apply the nodal displacements to the nodes belonging to the cut boundary (*Figure 3.12* right side represents the area of it), the following procedure is applied:

1. First of all, the nodes attached to the cut boundary are selected with the following commands:

Select→*Entities*→*Areas*→*From Full*→*Selection of the Cur boundary areas*

Select→*Entities*→*Node*→*Attached to*→*Areas All*

2. Subsequently, a file containing the coordinates of the cut boundary nodes is created:

Preprocessor→*Modelling*→*Create*→*Nodes*→*Write Node File*

where the file is saved with the extension *name-file.node*. However the submodel presents two issues:

- (a) The area highlighted in red on the *Figure 3.12* is characterised by a not converging displacements;
 - (b) The same problem is presents for the points in yellow in the *Figure 3.12*.
3. After that, the main model is opened again and solved. The displacements are interpolated in the cut boundary nodal coordinates and the file with these information is saved with *.cbdo* extension as the *Figure 3.13* shows and with the following commands:

General Postproc→*Submodelling*→*Interpolate DOF*

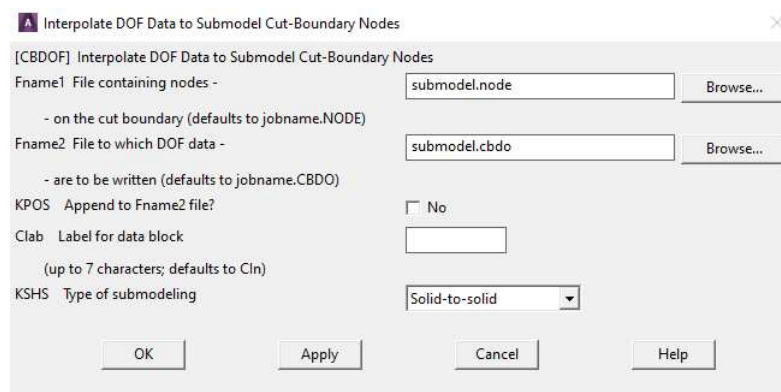


Figure 3.13: Window for configuration for *Interpolate DOF*.

4. The submodel is opened again and the nodal displacements are defined on the cut boundary with these commands:

File→*Read Input from*→*submodel.cbdo*

5. The system can be solved;

Solution→*Solve*→*Current LS*

3.1.2 PSM approach with Submodeling technique: results

Before the post-processing of the data, it is advised to disable the *PowerGraphics* option in Ansys®APDL toolbar, otherwise the output results are given by the average of only the superficial nodal stresses, without considering the inner ones.

In this analysis, the structure is subjected to pure mode I loading, so in this situation it can be demonstrated that, in the case that the stress flow is aligned with the external pressure direction, the first principal stress range $\Delta\sigma_{11}$ can be approximated equal to local stress $\Delta\sigma_{yy}$, evaluated with a local reference system with the origin placed on the V-notch. However, to obtain a more precise results, two local reference system are created on the node that represents the weld toe and the gusset with the following procedure:

1. The WorkPlane is displayed and is placed through a offset at one node of weld toe with the following commands:

Utility Menu→*Offset WorkPlane to*→*Node*

2. The WorkPlane is subjected to one rotation to obtain the correct orientation of the local system, by an angle equal to 105° about the z-axis. The commands to rotate the WorkPlane are:

Utility Menu→*Offset WP by Increments* →*Degrees*

3. Subsequently, the local reference coordinate system is created in the WorkPlane origin with the following commands:

Utility Menu→*Local Coordinate System*→*Created Local CS*→*At WP origin*

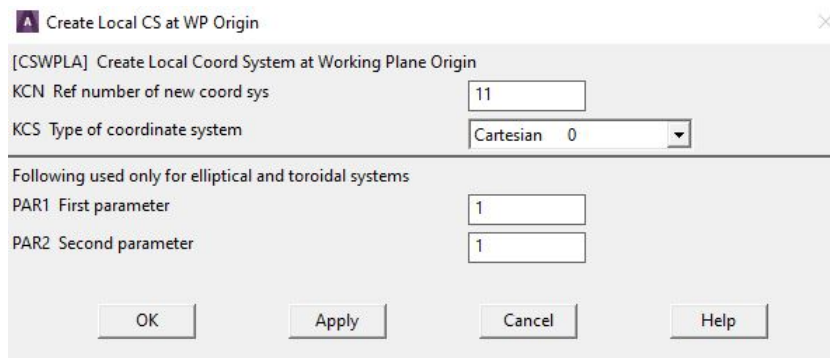


Figure 3.14: Creation of a local coordinate system at WP origin. As KCN option, a number greater than 10 must be chosen; so 11 is defined.

4. To plot the results in the new coordinate system, the following commands are executed:

General Postproc →*Option for Outp*

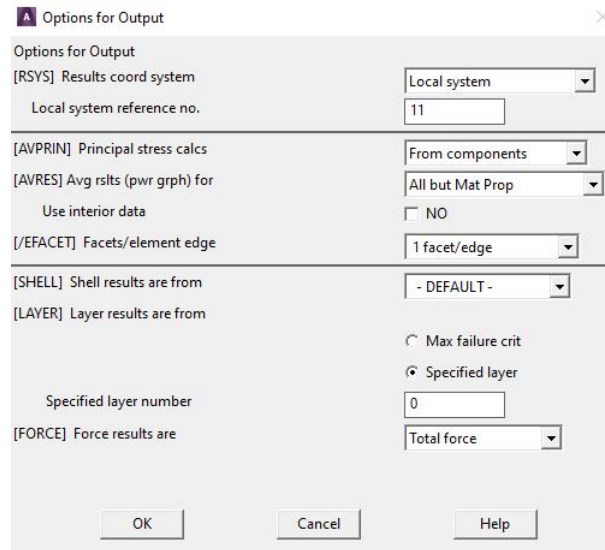


Figure 3.15: Option for Output window.

5. Before the creation of the local reference system at the gusset, is needed that the WorkPlane is aligned to the global reference system to avoid mistakes. The commands to execute this operation are:

Utility Menu→*Align WP with*→*Global Cartesian*

6. Subsequently, the same procedure is repeated with the only difference that the rotation angle is equal to 120°. The results are shown in the following figure:

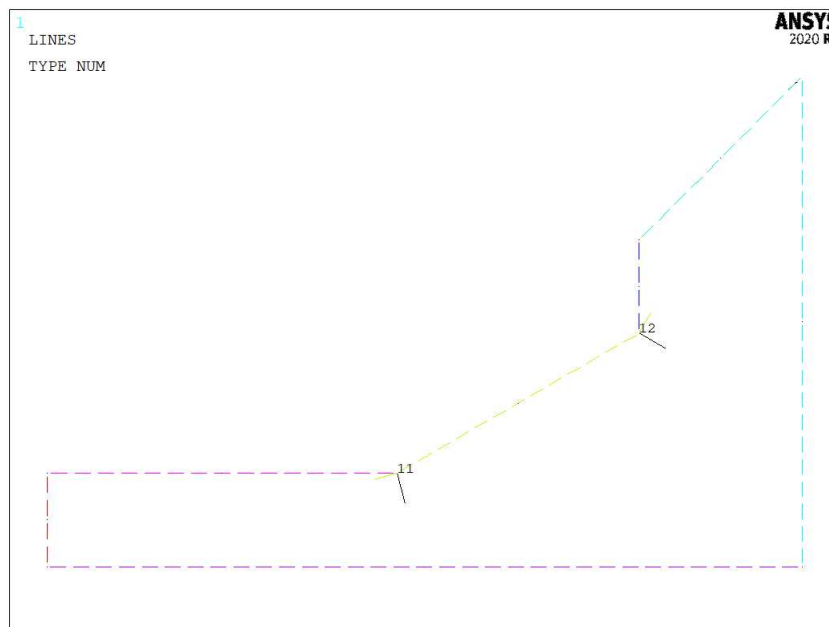


Figure 3.16: Local reference systems at the weld toe (11) and gusset (12).

During the analysis of the results, the first principal stress is evaluated and compared with $\Delta\sigma_{yy}$. The results of the first principal stress can be observed in the *Figure 3.17*, for an external applied pressure equal to 1 MPa:

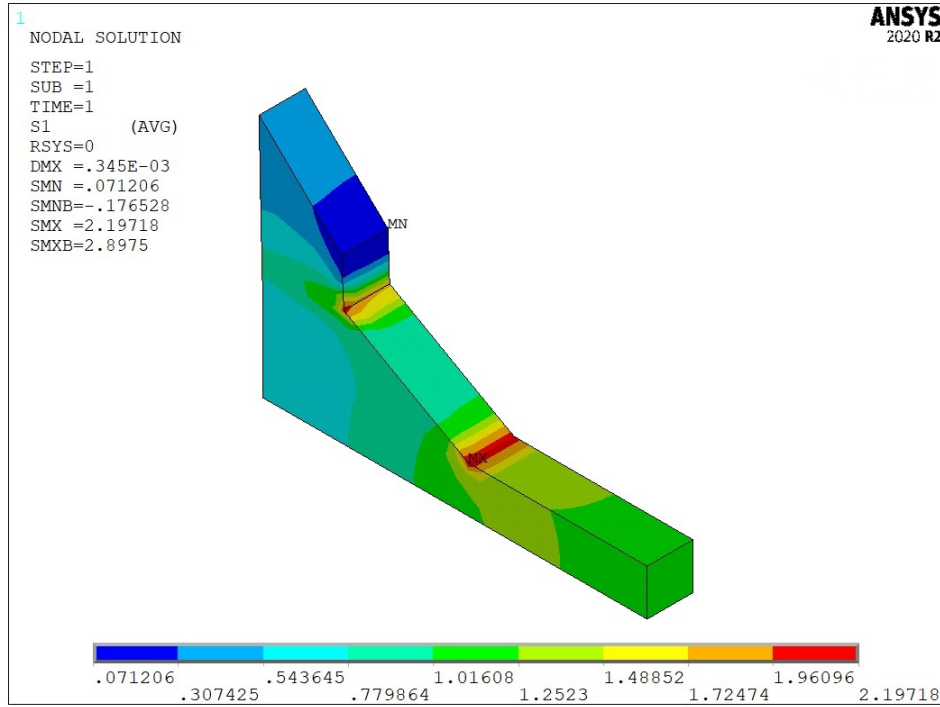


Figure 3.17: Plot of the first principal stress.

For an external applied pressure $\Delta\sigma_{nom} = 1MPa$, the results for weld toe and gusset are:

$$\Delta\sigma_{yy,weld-toe} = 2.10732MPa \quad (3.2)$$

$$\Delta\sigma_{11,weld-toe} = 2.11076MPa \quad (3.3)$$

$$\Delta\sigma_{yy,gusset} = 1.72814MPa \quad (3.4)$$

$$\Delta\sigma_{11,gusset} = 1.75698MPa \quad (3.5)$$

The equivalent peak stress are calculated by the formulae (2.23):

$$\Delta\sigma_{eq,peak,weld-toe} = \Delta\sigma_{\theta\theta,\theta=0,peak} \cdot f_{w1} = 2.10732 \cdot 0.900 = 1.897MPa \quad (3.6)$$

$$\Delta\sigma_{eq,peak,gusset} = \Delta\sigma_{\theta\theta,\theta=0,peak} \cdot f_{w1} = 1.72814 \cdot 1.203 = 2.079MPa \quad (3.7)$$

This result is not in good agreement with the value found in the literature [33]:

$$\Delta\sigma_{eq,peak,literature} = 2.307MPa \quad (3.8)$$

Thus, the relative error expresses in percentage between the calculated $\Delta\sigma_{eq,peak}$ and the $\Delta\sigma_{eq,peak,literature}$ is:

$$\Delta\% = \frac{\Delta\sigma_{eq,peak,calculated} - \Delta\sigma_{eq,peak,literature}}{\Delta\sigma_{eq,peak,literature}} \cdot 100 = -17.75\% \quad (3.9)$$

This high relative error is due to the two issues above-mentioned relative to the definition of the cut boundary.

To reduce the error, a new submodel is created with a more fine mesh than before, with a global element size equal to 0.2mm (Figure 3.18). The objective is to obtain a uniform cut boundary, indeed with the initial sub-model the nodes of cut boundary, near to the weld toe, are characterised by a non converging displacements, also called singular displacements.

The procedure to create the new submodel is the same of previous one.

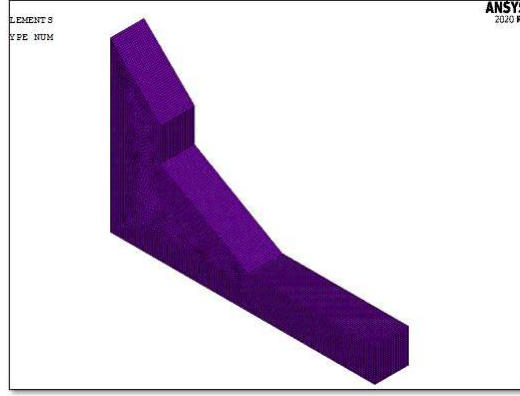


Figure 3.18: Submodel with global element size equal to 0.2 mm.

The results are:

$$\Delta\sigma_{yy,weld-toe} = 3.06095MPa \quad (3.10)$$

$$\Delta\sigma_{11,weld-toe} = 3.06183MPa \quad (3.11)$$

$$\Delta\sigma_{yy,gusset} = 3.12644MPa \quad (3.12)$$

$$\Delta\sigma_{11,gusset} = 3.13779MPa \quad (3.13)$$

The equivalent peak stress are calculated by the formulae (2.23):

$$\Delta\sigma_{eq,peak,weld-toe} = \Delta\sigma_{\theta\theta,\theta=0,peak} \cdot f_{w1} = 3.06095 \cdot 0.604 = 1.849MPa \quad (3.14)$$

$$\Delta\sigma_{eq,peak,gusset} = \Delta\sigma_{\theta\theta,\theta=0,peak} \cdot f_{w1} = 3.12644 \cdot 0.648 = 2.027MPa \quad (3.15)$$

This result is not, as before, in good agreement with the value found in the literature [33]:

$$\Delta\sigma_{eq,peak,literature} = 2.307MPa \quad (3.16)$$

The relative error expresses in percentage between the calculated $\Delta\sigma_{eq,peak}$ and the $\Delta\sigma_{eq,peak,literature}$ is:

$$\Delta\% = \frac{\Delta\sigma_{eq,peak,calculated} - \Delta\sigma_{eq,peak,literature}}{\Delta\sigma_{eq,peak,literature}} \cdot 100 = -19.84\% \quad (3.17)$$

As the results show, the error remain roughly constant because the PSM calibration constant $K_{FE}^* = 1.38 \pm 3\%$ is calibrated for a opening angle 2α lesser than 135° and in this case, it is extended for a angle of 150° . Indeed, the PSM Brick 185 approach has erroneously foreseen the experimental crack initiation point at gusset, instead the weld toe, as the experimental reality shows. Due to the important relative error between the value obtained from the PSM with submodelling technique and the value defined in literature, the data are not inserted inside the fatigue design PSM curve.

3.1.3 PSM approach with Tetra 187

The fatigue assessment for this model is performed by the application of Peak Stress Method for 3D structures with the adoption of ten-node quadratic elements, considering only the weld toe.

The element SOLID 187 is chosen from the Ansys®APDL library with *Pure Displacement* as Key Option 1, which means that the nodal forces are only dependent on the displacements.

As defined in the paragraph 3.1.1, the model is prevailing subjected to mode I. Under mode I, the PSM requirements, with Tetra elements SOLID 187, are define in the following table:

Location: weld toe $2\alpha = 150^\circ$		Mode I		
Element type	Mesh algorithm	$(a/d)_{min}$	2α	Mesh Pattern
Solid 187 KeyOpt:Pure Displacement	Free	1	150°	No particular indications

Table 3.9: Requirements for PSM with Tetra elements SOLID 187.

The mode I PSM calibration constant is calibrated at the weld toe where $2\alpha = 150^\circ$ and it is equal to $K_{FE}^* = 1.4423$.

To define the global element size of the model, the size of the element is obtained with the following procedure:

1. From literature the ratio $(a/d)_{min}$ is determined according to the Table 3.9. In this case the ratio for pure mode I is chosen and it is equal to 1;
2. The value of a is the reference dimension for selecting the maximal FE sizes d for PSM application and is defined as the half of the thickness t , so in this case is equal to 4 mm;
3. Subsequently, the minimum element size is defined as follow:

$$d_{min} = \frac{a}{3} = \frac{4}{3} = 1.33mm \quad (3.18)$$

4. The chosen dimension of elements is 1 mm

The λ_1 and e_1 values are depended on the opening angle 2α , that is 150° for the weld toe:

2α [°]	λ_1 (Mode I)	e_1 (Mode I)
150°	0.752	0.103

Table 3.10: Value of λ_1 and e_1 in function of the opening angle 2α

The corrective stress factors for mode I is calculated with the equation (2.24). The result is reported in the Table 3.11

2α [°]	f_{w1}
150°	0.941

Table 3.11: Value of the corrective stress factors f_{w1} in function of the opening angle 2α

Once the model is properly meshed, loaded and constraint, the system can be solved:

$$\text{Solution} \rightarrow \text{Solve} \rightarrow \text{Current LS}$$

3.1.4 PSM approach with Tetra 187: results

Before the post-processing of the data, it is advised to disable the *PowerGraphics* option in Ansys®APDL toolbar, otherwise the output results are given by the average of only the superficial nodal stresses, without considering the inner ones.

To obtain the correct value of the equivalent peak stress with the application of PSM Tetra 187, three considerations must be done:

1. The mesh is generate automatically by the *free-mesh* algorithm and it is intrinsically irregular, that is the node of the notch tip could be shared by different elements having a important different shape and size. For this reason, the peak stress could vary along the notch tip profile even in the case of a constant applied NSIF [24]. This problem can be solved by introducing an average peak stress value, which has been defined as the moving average on three adjacent vertex nodes, starting from the generic node $n=k$:

$$\bar{\sigma}_{i,j,peak,n=k} = \frac{\sigma_{i,j,peak,n=k-1} + \sigma_{i,j,peak,n=k} + \sigma_{i,j,peak,n=k+1}}{3} \Big|_{n=node} \quad (3.19)$$

2. Another important thing related to equation (3.19) is that only peak stresses calculated at vertex nodes of tetra elements have be introduced in this equation, thus the stresses at mid-side nodes must be neglected [30].
3. The V-notch profile edge nodes must be excluded from the average because they are affected by the nodal values in the adjacent areas.

In this analysis, the structure is subjected to pure mode I loading, so in this situation it can be demonstrated that, in the case that the stress flow is aligned with the external pressure direction, the first principal stress range $\Delta\sigma_{11}$ can be approximated equal to local stress $\Delta\sigma_{yy}$, evaluated with a local reference system with the origin placed on the V-notch. To reduce the post-processing time, the first principal stress is replaced by $\Delta\sigma_{yy}$ and the results can be observed in the *Figure 3.19*, for an external applied pressure equal to 1 MPa:

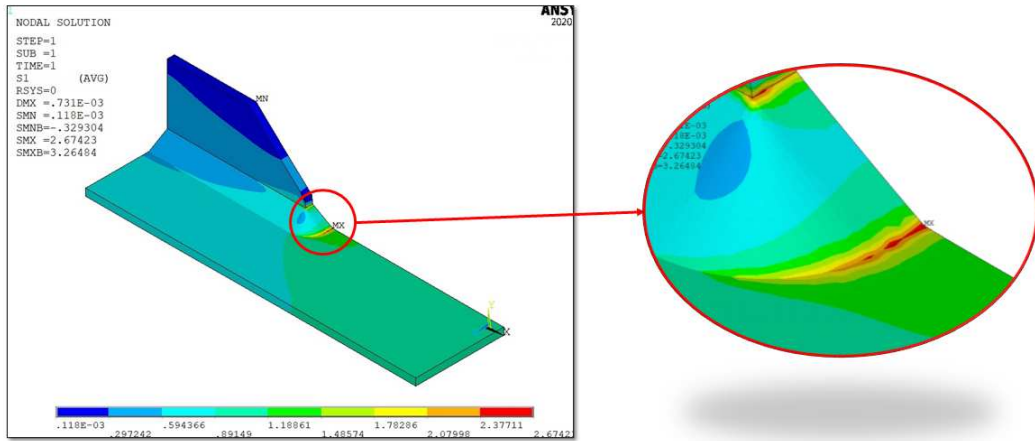


Figure 3.19: Plot of the first principal stress.

To obtain the trend of the nodal stress at the V-notch, the nodes attached to line that represents the weld toe (see *Figure 3.20*), is selected with the following commands:

Select→*Entities*→*Lines*→*From full*

Select→*Entities*→*Nodes*→*Attached to*→*Lines all*

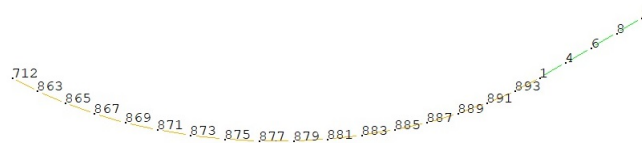


Figure 3.20: Selected nodes along the weld toe.

The results of the nodal tensions $\Delta\sigma_{11}$ and the relative average peak stress value are reported in the Appendix B.1.

For an external applied pressure $\Delta\sigma_{nom} = 1MPa$, the result at the weld toe is:

$$\overline{\Delta\sigma}_{11,weld-toe,peak} = 2.517MPa \quad (3.20)$$

The equivalent peak stress are calculated by the formulae (2.23):

$$\Delta\sigma_{eq,peak,weld-toe} = \overline{\Delta\sigma}_{\theta\theta,\theta=0,peak} \cdot f_{w1} = 2.517 \cdot 0.841 = 2.368MPa \quad (3.21)$$

This result is in good agreement with the value found in the literature [33]:

$$\Delta\sigma_{eq,peak,literature} = 2.307MPa \quad (3.22)$$

Thus, the relative error expresses in percentage between the calculated $\Delta\sigma_{eq,peak}$ and the $\Delta\sigma_{eq,peak,literature}$ is:

$$\Delta\sigma\% = \frac{\Delta\sigma_{eq,peak,calculated} - \Delta\sigma_{eq,peak,literature}}{\Delta\sigma_{eq,peak,literature}} \cdot 100 = 2.66\% \quad (3.23)$$

3.1.5 Data results for PSM curve

The previous model was characterised by a load equal to 1 MPa, applied to the main plate of the specimen. Thanks to the linear elasticity hypothesis, the equivalent peak stress can be defined for different loading conditions with the following expression:

$$\Delta\sigma_{eq,peak,gen} = \frac{\Delta\sigma_{gen}}{\Delta\sigma_{ref}} \cdot \Delta\sigma_{eq,peak,ref} \quad (3.24)$$

where:

- $\Delta\sigma_{eq,peak,gen}$ is a generic value of the equivalent peak stress for a generic loading condition that has to be detected;
- $\Delta\sigma_{gen}$ is the respective applied nominal stress;
- $\Delta\sigma_{eq,peak,ref}$ is the reference value of equivalent peak stress that are already detected;
- $\Delta\sigma_{ref}$ is the reference nominal stress, 1MPa.

The results in terms of equivalent peak stress calculated with PSM Tetra 187 approach, are defined in the Appendix C.1.

The all experimental data are collected inside the PSM design curve proposed by Meneghetti, Guzzella and Atzori for structure subjected to prevailing mode I.

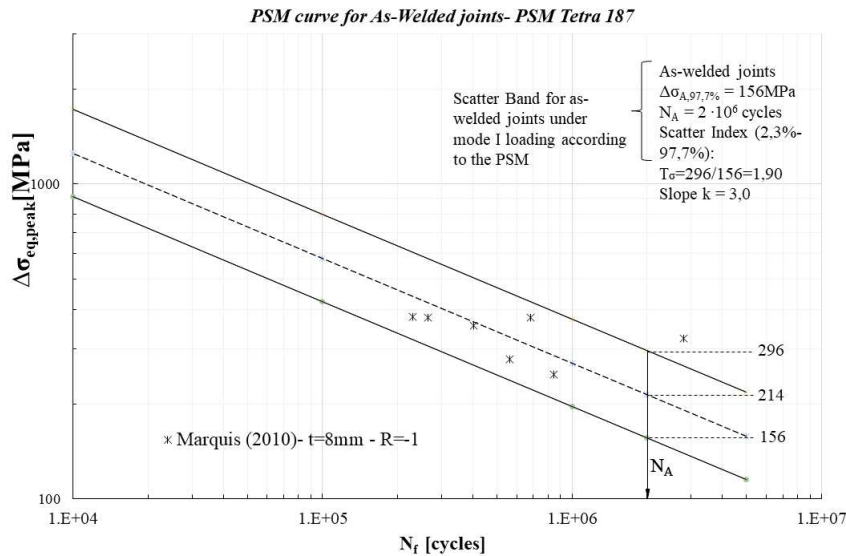


Figure 3.21: Experimental data inside the PSM design curve with Tetra 187 elements.

The following conclusion can be defined:

1. The all experimental data fall above the lines that represents the 97.7% of probability of survival. Thus the PSM design curve has demonstrated to be effective and conservative;
2. The PSM Brick 185 approach find results that are not in according with the literature due to the area of boundary condition that is characterised by a not converging displacements;
3. The PSM 187 approach gives more precise results thanks also to the presence of a calibration constant K_{FE}^* calibrated for angle higher than 135° . Indeed, the PSM Brick 185 method extends the K_{FE}^* for a opening angle $2\alpha = 135^\circ$, also for $2\alpha = 150^\circ$

3.1.6 SED (Strain Energy Density) approach

The fatigue assessment for this model is performed by the application of the Strain Energy Density approach. This method is an energetic criterion proposed by Lazzarin and Zambardi [25] in 2001 and it derives from the Neuber's theory of structural volume. Indeed, the averaged Strain Energy Density inside a circular volume of radius R_0 with the center in the V-notch tip, is the critical parameter to evaluate the fatigue strength of the welded components.

The element SOLID 187 is chosen from the Ansys®APDL with *Pure Displacement* as Key Option 1, which means that the nodal forces are only dependent on the displacements.

First of all, the control volume is created and it is characterised by a 3-dimensional circular sector shape with radius equal to $R_0 = 0.28\text{mm}$ and the deep is 0.28mm (0.14 in the model due to the symmetry condition). The center of the control volume is placed at the weld toe as the figure below shows:

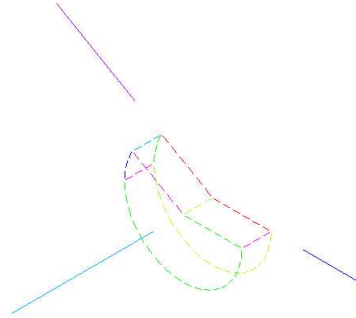


Figure 3.22: Control volume with the center at the V-notch tip.

The all model with the control volume has been modelled inside *SOLIDWORKS 2020* and after it has been imported in Ansys®APDL with *.IGS* extension.

To create the mesh of the model, the following procedure is executed:

1. The element inside the structural volume are characterised by a *global element size* equal to 0.05mm with a *free-mesh* algorithm;

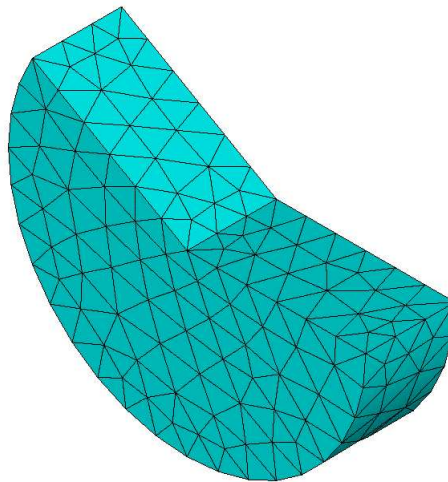


Figure 3.23: Mesh of the structural volume with global element size of 0.05.

2. The other volume is meshed with a *global element size* equal to 1 mm with a *free-mesh* algorithm.

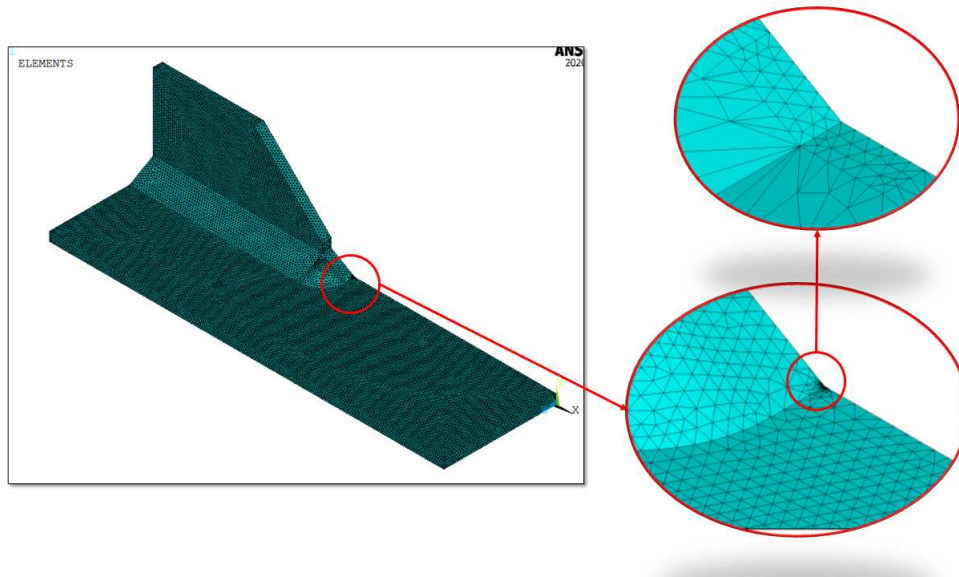


Figure 3.24: Mesh of the all structure.

Once the model is properly meshed, loaded and constraint, the system can be solved:

Solution→*Solve*→*Current LS*

3.1.7 SED (Strain Energy Density) approach: results

Before the post-processing of the data, it is advised to disable the *PowerGraphics* option in Ansys®APDL toolbar, otherwise the output results are given by the average of only the superficial nodal stresses, without considering the inner ones.

The averaged Strain Energy Density is defined as the energy contained inside the structural volume. To define this value, the element belonging to the structural volume have to be selected with the following commands:

Utility Menu→*Select*→*Entities*→*Volumes*→*By Num/Pick*→*From Full*

Utility Menu→*Select*→*Entities*→*Elements*→*Attached to*→*Volumes*

Subsequently, two *Element Table* are created :

1. The first one to define the energy inside each element selected. This Element Table is called *SENE*;
2. The second one to define the volume of each element selected. This Element Table is called *VOLU*;

The commands to create the Element Table are:

General Postproc→*Element Table*→*Define Element Table*→*SENE/VOLU*

Label	Item	Comp	Time Stamp	Status
SENE	SENE		Time= 1.0000	(Current)
VOLU	VOLU		Time= 1.0000	(Current)

Figure 3.25: Element Table in Ansys®APDL

After the creation of the Element Tables, each single element SENE and VOLU values must be summed with the following commands:

General Postproc → *Element Table* → *Sum of Each Item*

Finally, the averaged Strain Energy Density value can be calculated with the following expression:

$$\Delta \bar{W}_{FEM} = \frac{\sum_{V(R_0)} W_{FEM,i}}{V(R_0)} = \frac{SENE}{VOLU} \quad (3.25)$$

The result of SED for the weld toe when the specimen is subjected to a nominal stress of 1 MPa is:

$$SENE = 2.358 \cdot 10^{-7} MJ \quad (3.26)$$

$$VOLU = 0.0201144 mm^3 \quad (3.27)$$

$$SED = \frac{SENE}{VOLU} = \frac{2.358 \cdot 10^{-7}}{0.0201144} = 1.172 \cdot 10^{-5} \frac{MJ}{m^3} \quad (3.28)$$

From the SED, the equivalent peak stress is obtained with the following formula:

$$\Delta \sigma_{eq,peak} = \sqrt{\frac{2 \cdot E \cdot SED}{1 - \nu^2}} = \sqrt{\frac{2 \cdot 206000 \cdot 1.172 \cdot 10^{-5}}{1 - 0.3^2}} = 2.3036 MPa \quad (3.29)$$

This result is in good agreement with the value found in literature [33]:

$$\Delta \sigma_{eq,peak,literature} = 2.307 MPa \quad (3.30)$$

Thus, the relative error expresses in percentage between the calculated $\Delta \sigma_{eq,peak}$ and the $\Delta \sigma_{eq,peak,literature}$ is:

$$\Delta \% = \frac{\Delta \sigma_{eq,peak,calculated} - \Delta \sigma_{eq,peak,literature}}{\Delta \sigma_{eq,peak,literature}} \cdot 100 = -0.129\% \quad (3.31)$$

3.1.8 Data results for SED curve

The previous model was characterised by a load equal to 1 MPa, applied to the main plate of the specimen. Thanks to the linear elasticity hypothesis, the SED value can be defined for different loading conditions with the following expression:

$$SED_{gen} = \left(\frac{\Delta \sigma_{gen}}{\Delta \sigma_{ref}} \right)^2 \cdot SED_{ref} \quad (3.32)$$

where:

- SED_{gen} is a generic value of the SED for a generic loading condition that has to be detected;
- $\Delta \sigma_{gen}$ is the respective applied nominal stress;
- SED_{ref} is the reference value of SED that are already detected;
- $\Delta \sigma_{ref}$ is the reference nominal stress, 1 MPa.

The results in terms of SED are defined in the Appendix C.1.

The all experimental data are collected inside the SED design curve proposed by Lazzarin and Zambardi:

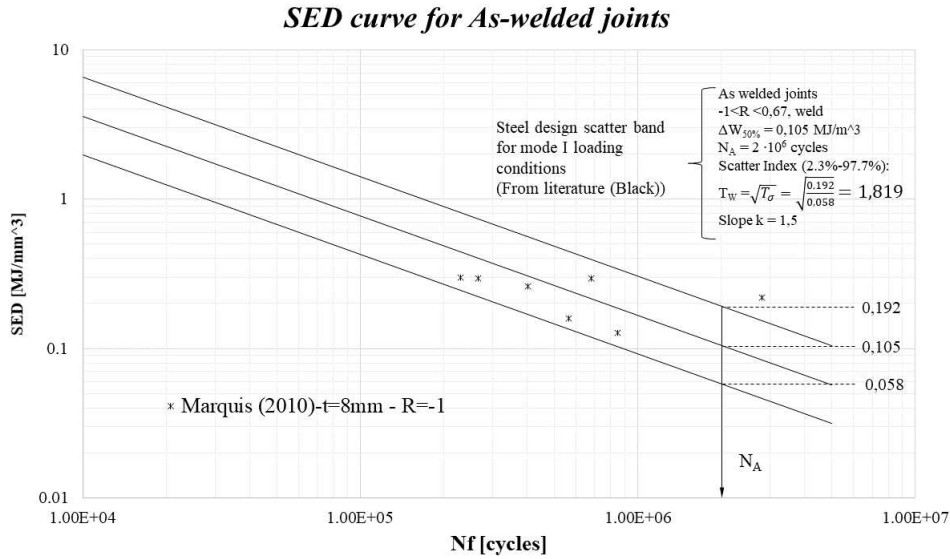


Figure 3.26: Experimental data inside the SED design curve.

The following conclusion can be defined:

1. The all experimental data fall above the lines that represents the 97.7% of probability of survival. Thus the PSM design curve has demonstrated to be effective and conservative;
2. The SED approach find results that are in according with the literature and it has correctly foreseen the experimental crack initiation point at weld toe.

3.1.9 SHSS (Structural Hot Spot Stress) approach

The fatigue assessment for this model is performed by the application of SHSS approach, following the IIW recommendation [1] to obtain the hot-spot stress. According to the guideline, the weld toe of the longitudinal stiffener FAT 71 is a hot-spot type *a* and the hot-spot stress value is detected with the employment of fine mesh, as Figure 1.4 shows.

The model of the longitudinal stiffener FAT 71 is divided in a series of volumes to allow the application of *Mapped-mesh* algorithm; indeed each volumes must be characterised by a number of face between 4 and 6 to obtain a *Mapped-mesh*. The eight-node linear element SOLID 185 is chosen in Ansys®APDL with *Simple Enhanced Strain* as Key Option 1.

The all informations about the mesh is reported in the following table:

Element type	Mesh algorithm	Main plate thickness <i>t</i>	Max element size	Adopted element size
Solid 185 KeyOpt:Simple Enhanced Strain	Mapped	8 mm (4 mm modelled)	$0.4 \cdot t = 0.4 \cdot 8 = 3.2\text{mm}$	1.6 mm

Table 3.12: Requirements for SHSS mesh.

The hot-spot stress is extrapolated at two reference points placed at $0.4t$ and $1.0t$ distance from the weld toe tip, so in this case at 3.2 mm and 8 mm from weld toe.

For the type of extrapolated stress, the graph in Figure 3.27 shows that, for an external applied pressure $\Delta\sigma_{nom} = 1\text{MPa}$, after 1.90 mm, the $\Delta\sigma_{xx}$ and the first principal stress $\Delta\sigma_{I1}$ are coincident. For this reason the choice is indifferent.

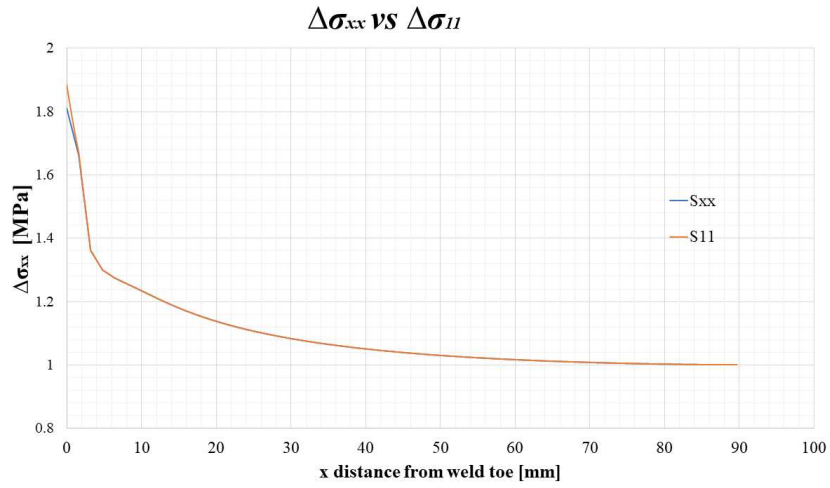


Figure 3.27: $\Delta\sigma_{xx}$ and $\Delta\sigma_{yy}$ plotted in function of the distance from weld toe tip

The mesh of the model is reported in the following figures:

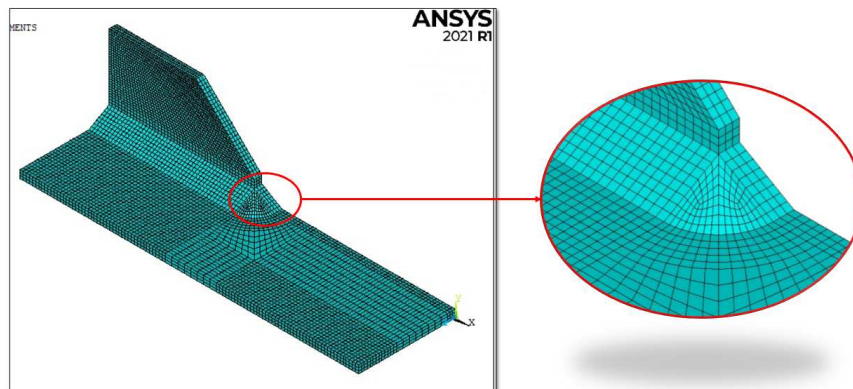


Figure 3.28: Mapped mesh for SHSS approach

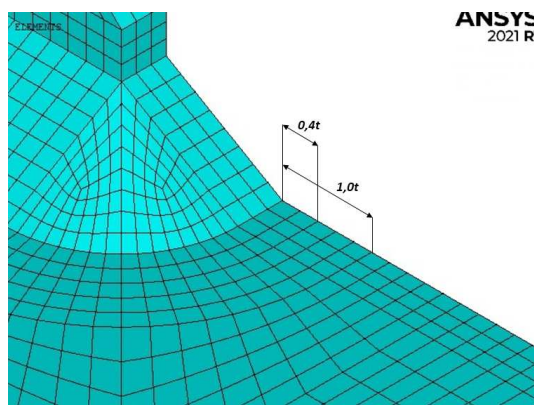


Figure 3.29: Mapped mesh for SHSS approach and reference points

Before the post-processing of the data, it is advised to disable the *PowerGraphics* option in Ansys®APDL toolbar, otherwise the output results are given by the average of only the superficial nodal stresses, without considering the inner ones.

For an external applied pressure $\Delta\sigma_{nom} = 1MPa$, the results of the tension at the reference points are:

$$\Delta\sigma_{xx,0.4t} = 1.36143MPa \quad (3.33)$$

$$\Delta\sigma_{xx,1.0t} = 1.25651MPa \quad (3.34)$$

$$\Delta\sigma_{11,0.4t} = 1.36192MPa \quad (3.35)$$

$$\Delta\sigma_{11,1.0t} = 1.25659MPa \quad (3.36)$$

$$(3.37)$$

The structural hot-spot stress is detected with the equation (1.2):

$$\Delta SHSS_{LSE,xx} = 1,67 \cdot \sigma_{xx,0.4t} - 0,67 \cdot \sigma_{xx,1.0t} = 1,67 \cdot 1,36143 - 0,67 \cdot 1,25651 = 1,4317MPa \quad (3.38)$$

$$\Delta SHSS_{LSE,11} = 1,67 \cdot \sigma_{11,0.4t} - 0,67 \cdot \sigma_{11,1.0t} = 1,67 \cdot 1,36192 - 0,67 \cdot 1,25659 = 1,4325MPa \quad (3.39)$$

This result is in good agreement with the value found in literature [33]:

$$\Delta\sigma_{xx,0.4t} = 1.336MPa \quad (3.40)$$

$$\Delta\sigma_{xx,1.0t} = 1.231MPa \quad (3.41)$$

$$(3.42)$$

$$\Delta SHSS_{LSE,literature} = 1,40635MPa$$

Thus, the relative errors expresses in percentage between the calculated $\Delta SHSS_{LSE,xx}$, $\Delta SHSS_{LSE,11}$ and the $\Delta SHSS_{LSE,literature}$ are:

$$\Delta\% = \frac{\Delta SHSS_{LSE,xx} - \Delta SHSS_{LSE,literature}}{\Delta SHSS_{LSE,literature}} \cdot 100 = 1.804\% \quad (3.43)$$

$$\Delta\% = \frac{\Delta SHSS_{LSE,11} - \Delta SHSS_{LSE,literature}}{\Delta SHSS_{LSE,literature}} \cdot 100 = 1.86\% \quad (3.44)$$

3.1.10 Data results for IIW curve

Nominal stress approach

The results are reported in terms of nominal stress, defined in the beginning of paragraph 3.1, inside the FAT 71 curve proposed by IIW guideline [1]:

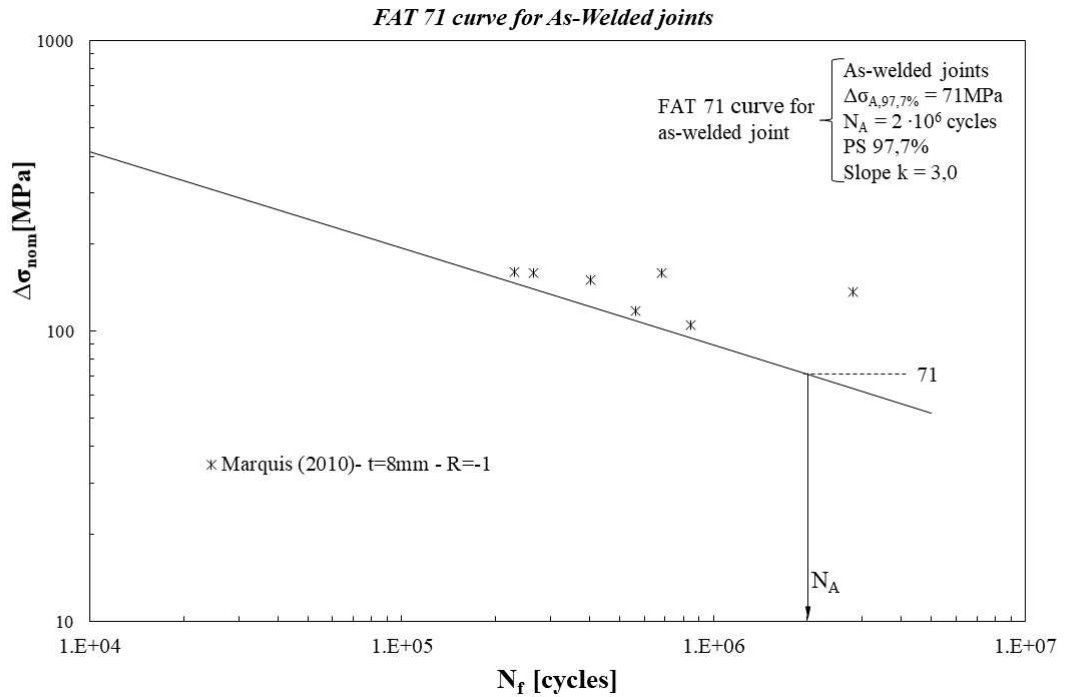


Figure 3.30: Experimental data inside the IIW nominal stress design curve.

SHSS approach

The previous model was characterised by a load equal to 1 MPa, applied to the main plate of the specimen. Thanks to the linear elasticity hypothesis, the SHSS value can be defined for different loading conditions with the following expression:

$$SHSS_{gen} = \left(\frac{\Delta\sigma_{gen}}{\Delta\sigma_{ref}} \right)^2 \cdot SHSS_{ref} \quad (3.45)$$

where:

- $SHSS_{gen}$ is a generic value of the SED for a generic loading condition that has to be detected;
- $\Delta\sigma_{gen}$ is the respective applied nominal stress;
- $SHSS_{ref}$ is the reference value of SED that are already detected;
- $\Delta\sigma_{ref}$ is the reference nominal stress, 1 MPa.

The results in terms of SHSS are defined in the Appendix C.1. The all experimental data are collected inside the SHSS design curve proposed by IIW guideline (Figure 3.31).

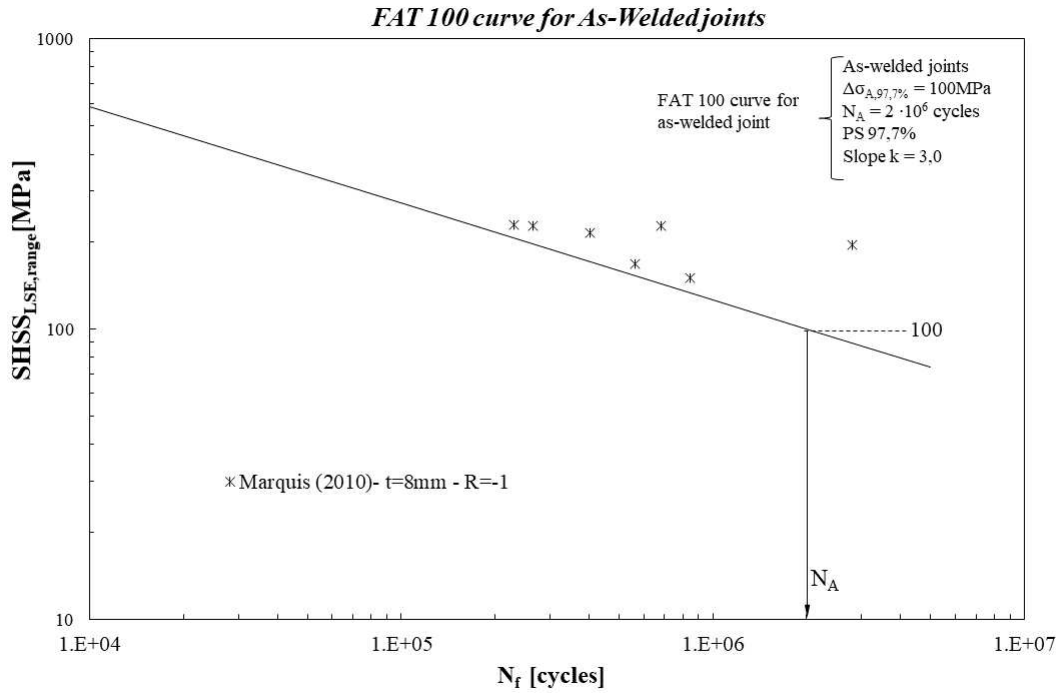


Figure 3.31: Experimental data inside the SHSS design curve.

The following conclusion can be defined:

1. These approaches have correctly been applied to FAT 63 welded joint, for weld toe fractures;
2. The nominal stress approach is characterised by the fact that all points fall above the lines that represents the 97.7% of probability of survival. For this reason, the nominal stress approach has proven to be conservative as the others methods;
3. The hot-spot stress method is characterised by the fact that all points fall above the lines that represents the 97.7% of probability of survival. For this reason, the SHSS approach has proven to be conservative as the others methods.

3.2 Vanrostenberghe 2015, longitudinal attachment FAT 63

The second joint analysed is a longitudinal stiffener characterised by a fatigue class FAT 63, studied by Yildirim in 2013 [42] under CAL (Constant Amplitude Loading) and subsequently by Vanrostenberghe in 2015. The principal information and mechanical properties about this typology of the joint are summarized in the Table 3.13 and Table 3.14:

Weld condition	Fracture location	Load application	Main plate/gusset thickness
As-welded, non-load carrying (NLC), full penetration	Weld toe	Axial, main plate, parent material	Main plate: 5-20mm Gusset: 5-20mm

Table 3.13: Information about the specimens

Material model	Yield strength f_y [MPa]	Young modulus [MPa]	Poisson's ratio ν
S700MC, HSS, Linear elastic, isotropic	700	206000	0.3
S690QL, HSS, Linear elastic, isotropic	690		

Table 3.14: Information about mechanical properties

Three different specimen are analysed:

- S700MC with main plate thickness equal to 10 mm;
- S690QL with main plate thickness equal to 10 mm;
- S690QL with main plate thickness equal to 20 mm;

The first two geometry are analysed together with a single model with thickness equal to 10mm, while the third one is studied separately as a model with main plate thickness equal to 20mm The dimensions of these joints are defined in the following table and figure:

Material	t [mm]	b [mm]	w [mm]	L [mm]	h [mm]	2 α [°]	z [mm]
S700MC	10	150	80	370	40	120	4.96
S690QL	10	150	80	370	40	120	4.96
S690QL	20	150	80	370	40	120	7.50

Table 3.15: Dimension of the longitudinal attachment FAT 63

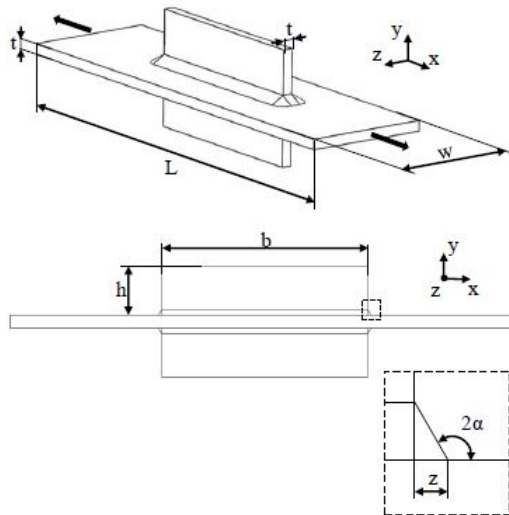


Figure 3.32: Vanrostenberghe 2015, longitudinal attachment FAT 63 [33].

The parameters of the weld profile is described in the following table:

t [mm]	ρ weld toe tip [mm]	Weld leg [mm]	Weld flack angle [°]
10	0	4.3	60
20	0	6.5	60

Table 3.16: Information about the weld profile

The radius ρ of the weld toe is defined equal to 0mm, as sharp V-notch at the weld toe. As described in the IIW recommendations [1], the effect of misalignment can be neglected in continuous welds longitudinally loaded.

The experimental data are defined in the following table in terms of nominal stress $\Delta\sigma_{nom}$:

$t=10mm$			
Material	Stress Ratio R	$\Delta\sigma_{nom}$ [MPa]	N_f [cycles]
S690QL	0.1	50	10000000
		70	10000000
		90	3466968
		200	204202
		250	112546
		350	47716
S700MC	0.5	50	10000000
		70	2333651
		90	893070
		200	88800
		250	49800
		300	33700
$t=20mm$			
Material	Stress Ratio R	$\Delta\sigma_{nom}$ [MPa]	N_f [cycles]
S690QL	0.1	70	3600954
		90	1513276
		200	125887
		250	113433
		350	41521
		S690QL	0.5
90	1612500		
125	828000		
200	136936		
250	85459		
300	49546		

Table 3.17: Experimental data of the 2nd joint, Vanrostenberghe 2015. The number barred represents the run-outs

FAT 63 are modelled in *SOLIDWORKS 2020* and subsequently, are imported inside Ansys®APDL with *.IGS* extension. The results are reported in the figure below:

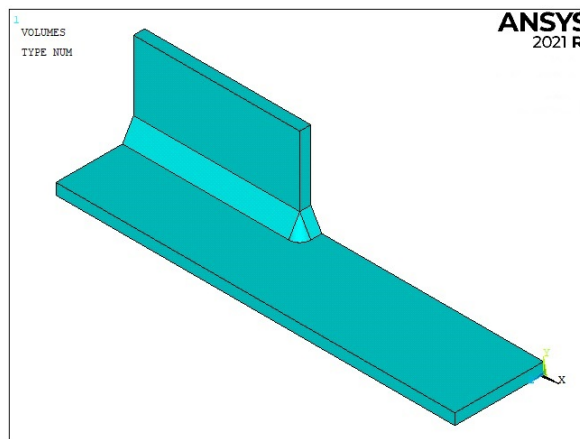


Figure 3.33: Model of longitudinal attachment FAT 63 with thickness equal to 10mm .

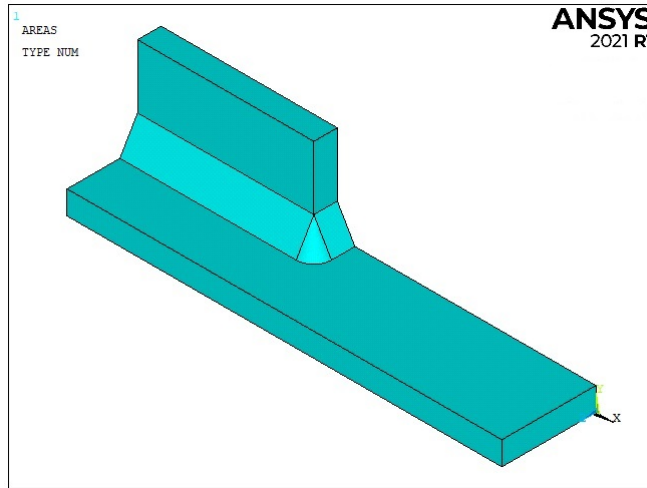


Figure 3.34: Model of longitudinal attachment FAT 63 with thickness equal to 20mm .

The procedure to define the boundary conditions of the model follows the same steps and dispositions defined for the longitudinal FAT71 (see paragraph 3.1). The results are reported in the following figures:

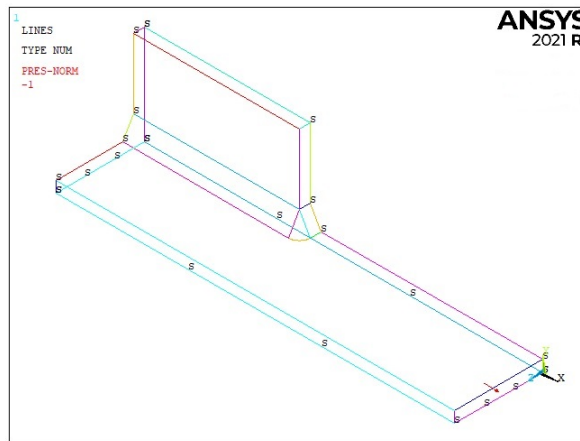


Figure 3.35: Boundary conditions of the model with thickness equal to 10mm. *S* indicate the symmetry boundary condition, while the red arrow represents the external pressure.

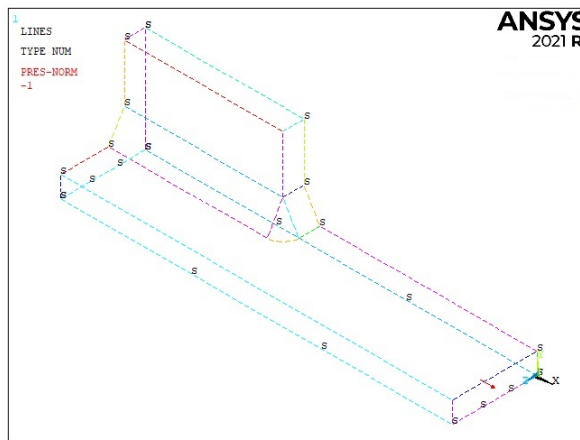


Figure 3.36: Boundary conditions of the model with thickness equal to 20mm. *S* indicate the symmetry boundary condition, while the red arrow represents the external pressure.

3.2.1 PSM approach with Submodeling technique

The fatigue assessment for the second joints (Vanrostenberghe 2015 with thickness equal to 10 and 20 mm) are initially performed by the application of Peak Stress Method for 3D structures with the adoption of eight-node linear elements. As describe in the paragraph 1.3.3, the submodelling technique is request.

The structures are prevailing subjected to mode I at the weld toe V-notch with a opening angle 2α equal to 120° . Indeed, referring to the graph of the Williams eigenvalues trend in *Figure 1.13*, mode II is not singular for V-notch opening angle greater than 102.5° , so $\lambda_2 = 0$. The mode III becomes singular in the junction part of the longitudinal stiffener, but its contribute is practically null, so it can be neglected.

The gusset is characterised by a opening angle equal to $2\alpha = 150^\circ$ and the PSM with the submodeling technique is not calibrated for V-notch opening angle higher than 135° . For this reason, the available calibration constants for $2\alpha = 135^\circ$ is extended for this case.

Main Model

First of all, is necessary to study the main model and the ten-node quadratic element SOLID 187 is chosen in Ansys@APDL with *Pure Displacement* Key Options 1, which means that the nodal forces are only dependent on the displacements.

The 10 mm and 20 mm main models are displayed on the *Figure 3.37-3.38*. The cut boundary for each main model is defined by a stress convergence analysis; indeed four different meshes, with global element size respectively equal to 5, 4, 3, 2 and 1 mm, are laid on the each main model.

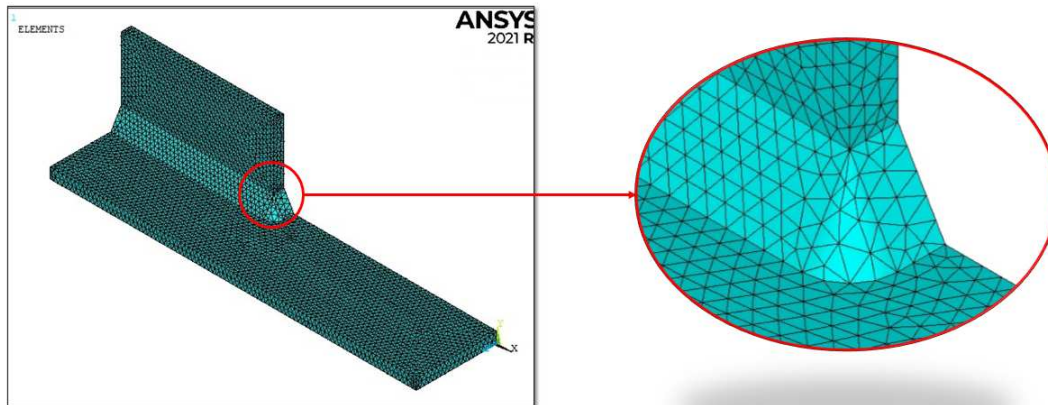


Figure 3.37: Example of 10mm main model with global element size equal to 2 mm.

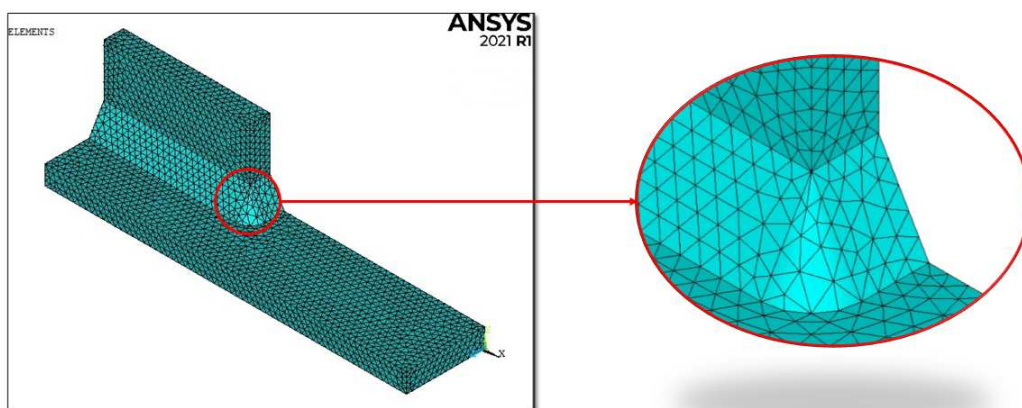


Figure 3.38: Example of 20mm main model with global element size equal to 3 mm.

The parameter to complete the convergence analysis is the first principal stress range $\Delta\sigma_{11}$, obtained along the x-axis that starts from the weld toe along the longitudinal direction, as *Figure 3.39* shows:

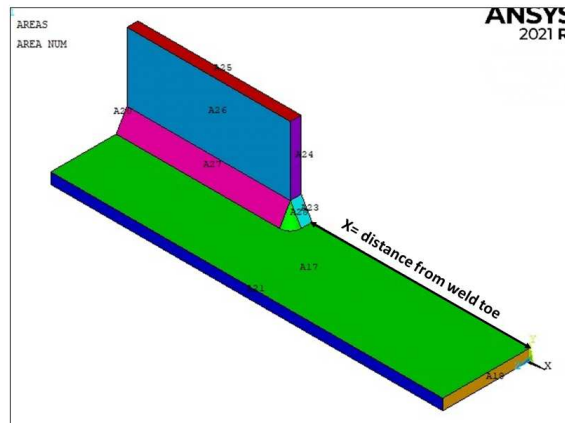


Figure 3.39: Direction of x-axis and path along which $\Delta\sigma_{11}$ is defined. This reference is valid also for the 20 mm main model

The results of the convergence stress analysis are reported in the following graph:

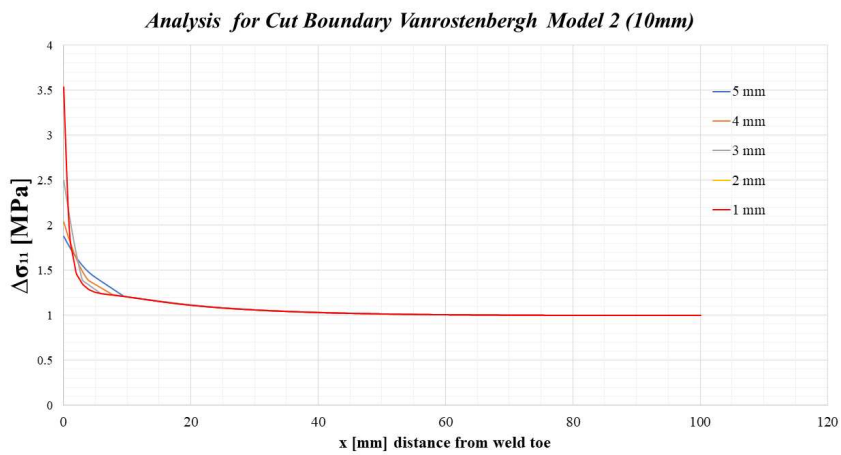


Figure 3.40: Results of convergence stress analysis for 10mm main model.

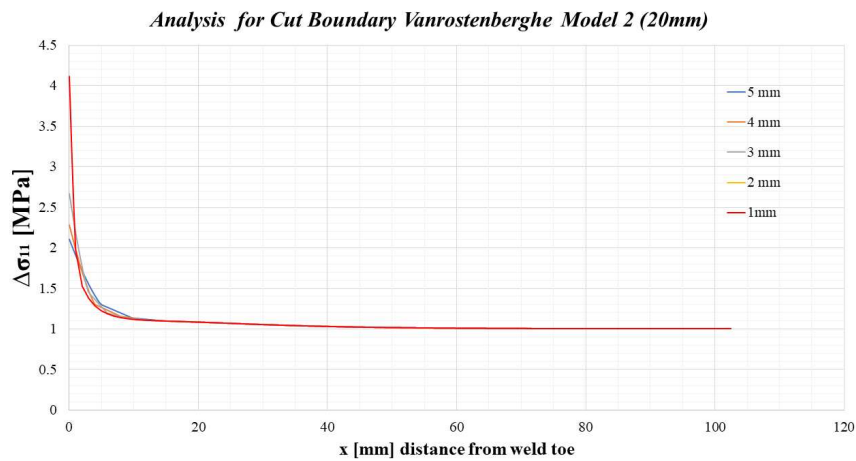


Figure 3.41: Results of convergence stress analysis for 20mm main model.

As Figure 3.40-3.41 shows, the cut boundary is placed at $x = 20.0mm$ from the weld toe for both models, where the compatibility between the results is achieved.

Submodel

The next step is to create and study the submodel. The eight-node linear element SOLID 185 is chosen in Ansys®APDL with *Simple Enhanced Strain* as Key Option 1.

As described in the paragraph 2.7, the reference system of the submodel must coincide with that of the main model because the submodel's boundary conditions are interpolated in the cut boundary with respect to the main model reference system.

Due to the same consideration of the main model, the weld toe is prevailing subjected to mode I because the opening angle 2α is equal to 120° , so mode II is null and mode III can be neglected due to its little contribute. Under mode I, the PSM, with Brick elements SOLID 185, requirements are define in the following table:

Location: weld toe $2\alpha = 120^\circ$				Mode I	
Element type	Mesh algorithm	$(a/d)_{min}$	2α	Mesh Pattern $2\alpha < 90^\circ$	Mesh Pattern $2\alpha > 90^\circ$
Solid 185 KeyOpt:Simple Enhanced Strain	Free	3	$0^\circ < 2\alpha < 135^\circ$	Four adjacent elements share the same node	Two adjacent elements share the same node
Location: gusset $2\alpha = 150^\circ$				Mode I	
Element type	Mesh algorithm	$(a/d)_{min}$	2α	Mesh Pattern $2\alpha < 90^\circ$	Mesh Pattern $2\alpha > 90^\circ$
Solid 185 KeyOpt:Simple Enhanced Strain	Free	3	135° extended to 150°	Four adjacent elements share the same node	Two adjacent elements share the same node

Table 3.18: Requirements for PSM with Brick elements SOLID 185.

The mode I PSM calibration constant is extended at the gusset where $2\alpha = 150^\circ$ and it is equal to $K_{FE}^* = 1.38 \pm 3\%$, at the weld toe, where $2\alpha = 120^\circ$, the PSM calibration constant for mode I is again equal to $K_{FE}^* = 1.38 \pm 3\%$.

To define the global element size of the 10 mm model, the following procedure is applied:

1. From literature the ratio $(a/d)_{min}$ is determined according to the Table 3.18. In this case the ratio for pure mode I is chosen and it is equal to 3;
2. The value of a is the reference dimension for selecting the maximal FE sizes d for PSM application and is defined as the half of the thickness t , so in this case is equal to 5 mm;
3. Subsequently, the minimum element size is defined as follow:

$$d_{min} = \frac{a}{3} = \frac{5}{3} = 1.667mm \quad (3.46)$$

4. The chosen dimension of elements is 1.67 mm

For the 20mm model, the size of the elements is obtained as following:

1. From literature the ratio $(a/d)_{min}$ is determined according to the Table 3.18. In this case the ratio for pure mode I is chosen and it is equal to 3;
2. The value of a is the reference dimension for selecting the maximal FE sizes d for PSM application and is defined as the half of the thickness t , so in this case is equal to 10 mm;
3. Subsequently, the minimum element size is defined as follow:

$$d_{min} = \frac{a}{3} = \frac{10}{3} = 3.33mm \quad (3.47)$$

4. The chosen dimension of elements is 3 mm

2α [°]	λ_1 (Mode I)	e_1 (Mode I)
120°	0.616	0.130
150°	0.752	0.103

Table 3.19: Value of λ_1 and e_1 in function of the opening angle 2α

The λ_1 and e_1 values are depended on the opening angle 2α , that is 120° for the weld toe and 150° for the gusset:

The corrective stress factors for mode I is calculated with the equation (2.24). The result is reported in the Table 3.20

$t=10$ mm	
2α [°]	f_{w1}
120°	1.464
150°	1.022
$t=20$ mm	
2α [°]	f_{w1}
120°	1.834
150°	1.182

Table 3.20: Value of the corrective stress factors f_{w1} in function of the opening angle 2α

The submodel is created by the extrusion by 5mm and 10 mm along the global z-axis of the sectional area for 10mm submodel and 20mm submodel respectively , reported in Figure 3.42-3.43, which is pre-meshed with the same requirements above-mentioned with elements PLANE 182 with *Simple Enhanced Strain* as Key Options 1 and *Plane Strain* as Key Options 3. These elements after the extrusion, will be SOLID 185. To obtain a correct extrusion in Ansys®APDL, the following commands are used:

Preprocessor→*Modelling*→*Operate*→*Extrude*→*Elem Ext Opts*

SOLID 185 is selected as Element type number and as the number of element extrusion is equal to 3 for 10 mm submodel and to 3 for 20 mm submodel, to obtain element with cube shape. The Figure 3.42-3.43 shows the correct options for the extrusion.

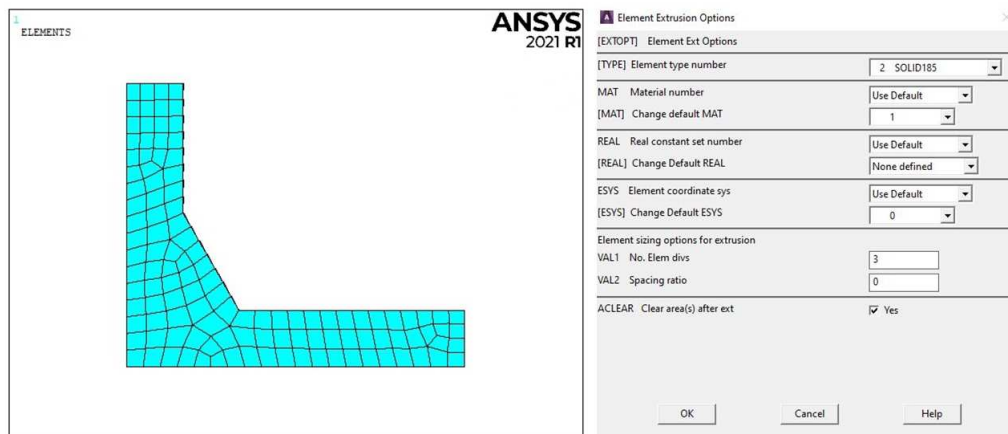


Figure 3.42: The element extrusion options and the sectional area that has to be extruded for 10mm submodel.

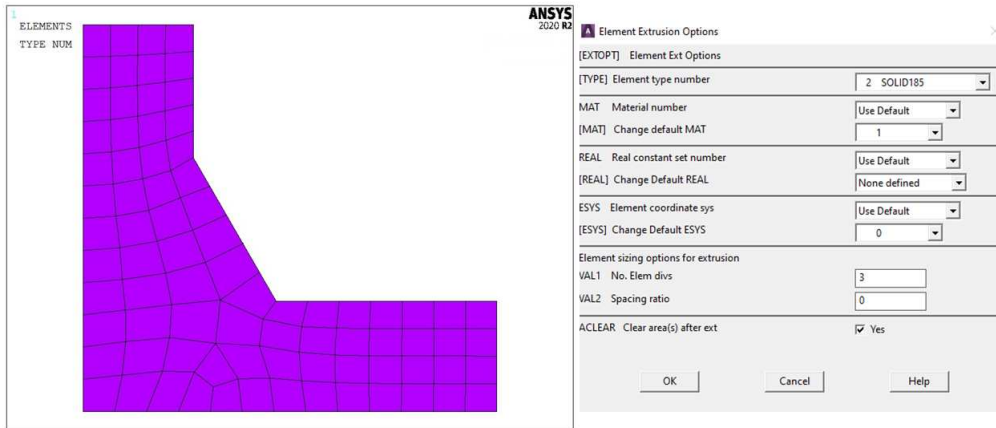


Figure 3.43: The element extrusion options and the sectional area that has to be extruded for 20mm submodel.

After that, the area can be extruded with the commands below:

Preprocessor→*Modelling*→*Operate*→*Extrude*→*Area*→*About Axis*

The boundary conditions and the modelling procedure of the models follow the same steps defined for the longitudinal FAT71.

3.2.2 PSM approach with Submodeling technique: results

Before the post-processing of the data, it is advised to disable the *PowerGraphics* option in Ansys®APDL toolbar, otherwise the output results are given by the average of only the superficial nodal stresses, without considering the inner ones.

In this analysis, the structures are subjected to pure mode I loading, so in these situations it can be demonstrated that, in the case that the stress flow is aligned with the external pressure direction, the first principal stress range $\Delta\sigma_{11}$ can be approximated equal to local stress $\Delta\sigma_{yy}$, evaluated with a local reference system with the origin placed on the V-notch. However, to obtain a more precise results, two local reference system are created on the node that represents the weld toe and the gusset with the same procedure described for the longitudinal joint FAT 71.

During the analysis of the results, the first principal stress is evaluated and compared with $\Delta\sigma_{yy}$. The results of the first principal stress can be observed in the *Figure 3.44-3.45*, for an external applied pressure equal to 1 MPa:

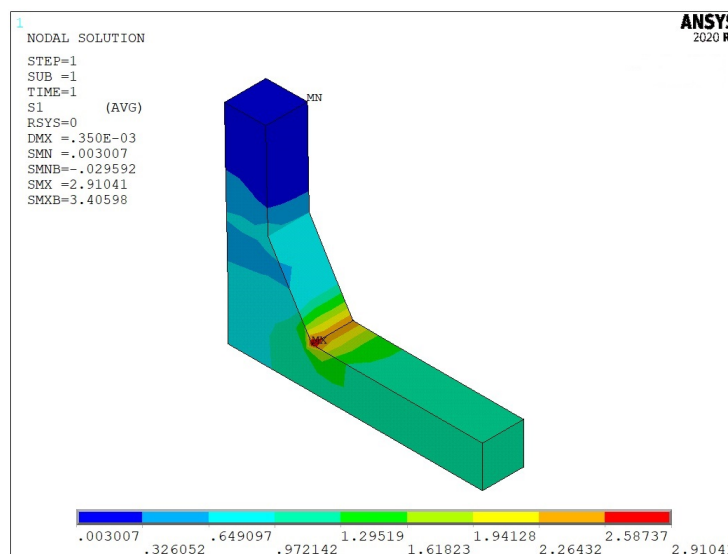


Figure 3.44: Plot of the first principal stress for 10 mm submodel.

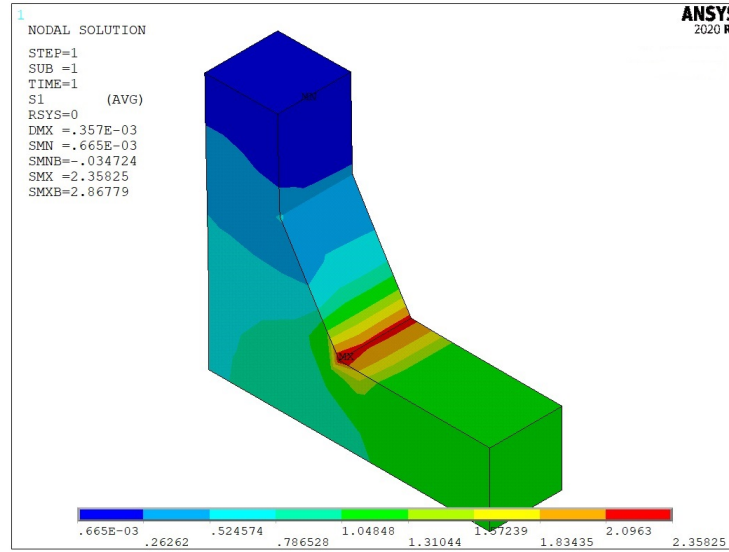


Figure 3.45: Plot of the first principal stress for 20 mm submodel.

Numerical results for 10mm submodel

For an external applied pressure $\Delta\sigma_{nom} = 1MPa$, the results for weld toe and gusset for 10mm submodel are:

$$\Delta\sigma_{yy,weld-toe} = 2.55334MPa \quad (3.48)$$

$$\Delta\sigma_{11,weld-toe} = 2.5523MPa \quad (3.49)$$

$$\Delta\sigma_{yy,gusset} = 0.642697MPa \quad (3.50)$$

$$\Delta\sigma_{11,gusset} = 0.652425MPa \quad (3.51)$$

The equivalent peak stress are calculated by the formulae (2.23):

$$\Delta\sigma_{eq,peak,weld-toe} = \Delta\sigma_{\theta\theta,\theta=0,peak} \cdot f_{w1} = 2.55334 \cdot 1.464 = 3.738MPa \quad (3.52)$$

$$\Delta\sigma_{eq,peak,gusset} = \Delta\sigma_{\theta\theta,\theta=0,peak} \cdot f_{w1} = 0.642697 \cdot 1.022 = 0.6568MPa \quad (3.53)$$

This result is not in good agreement with the value found in the literature [33]:

$$\Delta\sigma_{eq,peak,literature} = 3.274MPa \quad (3.54)$$

Thus, the relative error expresses in percentage between the calculated $\Delta\sigma_{eq,peak}$ and the $\Delta\sigma_{eq,peak,literature}$ is:

$$\Delta\% = \frac{\Delta\sigma_{eq,peak,calculated} - \Delta\sigma_{eq,peak,literature}}{\Delta\sigma_{eq,peak,literature}} \cdot 100 = 14.17\% \quad (3.55)$$

This high relative error is due to the two issues above-mentioned (paragraph 3.1.1) relative to the definition of the cut boundary.

To reduce the error, a new submodel is created with a more fine mesh than before, with a global element size equal to 0.2mm (Figure 3.46). The objective is to obtain a uniform cut boundary, indeed with the initial submodel the nodes of cut boundary, near to the weld toe, are characterised by a non converging displacements, also called singular displacements.

The procedure to create the new submodel is the same of previous one.

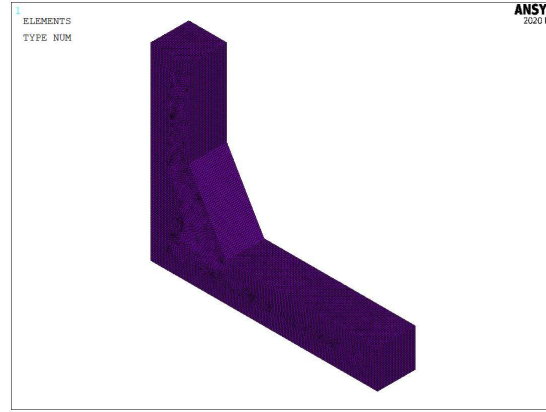


Figure 3.46: 10 mm submodel with global element size equal to 0.2 mm.

The results are:

$$\Delta\sigma_{yy,weld-toe} = 5.15851MPa \quad (3.56)$$

$$\Delta\sigma_{11,weld-toe} = 5.16062MPa \quad (3.57)$$

$$\Delta\sigma_{yy,gusset} = 1.05404MPa \quad (3.58)$$

$$\Delta\sigma_{11,gusset} = 1.05517MPa \quad (3.59)$$

$$\Delta\sigma_{eq,peak,weld-toe} = \Delta\sigma_{\theta\theta,\theta=0,peak} \cdot f_{w1} = 5.15851 \cdot 0.648 = 3.344MPa \quad (3.60)$$

$$\Delta\sigma_{eq,peak,gusset} = \Delta\sigma_{\theta\theta,\theta=0,peak} \cdot f_{w1} = 1.05404 \cdot 0.604 = 0.637MPa \quad (3.61)$$

$$\Delta\sigma_{eq,peak,literature} = 3.274MPa \quad (3.62)$$

$$\Delta\sigma\% = \frac{\Delta\sigma_{eq,peak,calculated} - \Delta\sigma_{eq,peak,literature}}{\Delta\sigma_{eq,peak,literature}} \cdot 100 = 2.12\% \quad (3.63)$$

As the results show, the relative error decreases and this approach has correctly foreseen the experimental crack initiation point at the weld toe, in according to the experimental reality. This results is due to that the PSM calibration constant $K_{FE}^* = 1.38 \pm 3\%$ is calibrated for a opening angle 2α lesser than 135° and in this case the value for weld toe ($2\alpha = 120^\circ$) is precise unlike the case of longitudinal joint FAT 71.

To decrease the relative error but with the initial global element size (1.67mm), a new submodel is created with a larger and greater cut boundary than the first submodel to obtain a converging displacements of the cut boundary nodes.

The procedure to create the new submodel is the same of previous one and the results is displayed on the following figure:.

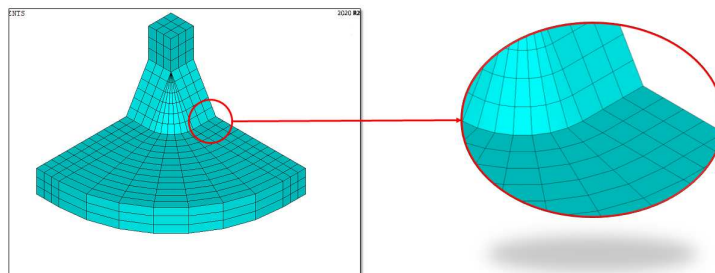


Figure 3.47: 10 mm submodel with a larger and greater cut boundary.

The results are:

$$\Delta\sigma_{yy,weld-toe} = 2.3608MPa \quad (3.64)$$

$$\Delta\sigma_{11,weld-toe} = 2.39427MPa \quad (3.65)$$

$$\Delta\sigma_{yy,gusset} = 0.911251MPa \quad (3.66)$$

$$\Delta\sigma_{11,gusset} = 0.95881MPa \quad (3.67)$$

$$\Delta\sigma_{eq,peak,weld-toe} = \Delta\sigma_{\theta\theta,\theta=0,peak} \cdot f_{w1} = 2.3608 \cdot 1.464 = 3.457MPa \quad (3.68)$$

$$\Delta\sigma_{eq,peak,gusset} = \Delta\sigma_{\theta\theta,\theta=0,peak} \cdot f_{w1} = 0.911251 \cdot 1.022 = 0.9317MPa \quad (3.69)$$

$$\Delta\sigma_{eq,peak,literature} = 3.274MPa \quad (3.70)$$

$$\Delta\% = \frac{\Delta\sigma_{eq,peak,calculated} - \Delta\sigma_{eq,peak,literature}}{\Delta\sigma_{eq,peak,literature}} \cdot 100 = 5.58\% \quad (3.71)$$

As the results show, the error decrease because the displacements of the cut boundary and so the boundary conditions of the submodel are more precise than the first type of submodel. The results obtained from the PSM with submodeling technique with a global element size equal to 0.2 mm, are subsequently inserted in the fatigue design PSM curve and compared with the results obtained from PSM Tetra 187.

Numerical results for 20 mm submodel

For an external applied pressure $\Delta\sigma_{nom} = 1MPa$, the results for weld toe and gusset for 20mm submodel are:

$$\Delta\sigma_{yy,weld-toe} = 2.17002MPa \quad (3.72)$$

$$\Delta\sigma_{11,weld-toe} = 2.20585MPa \quad (3.73)$$

$$\Delta\sigma_{yy,gusset} = 0.330816MPa \quad (3.74)$$

$$\Delta\sigma_{11,gusset} = 0.34869MPa \quad (3.75)$$

The equivalent peak stress are calculated by the formulae (2.23):

$$\Delta\sigma_{eq,peak,weld-toe} = \Delta\sigma_{\theta\theta,\theta=0,peak} \cdot f_{w1} = 2.17002 \cdot 1.834 = 3.979MPa \quad (3.76)$$

$$\Delta\sigma_{eq,peak,gusset} = \Delta\sigma_{\theta\theta,\theta=0,peak} \cdot f_{w1} = 0.330816 \cdot 1.182 = 0.391MPa \quad (3.77)$$

This result is not in good agreement with the value found in literature [33]:

$$\Delta\sigma_{eq,peak,literature} = 3.572MPa \quad (3.78)$$

Thus, the relative error expresses in percentage between the calculated $\Delta\sigma_{eq,peak}$ and the $\Delta\sigma_{eq,peak,literature}$ is:

$$\Delta\% = \frac{\Delta\sigma_{eq,peak,calculated} - \Delta\sigma_{eq,peak,literature}}{\Delta\sigma_{eq,peak,literature}} \cdot 100 = 11.40\% \quad (3.79)$$

This high relative error is due to the two issues above-mentioned (paragraph 3.1.1) relative to the definition of the cut boundary.

To reduce the error, a new submodel is created with a more fine mesh than before, with a global element size equal to 1 mm (Figure 3.48). The objective is to obtain a uniform cut boundary, indeed with the initial submodel the nodes of cut boundary, near to the weld toe, are characterised by a non converging displacements, also called singular displacements.

The procedure to create the new submodel is the same of previous one.

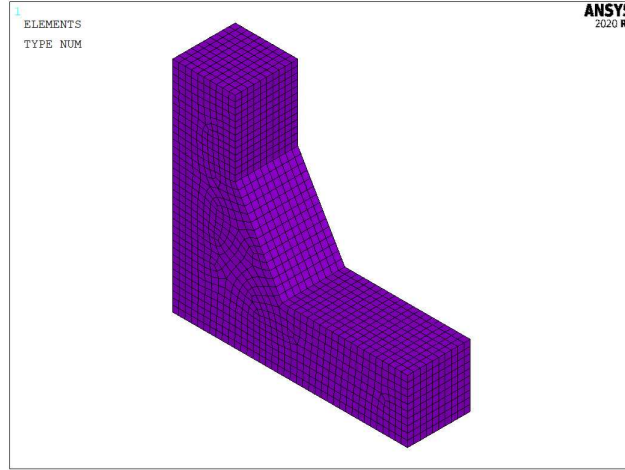


Figure 3.48: 10 mm submodel with global element size equal to 1 mm.

The results are:

$$\Delta\sigma_{yy,weld-toe} = 3.05506MPa \quad (3.80)$$

$$\Delta\sigma_{11,weld-toe} = 3.06593MPa \quad (3.81)$$

$$\Delta\sigma_{yy,gusset} = 0.418308MPa \quad (3.82)$$

$$\Delta\sigma_{11,gusset} = 0.4224MPa \quad (3.83)$$

$$\Delta\sigma_{eq,peak,weld-toe} = \Delta\sigma_{\theta\theta,\theta=0,peak} \cdot f_{w1} = 3.05506 \cdot 0.1.203 = 3.674MPa \quad (3.84)$$

$$\Delta\sigma_{eq,peak,gusset} = \Delta\sigma_{\theta\theta,\theta=0,peak} \cdot f_{w1} = 0.418308 \cdot 0.752 = 0.377MPa \quad (3.85)$$

$$\Delta\sigma_{eq,peak,literature} = 3.572MPa \quad (3.86)$$

$$\Delta\% = \frac{\Delta\sigma_{eq,peak,calculated} - \Delta\sigma_{eq,peak,literature}}{\Delta\sigma_{eq,peak,literature}} \cdot 100 = 2.86\% \quad (3.87)$$

As the results show, the relative error decreases and this approach has correctly foreseen the experimental crack initiation point at the weld toe, in according to the experimental reality. This results is due to that the PSM calibration constant $K_{FE}^* = 1.38 \pm 3\%$ is calibrated for a opening angle 2α lesser than 135° and in this case the value for weld toe ($2\alpha = 120^\circ$) is precise unlike the case of longitudinal joint FAT 71.

To decrease the relative error but with the initial global element size (3), a new submodel is created with a larger and greater cut boundary than the first submodel to obtain a converging displacements of the cut boundary nodes.

The procedure to create the new submodel is the same of previous one and the results is displayed on the following figure:

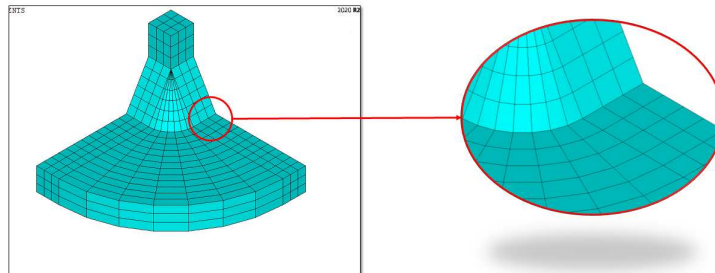


Figure 3.49: 20 mm submodel with a larger and greater cut boundary.

The results are:

$$\Delta\sigma_{yy,weld-toe} = 2.24836MPa \quad (3.88)$$

$$\Delta\sigma_{11,weld-toe} = 2.29424MPa \quad (3.89)$$

$$\Delta\sigma_{yy,gusset} = 0.796534MPa \quad (3.90)$$

$$\Delta\sigma_{11,gusset} = 0.835011MPa \quad (3.91)$$

$$\Delta\sigma_{eq,peak,weld-toe} = \Delta\sigma_{\theta\theta,\theta=0,peak} \cdot f_{w1} = 2.24836 \cdot 1.834 = 4.123MPa \quad (3.92)$$

$$\Delta\sigma_{eq,peak,gusset} = \Delta\sigma_{\theta\theta,\theta=0,peak} \cdot f_{w1} = 0.796534 \cdot 1.182 = 0.942MPa \quad (3.93)$$

$$\Delta\sigma_{eq,peak,literature} = 3.572MPa \quad (3.94)$$

$$\Delta\% = \frac{\Delta\sigma_{eq,peak,calculated} - \Delta\sigma_{eq,peak,literature}}{\Delta\sigma_{eq,peak,literature}} \cdot 100 = 15.42\% \quad (3.95)$$

As the results show, the error remains roughly constant. Thus, the best approach to obtain the minimum relative error is to reduce the global element size of the submodel. The results obtained from the PSM with submodeling technique with a global element size equal to 0.2 mm, are subsequently inserted in the fatigue design PSM curve and compared with the results obtained from PSM Tetra 187.

3.2.3 PSM approach Tetra 187

The fatigue assessment for these models are performed by the application of Peak Stress Method for 3D structures with the adoption of ten-node quadratic elements, considering only the weld toe.

The element SOLID 187 is chosen from the Ansys®APDL library with *Pure Displacement* as Key Option 1, which means that the nodal forces are only dependent on the displacements.

As defined in the paragraph 3.2.1, the model is prevailing subjected to mode I. Under mode I, the PSM requirements, with Tetra elements SOLID 187, are defined in the following table:

<i>Location: weld toe $2\alpha = 150^\circ$</i>			<i>Mode I</i>	
Element type	Mesh algorithm	$(a/d)_{min}$	2α	Mesh Pattern
Solid 187 KeyOpt:Pure Displacement	Free	1	150°	No particular indications

Table 3.21: Requirements for PSM with Tetra elements SOLID 187.

The mode I PSM calibration constant is calibrated at the weld toe where $2\alpha = 120^\circ$ and it is equal to $K_{FE}^* = 1.0901$.

To define the global element size of the 10 mm model, the following procedure is applied:

1. From literature the ratio $(a/d)_{min}$ is determined according to the *Table 3.21*. In this case the ratio for pure mode I is chosen and it is equal to 1;
2. The value of a is the reference dimension for selecting the maximal FE sizes d for PSM application and is defined as the half of the thickness t , so in this case is equal to 5 mm;
3. Subsequently, the minimum element size is defined as follow:

$$d_{min} = \frac{a}{1} = \frac{5}{1} = 5mm \quad (3.96)$$

4. The chosen dimension of elements is 1 mm

For the 20mm model, the size of the elements is obtained as following:

1. From literature the ratio $(a/d)_{min}$ is determined according to the *Table 3.21*. In this case the ratio for pure mode I is chosen and it is equal to 1;
2. The value of a is the reference dimension for selecting the maximal FE sizes d for PSM application and is defined as the half of the thickness t , so in this case is equal to 10 mm;
3. Subsequently, the minimum element size is defined as follow:

$$d_{min} = \frac{a}{3} = \frac{10}{1} = 10mm \quad (3.97)$$

4. The chosen dimension of elements is 1 mm

The λ_1 and e_1 values are depended on the opening angle 2α , that is 120° for the weld toe:

2α [°]	λ_1 (Mode I)	e_1 (Mode I)
120°	0.616	0.130

Table 3.22: Value of λ_1 and e_1 in function of the opening angle 2α

The corrective stress factors for mode I is calculated with the equation (2.24). The result is reported in the *Table 3.23*

$t=10$ mm	
2α [°]	f_{w1}
120	0.950
$t=20$ mm	
2α [°]	f_{w1}
120	0.950

Table 3.23: Value of the corrective stress factors f_{w1} in function of the opening angle 2α

Once the model is properly meshed, loaded and constraint, the system can be solved:

Solution → *Solve* → *Current LS*

3.2.4 PSM approach with Tetra 187: results

The method for the detection of the equivalent peak stress is characterized by the same considerations, procedure and dispositions of the previous longitudinal joints FAT 71 analysis, defined in the paragraph 3.1.3.

10 mm results

In this analysis, the structure is subjected to pure mode I loading, as describe in the paragraph 3.2.1, so the first principal stress range $\Delta\sigma_{11}$ can be approximated equal to local stress $\Delta\sigma_{yy}$, evaluated with a local reference system with the origin placed on the V-notch. To reduce the post-processing time, the first principal stress is replaced by $\Delta\sigma_{yy}$ and the results can be observed in the *Figure 3.50*, for an external applied pressure equal to 1 MPa:

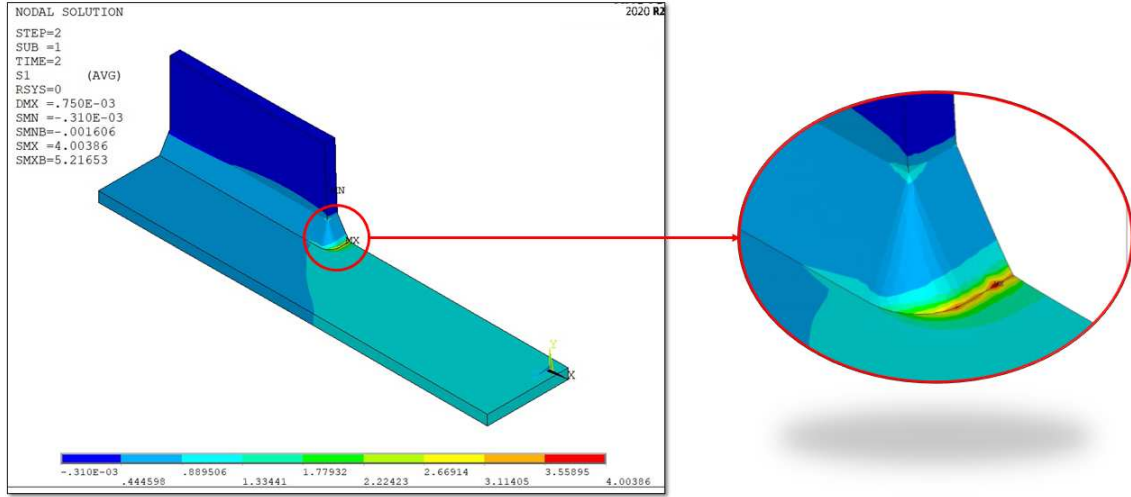


Figure 3.50: Plot of the first principal stress.

To obtain the trend of the nodal stress at the V-notch, the nodes attached to line that represents the weld toe (see Figure 3.51), is selected with the following commands:

Select → *Entities* → *Lines* → *From full*

Select → *Entities* → *Nodes* → *Attached to* → *Lines all*

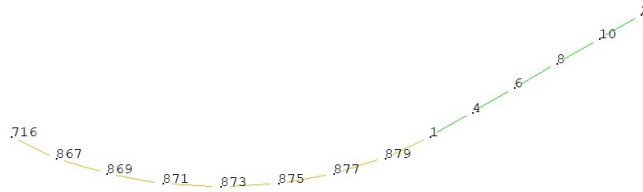


Figure 3.51: Selected nodes along the weld toe.

The results of the nodal tensions $\Delta\sigma_{11}$ and the relative average peak stress value are reported in the Appendix B.2.

For an external applied pressure $\Delta\sigma_{nom} = 1MPa$, the result at the weld toe is:

$$\overline{\Delta\sigma}_{11,weld-toe,peak} = 3.5503MPa \quad (3.98)$$

The equivalent peak stress are calculated by the formulae (2.23):

$$\Delta\sigma_{eq,peak,weld-toe} = \overline{\Delta\sigma}_{\theta\theta,\theta=0,peak} \cdot f_{w1} = 3.5503 \cdot 0.950 = 3.373MPa \quad (3.99)$$

This result is in good agreement with the value found in literature [33]:

$$\Delta\sigma_{eq,peak,literature} = 3.2747MPa \quad (3.100)$$

Thus, the relative error expresses in percentage between the calculated $\Delta\sigma_{eq,peak}$ and the $\Delta\sigma_{eq,peak,literature}$ is:

$$\Delta\% = \frac{\Delta\sigma_{eq,peak,calculated} - \Delta\sigma_{eq,peak,literature}}{\Delta\sigma_{eq,peak,literature}} \cdot 100 = 3.01\% \quad (3.101)$$

20 mm results

In this analysis, the structure is subjected to pure mode I loading, as describe in the paragraph 3.2.1,so the first principal stress range $\Delta\sigma_{11}$ can be approximated equal to local stress $\Delta\sigma_{yy}$, evaluated with a local reference system with the origin placed on the V-notch. To reduce the post-processing time, the first principal stress is replaced by $\Delta\sigma_{yy}$ and the results can be observed in the *Figure 3.52*, for an external applied pressure equal to 1 MPa:

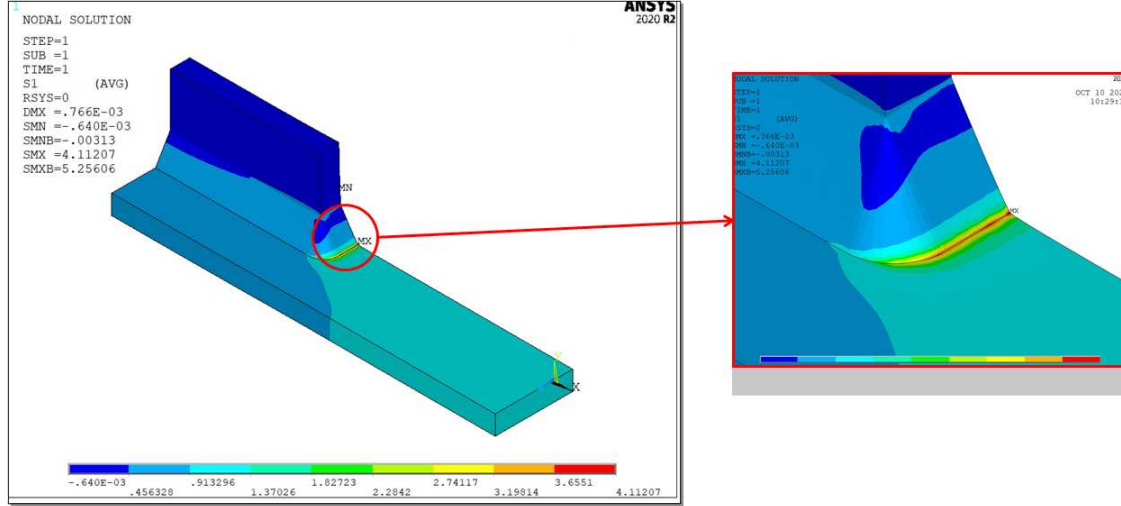


Figure 3.52: Plot of the first principal stress.

To obtain the trend of the nodal stress at the V-notch, the nodes attached to line that represents the weld toe (see *Figure3.53*), is selected with the same procedure described before.

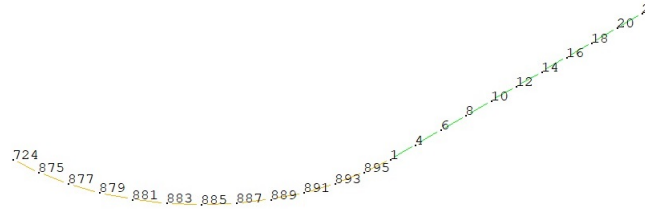


Figure 3.53: Selected nodes along the weld toe.

The results of the nodal tensions $\Delta\sigma_{11}$ and the relative average peak stress value are reported in the Appendix B.2.

For an external applied pressure $\Delta\sigma_{nom} = 1MPa$, the result at the weld toe is:

$$\overline{\Delta\sigma}_{11,weld-toe,peak} = 3.7781MPa \quad (3.102)$$

The equivalent peak stress are calculated by the formulae (2.23):

$$\Delta\sigma_{eq,peak,weld-toe} = \overline{\Delta\sigma}_{\theta\theta,\theta=0,peak} \cdot f_{w1} = 3.7781 \cdot 0.950 = 3589MPa \quad (3.103)$$

This result is in good agreement with the value found in literature [33]:

$$\Delta\sigma_{eq,peak,literature} = 3.572MPa \quad (3.104)$$

Thus, the relative error expresses in percentage between the calculated $\Delta\sigma_{eq,peak}$ and the $\Delta\sigma_{eq,peak,literature}$ is:

$$\Delta\% = \frac{\Delta\sigma_{eq,peak,calculated} - \Delta\sigma_{eq,peak,literature}}{\Delta\sigma_{eq,peak,literature}} \cdot 100 = 0.47\% \quad (3.105)$$

3.2.5 Data results for PSM curve

The previous model was characterised by a load equal to 1 MPa, applied to the main plate of the specimen; to obtain the value of the peak stress related to the applied nominal stress, the equation (3.24) is applied.

The results in terms of equivalent peak stress calculated with PSM Tetra 187 approach, are defined in the Appendix C.2.

The all experimental data are collected inside the PSM design curve proposed by Meneghetti, Guzzella and Atzori for structure subjected to prevailing mode I.

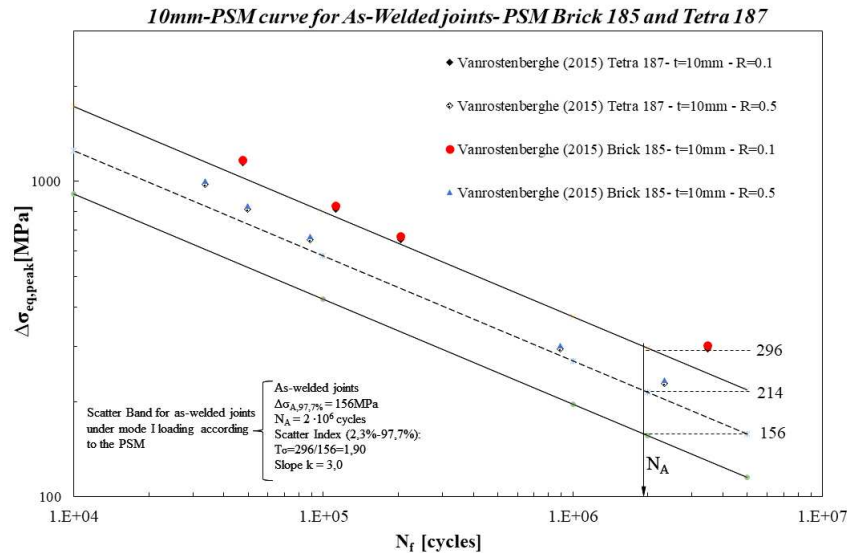


Figure 3.54: Experimental data inside the PSM design curve with Brick 185 and Tetra 185 elements for 10mm model.

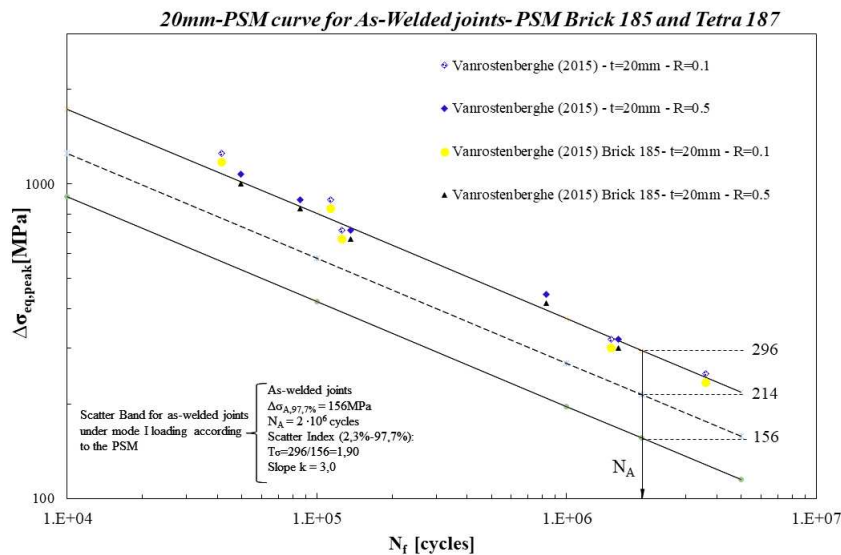


Figure 3.55: Experimental data inside the PSM design curve with Brick 185 and Tetra 185 elements for 20mm model.

The following conclusion can be defined:

1. The all experimental data fall above the lines that represents the 50% of probability of survival. Thus the PSM design curve has demonstrated to be effective and conservative;
2. The PSM Brick 185 approach have correctly foreseen the experimental crack initiation point at the weld toe. The best PSM Brick 185 approach is characterised by a submodel global element size equal to 0.2 mm for 10 mm model and to 1mm for 20 mm model. Indeed, with this method the relative error between the analytical results and literature results is acceptable.

3.2.6 SED (Strain Energy Density) approach

The fatigue assessment for these models are performed by the application of the Strain Energy Density approach.

The element SOLID 187 is chosen from the Ansys®APDL with *Pure Displacement* as Key Option 1, which means that the nodal forces are only dependent on the displacements.

First of all, the control volume is created and it is characterised by a 3-dimensional circular sector shape with radius equal to $R_0 = 0.28\text{mm}$ and the deep is 0.28mm (0.14 in the model due to the symmetry condition). The center of the control volume is placed at the weld toe for the both models (10 mm and 20 mm) as the figures below show:

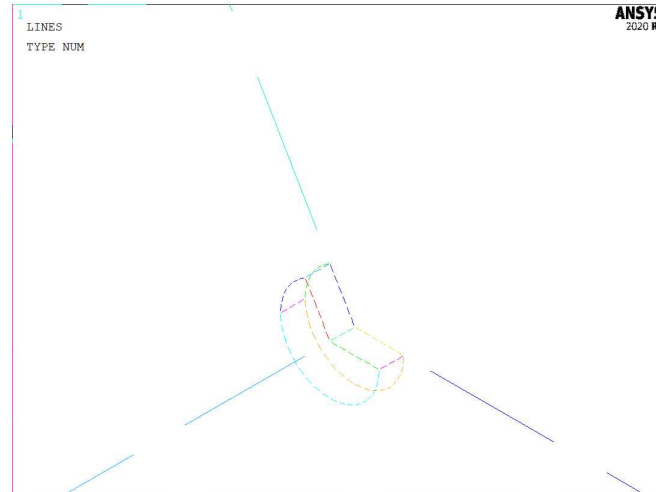


Figure 3.56: Control volume for the 10 mm model with the center at the V-notch tip.

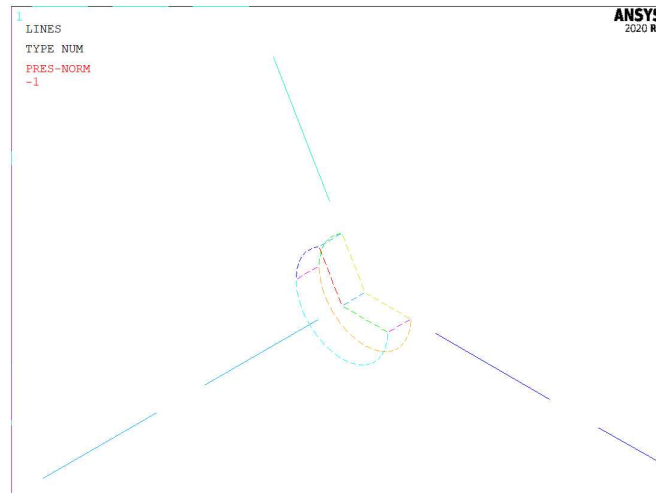


Figure 3.57: Control volume for the 20 mm model with the center at the V-notch tip.

The models with the control volume have been modelled inside *SOLIDWORKS 2020* and after they have been imported in Ansys®APDL with *.IGS* extension.

To create the mesh of the model, the procedure is the same for the 10 mm and 20 mm model and is characterised by the following steps:

1. The element inside the structural volume are characterised by a *global element size* equal to 0.05mm with a *free-mesh* algorithm;

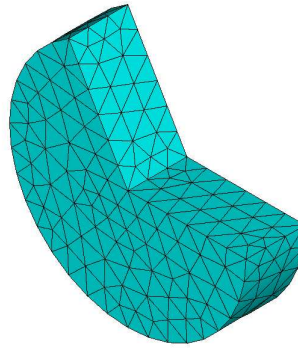


Figure 3.58: Mesh of the structural volume with global element size of 0.05, the structural volume is the same for 10 and 20 mm model.

2. The other volume is meshed with a global element size equal to 1 mm with a free-mesh algorithm.

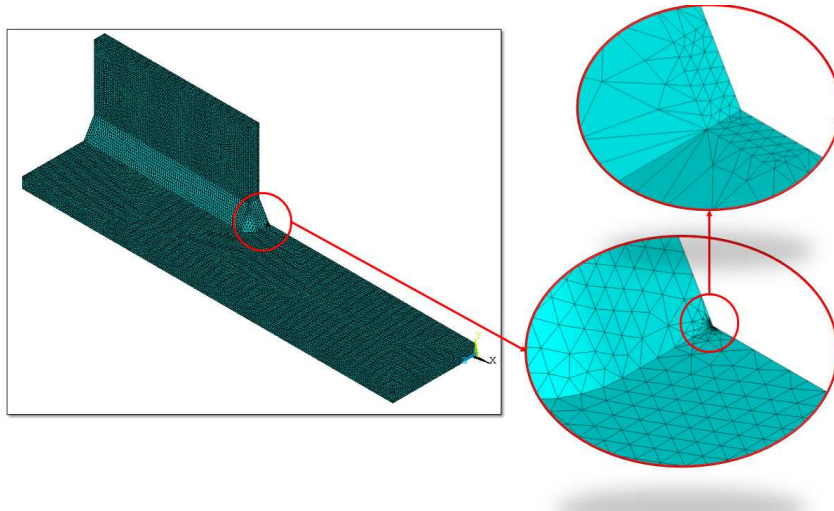


Figure 3.59: Mesh of the all 10 mm structure.

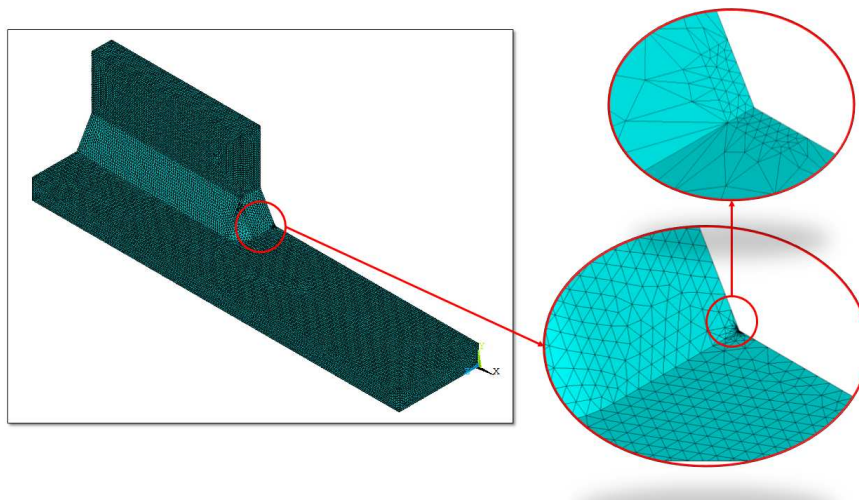


Figure 3.60: Mesh of the all 20 mm structure.

Once the model is properly meshed, loaded and constraint, the system can be solved:

Solution→*Solve*→*Current LS*

3.2.7 SED (Strain Energy Density) approach: results

Before the post-processing of the data, it is advised to disable the *PowerGraphics* option in Ansys®APDL toolbar, otherwise the output results are given by the average of only the superficial nodal stresses, without considering the inner ones.

The method for the detection of the SED (Strain Energy Density) is characterised by the same considerations, procedure and dispositions of the previous longitudinal joint FAT 71 analysis, defined in the paragraph 3.1.8

10 mm results

The result of SED for the 10 mm model weld toe when the specimen is subjected to a nominal stress of 1 MPa is:

$$SENE = 5.4255 \cdot 10^{-7} MJ \quad (3.106)$$

$$VOLU = 0.0229879 mm^3 \quad (3.107)$$

$$SED = \frac{SENE}{VOLU} = \frac{5.4255 \cdot 10^{-7}}{0.0229879} = 2.3602 \cdot 10^{-5} \frac{MJ}{m^3} \quad (3.108)$$

From the SED, the equivalent peak stress is obtained with the following formula:

$$\Delta\sigma_{eq,peak} = \sqrt{\frac{2 \cdot E \cdot SED}{1 - \nu^2}} = \sqrt{\frac{2 \cdot 206000 \cdot 2.3602 \cdot 10^{-5}}{1 - 0.3^2}} = 3.2689 MPa \quad (3.109)$$

This result is in good agreement with the value found in literature [33]:

$$\Delta\sigma_{eq,peak,literature} = 3.274 MPa \quad (3.110)$$

Thus, the relative error expresses in percentage between the calculated $\Delta\sigma_{eq,peak}$ and the $\Delta\sigma_{eq,peak,literature}$ is:

$$\Delta\% = \frac{\Delta\sigma_{eq,peak,calculated} - \Delta\sigma_{eq,peak,literature}}{\Delta\sigma_{eq,peak,literature}} \cdot 100 = -0.168\% \quad (3.111)$$

20 mm results

The result of SED for the 20 mm model weld toe when the specimen is subjected to a nominal stress of 1 MPa is:

$$SENE = 6.4728 \cdot 10^{-7} MJ \quad (3.112)$$

$$VOLU = 0.0229879 mm^3 \quad (3.113)$$

$$SED = \frac{SENE}{VOLU} = \frac{6.4728 \cdot 10^{-7}}{0.0229879} = 2.8157 \cdot 10^{-5} \frac{MJ}{m^3} \quad (3.114)$$

From the SED, the equivalent peak stress is obtained with the following formula:

$$\Delta\sigma_{eq,peak} = \sqrt{\frac{2 \cdot E \cdot SED}{1 - \nu^2}} = \sqrt{\frac{2 \cdot 206000 \cdot 2.8157 \cdot 10^{-5}}{1 - 0.3^2}} = 3.5705 MPa \quad (3.115)$$

This result is in good agreement with the value found in literature [33]:

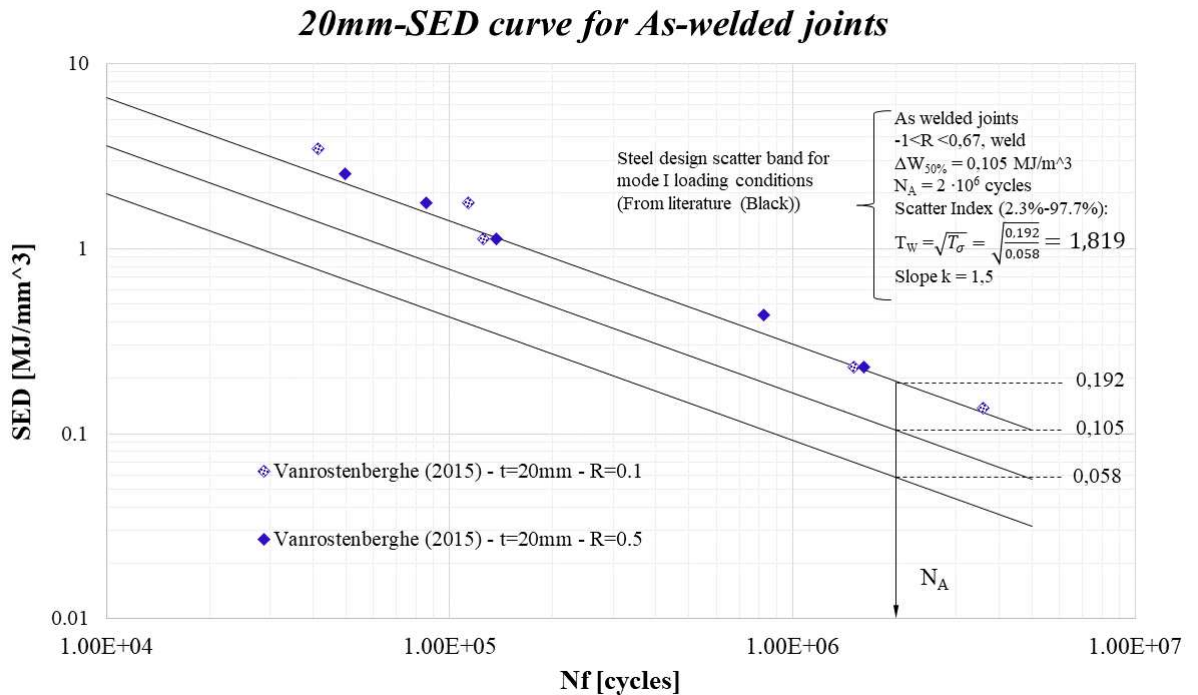
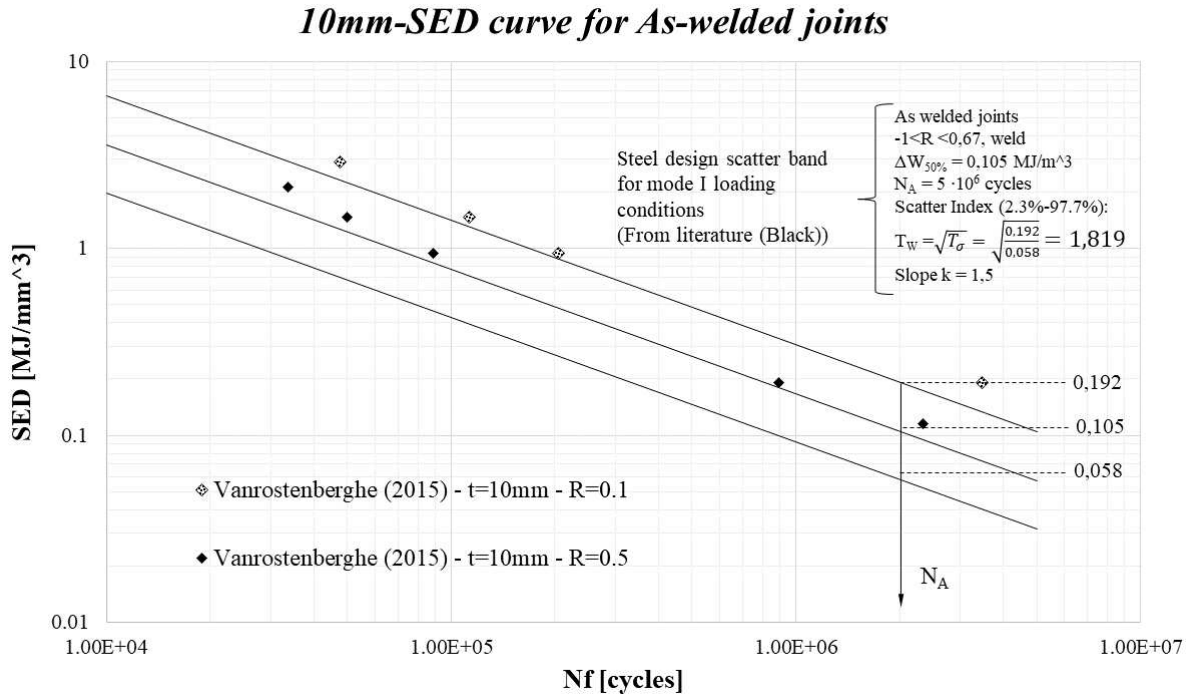
$$\Delta\sigma_{eq,peak,literature} = 3.572 MPa \quad (3.116)$$

Thus, the relative error expresses in percentage between the calculated $\Delta\sigma_{eq,peak}$ and the $\Delta\sigma_{eq,peak,literature}$ is:

$$\Delta\% = \frac{\Delta\sigma_{eq,peak,calculated} - \Delta\sigma_{eq,peak,literature}}{\Delta\sigma_{eq,peak,literature}} \cdot 100 = -0.049\% \quad (3.117)$$

3.2.8 Data results for SED curve

The previous model was characterised by a load equal to 1 MPa, applied to the main plate of the specimen; to obtain the value of the peak stress related to the applied nominal stress, the equation (3.32) is applied. The results in terms of SED are defined in the Appendix C.2. The all experimental data are collected inside the SED design curve proposed by Lazzarin and Zambarandi:



The following conclusion can be defined:

1. The all experimental data fall above the lines that represents the 50% of probability of survival. Thus the PSM design curve has demonstrated to be effective and conservative;
2. The SED approach find results that are in according with the literature and it has correctly foreseen the experimental crack initiation point at weld toe.

3.2.9 SHSS (Structural Hot Spot Stress) approach

The fatigue assessment for these models are performed by the application of SHSS approach, following the IIW recommendation [1] to obtain the hot-spot stress. According to the guideline, the weld toe of the longitudinal stiffener FAT 63 is a hot-spot type *a* and the hot-spot stress value is detected with the employment of fine mesh, as *Figure 1.4* shows.

The models of the longitudinal stiffener FAT 63 10 mm and 20 mm are divided in a series of volumes to allow the application of *Mapped-mesh* algorithm; indeed each volumes must be characterised by a number of face between 4 and 6 to obtain a *Mapped-mesh*. The eight-node linear element SOLID 185 is chosen in Ansys®APDL with *Simple Enhanced Strain* as Key Option 1.

10 mm model

The all informations about the mesh for 10mm model is reported in the following table:

Element type	Mesh algorithm	Main plate thickness <i>t</i>	Max element size	Adopted element size
Solid 185 KeyOpt:Simple Enhanced Strain	Mapped	10 mm (5 mm modelled)	$0.4 \cdot t =$ $0.4 \cdot 10 = 4mm$	2 mm

Table 3.24: Requirements for SHSS mesh.

The hot-spot stress is extrapolated at two reference points placed at $0.4t$ and $1.0t$ distane from the weld toe tip, so in this case at 4 mm and 10 mm from weld toe.

For the type of extrapolated stress, the graph in *Figure 3.63* shows that, for an external applied pressure $\Delta\sigma_{nom} = 1MPa$, after 1.95 mm, the $\Delta\sigma_{xx}$ and the first principal stress $\Delta\sigma_{11}$ are coincident. For this reason the choice is indifferent.

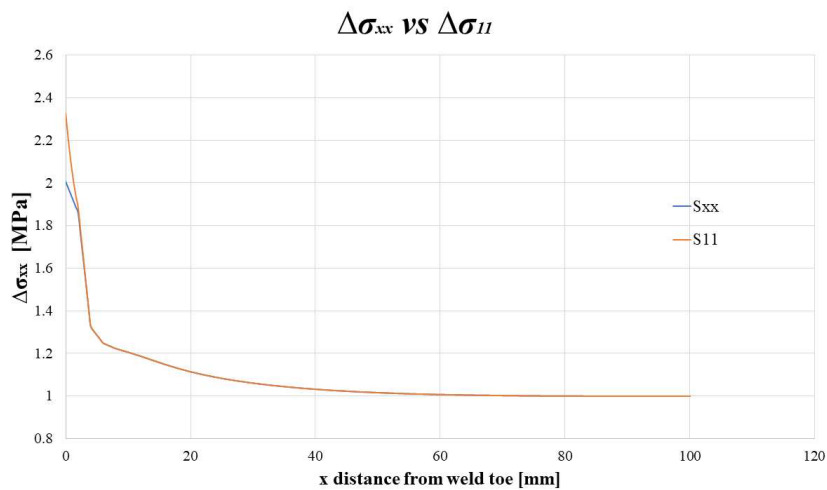


Figure 3.63: $\Delta\sigma_{xx}$ and $\Delta\sigma_{yy}$ plotted in function of the distance from weld toe tip

The mesh of the model is reported in the following figures:

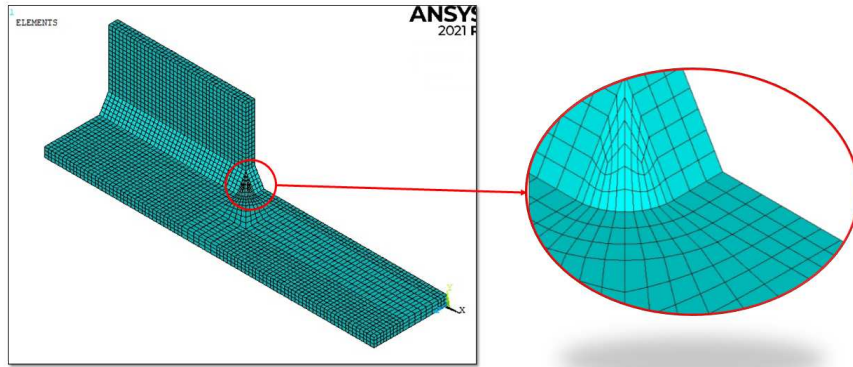


Figure 3.64: Mapped mesh for SHSS approach

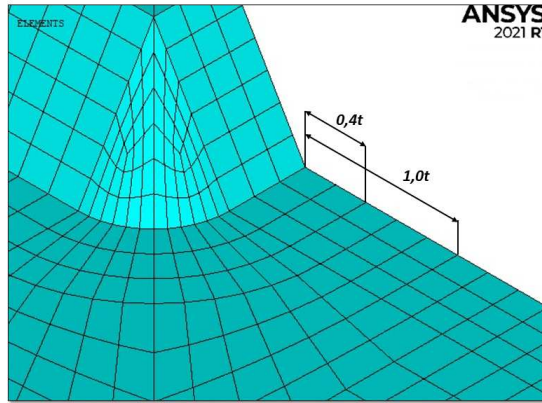


Figure 3.65: Mapped mesh for SHSS approach and reference points

Before the post-processing of the data, it is advised to disable the *PowerGraphics* option in Ansys®APDL toolbar, otherwise the output results are given by the average of only the superficial nodal stresses, without considering the inner ones.

For an external applied pressure $\Delta\sigma_{nom} = 1MPa$, the results of the tension at the reference points are:

$$\Delta\sigma_{xx,0.4t} = 1.3246MPa \quad (3.118)$$

$$\Delta\sigma_{xx,1.0t} = 1.20659MPa \quad (3.119)$$

$$\Delta\sigma_{11,0.4t} = 1.32561MPa \quad (3.120)$$

$$\Delta\sigma_{11,1.0t} = 1.20673MPa \quad (3.121)$$

$$(3.122)$$

The structural hot-spot stress is detected with the equation 1.2:

$$\Delta SHSS_{LSE,xx} = 1,67 \cdot \sigma_{xx,0.4t} - 0.67 \cdot \sigma_{xx,1.0t} = 1.67 \cdot 1.3246 - 0.67 \cdot 1.20659 = 1.4037MPa \quad (3.123)$$

$$\Delta SHSS_{LSE,11} = 1,67 \cdot \sigma_{11,0.4t} - 0.67 \cdot \sigma_{11,1.0t} = 1.67 \cdot 1.32561 - 0.67 \cdot 1.20673 = 1.4053MPa \quad (3.124)$$

This result is in good agreement with the value found in literature [33]:

$$\Delta\sigma_{xx,0.4t} = 1.312MPa \quad (3.125)$$

$$\Delta\sigma_{xx,1.0t} = 1.205MPa \quad (3.126)$$

$$(3.127)$$

$$\Delta SHSS_{LSE,literature} = 1,384MPa$$

Thus, the relative errors expresses in percentage between the calculated $\Delta SHSS_{LSE,xx}$, $\Delta SHSS_{LSE,11}$ and the $\Delta SHSS_{LSE,literature}$ are:

$$\Delta\% = \frac{\Delta SHSS_{LSE,xx} - \Delta SHSS_{LSE,literature}}{\Delta SHSS_{LSE,literature}} \cdot 100 = 1.44\% \quad (3.128)$$

$$\Delta\% = \frac{\Delta SHSS_{LSE,11} - \Delta SHSS_{LSE,literature}}{\Delta SHSS_{LSE,literature}} \cdot 100 = 1.56\% \quad (3.129)$$

20 mm model

The all informations about the mesh for 10mm model is reported in the following table:

Element type	Mesh algorithm	Main plate thickness t	Max element size	Adopted element size
Solid 185 KeyOpt:Simple Enhanced Strain	Mapped	20 mm (10 mm modelled)	$0.4 \cdot t = 0.4 \cdot 20 = 8mm$	2 mm

Table 3.25: Requirements for SHSS mesh.

The hot-spot stress is extrapolated at two reference points placed at $0.4t$ and $1.0t$ distance from the weld toe tip, so in this case at 8 mm and 20 mm from weld toe.

For the type of extrapolated stress, the graph in *Figure 3.66* shows that, for an external applied pressure $\Delta\sigma_{nom} = 1MPa$, after 1.95 mm, the $\Delta\sigma_{xx}$ and the first principal stress $\Delta\sigma_{11}$ are coincident. For this reason the choice is indifferent.

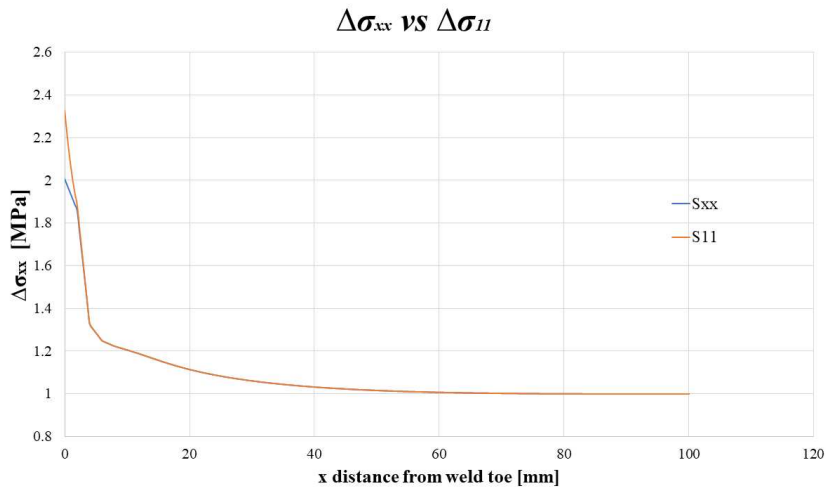


Figure 3.66: $\Delta\sigma_{xx}$ and $\Delta\sigma_{yy}$ plotted in function of the distance from weld toe tip

The mesh of the model is reported in the following figures:

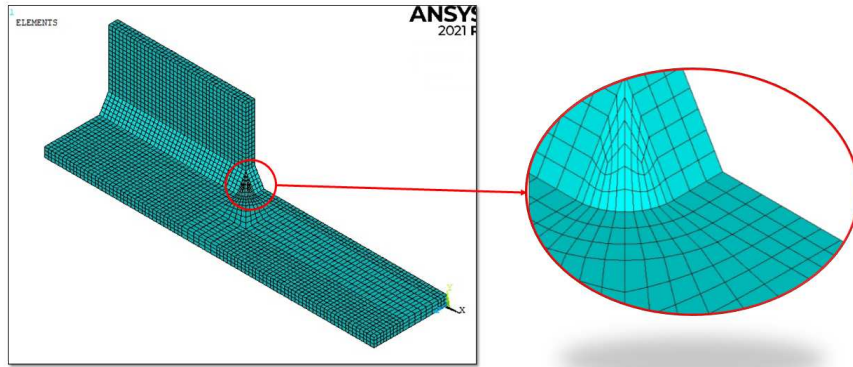


Figure 3.67: Mapped mesh for SHSS approach

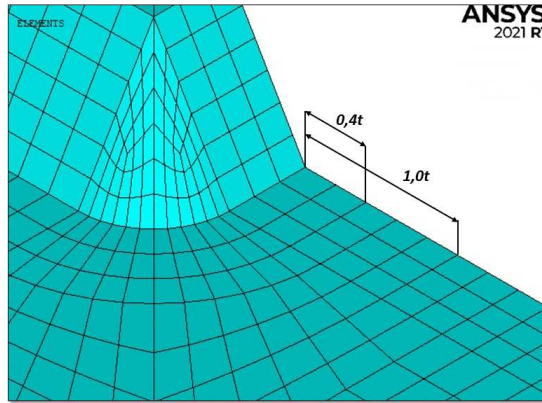


Figure 3.68: Mapped mesh for SHSS approach and reference points

Before the post-processing of the data, it is advised to disable the *PowerGraphics* option in Ansys®APDL toolbar, otherwise the output results are given by the average of only the superficial nodal stresses, without considering the inner ones.

For an external applied pressure $\Delta\sigma_{nom} = 1MPa$, the results of the tension at the reference points are:

$$\Delta\sigma_{xx,0.4t} = 1.15154MPa \quad (3.130)$$

$$\Delta\sigma_{xx,1.0t} = 1.08205MPa \quad (3.131)$$

$$\Delta\sigma_{11,0.4t} = 1.15175MPa \quad (3.132)$$

$$\Delta\sigma_{11,1.0t} = 1.08207MPa \quad (3.133)$$

$$(3.134)$$

The structural hot-spot stress is detected with the equation 1.2:

$$\Delta SHSS_{LSE,xx} = 1,67 \cdot \sigma_{xx,0.4t} - 0,67 \cdot \sigma_{xx,1.0t} = 1,67 \cdot 1.15154 - 0,67 \cdot 1.08205 = 1.1981MPa \quad (3.135)$$

$$\Delta SHSS_{LSE,11} = 1,67 \cdot \sigma_{11,0.4t} - 0,67 \cdot \sigma_{11,1.0t} = 1,67 \cdot 1.15175 - 0,67 \cdot 1.08207 = 1.1984MPa \quad (3.136)$$

This result is in good agreement with the value found in literature [33]:

$$\Delta\sigma_{xx,0.4t} = 1.154MPa \quad (3.137)$$

$$\Delta\sigma_{xx,1.0t} = 1.082MPa \quad (3.138)$$

$$(3.139)$$

$$\Delta SHSS_{LSE,literature} = 1,202MPa$$

Thus, the relative errors expresses in percentage between the calculated $\Delta SHSS_{LSE,xx}$, $\Delta SHSS_{LSE,11}$ and the $\Delta SHSS_{LSE,literature}$ are:

$$\Delta\% = \frac{\Delta SHSS_{LSE,xx} - \Delta SHSS_{LSE,literature}}{\Delta SHSS_{LSE,literature}} \cdot 100 = -0.345\% \quad (3.140)$$

$$\Delta\% = \frac{\Delta SHSS_{LSE,11} - \Delta SHSS_{LSE,literature}}{\Delta SHSS_{LSE,literature}} \cdot 100 = -0.316\% \quad (3.141)$$

3.2.10 Data results for IIW curve

Nominal stress approach

The results are reported in terms of nominal stress, defined in the beginning of paragraph 3.2, inside the FAT 63 curve proposed by IIW guideline [1]:

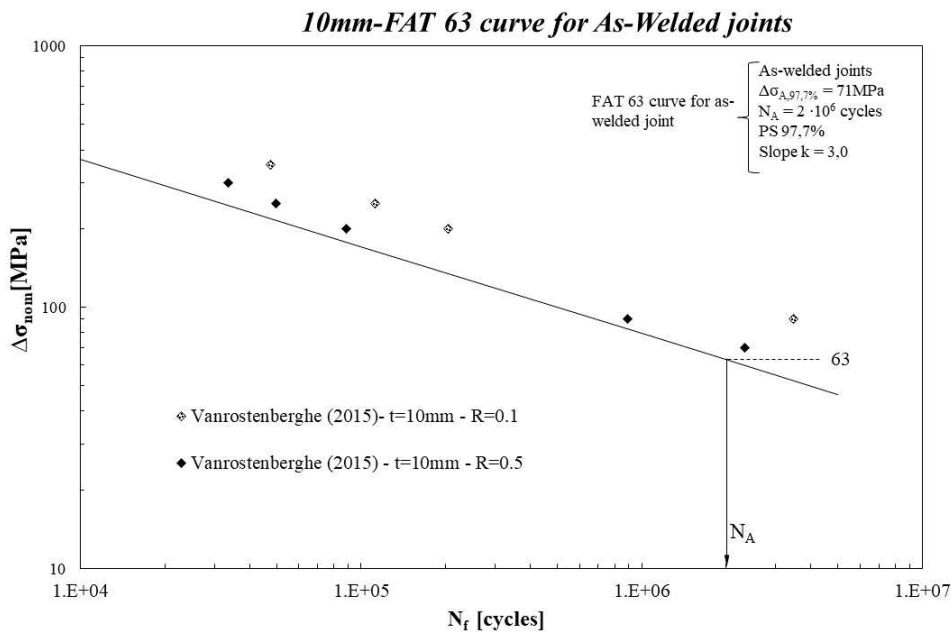


Figure 3.69: Experimental data inside the IIW nominal stress design curve.

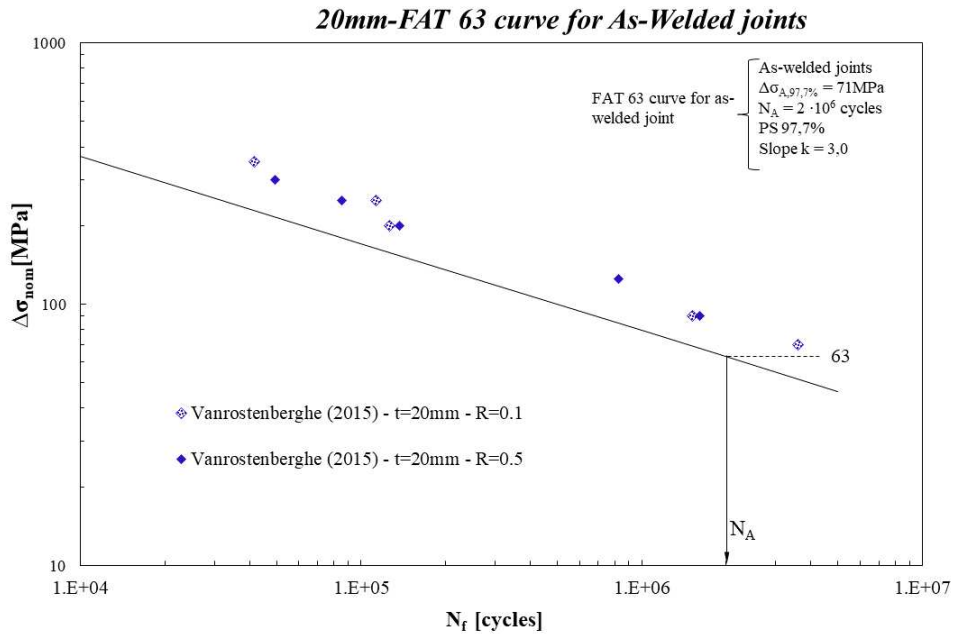


Figure 3.70: Experimental data inside the IIW nominal stress design curve.

SHSS approach

The previous model was characterised by a load equal to 1 MPa, applied to the main plate of the specimen; to obtain the value of the hot-spot stress related to the applied nominal stress, the equation (3.45) is applied.

The results in terms of SHSS are defined in the Appendix C.2.

The all experimental data are collected inside the SHSS design curve proposed by IIW guideline:

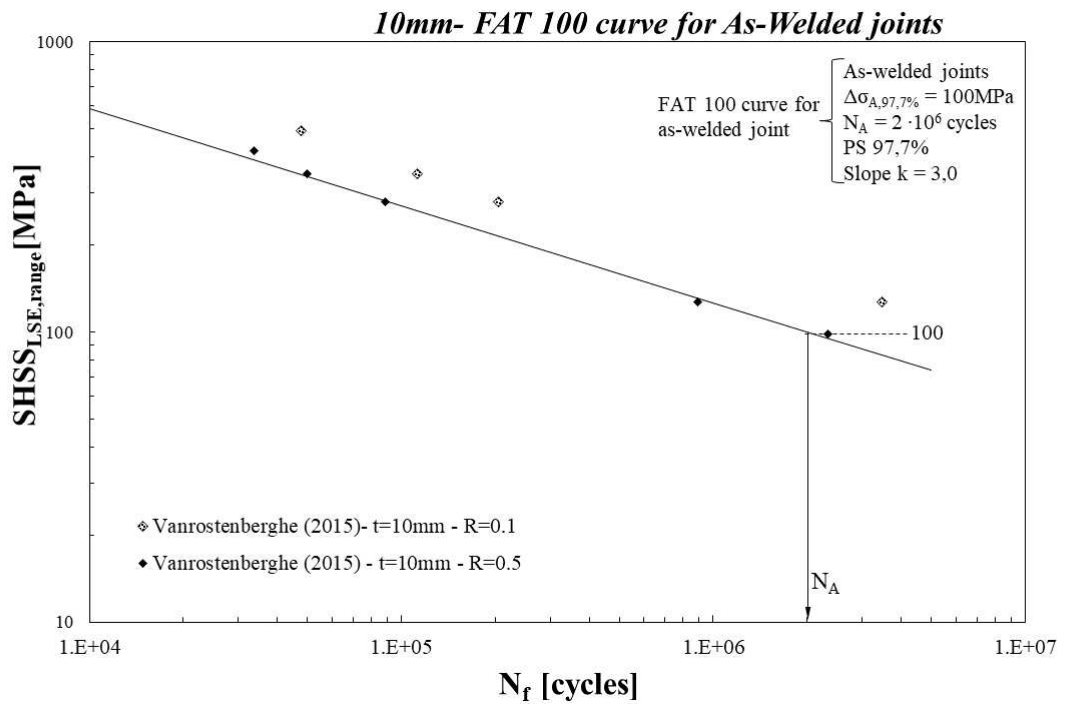


Figure 3.71: Experimental data inside the SHSS design curve.

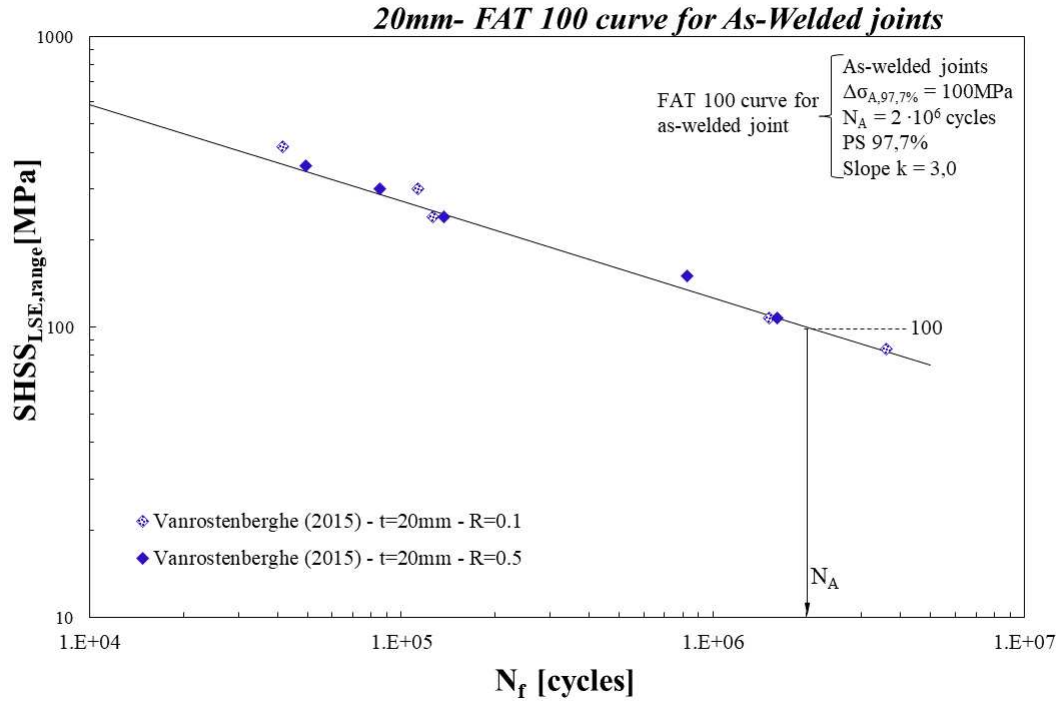


Figure 3.72: Experimental data inside the SHSS design curve.

The following conclusion can be defined:

1. These approaches have correctly been applied to FAT 63 welded joint, for weld toe fractures;
2. The nominal stress approach is characterised by the fact that all points fall above the lines that represents the 97.7% of probability of survival. For this reason, the nominal stress approach has proven to be conservative as the others methods;
3. The hot-spot stress method is characterised by the fact that some points fall below the lines that represents the 97.7% of probability of survival. For this reason, the SHSS approach has not proven to be conservative as the others methods.

3.3 Yildirim 2020, transverse attachment FAT 80

The third joint analysed is a transverse attachment characterised by a fatigue class FAT 80, studied by Yildirim in 2020 [18] under CAL (Constant Amplitude Loading).

The principal information and mechanical properties about this typology of the joint are summarized in the Table 3.26 and Table 3.27:

Weld condition	Fracture location	Load application	Main plate/gusset thickness
As-welded, non-load carrying (NLC), full penetration	Weld toe	Axial, main plate, parent material	Main plate: 6mm Gusset: 6mm

Table 3.26: Information about the specimens

Material model	Yield strength f_y [MPa]	Young modulus [MPa]	Poisson's ratio ν
AH36, HSS, Linear elastic, isotropic	392	206000	0.3

Table 3.27: Information about mechanical properties

The dimensions of this joint are defined in the following table and figure:

t [mm]	b [mm]	w [mm]	L [mm]	h [mm]	2α [°]	z [mm]
6	6	40	600	40	135	5.50

Table 3.28: Dimension of the transverse attachment FAT 80, studied by Yildirim in 2020.

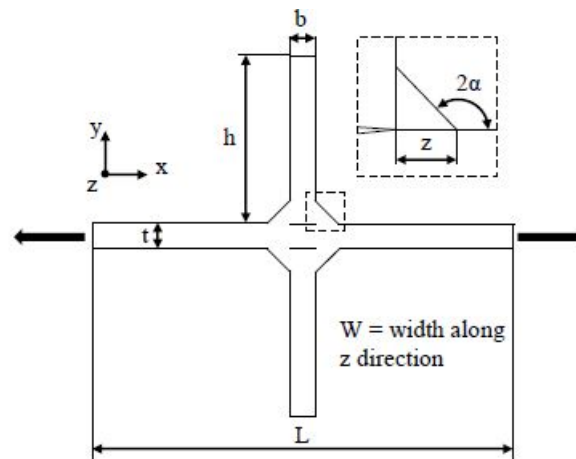


Figure 3.73: Yildirim 2020, transverse attachment FAT 80 [33].

The parameters of the weld profile is described in the following table:

ρ weld toe tip [mm]	Weld leg [mm]	Weld flack angle [°]	2α
$\cong 0$	5.50	45	Weld toe: 135° Gusset: 135°

Table 3.29: Information about the weld profile

The radius ρ of the weld toe is lower than 1.5mm, so the assumption of a sharp V-notch ($\rho = 0mm$) at the weld toe is acceptable with the non conventional LEFM extension to welded joints. The effect of misalignment can not be neglected in transverse joint, however in this first analysis it is neglected. The experimental data are defined in the following table in terms of nominal stress $\Delta\sigma_{nom}$:

Stress Ratio R	$\Delta\sigma_{nom}$ [MPa]	N_f [cycles]
0.1	153	827502
	190	334910
	153	837466
	190	383736
	117	11700000
	125	10052008
-0.46	190	608805
	243	201094
	153	1723400
	243	217785
	190	710346
	136	10122344

Table 3.30: Experimental data of the 3rd joint, Yildirim 2020. The number barred represents the run-outs

Yildirim FAT 80 is modelled in *SOLIDWORKS 2020* and subsequently, is imported inside Ansys®APDL with *.IGS* extension. The results is reported in the figure below:

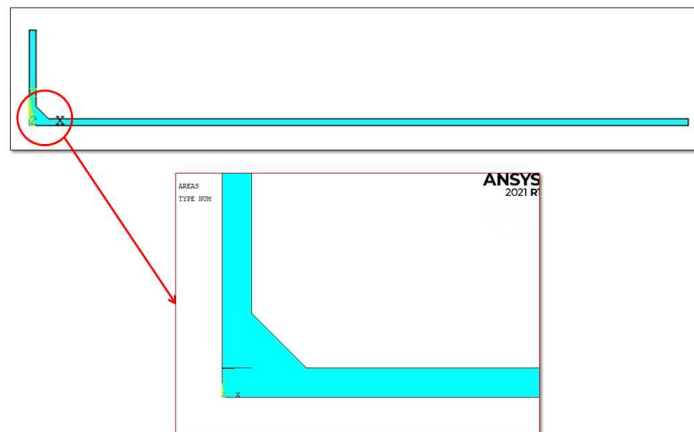


Figure 3.74: Model of transverse attachment FAT 80, studied by Yildirim in 2020.

The modelling procedure in Ansys®APDL is briefly described:

- Thanks to the double symmetry of the longitudinal stiffener, only 1/4 of the geometry is modelled to reduce the computational time;
- A root has been created and it is characterized by a initial opening length equal to 0.1mm;
- The first joint is subjected to an axial load and it is applied on the main plate as a constant pressure equal to $p = \Delta\sigma_{nom}$, on the Line L2 as *Figure 3.75* shows;
- Symmetry boundary conditions are applied on the lines L1, L7 and L10(*Figure 3.76*).



Figure 3.75: Load of the model of transverse attachment FAT 80, studied by Yildirim in 2020.

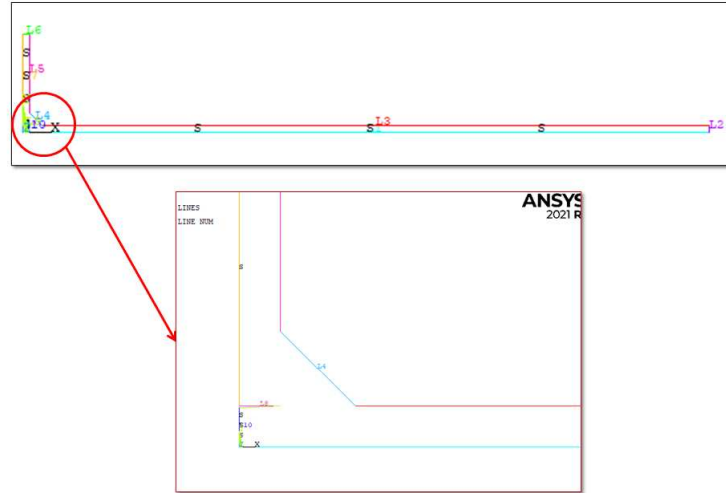


Figure 3.76: Symmetry condition of the model of transverse attachment FAT 80 studied by Yildirim in 2020.

3.3.1 PSM approach Plane 182

The fatigue assessment for this model is performed by the application of Peak Stress Method for 2D structures with the adoption of four-node linear elements.

The element PLANE 182 is chosen from the Ansys®APDL library with *Simple Enhanced Strain* as Key Option 1 and *Plane Strain* as Key Option 3.

The model is prevailing subjected to mode I at the attachment edge with a opening angle 2α equal to 135° . Indeed, referring to the graph of the Williams eigenvalues trend in *Figure 1.13*, mode II is not singular for V-notch opening angle greater than 102.5° , so $\lambda_2 = 0$; the mode III can be neglected because is irrelevant.

Under mode I, the PSM requirements, with Tetra elements PLANE 182, are define in the following table:

Element type	Mesh algorithm	Mode I			
		$(a/d)_{min}$	2α	Mesh Pattern $2\alpha < 90^\circ$	Mesh Pattern $2\alpha > 90^\circ$
Plane 182 KeyOpt: <i>Simple Enhanced Strain</i> + <i>Plane Strain</i>	Free	3	$0^\circ < 2\alpha < 135^\circ$	Four adjacent elements share the same node	Two adjacent elements share the same node

Table 3.31: Requirements for PSM.

The mode I PSM calibration constant is calibrated at the weld toe where $2\alpha = 135^\circ$ and it is equal to $K_{FE}^* = 1.38 \pm 3\%$.

To define the global element size of the model, the following procedure is applied:

1. From literature the ratio $(a/d)_{min}$ is determined according to the *Table 3.31*. In this case the ratio for pure mode I is chosen and it is equal to 3;
2. The value of a is the reference dimension for selecting the maximal FE sizes d for PSM application and is defined as the half of the thickness t , so in this case is equal to 3 mm;

3. Subsequently, the minimum element size is defined as follow:

$$d_{min} = \frac{a}{3} = \frac{3}{3} = 1mm \quad (3.142)$$

4. The chosen dimension of elements is 1 mm

The λ_1 and e_1 values are depended on the opening angle 2α , that is 135° for the weld toe:

2α [°]	λ_1 (Mode I)	e_1 (Mode I)
135°	0.674	0.117

Table 3.32: Value of λ_1 and e_1 in function of the opening angle 2α

The corrective stress factors for mode I is calculated with the equation (2.24). The result is reported in the Table 3.33

2α [°]	f_{wI}
135°	1.06

Table 3.33: Value of the corrective stress factors f_{wI} in function of the opening angle 2α

Once the model is properly meshed, loaded and constraint, the system can be solved:

Solution → *Solve* → *Current LS*

3.3.2 PSM approach with Plane 182: results

In this analysis, the structures are subjected to pure mode I loading, so in these situations it can be demonstrated that, in the case that the stress flow is aligned with the external pressure direction, the first principal stress range $\Delta\sigma_{11}$ can be approximated equal to local stress $\Delta\sigma_{yy}$, evaluated with a local reference system with the origin placed on the V-notch. However, to obtain a more precise results, a local reference system is created on the node that represents the weld toe with the same procedure described in the paragraph 2.2.1 (see Figure 3.77).

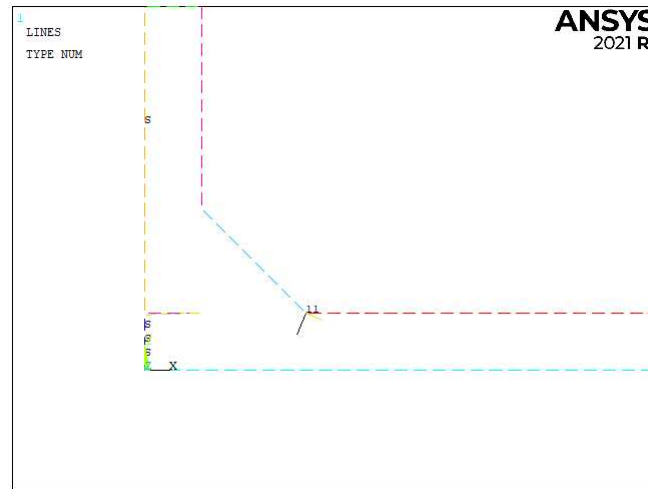


Figure 3.77: Local reference system with the origin at the weld toe.

During the analysis of the results, the first principal stress is evaluated and compared with $\Delta\sigma_{yy}$. The results of the first principal stress can be observed in the Figure 3.78, for an external applied pressure equal to 1 MPa:

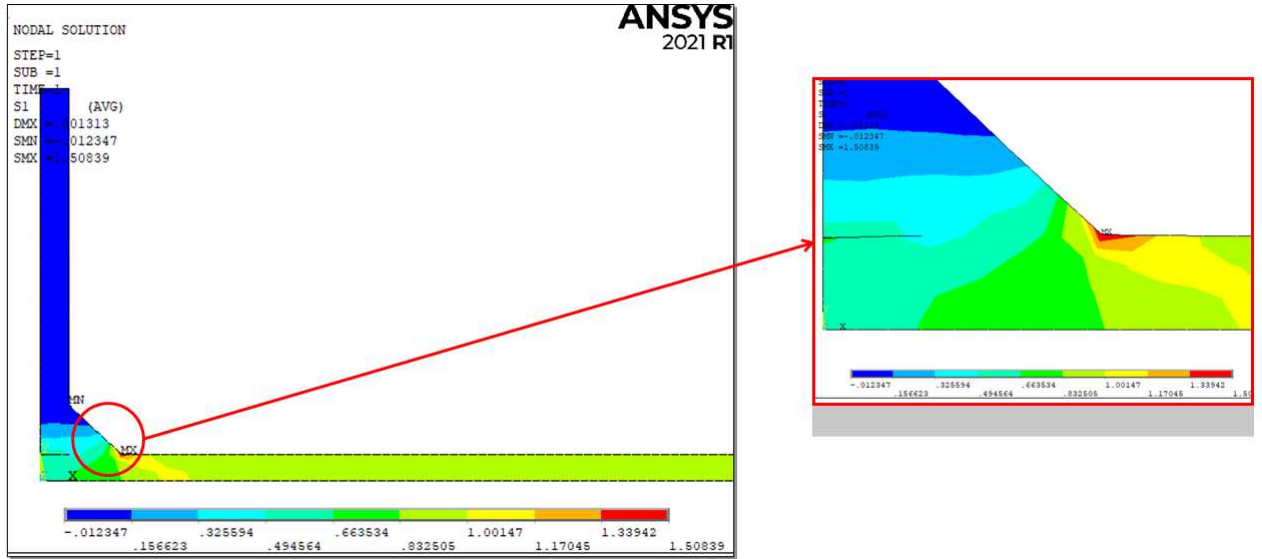


Figure 3.78: Plot of the first principal stress.

For an external applied pressure $\Delta\sigma_{nom} = 1MPa$, the result at the weld toe is:

$$\overline{\Delta\sigma}_{yy,weld-toe,peak} = 1.49156MPa \quad (3.143)$$

$$\overline{\Delta\sigma}_{11,weld-toe,peak} = 1.50839MPa \quad (3.144)$$

$$(3.145)$$

The equivalent peak stress are calculated by the formulae (2.23):

$$\Delta\sigma_{eq,peak,weld-toe} = \overline{\Delta\sigma}_{\theta\theta,\theta=0,peak} \cdot f_{w1} = 1.49156 \cdot 1.06 = 1.5985MPa \quad (3.146)$$

This result is in good agreement with the value found in literature [33]:

$$\Delta\sigma_{eq,peak,literature} = 1.620MPa \quad (3.147)$$

Thus, the relative error expresses in percentage between the calculated $\Delta\sigma_{eq,peak}$ and the $\Delta\sigma_{eq,peak,literature}$ is:

$$\Delta\% = \frac{\Delta\sigma_{eq,peak,calculated} - \Delta\sigma_{eq,peak,literature}}{\Delta\sigma_{eq,peak,literature}} \cdot 100 = -1.37\% \quad (3.148)$$

3.3.3 Data results for PSM curve

The previous model was characterised by a load equal to 1 MPa, applied to the main plate of the specimen; to obtain the value of the peak stress related to the applied nominal stress, the equation (3.24) is applied.

The results in terms of equivalent peak stress calculated with PSM Plane 182 approach, are defined in the Appendix C.3.

The all experimental data are collected inside the PSM design curve proposed by Meneghetti and Lazzarin for structure subjected to prevailing mode I.

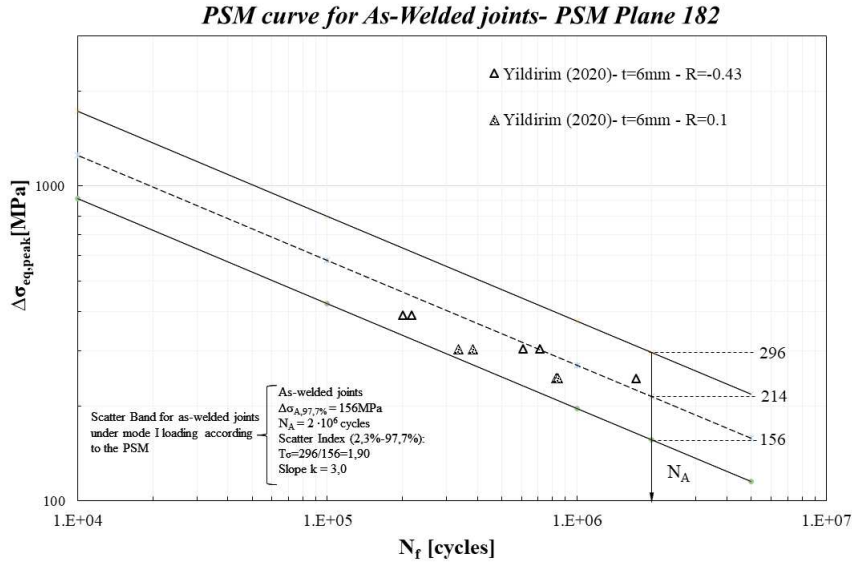


Figure 3.79: Experimental data inside the PSM design curve with Plane 182 elements.

The following conclusion can be defined:

1. The all experimental data fall above the lines that represents the 97.7% of probability of survival. Thus the PSM design curve has demonstrated to be effective and conservative;
2. The PSM Plane 182 approach have correctly foreseen the experimental crack initiation point at the weld toe.

3.3.4 SHSS (Structural Hot Spot Stress) approach

The fatigue assessment for this model is performed by the application of SHSS approach, following the IIW recommendation [1] to obtain the hot-spot stress. According to the guideline, the weld toe of the transverse attachment FAT 80 studied by Yildirim in 2020, is a hot-spot type *a* and the hot-spot stress value is detected with the employment of fine mesh, as *Figure 1.4* shows.

The model is divided in a series of areas to allow the application of *Mapped-mesh* algorithm; indeed each areas must be characterised by a number of side between 3 and 4 to obtain a *Mapped-mesh*. The eight-node linear element PLANE 182 is chosen in Ansys®APDL with *Simple Enhanced Strain* as Key Option 1 and *Plane Strain* as Key Option 3.

The all informations about the mesh is reported in the following table:

Element type	Mesh algorithm	Main plate thickness <i>t</i>	Max element size	Adopted element size
Plane 182 KeyOpt: <i>Simple Enhanced Strain</i> + <i>Plane Strain</i>	Mapped	6 mm (3 mm modelled)	$0.4 \cdot t = 0.4 \cdot 6 = 2.4 \text{ mm}$	1.2 mm

Table 3.34: Requirements for SHSS mesh.

The hot-spot stress is extrapolated at two reference points placed at $0.4t$ and $1.0t$ distance from the weld toe tip, so in this case at 2.4 mm and 6 mm from weld toe.

For the type of extrapolated stress, the graph in *Figure 3.80* shows that, for an external applied pressure $\Delta\sigma_{nom} = 1 \text{ MPa}$, after 1.50 mm, the $\Delta\sigma_{xx}$ and the first principal stress $\Delta\sigma_{I1}$ are coincident. For this reason the choice is indifferent.

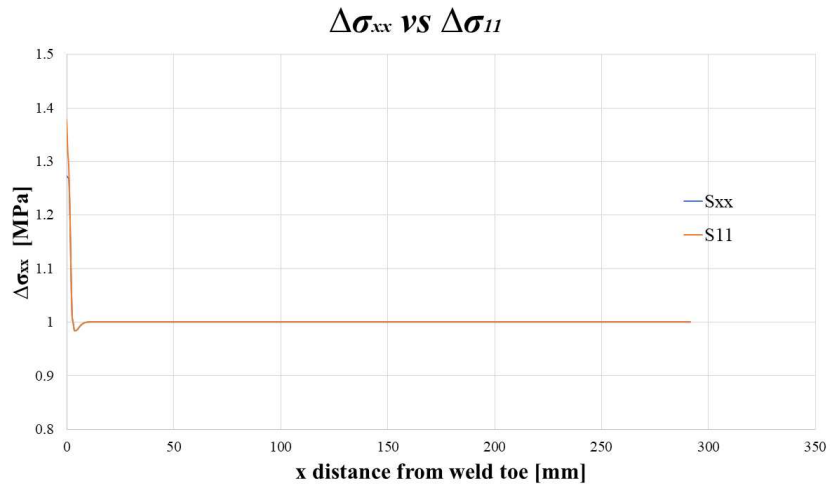


Figure 3.80: $\Delta\sigma_{xx}$ and $\Delta\sigma_{yy}$ plotted in function of the distance from weld toe tip

The mesh of the model is reported in the following figures:

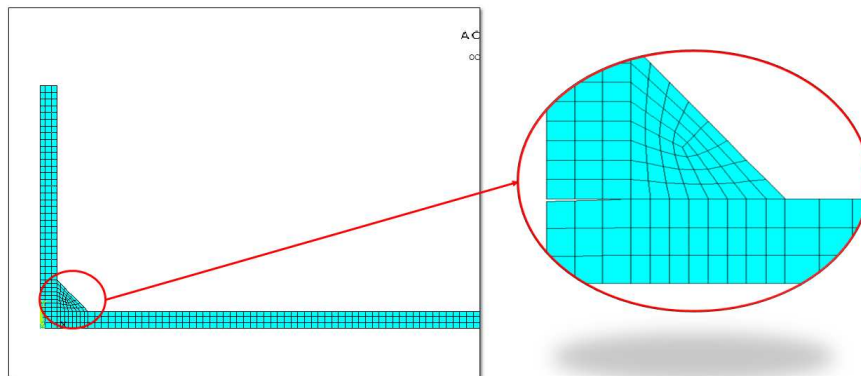


Figure 3.81: Mapped mesh for SHSS approach

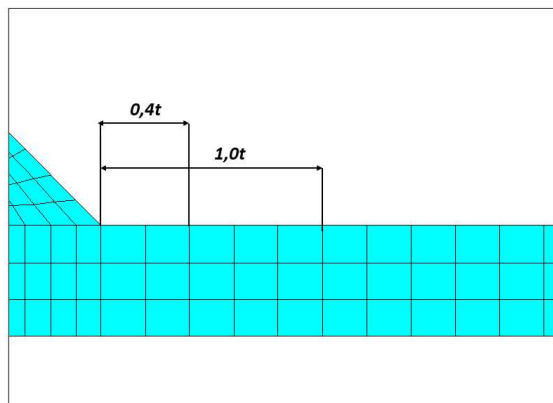


Figure 3.82: Mapped mesh for SHSS approach and reference points

For an external applied pressure $\Delta\sigma_{nom} = 1MPa$, the results of the tension at the reference points are:

$$\Delta\sigma_{xx,0.4t} = 1.01433MPa \quad (3.149)$$

$$\Delta\sigma_{xx,1.0t} = 0.99117MPa \quad (3.150)$$

$$\Delta\sigma_{11,0.4t} = 1.01476MPa \quad (3.151)$$

$$\Delta\sigma_{11,1.0t} = 0.99118MPa \quad (3.152)$$

$$(3.153)$$

The structural hot-spot stress is detected with the equation 1.2:

$$\Delta SHSS_{LSE,xx} = 1,67 \cdot \sigma_{xx,0.4t} - 0,67 \cdot \sigma_{xx,1.0t} = 1,67 \cdot 1,01433 - 0,67 \cdot 0,99117 = 1,0298MPa \quad (3.154)$$

$$\Delta SHSS_{LSE,11} = 1,67 \cdot \sigma_{11,0.4t} - 0,67 \cdot \sigma_{11,1.0t} = 1,67 \cdot 1,01476 - 0,67 \cdot 0,99118 = 1,03056MPa \quad (3.155)$$

This result is in good agreement with the value found in literature [33]:

$$\Delta\sigma_{xx,0.4t} = 1.017MPa \quad (3.156)$$

$$\Delta\sigma_{xx,1.0t} = 0.991MPa \quad (3.157)$$

$$(3.158)$$

$$\Delta SHSS_{LSE,literature} = 1,035MPa$$

Thus, the relative errors expresses in percentage between the calculated $\Delta SHSS_{LSE,xx}$, $\Delta SHSS_{LSE,11}$ and the $\Delta SHSS_{LSE,literature}$ are:

$$\Delta\% = \frac{\Delta SHSS_{LSE,xx} - \Delta SHSS_{LSE,literature}}{\Delta SHSS_{LSE,literature}} \cdot 100 = -0.50\% \quad (3.159)$$

$$\Delta\% = \frac{\Delta SHSS_{LSE,11} - \Delta SHSS_{LSE,literature}}{\Delta SHSS_{LSE,literature}} \cdot 100 = -0.43\% \quad (3.160)$$

3.3.5 Data results for IIW curve

Nominal stress approach

The results are reported in terms of nominal stress, defined in the beginning of paragraph 3.3, inside the FAT 80 curve proposed by IIW guideline [1]:

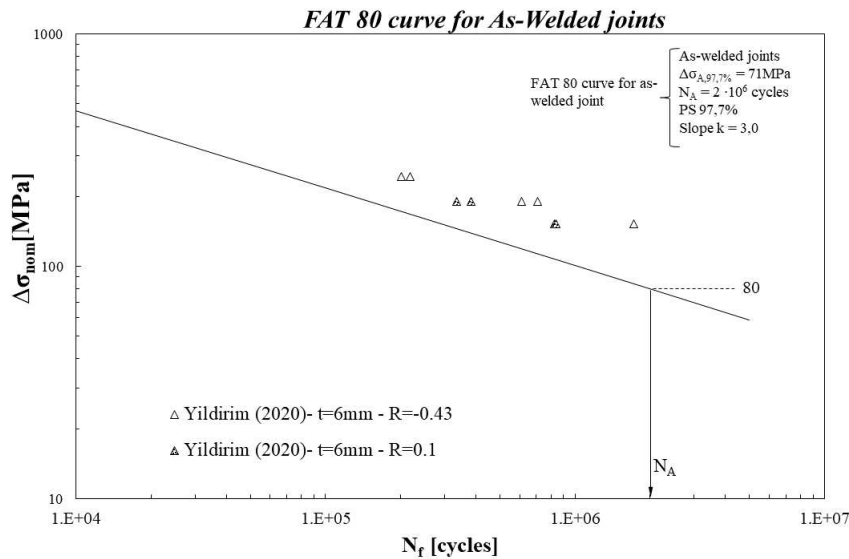


Figure 3.83: Experimental data inside the IIW nominal stress design curve.

SHSS approach

The previous model was characterised by a load equal to 1 MPa, applied to the main plate of the specimen; to obtain the value of the hot-spot stress related to the applied nominal stress, the equation (3.45) is applied.

The results in terms of SHSS are defined in the Appendix C.3.
 The all experimental data are collected inside the SHSS design curve proposed by IIW guideline:

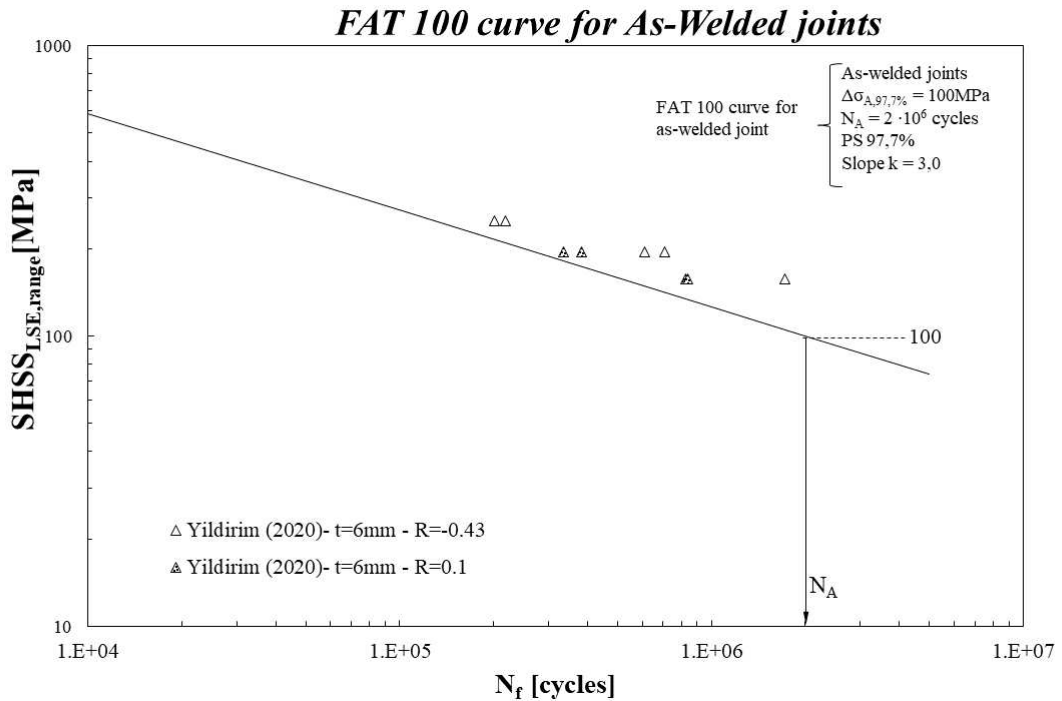


Figure 3.84: Experimental data inside the SHSS design curve.

The following conclusion can be defined:

1. These approaches have correctly been applied to FAT 80 welded joint, for weld toe fractures;
2. The nominal stress approach is characterised by the fact that all points fall above the lines that represents the 97.7% of probability of survival. For this reason, the nominal stress approach has proven to be conservative as the others methods.
3. The hot-spot stress method is characterised by the fact that all points fall above the lines that represents the 97.7% of probability of survival. For this reason, the SHSS approach has proven to be conservative as the others methods.

3.4 Okawa 2013, transverse attachment FAT 80

The fourth joint analysed is a transverse attachment characterised by a fatigue class FAT 80, studied by Okawa in 2013 [43] under CAL (Constant Amplitude Loading).

The principal information and mechanical properties about this typology of the joint are summarized in the Table 3.35 and Table 3.36:

Weld condition	Fracture location	Load application	Main plate/gusset thickness
As-welded, non-load carrying (NLC), full penetration	Weld toe	Axial, main plate, parent material	Main plate: 20mm Gusset: 10mm

Table 3.35: Information about the specimens

Material model	Yield strength f_y [MPa]	Young modulus [MPa]	Poisson's ratio ν
AH36, HSS, Linear elastic, isotropic	392	206000	0.3

Table 3.36: Information about mechanical properties

The dimensions of this joint are defined in the following table and figure:

t [mm]	b [mm]	w [mm]	L [mm]	h [mm]	2α [°]	z [mm]
20	10	75	700	50	135	8

Table 3.37: Dimension of the transverse attachment FAT 80, studied by Okawa in 2013.

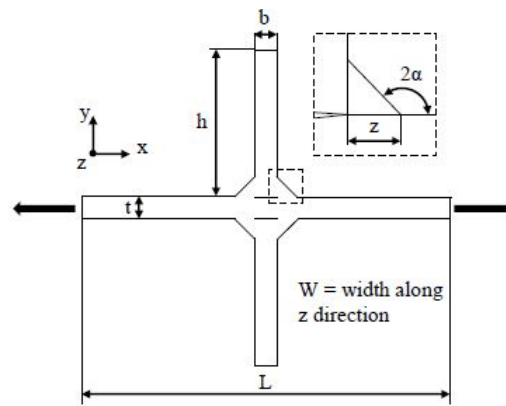


Figure 3.85: Okawa 2013, transverse attachment FAT 80 [33].

The parameters of the weld profile is described in the following table:

ρ weld toe tip [mm]	Weld leg [mm]	Weld flack angle [°]	2α
$\cong 0$	8	45	Weld toe: 135° Gusset: 135°

Table 3.38: Information about the weld profile

The radius ρ of the weld toe is lower than 1.5mm, so the assumption of a sharp V-notch ($\rho = 0\text{mm}$) at the weld toe is acceptable with the non conventional LEFM extension to welded joints. The effect of misalignment can not be neglected in transverse joint, however in this first analysis it is neglected. The experimental data are defined in the following table in terms of nominal stress $\Delta\sigma_{nom}$:

Stress Ratio R	$\Delta\sigma_{nom}$ [MPa]	N_f [cycles]
0.1	200	164000
	150	354000
	100	1320000
	80	5000000

Table 3.39: Experimental data of the 4th joint, Okawa 2013. The number barred represents the run-outs

OKawa FAT 80 is modelled in SOLIDWORKS 2020 and subsequently, is imported inside Ansys®APDL with .JGS extension. The results is reported in the figure below:

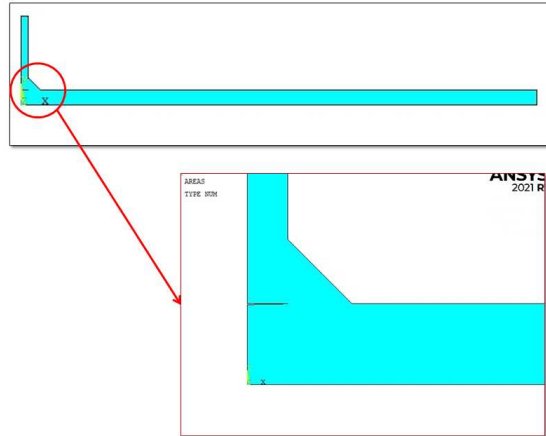


Figure 3.86: Model of transverse attachment FAT 80, studied by Okawa in 2013.

The procedure to define the boundary conditions of the model follows the same steps and dispositions defined for the transverse attachment FAT 80, studied by Yildirim in 2020 (see paragraph 3.3). The results are reported in the following figures:



Figure 3.87: Load of the model of transverse attachment FAT 80, studied by Okawa in 2013.

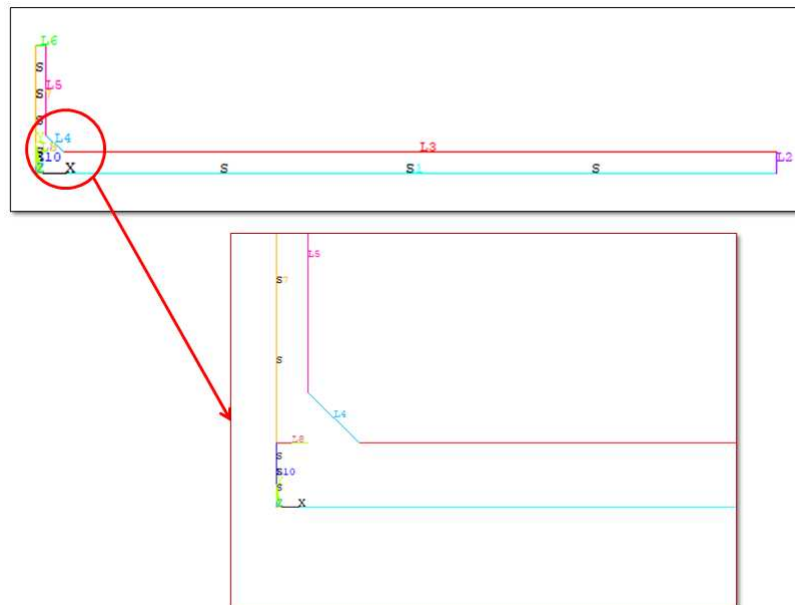


Figure 3.88: Symmetry condition of the model of transverse attachment FAT 80 studied by Okawa in 2013.

3.4.1 PSM approach Plane 182

The fatigue assessment for this model is performed by the application of Peak Stress Method for 2D structures with the adoption of four-node linear elements.

The element PLANE 182 is chosen from the Ansys®APDL library with *Simple Enhanced Strain* as Key Option 1 and *Plane Strain* as Key Option 3.

The model is prevailing subjected to mode I at the attachment edge with a opening angle 2α equal to 135° . Indeed, referring to the graph of the Williams eigenvalues trend in *Figure 1.13*, mode II is not singular for V-notch opening angle greater than 102.5° , so $\lambda_2 = 0$; the mode III can be neglected because is irrelevant.

Under mode I, the PSM requirements, with Tetra elements PLANE 182, are define in the following table:

Element type	Mesh algorithm	Mode I			
		$(a/d)_{min}$	2α	Mesh Pattern $2\alpha < 90^\circ$	Mesh Pattern $2\alpha > 90^\circ$
Plane 182 KeyOpt:Simple Enhanced Strain + Plane Strain	Free	3	$0^\circ < 2\alpha < 135^\circ$	Four adjacent elements share the same node	Two adjacent elements share the same node

Table 3.40: Requirements for PSM.

The mode I PSM calibration constant is calibrated at the weld toe where $2\alpha = 135^\circ$ and it is equal to $K_{FE}^* = 1.38 \pm 3\%$.

To define the global element size of the model, the following procedure is applied:

1. From literature the ratio $(a/d)_{min}$ is determined according to the *Table 3.40*. In this case the ratio for pure mode I is chosen and it is equal to 3;
2. The value of a is the reference dimension for selecting the maximal FE sizes d for PSM application and is defined as the half of the thickness t , so in this case is equal to 10 mm;
3. Subsequently, the minimum element size is defined as follow:

$$d_{min} = \frac{a}{3} = \frac{10}{3} = 3.33mm \quad (3.161)$$

4. The chosen dimension of elements is 3 mm

The λ_1 and e_1 values are depended on the opening angle 2α , that is 135° for the weld toe:

2α [°]	λ_1 (Mode I)	e_1 (Mode I)
135°	0.674	0.117

Table 3.41: Value of λ_1 and e_1 in function of the opening angle 2α

The corrective stress factors for mode I is calculated with the equation (2.24). The result is reported in the *Table 3.42*

2α [°]	f_{w1}
135°	1.569

Table 3.42: Value of the corrective stress factors f_{w1} in function of the opening angle 2α

Once the model is properly meshed, loaded and constraint, the system can be solved:

Solution → *Solve* → *Current LS*

3.4.2 PSM approach with Plane 182: results

In this analysis, the structures are subjected to pure mode I loading, so in these situations it can be demonstrated that, in the case that the stress flow is aligned with the external pressure direction, the first principal stress range $\Delta\sigma_{11}$ can be approximated equal to local stress $\Delta\sigma_{yy}$, evaluated with a local reference system with the origin placed on the V-notch. However, to obtain a more precise results, a local reference system is created on the node that represents the weld toe with the same procedure described in the paragraph 2.2.1 (see Figure 3.89).

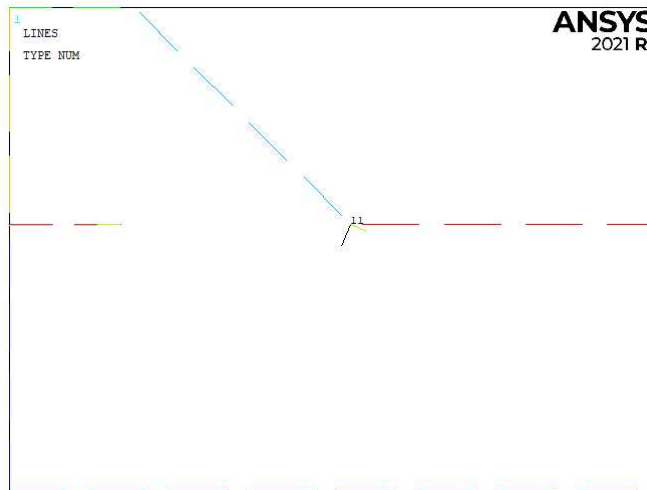


Figure 3.89: Local reference system with the origin at the weld toe.

During the analysis of the results, the first principal stress is evaluated and compared with $\Delta\sigma_{yy}$. The results of the first principal stress can be observed in the Figure 3.90, for an external applied pressure equal to 1 MPa:

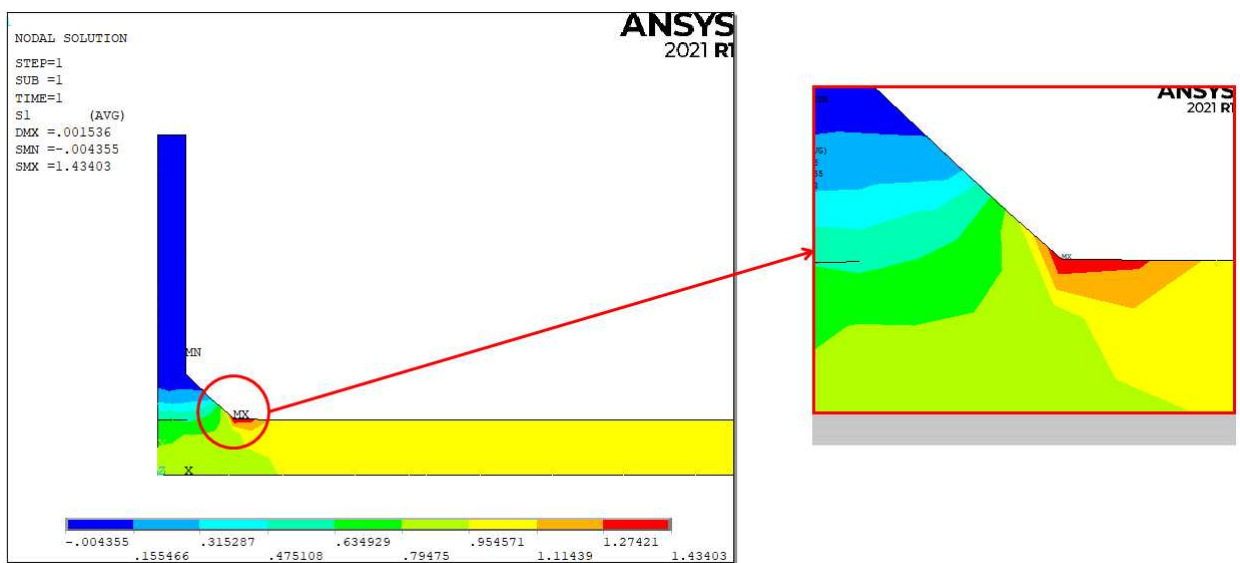


Figure 3.90: Plot of the first principal stress.

For an external applied pressure $\Delta\sigma_{nom} = 1MPa$, the result at the weld toe is:

$$\overline{\Delta\sigma}_{yy,weld-toe,peak} = 1.43403MPa \quad (3.162)$$

$$\overline{\Delta\sigma}_{11,weld-toe,peak} = 1.41986MPa \quad (3.163)$$

$$(3.164)$$

The equivalent peak stress are calculated by the formulae (2.23):

$$\Delta\sigma_{eq,peak,weld-toe} = \overline{\Delta\sigma}_{\theta\theta,\theta=0,peak} \cdot f_{w1} = 1.434303 \cdot 1.569 = 2.17417MPa \quad (3.165)$$

This result is in good agreement with the value found in literature [33]:

$$\Delta\sigma_{eq,peak,literature} = 2.1785MPa \quad (3.166)$$

Thus, the relative error expresses in percentage between the calculated $\Delta\sigma_{eq,peak}$ and the $\Delta\sigma_{eq,peak,literature}$ is:

$$\Delta\% = \frac{\Delta\sigma_{eq,peak,calculated} - \Delta\sigma_{eq,peak,literature}}{\Delta\sigma_{eq,peak,literature}} \cdot 100 = -0.20\% \quad (3.167)$$

3.4.3 Data results for PSM curve

The previous model was characterised by a load equal to 1 MPa, applied to the main plate of the specimen; to obtain the value of the peak stress related to the applied nominal stress, the equation (3.24) is applied.

The results in terms of equivalent peak stress calculated with PSM Plane 182 approach, are defined in the Appendix C.4.

The all experimental data are collected inside the PSM design curve proposed by Meneghetti and Lazzarin for structure subjected to prevailing mode I.

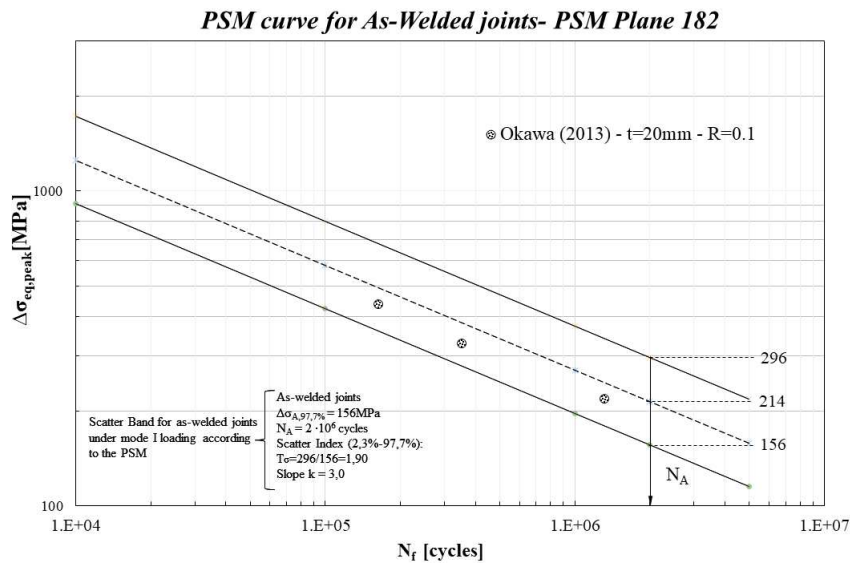


Figure 3.91: Experimental data inside the PSM design curve with Plane 182 elements.

The following conclusion can be defined:

1. The all experimental data fall above the lines that represents the 97.7% of probability of survival. Thus the PSM design curve has demonstrated to be effective and conservative;
2. The PSM Plane 182 approach have correctly foreseen the experimental crack initiation point at the weld toe.

3.4.4 SHSS (Structural Hot Spot Stress) approach

The fatigue assessment for this model is performed by the application of SHSS approach, following the IIW recommendation [1] to obtain the hot-spot stress. According to the guideline, the weld toe of the transverse attachment FAT 80 studied by Okawa in 2013, is a hot-spot type *a* and the hot-spot stress value is detected with the employment of fine mesh, as *Figure 1.4* shows.

The model is divided in a series of areas to allow the application of *Mapped-mesh* algorithm; indeed each areas must be characterised by a number of side between 3 and 4 to obtain a *Mapped-mesh*. The eight-node linear element PLANE 182 is chosen in Ansys®APDL with *Simple Enhanced Strain* as Key Option 1 and *Plane Strain* as Key Option 3.

The all informations about the mesh is reported in the following table:

Element type	Mesh algorithm	Main plate thickness <i>t</i>	Max element size	Adopted element size
Plane 182 KeyOpt:Simple Enhanced Strain + Plane Strain	Mapped	20 mm (10 mm modelled)	$0.4 \cdot t = 0.4 \cdot 20 = 8mm$	4 mm

Table 3.43: Requirements for SHSS mesh.

The hot-spot stress is extrapolated at two reference points placed at $0.4t$ and $1.0t$ distance from the weld toe tip, so in this case at 8 mm and 20 mm from weld toe.

For the type of extrapolated stress, the graph in *Figure 3.92* shows that, for an external applied pressure $\Delta\sigma_{nom} = 1MPa$, after 1.10 mm, the $\Delta\sigma_{xx}$ and the first principal stress $\Delta\sigma_{11}$ are coincident. For this reason the choice is indifferent.

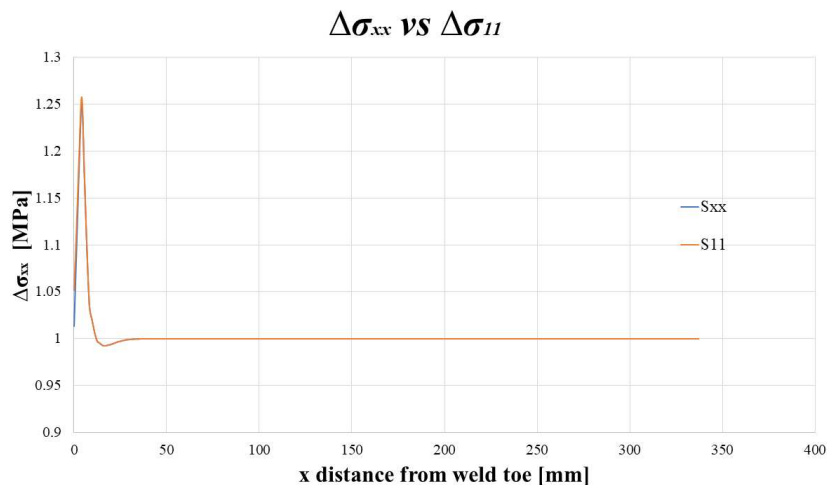


Figure 3.92: $\Delta\sigma_{xx}$ and $\Delta\sigma_{yy}$ plotted in function of the distance from weld toe tip

The mesh of the model is reported in the following figures:

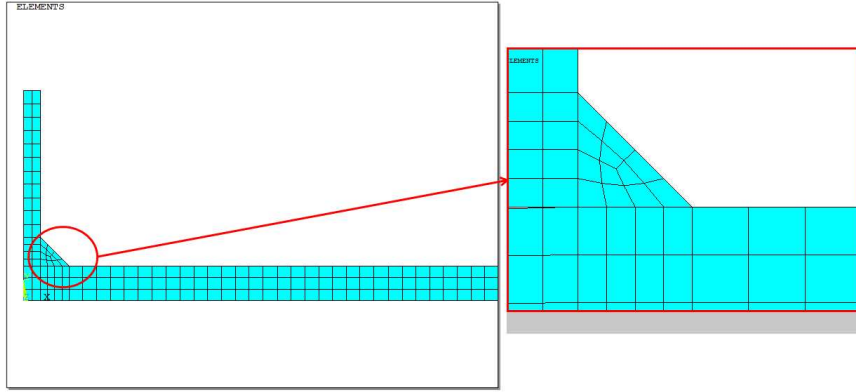


Figure 3.93: Mapped mesh for SHSS approach

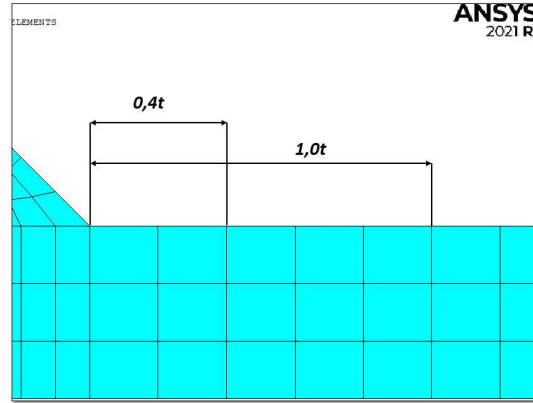


Figure 3.94: Mapped mesh for SHSS approach and reference points

For an external applied pressure $\Delta\sigma_{nom} = 1MPa$, the results of the tension at the reference points are:

$$\Delta\sigma_{xx,0.4t} = 1.03714MPa \quad (3.168)$$

$$\Delta\sigma_{xx,1.0t} = 0.99394MPa \quad (3.169)$$

$$\Delta\sigma_{11,0.4t} = 1.03759MPa \quad (3.170)$$

$$\Delta\sigma_{11,1.0t} = 0.99394MPa \quad (3.171)$$

$$(3.172)$$

The structural hot-spot stress is detected with the equation 1.2:

$$\Delta SHSS_{LSE,xx} = 1,67 \cdot \sigma_{xx,0.4t} - 0,67 \cdot \sigma_{xx,1.0t} = 1,67 \cdot 1.03714 - 0,67 \cdot 0.99394 = 1.0661MPa \quad (3.173)$$

$$\Delta SHSS_{LSE,11} = 1,67 \cdot \sigma_{11,0.4t} - 0,67 \cdot \sigma_{11,1.0t} = 1,67 \cdot 1.03759 - 0,67 \cdot 0.99394 = 1.0668MPa \quad (3.174)$$

This result is in good agreement with the value found in literature [33]:

$$\Delta\sigma_{xx,0.4t} = 1.037MPa \quad (3.175)$$

$$\Delta\sigma_{xx,1.0t} = 0.994MPa \quad (3.176)$$

$$(3.177)$$

$$\Delta SHSS_{LSE,literature} = 1,066MPa$$

Thus, the relative errors expresses in percentage between the calculated $\Delta SHSS_{LSE,xx}$, $\Delta SHSS_{LSE,11}$ and the $\Delta SHSS_{LSE,literature}$ are:

$$\Delta\% = \frac{\Delta SHSS_{LSE,xx} - \Delta SHSS_{LSE,literature}}{\Delta SHSS_{LSE,literature}} \cdot 100 = -0.008\% \quad (3.178)$$

$$\Delta\% = \frac{\Delta SHSS_{LSE,11} - \Delta SHSS_{LSE,literature}}{\Delta SHSS_{LSE,literature}} \cdot 100 = -0.078\% \quad (3.179)$$

3.4.5 Data results for IIW curve

Nominal stress approach

The results are reported in terms of nominal stress, defined in the beginning of paragraph 3.4, inside the FAT 80 curve proposed by IIW guideline [1]:

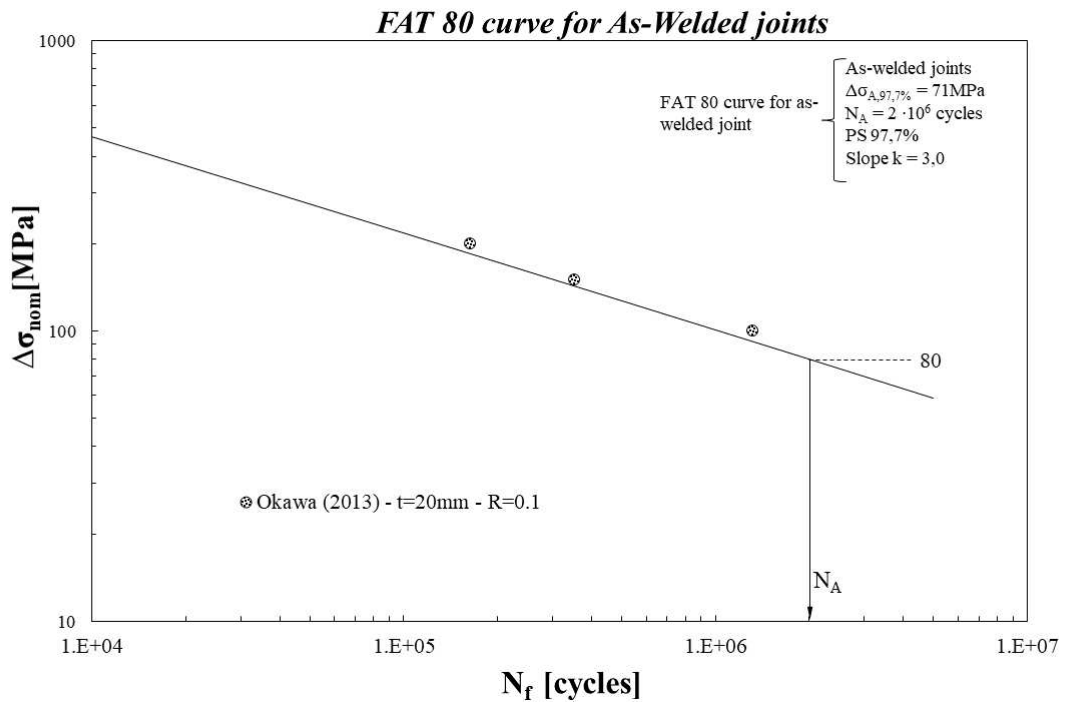


Figure 3.95: Experimental data inside the IIW nominal stress design curve.

SHSS approach

The previous model was characterised by a load equal to 1 MPa, applied to the main plate of the specimen; to obtain the value of the hot-spot stress related to the applied nominal stress, the equation (3.45) is applied.

The results in terms of SHSS are defined in the Appendix C.4. The all experimental data are collected inside the SHSS design curve proposed by IIW guideline:

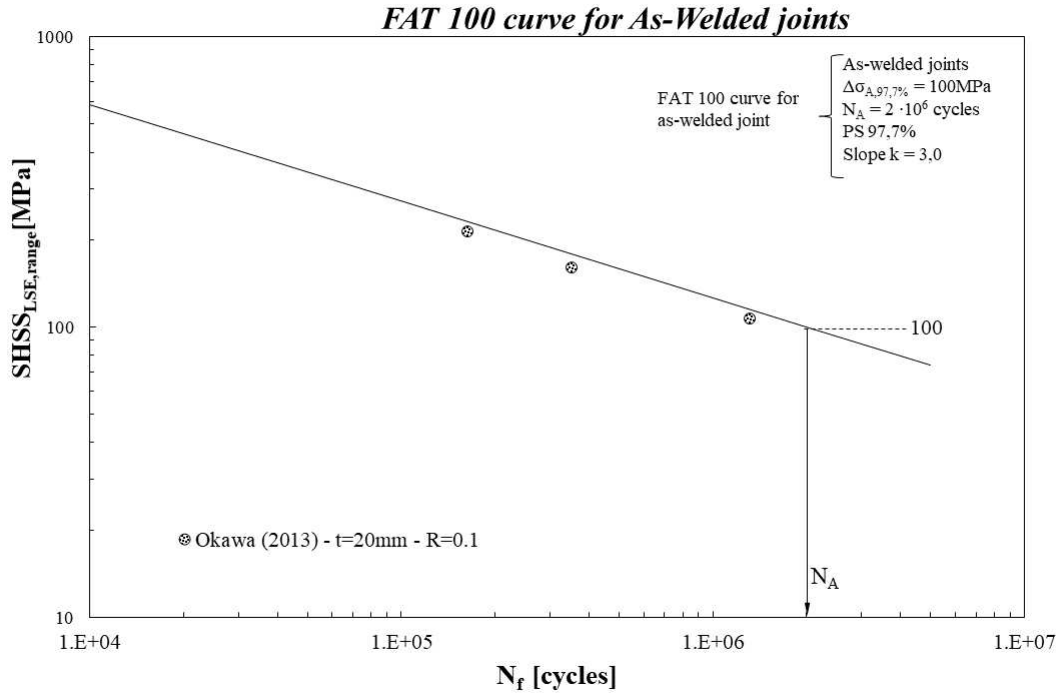


Figure 3.96: Experimental data inside the SHSS design curve.

The following conclusion can be defined:

1. These approaches have correctly been applied to FAT 80 welded joint, for weld toe fractures;
2. The nominal stress approach is characterised by the fact that all points fall above the lines that represents the 97.7% of probability of survival. For this reason, the nominal stress approach has proven to be conservative as the others methods.
3. The hot-spot stress method is characterised by the fact that all points fall below the lines that represents the 97.7% of probability of survival. For this reason, the SHSS approach has not proven to be conservative as the others methods.

3.5 Kuhlmann-Gunther 2009, transverse attachment FAT 80

The fifth joint analysed is a transverse attachment characterised by a fatigue class FAT 80, studied by Kuhlmann and Gunther in 2009 [44] under CAL (Constant Amplitude Loading).

The principal information and mechanical properties about this typology of the joint are summarized in the Table 3.44 and Table 3.45:

Weld condition	Fracture location	Load application	Main plate/gusset thickness
As-welded, non-load carrying (NLC), full penetration	Weld toe	Axial, main plate, parent material	Main plate: 12mm Gusset: 12mm

Table 3.44: Information about the specimens

Material model	Yield strength f_y [MPa]	Young modulus [MPa]	Poisson's ratio ν
S355J2, linear elastic, isotropic	355	206000	0.3
S690QL, linear elastic, isotropic	690		

Table 3.45: Information about mechanical properties

The dimensions of this joint are defined in the following table and figure:

t [mm]	b [mm]	w [mm]	L [mm]	h [mm]	2α [°]	z [mm]
12	12	80	450	40	135	7

Table 3.46: Dimension of the transverse attachment FAT 80, studied by Kuhlmann and Gunther in 2009.

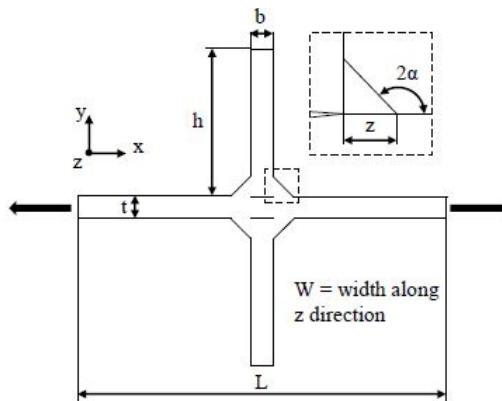


Figure 3.97: Kuhlmann-Gunther 2009, transverse attachment FAT 80 [33].

The parameters of the weld profile is described in the following table:

ρ weld toe tip [mm]	Weld leg [mm]	Weld flack angle [°]	2α
$\cong 0$	7	45	Weld toe: 135° Gusset: 135°

Table 3.47: Information about the weld profile

The radius ρ of the weld toe is lower than 1.5mm, so the assumption of a sharp V-notch ($\rho = 0mm$) at the weld toe is acceptable with the non conventional LEFM extension to welded joints. The effect of misalignment can not be neglected in transverse joint, however in this first analysis it is neglected. The experimental data are defined in the following table in terms of nominal stress $\Delta\sigma_{nom}$:

Stress Ratio R	Material	$\Delta\sigma_{nom}$ [MPa]	N_f [cycles]
0.1	S355J2	300	67921
		300	64159
		170	574631
		170	456289
		125	1400261
		125	3712215
		225	185219
		225	168630
		125	1933751
0.1	S690QL	300	106797
		300	123652
		225	537534
		225	415746
		190	1028720
		190	575000
		190	1034355
		150	3517443
		150	1833757

Table 3.48: Experimental data of the 5th joint, Kuhlmann-Gunther 2009. The number barred represents the run-outs

Kuhlmann-Gunther FAT 80 is modelled in *SOLIDWORKS 2020* and subsequently, is imported inside Ansys®APDL with *.IGS* extension. The results is reported in the figure below:

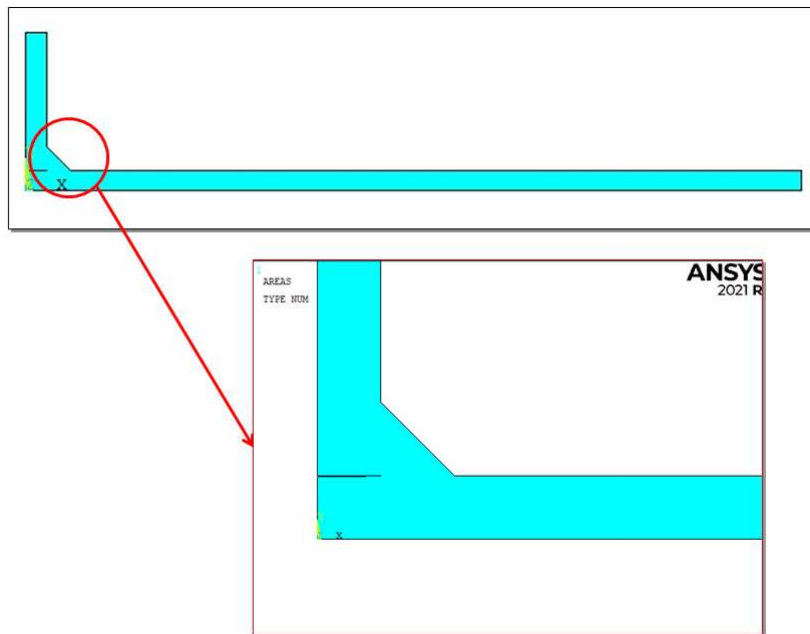


Figure 3.98: Model of transverse attachment FAT 80, studied by Kuhlmann and Gunther in 2009.

The procedure to define the boundary conditions of the model follows the same steps and dispositions defined for the transverse attachment FAT 80, studied by Yildirim in 2020 (see paragraph 3.3). The results are reported in the following figures:



Figure 3.99: Load of the model of transverse attachment FAT 80, studied by Kuhlmann and Gunther in 2009.

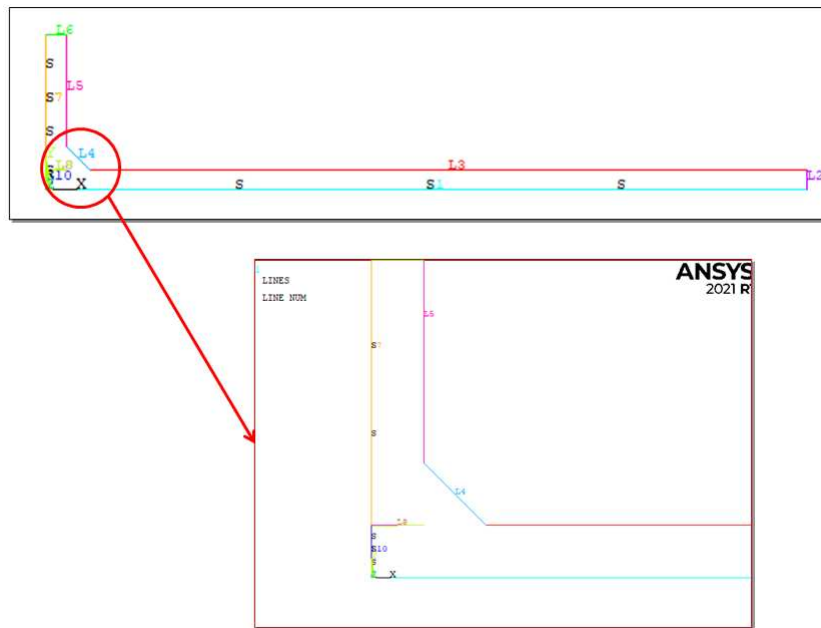


Figure 3.100: Symmetry condition of the model of transverse attachment FAT 80 studied by Kuhlmann and Gunther in 2009.

3.5.1 PSM approach Plane 182

The fatigue assessment for this model is performed by the application of Peak Stress Method for 2D structures with the adoption of four-node linear elements.

The element PLANE 182 is chosen from the Ansys®APDL library with *Simple Enhanced Strain* as Key Option 1 and *Plane Strain* as Key Option 3.

The model is prevailing subjected to mode I at the attachment edge with a opening angle 2α equal to 135° . Indeed, referring to the graph of the Williams eigenvalues trend in *Figure 1.13*, mode II is not singular for V-notch opening angle greater than 102.5° , so $\lambda_2 = 0$; the mode III can be neglected because is irrelevant.

Under mode I, the PSM requirements, with Tetra elements PLANE 182, are define in the following table:

Element type	Mesh algorithm	Mode I			
		$(a/d)_{min}$	2α	Mesh Pattern $2\alpha < 90^\circ$	Mesh Pattern $2\alpha > 90^\circ$
Plane 182 KeyOpt:Simple Enhanced Strain + Plane Strain	Free	3	$0^\circ < 2\alpha < 135^\circ$	Four adjacent elements share the same node	Two adjacent elements share the same node

Table 3.49: Requirements for PSM.

The mode I PSM calibration constant is calibrated at the weld toe where $2\alpha = 135^\circ$ and it is equal to $K_{FE}^* = 1.38 \pm 3\%$.

To define the global element size of the model, the size of the element is obtained with the following procedure:

1. From literature the ratio $(a/d)_{min}$ is determined according to the *Table 3.49*. In this case the ratio for pure mode I is chosen and it is equal to 3;
2. The value of a is the reference dimension for selecting the maximal FE sizes d for PSM application and is defined as the half of the thickness t , so in this case is equal to 6 mm;
3. Subsequently, the minimum element size is defined as follow:

$$d_{min} = \frac{a}{3} = \frac{6}{3} = 2mm \quad (3.180)$$

4. The chosen dimension of elements is 2 mm

The λ_1 and e_1 values are depended on the opening angle 2α , that is 135° for the weld toe:

2α [°]	λ_1 (Mode I)	e_1 (Mode I)
135°	0.674	0.117

Table 3.50: Value of λ_1 and e_1 in function of the opening angle 2α

The corrective stress factors for mode I is calculated with the equation (2.24). The result is reported in the *Table 3.51*

2α [°]	f_{w1}
135°	1.328

Table 3.51: Value of the corrective stress factors f_{w1} in function of the opening angle 2α

Once the model is properly meshed, loaded and constraint, the system can be solved:

Solution→*Solve*→*Current LS*

3.5.2 PSM approach with Plane 182: results

In this analysis, the structures are subjected to pure mode I loading, so in these situations it can be demonstrated that, in the case that the stress flow is aligned with the external pressure direction, the first principal stress range $\Delta\sigma_{11}$ can be approximated equal to local stress $\Delta\sigma_{yy}$, evaluated with a local reference system with the origin placed on the V-notch. However, to obtain a more precise results, a local reference system is created on the node that represents the weld toe with the same procedure described in the paragraph 2.2.1 (see *Figure 3.101*).

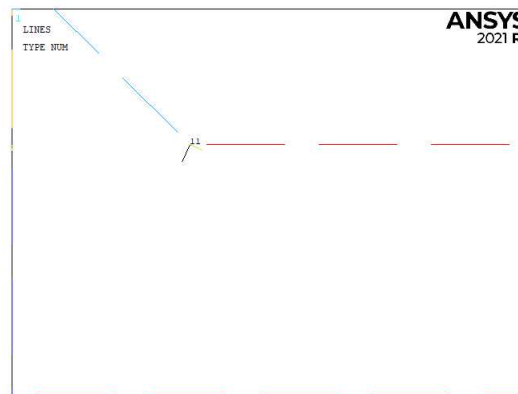


Figure 3.101: Local reference system with the origin at the weld toe.

During the analysis of the results, the first principal stress is evaluated and compared with $\Delta\sigma_{yy}$. The results of the first principal stress can be observed in the *Figure 3.102*, for an external applied pressure equal to 1 MPa:

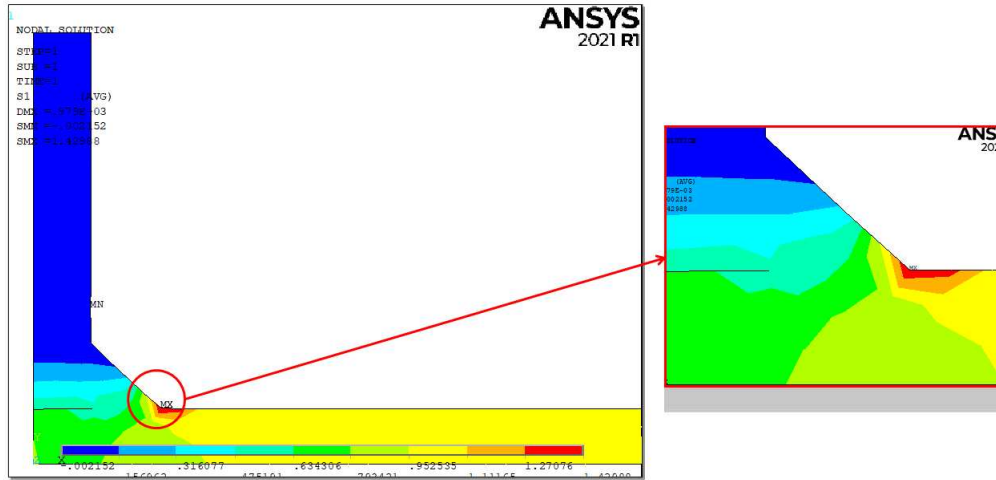


Figure 3.102: Plot of the first principal stress.

For an external applied pressure $\Delta\sigma_{nom} = 1MPa$, the result at the weld toe is:

$$\overline{\Delta\sigma}_{yy,weld-toe,peak} = 1.42988MPa \quad (3.181)$$

$$\overline{\Delta\sigma}_{11,weld-toe,peak} = 1.41695MPa \quad (3.182)$$

$$(3.183)$$

The equivalent peak stress are calculated by the formulae (2.23):

$$\Delta\sigma_{eq,peak,weld-toe} = \overline{\Delta\sigma}_{\theta\theta,\theta=0,peak} \cdot f_{w1} = 1.42988 \cdot 1.328 = 1.899MPa \quad (3.184)$$

This result is in good agreement with the value found in literature [33]:

$$\Delta\sigma_{eq,peak,literature} = 1.968MPa \quad (3.185)$$

Thus, the relative error expresses in percentage between the calculated $\Delta\sigma_{eq,peak}$ and the $\Delta\sigma_{eq,peak,literature}$ is:

$$\Delta\% = \frac{\Delta\sigma_{eq,peak,calculated} - \Delta\sigma_{eq,peak,literature}}{\Delta\sigma_{eq,peak,literature}} \cdot 100 = -3.488\% \quad (3.186)$$

3.5.3 Data results for PSM curve

The previous model was characterised by a load equal to 1 MPa, applied to the main plate of the specimen; to obtain the value of the peak stress related to the applied nominal stress, the equation (3.24) is applied. The results in terms of equivalent peak stress calculated with PSM Plane 182 approach, are defined in the Appendix C.5.

The all experimental data are collected inside the PSM design curve proposed by Meneghetti and Lazzarin for structure subjected to prevailing mode I.

The following conclusion can be defined:

1. The all experimental data fall above the lines that represents the 97.7% of probability of survival. Thus the PSM design curve has demonstrated to be effective and conservative;
2. The PSM Plane 182 approach have correctly foreseen the experimental crack initiation point at the weld toe.

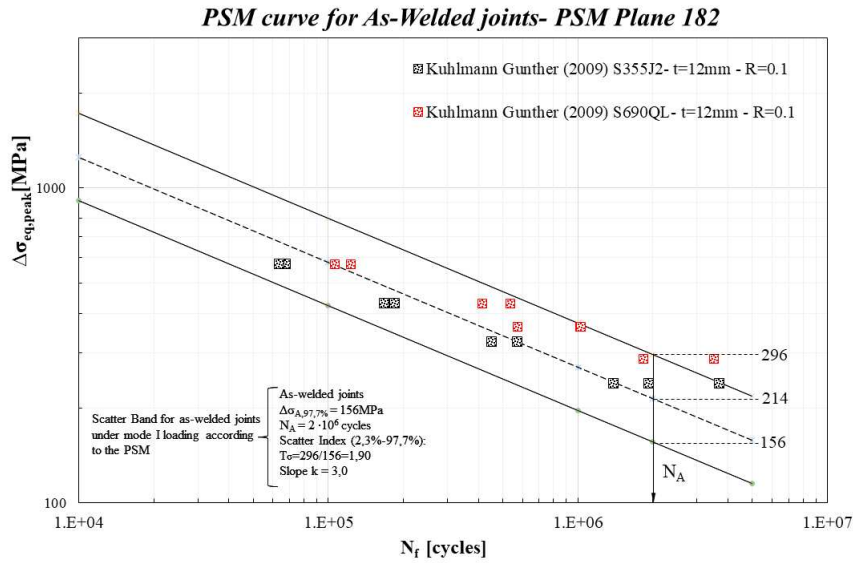


Figure 3.103: Experimental data inside the PSM design curve with Plane 182 elements.

3.5.4 SHSS (Structural Hot Spot Stress) approach

The fatigue assessment for this model is performed by the application of SHSS approach, following the IIW recommendation [1] to obtain the hot-spot stress. According to the guideline, the weld toe of the transverse attachment FAT 80 studied by Kuhlmann and Gunther in 2009, is a hot-spot type *a* and the hot-spot stress value is detected with the employment of fine mesh, as *Figure 1.4* shows.

The model is divided in a series of areas to allow the application of *Mapped-mesh* algorithm; indeed each areas must be characterised by a number of side between 3 and 4 to obtain a *Mapped-mesh*. The eight-node linear element PLANE 182 is chosen in Ansys®APDL with *Simple Enhanced Strain* as Key Option 1 and *Plane Strain* as Key Option 3.

The all informations about the mesh is reported in the following table:

Element type	Mesh algorithm	Main plate thickness <i>t</i>	Max element size	Adopted element size
Plane 182 KeyOpt:Simple Enhanced Strain + Plane Strain	Mapped	12 mm (6 mm modelled)	$0.4 \cdot t =$ $0.4 \cdot 12 = 4.8mm$	2.4 mm

Table 3.52: Requirements for SHSS mesh.

The hot-spot stress is extrapolated at two reference points placed at $0.4t$ and $1.0t$ distance from the weld toe tip, so in this case at 4.8 mm and 12 mm from weld toe. For the type of extrapolated stress, the graph in *Figure 3.104* shows that, for an external applied pressure $\Delta\sigma_{nom} = 1MPa$, after 1.10 mm, the $\Delta\sigma_{xx}$ and the first principal stress $\Delta\sigma_{11}$ are coincident. For this reason the choice is indifferent.

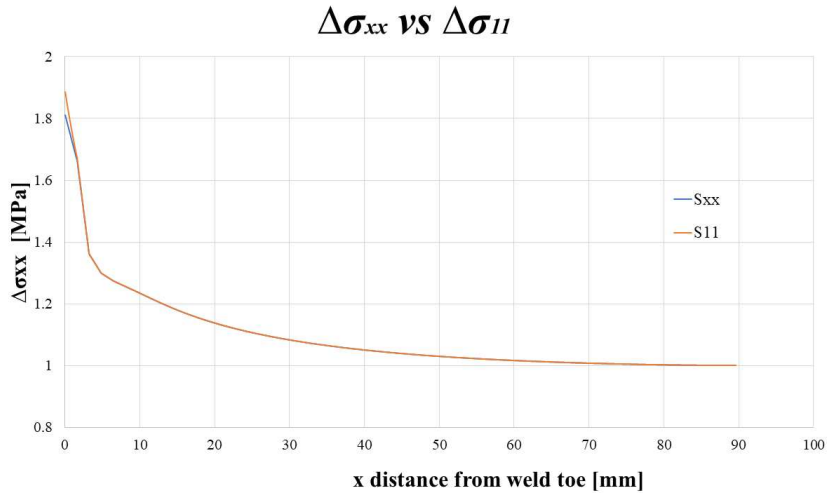


Figure 3.104: $\Delta\sigma_{xx}$ and $\Delta\sigma_{yy}$ plotted in function of the distance from weld toe tip

The mesh of the model is reported in the following figures:

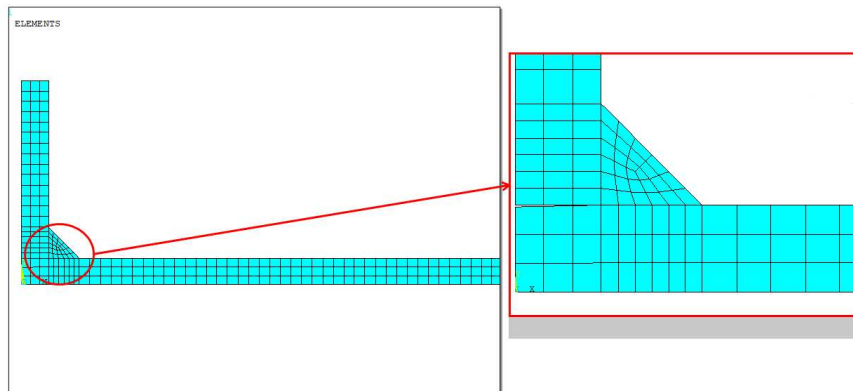


Figure 3.105: Mapped mesh for SHSS approach

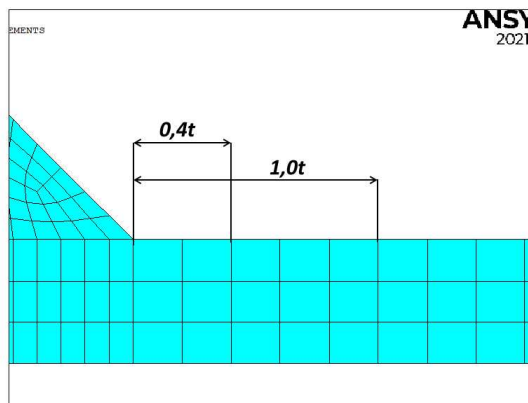


Figure 3.106: Mapped mesh for SHSS approach and reference points

For an external applied pressure $\Delta\sigma_{nom} = 1MPa$, the results of the tension at the reference points are:

$$\Delta\sigma_{xx,0.4t} = 1.02291MPa \quad (3.187)$$

$$\Delta\sigma_{xx,1.0t} = 0.99199MPa \quad (3.188)$$

$$\Delta\sigma_{11,0.4t} = 1.02336MPa \quad (3.189)$$

$$\Delta\sigma_{11,1.0t} = 0.99199MPa \quad (3.190)$$

$$(3.191)$$

The structural hot-spot stress is detected with the equation 1.2:

$$\Delta SHSS_{LSE,xx} = 1,67 \cdot \sigma_{xx,0.4t} - 0.67 \cdot \sigma_{xx,1.0t} = 1.67 \cdot 1.02291 - 0.67 \cdot 0.99199 = 1.04363MPa \quad (3.192)$$

$$\Delta SHSS_{LSE,11} = 1,67 \cdot \sigma_{11,0.4t} - 0.67 \cdot \sigma_{11,1.0t} = 1.67 \cdot 1.02336 - 0.67 \cdot 0.99199 = 1.04438MPa \quad (3.193)$$

This result is in good agreement with the value found in literature [33]:

$$\Delta\sigma_{xx,0.4t} = 1.021MPa \quad (3.194)$$

$$\Delta\sigma_{xx,1.0t} = 0.992MPa \quad (3.195)$$

$$(3.196)$$

$$\Delta SHSS_{LSE,literature} = 1,041MPa$$

Thus, the relative errors expresses in percentage between the calculated $\Delta SHSS_{LSE,xx}$, $\Delta SHSS_{LSE,11}$ and the $\Delta SHSS_{LSE,literature}$ are:

$$\Delta\% = \frac{\Delta SHSS_{LSE,xx} - \Delta SHSS_{LSE,literature}}{\Delta SHSS_{LSE,literature}} \cdot 100 = 0.25\% \quad (3.197)$$

$$\Delta\% = \frac{\Delta SHSS_{LSE,11} - \Delta SHSS_{LSE,literature}}{\Delta SHSS_{LSE,literature}} \cdot 100 = 0.32\% \quad (3.198)$$

3.5.5 Data results for IIW curve

Nominal stress approach

The results are reported in terms of nominal stress, defined in the beginning of paragraph 3.5, inside the FAT 80 curve proposed by IIW guideline [1]:

SHSS approach

The previous model was characterised by a load equal to 1 MPa, applied to the main plate of the specimen; to obtain the value of the hot-spot stress related to the applied nominal stress, the equation (3.45) is applied.

The results in terms of SHSS are defined in the Appendix C.5.
The all experimental data are collected inside the SHSS design curve proposed by IIW guideline:

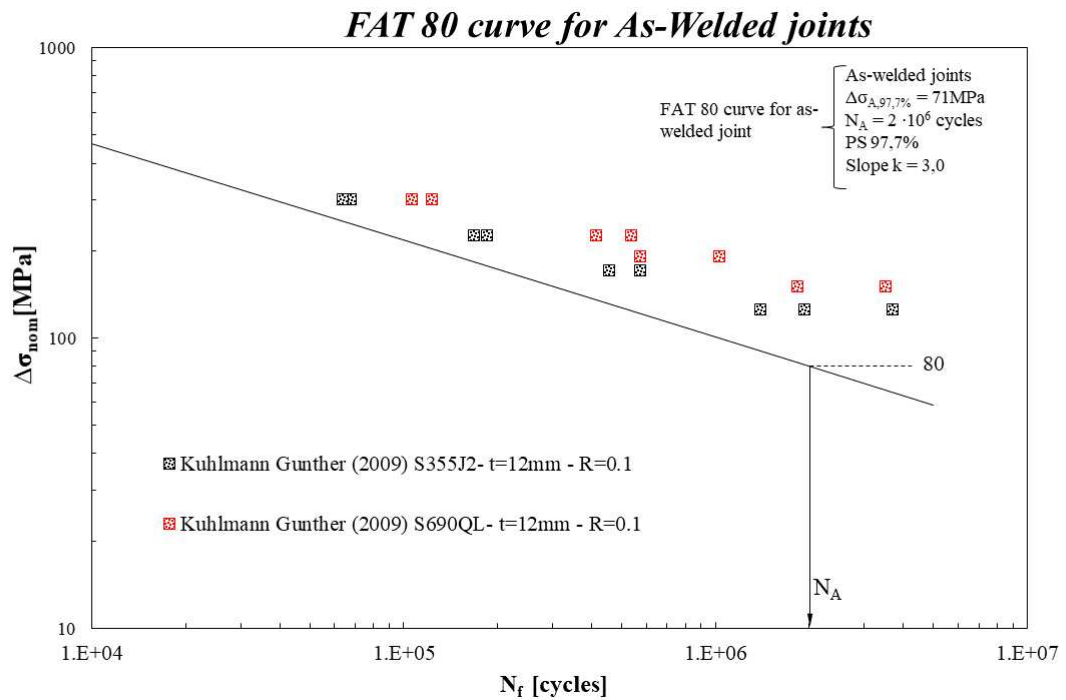


Figure 3.107: Experimental data inside the IIW nominal stress design curve.

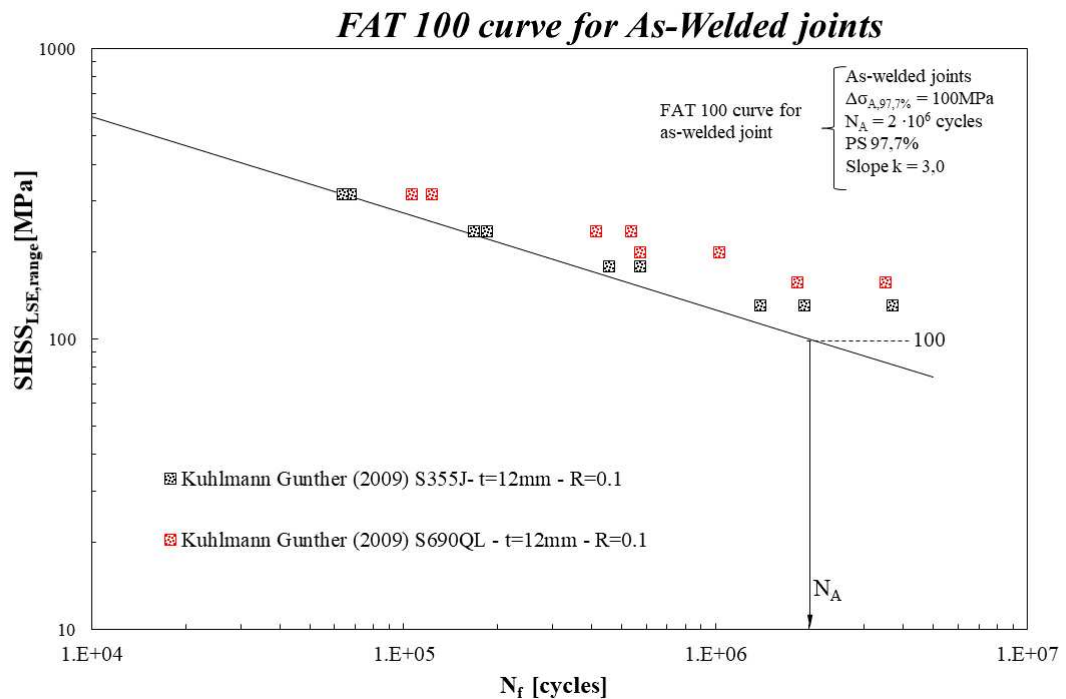


Figure 3.108: Experimental data inside the SHSS design curve.

The following conclusion can be defined:

1. These approaches have correctly been applied to FAT 80 welded joint, for weld toe fractures;
2. The nominal stress approach is characterised by the fact that all points fall above the lines that represents the 97.7% of probability of survival. For this reason, the nominal stress approach has proven to be conservative as the others methods.
3. The hot-spot stress method is characterised by the fact that all points fall below the lines that represents

the 97.7% of probability of survival. For this reason, the SHSS approach has proven to be conservative as the others methods.

3.6 Kuhlmann 2006, transverse attachment FAT 80

The sixth joint analysed is a transverse attachment characterised by a fatigue class FAT 80, studied by Kuhlmann in 2006 [44] under CAL (Constant Amplitude Loading).

The principal information and mechanical properties about this typology of the joint are summarized in the Table 3.53 and Table 3.54:

Weld condition	Fracture location	Load application	Main plate/gusset thickness
As-welded, non-load carrying (NLC), full penetration	Weld toe	Axial, main plate, parent material	Main plate: 12mm Gusset: 12mm

Table 3.53: Information about the specimens

Material model	Yield strength f_y [MPa]	Young modulus [MPa]	Poisson's ratio ν
S355, linear elastic, isotropic	355	0.3	
S460, linear elastic, isotropic	460		

Table 3.54: Information about mechanical properties

The dimensions of this joint are defined in the following table and figure:

t [mm]	b [mm]	w [mm]	L [mm]	h [mm]	2α [°]	z [mm]
12	12	40	500	50	135	5.66

Table 3.55: Dimension of the transverse attachment FAT 80, studied by Kuhlmann in 2006.

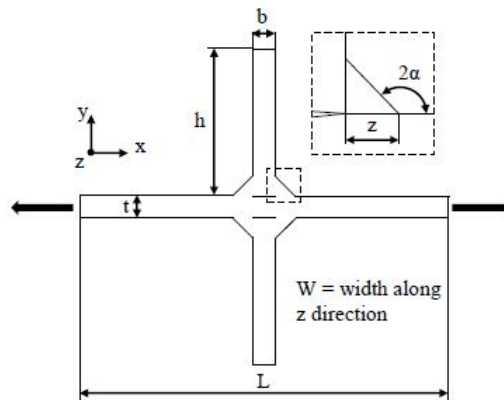


Figure 3.109: Kuhlmann 2006, transverse attachment FAT 80 [33].

The parameters of the weld profile is described in the following table:

ρ weld toe tip [mm]	Weld leg [mm]	Weld flack angle [°]	2α
$\cong 0$	7	45	Weld toe: 135° Gusset: 135°

Table 3.56: Information about the weld profile

The radius ρ of the weld toe is lower than 1.5mm, so the assumption of a sharp V-notch ($\rho = 0mm$) at the weld toe is acceptable with the non conventional LEFM extension to welded joints. The effect of misalignment can not be neglected in transverse joint, however in this first analysis it is neglected. The experimental data are not available. Kuhlmann FAT 80 is modelled in *SOLIDWORKS 2020* and subsequently, is imported inside Ansys®APDL with *.IGS* extension. The results is reported in the figure below:

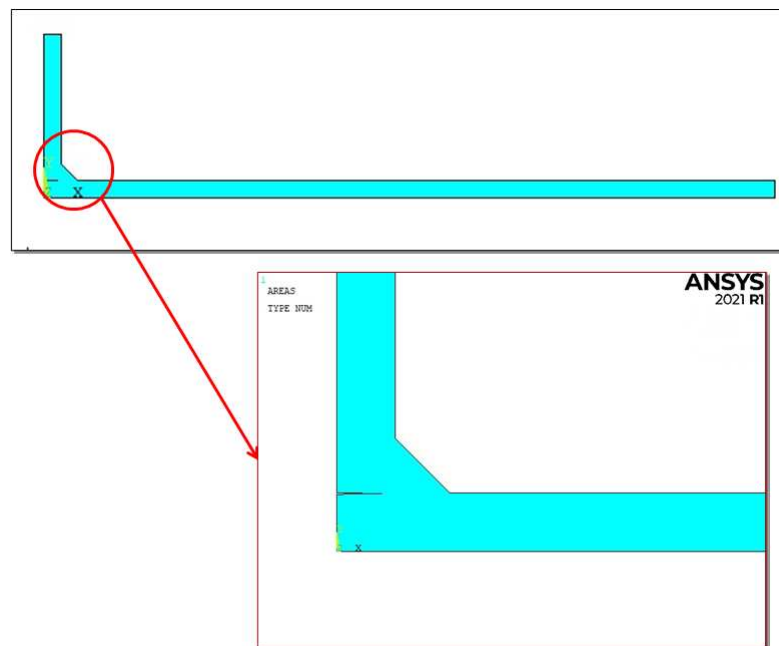


Figure 3.110: Model of transverse attachment FAT 80, studied by Kuhlmann in 2006.

The procedure to define the boundary conditions of the model follows the same steps and dispositions defined for the transverse attachment FAT 80, studied by Yildirim in 2020 (see paragraph 3.3). The results are reported in the following figures:



Figure 3.111: Load of the model of transverse attachment FAT 80, studied by Kuhlmann 2006.

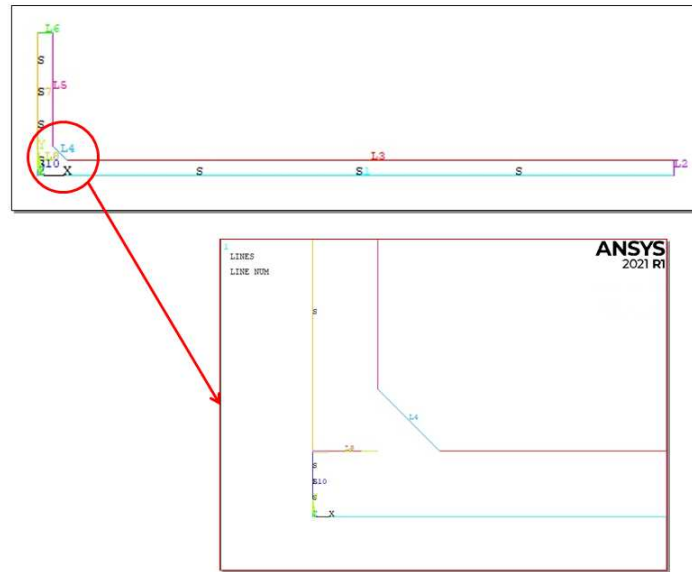


Figure 3.112: Symmetry condition of the model of transverse attachment FAT 80 studied by Kuhlmann 2006.

3.6.1 SHSS (Structural Hot Spot Stress) approach

The fatigue assessment for this model is performed by the application of SHSS approach, following the IIW recommendation [1] to obtain the hot-spot stress. According to the guideline, the weld toe of the transverse attachment FAT 80 studied by Kuhlmann in 2006, is a hot-spot type *a* and the hot-spot stress value is detected with the employment of fine mesh, as *Figure 1.4* shows.

The model is divided in a series of areas to allow the application of *Mapped-mesh* algorithm; indeed each areas must be characterised by a number of side between 3 and 4 to obtain a *Mapped-mesh*. The eight-node linear element PLANE 182 is chosen in Ansys®APDL with *Simple Enhanced Strain* as Key Option 1 and *Plane Strain* as Key Option 3.

The all informations about the mesh is reported in the following table:

Element type	Mesh algorithm	Main plate thickness <i>t</i>	Max element size	Adopted element size
Plane 182 KeyOpt:Simple Enhanced Strain + Plane Strain	Mapped	12 mm (6 mm modelled)	$0.4 \cdot t =$ $0.4 \cdot 12 = 4.8mm$	2.4 mm

Table 3.57: Requirements for SHSS mesh.

The hot-spot stress is extrapolated at two reference points placed at $0.4t$ and $1.0t$ distance from the weld toe tip, so in this case at 4.8 mm and 12 mm from weld toe.

For the type of extrapolated stress, the graph in *Figure 3.113* shows that, for an external applied pressure $\Delta\sigma_{nom} = 1MPa$, after 1.25 mm, the $\Delta\sigma_{xx}$ and the first principal stress $\Delta\sigma_{11}$ are coincident. For this reason the choice is indifferent.

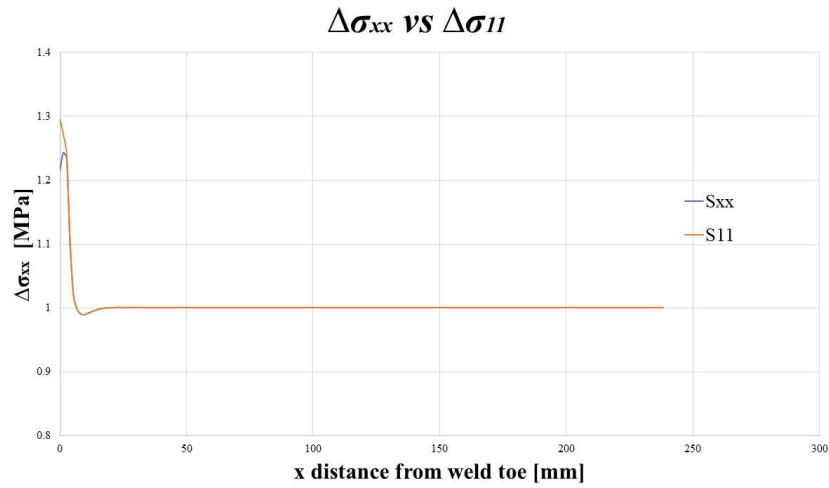


Figure 3.113: $\Delta\sigma_{xx}$ and $\Delta\sigma_{yy}$ plotted in function of the distance from weld toe tip

The mesh of the model is reported in the following figures:

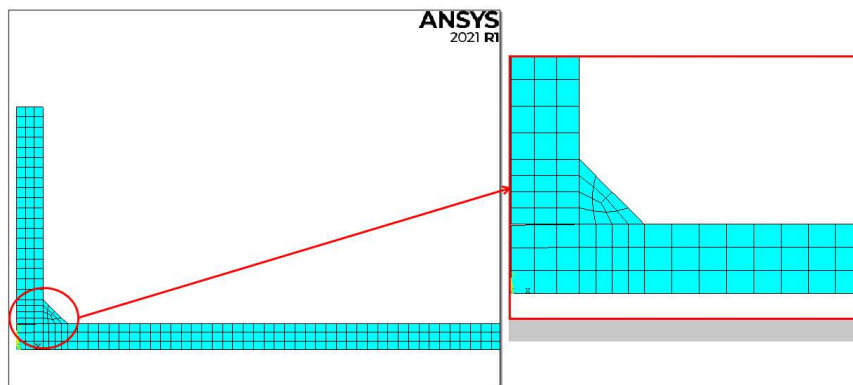


Figure 3.114: Mapped mesh for SHSS approach

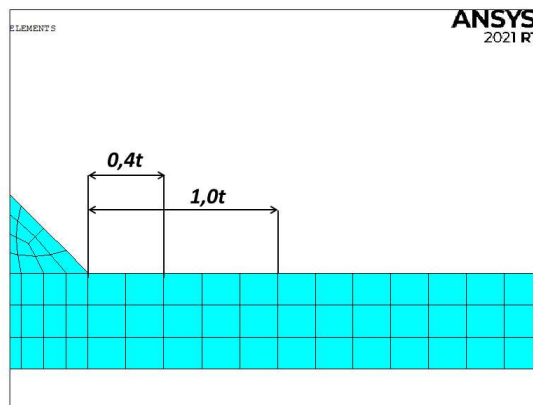


Figure 3.115: Mapped mesh for SHSS approach and reference points

For an external applied pressure $\Delta\sigma_{nom} = 1MPa$, the results of the tension at the reference points are:

$$\Delta\sigma_{xx,0.4t} = 1.02783MPa \quad (3.199)$$

$$\Delta\sigma_{xx,1.0t} = 0.99254MPa \quad (3.200)$$

$$\Delta\sigma_{11,0.4t} = 1.02829MPa \quad (3.201)$$

$$\Delta\sigma_{11,1.0t} = 0.99254MPa \quad (3.202)$$

$$(3.203)$$

The structural hot-spot stress is detected with the equation 1.2:

$$\Delta SHSS_{LSE,xx} = 1,67 \cdot \sigma_{xx,0.4t} - 0.67 \cdot \sigma_{xx,1.0t} = 1.67 \cdot 1.02783 - 0.67 \cdot 0.99254 = 1.05147MPa \quad (3.204)$$

$$\Delta SHSS_{LSE,11} = 1,67 \cdot \sigma_{11,0.4t} - 0.67 \cdot \sigma_{11,1.0t} = 1.67 \cdot 1.02829 - 0.67 \cdot 0.99254 = 1.05224MPa \quad (3.205)$$

This result is in good agreement with the value found in literature [33]:

$$\Delta\sigma_{xx,0.4t} = 1.025MPa \quad (3.206)$$

$$\Delta\sigma_{xx,1.0t} = 0.992MPa \quad (3.207)$$

$$(3.208)$$

$$\Delta SHSS_{LSE,literature} = 1,046MPa$$

Thus, the relative errors expresses in percentage between the calculated $\Delta SHSS_{LSE,xx}$, $\Delta SHSS_{LSE,11}$ and the $\Delta SHSS_{LSE,literature}$ are:

$$\Delta\% = \frac{\Delta SHSS_{LSE,xx} - \Delta SHSS_{LSE,literature}}{\Delta SHSS_{LSE,literature}} \cdot 100 = 0.52\% \quad (3.209)$$

$$\Delta\% = \frac{\Delta SHSS_{LSE,11} - \Delta SHSS_{LSE,literature}}{\Delta SHSS_{LSE,literature}} \cdot 100 = 0.60\% \quad (3.210)$$

Due to the lack of the experimental data, the results can not be imported inside the FAT 100 curve proposed by IIW guideline [1].

3.7 Summary of the results

SHSS results

The Hot-spot stress results of the all models are collected together in the following table with the type of mesh algorithm, the type of element, the thickness t , the global element size d and the relative error.

Name of model	Mesh Pattern	FE type	t [mm]	d [mm]	$SHSS_{LSE,paper}$ [MPa]	$SHSS_{LSE,calc.}$ [MPa]	$\Delta\%$
Marquis (2010)	Mapped	Solid 185	8	1.6	1.406	1.432	1.80%
Vanrostenberghe (2015)	Mapped	Solid 185	10	2	1.384	1.404	1.44%
Vanrostenberghe (2015)	Mapped	Solid 185	20	2	1.203	1.198	-0.35%
Yildirim (2020)	Mapped	Plane 182	6	1.2	1.035	1.0298	-0.50%
Okawa (2013)	Mapped	Plane 182	20	4	1.066	1.0661	0.026%
Kuhlmann-Gunther (2009)	Mapped	Plane 182	12	2.4	1.041	1.0436	0.25%
Kuhlmann(2006)	Mapped	Plane 182	12	2.4	1.046	1.0515	0.52%

Table 3.58: Summary of SHSS results of the all models

The all experimental data of the all models are collected inside the SHSS design curve proposed by IIW guideline:

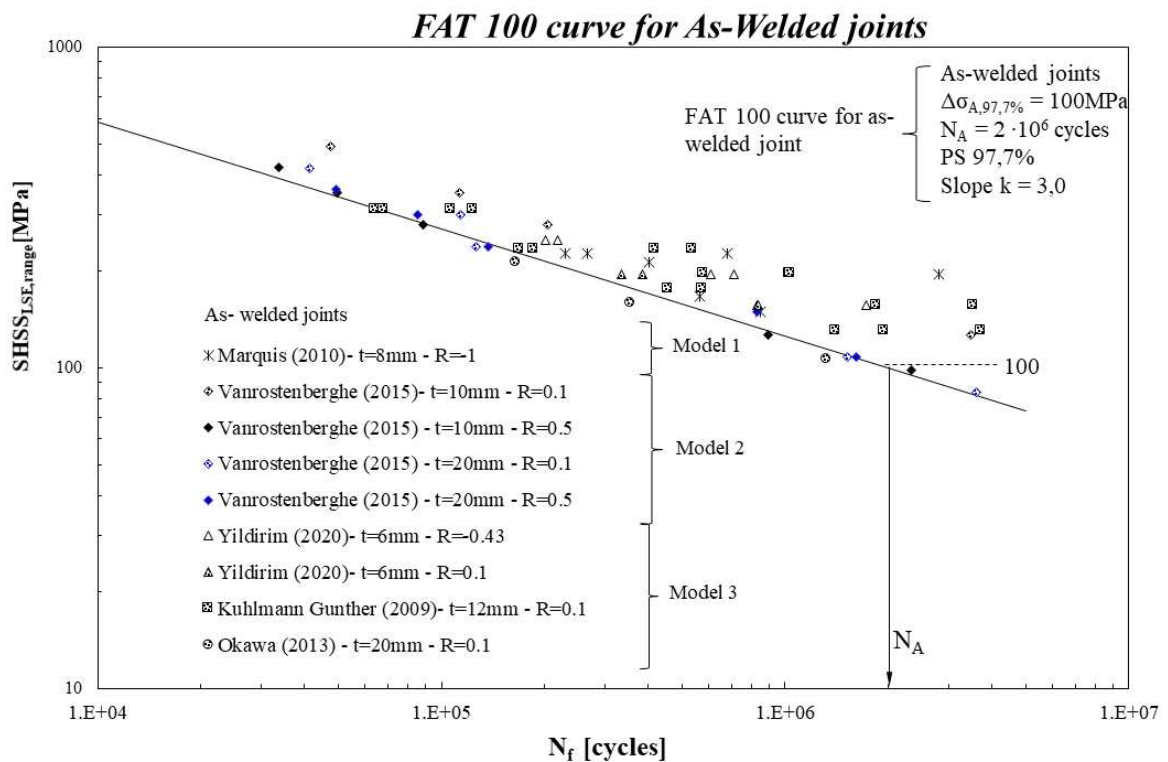


Figure 3.116: Experimental data inside the SHSS design curve.

PSM results

The PSM results of the all models are collected in three tables :

1. The first two tables collect the PSM results of 3D models. Indeed there are the values of the equivalent peak stress obtained from PSM Brick 185 ($\Delta\sigma_{eq,peak,Sub}$), PSM Tetra 187 ($\Delta\sigma_{eq,peak,Tetra}$) and from SED ($\Delta\sigma_{eq,peak,SED}$) with the relative errors;
2. The third table collect the PSM results of 2D models with the relative errors.

Name of model	$\Delta\sigma_{eq,peak,paper}$ [MPa]	$\Delta\sigma_{eq,peak,Sub}$ [MPa]	$\Delta\%$	$\Delta\sigma_{eq,peak,Tetra}$ [MPa]	$\Delta\%$
Marquis (2010)	2.307	1.897	-17.74%	2.368	2.66%
Vanrostenberghe (2015)	3.274	3.738	-14.17%	3.274	3.01%
Vanrostenberghe (2015)	3.571	3.979	-11.40%	3.589	0.47%

Table 3.59: Summary of PSM results of the all 3D models

Name of model	$\Delta\sigma_{eq,peak,paper}$ [MPa]	$\Delta\sigma_{eq,peak,SED}$ [MPa]	$\Delta\%$
Marquis (2010)	2.307	2.304	-0.129%
Vanrostenberghe (2015)	3.274	3.269	-0.168%
Vanrostenberghe (2015)	3.571	3.571	-0.049%

Table 3.60: Summary of PSM results of the all 3D models

Name of model	$\Delta\sigma_{eq,peak,paper}$ [MPa]	$\Delta\sigma_{eq,peak,PSM}$ [MPa]	$\Delta\%$
Yildirim (2020)	1.620	1.5985	-1.37%
Okawa (2013)	1.969	1.899	-3.488%
Kuhlmann-Gunther (2009)	2.178	2.179	0.20%

Table 3.61: Summary of PSM results of the all 2D models

The all experimental data are collected inside the PSM design curve proposed by Meneghetti and Lazzarin for structure subjected to prevailing mode I.

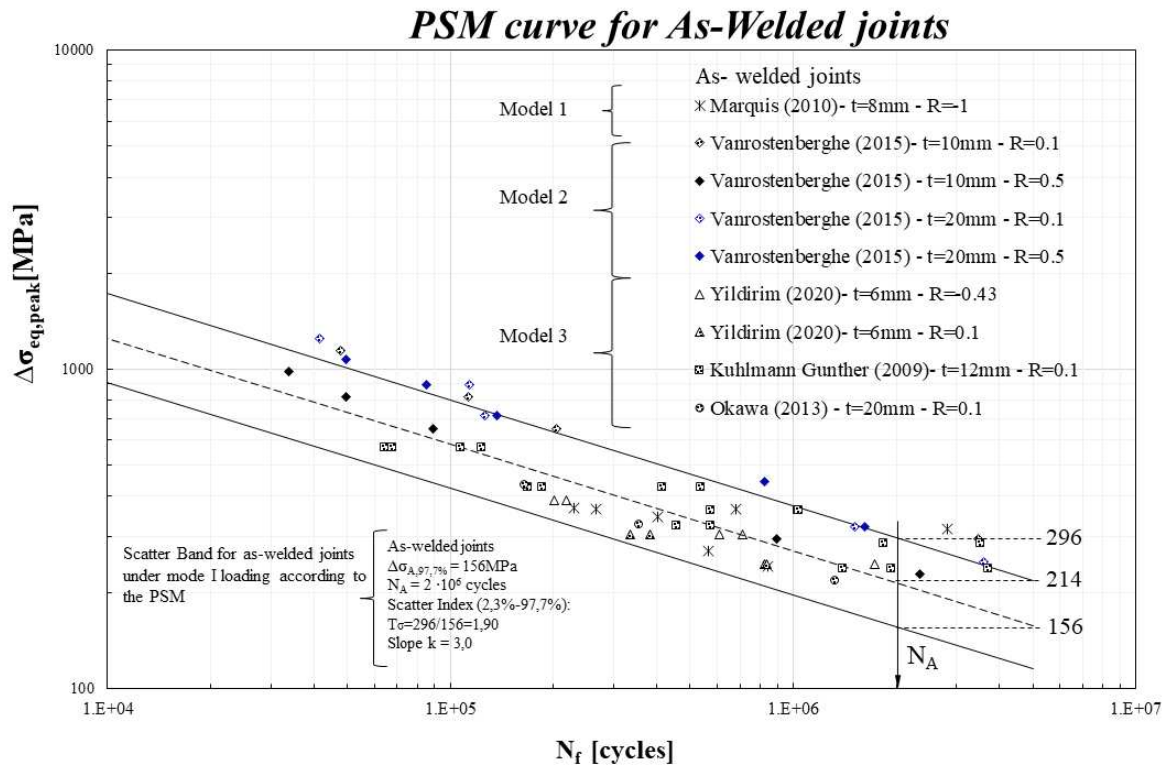


Figure 3.117: Experimental data inside the PSM design curve.

Chapter 4

Numerical analysis of experimental data and fatigue assessment of HFMI-treated joint by local approaches

The objective of this chapter is to perform a fatigue assessment on various HFMI-treated joint in terms of Equivalent Peak Stress and Structural Hot-Spot stress. The re-elaborated data are collected together and entered inside their respective design curve, available in the literature. Subsequently, a fatigue life N_f comparison with the experimental data, is elaborated to identify the grade of conservatives defined by each method. The Equivalent Peak Stress is calculated through the SED approach, the same method used for as-welded joint. The fatigue assessment with the SHSS method refers to the rule and dispositions defined in the IIW guideline [3].

The analysed joint are the same of the as-welded analysed joint in the *Chapter 3*.

The assessment are performed with the application of local approaches above-mentioned through the use of the finite element software Ansys®Mechanical APDL with the license of the University of Padua. For the modelling and study of 2D geometries, the four-node linear element PLANE 182 is adopted with *Simple Enhanced Strain* as Key Options 1 and *Plane Strain* as Key Options 3; on the other hand, in the case of 3D structure, the eight-node linear element SOLID 185 (also called Brick 185) is used with *Simple Enhanced Strain* as Key Options 1 and also the ten-node quadratic element SOLID 187 (also called Tetra 187) is adopted with *Pure displacement* as Key Options 1.

The all specimens have been modelled inside *SOLIDWORKS 2020* and after they have been imported inside Ansys®APDL with *.IGS* extension.

The dimensions of the HFMI groove are defined in the literature [33] and in order to correctly apply the PSM with the SED approach, the hypothesis of blunt V-notches has to be made.

The SHSS method for HFMI-treated joints is characterised by the same procedures described in the *Chapter 3*.

The misalignment effect on the HFMI-treated joints is neglected because is not considered critical.

Before the description of the equivalent peak stress detection, the HFMI treatment is explained and described.

4.1 Principles of HFMI post-weld treatments on welded joints to improve the weld toe

The structures are subjected to severe cyclic and dynamic loading conditions during their service life, which can result in fatigue damage at welded joints, where the local stress concentration are significant effect due to the joint geometry (weld toes and roots). In order to overcome this problem, several thermal and mechanical post-weld treatment are proposed to improve the stress field and/or the surface geometry in and around the welds. Some of this techniques are applied during the welding process, others are performed after the welding process.

The High-frequency mechanical impact (HFMI) is a novel, reliable and effective post-treatment technique to improve the fatigue strength of welded structures.

The reference guideline for this technique is *IIW Recommendations for the HFMI Treatment* [3].

4.1.1 Description of HFMI treatment

The HFMI treatment was developed at the Northern Scientific and Technological Foundation in Russia in association with Paton Welding Institute in Ukraine.

In the past ten years, the HFMI treatment has been defined as a reliable, user-friendly and efficient technique for post-weld fatigue life improvement of welded joints. Indeed, the past decade has seen steady increase in the number of HFMI peening equipment manufactures. There are different type of power sources for peening devices: ultrasonic impact treatment (UIT), ultrasonic peening (UP), ultrasonic peening treatment (UPT), high frequency impact treatment (HiFiT), pneumatic impact treatment (PIT) and ultrasonic needle peening (UNP). The working principle of the High-frequency mechanical impact technique is identical for every power sources: a cylindrical indenters are accelerated against a component or structure at the potential fatigue crack initiation sites with high frequency (>90 Hz), so that the impacted material endures a local plastic deformation. The cylindrical indenters can be different diameters and can be single or multiple, depending on the manufacturer of the device and the purpose of the use.

The benefits of HFMI treatment are:

1. The imposed of a beneficial compressive residual stress state near to the weld toe;
2. The establishment of a smooth transition from parent material to the weld metal (same thing for the cold-worked surface region);
3. The material microstructure modifies, as well as the local weld toe geometry.

In the following figure are reported some example of HFMI treatment joint from different companies:

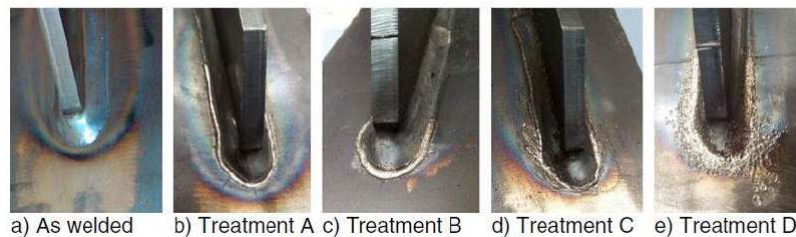


Figure 4.1: Different HFMI grooves [46].

The reference guideline for this technique is *IIW Recommendations for the HFMI Treatment* [3] and it has been published in the 2006. The guideline defined that the HFMI treatment is applicable to joint made of structural steel, main plate ranging between 5 and 50 mm and steel grade f_y ranges from 235 MPa to 960 MPa. However, during the last years, a research is conducted also on aluminium and stainless-steel structures.

This technique can solely be applied to weld toe. For this reason, if a joint is characterised by a potential fracture at the root, the HFMI treatment can not be effective for this joint.

The weld toe treatment procedures can vary from application to application and depending on the tool being used. The *Table 4.1* defines example procedure parameter for two HFMI tools with alternate power sources and indenter configuration (*Figure 4.2*).

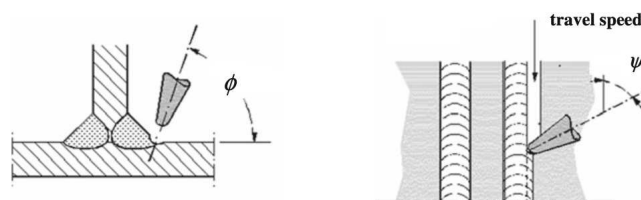


Figure 4.2: Orientation of the HFMI tool respect to weld being treated [3].

Parameter	HFMI tool	
	HiFIT	UIT
Power source	Pneumatic	Ultrasonic magnetostrictive
Number of indenters	1	1-4
Angle of the axis of the indenters with respect to the plate surface, Φ	60°-80°	30-60° 40°-80°
Angle of the axis of the indenters with respect to the direction of travel, Ψ	70°-90°	90° (all pins should contact the weld toe)
Working speed	3-5 mm/s	5-10 mm/s 5-25 mm/s
Other		The self-weight of the tool is sufficient. Minimum of 5 passes

Table 4.1: Comparison between HiFIT and UIT [3].

The inclination angle of the indenter with respect to plate surface Φ is common practise to match it to the V-notch bisector.

The guideline define some advices on visual inspections for the qualitative and quantitative measurement of weld toe groove due to HFMI treatment. The resulting groove must be smooth along all defined weld, shiny, continuous, with no breaks or visible lines as undercuts or porosity. *Figure 4.3-4.4* show some example of no well-treated weld toe.

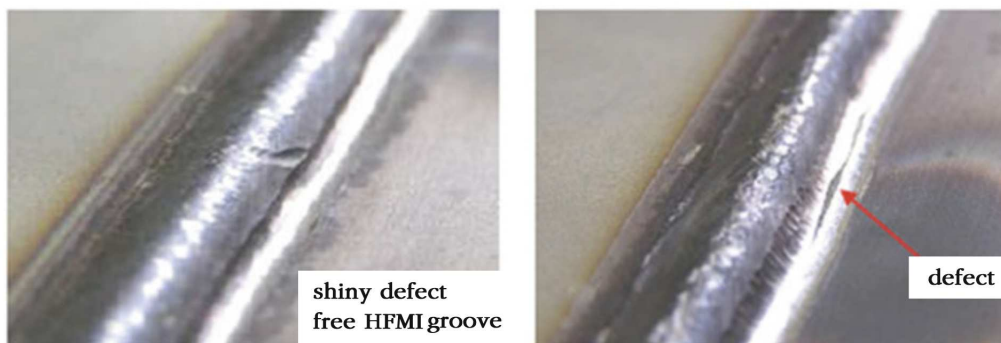


Figure 4.3: A shiny and defect free HFMI groove [3].

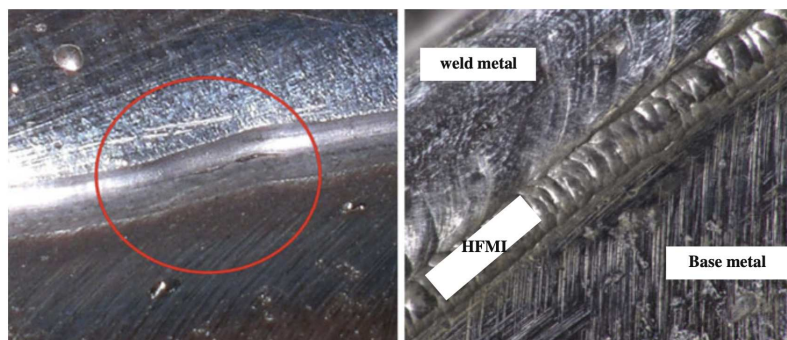


Figure 4.4: On the left, the HFMI groove shows a thin crack-like defect which can reduce or eliminate the benefits of HFMI treatment. On the right, a non-smooth HFMI groove which needs further peening [3].

HFMI treatment produces significant local cold-forming of the material near the weld fusion line. In the case that the indenters are excessively impacted in one single location at the weld toe, the resulting plastic displacement of the metal can result in a crack-like feature at the side of HFMI groove as *Figure 4.5* shows. This defect must be removed by light grinding and the weld toe should be retreated

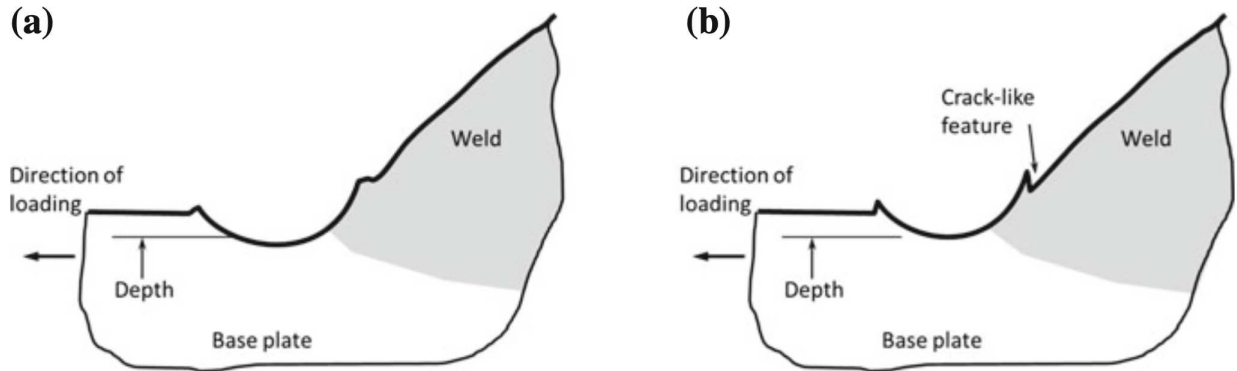


Figure 4.5: On the left, the proper profile of HFMI groove. On the right, an improper profile of HFMI groove where there is a crack-like feature due to plastic deformation of the material [3].

Concerning quantitative aspects, the guideline defines some typical post-weld treatment geometrical dimensions with reference to *Figure 4.6*:

- Groove depth: 0.1-0.6 mm;
- Groove width; 3-6 mm;
- Groove radius: depends on the type of pin tip and the number of passes.

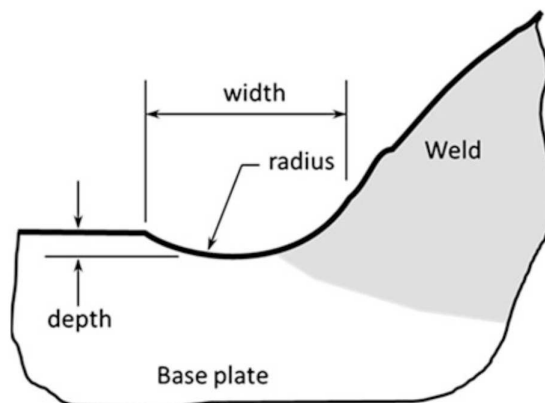


Figure 4.6: Reference to define the dimension of HFMI groove [3].

The guideline defines that no single groove dimension is optimal in all situations because each configuration depends on the steel yield strength and the diameter of indenter. Furthermore, a minimum groove depth of about 0.1-0.2 mm is necessary to guarantee a complete weld toe treatment.

4.1.2 Fatigue assessment of HFMI-treated joints (IIW recommendations)

The fatigue assessment of HFMI-treated joints is defined in terms of nominal stress, structural hot-spot method and effective notch stress. The guideline includes the fatigue design curve for each assessment method. The HFMI improvements is applied to the weld toe and its objective is to increase the fatigue lives of weld treated from the point of view of potential fatigue failure from the weld toe.

Nominal stress approach

The advantages of HFMI treatment are available only for welded joints characterised by FAT classes between FAT 50 and FAT 90. This limitation is due to the fact that the upper classes include complex structural geometries or non-welded details, that are not governed by a weld toe failure; instead, the lower classes have not been studied with respect the HFMI improvement yet.

There are many factors that can reduce and modify the reference nominal FAT classes for the HFMI-treated joints:

1. **Thickness and size effect:** plate thickness and weld size influence the local stress concentration at the weld toe and the stress gradient through the plate thickness. These effects can reduce the fatigue strength of the joint. For this reason the nominal stress assessment method and also the structural hot-spot method require a thickness reduction factor for plate characterised by a thickness greater then 25 mm and it is defined in the following equation:

$$f(t) = \left(\frac{25}{t_{eff}} \right)^{0.2} \quad (4.1)$$

where:

- $t_{eff} = \frac{L}{2}$ for $\frac{L}{t} < 2$;
- $t_{eff} = t$ for $\frac{L}{t} \geq 2$.

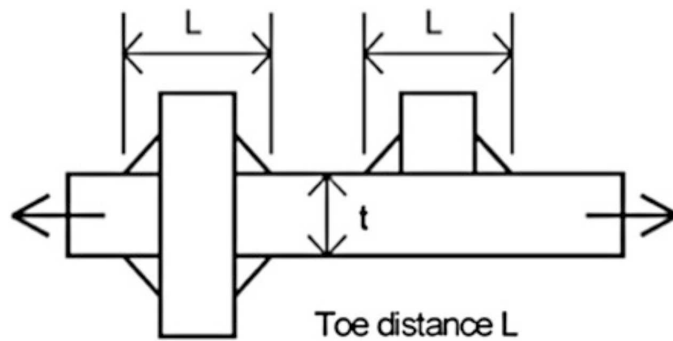


Figure 4.7: Description of L and t [3].

2. **Steel Strength:** the effect of the material steel strength on the grade of improvement is reported in the Figure 4.8 and the recommendation defines that:

- for $f_y < 355MPa$, four fatigue classes FAT increase in strength respect to the nominal fatigue class in the as-welded condition;
- for $f_y > 355MPa$, one fatigue class FAT increase in strength (about 12.5%) for every 200 MPa increment in yield resistance f_y is recommended.

The HFMI benefit effect have the tendency to increase with the material steel grade.

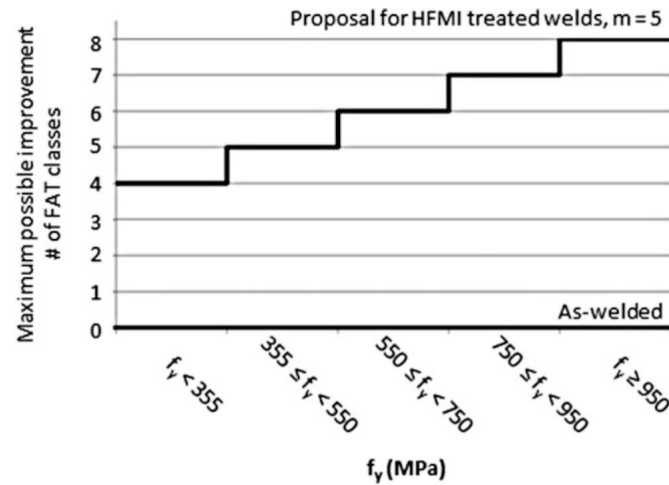


Figure 4.8: Maximum increase in the number of FAT classes as a function of f_y [3].

3. **Loading effects:** the overloads on the structures can conduct to a plastic redistribution of the material around the weld toe area and this effect can cause a decrease of the beneficial compressive residual stress, so the structures can have a reduction of the benefit effect of HFMI treatment. The following table explains the limitation on the maximum applied stress:

Type of load	As-welded condition	HFMI + hammer/needle peening
$\Delta\sigma_{nom,max}$ [MPa]	$1.5 \cdot f_y$	$0.8 \cdot f_y$ due to overloads, $R < 0.5$
$\Delta\tau_{nom,max}$ [MPa]	$1.5 \cdot \frac{f_y}{\sqrt{3}}$	
$\Delta\sigma_{hs,max}$ [MPa]	$2 \cdot f_y$	

Table 4.2: Maximum applied stress [3].

4. **Stress ratio R:** the effect of stress ratio R is expressed as a penalty with respect to the maximum increase in the number of FAT classes as a function of f_y . Indeed, this effect can strongly change the service life of the component.

The graph in the Figure 4.9 expresses that the higher the stress ratio is, the lower the fatigue endurance in terms of maximum applicable nominal stress becomes.

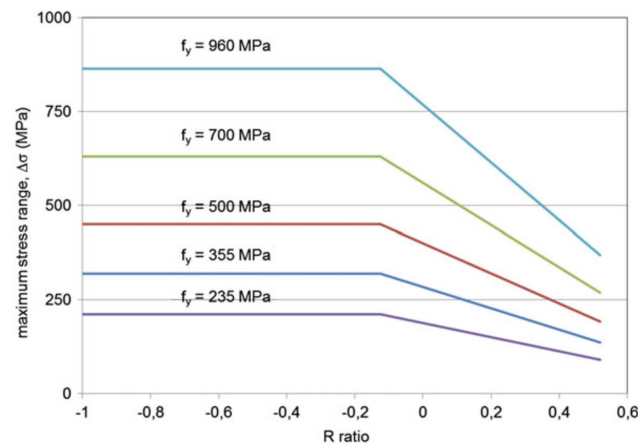


Figure 4.9: Influence of stress Ratio in CAL condition and in terms of $\Delta\sigma_{nom,max}$ [3].

The penalty effect of the stress ratio R is expressed in the following table:

Stress Ratio R	Minimum FAT classes reduction
$R \leq 0.15$	No reduction
$0.15 < R \leq 0.28$	One FAT class reduction
$0.28 < R \leq 0.4$	Two FAT classes reduction
$0.4 < R \leq 0.52$	Three FAT classes reduction
$R < 0.52$	No data available

Table 4.3: Effect of stress ratio R [3].

5. **Variable Amplitude Loading:** in many situation it is convenient to express the variable amplitude loading in terms of an equivalent constant amplitude loading history with the following equation, based on Miner's damage sum hypothesis:

$$\Delta\sigma_{eq} = \left(\frac{1}{D} \cdot \frac{\sum \Delta\sigma_i^m \cdot N_i + \Delta\sigma_k^{m-m'} + \sum \Delta\sigma_j^{m'} \cdot N_j}{\sum N_i + \sum N_j} \right)^{\frac{1}{m}} \quad (4.2)$$

where:

- $\Delta\sigma_{eq}$ is the equivalent applied stress in terms of Constant Amplitude Loading (CAL);
- $N_{i,j}$ are the number of cycles spent at their respective stress range $\Delta\sigma_{i,j}$;
- $\Delta\sigma_k$ is the stress range that corresponds to the knee point at $N = 1 \cdot 10^7$ cycles;
- D is the damage sum, ranging from 0 to 1;
- m is the inverse slope above the knee point;
- m' is the inverse slope below the knee point;

All fatigue design methods for HFMI-treated joints are based on an assumed inverse slope of the nominal FAT classes equal to $m = 5$ and, as for the as-welded condition, FAT classes are defined at $N_A = 2 \cdot 10^6$ cycles. For Constant Amplitude Loading (CAL) condition, it is recommended that the slope parameter m is changed to 22 at $N_D = 1 \cdot 10^7$ cycles; while for VAL condition the inverse slope is changed to $m' = (2m - 1)$. The nominal S-N curves for HFMI-treated joints in CAL condition, are illustrated from *Figure 4.10* to *Figure 4.14* to changing of the steel grade f_y and for a Stress Ratio R lower than 0.15.

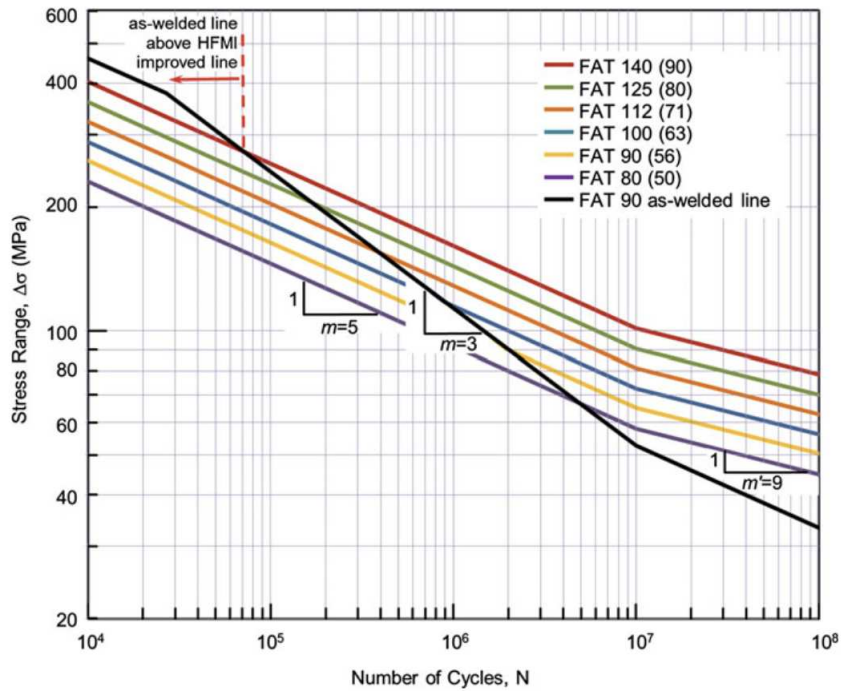


Figure 4.10: Nominal stress S-N curve for HFMI improved welded joints, $f_y < 355 \text{ MPa}$, $R < 0.15$. The value in the brackets represents the reference FAT class in As-welded condition. In black, the FAT 90 as-welded line with a inverse slope m equal to 3 [3].

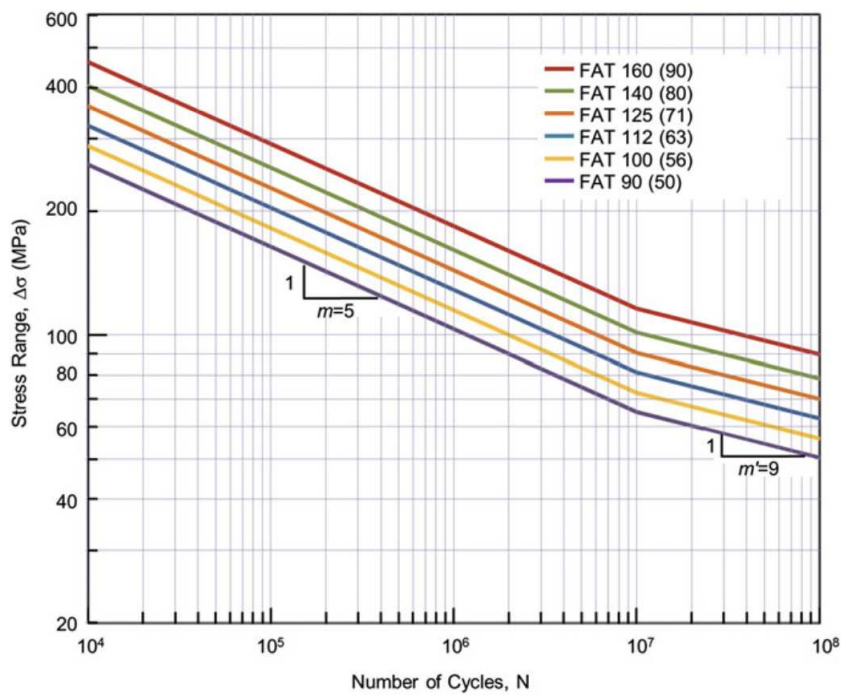


Figure 4.11: Nominal stress S-N curve for HFMI improved welded joints, $355 \text{ MPa} \leq f_y < 550 \text{ MPa}$, $R < 0.15$. The value in the brackets represents the reference FAT class in As-welded condition [3].

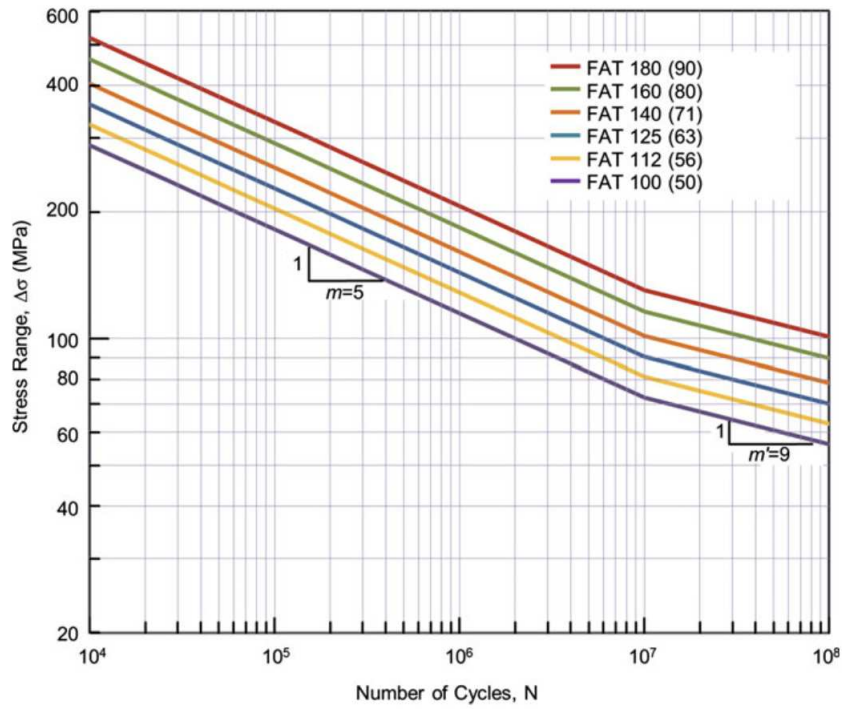


Figure 4.12: Nominal stress S - N curve for HFMI improved welded joints, $550\text{MPa} \leq f_y < 750\text{MPa}$, $R < 0.15$. The value in the brackets represents the reference FAT class in As-welded condition [3].

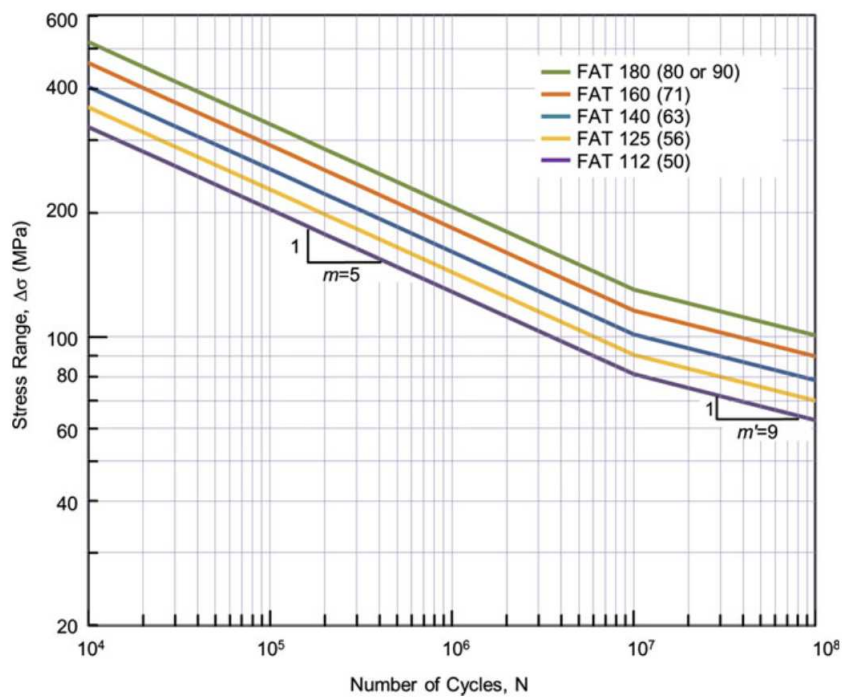


Figure 4.13: Nominal stress S - N curve for HFMI improved welded joints, $750\text{MPa} \leq f_y < 950\text{MPa}$, $R < 0.15$. The value in the brackets represents the reference FAT class in As-welded condition [3].

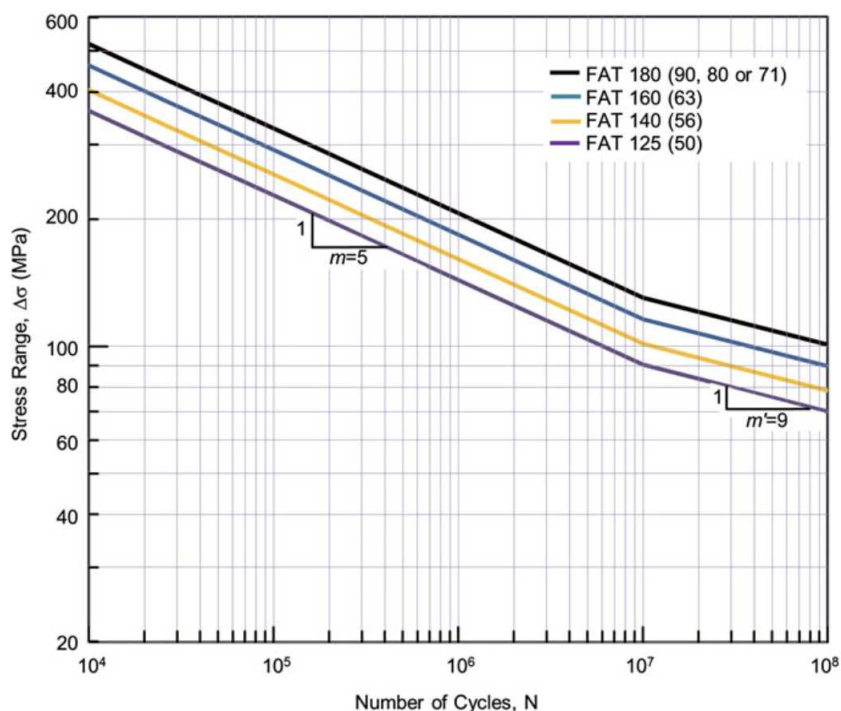


Figure 4.14: Nominal stress S-N curve for HFMI improved welded joints, $950\text{MPa} \leq f_y$, $R < 0.15$. The value in the brackets represents the reference FAT class in As-welded condition [3].

In the *Figure 4.10* is reported the as-welded FAT 90 and its respective HFMI FAT 140 curve. These two curves are characterised by a different slope and due to this, there is an intersection point, called N_I in this thesis. Thus, for a number of cycles $N < N_I$, the as-welded line define a higher number of cycles to failure than the respective HFMI curve. Indeed, for welded structures in low strength steel, fatigue strength improvement due to the HFMI treatment will not be expected if the fatigue life is less than N_I . In the following table are reported the specific value to varying the steel grade f_y :

f_y [MPa]	N_I [cycles]
$f_y < 355$	72 000
$355 \leq f_y < 550$	30 000
$550 \leq f_y < 750$	12 500
$750 \leq f_y$	<10 000

Table 4.4: Computed cycles limit below which HFMI is not expected to result in fatigue strength improvement as a function of steel strength [3].

Structural Hot-Spot Stress approach

The procedure for the numerical extrapolation with the used of FE software for HFMI-treated joints is the same of the as-welded joint, describe in the paragraph 1.2.1.

In as-welded condition, the different nominal FAT classes are collapsed in only two FAT classes for the hot-spot method: FAT 90 and FAT 100. In the case of HFMI-treated joints, the IIW guideline defined that the FAT classes depend on the steel grade range as the following table shows:

f_y [MPa]	LC fillet welds		NLC fillet welds	
	FAT	$L_{S,min}$	FAT	$L_{S,min}$
<i>As-welded, m=3</i>				
All f_y	90	-	100	-
<i>Improved by HFMI, m=5</i>				
$f_y < 355$	140	-	160	-
$355 \leq f_y < 550$	160	-	180	-
$550 \leq f_y < 750$	180	-	200	1.15
$750 \leq f_y < 950$	200	1.15	225	1.25
$950 \leq f_y$	225	1.25	250	1.40

Table 4.5: FAT classes for structural hot-spot approach for as-welded and HFMI conditions [3].

After the extrapolation of the SHSS, the verification of the value is recommended with the following equation, that represents the structural hot-spot stress concentration k_S :

$$k_S = \frac{\sigma_{hs}}{\sigma_{nom}} > k_{S,min} \quad (4.3)$$

When the SHSS method is used a computation problem may arise for welded details with small structural stress concentrations, the hot spot stress system must be limited so as not result in a S-N curve greater than FAT 180 in the nominal stress system [3].

The fatigue class reduction for nominal stress approach due to the stress ratio R and the loading conditions can be used also for SHSS approach.

Effective Notch Stress approach

The procedure for the numerical extrapolation of Effective Notch Stress with the used of FE software for HFMI-treated joints is the same of the as-welded joint, describe in the paragraph 1.2.2.

In as-welded condition, the different nominal FAT classes are collapsed in only one FAT class for the ENS method: FAT 225. In the case of HFMI-treated joints, the IIW guideline defined that the FAT classes depend on the steel grade range as the following table shows with the assumption that $\Delta\sigma$ is computed in terms of maximum principal stress range at the notch:

f_y [MPa]	Effective Notch Stress characteristic curve modelled using $\rho_f = 1mm$
<i>As-welded, m=3</i>	
All f_y	225
<i>Improved by HFMI, m=5</i>	
$f_y < 355$	320
$355 \leq f_y < 550$	360
$550 \leq f_y < 750$	400
$750 \leq f_y < 950$	450
$950 \leq f_y$	500

Table 4.6: FAT classes for structural ENS approach for as-welded and HFMI conditions [3].

Fricke [2] defines the effective notch stress concentration as the ratio of effective notch stress to structural stress:

$$K_W = \frac{\sigma_W}{\sigma_S} \quad (4.4)$$

Fricke proposes that a minimum K_W of at least 1.6 should be used for low stress concentration details. Indeed, if the computed K_W is lower than 1.6, the minimum value of $K_W = 1.6$ is used for fatigue assessment.

When the ENS method is used, a computation problem may arise for welded details with small structural stress concentrations, the effective notch stress system must be limited so as not result in a S-N curve greater than FAT 180 in the nominal stress system [3].

The fatigue class reduction for nominal stress approach due to the stress ratio R and the loading conditions can be used also for ENS approach.

4.1.3 Fatigue assessment of HFMI-treated joints: University of Padua approach

The Peak Stress method and the Strain Energy Density approach have been employed for the fatigue assessment of welded joints in as-welded condition. In 2020, Meneghetti, Campagnolo, Yildirim and Belluzzo [33] studied and applied the PSM and SED approaches for the fatigue assessment of HFMI-treated welded joints.

The HFMI groove radius at weld toe is typically defined between 1.5 mm and 4.5 mm. The hypothesis assumed that the weld toe radius equal to zero as the as-welded condition, is too restrictive; for this reason the weld toe of HFMI-treated joints is considered as a blunt V-notch. Thanks to this, the PSM can be employed in combination with the SED approach for blunt notches as describe in [33].

SED approach for blunt notches

Initially, the Strain Energy Density approach was proposed by Lazzarin and Zambardi [25] in 2001 for sharp V-notches but subsequently, it was extended also to blunt notches in 2005 [27]. The theory defined in 2005, follows the same principles of the previous one in 2001 for sharp V-notches in steel and aluminium alloys structure. A scheme of a blunt notch is displayed on the *Figure 4.15* with a polar reference system:

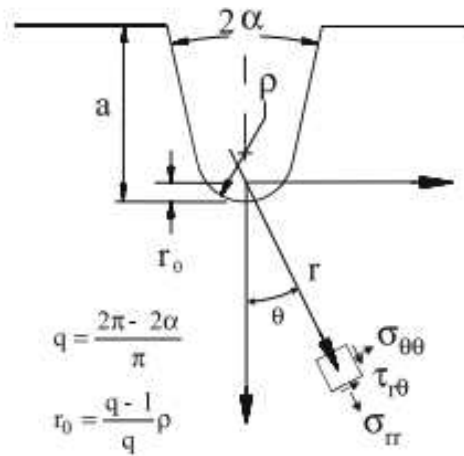


Figure 4.15: Polar coordinate system and stress components [27].

In the *Figure 4.15* are expressed two fundamental parameter to model correctly the rounded circular sector. These expression were defined by Neuber in 1958 and they are reported in the following equations:

$$q = \frac{2\pi - 2\alpha}{\pi} \quad (4.5)$$

$$r_0 = \frac{q-1}{q} \cdot \rho \quad (4.6)$$

where:

- 2α is the notch opening angle;
- ρ is the notch radius;
- r_0 is the distance between the origin of the analytical frame and the notch tip.

In the following figure are represented different examples of a structural volume in the case of sharp V-notch and blunt notch:

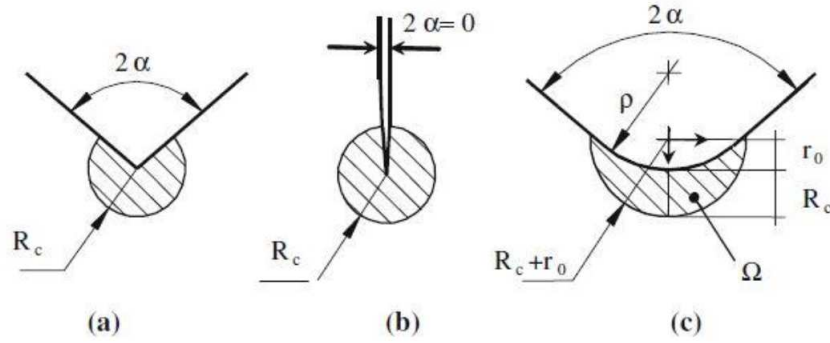


Figure 4.16: From left to right: schematic representation of sharp V-notch, a crack and blunt notch [27].

As described by Lazzarin in 2005, when a structure is subjected to different modes, at the notch the maximum principal stress is not aligned with the blunt notch bisector but it is characterised by a inclination angle ϕ . In this case, the structural volume must be rigidly rotate by a certain angle ϕ about the centre of the blunt notch. In this way, the maximum principal stress is entirely included in the volume, as the following figure shows:

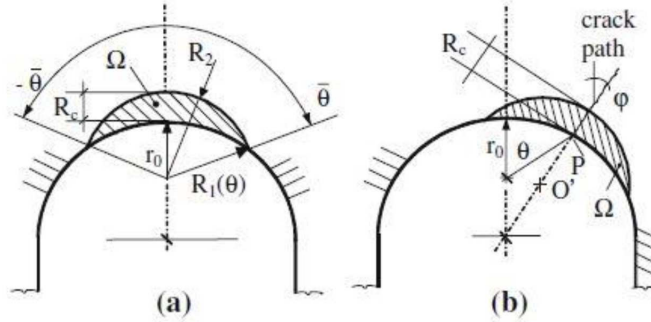


Figure 4.17: On the left, an example of structural volume under pure mode I, on the right, under combined modes [27].

In the case of a HFMI-treated joint, the averaged strain energy density $\Delta\bar{W}$ inside the structural volume can be calculated with the equation (1.9). In the FE environment, the average SED is calculated with the so-called "direct approach", with the following formula:

$$\Delta\bar{W}_{FEM} = \frac{\sum_{V(R_0)} W_{FEM,i}}{V(R_0)} \quad (4.7)$$

PSM combined with SED for blunt notches

Thanks to the linear elastic hypothesis, the equivalent peak stress can be defined as follows:

$$c_w \cdot \Delta\bar{W}_{FEM} = \frac{1 - \nu^2}{2E} \cdot \Delta\sigma_{eq,peak}^2 \quad (4.8)$$

$$\Delta\sigma_{eq,peak} = \sqrt{c_w \cdot \frac{2E \cdot \Delta\bar{W}_{FEM}}{1 - \nu^2}} \quad (4.9)$$

where:

- $\Delta\sigma_{eq,peak}$ is the equivalent peak stress;
- $\Delta\bar{W}_{FEM}$ is the average strain energy density inside the structural volume;
- c_w is the parameter accounting of the stress ratio R;
- E is the Young modulus;
- ν is the Poisson's ratio.

4.2 Marquis 2010, longitudinal attachment FAT 71

The first joint analysed is a longitudinal stiffener characterised by a fatigue class FAT 71, studied by Marquis and Yildirim in 2010 [41] under CAL (Constant Amplitude Loading).

The principal information and mechanical properties about this typology of the joint are summarized in the *Table 3.1* and *Table 3.2*:

Weld condition	Fracture location	Load application	Main plate/gusset thickness
HFMI, non-load carrying (NLC), full penetration	Weld toe	Axial, main plate, parent material	Main plate: 8mm Gusset: 8mm

Table 4.7: Information about the specimens

Material model	Yield strength f_y [MPa]	Young modulus [MPa]	Poisson's ratio ν
S700, HSS, Linear elastic, isotropic	700	206000	0.3

Table 4.8: Information about mechanical properties

The dimensions of this joint are defined and described in the paragraph 3.1 (*Table 3.3* and *Figure 3.1*). Regarding the HFMI groove geometry, the dimensions (radius, depth and width) are taken from [33] and the values are expressed in the following table with reference to *Figure 4.18*

depth [mm]	ρ_{HFMI} [mm]	width [mm]	2α [°]
0.21	3.31	3.71	150

Table 4.9: Dimension of HFMI groove for the longitudinal attachment FAT 71

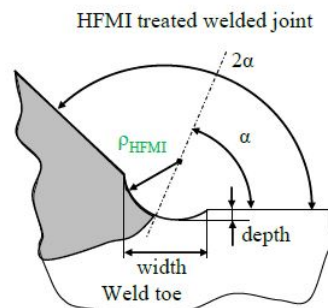


Figure 4.18: Reference to define the dimension of HFMI groove [33].

The inclination angle of the indenters is assumed to be performed along the V-notch bisector, i.e. 75° in this case.

The experimental data are defined in the following table in terms of nominal stress $\Delta\sigma_{nom}$:

Stress Ratio R	$\Delta\sigma_{nom}$ [MPa]	N_f [cycles]
-1	464	499 700
	450	552 400
	446	208 600
	410	1 949 000
	337	964 800
	337	858 400
	317	447 500
	305	469 700
	257	290 7000
	255	1 980 000

Table 4.10: Experimental data of the 1st joint, Marquis 2010 in HFMI treated condition.

FAT 71 is modelled in *SOLIDWORKS 2020* with the HFMI groove and subsequently, is imported inside Ansys®APDL with *.IGS* extension. The results is reported in the figure below:

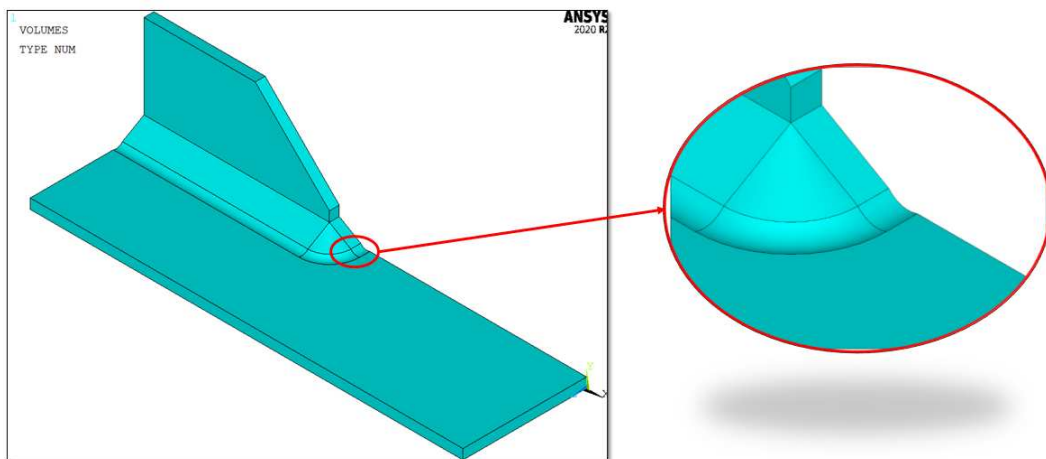


Figure 4.19: Model of longitudinal attachment FAT 71 in HFMI treated condition.

The procedure to define the boundary conditions of the model follows the same steps and dispositions defined for the same joint in as-welded condition described in the paragraph 3.1.

4.2.1 PSM combined with SED for blunt notches

The fatigue assessment for this model is performed by the application of Peak Stress Method in combination with the SED approach with the adoption of ten-node quadratic elements, considering only the weld toe.

The element SOLID 187 is chosen from the Ansys®APDL library with *Pure Displacement* as Key Option 1, which means that the nodal forces are only dependent on the displacements.

The SED approach for blunt notches is based on the creation of a structural volume at the radiused weld toe, that can be rigidly rotated (*Figure 4.20*) to included the whole maximum principal stress, which is related to the highest strain energy density.

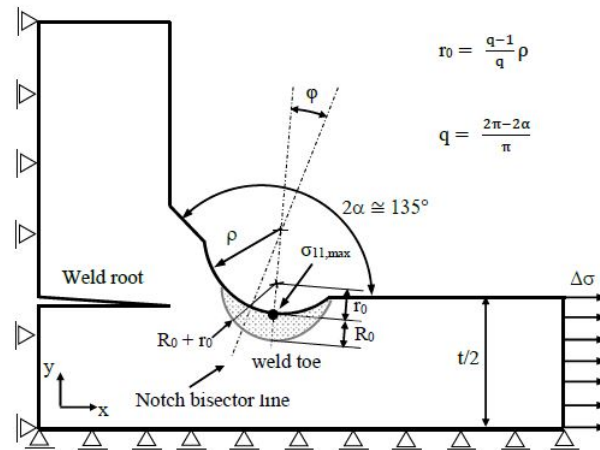


Figure 4.20: The "crescent shape" structural volume to calculate the averaged SED at the radiused weld toe of HFMI treated transverse NLC fillet welded joint [33].

The first step is to determinate the inclination angle Φ with respect to the blunt notch bisector of the most stressed area that is indicated in red in Ansys®APDL. To define the inclination angle, the model is meshed with a global element size equal to 1 mm. Subsequently, two refinements with depth equal to 5 (see Figure 4.21 for the refine options) are applied to the arc that represents the groove due to HFMI treatment (Figure 4.22) with the following commands:

Preprocessor→*Meshing*→*Modify Mesh*→*Refine At*→*Lines*

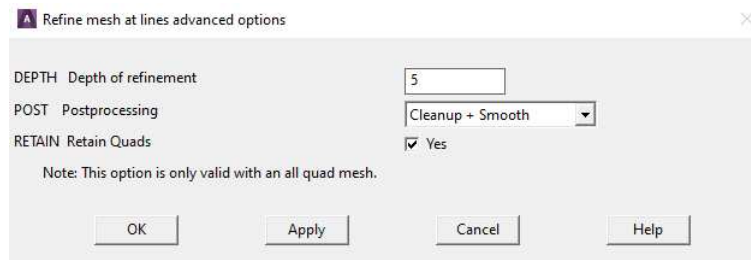


Figure 4.21: Options for the refinement.

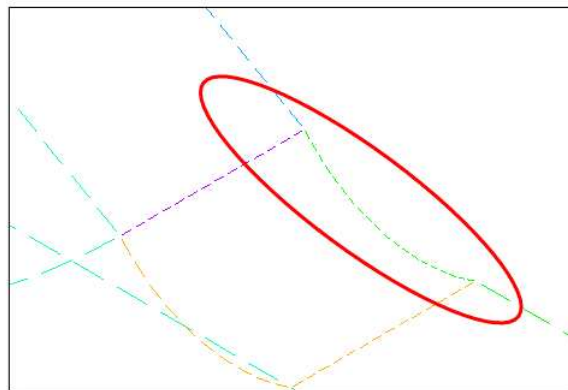


Figure 4.22: Arc that represents the HFMI groove where the refinements are applied.

The meshed model is displayed on the following figure:

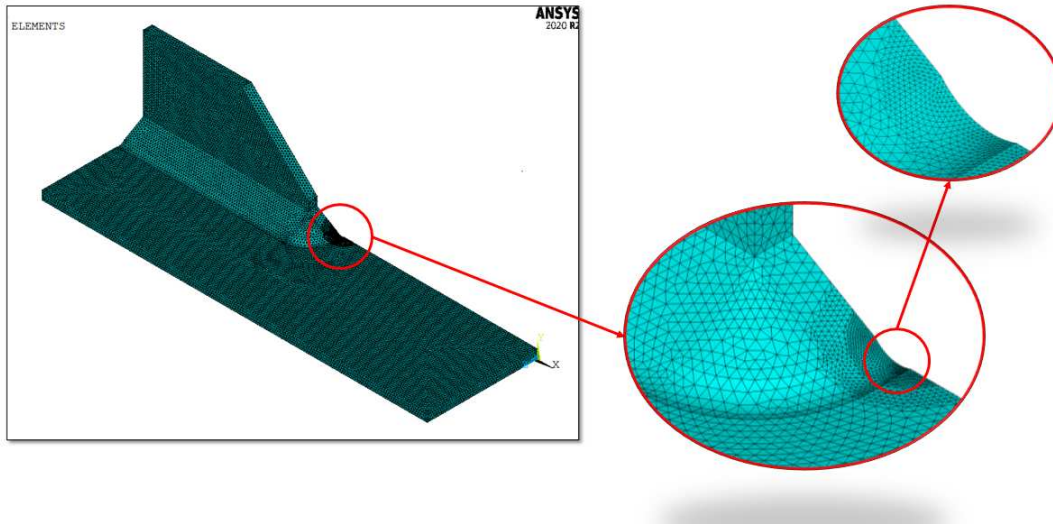


Figure 4.23: Mesh of the model to define the inclination angle.

The model is subjected to an external nominal stress $\Delta\sigma_{nom} = 1MPa$ applied on the main plate. Once the model is properly meshed, loaded and constraint, the system can be solve:

Solution → *Solve* → *Current LS*

The first principal stress $\Delta\sigma_{11}$ is plotted:

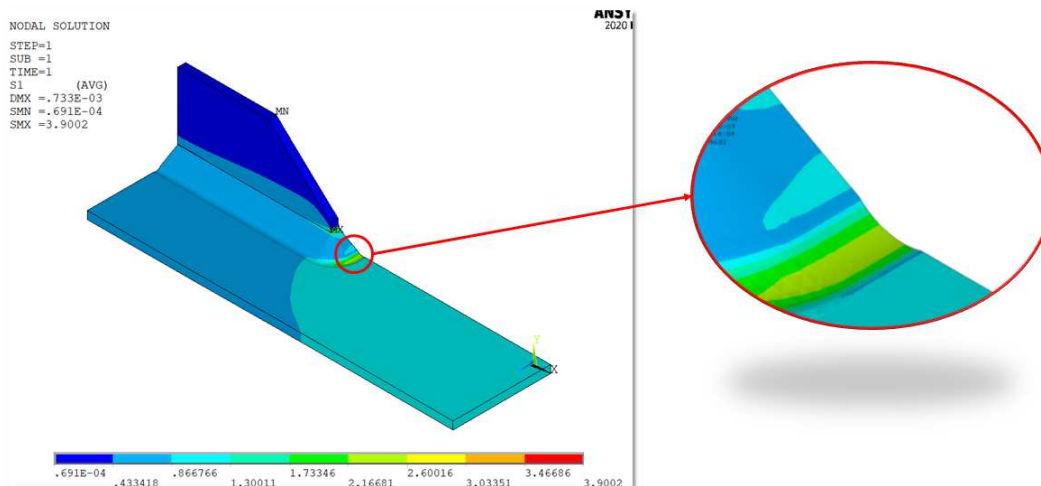


Figure 4.24: Plot of the first principal stress.

The highest stress is not located exactly around the blunt notch bisector, so it is matter of quantifying the grades of rotation. The value of the angle is reported in the following equation and represents a clockwise rotation about the global z-axis:

$$\Phi = 7.06^\circ \quad (4.10)$$

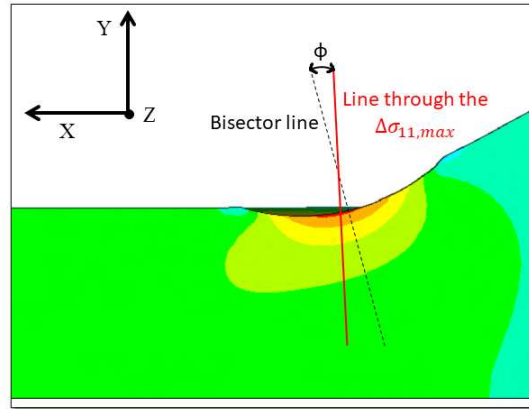


Figure 4.25: Inclination angle Φ

The circular sector is created according to equations (4.5) and (4.6):

$$q = \frac{2\pi - 2\alpha}{\pi} = 2 - \frac{150}{180} = 1.1667 \quad (4.11)$$

$$r_0 = \frac{q-1}{q} \cdot \rho_{HFMI} = \frac{1.1667-1}{1.1667} \cdot 3.31 = 0.53\text{mm} \quad (4.12)$$

$$R_0 + r_0 = 0.28 + 0.53 = 0.81\text{mm} \quad (4.13)$$

Subsequently, the control volume to calculate the averaged Strain Energy Density (SED) is created with a deep equal to 0.14 due to the symmetries of the model. The result is reported in the following figure:

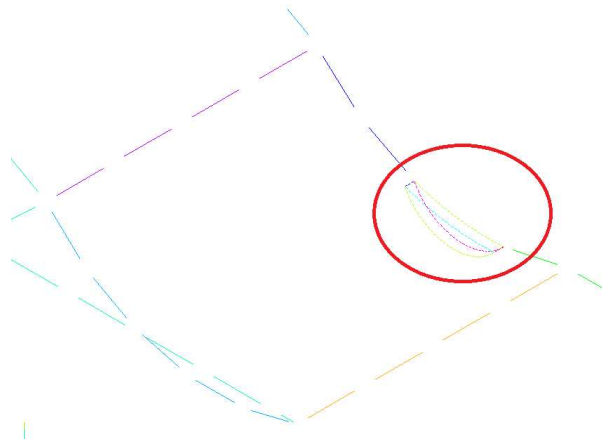


Figure 4.26: Illustration of the control volume to calculate the SED.

To create the mesh of the model, the following procedure is executed:

1. The element inside the structural volume are characterised by a *global element size* equal to 0.05mm with a *free-mesh* algorithm;

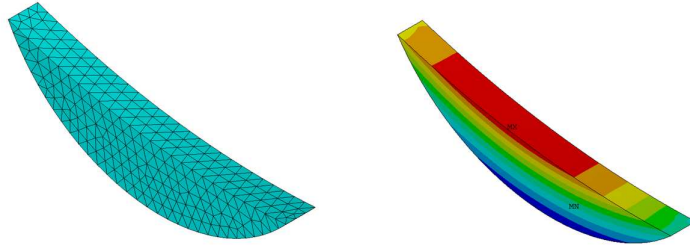


Figure 4.27: On the left, the mesh of the structural volume with global element size of 0.05. On the right, the proof that the highest stress is contained inside the volume.

2. The other volume is meshed with a global element size equal to 1 mm with a free-mesh algorithm.

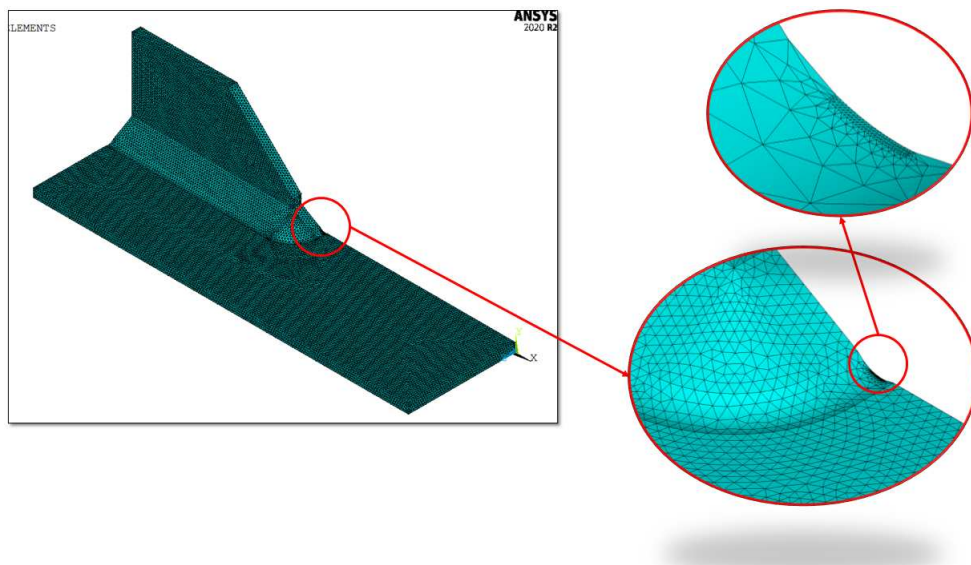


Figure 4.28: Mesh of the all structure.

Once the model is properly meshed, loaded and constraint, the system can be solved:

Solution → *Solve* → *Current LS*

Before the post-processing of the data, it is advised to disable the *PowerGraphics* option in Ansys®APDL toolbar, otherwise the output results are given by the average of only the superficial nodal stresses, without considering the inner ones.

The averaged Strain Energy Density is defined as the energy contained inside the structural volume. To define this value, the element belonging the structural volume have to be selected with the following commands:

Utility Menu → *Select* → *Entities* → *Volumes* → *By Num/Pick* → *From Ful*

Utility Menu → *Select* → *Entities* → *Elements* → *Attached to* → *Volumes*

Subsequently, two *Element Table* are created :

1. The first one to define the energy inside each element selected. This Element Table is called *SENE*;
2. The second one to define the volume of each element selected. This Element Table is called *VOLU*;

The commands to create the Element Table are:

General Postproc → *Element Table* → *Define Element Table* → *SENE/VOLU*

Label	Item	Comp	Time Stamp	Status
SENE	SENE		Time= 1.0000	(Current)
VOLU	VOLU		Time= 1.0000	(Current)

Figure 4.29: Element Table in Ansys®APDL

After the creation of the Element Tables, each single element SENE and VOLU values must be summed with the following commands:

General Postproc → *Element Table* → *Sum of Each Item*

Finally, the averaged Strain Energy Density value can be calculated with the following expression:

$$\Delta \bar{W}_{FEM} = \frac{\sum_{V(R_0)} W_{FEM,i}}{V(R_0)} = \frac{SENE}{VOLU} \quad (4.14)$$

The result of SED for the weld toe when the specimen is subjected to a nominal stress of 1 MPa is:

$$SENE = 3.98752 \cdot 10^{-7} MJ \quad (4.15)$$

$$VOLU = 0.0370094 mm^3 \quad (4.16)$$

$$SED = \frac{SENE}{VOLU} = \frac{3.98752 \cdot 10^{-7}}{0.0370094} = 1.07743 \cdot 10^{-5} \frac{MJ}{m^3} \quad (4.17)$$

From the SED, the equivalent peak stress is obtained with the following formula:

$$\Delta \sigma_{eq,peak} = \sqrt{\frac{2 \cdot E \cdot SED}{1 - \nu^2}} = \sqrt{\frac{2 \cdot 206000 \cdot 1.07743 \cdot 10^{-5}}{1 - 0.3^2}} = 2.2086 MPa \quad (4.18)$$

This result is in good agreement with the value found in literature [33]:

$$\Delta \sigma_{eq,peak,literature} = 2.219 MPa \quad (4.19)$$

Thus, the relative error expresses in percentage between the calculated $\Delta \sigma_{eq,peak}$ and the $\Delta \sigma_{eq,peak,literature}$ is:

$$\Delta \% = \frac{\Delta \sigma_{eq,peak,calculated} - \Delta \sigma_{eq,peak,literature}}{\Delta \sigma_{eq,peak,literature}} \cdot 100 = -0.47\% \quad (4.20)$$

4.2.2 Data results for SED curve

The previous model was characterised by a load equal to 1 MPa, applied to the main plate of the specimen; to obtain the value of the peak stress related to the applied nominal stress, the equation (3.24) is applied.

The results in terms of equivalent peak stress are defined in the Appendix D.1.

The all experimental data are collected inside the PSM design curve proposed by Meneghetti, Camagnolo, Yildirim and Belluzzo [33]. The black lines are the PSM-based scatter band calculated in HFMI condition with a inverse slope equal to 5 [33], the dotted blue lines are the PSM design curve proposed by Meneghetti, Guzzella and Atzori for structure subjected to prevailing mode I [10]:

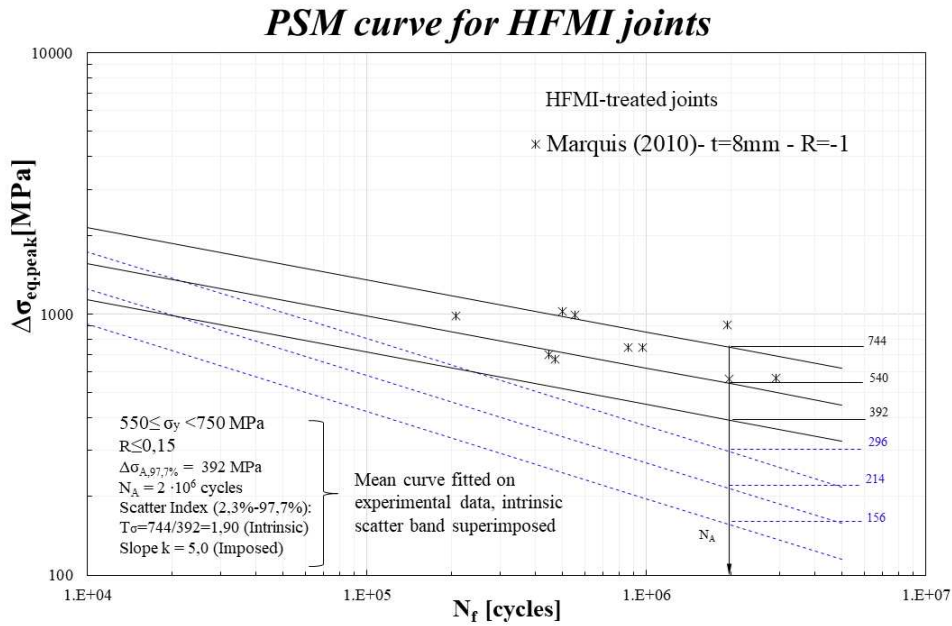


Figure 4.30: Experimental data inside the PSM design curve.

The following conclusion can be defined:

1. The all experimental data fall above the lines that represents the 2.3% of probability of survival in as-welded condition with a inverse slope equal to 3. Thus the PSM design curve has demonstrated to be effective and very conservative. This result is expected because the PSM fatigue design curve proposed by Meneghetti, Guzzella and Atzori is calibrated for as-welded joints and the considerations of the HFMI benefits are not present;
2. The all experimental data fall above the lines that represents the 97.7% of probability of survival in HFMI-treated condition with a inverse slope equal to 5. Thus the PSM design curve has demonstrated to be effective and conservative;
3. The Peak Stress Method combined with SED approach find results that are in according with the literature and it has correctly foreseen the experimental crack initiation point at weld toe.

4.2.3 SHSS(Structural Hot Spot Stress) approach

According to the IIW Recommendations, the SHSS approach procedure is the same adopted for as-welded joints, described in the paragraph 3.1.10.

The previous model was characterised by a load equal to 1 MPa, applied to the main plate of the specimen; to obtain the value of the hot-spot stress related to the applied nominal stress, the equation (3.45) is applied.

The results in terms of SHSS are defined in the Appendix D.1.

In agreement with the IIW Recommendations on the HFMI-treated joints [3], the design curve is increased of a FAT class. The hot-spot FAT class for $550 \leq f_y < 750$, non-load carrying fillet welds, is FAT 200 (see Table 4.5):

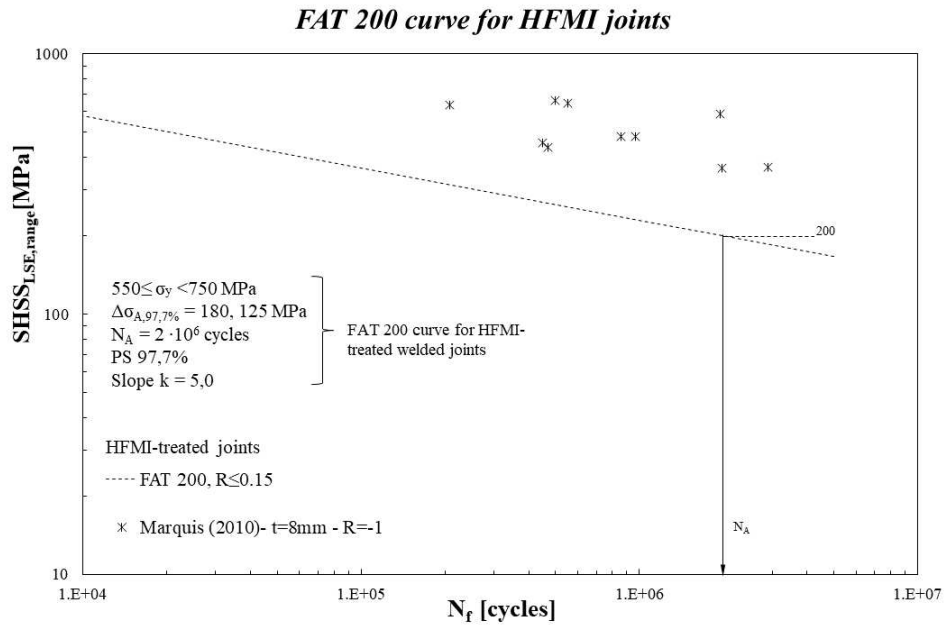


Figure 4.31: Experimental data inside the SHSS design curve.

The following conclusion can be defined:

1. The all experimental data fall above the lines that represents the 97.7% of probability of survival in HFMI-treated condition with a inverse slope equal to 5. Thus the PSM design curve has demonstrated to be effective and conservative;
2. The SHSS approach find results that are in according with the literature and it has correctly foreseen the experimental crack initiation point at weld toe.

4.3 Vanrostenberghe 2015, longitudinal attachment FAT 63

The second joint analysed is a longitudinal stiffener characterised by a fatigue class FAT 63, studied by Yildirim in 2013 [42] under CAL (Constant Amplitude Loading) and subsequently by Vanrostenberghe in 2015. The principal information and mechanical properties about this typology of the joint are summarized in the Table 4.11 and Table 4.12:

Weld condition	Fracture location	Load application	Main plate/gusset thickness
HFMI, non-load carrying (NLC), full penetration	Weld toe	Axial, main plate, parent material	Main plate: 5-20mm Gusset: 5-20mm

Table 4.11: Information about the specimens

Material model	Yield strength f_y [MPa]	Young modulus [MPa]	Poisson's ratio ν
S700MC, HSS, Linear elastic, isotropic	700	206000	0.3
S690QL, HSS, Linear elastic, isotropic	690		

Table 4.12: Information about mechanical properties

Three different specimen are analysed:

- S700MC with main plate thickness equal to 10 mm;
- S690QL with main plate thickness equal to 10 mm;
- S690QL with main plate thickness equal to 20 mm;

The first two geometry are analysed together with a single model with thickness equal to 10mm, while the third one is studied separately as a model with main plate thickness equal to 20mm.

The dimensions of this joint are defined and described in the paragraph 3.2 (Table 3.15 and Figure 3.32).

Regarding the HFMI groove geometry, the dimensions (radius, depth and width) are taken from [33] and the values are expressed in the following table with reference to Figure 4.32

t [mm]	depth [mm]	ρ_{HFMI} [mm]	width [mm]	2α [°]
10	0.21	3.31	4.42	120
20	0.21	3.31	4.42	120

Table 4.13: Dimension of HFMI groove for the longitudinal attachment FAT 63

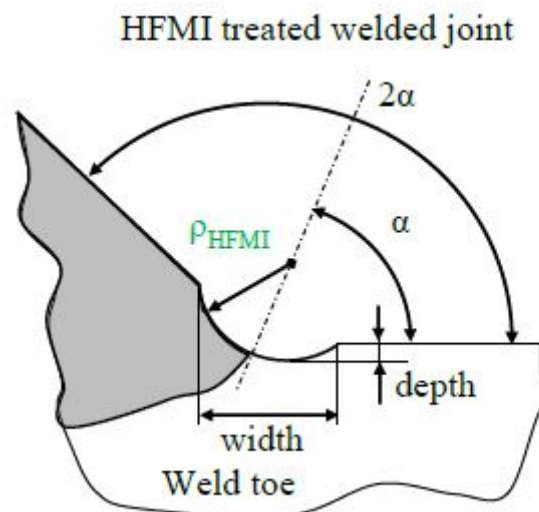


Figure 4.32: Reference to define the dimension of HFMI groove [33].

The inclination angle of the indenters is assumed to be performed along the V-notch bisector, i.e. 60° in this case.

The experimental data are defined in the following table in terms of nominal stress $\Delta\sigma_{nom}$:

<i>t=10mm</i>			
Material	Stress Ratio R	$\Delta\sigma_{nom}$ [MPa]	N_f [cycles]
S700MC S690QL	0.1	90	10 000 000
		175	10 000 000
		90	6 000 000
		150	6 000 000
		90	2 000 000
		200	6 000 000
		225	10 000 000
		90	10 000 000
		200	10 000 000
		70	2 000 000
		90	2 000 000
		300	158 200
		150	2 031 700
		250	3 547 800
		350	101 200
		150	532 122
		350	187 828
		250	855 162
350	82 506		
400	98 500		
250	317 200		
350	223 100		
225	18 010		
350	134 300		
S700MC	0.5	250	33 391
		200	84 895
<i>t=20mm</i>			
Material	Stress Ratio R	$\Delta\sigma_{nom}$ [MPa]	N_f [cycles]
S690QL	0.1	150	10 000 000
		250	10 000 000
		275	141 700
		200	480 200
		250	232 323
		350	80 830
		400	184 642
		300	470 640
S690QL	0.5	350	123 655
		200	343 210
		125	1 019 256
		150	644 530
		275	56 926

Table 4.14: Experimental data of the 2nd joint, Vanrostenberghe 2015 in HFMI-treated condition. The number barred represents the run-outs

FAT 63 is modelled in *SOLIDWORKS 2020* with the HFMI groove and subsequently, is imported inside Ansys®APDL with *.IGS* extension. The results is reported in the figure below:

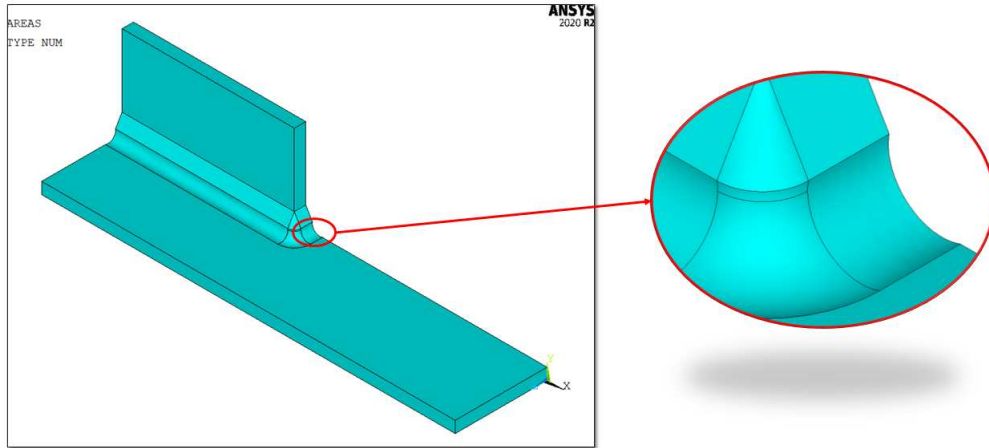


Figure 4.33: Model of longitudinal attachment 10 mm FAT 63 in HFMI treated condition.

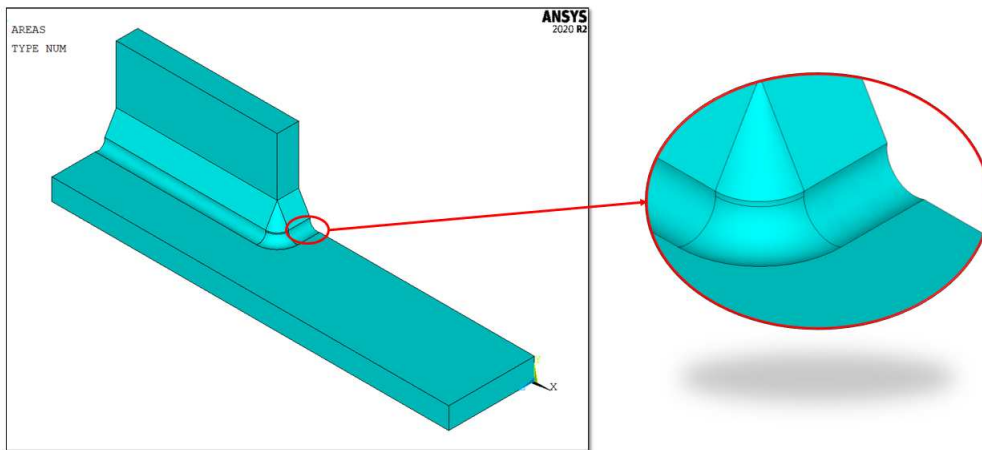


Figure 4.34: Model of longitudinal attachment 20 mm FAT 63 in HFMI treated condition.

The procedure to define the boundary conditions of the models follow the same steps and dispositions defined for the same joints in as-welded condition described in the paragraph 3.2.

4.3.1 PSM combined with SED for blunt notches

The fatigue assessment for this model is performed by the application of Peak Stress Method in combination with the SED approach with the adoption of ten-node quadratic elements, considering only the weld toe.

The element SOLID 187 is chosen from the Ansys®APDL library with *Pure Displacement* as Key Option 1, which means that the nodal forces are only dependent on the displacements.

The SED approach for blunt notches is based on the creation of a structural volume at the radiused weld toe, that can be rigidly rotated (*Figure 4.20*) to included the whole maximum principal stress, which is related to the highest strain energy density.

The first step is to determinate the inclination angle Φ with respect to the blunt notch bisector of the most stressed area that is indicated in red in Ansys®APDL.

To define the inclination angle, the 10mm model is meshed with a global element size equal to 1 mm and equal to 2 mm for 20mm model. Subsequently, two refinements with depth equal to 5 (see *Figure 4.35* for the refine options) are applied to the arc that represents the groove due to HFMI treatment (*Figure 4.36-4.36*) with the following commands:

Preprocessor → *Meshing* → *Modify Mesh* → *Refine At* → *Lines*

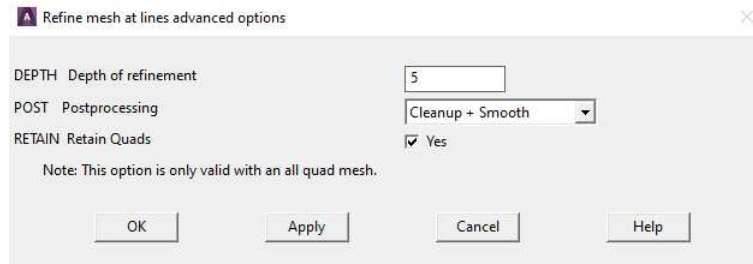


Figure 4.35: Options for the refinement for 10mm and 20mm model.

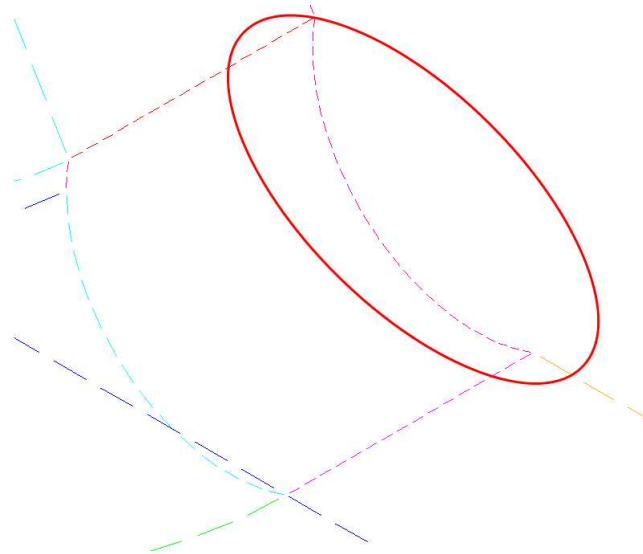


Figure 4.36: Arc that represents the HFMI groove where the refinements are applied for 10mm model.

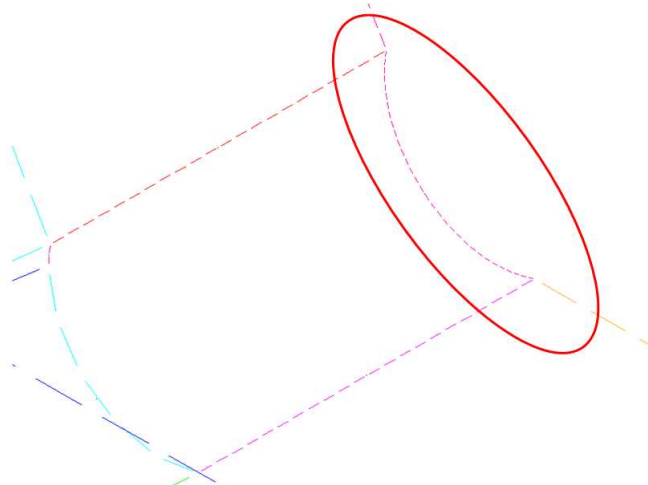


Figure 4.37: Arc that represents the HFMI groove where the refinements are applied for 20mm model.

The meshed models are displayed on the following figure:

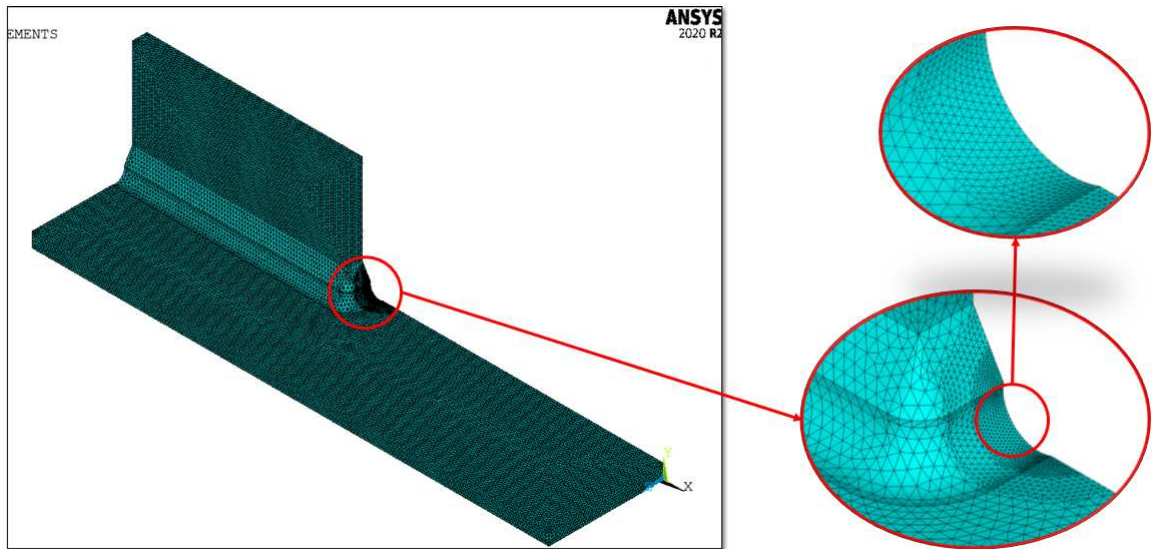


Figure 4.38: Mesh of the 10mm model to define the inclination angle.

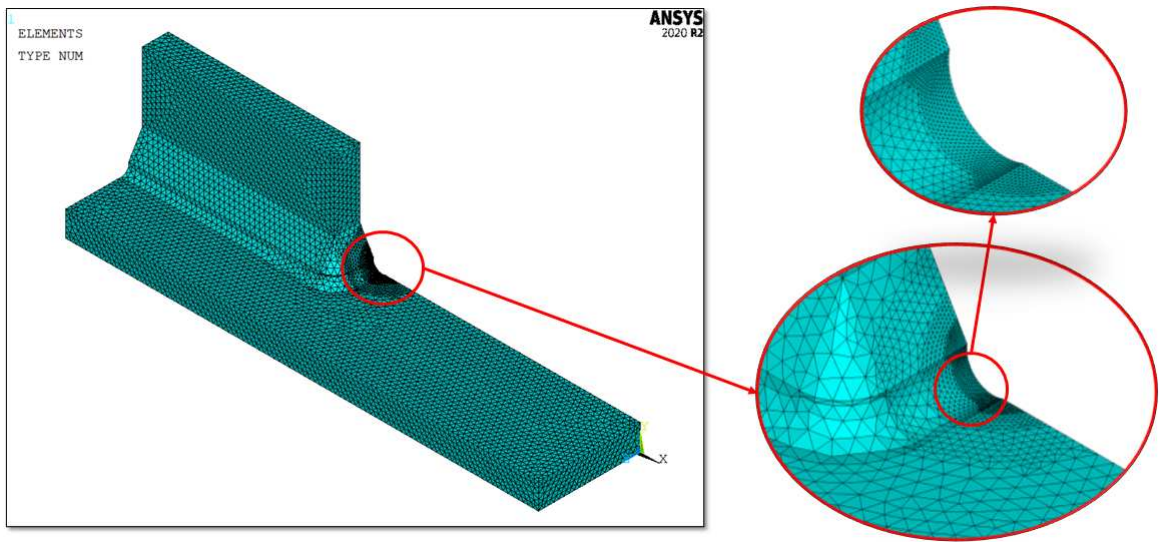


Figure 4.39: Mesh of the 20mm model to define the inclination angle.

The models are subjected to an external nominal stress $\Delta\sigma_{nom} = 1MPa$ applied on the main plate. Once the model is properly meshed, loaded and constraint, the system can be solve:

Solution→*Solve*→*Current LS*

The first principal stress $\Delta\sigma_{11}$ is plotted:

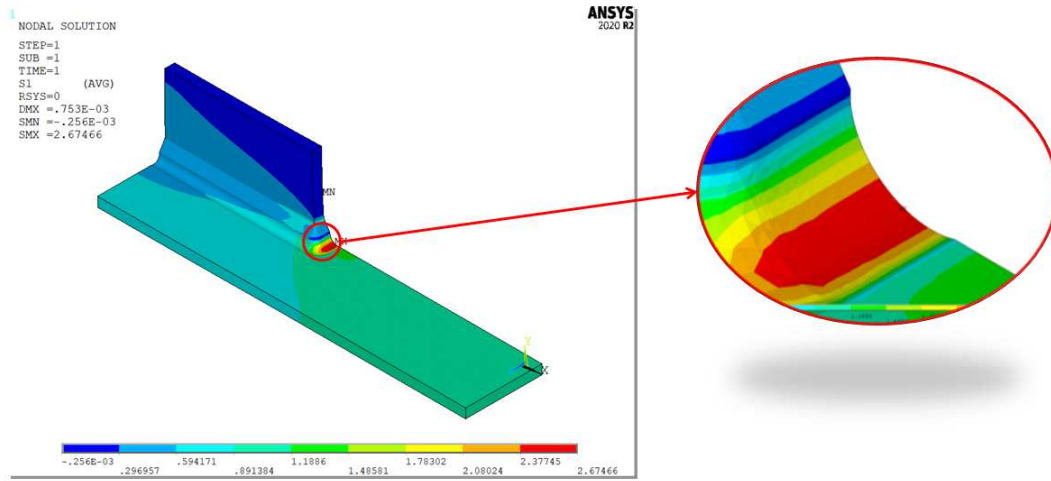


Figure 4.40: Plot of the first principal stress on the 10mm model.

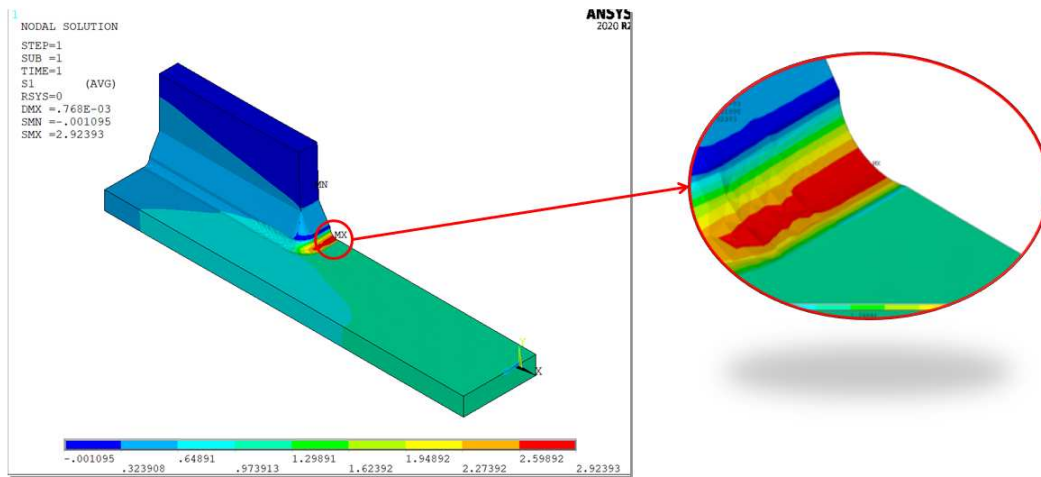


Figure 4.41: Plot of the first principal stress on the 20mm model.

The highest stresses are not located exactly around the blunt notch bisector, so it is matter of quantifying the grades of rotation. The values of the angles are reported in the following equations and represent a clockwise rotation about the global z-axis:

$$\Phi_{10mm} = 11.78^\circ \quad (4.21)$$

$$\Phi_{20mm} = 9.09^\circ \quad (4.22)$$

The circular sector is created according to equations (4.5) and (4.6) and the results are the same for 10mm and 20mm models:

$$q = \frac{2\pi - 2\alpha}{\pi} = 2 - \frac{120}{180} = 1.333 \quad (4.23)$$

$$r_0 = \frac{q-1}{q} \cdot \rho_{HFMI} = \frac{1.333-1}{1.333} \cdot 3.31 = 0.8275mm \quad (4.24)$$

$$R_0 + r_0 = 0.28 + 0.8275 = 1.1075mm \quad (4.25)$$

Subsequently, the control volume to calculate the averaged Strain Energy Density (SED) is created with a deep equal to 0.14 due to the symmetries of the model. The results for 10mm and 20mm models are reported in the following figures:

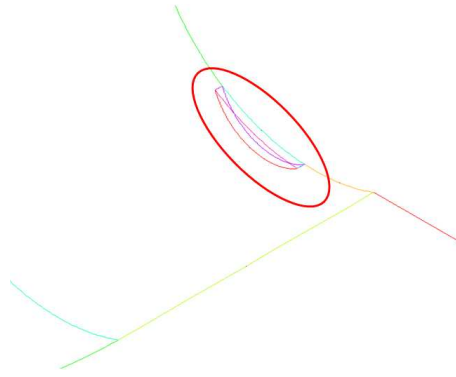


Figure 4.42: Illustration of the control volume to calculate the SED for 10mm model.

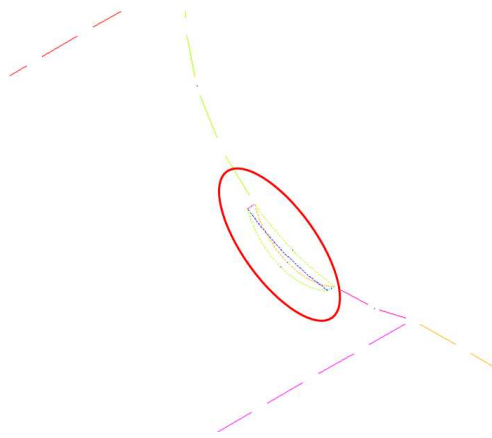


Figure 4.43: Illustration of the control volume to calculate the SED for 20mm model.

To create the mesh of the two models, the following procedure is executed:

1. The element inside the structural volume are characterised by a *global element size* equal to 0.05mm with a *free-mesh* algorithm;

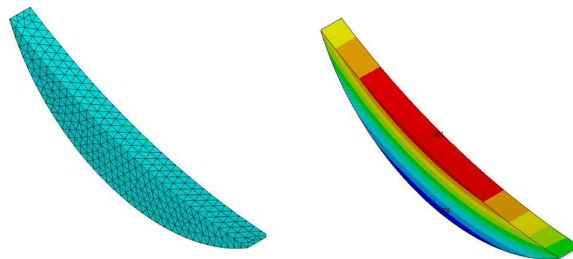


Figure 4.44: On the left, the mesh of the structural volume of 10mm model with global element size of 0.05. On the right, the proof that the highest stress is contained inside the volume.

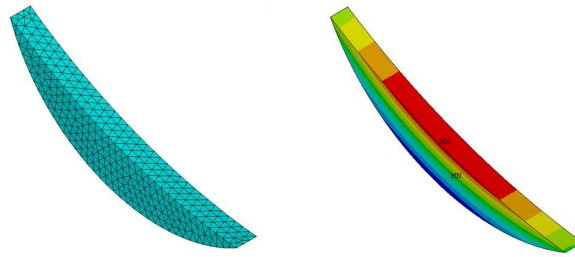


Figure 4.45: On the left, the mesh of the structural volume of 20mm model with global element size of 0.05. On the right, the proof that the highest stress is contained inside the volume.

2. The other volume is meshed with a global element size equal to 1 mm with a free-mesh algorithm.

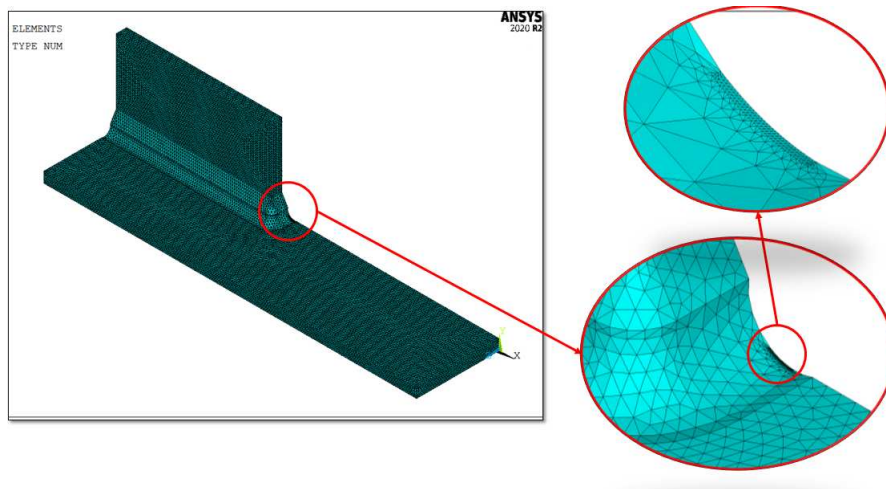


Figure 4.46: Mesh of the all 10mm model.

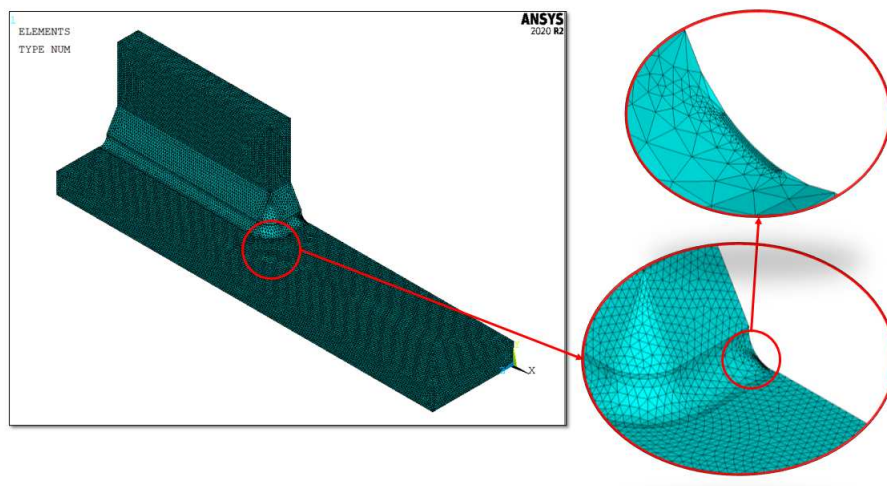


Figure 4.47: Mesh of the all 20mm model.

Once the model is properly meshed, loaded and constraint, the system can be solved:

Solution → *Solve* → *Current LS*

Before the post-processing of the data, it is advised to disable the *PowerGraphics* option in Ansys®APDL toolbar, otherwise the output results are given by the average of only the superficial nodal stresses, without considering the inner ones.

The averaged Strain Energy Density is defined as the energy contained inside the structural volume. The same procedure used for FAT 71 is applied to detect the SED value.

10mm results

The result of SED for the weld toe when the specimen is subjected to a nominal stress of 1 MPa is:

$$SENE = 6.45882 \cdot 10^{-7} MJ \quad (4.26)$$

$$VOLU = 0.046614 mm^3 \quad (4.27)$$

$$SED = \frac{SENE}{VOLU} = \frac{6.45882 \cdot 10^{-7}}{0.046614} = 1.3856 \cdot 10^{-5} \frac{MJ}{m^3} \quad (4.28)$$

From the SED, the equivalent peak stress is obtained with the following formula:

$$\Delta\sigma_{eq,peak} = \sqrt{\frac{2 \cdot E \cdot SED}{1 - \nu^2}} = \sqrt{\frac{2 \cdot 206000 \cdot 1.3856 \cdot 10^{-5}}{1 - 0.3^2}} = 2.5046 MPa \quad (4.29)$$

This result is in good agreement with the value found in literature [33]:

$$\Delta\sigma_{eq,peak,literature} = 2.501 MPa \quad (4.30)$$

Thus, the relative error expresses in percentage between the calculated $\Delta\sigma_{eq,peak}$ and the $\Delta\sigma_{eq,peak,literature}$ is:

$$\Delta\% = \frac{\Delta\sigma_{eq,peak,calculated} - \Delta\sigma_{eq,peak,literature}}{\Delta\sigma_{eq,peak,literature}} \cdot 100 = -0.15\% \quad (4.31)$$

20mm results

The result of SED for the weld toe when the specimen is subjected to a nominal stress of 1 MPa is:

$$SENE = 7.50133 \cdot 10^{-7} MJ \quad (4.32)$$

$$VOLU = 0.046614 mm^3 \quad (4.33)$$

$$SED = \frac{SENE}{VOLU} = \frac{7.50133 \cdot 10^{-7}}{0.046614} = 1.60923 \cdot 10^{-5} \frac{MJ}{m^3} \quad (4.34)$$

From the SED, the equivalent peak stress is obtained with the following formula:

$$\Delta\sigma_{eq,peak} = \sqrt{\frac{2 \cdot E \cdot SED}{1 - \nu^2}} = \sqrt{\frac{2 \cdot 206000 \cdot 1.60923 \cdot 10^{-5}}{1 - 0.3^2}} = 2.6992 MPa \quad (4.35)$$

This result is in good agreement with the value found in literature [33]:

$$\Delta\sigma_{eq,peak,literature} = 2.699 MPa \quad (4.36)$$

Thus, the relative error expresses in percentage between the calculated $\Delta\sigma_{eq,peak}$ and the $\Delta\sigma_{eq,peak,literature}$ is:

$$\Delta\% = \frac{\Delta\sigma_{eq,peak,calculated} - \Delta\sigma_{eq,peak,literature}}{\Delta\sigma_{eq,peak,literature}} \cdot 100 = -0.008\% \quad (4.37)$$

4.3.2 Data results for SED curve

The previous model was characterised by a load equal to 1 MPa, applied to the main plate of the specimen; to obtain the value of the peak stress related to the applied nominal stress, the equation (3.24) is applied.

The results in terms of equivalent peak stress are defined in the Appendix D.2.

The all experimental data are collected inside the PSM design curve proposed by Meneghetti, Camapgnolo, Yildirim and Belluzzo [33]. The black lines are the PSM-based scatter band calculated in HFMI condition with a inverse slope equal to 5 [33], the dotted blue lines are the PSM design curve proposed by Meneghetti, Guzzella and Atzori for structure subjected to prevailing mode I [10]. The curve proposed by Meneghetti, Camapgnolo, Yildirim and Belluzzo [33] are different based on the stress ratio and the material steel strength:

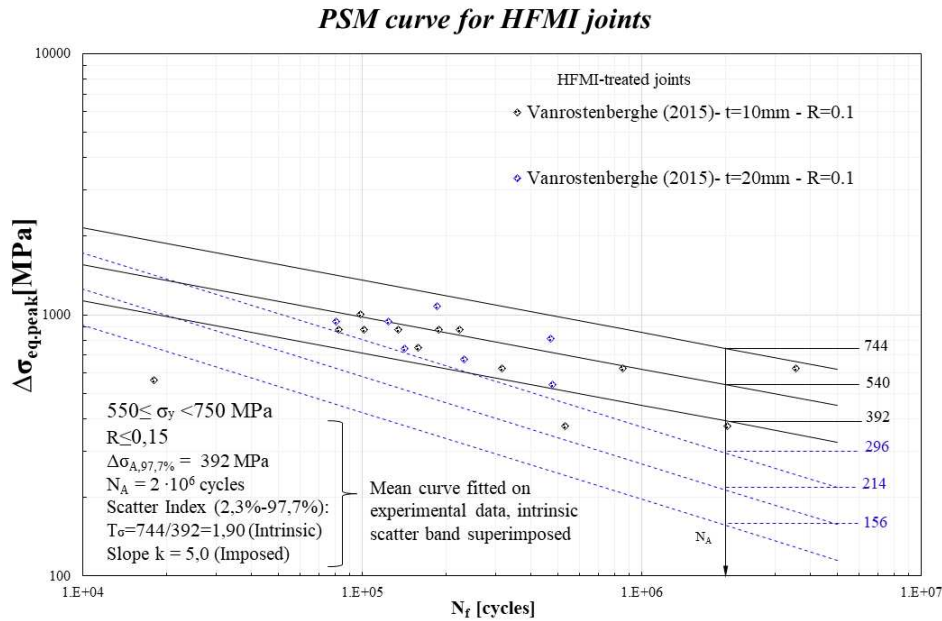


Figure 4.48: Experimental data inside the PSM design curve.

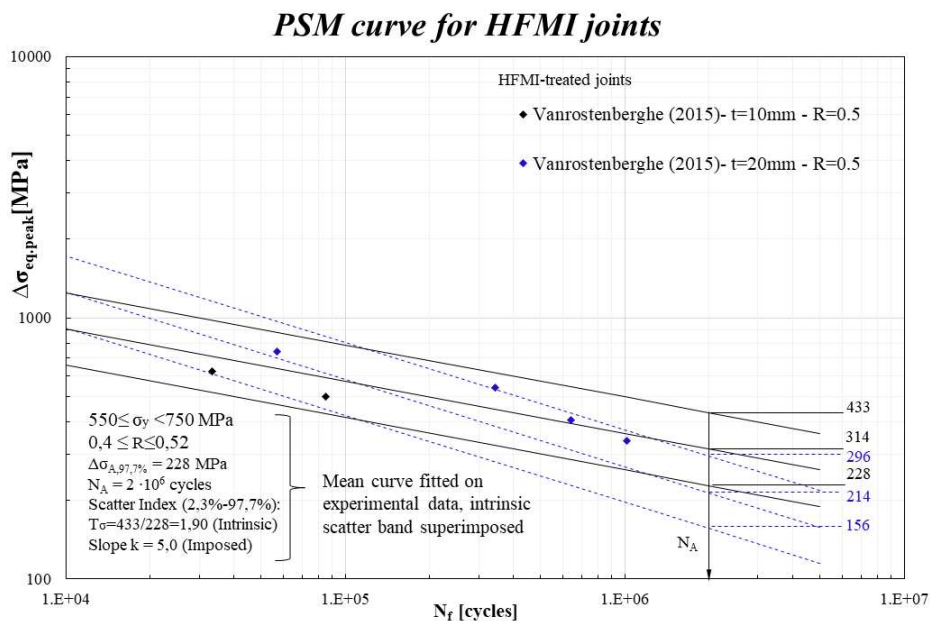


Figure 4.49: Experimental data inside the PSM design curve.

The following conclusion can be defined:

1. The all experimental data fall above the lines that represents the 97.7% of probability of survival in as-welded condition with a inverse slope equal to 3. Thus the PSM design curve has demonstrated to be effective and very conservative. This result is expected because the PSM fatigue design curve proposed by Meneghetti, Guzzella and Atzori is calibrated for as-welded joints and the considerations of the HFMI benefits are not present;
2. Several experimental data fall above the lines that represents the 97.7% of probability of survival in HFMI-treated condition with a inverse slope equal to 5. Thus the PSM design curve has demonstrated to be partially effective and conservative due to the misalignment effect have been neglected;
3. The Peak Stress Method combined with SED approach find results that are in according with the literature

and it has correctly foreseen the experimental crack initiation point at weld toe.

4.3.3 SHSS(Structural Hot Spot Stress) approach

According to the IIW Recommendations, the SHSS approach procedure is the same adopted for as-welded joints, described in the paragraph 3.2.9.

The previous model was characterised by a load equal to 1 MPa, applied to the main plate of the specimen; to obtain the value of the hot-spot stress related to the applied nominal stress, the equation (3.45) is applied.

The results in terms of SHSS are defined in the Appendix D.2.

In agreement with the IIW Recommendations on the HFMI-treated joints [3], the design curve is increased of a FAT class. The hot-spot FAT class for $550 \leq f_y < 750$, non-load carrying fillet welds, is FAT 200 (see Table 4.5) for $R \leq 0.15$ and FAT 140 for $0.4 < R \leq 0.52$:

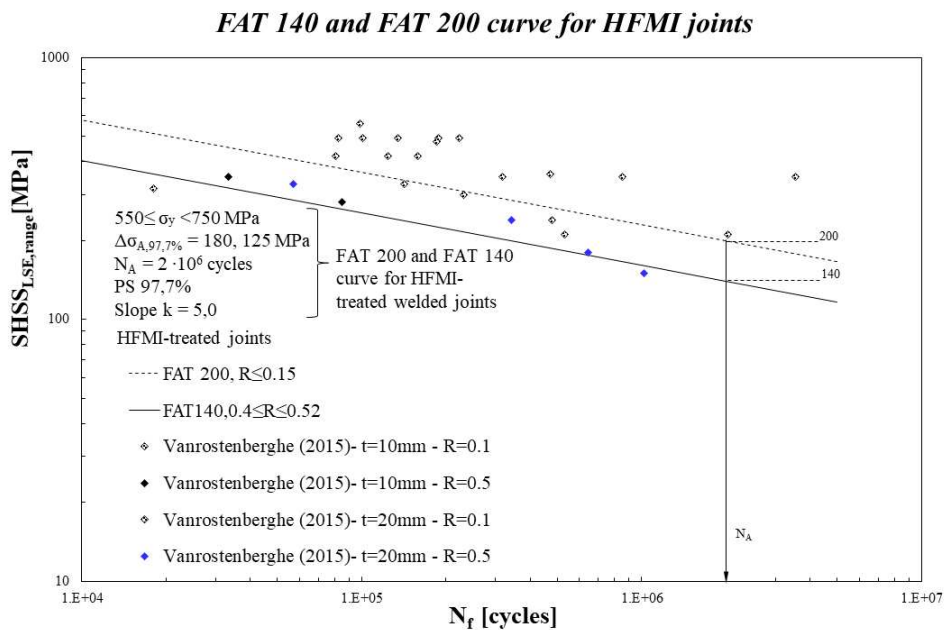


Figure 4.50: Experimental data inside the SHSS design curve.

The following conclusion can be defined:

1. Several experimental data fall above the lines that represents the 97.7% of probability of survival in HFMI-treated condition with a inverse slope equal to 5. Thus the PSM design curve has demonstrated to be partially effective and conservative due to the misalignment effect have been neglected;
2. The SHSS approach find results that are in according with the literature and it has correctly foreseen the experimental crack initiation point at weld toe.

4.4 Yildirim 2020, transverse attachment FAT 80

The third joint analysed is a transverse attachment characterised by a fatigue class FAT 80, studied by Yildirim in 2020 [18] under CAL (Constant Amplitude Loading).

The principal information and mechanical properties about this typology of the joint are summarized in the Table 4.15 and Table 4.16:

Weld condition	Fracture location	Load application	Main plate/gusset thickness
HFMI, non-load carrying (NLC), full penetration	Weld toe	Axial, main plate, parent material	Main plate: 6mm Gusset: 6mm

Table 4.15: Information about the specimens

Material model	Yield strength f_y [MPa]	Young modulus [MPa]	Poisson's ratio ν
AH36, HSS, Linear elastic, isotropic	392	206000	0.3

Table 4.16: Information about mechanical properties

The dimensions of this joint are defined and described in the paragraph 3.3 (Table 3.28 and Figure 3.73). Regarding the HFMI groove geometry, the dimensions (radius, depth and width) are taken from [33] and the values are expressed in the following table with reference to Figure 4.18

depth [mm]	ρ_{HFMI} [mm]	width [mm]	2α [°]
0.16	1.80	2.43	135

Table 4.17: Dimension of HFMI groove for the transverse attachment FAT 80, studied by Yildirim in 2020

The inclination angle of the indenters is assumed to be performed along the V-notch bisector, i.e. 67.5° in this case.

The experimental data are defined in the following table in terms of nominal stress $\Delta\sigma_{nom}$:

Stress Ratio R	$\Delta\sigma_{nom}$ [MPa]	N_f [cycles]
-0.43	242	798 406
	181	1 346 563
	242	433 673
	181	1 351 325
	181	1 695 096

Table 4.18: Experimental data of the 3rd joint, Yildirim 2020 in HFMI treated condition.

FAT 80 is modelled in *SOLIDWORKS 2020* with the HFMI groove and subsequently, is imported inside Ansys®APDL with .IGS extension. The results is reported in the figure below:

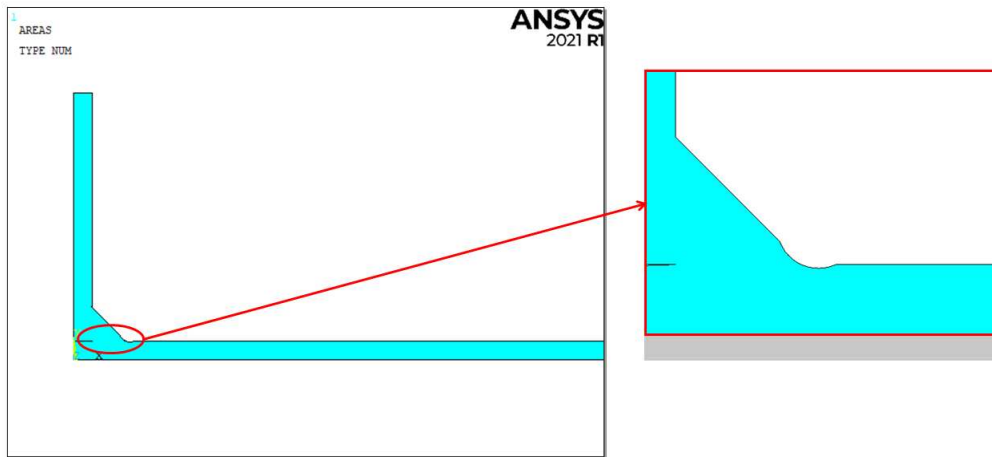


Figure 4.51: Model of longitudinal attachment FAT 80 studied by Yildirim in HFMI treated condition.

The procedure to define the boundary conditions of the model follows the same steps and dispositions defined for the same joint in as-welded condition described in the paragraph 3.3.

4.4.1 PSM combined with SED for blunt notches

The fatigue assessment for this model is performed by the application of Peak Stress Method in combination with the SED approach with the adoption of four-node linear elements, considering only the weld toe.

The element PLANE 182 is chosen from the Ansys®APDL library with *Simple Enhanced Strain* as Key Option 1 and *Plane Strain* as Key Option 3.

The SED approach for blunt notches is based on the creation of a structural volume at the radiused weld toe, that can be rigidly rotated (*Figure 4.20*) to included the whole maximum principal stress, which is related to the highest strain energy density.

The first step is to determinate the inclination angle Φ with respect to the blunt notch bisector of the most stressed area that is indicated in red in Ansys®APDL.

To define the inclination angle, the model is meshed with a global element size equal to 0.8 mm and subsequently, two refinements with depth equal to 5 (see *Figure 4.52* for the refine options) are applied to the arc that represents the groove due to HFMI treatment (*Figure 4.53*) with the following commands:

Preprocessor → *Meshing* → *Modify Mesh* → *Refine At* → *Lines*

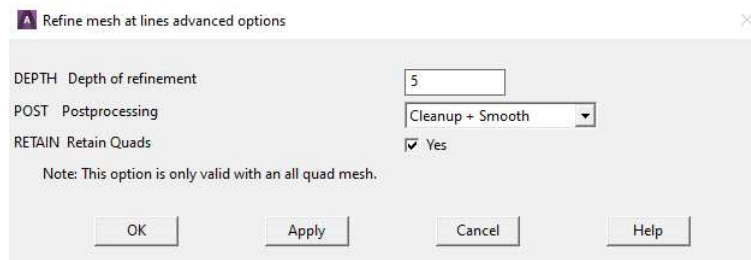


Figure 4.52: Options for the refinement.

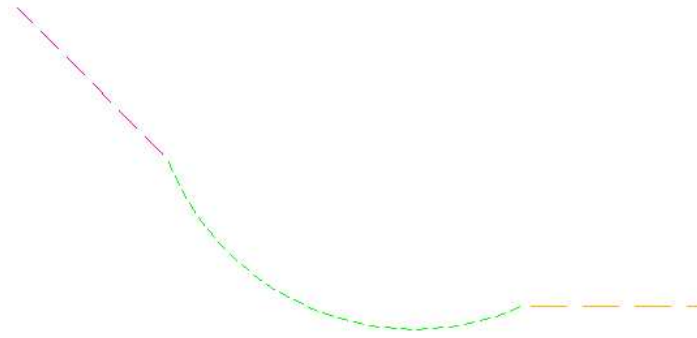


Figure 4.53: Arc that represents the HFMI groove where the refinements are applied.

The meshed model is displayed on the following figure:

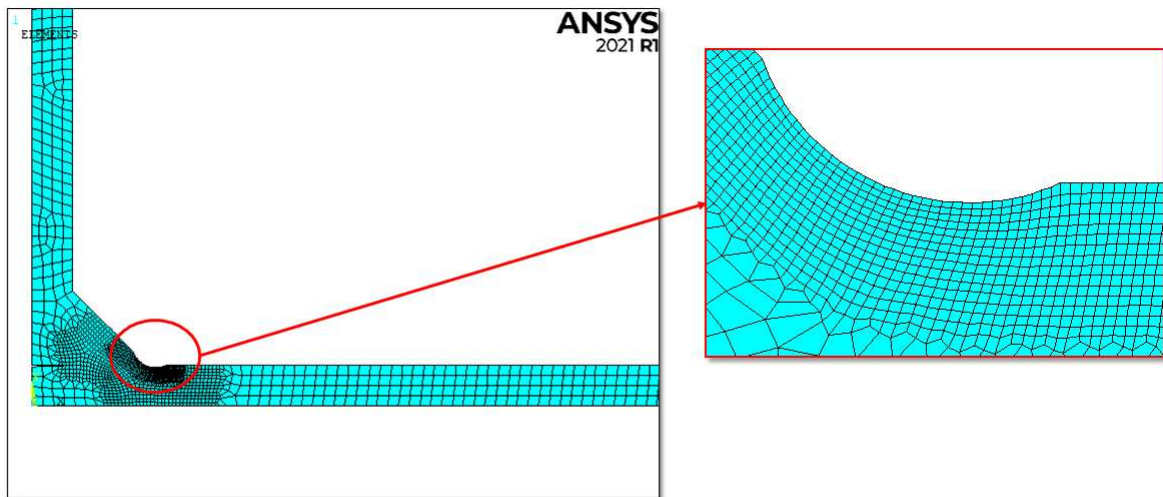


Figure 4.54: Mesh of the model to define the inclination angle.

The model is subjected to an external nominal stress $\Delta\sigma_{nom} = 1MPa$ applied on the main plate. Once the model is properly meshed, loaded and constraint, the system can be solve:

Solution→*Solve*→*Current LS*

The first principal stress $\Delta\sigma_{11}$ is plotted:

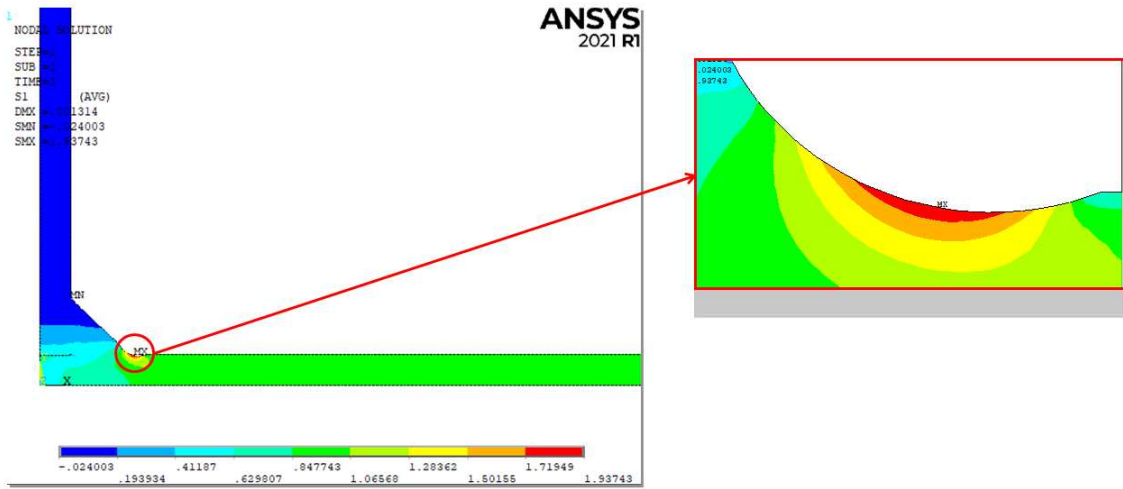


Figure 4.55: Plot of the first principal stress.

The highest stress is not located exactly around the blunt notch bisector, so it is matter of quantifying the grades of rotation. The value of the angle is reported in the following equation and represents a clockwise rotation about the global z-axis:

$$\Phi = 10.5^\circ \quad (4.38)$$

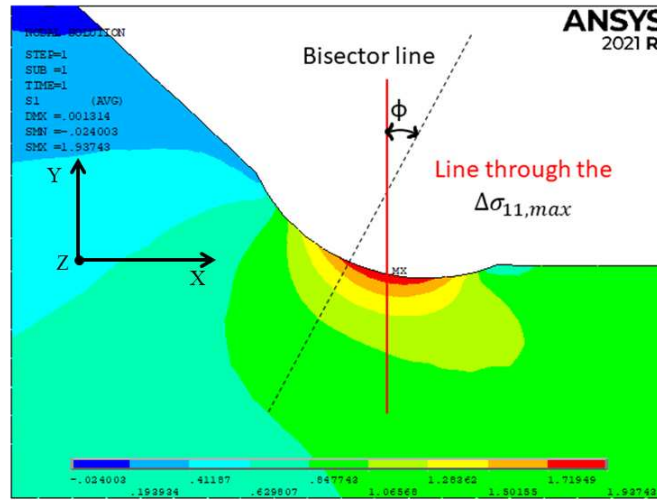


Figure 4.56: Inclination angle Φ

The circular sector is created according to equations (4.5) and (4.6):

$$q = \frac{2\pi - 2\alpha}{\pi} = 2 - \frac{135}{180} = 1.25 \quad (4.39)$$

$$r_0 = \frac{q-1}{q} \cdot \rho_{HFMI} = \frac{1.25-1}{1.25} \cdot 1.80 = 0.4mm \quad (4.40)$$

$$R_0 + r_0 = 0.28 + 0.4 = 0.68mm \quad (4.41)$$

Subsequently, the control volume to calculate the averaged Strain Energy Density (SED) is created. The result is reported in the following figure:

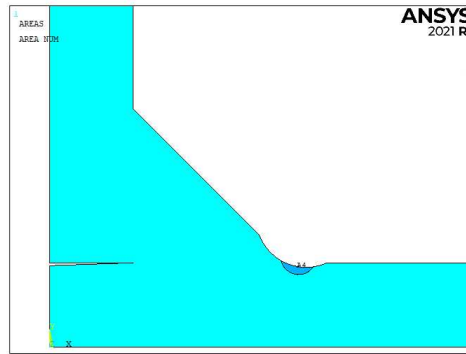


Figure 4.57: Illustration of the control Area to calculate the SED.

To create the mesh of the model, the following procedure is executed:

1. The element inside the structural volume are characterised by a *global element size* equal to 0.01mm with a *free-mesh* algorithm;

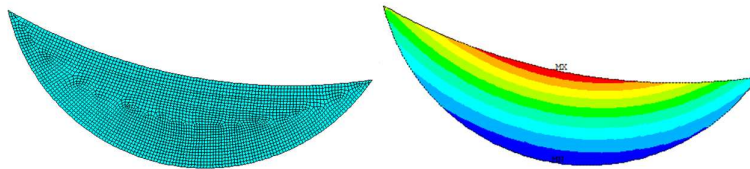


Figure 4.58: On the left, the mesh of the structural volume with global element size of 0.01. On the right, the proof that the highest stress is contained inside the volume.

2. The other volume is meshed with a *global element size* equal to 0.1 mm with a *free-mesh* algorithm.

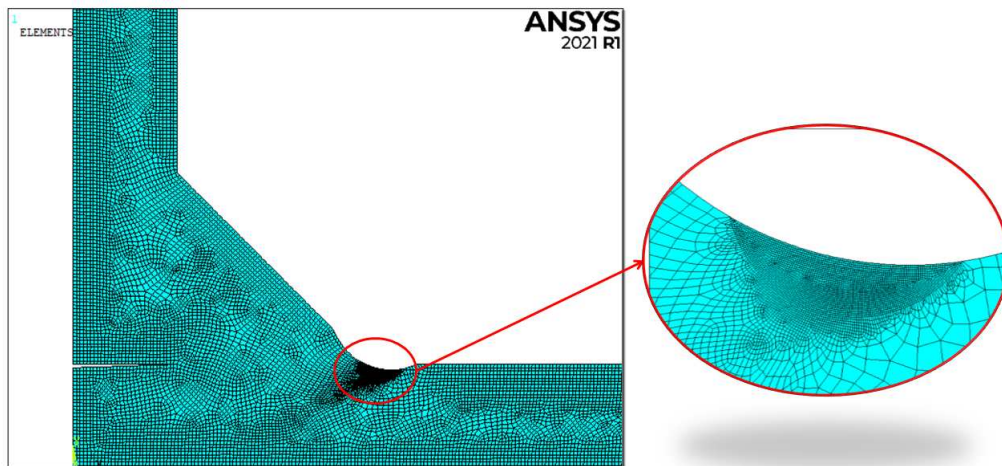


Figure 4.59: Mesh of the all structure.

Once the model is properly meshed, loaded and constraint, the system can be solved:

Solution → *Solve* → *Current LS*

The averaged Strain Energy Density is defined as the energy contained inside the structural volume. The same procedure used for FAT 71 is applied to detect the SED value.

The result of SED for the weld toe when the specimen is subjected to a nominal stress of 1 MPa is:

$$SENE = 1.44139 \cdot 10^{-6} MJ \quad (4.42)$$

$$VOLUME = 0.245309 mm^3 \quad (4.43)$$

$$SED = \frac{SENE}{VOLU} = \frac{1.44139 \cdot 10^{-6}}{0.245309} = 5.87581 \cdot 10^{-6} \frac{MJ}{m^3} \quad (4.44)$$

From the SED, the equivalent peak stress is obtained with the following formula:

$$\Delta\sigma_{eq,peak} = \sqrt{\frac{2 \cdot E \cdot SED}{1 - \nu^2}} = \sqrt{\frac{2 \cdot 206000 \cdot 5.87581 \cdot 10^{-6}}{1 - 0.3^2}} = 1.6310 MPa \quad (4.45)$$

This result is in good agreement with the value found in literature [33]:

$$\Delta\sigma_{eq,peak,literature} = 1.611 MPa \quad (4.46)$$

Thus, the relative error expresses in percentage between the calculated $\Delta\sigma_{eq,peak}$ and the $\Delta\sigma_{eq,peak,literature}$ is:

$$\Delta\% = \frac{\Delta\sigma_{eq,peak,calculated} - \Delta\sigma_{eq,peak,literature}}{\Delta\sigma_{eq,peak,literature}} \cdot 100 = 1.24\% \quad (4.47)$$

4.4.2 Data results for SED curve

The previous model was characterised by a load equal to 1 MPa, applied to the main plate of the specimen; to obtain the value of the peak stress related to the applied nominal stress, the equation (3.24) is applied. The results in terms of equivalent peak stress are defined in the Appendix D.3. The all experimental data are collected inside the PSM design curve proposed by Meneghetti, Camagnolo, Yildirim and Belluzzo [33]. The black lines are the PSM-based scatter band calculated in HFMI condition with a inverse slope equal to 5 [33], the dotted blue lines are the PSM design curve proposed by Meneghetti, Guzzella and Atzori for structure subjected to prevailing mode I [10]:

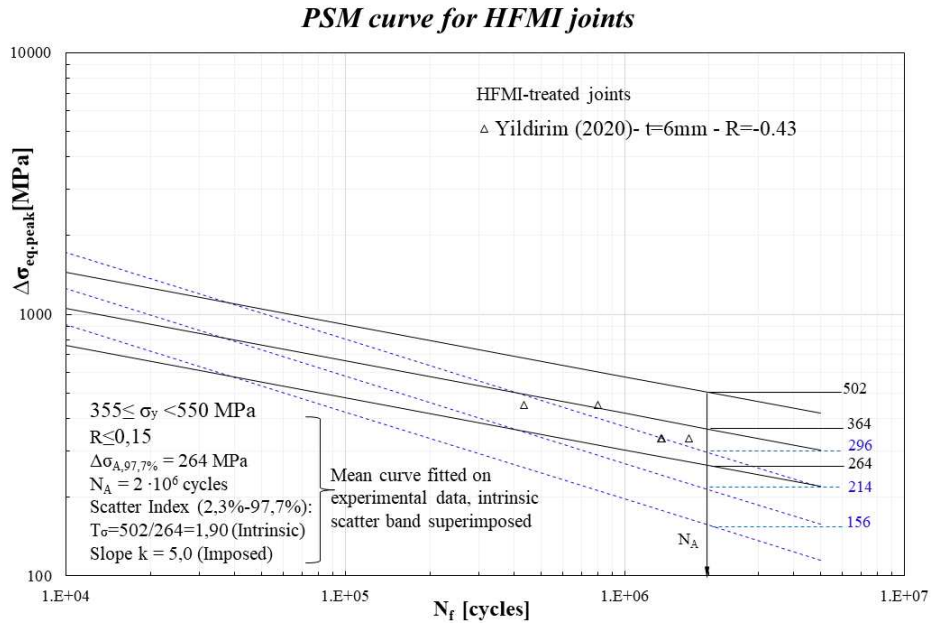


Figure 4.60: Experimental data inside the PSM design curve.

The following conclusion can be defined:

1. The all experimental data fall above the lines that represents the 50% of probability of survival in as-welded condition with a inverse slope equal to 3. Thus the PSM design curve has demonstrated to be effective and very conservative. This result is expected because the PSM fatigue design curve proposed by Meneghetti, Guzzella and Atzori is calibrated for as-welded joints and the considerations of the HFMI benefits are not present;
2. The all experimental data fall above the lines that represents the 97.7% of probability of survival in HFMI-treated condition with a inverse slope equal to 5. Thus the PSM design curve has demonstrated to be effective and conservative;
3. The Peak Stress Method combined with SED approach find results that are in according with the literature and it has correctly foreseen the experimental crack initiation point at weld toe.

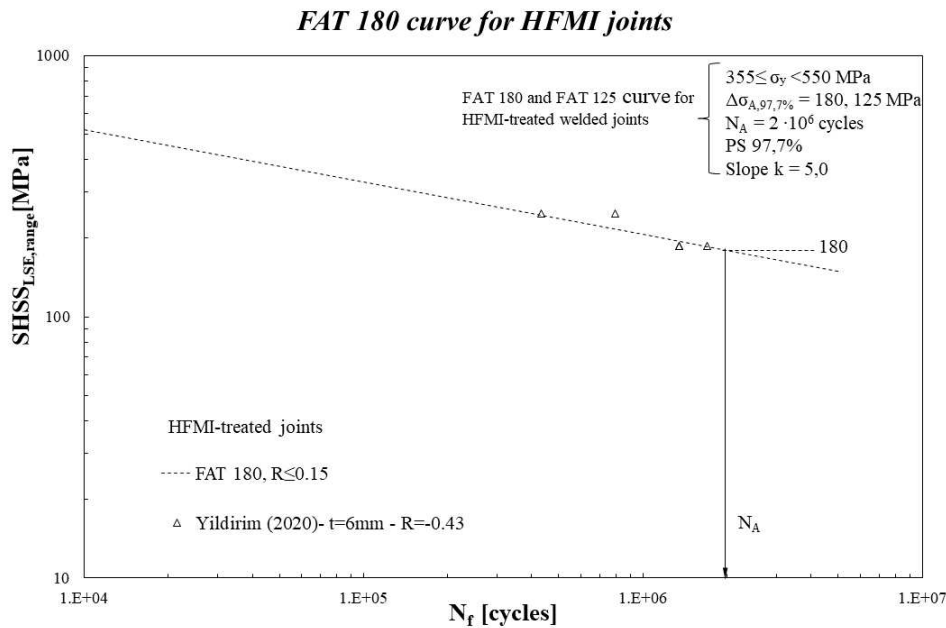
4.4.3 SHSS(Structural Hot Spot Stress) approach

According to the IIW Recommendations, the SHSS approach procedure is the same adopted for as-welded joints, described in the paragraph 3.3.4.

The previous model was characterised by a load equal to 1 MPa, applied to the main plate of the specimen; to obtain the value of the hot-spot stress related to the applied nominal stress, the equation (3.45) is applied.

The results in terms of SHSS are defined in the Appendix D.3.

In agreement with the IIW Recommendations on the HFMI-treated joints [3], the design curve is increased of a FAT class. The hot-spot FAT class for $355 \leq \sigma_y < 550$, non-load carrying fillet welds, is FAT 180 (see Table 4.5) for the stress ratio $R \leq 0.15$:



The following conclusion can be defined:

1. Several experimental data fall above the lines that represents the 97.7% of probability of survival in HFMI-treated condition with a inverse slope equal to 5. Thus the PSM design curve has demonstrated to be partially effective and conservative due to the misalignment effect have been neglected;
2. The SHSS approach find results that are in according with the literature and it has correctly foreseen the experimental crack initiation point at weld toe.

4.5 Okawa 2013, transverse attachment FAT 80

The fourth joint analysed is a transverse attachment characterised by a fatigue class FAT 80, studied by Okawa in 2013 [43] under CAL (Constant Amplitude Loading).

The principal information and mechanical properties about this typology of the joint are summarized in the *Table 4.19* and *Table 4.20*:

Weld condition	Fracture location	Load application	Main plate/gusset thickness
HFMI, non-load carrying (NLC), full penetration	Weld toe	Axial, main plate, parent material	Main plate: 20mm Gusset: 10mm

Table 4.19: Information about the specimens

Material model	Yield strength f_y [MPa]	Young modulus [MPa]	Poisson's ratio ν
AH36, HSS, Linear elastic, isotropic	392	206000	0.3

Table 4.20: Information about mechanical properties

The dimensions of this joint are defined and described in the paragraph 3.4 (*Table 3.37* and *Figure 3.85*). Regarding the HFMI groove geometry, the dimensions (radius, depth and width) are taken from [33] and the values are expressed in the following table with reference to *Figure 4.18*

depth [mm]	ρ_{HFMI} [mm]	width [mm]	2α [°]
0.186	2.00	2.72	135

Table 4.21: Dimension of HFMI groove for the transverse attachment FAT 80, studied by Okawa in 2013

The inclination angle of the indenters is assumed to be performed along the V-notch bisector, i.e. 67.5° in this case.

The experimental data are defined in the following table in terms of nominal stress $\Delta\sigma_{nom}$:

Stress Ratio R	$\Delta\sigma_{nom}$ [MPa]	N_f [cycles]
-1	420	378 000
	400	990 000
	380	2 295 000
0.1	250	5 000 000
	270	818 000
	260	1 067 000
	300	304 000
0.5	125	346 000
	175	346 000
	150	503 000
	135	3 450 000

Table 4.22: Experimental data of the 4th joint, Okawa 2013 in HFMI treated condition.

FAT 80 is modelled in *SOLIDWORKS 2020* with the HFMI groove and subsequently, is imported inside Ansys®APDL with *.IGS* extension. The results is reported in the figure below:

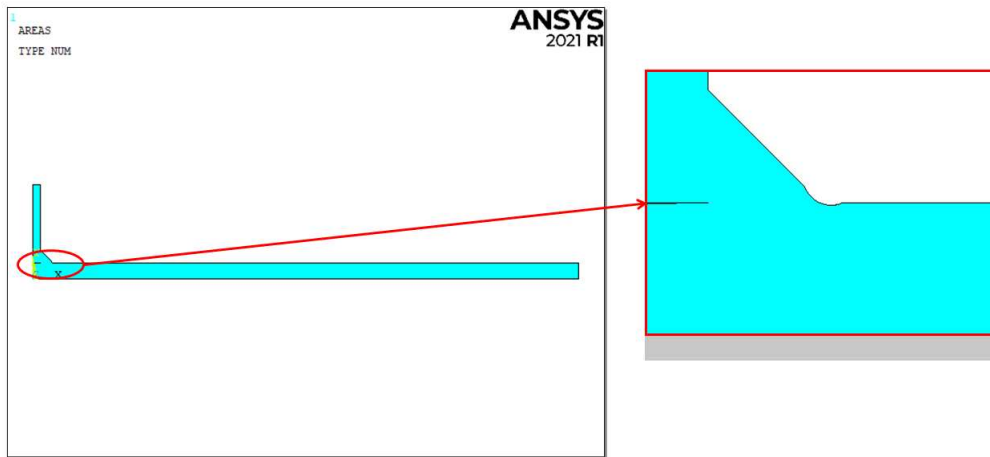


Figure 4.62: Model of longitudinal attachment FAT 80 studied by Okawa in HFMI treated condition.

The procedure to define the boundary conditions of the model follows the same steps and dispositions defined for the same joint in as-welded condition described in the paragraph 3.4.

4.5.1 PSM combined with SED for blunt notches

The fatigue assessment for this model is performed by the application of Peak Stress Method in combination with the SED approach with the adoption of four-node linear elements, considering only the weld toe.

The element PLANE 182 is chosen from the Ansys®APDL library with *Simple Enhanced Strain* as Key Option 1 and *Plane Strain* as Key Option 3.

The SED approach for blunt notches is based on the creation of a structural volume at the radiused weld toe, that can be rigidly rotated (*Figure 4.20*) to included the whole maximum principal stress, which is related to the highest strain energy density.

The first step is to determinate the inclination angle Φ with respect to the blunt notch bisector of the most stressed area that is indicated in red in Ansys®APDL.

To define the inclination angle, the model is meshed with a global element size equal to 0.6 mm and subsequently, two refinements with depth equal to 5 (see *Figure 4.63* for the refine options) are applied to the arc that represents the groove due to HFMI treatment (*Figure 4.64*) with the following commands:

Preprocessor → *Meshing* → *Modify Mesh* → *Refine At* → *Lines*

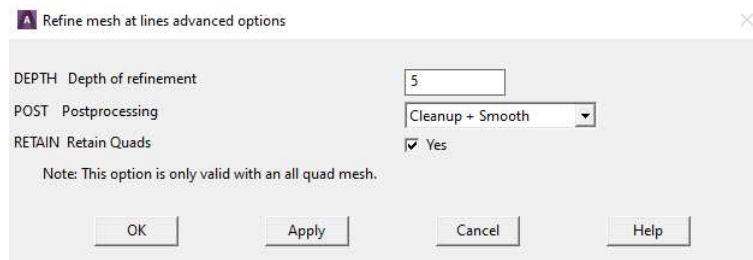


Figure 4.63: Options for the refinement.

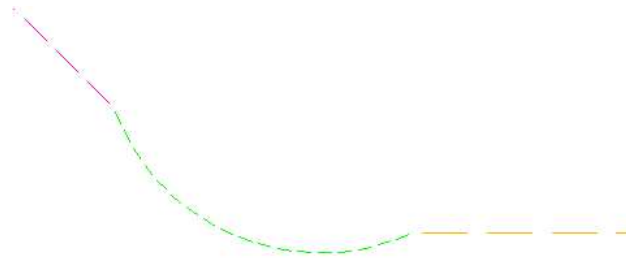


Figure 4.64: Arc that represents the HFMI groove where the refinements are applied.

The meshed model is displayed on the following figure:

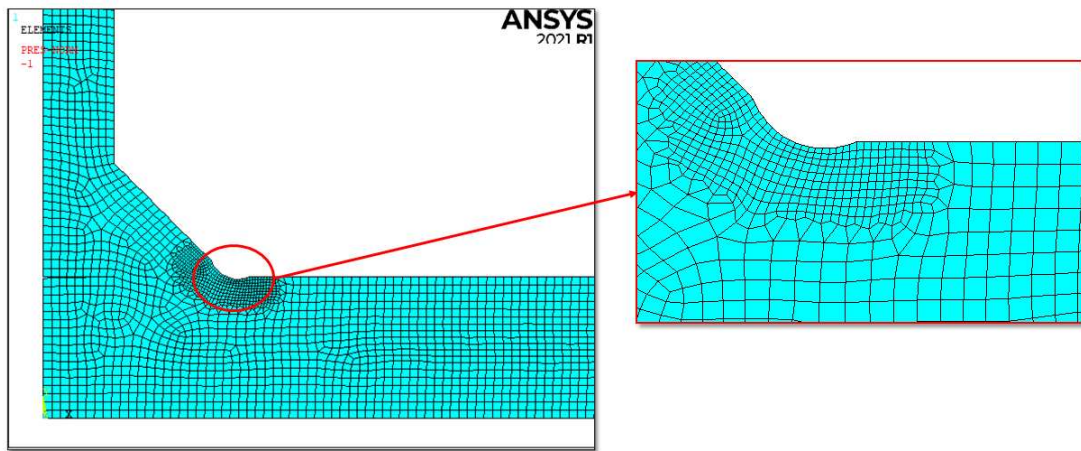


Figure 4.65: Mesh of the model to define the inclination angle.

The model is subjected to an external nominal stress $\Delta\sigma_{nom} = 1MPa$ applied on the main plate. Once the model is properly meshed, loaded and constraint, the system can be solve:

Solution → *Solve* → *Current LS*

The first principal stress $\Delta\sigma_{11}$ is plotted:

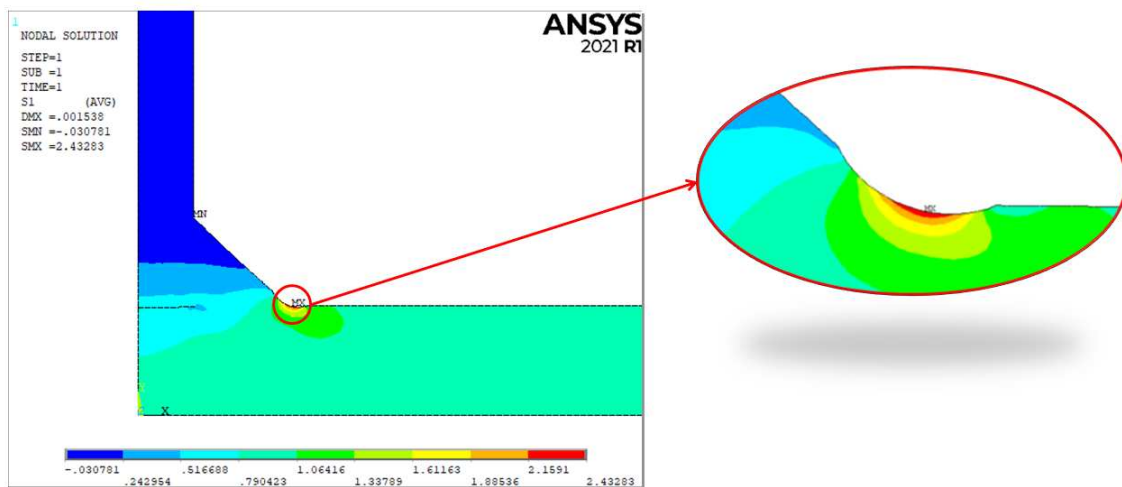


Figure 4.66: Plot of the first principal stress.

The highest stress is not located exactly around the blunt notch bisector, so it is matter of quantifying the grades of rotation. The value of the angle is reported in the following equation and represents a clockwise rotation about the global z-axis:

$$\Phi = 10.5^\circ \quad (4.48)$$

The circular sector is created according to equations (4.5) and (4.6):

$$q = \frac{2\pi - 2\alpha}{\pi} = 2 - \frac{135}{180} = 1.25 \quad (4.49)$$

$$r_0 = \frac{q-1}{q} \cdot \rho_{HFMI} = \frac{1.25-1}{1.25} \cdot 2.00 = 0.4mm \quad (4.50)$$

$$R_0 + r_0 = 0.28 + 0.4 = 0.68mm \quad (4.51)$$

Subsequently, the control volume to calculate the averaged Strain Energy Density (SED) is created. The result is reported in the following figure:

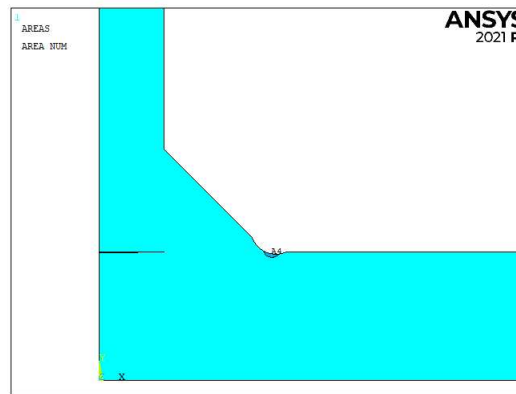


Figure 4.67: Illustration of the control Area to calculate the SED.

To create the mesh of the model, the following procedure is executed:

1. The element inside the structural volume are characterised by a *global element size* equal to 0.01mm with a *free-mesh* algorithm;

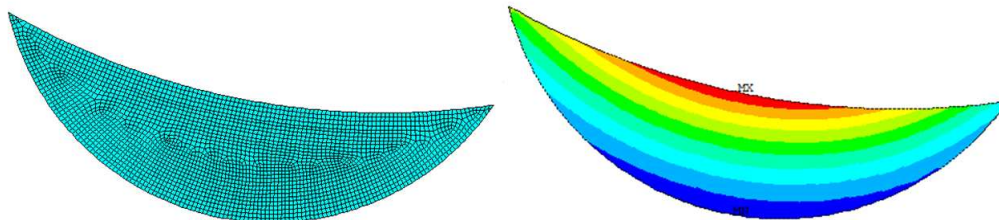


Figure 4.68: On the left, the mesh of the structural volume with global element size of 0.01. On the right, the proof that the highest stress is contained inside the volume.

2. The other volume is meshed with a *global element size* equal to 0.2 mm with a *free-mesh* algorithm.

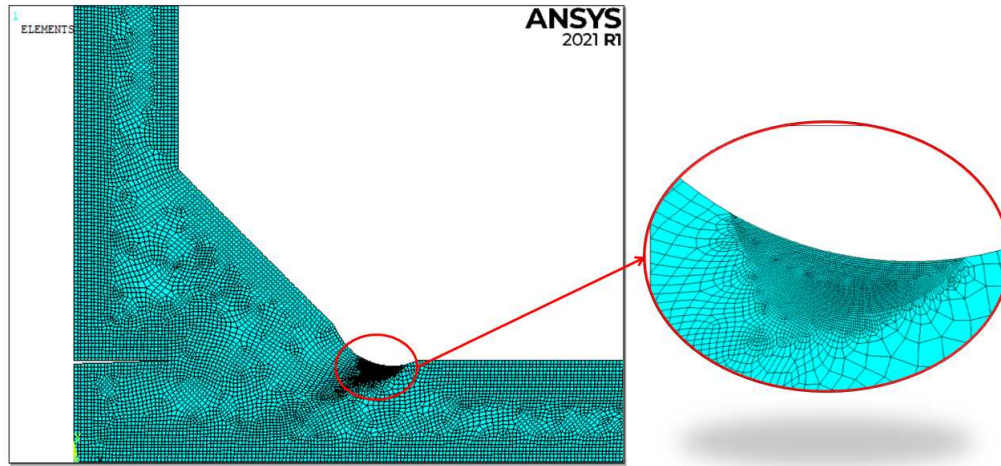


Figure 4.69: Mesh of the all structure.

Once the model is properly meshed, loaded and constraint, the system can be solved:

Solution→*Solve*→*Current LS*

The averaged Strain Energy Density is defined as the energy contained inside the structural volume. The same procedure used for FAT 71 is applied to detect the SED value.

The result of SED for the weld toe when the specimen is subjected to a nominal stress of 1 MPa is:

$$SENE = 2.46788 \cdot 10^{-6} MJ \quad (4.52)$$

$$VOLUME = 0.2476 mm^3 \quad (4.53)$$

$$SED = \frac{SENE}{VOLUME} = \frac{2.46788 \cdot 10^{-6}}{0.2476} = 9.96721 \cdot 10^{-6} \frac{MJ}{m^3} \quad (4.54)$$

From the SED, the equivalent peak stress is obtained with the following formula:

$$\Delta\sigma_{eq,peak} = \sqrt{\frac{2 \cdot E \cdot SED}{1 - \nu^2}} = \sqrt{\frac{2 \cdot 206000 \cdot 9.96721 \cdot 10^{-6}}{1 - 0.3^2}} = 2.1243 MPa \quad (4.55)$$

This result is in good agreement with the value found in literature [33]:

$$\Delta\sigma_{eq,peak,literature} = 2.10 MPa \quad (4.56)$$

Thus, the relative error expresses in percentage between the calculated $\Delta\sigma_{eq,peak}$ and the $\Delta\sigma_{eq,peak,literature}$ is:

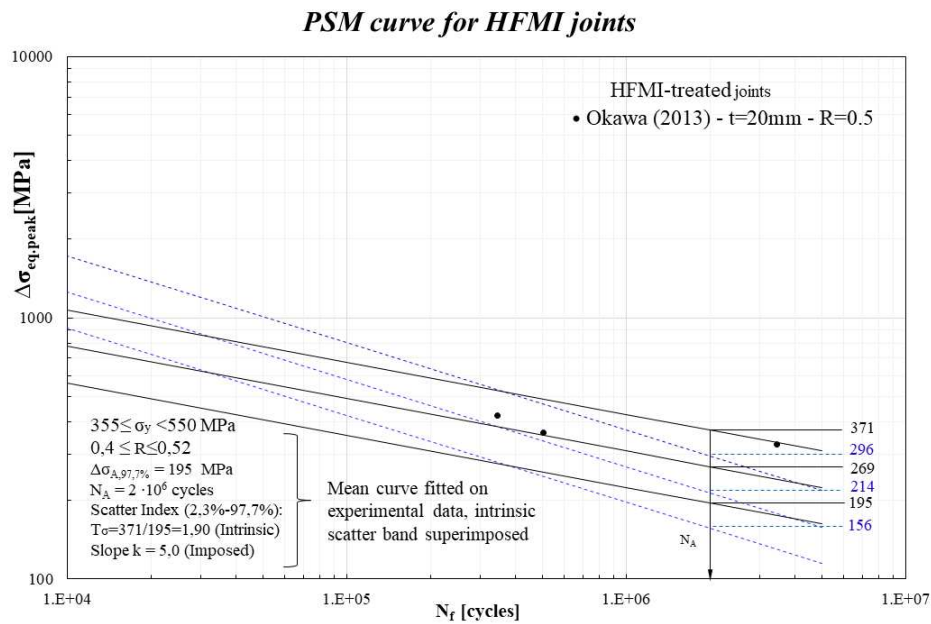
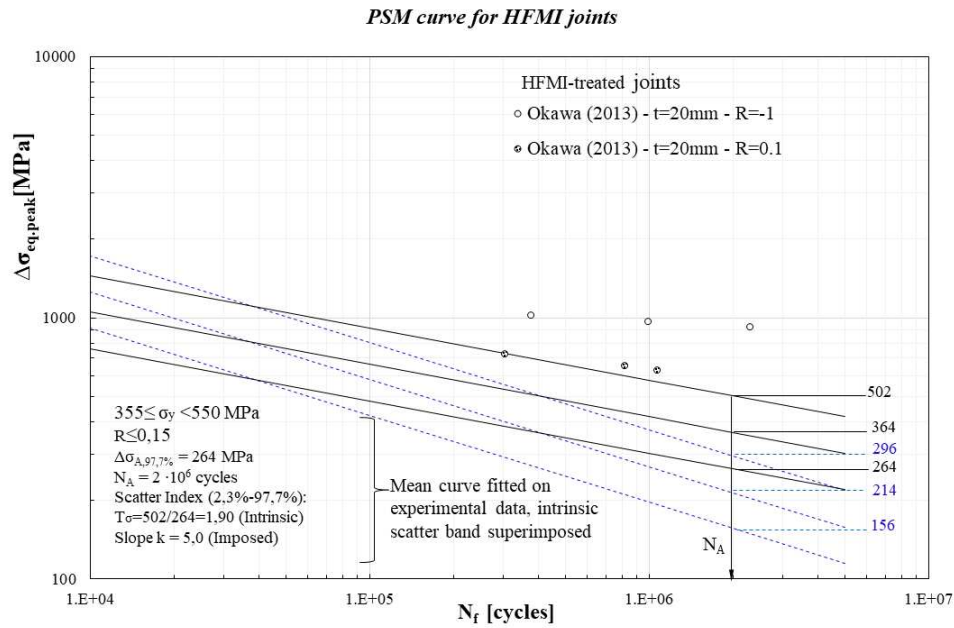
$$\Delta\% = \frac{\Delta\sigma_{eq,peak,calculated} - \Delta\sigma_{eq,peak,literature}}{\Delta\sigma_{eq,peak,literature}} \cdot 100 = 1.16\% \quad (4.57)$$

4.5.2 Data results for SED curve

The previous model was characterised by a load equal to 1 MPa, applied to the main plate of the specimen; to obtain the value of the peak stress related to the applied nominal stress, the equation (3.24) is applied.

The results in terms of equivalent peak stress are defined in the Appendix D.4.

The all experimental data are collected inside the PSM design curve proposed by Meneghetti, Camagnolo, Yildirim and Belluzzo [33]. The black lines are the PSM-based scatter band calculated in HFMI condition with a inverse slope equal to 5 [33], the dotted blue lines are the PSM design curve proposed by Meneghetti, Guzzella and Atzori for structure subjected to prevailing mode I [10]. The curve proposed by Meneghetti, Camagnolo, Yildirim and Belluzzo [33] are different based on the stress ratio and the material steel strength:



The following conclusion can be defined:

1. The all experimental data fall above the lines that represents the 97.7% of probability of survival in as-welded condition with a inverse slope equal to 3 for stress ratio $R \leq 0.15$. For $0.4 \leq R \leq 0.52$, the all experimental data fall above the lines that represents the 50% of probability of survival in as-welded condition. Thus the PSM design curve has demonstrated to be effective and very conservative. This result is expected because the PSM fatigue design curve proposed by Meneghetti, Guzzella and Atzori is calibrated for as-welded joints and the considerations of the HFMI benefits are not present;
2. The all experimental data fall above the lines that represents the 50% of probability of survival in HFMI-treated condition with a inverse slope equal to 5. Thus the PSM design curve has demonstrated to be effective and conservative;

3. The Peak Stress Method combined with SED approach find results that are in according with the literature and it has correctly foreseen the experimental crack initiation point at weld toe.

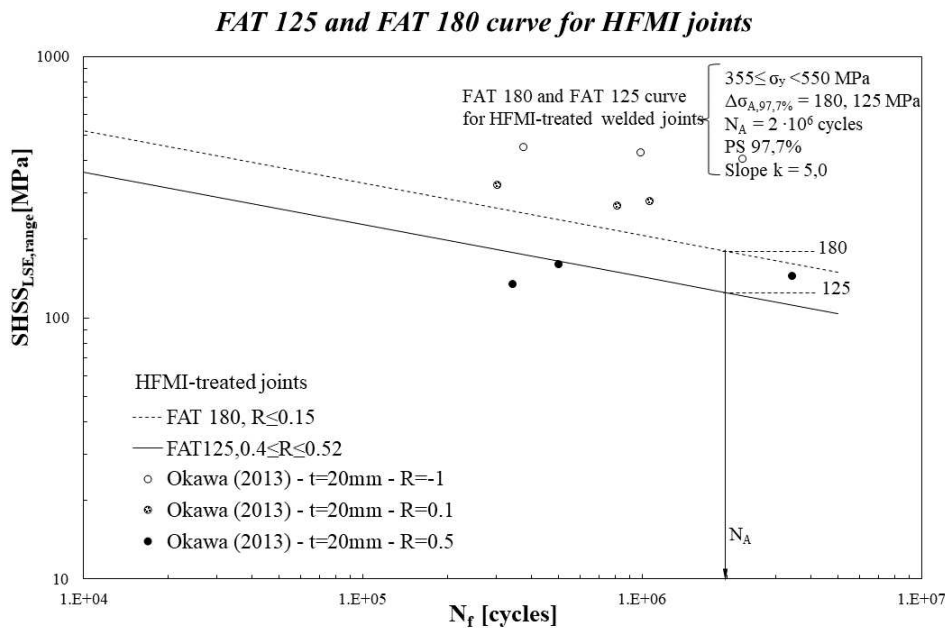
4.5.3 SHSS(Structural Hot Spot Stress) approach

According to the IIW Recommendations, the SHSS approach procedure is the same adopted for as-welded joints, described in the paragraph 3.4.5.

The previous model was characterised by a load equal to 1 MPa, applied to the main plate of the specimen; to obtain the value of the hot-spot stress related to the applied nominal stress, the equation (3.45) is applied.

The results in terms of SHSS are defined in the Appendix D.4.

In agreement with the IIW Recommendations on the HFMI-treated joints [3], the design curve is increased of a FAT class. The hot-spot FAT class for $355 \leq f_y < 550$, non-load carrying fillet welds, is FAT 180 (see Table 4.5) for the stress ratio $R \leq 0.15$ and FAT 125 for $0.4 \leq R \leq 0.52$:



The following conclusion can be defined:

1. The all experimental data fall above the lines that represents the 97.7% of probability of survival in HFMI-treated condition with a inverse slope equal to 5. Thus the PSM design curve has demonstrated to be effective and conservative due to the misalignment effect have been neglected;
2. The SHSS approach find results that are in according with the literature and it has correctly foreseen the experimental crack initiation point at weld toe.

4.6 Kuhlmann-Gunther 2009, transverse attachment FAT 80

The fifth joint analysed is a transverse attachment characterised by a fatigue class FAT 80, studied by Kuhlmann and Gunther in 2009 [44] under CAL (Constant Amplitude Loading).

The principal information and mechanical properties about this typology of the joint are summarized in the Table 4.23 and Table 4.24:

Weld condition	Fracture location	Load application	Main plate/gusset thickness
HFMI, non-load carrying (NLC), full penetration	Weld toe	Axial, main plate, parent material	Main plate: 12mm Gusset: 12mm

Table 4.23: Information about the specimens

Material model	Yield strength f_y [MPa]	Young modulus [MPa]	Poisson's ratio ν
S355J2, linear elastic, isotropic	355	206000	0.3
S690QL, linear elastic, isotropic	690		

Table 4.24: Information about mechanical properties

The dimensions of this joint are defined and described in the paragraph 3.5 (Table 3.46 and Figure 3.97). Regarding the HFMI groove geometry, the dimensions (radius, depth and width) depend on the material type and are taken from [33]. The values are expressed in the following table with reference to Figure 4.18:

Material	depth [mm]	ρ_{HFMI} [mm]	width [mm]	2α [°]
S355J2	0.17	2	2.7	135
S690QL	0.12	2	2.58	

Table 4.25: Dimension of HFMI groove for the transverse attachment FAT 80, studied by Kuhlmann and Gunther in 2009

The inclination angle of the indenters is assumed to be performed along the V-notch bisector, i.e. 67.5° in this case.

The experimental data are defined in the following table in terms of nominal stress $\Delta\sigma_{nom}$:

Material	Stress Ratio R	$\Delta\sigma_{nom}$ [MPa]	N_f [cycles]
S355J2	0.1	300	1 426 998
		340	137 721
		340	116 159
		315	711 012
		315	298 866
		280	799 250
S690QL	0.1	340	768 457
		340	478 283
		315	759 450
		315	1 270 270
		400	193 512
		400	228 100
		280	2 119 665

Table 4.26: Experimental data of the 5th joint, Kuhlmann-Gunther 2009 in HFMI treated condition.

FAT 80 is modelled in *SOLIDWORKS 2020* with the HFMI groove and subsequently, is imported inside Ansys®APDL with .IGS extension. Due to the different dimensions of the groove, two models are created: the

first one for the S355J2 material; the second one for the S690QL material. The results are reported in the figures below:

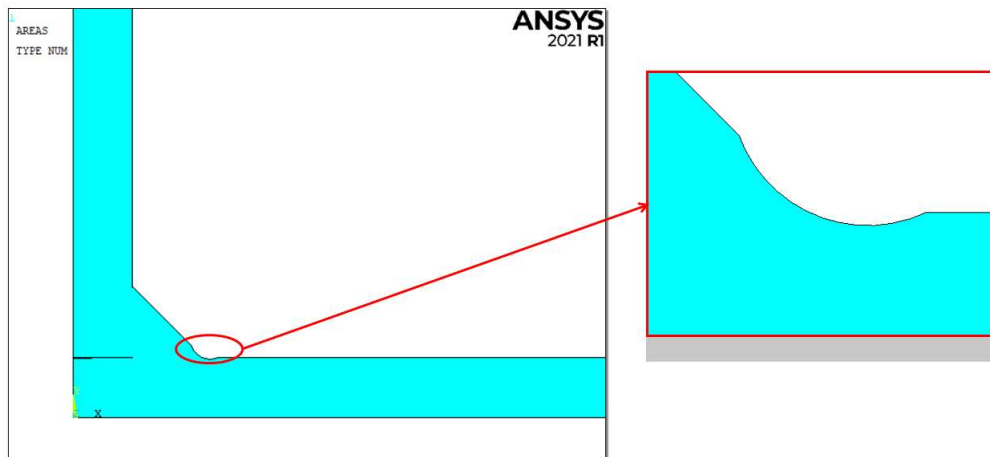


Figure 4.73: Model of longitudinal attachment FAT 80 S355J2 studied by Kuhlmann and Gunther in HFMI treated condition.

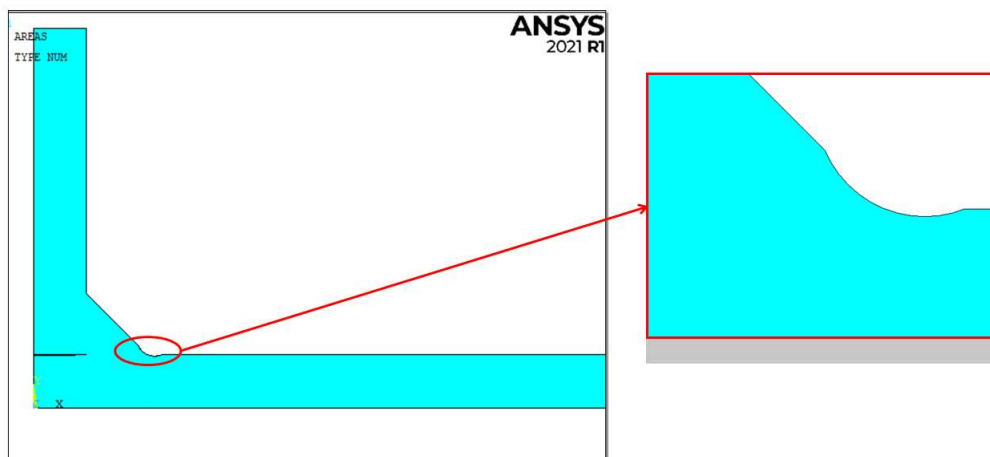


Figure 4.74: Model of longitudinal attachment FAT 80 S690QL studied by Kuhlmann and Gunther in HFMI treated condition.

The procedure to define the boundary conditions of the model follows the same steps and dispositions defined for the same joint in as-welded condition described in the paragraph 3.5.

4.6.1 PSM combined with SED for blunt notches

The fatigue assessment for this model is performed by the application of Peak Stress Method in combination with the SED approach with the adoption of four-node linear elements, considering only the weld toe.

The element PLANE 182 is chosen from the Ansys®APDL library with *Simple Enhanced Strain* as Key Option 1 and *Plane Strain* as Key Option 3.

The SED approach for blunt notches is based on the creation of a structural volume at the radiused weld toe, that can be rigidly rotated (*Figure 4.20*) to include the whole maximum principal stress, which is related to the highest strain energy density.

The first step is to determine the inclination angle Φ with respect to the blunt notch bisector of the most stressed area that is indicated in red in Ansys®APDL.

To define the inclination angle, the models are meshed with a global element size equal to 0.5 mm and subsequently, two refinements with depth equal to 5 (see *Figure 4.75* for the refine options) are applied to the arc that represents the groove due to HFMI treatment (*Figure 4.76-4.77*) with the following commands:

Preprocessor→Meshing→Modify Mesh→Refine At→Lines

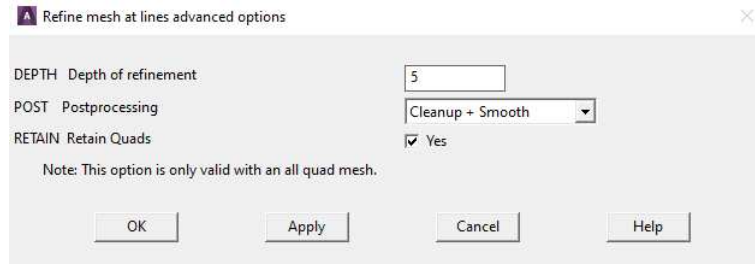


Figure 4.75: Options for the refinement.

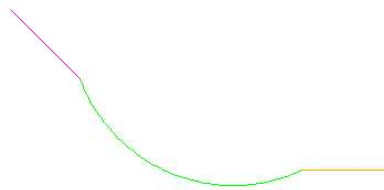


Figure 4.76: Arc that represents the HFMI groove where the refinements are applied for S355J2 model.

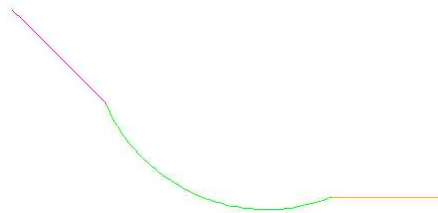


Figure 4.77: Arc that represents the HFMI groove where the refinements are applied for S690QL model.

The meshed models are displayed on the following figures:

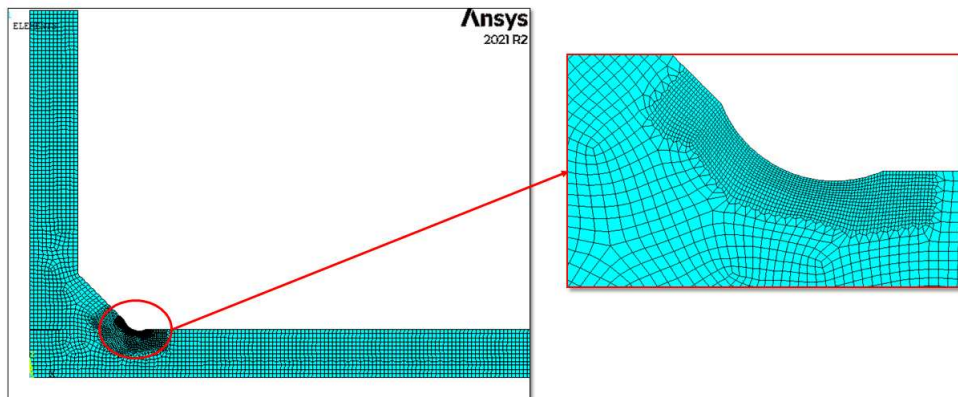


Figure 4.78: Mesh of the model S355J2 to define the inclination angle.

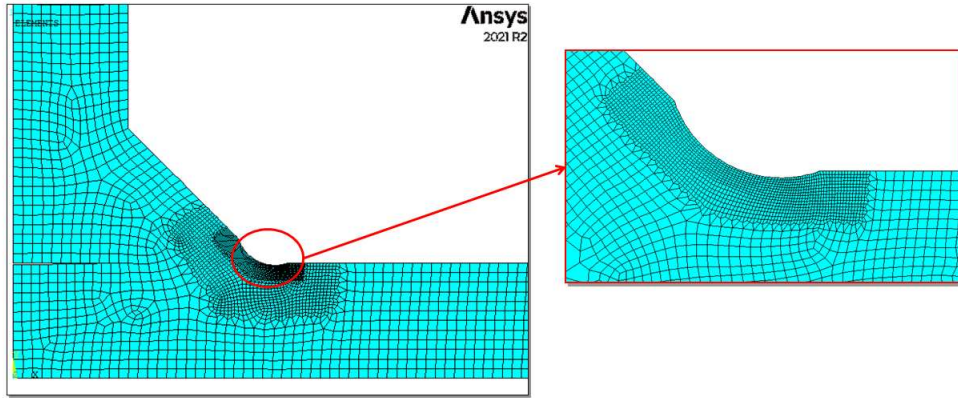


Figure 4.79: Mesh of the model S690QL to define the inclination angle.

The model is subjected to an external nominal stress $\Delta\sigma_{nom} = 1MPa$ applied on the main plate. Once the model is properly meshed, loaded and constraint, the system can be solve:

Solution → Solve → Current LS

The first principal stress $\Delta\sigma_{11}$ is plotted:

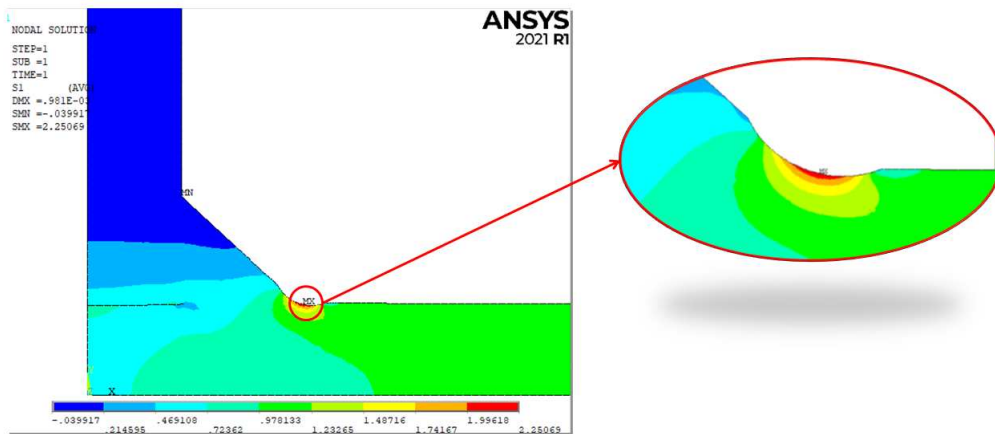


Figure 4.80: Plot of the first principal stress for the model S355J2.

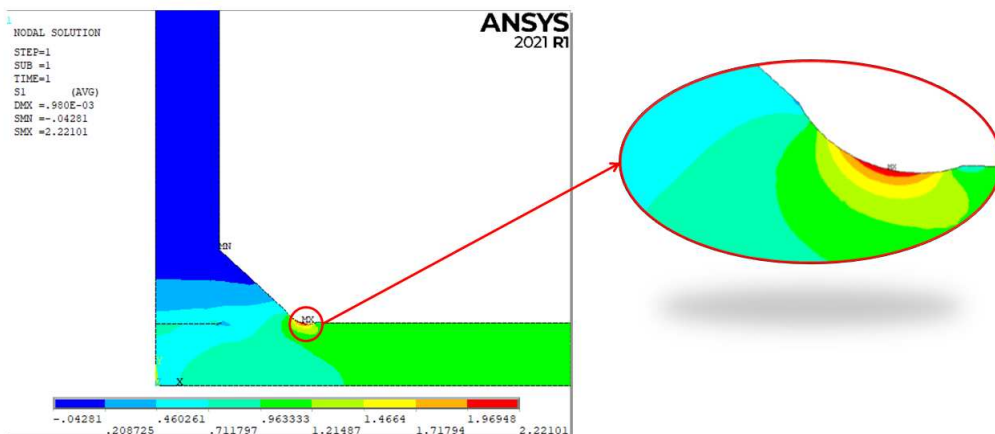


Figure 4.81: Plot of the first principal stress for the model S690QL.

The highest stress is not located exactly around the blunt notch bisector, so it is matter of quantifying the grades of rotation. The value of the angle is reported in the following equation and represents a clockwise rotation about the global z-axis:

$$\Phi_{S355J2} = 9.50^\circ \quad (4.58)$$

$$\Phi_{S690QL} = 8.18^\circ \quad (4.59)$$

The circular sector is created according to equations (4.5) and (4.6) and the results are the same for S355J2 and S690QL models:

$$q = \frac{2\pi - 2\alpha}{\pi} = 2 - \frac{135}{180} = 1.25 \quad (4.60)$$

$$r_0 = \frac{q-1}{q} \cdot \rho_{HFMI} = \frac{1.25-1}{1.25} \cdot 2 = 0.4mm \quad (4.61)$$

$$R_0 + r_0 = 0.28 + 0.4 = 0.68mm \quad (4.62)$$

Subsequently, the control volume to calculate the averaged Strain Energy Density (SED) is created. The result is reported in the following figure:

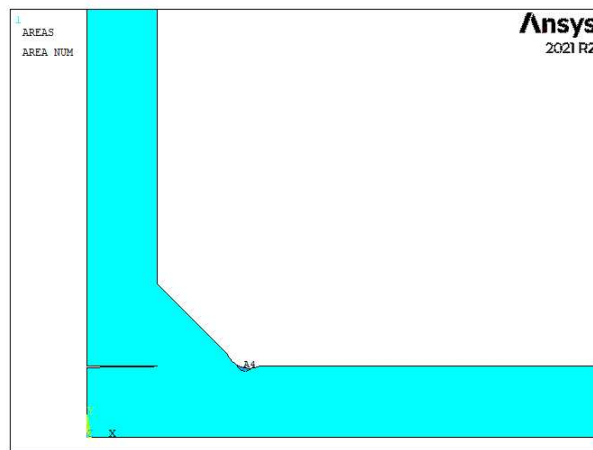


Figure 4.82: Illustration of the control Area to calculate the SED for S355J2.

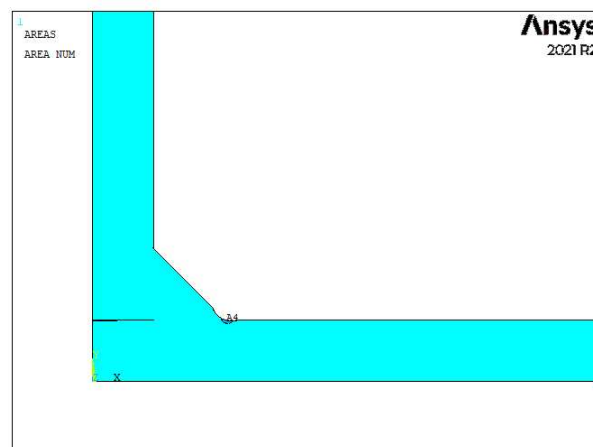


Figure 4.83: Illustration of the control Area to calculate the SED for S690QL.

To create the mesh of the model, the following procedure is executed:

1. The element inside the structural volume are characterised by a *global element size* equal to 0.01mm with a *free-mesh* algorithm;

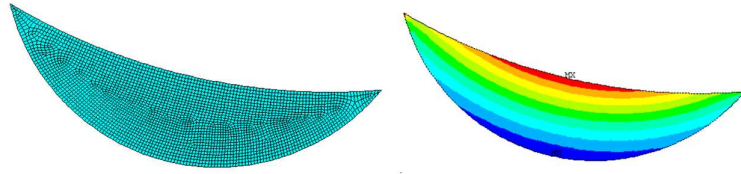


Figure 4.84: On the left, the mesh of the structural volume with global element size of 0.01. On the right, the proof that the highest stress is contained inside the volume for the model S355J2.

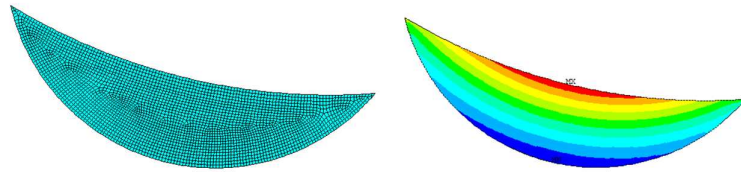


Figure 4.85: On the left, the mesh of the structural volume with global element size of 0.01. On the right, the proof that the highest stress is contained inside the volume for the model S690QL.

2. The other volume is meshed with a *global element size* equal to 0.2 mm with a *free-mesh* algorithm.

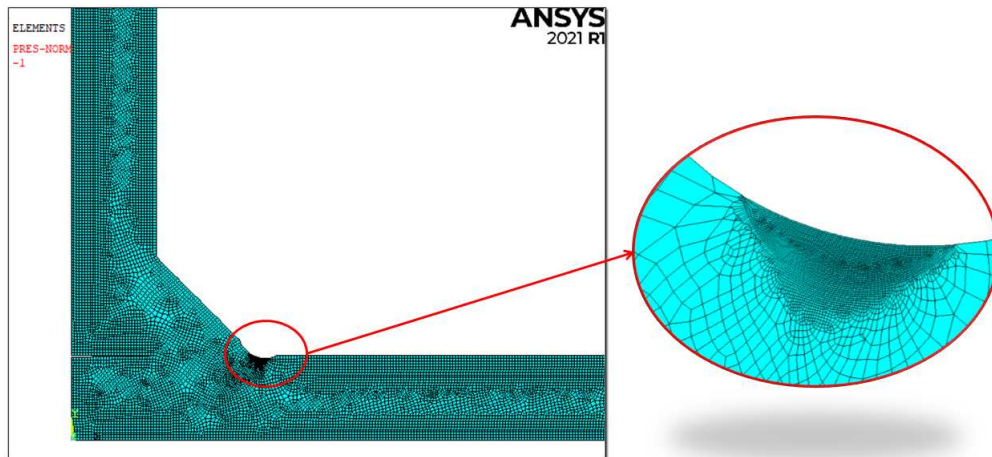


Figure 4.86: Mesh of the all structure S355J2.

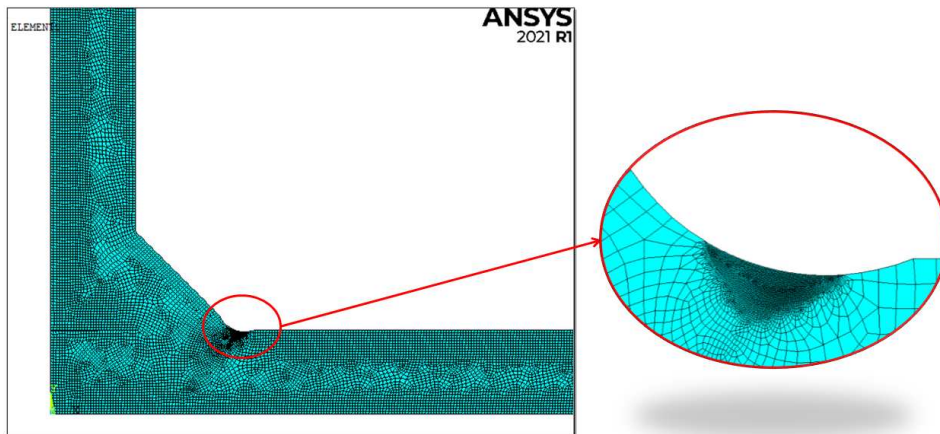


Figure 4.87: Mesh of the all structure S690QL.

Once the model is properly meshed, loaded and constraint, the system can be solved:

Solution → *Solve* → *Current LS*

The averaged Strain Energy Density is defined as the energy contained inside the structural volume. The same procedure used for FAT 71 is applied to detect the SED value.

Results for S355J2 model

The result of SED for the weld toe when the specimen is subjected to a nominal stress of 1 MPa is:

$$SENE = 2.06236 \cdot 10^{-6} MJ \quad (4.63)$$

$$VOLU = 0.24673 mm^3 \quad (4.64)$$

$$SED = \frac{SENE}{VOLU} = \frac{2.06236 \cdot 10^{-6}}{0.24673} = 8.35877 \cdot 10^{-6} \frac{MJ}{m^3} \quad (4.65)$$

From the SED, the equivalent peak stress is obtained with the following formula:

$$\Delta\sigma_{eq,peak} = \sqrt{\frac{2 \cdot E \cdot SED}{1 - \nu^2}} = \sqrt{\frac{2 \cdot 206000 \cdot 8.35877 \cdot 10^{-6}}{1 - 0.3^2}} = 1.9454 MPa \quad (4.66)$$

This result is in good agreement with the value found in literature [33]:

$$\Delta\sigma_{eq,peak,literature} = 1.909 MPa \quad (4.67)$$

Thus, the relative error expresses in percentage between the calculated $\Delta\sigma_{eq,peak}$ and the $\Delta\sigma_{eq,peak,literature}$ is:

$$\Delta\% = \frac{\Delta\sigma_{eq,peak,calculated} - \Delta\sigma_{eq,peak,literature}}{\Delta\sigma_{eq,peak,literature}} \cdot 100 = 1.90\% \quad (4.68)$$

Results for S690QL model

The result of SED for the weld toe when the specimen is subjected to a nominal stress of 1 MPa is:

$$SENE = 2.01481 \cdot 10^{-6} MJ \quad (4.69)$$

$$VOLU = 0.248067 mm^3 \quad (4.70)$$

$$SED = \frac{SENE}{VOLU} = \frac{2.01481 \cdot 10^{-6}}{0.248067} = 8.12204 \cdot 10^{-6} \frac{MJ}{m^3} \quad (4.71)$$

From the SED, the equivalent peak stress is obtained with the following formula:

$$\Delta\sigma_{eq,peak} = \sqrt{\frac{2 \cdot E \cdot SED}{1 - \nu^2}} = \sqrt{\frac{2 \cdot 206000 \cdot 8.12204 \cdot 10^{-6}}{1 - 0.3^2}} = 1.9176 MPa \quad (4.72)$$

This result is in good agreement with the value found in literature [33]:

$$\Delta\sigma_{eq,peak,literature} = 1.909 MPa \quad (4.73)$$

Thus, the relative error expresses in percentage between the calculated $\Delta\sigma_{eq,peak}$ and the $\Delta\sigma_{eq,peak,literature}$ is:

$$\Delta\% = \frac{\Delta\sigma_{eq,peak,calculated} - \Delta\sigma_{eq,peak,literature}}{\Delta\sigma_{eq,peak,literature}} \cdot 100 = 1.91\% \quad (4.74)$$

4.6.2 Data results for SED curve

The previous model was characterised by a load equal to 1 MPa, applied to the main plate of the specimen; to obtain the value of the peak stress related to the applied nominal stress, the equation (3.24) is applied. The results in terms of equivalent peak stress are defined in the Appendix D.4. The all experimental data are collected inside the PSM design curve proposed by Meneghetti, Camagnolo, Yildirim and Belluzzo [33]. The black lines are the PSM-based scatter band calculated in HFMI condition with a inverse slope equal to 5 [33], the dotted blue lines are the PSM design curve proposed by Meneghetti, Guzzella and Atzori for structure subjected to prevailing mode I [10]. The curve proposed by Meneghetti, Camagnolo, Yildirim and Belluzzo [33] are different based on the stress ratio and the material steel strength:

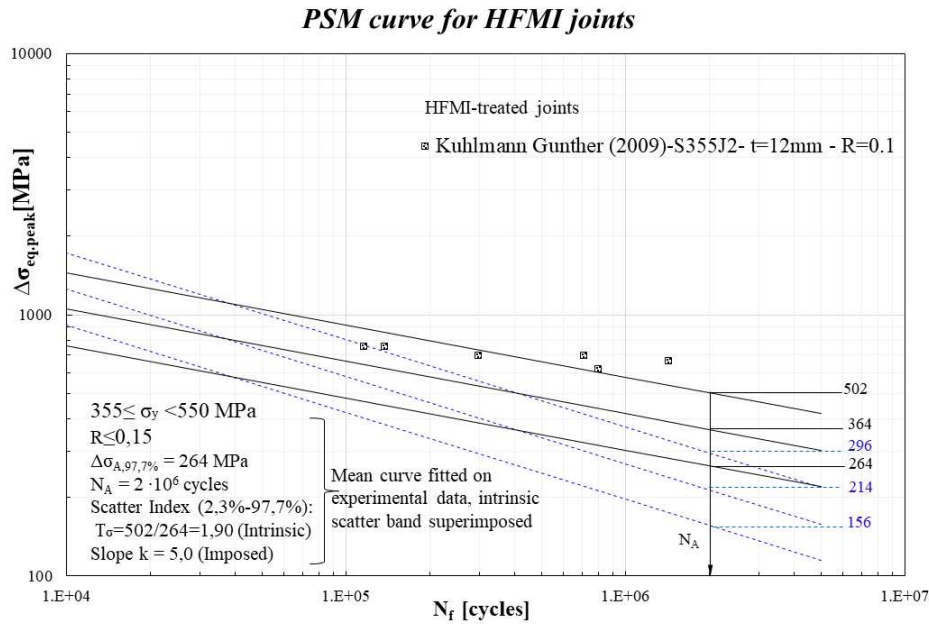


Figure 4.88: Experimental data inside the PSM design curve.

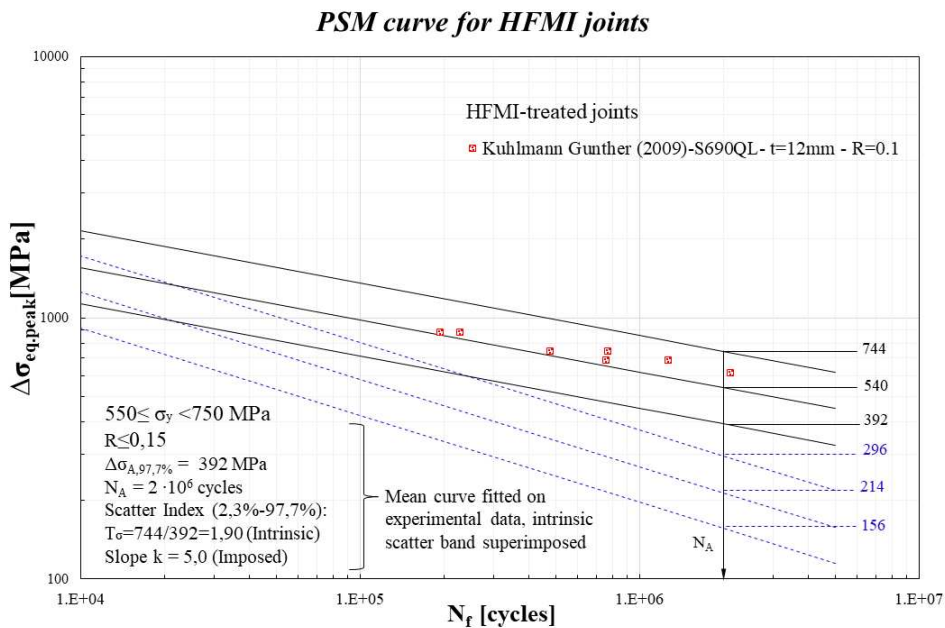


Figure 4.89: Experimental data inside the PSM design curve.

The following conclusion can be defined:

1. The all experimental data fall above the lines that represents the 50% of probability of survival in as-welded condition with a inverse slope equal to 3 for yield strength $355 \leq f_y < 550MPa$. The all experimental data fall above the lines that represents the 2.3% of probability of survival in as-welded condition for yield strength $550 \leq f_y < 750MPa$. Thus the PSM design curve has demonstrated to be effective and very conservative. This result is expected because the PSM fatigue design curve proposed by Meneghetti, Guzzella and Atzori is calibrated for as-welded joints and the considerations of the HFMI benefits are not present;
2. The all experimental data fall above the lines that represents the 50% of probability of survival in HFMI-treated condition with a inverse slope equal to 5. Thus the PSM design curve has demonstrated to be effective and conservative;
3. The Peak Stress Method combined with SED approach find results that are in according with the literature and it has correctly foreseen the experimental crack initiation point at weld toe.

4.6.3 SHSS(Structural Hot Spot Stress) approach

According to the IIW Recommendations, the SHSS approach procedure is the same adopted for as-welded joints, described in the paragraph 3.5.4.

The previous model was characterised by a load equal to 1 MPa, applied to the main plate of the specimen; to obtain the value of the hot-spot stress related to the applied nominal stress, the equation (3.45) is applied.

The results in terms of SHSS are defined in the Appendix D.5.

In agreement with the IIW Recommendations on the HFMI-treated joints [3], the design curve is increased of a FAT class. The hot-spot FAT class for non-load carrying fillet welds, is FAT 180 (see Table4.5) for the yield strength $355 \leq f_y < 550MPa$ and FAT 200 $550 \leq f_y < 750MPa$:

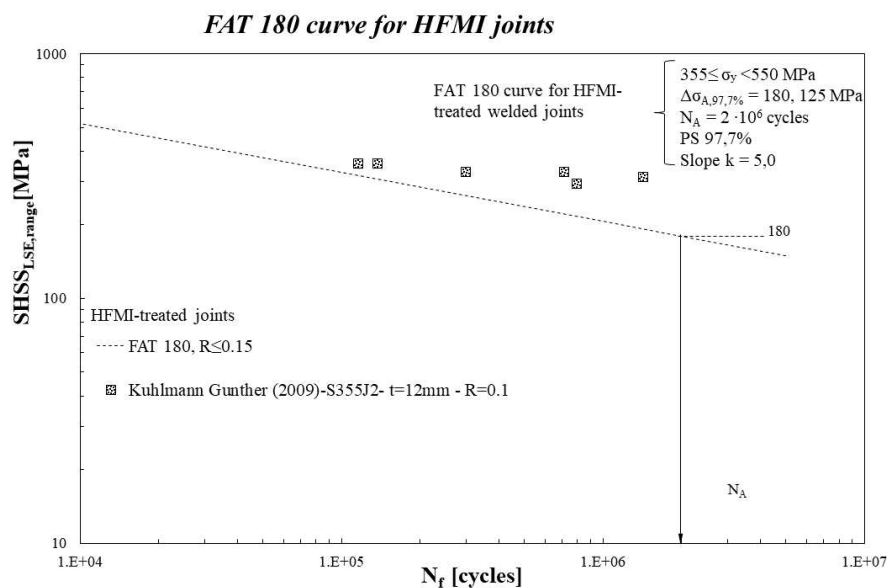


Figure 4.90: Experimental data inside the SHSS design curve.

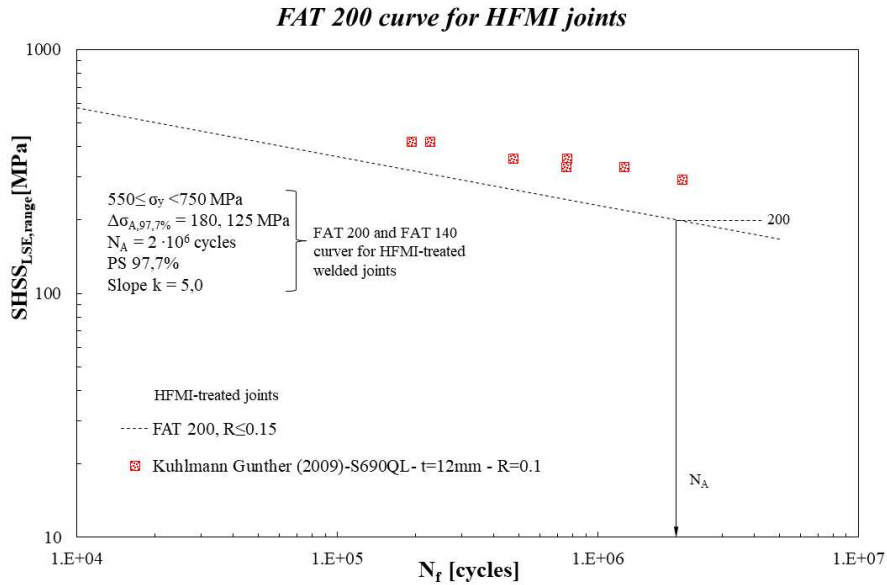


Figure 4.91: Experimental data inside the SHSS design curve.

The following conclusion can be defined:

1. The all experimental data fall above the lines that represents the 97.7% of probability of survival in HFMI-treated condition with a inverse slope equal to 5. Thus the PSM design curve has demonstrated to be effective and conservative due to the misalignment effect have been neglected;
2. The SHSS approach find results that are in according with the literature and it has correctly foreseen the experimental crack initiation point at weld toe.

4.7 Kuhlmann 2006, transverse attachment FAT 80

The sixth joint analysed is a transverse attachment characterised by a fatigue class FAT 80, studied by Kuhlmann in 2006 [44] under CAL (Constant Amplitude Loading).

The principal information and mechanical properties about this typology of the joint are summarized in the *Table 4.27* and *Table 4.28*:

Weld condition	Fracture location	Load application	Main plate/gusset thickness
HFMI, non-load carrying (NLC), full penetration	Weld toe	Axial, main plate, parent material	Main plate: 12mm Gusset: 12mm

Table 4.27: Information about the specimens

Material model	Yield strength f_y [MPa]	Young modulus [MPa]	Poisson's ratio ν
S355, linear elastic, isotropic	355	206000	0.3
S460, linear elastic, isotropic	460		

Table 4.28: Information about mechanical properties

The dimensions of this joint are defined and described in the paragraph 3.6 (*Table 3.55* and *Figure 3.109*). Regarding the HFMI groove geometry, the dimensions (radius, depth and width) are taken from [33] and the values are expressed in the following table with reference to *Figure 4.18*

depth [mm]	ρ_{HFMI} [mm]	width [mm]	2α [°]
0.10	2.50	3.00	135

Table 4.29: Dimension of HFMI groove for the transverse attachment FAT 80, studied by Kuhlmann in 2006

The inclination angle of the indenters is assumed to be performed along the V-notch bisector, i.e. 67.5° in this case.

The experimental data are defined in the following table in terms of nominal stress $\Delta\sigma_{nom}$:

Material	Stress Ratio R	$\Delta\sigma_{nom}$ [MPa]	N_f [cycles]
S355	0.1	306	108 489
		278	363 274
		253	455 624
		230	977 946
		261	349,432
		264	315 592
		217	1 146 656
		260	845 460
		320	89,949
		250	1 365 764
		294	200 637
		S460	0.1
320	174 924		
287	346 406		
250	992 769		
240	1 077822		
387	51 593		
294	221 726		
332	260 850		
356	162 744		
271	522 654		

Table 4.30: Experimental data of the 6th joint, Kuhlmann 2006 in HFMI treated condition.

FAT 80 is modelled in *SOLIDWORKS 2020* with the HFMI groove and subsequently, is imported inside Ansys®APDL with .IGS extension. The results is reported in the figure below:

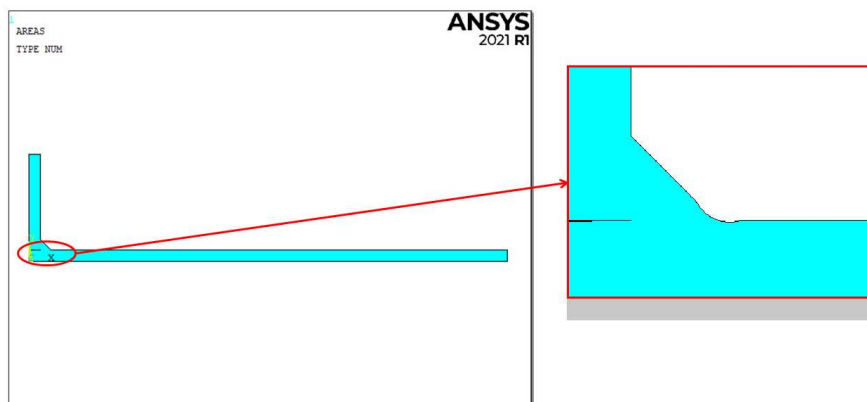


Figure 4.92: Model of longitudinal attachment FAT 80 studied by Okawa in HFMI treated condition.

The procedure to define the boundary conditions of the model follows the same steps and dispositions defined for the same joint in as-welded condition described in the paragraph 3.6.

4.7.1 PSM combined with SED for blunt notches

The fatigue assessment for this model is performed by the application of Peak Stress Method in combination with the SED approach with the adoption of four-node linear elements, considering only the weld toe.

The element PLANE 182 is chosen from the Ansys®APDL library with *Simple Enhanced Strain* as Key Option 1 and *Plane Strain* as Key Option 3.

The SED approach for blunt notches is based on the creation of a structural volume at the radiused weld toe, that can be rigidly rotated (*Figure 4.20*) to include the whole maximum principal stress, which is related to the highest strain energy density.

The first step is to determine the inclination angle Φ with respect to the blunt notch bisector of the most stressed area that is indicated in red in Ansys®APDL.

To define the inclination angle, the model is meshed with a global element size equal to 0.5 mm and subsequently, two refinements with depth equal to 5 (see *Figure 4.93* for the refine options) are applied to the arc that represents the groove due to HFMI treatment (*Figure 4.94*) with the following commands:

Preprocessor → *Meshing* → *Modify Mesh* → *Refine At* → *Lines*

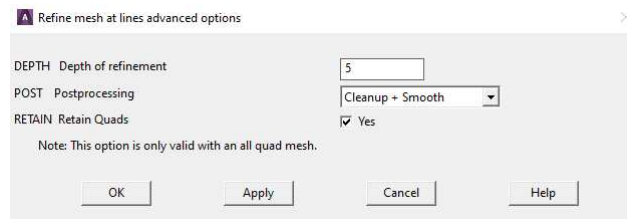


Figure 4.93: Options for the refinement.

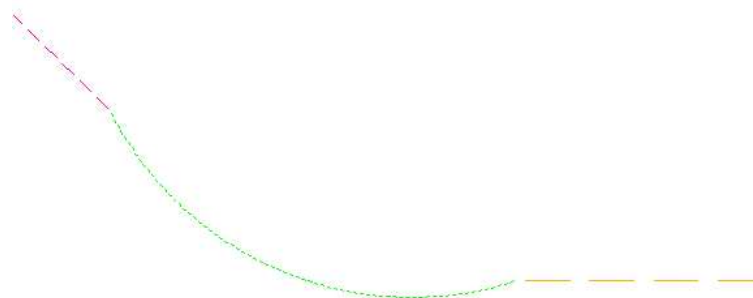


Figure 4.94: Arc that represents the HFMI groove where the refinements are applied.

The meshed model is displayed on the following figure:

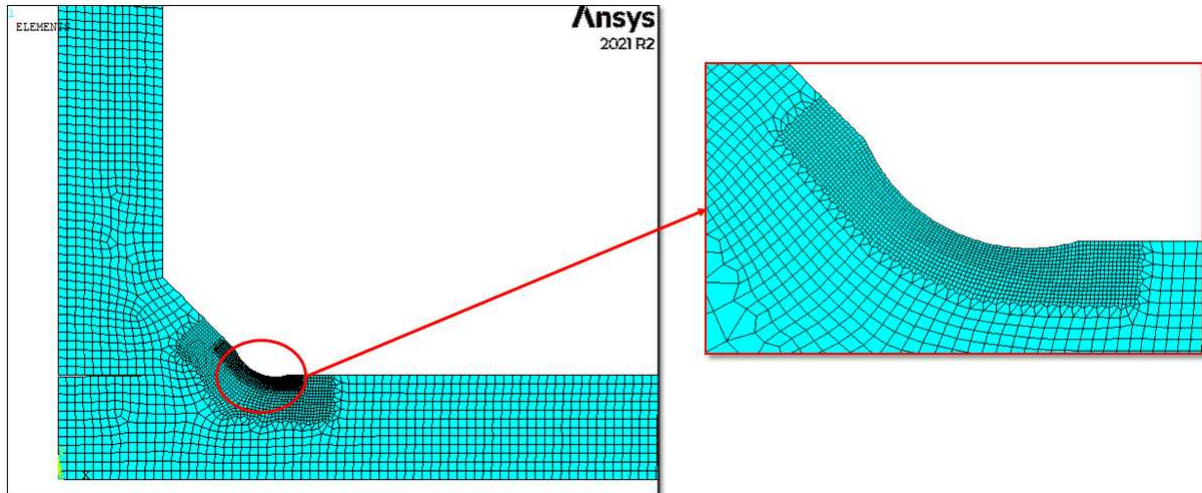


Figure 4.95: Mesh of the model to define the inclination angle.

The model is subjected to an external nominal stress $\Delta\sigma_{nom} = 1MPa$ applied on the main plate. Once the model is properly meshed, loaded and constraint, the system can be solve:

Solution→*Solve*→*Current LS*

The first principal stress $\Delta\sigma_{11}$ is plotted:

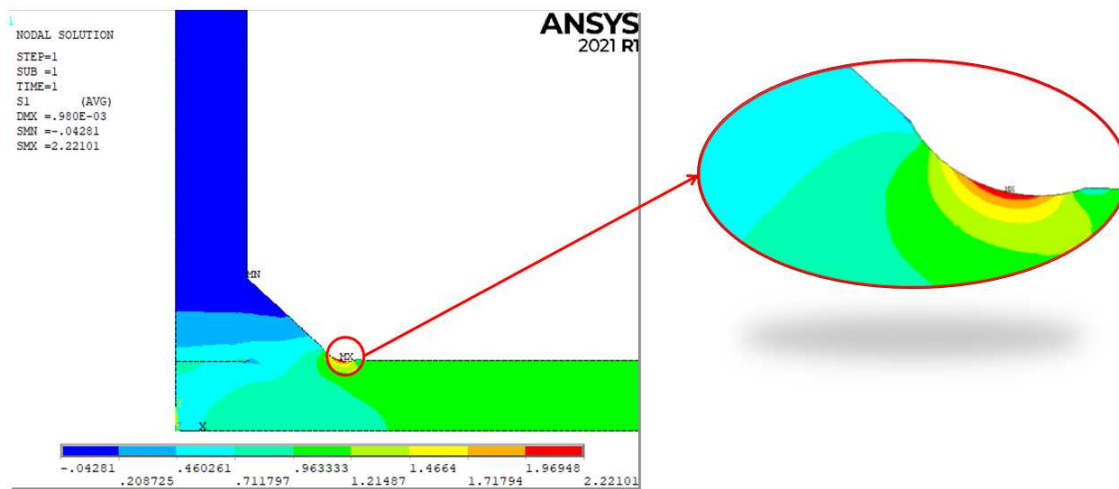


Figure 4.96: Plot of the first principal stress.

The highest stress is not located exactly around the blunt notch bisector, so it is matter of quantifying the grades of rotation. The value of the angle is reported in the following equation and represents a clockwise rotation about the global z-axis:

$$\Phi = 9.88^\circ \quad (4.75)$$

The circular sector is created according to equations (4.5) and (4.6):

$$q = \frac{2\pi - 2\alpha}{\pi} = 2 - \frac{135}{180} = 1.25 \quad (4.76)$$

$$r_0 = \frac{q-1}{q} \cdot \rho_{HFMI} = \frac{1.25-1}{1.25} \cdot 2.5 = 0.5mm \quad (4.77)$$

$$R_0 + r_0 = 0.28 + 0.4 = 0.78mm \quad (4.78)$$

Subsequently, the control volume to calculate the averaged Strain Energy Density (SED) is created. The result is reported in the following figure:

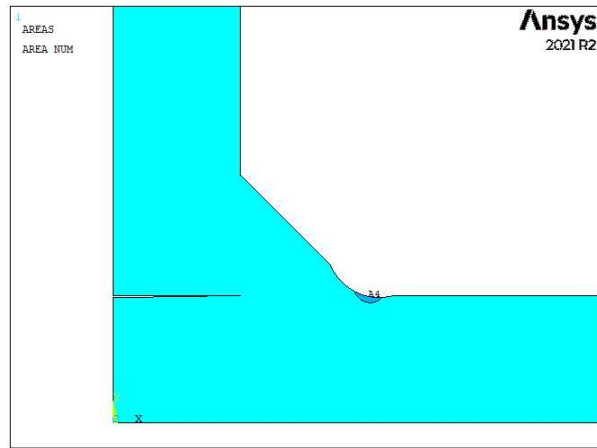


Figure 4.97: Illustration of the control Area to calculate the SED.

To create the mesh of the model, the following procedure is executed:

1. The element inside the structural volume are characterised by a *global element size* equal to 0.01mm with a *free-mesh* algorithm;

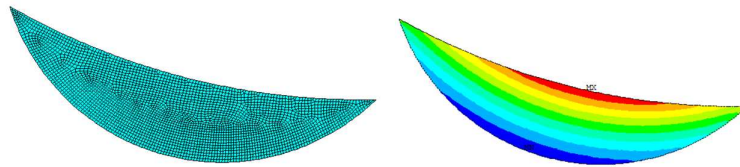


Figure 4.98: On the left, the mesh of the structural volume with global element size of 0.01. On the right, the proof that the highest stress is contained inside the volume.

2. The other volume is meshed with a *global element size* equal to 0.2 mm with a *free-mesh* algorithm.

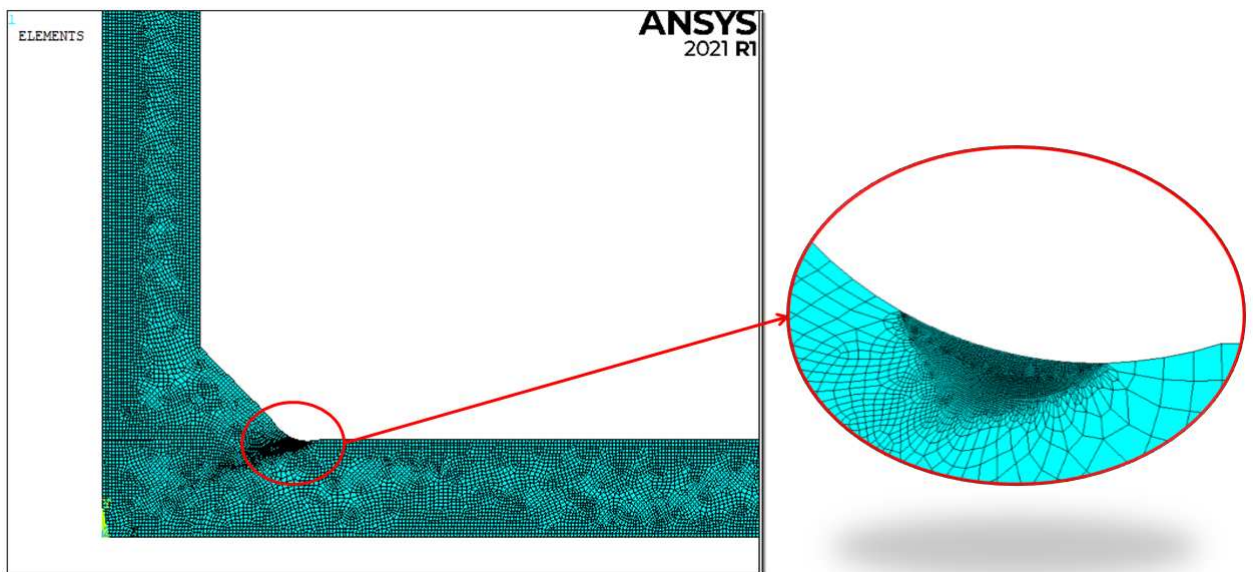


Figure 4.99: Mesh of the all structure.

Once the model is properly meshed, loaded and constraint, the system can be solved:

Solution → Solve → Current LS

The averaged Strain Energy Density is defined as the energy contained inside the structural volume. The same procedure used for FAT 71 is applied to detect the SED value.

The result of SED for the weld toe when the specimen is subjected to a nominal stress of 1 MPa is:

$$SENE = 1.89439 \cdot 10^{-6} MJ \quad (4.79)$$

$$VOLU = 0.266519 mm^3 \quad (4.80)$$

$$SED = \frac{SENE}{VOLU} = \frac{1.89439 \cdot 10^{-6}}{0.266519} = 7.1079 \cdot 10^{-6} \frac{MJ}{m^3} \quad (4.81)$$

From the SED, the equivalent peak stress is obtained with the following formula:

$$\Delta\sigma_{eq,peak} = \sqrt{\frac{2 \cdot E \cdot SED}{1 - \nu^2}} = \sqrt{\frac{2 \cdot 206000 \cdot 7.1079 \cdot 10^{-6}}{1 - 0.3^2}} = 1.7939 MPa \quad (4.82)$$

This result is in good agreement with the value found in literature [33]:

$$\Delta\sigma_{eq,peak,literature} = 1.773 MPa \quad (4.83)$$

Thus, the relative error expresses in percentage between the calculated $\Delta\sigma_{eq,peak}$ and the $\Delta\sigma_{eq,peak,literature}$ is:

$$\Delta\% = \frac{\Delta\sigma_{eq,peak,calculated} - \Delta\sigma_{eq,peak,literature}}{\Delta\sigma_{eq,peak,literature}} \cdot 100 = 1.18\% \quad (4.84)$$

4.7.2 Data results for SED curve

The previous model was characterised by a load equal to 1 MPa, applied to the main plate of the specimen; to obtain the value of the peak stress related to the applied nominal stress, the equation (3.24) is applied.

The results in terms of equivalent peak stress are defined in the Appendix D.6.

The all experimental data are collected inside the PSM design curve proposed by Meneghetti, Camagnolo, Yildirim and Belluzzo [33]. The black lines are the PSM-based scatter band calculated in HFMI condition with a inverse slope equal to 5 [33], the dotted blue lines are the PSM design curve proposed by Meneghetti, Guzzella and Atzori for structure subjected to prevailing mode I [10]:

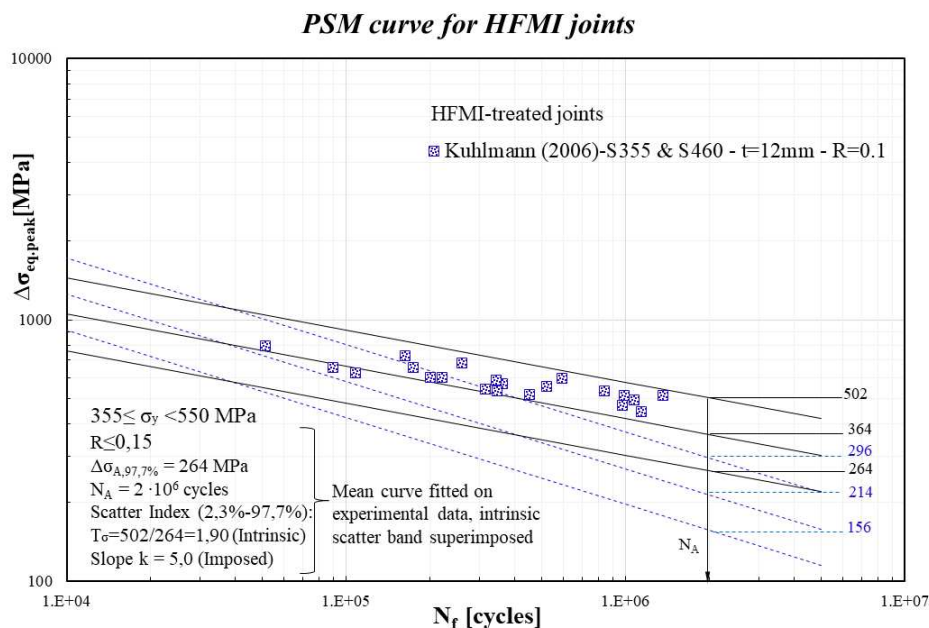


Figure 4.100: Experimental data inside the PSM design curve.

The following conclusion can be defined:

1. The all experimental data fall above the lines that represents the 50% of probability of survival in as-welded condition with a inverse slope equal to 3. Thus the PSM design curve has demonstrated to be effective and very conservative. This result is expected because the PSM fatigue design curve proposed by Meneghetti, Guzzella and Atzori is calibrated for as-welded joints and the considerations of the HFMI benefits are not present;
2. The all experimental data fall above the lines that represents the 97.7% of probability of survival in HFMI-treated condition with a inverse slope equal to 5. Thus the PSM design curve has demonstrated to be effective and conservative;
3. The Peak Stress Method combined with SED approach find results that are in according with the literature and it has correctly foreseen the experimental crack initiation point at weld toe.

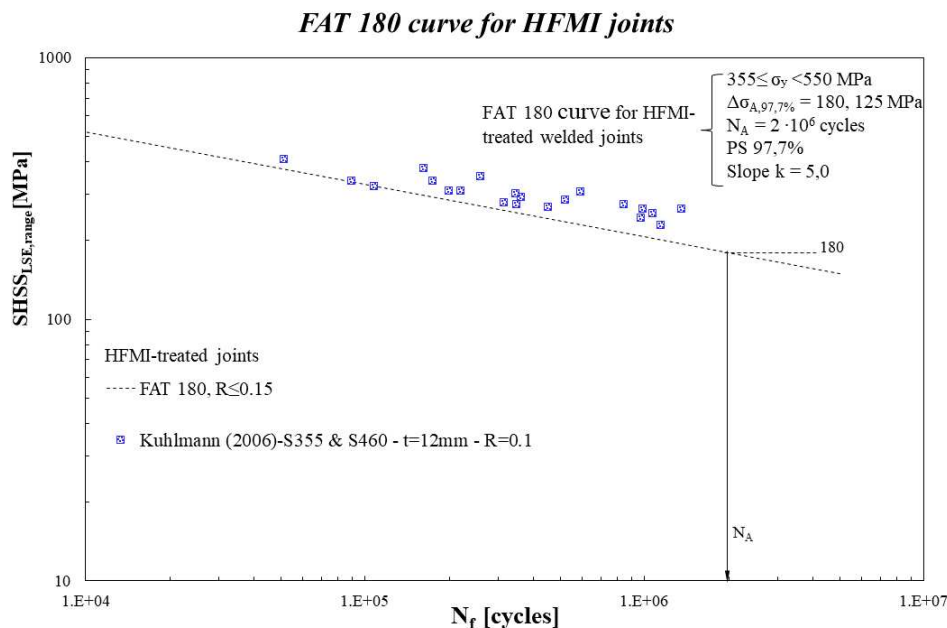
4.7.3 SHSS(Structural Hot Spot Stress) approach

According to the IIW Recommendations, the SHSS approach procedure is the same adopted for as-welded joints, described in the paragraph 3.6.1.

The previous model was characterised by a load equal to 1 MPa, applied to the main plate of the specimen; to obtain the value of the hot-spot stress related to the applied nominal stress, the equation (3.45) is applied.

The results in terms of SHSS are defined in the Appendix D.6.

In agreement with the IIW Recommendations on the HFMI-treated joints [3], the design curve is increased of a FAT class. The hot-spot FAT class for $355 \leq f_y < 550$, non-load carrying fillet welds, is FAT 180 (see Table 4.5) for the stress ratio $R \leq 0.15$:



The following conclusion can be defined:

1. The all experimental data fall above the lines that represents the 97.7% of probability of survival in HFMI-treated condition with a inverse slope equal to 5. Thus the PSM design curve has demonstrated to be effective and conservative due to the misalignment effect have been neglected;
2. The SHSS approach find results that are in according with the literature and it has correctly foreseen the experimental crack initiation point at weld toe.

4.8 Summary of the results

SHSS results

The Hot-spot stress results of the all models are collected together in the following table with the type of mesh algorithm, the type of element, the thickness t , the global element size d and the relative error.

Name of model	Mesh Pattern	FE type	t [mm]	d [mm]	SHSS _{LSE,paper} [MPa]	SHSS _{LSE,calc.} [MPa]	Δ %
Marquis (2010)	Mapped	Solid 185	8	1.6	1.406	1.432	1.80%
Vanrostenberghe (2015)	Mapped	Solid 185	10	2	1.384	1.404	1.44%
Vanrostenberghe (2015)	Mapped	Solid 185	20	2	1.203	1.198	-0.35%
Yildirim (2020)	Mapped	Plane 182	6	1.2	1.035	1.0298	-0.50%
Okawa (2013)	Mapped	Plane 182	20	4	1.066	1.0661	0.026%
Kuhlmann-Gunther (2009)	Mapped	Plane 182	12	2.4	1.041	1.0436	0.25%
Kuhlmann (2006)	Mapped	Plane 182	12	2.4	1.046	1.0515	0.52%

Table 4.31: Summary of SHSS results of the all models

In agreement with the IIW Recommendations on the HFMI-treated joints [3], the design curve is increased of a FAT class and it depends on the steel grade range and the stress ratio. The improvement of FAT class for each joint are reported in the following table:

Name of model	Material	f_y [MPa]	R				FAT Class AW	FAT class Improvement			
								Only f_y effect	R effect		
Marquis (2010)	S7000	$550 \leq f_y < 750$		-1			100	200		200	
Vanrosten. 10mm(2015)	S7000	$550 \leq f_y < 750$	0.1		0.5		100	200	200		140
Vanrosten. 20mm(2015)	S7000	$550 \leq f_y < 750$	0.1		0.5		100	200	200		140
Vanrosten. 10mm(2015)	S690QL	$550 \leq f_y < 750$	0.1		0.5		100	200	200		140
Vanrosten. 20mm(2015)	S690QL	$550 \leq f_y < 750$	0.1		0.5		100	200	200		140
Yildirim (2020)	AH36	423		-0.43			100	180		180	
Okawa (2013)	AH36	423	-1	0.1	0.5		100	180	180	180	125
Kuhlmann-Gunther (2009)	S355J2	$355 \leq f_y < 550$		0.1			100	180		180	
Kuhlmann-Gunther (2009)	S690QL	$550 \leq f_y < 750$		0.1			100	200		200	
Kuhlmann (2006)	S460	460		0.1			100	180		180	
Kuhlmann (2006)	S355	355		0.1			100	180		180	

Table 4.32: FAT class improvement for each model.

The all experimental data of the all models are collected inside the SHSS design curve proposed by IIW guideline. In agreement with the IIW Recommendations on the HFMI-treated joints [3], the design curve is increased of a FAT class as shown in Table 4.32:

FAT 125 and FAT 180 curve for HFMI joints

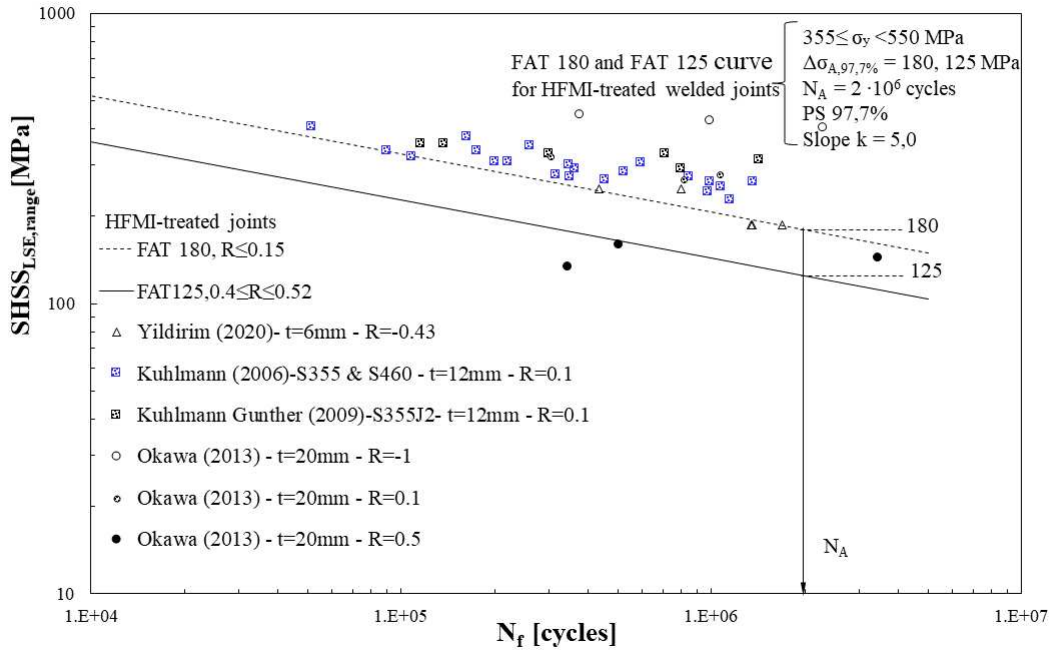


Figure 4.102: Experimental data inside the SHSS design curve for $355 \leq f_y < 550$ MPa.

FAT 140 and FAT 200 curve for HFMI joints

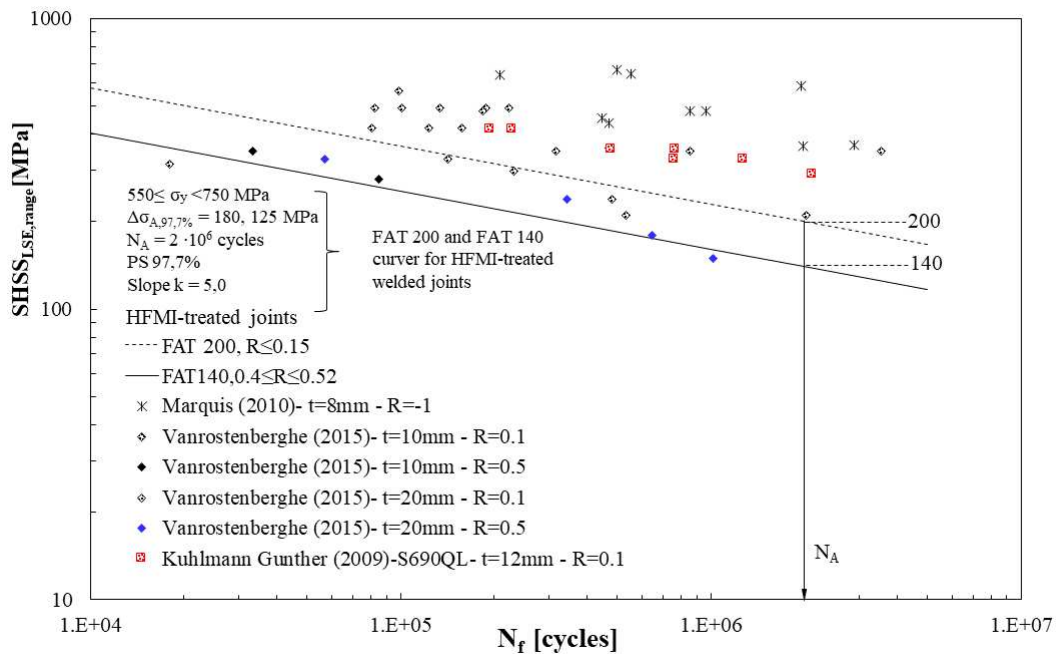


Figure 4.103: Experimental data inside the SHSS design curve for $550 \leq f_y < 750$ MPa.

PSM results

The PSM results of the all models are collected together in the following table with the thickness t , the global element size d_{global} and the element size inside the SED volume d_{local} , inclination angle of the SED volume and the relative error:

Name of model	t [mm]	d_{global} [mm]	d_{local} [mm]	Φ_{paper} [°]	$\Phi_{calc.}$ [°]	$\Delta\sigma_{eq,peak,paper}$ [MPa]	$\Delta\sigma_{eq,peak,calc.}$ [MPa]	$\Delta\%$
Marquis (2010)	8	1	0.05	3.57	7.06	2.219	2.2086	-0.47%
Vanrostenberghe (2015)	10	1	0.05	11.9	11.78	2.501	2.5046	0.15%
Vanrostenberghe (2015)	20	1	0.05	7.57	9.09	2.699	2.6992	0.008%
Yildirim (2020)	6	1	0.05	11.7	11.73	1.611	1.6310	1.24%
Okawa (2013)	20	1	0.05	10.5	10.5	2.100	2.1243	1.16%
Kuhlmann-Gunther (2009) S355J2	12	1	0.05	9.00	9.5	1.909	1.9454	1.90%
Kuhlmann-Gunther (2009) S690QL	12	1	0.05	9.00	8.18	1.909	1.9176	0.45%
Kuhlmann (2006)	12	1	0.05	8.3	9.88	1.773	1.7939	1.18%

Table 4.33: Summary of ϵ SM results of the all models

The all experimental data are collected inside the PSM design curve proposed by Meneghetti, Camapgnolo, Yildirim and Belluzzo [33] for HFMI-treated joints. The curves are divided in based on the stress Ratio R and the steel grade range:

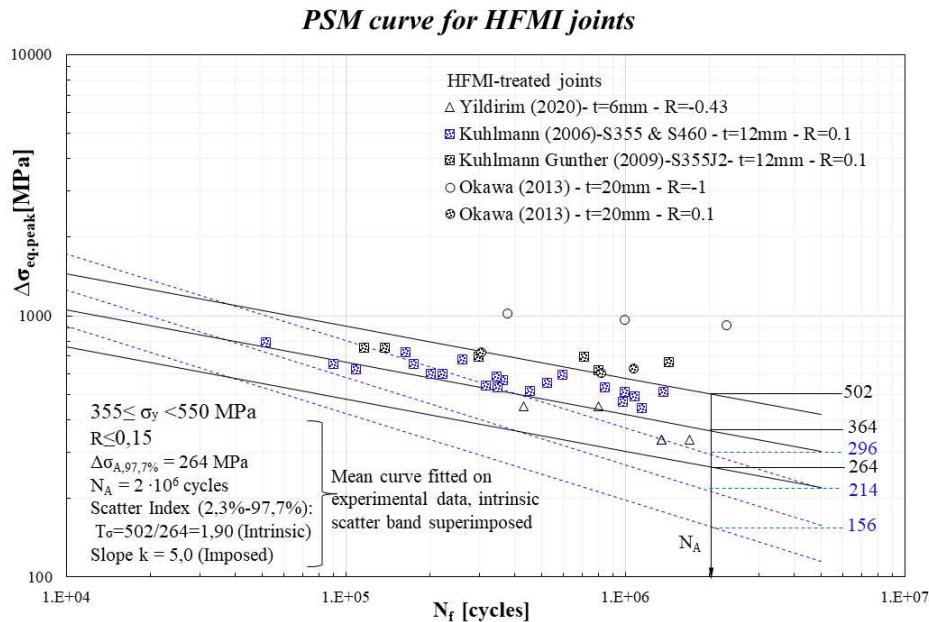


Figure 4.104: Experimental data inside the PSM design curve for $355 \leq f_y < 550\text{MPa}$ and $R \leq 0.15$.

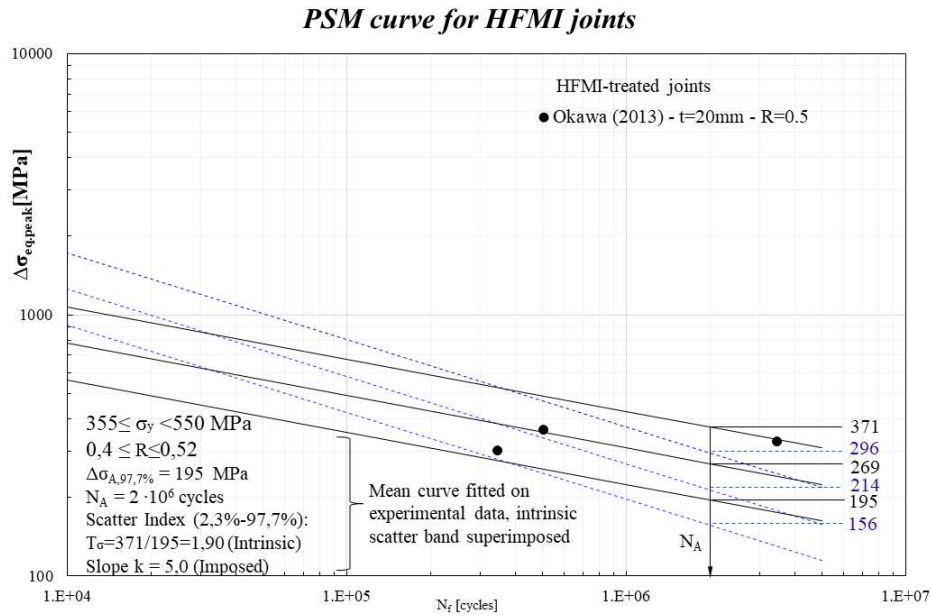


Figure 4.105: Experimental data inside the PSM design curve for $355 \leq f_y < 550$ MPa and $0.4 \leq R \leq 0.52$.

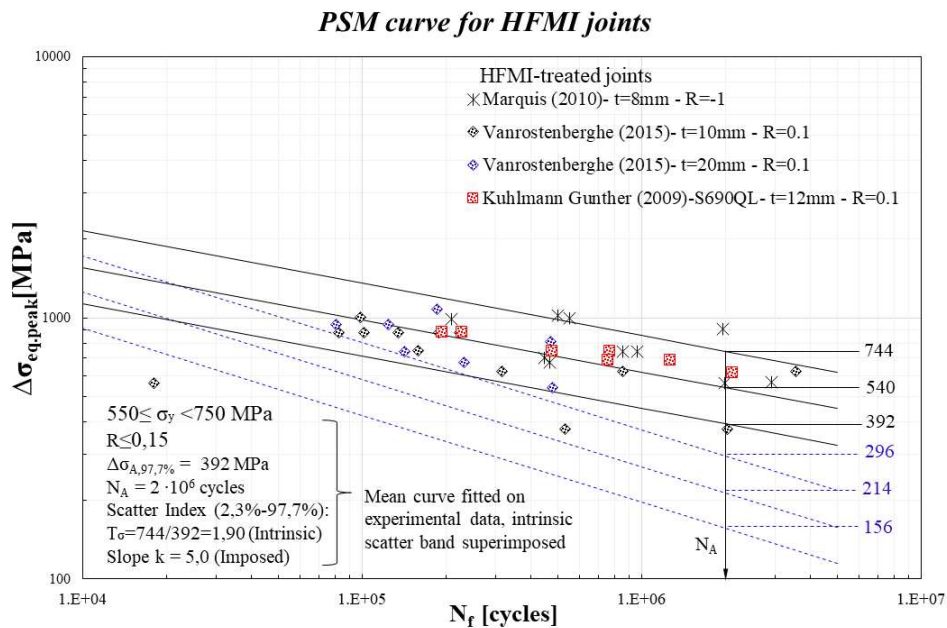


Figure 4.106: Experimental data inside the PSM design curve for $550 \leq f_y < 750$ MPa and $R \leq 0.15$.

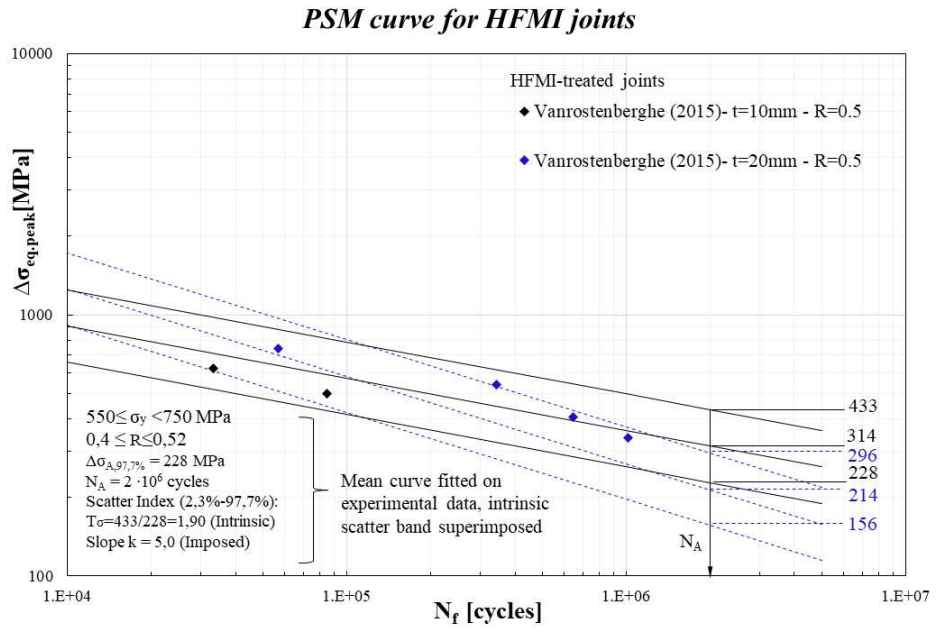


Figure 4.107: Experimental data inside the PSM design curve for $550 \leq f_y < 750$ MPa and $0.4 \leq R \leq 0.52$.

Chapter 5

Assessment of misalignment effect of cruciform joints in HFMI condition

The objective of this chapter is to perform an assessment of the misalignment effect on several cruciform joints in HFMI condition in terms of Effective Notch Stress (ENS), Structural Hot-Spot stress and Equivalent Peak Stress. This chapter aims to detect a k_{mis} factor in function of the angular misalignment α , the axial misalignment e and the thickness t of the joints. This factor considers the misalignment effect on the fatigue life of the welded joints.

The Equivalent Peak Stress for the HFMI joints is calculated through the SED approach, the same method used in the *Chapter 4*.

The assessment are performed with the application of local approaches above-mentioned through the use of finite element software Ansys®Mechanical APDL and MatLab with the license of the University of Padua. For the modelling and the study of the 2D cruciform joints with the PSM approach, Hot-Spot stress method and ENS approach, the four-node element PLANE 182 is adopted with *Simple Enhanced Strain* as Key Options 1 and *Plane Strain* as Key Options 3. Furthermore, the ENS method is applied also with the use of the eight-node quadratic element PLANE 183, with *Quadrilateral* as Key Options 1, *Plane Strain* as Key Options 3 and *Pure Displacement* as Key Options 6.

The all specimens have been modelled inside MatLab code, where a *.txt* file with the APDL commands has been created and after it has been imported inside Ansys®APDL.

Before the description of the procedure for the detection of k_{mis} factor, the misalignment effect is explained and described.

5.1 Definition of angular and linear misalignment

All structures which will be subjected to stress fluctuations during them employment, must be designed against the possibility of fatigue failure. Most of today's steel structures are characterised by the presence of welded connections, which will involve ensuring that each welded joints will possess an adequate fatigue strength to avoid failure.

The fatigue strength of some welded joints, can be reduced by the presence of welding defects, such as slag inclusions, gas pores, undercuts or misalignment. The misalignment in welded components is a results of the thermal-input during welding and also its mechanical restraints. In many cases the misalignment effect can not be completely avoided because they have a influence on the fatigue life of the welded joint.

The main cause for the reduction in fatigue strength of misaligned welded joints is thought to be the introduction of additional tensile stress due to the presence of a secondary bending. These effect also increase the degree of stress and strain concentration, which deteriorates the fatigue properties of the welded joints.

There are two different types of misalignment: the axial misalignment, called in this thesis e , and the angular misalignment, called α , as illustrated in the following figures:

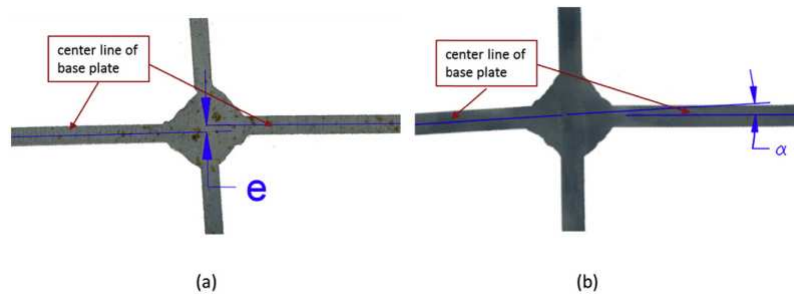


Figure 5.1: Definition of two types of joint misalignment in fillet welded connection: (a)axial misalignment; (b) angular misalignment [53]

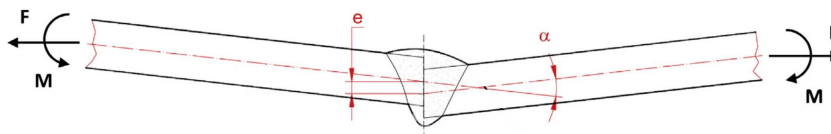


Figure 5.2: Definition of two types of joint misalignment in butt welded connection [54].

Thus, the fatigue of welded connection can be significantly influenced by joint misalignments which introduce a secondary bending at the presence of axial tension.

5.2 Procedure for the detection of misalignment effect

5.2.1 Definition of sample's geometry

The samples analysed are cruciform joints that are made of AH36 steel grades having 6 mm of thickness, which are provided by SSAB in Finland. This joints have been studied by Yildirim under VAL (Variable Amplitude Loading).

The mechanical properties and chemical composition of the AH36 are reported in the following tables:

Material model	Yield strength f_y [MPa]	Ultimate strength f_U [MPa]	Elongation [%]	Young modulus [MPa]	Poisson's ratio ν
AH36	423	546	0	206000	0.3

Table 5.1: Information about mechanical properties.

Material	C	Si	Mn	P	S	Al	Nb	V	Ti	Cu	Cr	Ni	Mo	Ca
AH36	0.14	0.39	1.43	0.008	0.007	0.034	0.013	0.008	0.04	0.02	0.08	0.06	0.007	0.0

Table 5.2: Information about chemical composition.

Geometry measurements are carried out with an ATOS Scanbox from GmbH having an optical measuring system with an accuracy of 0.02mm. From this measurement, 13 clouds of points are obtained, one for each samples. Indeed, the model of the joints is created from the relative cloud of points and for each model, the principal geometrical dimensions are obtained. The ideal model without misalignment and the dimensions that are obtained from the model, are displayed on the following figure:

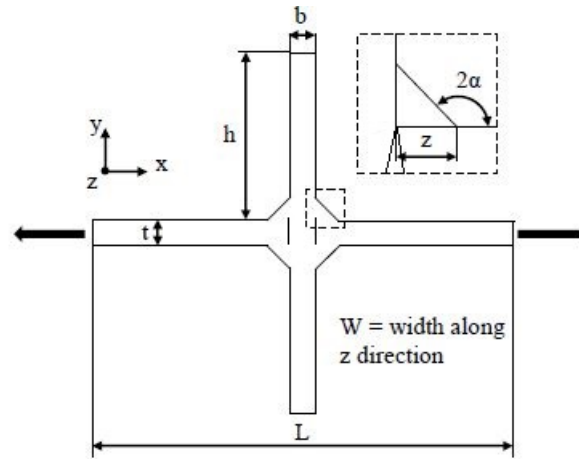


Figure 5.3: Definition of the principal dimension of the samples.

To obtain the values of the principal geometrical dimensions, the *.txt* file with the coordinates of the points is read from MatLab and subsequently, a sampling is applied to reduce the number of points. The sampling parameter n is chosen equal to 10, meaning that every 10 points of the cloud, the tenth is taken and used to build the model. This value of the sampling parameter is obtained thanks to an analysis of the sensitivity. Indeed, if the sampling parameter changes, the maximum principal stress at the weld toe will be roughly constant, as the following graph shows:

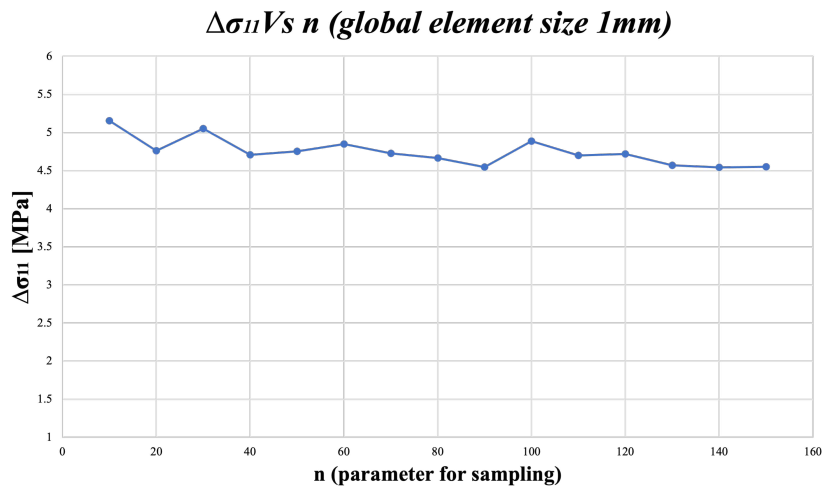


Figure 5.4: Graph to understand the influence of sampling parameter.

The MatLab code used is reported in the Appendix E.1. Furthermore, the specimen must be extended to obtain the real length of the sample (600 mm). Indeed, the total length of the cloud of points is characterised by a length equal to 300 mm. This operation is done inside MatLab and the code is reported in the Appendix E.1.

The dimension of each samples are reported in the following table with the name of the *.txt* file:

Name of .txt file	L [mm]	t [mm]	b [mm]	z [mm]	h [mm]	2 α [°]
355-WH-2	600	6	6	6	33	135
355-WH-3	600	6	6	6.8	32	135
355-WH-4	600	6	6	5.8	33	135
355-WH-5	600	6	6	6	34	135
355-WH-8	600	6	6	6.8	33	135
355-WH-11	600	6	6	6.41	33	135
355-WH-14	600	6	6	6.5	33	135
355-WH-16	600	6	6	6.45	33	135
355-WH-17	600	6	6	6.45	33	135
355-WH-18	600	6	6	7	32.6	135
355-WH-20	600	6	6	6.2	34	135
355-WH-21	600	6	6	6.2	34	135
355-WH-22	600	6	6	7	33	135

Table 5.3: Dimension of the samples.

After the detection of the geometrical dimension of the samples, the angular misalignment is obtained from the calculation of the angular coefficient of the longer arm of the welded joints, as Figure 5.5 shows.

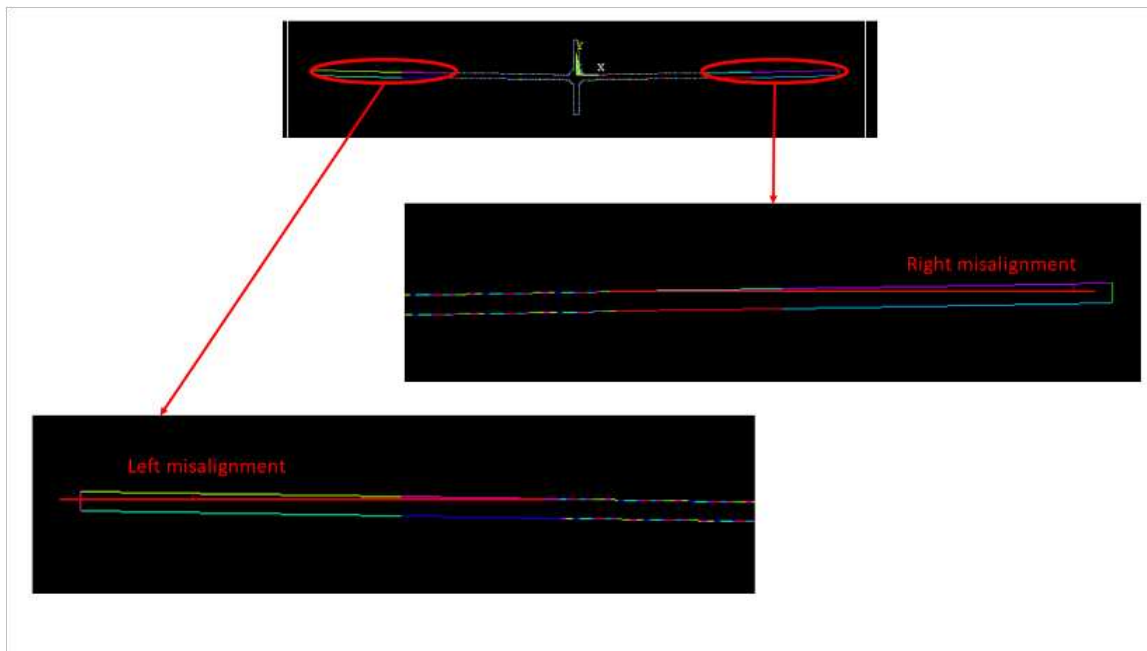


Figure 5.5: Definition of the angular misalignment.

Thus, the angular misalignment is obtained from the following equation:

$$\alpha = \tan^{-1} m \quad (5.1)$$

where:

- α is the angular misalignment;
- m is the angular coefficient of the longer arm, obtained from MatLab code in Appendix E.1.

The results of the angular misalignment are reported in the following tables:

Name of .txt file	Right misalignment α_R [°]	Left misalignment α_L [°]
355-WH-2	1.16	1.48
355-WH-3	1.03	1.42
355-WH-4	0.91	1.32
355-WH-5	0.87	1.27
355-WH-8	0.64	1.25
355-WH-11	0.76	1.09
355-WH-14	1.03	1.51
355-WH-16	0.78	1.29
355-WH-17	0.80	1.23
355-WH-18	0.86	1.24
355-WH-20	0.86	1.07
355-WH-21	0.96	1.01
355-WH-22	1.01	0.94

Table 5.4: Value of the right and left angular misalignment.

The samples are tested in VAL (Variable Amplitude Loading) condition and the experimental results are defined in the following tables:

Name of .txt file	σ_{max} [MPa]	σ_{min} [MPa]	$\Delta\sigma$ [MPa]	N_f [cycles]
355-WH-2	258.33	-116.67	375.00	2 799 750
355-WH-3	258.33	-116.67	375.00	3 387 000
355-WH-5	233.33	-100.00	333.33	3 410 280
355-WH-8	200.00	-83.33	283.33	8 750 324
355-WH-14	175.00	-75.00	250.00	6 673 500
355-WH-16	175.00	-75.00	250.00	7 085 250
355-WH-17	200.00	-83.33	283.33	4 420 500
355-WH-18	233.33	-100.00	333.33	3 607 500
355-WH-20	233.33	-100.00	333.33	3 261 000
355-WH-21	200.00	-83.33	283.33	4 446 750
355-WH-22	258.33	-116.67	375.00	2 341 500

Table 5.5: Experimental data of the samples with angular misalignment.

5.2.2 Preliminary analysis of the samples

The samples are initially subjected to a preliminary analysis. First of all, thanks to the MatLab code (see Appendix E.1), the model of the welded joint is created inside Ansys®APDL.

The modelling procedure in Ansys®APDL is briefly described:

- Due to the presence of angular misalignment, the symmetries are not present, so the whole model is created;
- The boundary conditions are taken from the reference [50]. Thus, the constraint are:
 1. $u_x = 0$ for the Line 168 (Figure 5.6);
 2. $u_y = 0$ for the Line 161 and 167 (Figure 5.6);
 3. The specimens is subjected to a pressure $p = -\Delta\sigma_{nom} = 1MPa$ on the Line 169 (Figure 5.7)
- All APDL commands are defined inside the MatLab code, which creates a .txt file that it is imported inside Ansys.

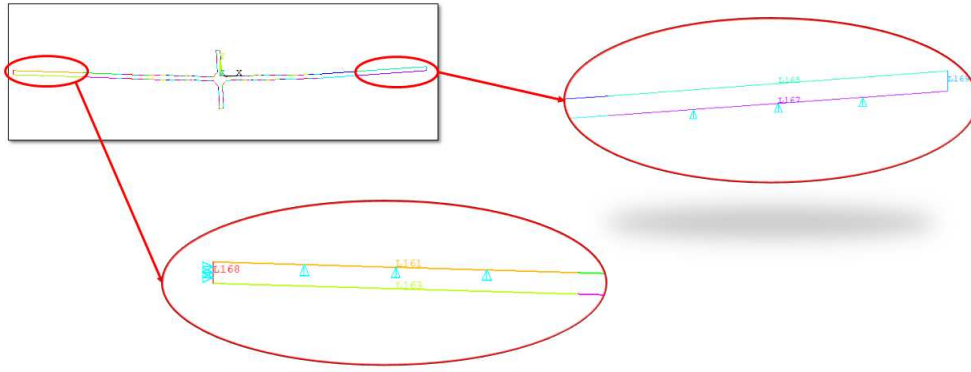


Figure 5.6: Boundary condition of the model inside Ansys®APDL.

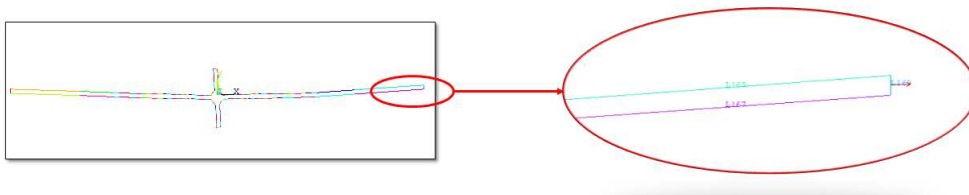


Figure 5.7: Boundary condition of the model inside Ansys®APDL.

In the following figure, there are the all boundary conditions applied:

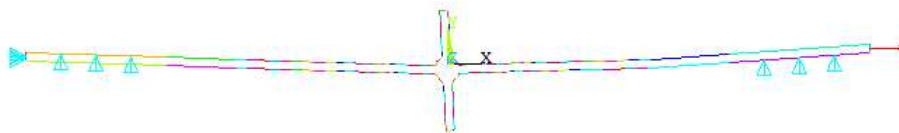


Figure 5.8: Boundary condition of the model inside Ansys®APDL. The red arrow represents the external pressure.

During this preliminary analysis, each model is meshed with a global element size equal to 0.5 mm with the following commands:

Preprocessr→*Meshing*→*Size Cntrl*s→*Manual Size*→*Global*→*Size*→0.5

Meshing→*Mesh*→*Area*→*Free*

The results is displayed on the following figure:

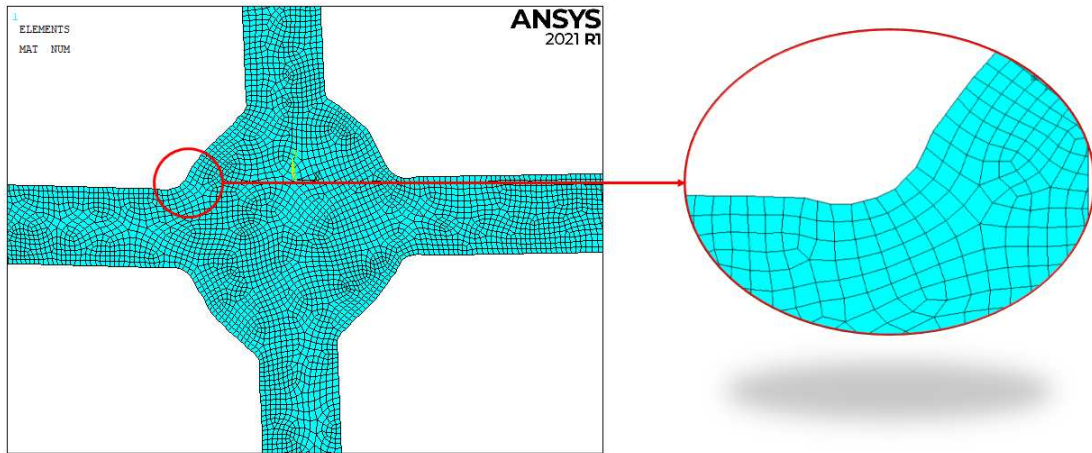


Figure 5.9: Mesh of the model with a global element size equal to 0.5 mm.

Once the model is properly meshed, loaded and constraint, the system can be solved:

Solution → *Solve* → *Current LS*

The results of the first principal stress can be observed in the *Figure 5.10*, for an external applied pressure equal to 1 MPa:

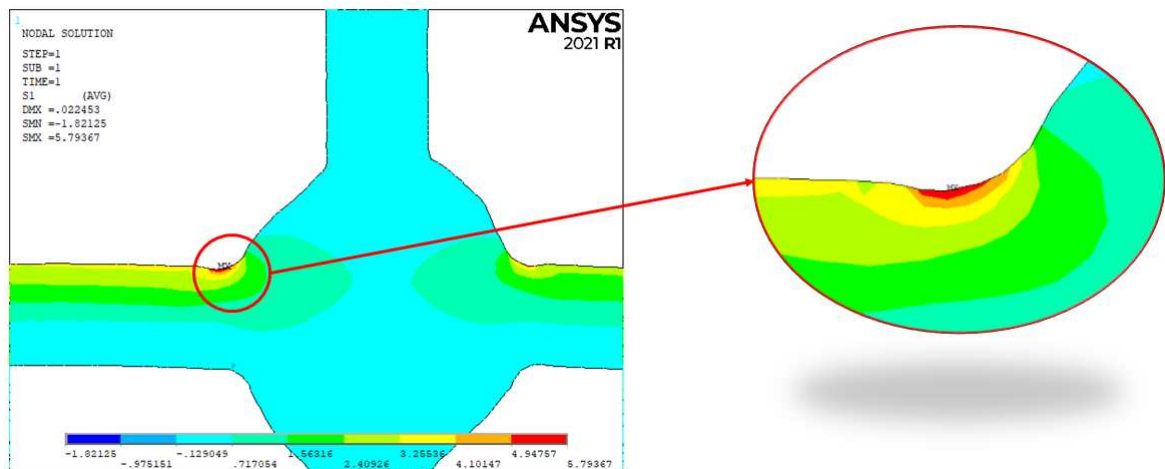


Figure 5.10: Plot of the first principal stress.

The results of the preliminary analysis for each model are reported in the following table:

Name of .txt file	$\Delta\sigma_{11,max,weldtoe}$ [MPa]	Right misalignment α_R [°]	Left misalignment α_L [°]
355-WH-2	5.7937	1.16	1.48
355-WH-3	5.7993	1.03	1.42
355-WH-4	5.8974	0.91	1.32
355-WH-5	4.5343	0.87	1.27
355-WH-8	4.92	0.64	1.25
355-WH-11	4.8354	0.76	1.09
355-WH-14	5.6188	1.03	1.51
355-WH-16	5.4915	0.78	1.29
355-WH-17	5.0055	0.80	1.23
355-WH-18	5.0221	0.86	1.24
355-WH-20	4.6786	0.86	1.07
355-WH-21	4.5449	0.96	1.01
355-WH-22	4.4553	1.01	0.94

Table 5.6: Results of preliminary analysis.

5.2.3 Ideal model and application of local approaches

The next step for the detection of the misalignment effect is to create a ideal model. Indeed, for each points cloud, an ideal model is built without the angular misalignment and with a sharp V-notch at the weld toe. Furthermore, a ideal model without misalignment but with the groove due to the HFMI treatment is created and the PSM approach combine with the SED is applied on it.

One example of the ideal model with a sharp V-notch is represented in the *Figure5.11*. Thanks to the lack of angular misalignment, the cruciform joint is characterised by a double symmetry; for this reason only 1/4 of the joint is created:



Figure 5.11: Geometry of the ideal model inside Ansys®APDL.

The modelling procedure in Ansys®APDL is briefly described:

- The ideal model is subjected to an axial load on the main plate as a constant pressure equal to $p = -\Delta\sigma_{nom} = 1MPa$, on the Line L2 as *Figure 5.12* shows;
- Symmetry boundary condition are applied on the lines L1 and L7 (*Figure 5.12*);



Figure 5.12: Boundary condition of the ideal model inside Ansys®APDL.

Subsequently, each ideal model is analysed and the Peak Stress Method (PSM), Effective Notch Stress (ENS) approach and Structural Hot-Spot Stress (SHSS) approach are applied. In the next paragraphs, the

application of local approaches will be described and each procedure refers to the ideal model that comes from the points cloud called 355-WH-2, but it can be similarly extended for the other joints. All procedures are implemented in MatLab to reduce the working time and to parameterize the procedure. The idea of MatLab code is to create a .txt file with the APDL commands, allowing the creation of the model, mesh and to extract the results from the model. All MatLab codes are reported in the Appendix E.2.

Effective Notch Stress (ENS) approach

The fatigue assessment for this model is performed by the application of the Effective Notch Stress approach. Two different analysis are done:

1. The first one is characterised by the using of 4-node linear element PLANE 182 with *Simple Enhanced Strain* as Key Option 1 and *Plane Strain* as Key Option 3;

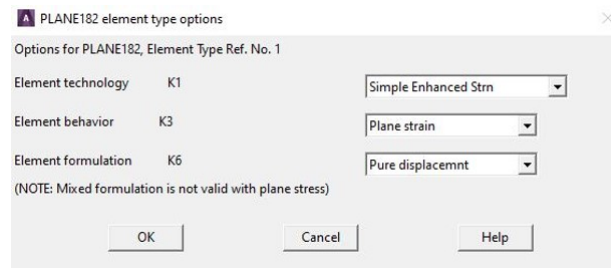


Figure 5.13: Options for the element PLANE 182.

2. The second one is characterised by the using of 8-node quadratic element PLANE 183 with *Quadrilateral* as Key Option 1, *Plane Strain* as Key Option 2 and *Pure Displacement* as Key Option 6.

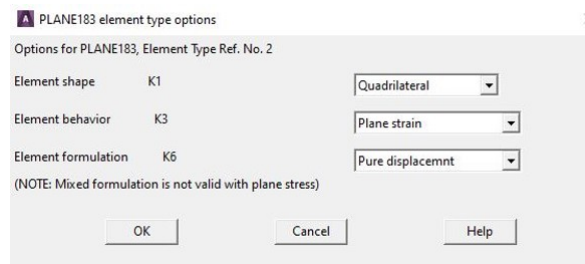


Figure 5.14: Options for the element PLANE 183.

To apply this approach, the *IIW Recommendations for Fatigue Assessment by Notch Stress Analysis for welded Structures* [2] is followed. The guideline defines that the rounding of the roots of non-penetrating fillet welds can be of three different types, as *Figure 5.15* shows.

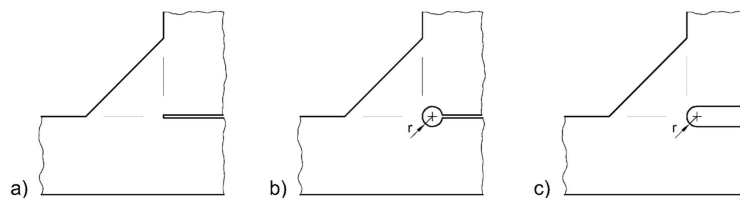


Figure 5.15: Rounding of weld root of non penetrating fillet weld by a keyhole and an U-shaped notch [2].

In this case the rounding of the weld root displayed on the *Figure 5.15c* is chosen. The effective radius, which is implemented to finite element model, is defined as follows:

$$\rho_f = \rho + 1\text{mm} \quad (5.2)$$

where:

- ρ_f is the effective radius;
- ρ is the actual radius of weld toe.

For the worst case and practical applications, the actual radius ρ is assumed equal to zero. Thus, the ENS approach for fatigue assessment is reduced to $\rho_f = 1\text{mm}$ at weld toe or root.

The IIW recommendations gives some rules for the global element size and mesh pattern as *Figure 5.16* shows. The rule for the size are expressed in *Table 5.7* and have to be observed in the curved part and straight part of the notch surfaces in normal and tangential direction.

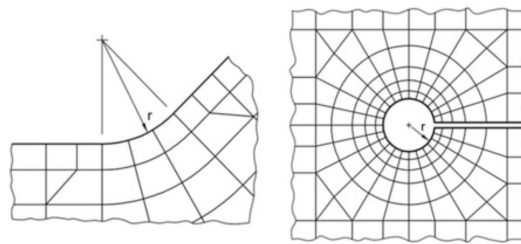


Figure 5.16: Recommended meshing at weld toes and roots [2].

Element type	Relative size	Absolute size [mm]	No. of elements in 45° arc	No. of elements in 360° arc
Quadratic with mid-side nodes	$\leq r/4$	≤ 0.25	≥ 3	≥ 24
Linear	$\leq r/6$	≤ 0.15	≥ 5	≥ 40

Table 5.7: Recommended size of elements on surface [1].

The ideal model for the application of ENS approach is displayed on the following figure:

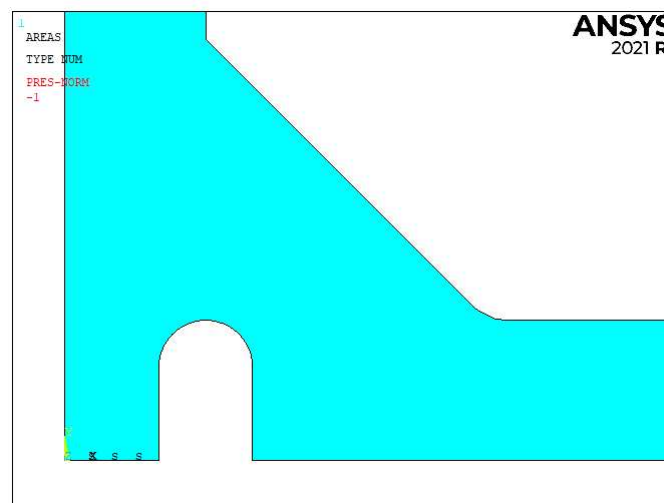


Figure 5.17: Ideal model for the application of ENS approach.

For the analysis with the element PLANE 182, the global element size is equal to 0.1 mm, according to the IIW Recommendations [2]. To obtain the correct number of elements along the roots and the weld toe, two refinements are applied with depth of two elements. The mesh of the model is displayed on the following figure:

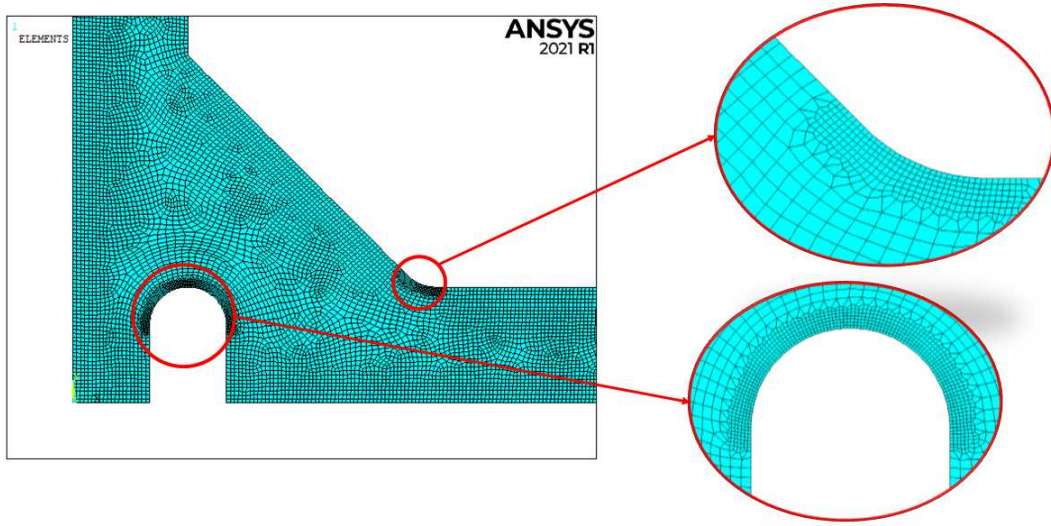


Figure 5.18: Mesh of ideal model with element PLANE 182.

Once the model is properly meshed, loaded and constraint, the system can be solved:

Solution → *Solve* → *Current LS*

The results of the first principal stress can be observed in the *Figure 5.19*, for an external applied pressure equal to 1 MPa:

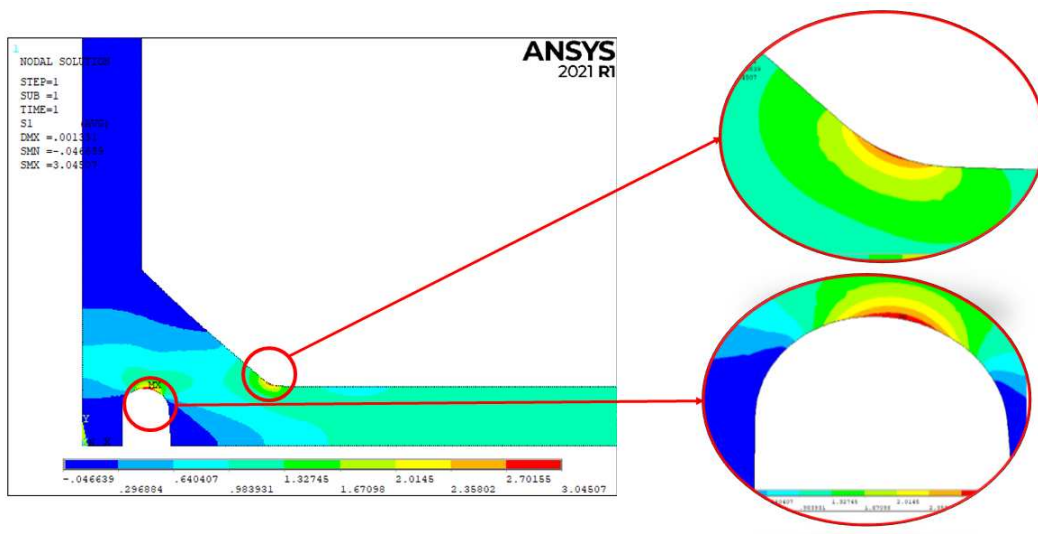


Figure 5.19: Plot of the first principal stress of ideal model with element PLANE 182.

The maximum first principal stress at the weld toe and root are:

$$\Delta\sigma_{11,Toe,max} = 2.7779MPa \quad (5.3)$$

$$\Delta\sigma_{11,Root,max} = 3.0455MPa \quad (5.4)$$

For the analysis with the element PLANE 183, the global element size is equal to 0.2 mm, according to the IIW Recommendations [2]. To obtain the correct number of elements along the roots and the weld toe, two refinements are applied with depth of two elements. The mesh of the model is displayed on the following figure:

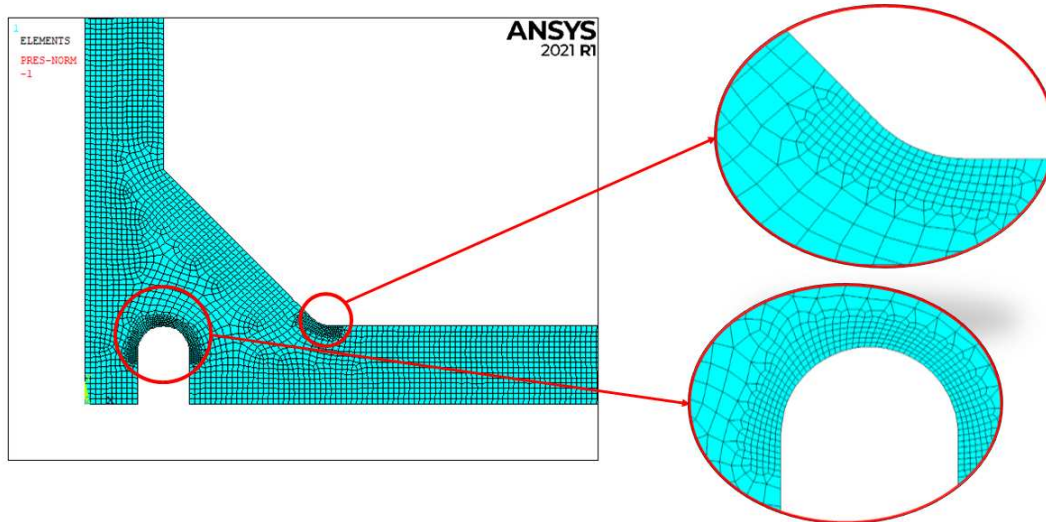


Figure 5.20: Mesh of ideal model with element PLANE 183.

Once the model is properly meshed, loaded and constraint, the system can be solved:

Solution→*Solve*→*Current LS*

The results of the first principal stress can be observed in the *Figure 5.21*, for an external applied pressure equal to 1 MPa:

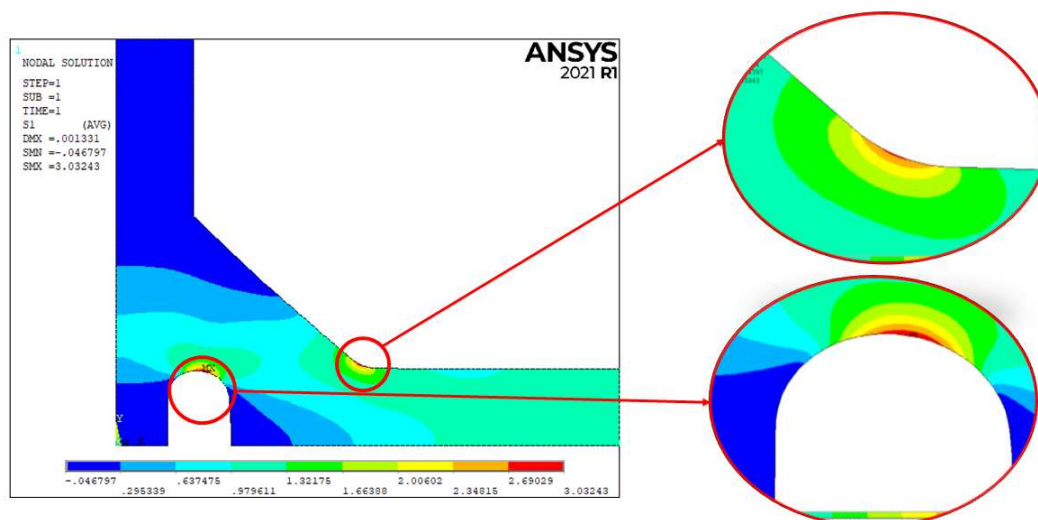


Figure 5.21: Plot of the first principal stress of ideal model with element PLANE 183.

The maximum first principal stress at the weld toe and root are:

$$\Delta\sigma_{11,Toe,max} = 2.7615MPa \tag{5.5}$$

$$\Delta\sigma_{11,Root,max} = 3.0324MPa \tag{5.6}$$

The results of the all ideal model are reported in the Appendix F.2.

Structural Hot-Spot Stress (SHSS) approach

The fatigue assessment for this model is performed by the application of SHSS approach, following the IIW recommendation [1] to obtain the hot-spot stress. The hot-spot stress value is detected with the employment of fine mesh, as *Figure 1.4* shows, and the hot-spot stress is detected with the formulas for hot-spot type *a* and also type *b*.

The model is divided in a series of areas to allow the application of *Mapped-mesh* algorithm; indeed each areas must be characterised by a number of side between 3 and 4 to obtain a *Mapped-mesh*. The four-node linear element PLANE 182 is chosen in Ansys®APDL with *Simple Enhanced Strain* as Key Option 1 and *Plane Strain* as Key Option 3.

The all informations about the mesh is reported in the following table:

Element type	Mesh algorithm	Main plate thickness <i>t</i>	Max element size	Adopted element size
Plane 182 KeyOpt:Simple Enhanced Strain + Plane Strain	Mapped	6 mm	$0.4 \cdot t = 0.4 \cdot 6 = 2.4mm$	0.4 mm

Table 5.8: Requirements for SHSS mesh.

The hot-spot stress is extrapolated at two reference points placed at $0.4t$ and $1.0t$ distance from the weld tip, so in this case at 2.4 mm and 6 mm from weld toe. These reference points are used for the hot-spot type *a*. For type *b*, the structural hot-spot stress is extrapolated at three reference points located at 4mm, 8mm and 12mm distance from the weld toe.

For the type of extrapolated stress, the graph in *Figure 5.22* shows that, for an external applied pressure $\Delta\sigma_{nom} = 1MPa$, the $\Delta\sigma_{xx}$ and the first principal stress $\Delta\sigma_{11}$ are coincident. For this reason the choice is indifferent.

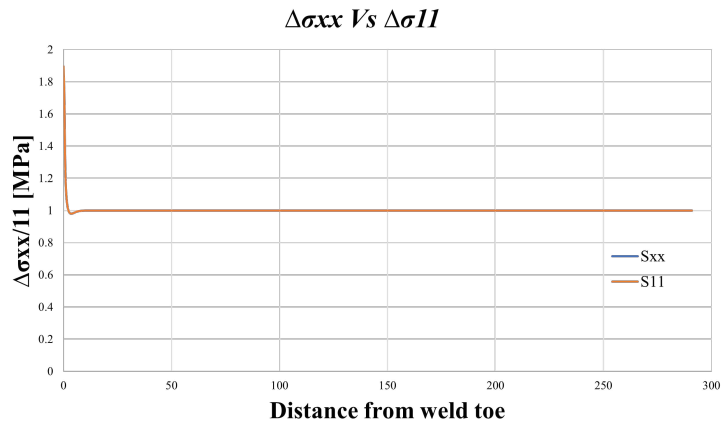


Figure 5.22: $\Delta\sigma_{xx}$ and $\Delta\sigma_{yy}$ plotted in function of the distance from weld toe tip.

The mesh of the model is reported in the following figures:

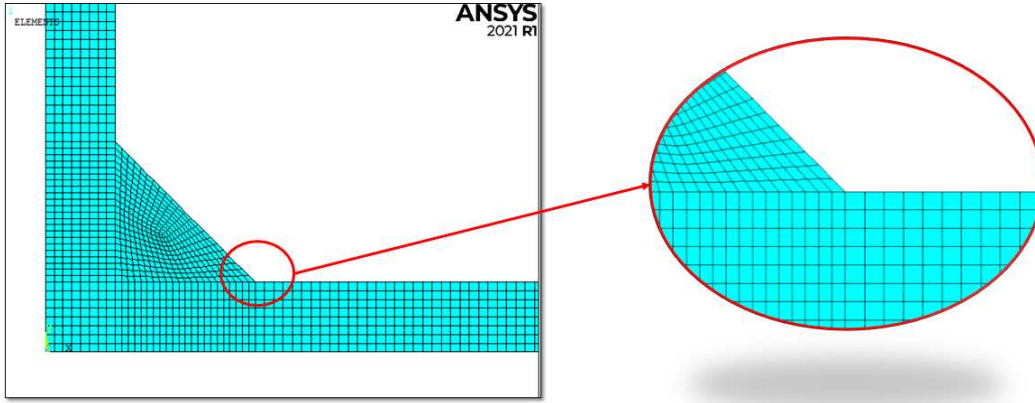


Figure 5.23: Mapped mesh for SHSS approach.

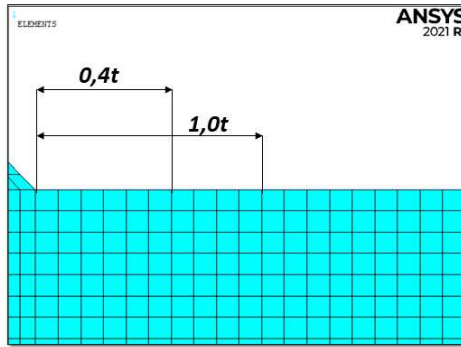


Figure 5.24: Mapped mesh for SHSS approach and reference points.

For an external applied pressure $\Delta\sigma_{nom} = 1MPa$, the results of the tension at the reference points for hot spot type *a* are:

$$\Delta\sigma_{xx,0.4t} = 0.99384MPa \quad (5.7)$$

$$\Delta\sigma_{xx,1.0t} = 0.99285MPa \quad (5.8)$$

$$\Delta\sigma_{11,0.4t} = 0.99388MPa \quad (5.9)$$

$$\Delta\sigma_{11,1.0t} = 0.99285MPa \quad (5.10)$$

The structural hot-spot stress type *a* is detected with the equation (1.2):

$$\Delta SHSS_{LSE,xx} = 1,67 \cdot \sigma_{xx,0.4t} - 0.67 \cdot \sigma_{xx,1.0t} = 1.67 \cdot 0.99384 - 0.67 \cdot 0.99285 = 0.99450MPa \quad (5.11)$$

$$\Delta SHSS_{LSE,11} = 1,67 \cdot \sigma_{11,0.4t} - 0.67 \cdot \sigma_{11,1.0t} = 1.67 \cdot 0.99388 - 0.67 \cdot 0.99285 = 1.03056MPa \quad (5.12)$$

For an external applied pressure $\Delta\sigma_{nom} = 1MPa$, the results of the tension at the reference points for hot spot type *b* are:

$$\Delta\sigma_{xx,4mm} = 0.98176MPa \quad (5.13)$$

$$\Delta\sigma_{xx,8mm} = 0.99855MPa \quad (5.14)$$

$$\Delta\sigma_{xx,12mm} = 1.00006MPa \quad (5.15)$$

$$\Delta\sigma_{11,4mm} = 0.98176MPa \quad (5.16)$$

$$\Delta\sigma_{11,8mm} = 0.99855MPa \quad (5.17)$$

$$\Delta\sigma_{11,12mm} = 1.00006MPa \quad (5.18)$$

The structural hot-spot stress type b is detected with the following equation:

$$\Delta SHSS_{LSE} = 3 \cdot \Delta \sigma_{xx,4mm} - 3 \cdot \Delta \sigma_{xx,8mm} + \Delta \sigma_{xx,12mm} \quad (5.19)$$

$$\Delta SHSS_{LSE,xx} = 3 \cdot \Delta \sigma_{xx,4mm} - 3 \cdot \Delta \sigma_{xx,8mm} + \Delta \sigma_{xx,12mm} = 3 \cdot 0.98176 - 3 \cdot 0.99855 + 1.00006 = 0.9497 \quad (5.20)$$

$$\Delta SHSS_{LSE,11} = 3 \cdot \Delta \sigma_{11,4mm} - 3 \cdot \Delta \sigma_{11,8mm} + \Delta \sigma_{11,12mm} = 3 \cdot 0.98176 - 3 \cdot 0.99855 + 1.00006 = 0.9497 \quad (5.21)$$

The results of the all ideal model are reported in the Appendix F.2.

Peak Stress Method (PSM) for ideal model with sharp V-notch

The fatigue assessment for this model is performed by the application of the PSM approach for 2D structure with the adoption of four-node linear elements. The element PLANE 182 is chosen from the Ansys®APDL library with *Simple Enhanced Strain* as Key Option 1 and *Plane Strain* as Key Option 3. The model is characterised by a root with an initial opening length equal to 0.1 mm.

The weld toe is subjected to pure mode I because it is characterised by a V-notch opening angle 2α equal to 135° . On the other hand, the root is characterised by a V-notch opening angle equal to 0° , so it is subjected to mode I and also mode II.

Under mode I and mode II, the PSM requirements are defined in the following table:

Element type	Mesh algorithm	$(a/d)_{min}$	2α	Mode I	
				Mesh Pattern $2\alpha < 90^\circ$	Mesh Pattern $2\alpha > 90^\circ$
Plane 182 KeyOpt:Simple Enhanced Strain + Plane Strain	Free	3	$0^\circ < 2\alpha < 135^\circ$	Four adjacent elements share the same node	Two adjacent elements share the same node
Mode II					
Plane 182 KeyOpt:Simple Enhanced Strain + Plane Strain	Free	14	$0^\circ < 2\alpha < 135^\circ$	Four adjacent elements share the same node	Four adjacent elements share the same node up to $2\alpha = 102.5^\circ$

Table 5.9: Requirements for PSM.

The mode I PSM calibration constant is equal to $K_{FE}^* = 1.38 \pm 3\%$, instead for mode II, the calibration constant is equal to $K_{FE}^{**} = 3.38 \pm 3\%$.

The size of the element is obtained with the following procedure:

1. From literature the ratio $(a/d)_{min}$ is determined. In this case there are 2 ratio: the first one for mode I and the second for mode II. The highest ratio is chosen;
2. The value of a is the reference dimension for selecting the maximal FE sizes d for PSM application and is defined as the half of the thickness t ;
3. Subsequently, the minimum element size is defined as follow:

$$d_{min} = \frac{a}{14} = \frac{6}{14} = 0.214mm \quad (5.22)$$

4. The chosen dimension of elements is 0.2mm.

The λ_1 , e_1 , λ_2 and e_2 values are depended on the V-notch opening angle 2α , that is 135° for the weld toe and 0° for the root:

2α [°]	λ_1 (Mode I)	e_1 (Mode I)	λ_2 (Mode II)	e_2 (Mode II)
135°	0.674	0.117	/	/
0°	0.5	0.133	0.5	0.341

Table 5.10: Value of $\lambda_1, e_1, \lambda_2$ and e_2 in function of the opening angle 2α .

The corrective stress factors for mode I and II are calculated with the equation (2.24) for the weld toe and root. The results are reported in the *Table 5.11*

2α [°]	f_{w1}	f_{w2}
135°	0.627	/
0°	0.633	2.473

Table 5.11: Values of the corrective stress factors f_{w1} and f_{w2} in function of the opening angle 2α .

Finally, the mesh can be laid on the model and the results is displayed on the *Figure 5.25*:

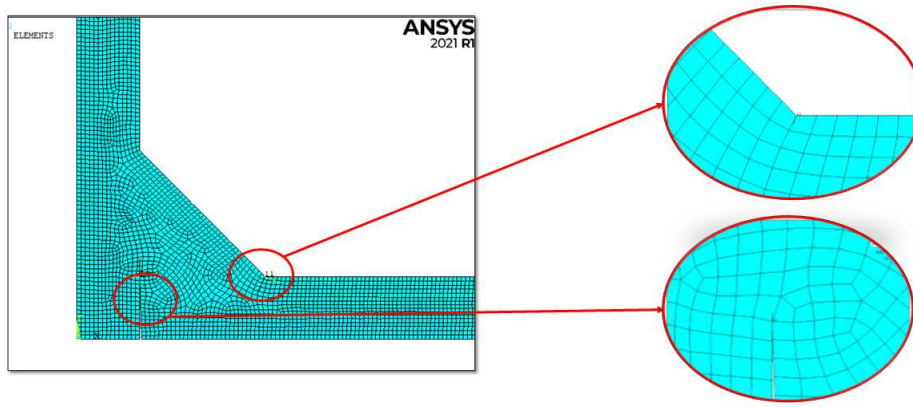


Figure 5.25: Mesh conformation with global element size $d = 0.2\text{mm}$.

After the application of load and constraint, the system can be solved:

Solution → *Solve* → *Current LS*

The results of the first principal stress is plotted in the *Figure 5.26*:

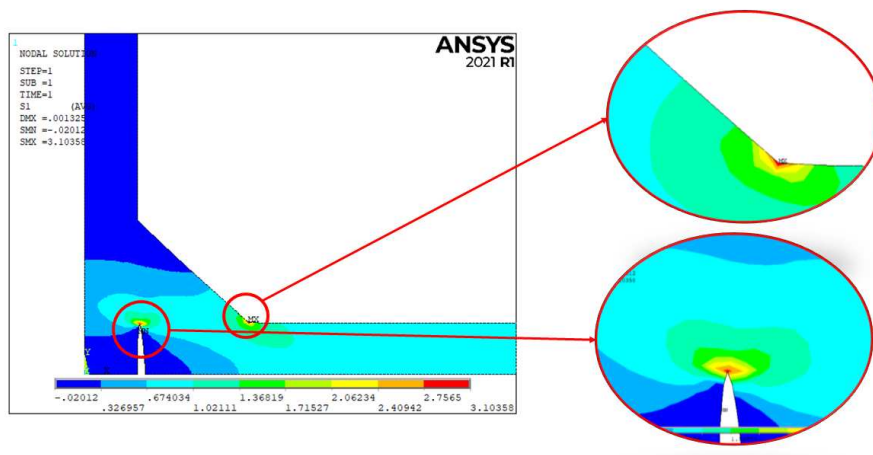


Figure 5.26: Plot of 1st principal stress for an external applied nominal stress range of 1MPa.

Two local reference systems (*Figure 5.27*) are created on the nodes that represent the weld toe and the apex of the root. The *WorkPlane* is rotated by an angle equal to 112.5° for the toe and by an angle equal to 90° for

the root. The procedure for the creation of the local reference systems is the same as described in the paragraph 3.1.2.

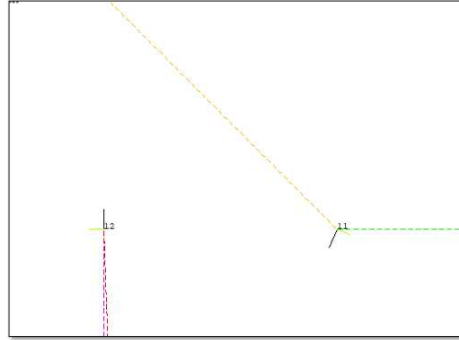


Figure 5.27: Local reference system at the weld toe and root.

Thanks to the creation of the local reference system, the tension $\Delta\sigma_{yy}$ can be extracted:

$$\Delta\sigma_{yy,weldtoe} = 3.10342MPa \quad (5.23)$$

$$\Delta\sigma_{yy,root} = 2.83454MPa \quad (5.24)$$

$$\Delta\tau_{xy,root} = 0.30412MPa \quad (5.25)$$

The equivalent peak stresses are calculated by the formula (2.23):

$$\Delta\sigma_{eq,peak,toe} = f_{w1} \cdot \sigma_{\theta\theta,\theta=0,peak} = 1.946MPa \quad (5.26)$$

$$\Delta\sigma_{eq,peak,root} = \sqrt{f_{w1}^2 \cdot \sigma_{\theta\theta,\theta=0,peak}^2 + f_{w2}^2 \cdot \tau_{r\theta,\theta=0,peak}^2} = 1.945MPa \quad (5.27)$$

The results of the all ideal model are reported in the Appendix F.2.

Peak Stress Method (PSM) for ideal model with HFMI groove

The fatigue assessment for this model is performed by the application of Peak Stress Method in combination with the SED approach with the adoption of four-node linear elements, considering only the weld toe. First of all, the dimensions of the HFMI groove are taken from the reference [47] and are reported in the following table:

depth [mm]	ρ_{HFMI} [mm]	width [mm]	2α [°]
0.3	3.31	4.48	135

Table 5.12: Dimension of HFMI groove.

The element PLANE 182 is chosen from the Ansys®APDL library with *Simple Enhanced Strain* as Key Option 1 and *Plane Strain* as Key Option 3.

The SED approach for blunt notches is based on the creation of a structural volume at the radiused weld toe, that can be rigidly rotated (*Figure 4.20*) to included the whole maximum principal stress, which is related to the highest strain energy density.

The first step is to determinate the inclination angle Φ with respect to the blunt notch bisector of the most stressed area that is indicated in red in Ansys®APDL.

To define the inclination angle, the model is meshed with a global element size equal to 0.5 mm and subsequently, two refinements with depth equal to 5 (see *Figure 5.28* for the refine options) are applied to the arc that represents the groove due to HFMI treatment (*Figure 5.29*) with the following commands:

Preprocessor→*Meshing*→*Modify Mesh*→*Refine At*→*Lines*

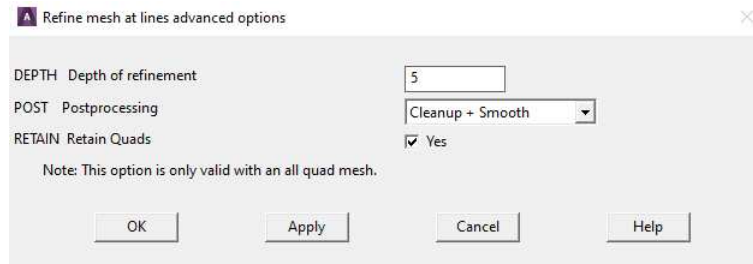


Figure 5.28: Options for the refinement.

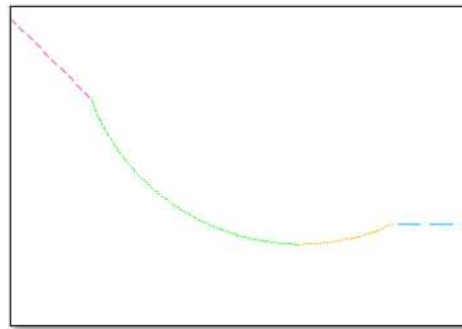


Figure 5.29: Arc that represents the HFMI groove where the refinements are applied.

The meshed model is displayed on the following figure:

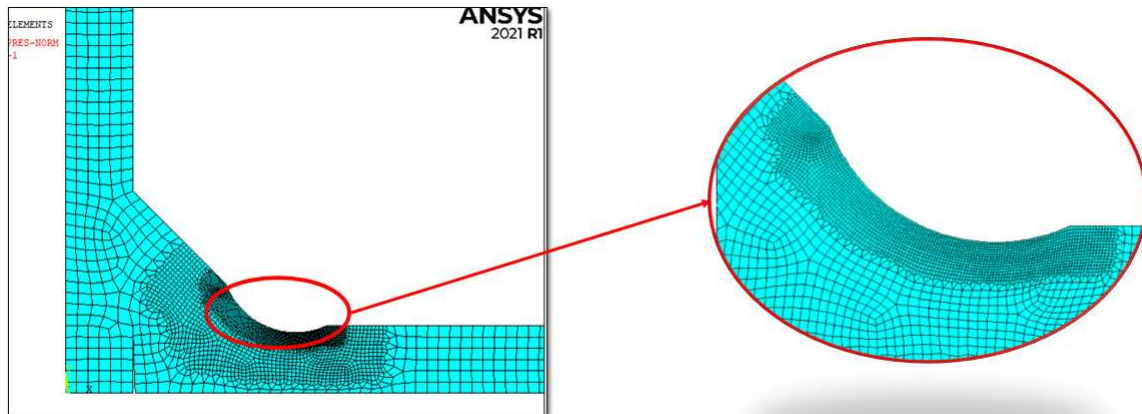


Figure 5.30: Mesh of the model to define the inclination angle.

The model is subjected to an external nominal stress $\Delta\sigma_{nom} = 1MPa$ applied on the main plate. Once the model is properly meshed, loaded and constraint, the system can be solve:

Solution→*Solve*→*Current LS*

The highest stress is not located exactly around the blunt notch bisector, so it is matter of quantifying the grades of rotation. The value of the angle is reported in the following equation and represents a clockwise rotation about the global z-axis:

$$\Phi = 2.411^\circ \tag{5.28}$$

The circular sector is created according to equations (4.5) and (4.6):

$$q = \frac{2\pi - 2\alpha}{\pi} = 2 - \frac{135}{180} = 1.25 \tag{5.29}$$

$$r_0 = \frac{q-1}{q} \cdot \rho_{HFMI} = \frac{1.25-1}{1.25} \cdot 3.31 = 0.662mm \quad (5.30)$$

$$R_0 + r_0 = 0.28 + 0.662 = 0.942mm \quad (5.31)$$

Subsequently, the control volume to calculate the averaged Strain Energy Density (SED) is created. The result is reported in the following figure:

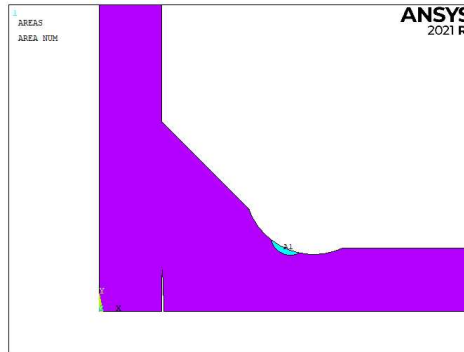


Figure 5.31: Illustration of the control Area to calculate the SED.

To create the mesh of the model, the following procedure is executed:

1. The element inside the structural volume are characterised by a *global element size* equal to 0.01mm with a *free-mesh* algorithm;

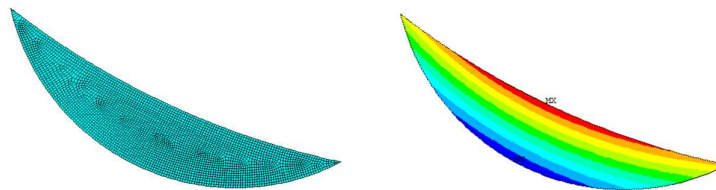


Figure 5.32: On the left, the mesh of the structural volume with global element size of 0.01. On the right, the proof that the highest stress is contained inside the volume.

2. The other volume is meshed with a *global element size* equal to 0.1 mm with a *free-mesh* algorithm.

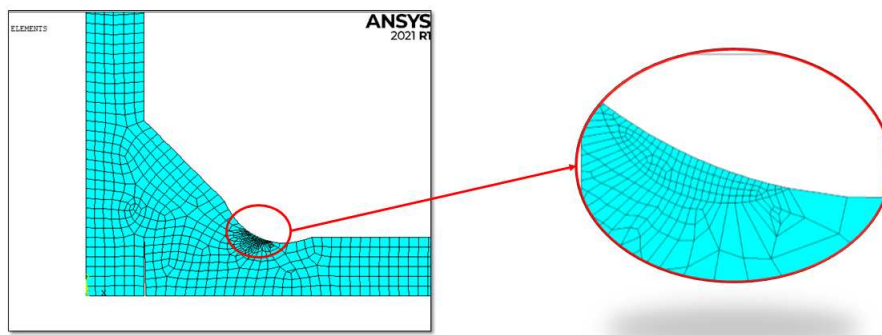


Figure 5.33: Mesh of the all structure.

Once the model is properly meshed, loaded and constraint, the system can be solved:

Solution → *Solve* → *Current LS*

The averaged Strain Energy Density is defined as the energy contained inside the structural volume. The same procedure described in the paragraph 4.2.2 is applied to detect the SED value.

The result of SED for the weld toe when the specimen is subjected to a nominal stress of 1 MPa is:

$$SENE = 1.84529 \cdot 10^{-6} MJ \quad (5.32)$$

$$VOLUME = 0.294241 mm^3 \quad (5.33)$$

$$SED = \frac{SENE}{VOLUME} = \frac{1.84529 \cdot 10^{-6}}{0.294241} = 6.2713 \cdot 10^{-6} \frac{MJ}{m^3} \quad (5.34)$$

From the SED, the equivalent peak stress is obtained with the following formula:

$$\Delta\sigma_{eq,peak} = \sqrt{\frac{2 \cdot E \cdot SED}{1 - \nu^2}} = \sqrt{\frac{2 \cdot 206000 \cdot 6.2713 \cdot 10^{-6}}{1 - 0.3^2}} = 1.685 MPa \quad (5.35)$$

Subsequently, the equivalent peak stress at the weld root is detected with the same procedure used for the ideal model with sharp V-notch. Thus, the results are:

$$\Delta\sigma_{yy,root} = 2.93004 MPa \quad (5.36)$$

$$\Delta\tau_{xy,root} = 0.331525 MPa \quad (5.37)$$

The equivalent peak stresses are calculated by the formula (2.23):

$$\Delta\sigma_{eq,peak,root} = \sqrt{f_{w1}^2 \cdot \sigma_{\theta\theta,\theta=0,peak}^2 + f_{w2}^2 \cdot \tau_{r\theta,\theta=0,peak}^2} = 2.028 MPa \quad (5.38)$$

The results of the all ideal model are reported in the Appendix F.2.

5.2.4 Ideal model with Misalignment and application of local approaches

The next step for the detection of the misalignment effect is to create a ideal model with angular misalignment, detected in the paragraph 5.2.1. With the terminology *ideal model* means that it does not come from the cloud of points.

For each ideal model defined in the paragraph 5.2.3, a new ideal model is built with the angular misalignment and with a sharp V-notch at the weld toe. Furthermore, a ideal model with misalignment but with the groove due to the HFMI treatment is created and the PSM approach combine with the SED is applied on it.

One example of the ideal model with a sharp V-notch is represented in the following figure. Due to the angular misalignment, the cruciform joint is not characterised by a double symmetry as before:

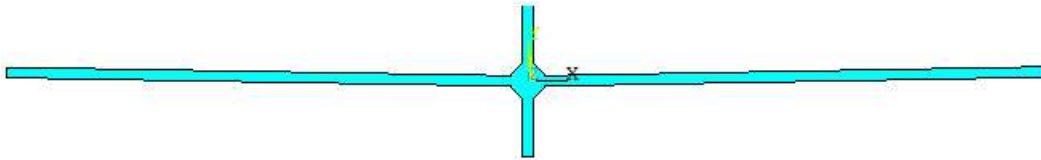


Figure 5.34: Geometry of the ideal model with misalignment inside Ansys®APDL.

The modelling procedure in Ansys®APDL is briefly described:

- The ideal model is subjected to an axial load on the main plate as a constant pressure equal to $p = -\Delta\sigma_{nom} = 1 MPa$, on the Line L4 as *Figure 5.35* shows;
- $u_x = 0$ for the Line 13 (*Figure 5.6*);
- $u_y = 0$ for the Line 14 and 5 (*Figure 5.35*);

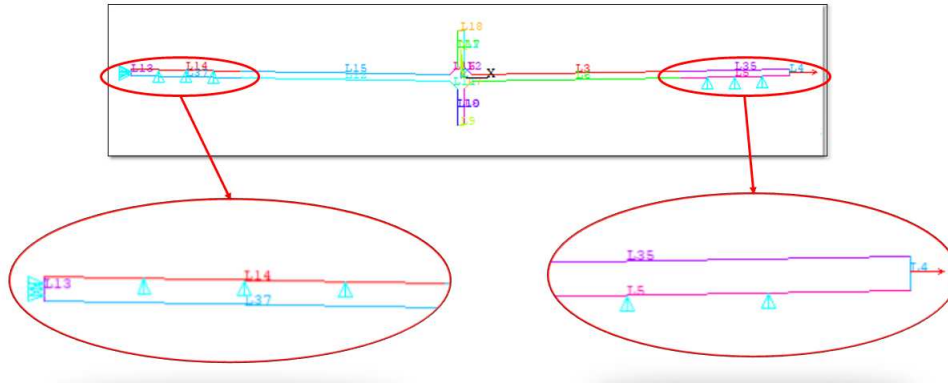


Figure 5.35: Boundary condition of the ideal model with misalignment inside Ansys®APDL.

Subsequently, each ideal model with angular misalignment is analysed and the Peak Stress Method (PSM), Effective Notch Stress (ENS) approach and Structural Hot-Spot Stress (SHSS) approach are applied. In the next paragraphs, the application of local approaches will be described and each procedure refers to the ideal model with misalignment with the dimensions that comes from the points cloud called 355-WH-2, but it can be similarly extended for the other joints. All procedures are implemented in MatLab to reduce the working time and to parameterize the procedure. The idea of MatLab code is to create a *.txt* file with the APDL commands, allowing the creation of the model, mesh and to extract the results from the model. All MatLab codes are reported in the Appendix E.3.

Effective Notch Stress (ENS) approach

The fatigue assessment for this model is performed by the application of the Effective Notch Stress approach. As before, two different analysis are done:

1. The first one is characterised by the using of 4-node linear element PLANE 182 with *Simple Enhanced Strain* as Key Option 1 and *Plane Strain* as Key Option 3;
2. The second one is characterised by the using of 8-node quadratic element PLANE 183 with *Quadrilateral* as Key Option 1, *Plane Strain* as Key Option 2 and *Pure Displacement* as Key Option 6.

To apply this approach, the *IIW Recommendations for Fatigue Assessment by Notch Stress Analysis for welded Structures* [2] is followed and the same rules of ideal model (see paragraph 5.2.3) are followed. As before, for the worst case and practical applications, the actual radius ρ is assumed equal to zero. Thus, the ENS approach for fatigue assessment is reduced to $\rho_f = 1\text{mm}$ at weld toe or root.

To define the global element size of the model, the same rules used for the ideal model, are followed in this case.

The ideal model for the application of ENS approach is displayed on the following figure:

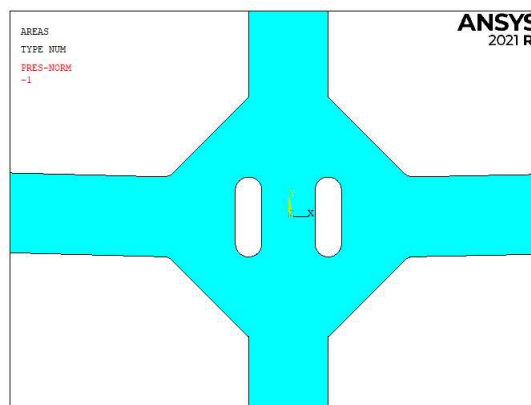


Figure 5.36: Ideal model with angular misalignment for the application of ENS approach.

For the analysis with the element PLANE 182, the global element size is equal to 0.1 mm, according to the IIW Recommendations [2]. To obtain the correct number of elements along the roots and the weld toe, two refinements are applied with depth of two elements. The mesh of the model is displayed on the following figure:

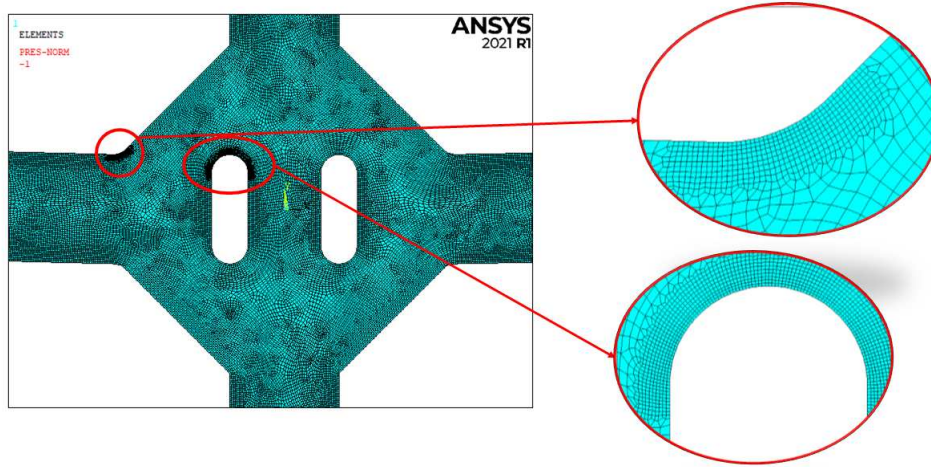


Figure 5.37: Mesh of ideal model with misalignment with element PLANE 182.

Once the model is properly meshed, loaded and constraint, the system can be solved:

Solution → *Solve* → *Current LS*

The results of the first principal stress can be observed in the Figure 5.38, for an external applied pressure equal to 1 MPa:

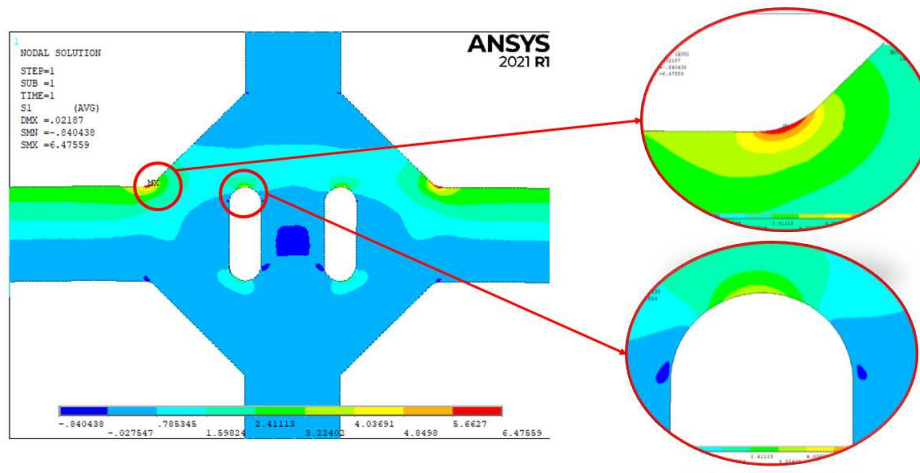


Figure 5.38: Plot of the first principal stress of ideal model with angular misalignment with element PLANE 182.

The maximum first principal stress at the weld toe and root are:

$$\Delta\sigma_{11,Toe,max} = 6.4756\text{MPa} \quad (5.39)$$

$$\Delta\sigma_{11,Root,max} = 3.9549\text{MPa} \quad (5.40)$$

For the analysis with the element PLANE 183, the global element size is equal to 0.2 mm, according to the IIW Recommendations [2]. To obtain the correct number of elements along the roots and the weld toe, two refinements are applied with depth of two elements. The mesh of the model is displayed on the following figure:

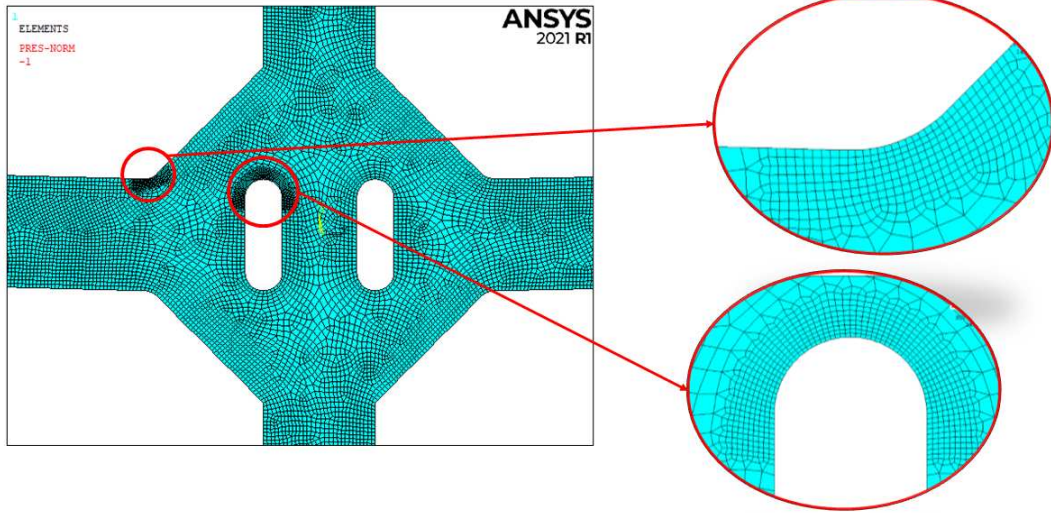


Figure 5.39: Mesh of ideal model with angular misalignment with element PLANE 183.

Once the model is properly meshed, loaded and constraint, the system can be solved:

Solution→*Solve*→*Current LS*

The results of the first principal stress can be observed in the *Figure 5.40*, for an external applied pressure equal to 1 MPa:

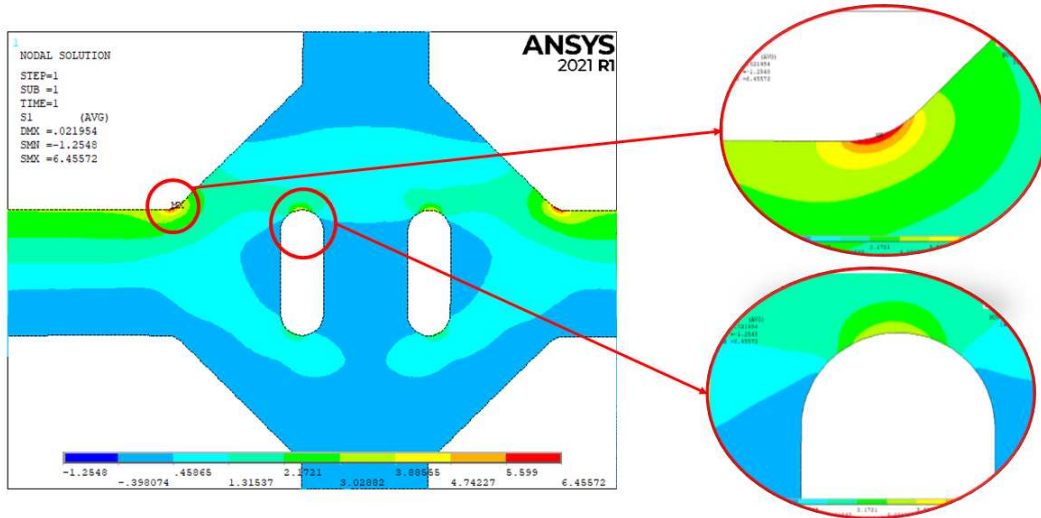


Figure 5.40: Plot of the first principal stress of ideal model with angular misalignment with element PLANE 183.

The maximum first principal stress at the weld toe and root are:

$$\Delta\sigma_{11,Toe,max} = 6.4557MPa \quad (5.41)$$

$$\Delta\sigma_{11,Root,max} = 3.9365MPa \quad (5.42)$$

The results of the all ideal model with angular misalignment are reported in the Appendix F.3.

Structural Hot-Spot Stress (SHSS) approach

The fatigue assessment for this model is performed by the application of SHSS approach, following the IIW recommendation [1] to obtain the hot-spot stress. The hot-spot stress value is detected with the employment of fine mesh, as *Figure 1.4* shows, and the hot-spot stress is detected with the formulas for hot-spot type *a* and also type *b*.

The model is divided in a series of areas to allow the application of *Mapped-mesh* algorithm; indeed each areas must be characterised by a number of side between 3 and 4 to obtain a *Mapped-mesh* (see *Figure 5.41*). The four-node linear element PLANE 182 is chosen in Ansys®APDL with *Simple Enhanced Strain* as Key Option 1 and *Plane Strain* as Key Option 3.

The all informations about the mesh is reported in the following table:

Element type	Mesh algorithm	Main plate thickness t	Max element size	Adopted element size
Plane 182 KeyOpt:Simple Enhanced Strain + Plane Strain	Mapped	6 mm	$0.4 \cdot t = 0.4 \cdot 6 = 2.4\text{mm}$	0.4 mm

Table 5.13: Requirements for SHSS mesh.

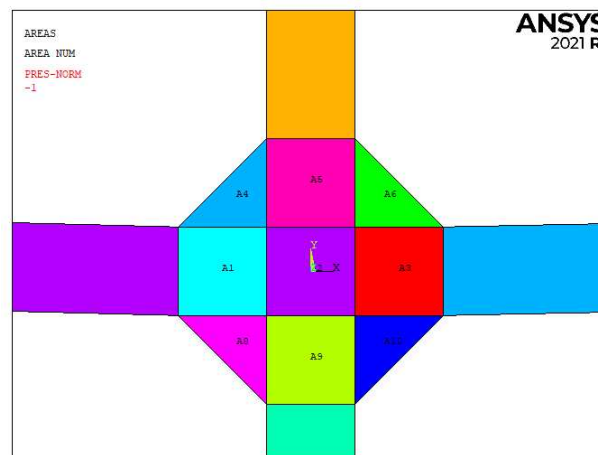


Figure 5.41: Subdivision of area for Mapped mesh.

The hot-spot stress is extrapolated at two reference points placed at $0.4t$ and $1.0t$ distance from the weld toe tip, so in this case at 2.4 mm and 6 mm from weld toe. These reference points are used for the hot-spot type *a*. For type *b*, the structural hot-spot stress is extrapolated at three reference points located at 4mm, 8mm and 12mm distance from the weld toe.

For the type of extrapolated stress, the graph in *Figure 5.42* shows that, for an external applied pressure $\Delta\sigma_{nom} = 1\text{MPa}$, the $\Delta\sigma_{xx}$ and the first principal stress $\Delta\sigma_{11}$ are coincident. For this reason the choice is indifferent.

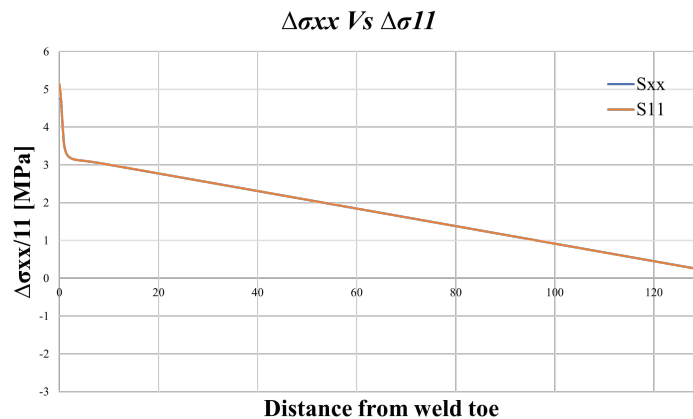


Figure 5.42: $\Delta\sigma_{xx}$ and $\Delta\sigma_{yy}$ plotted in function of the distance from weld toe tip.

The mesh of the model is reported in the following figures:

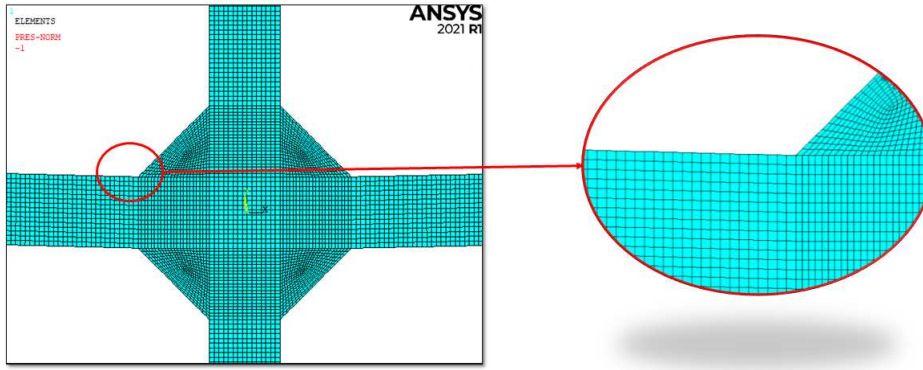


Figure 5.43: Mapped mesh for SHSS approach.

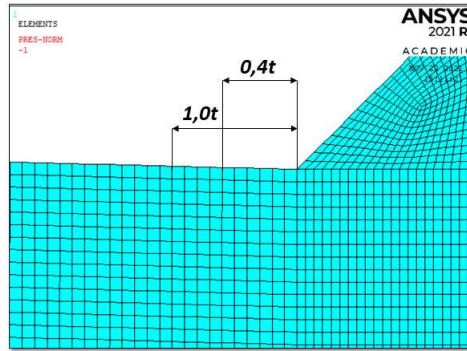


Figure 5.44: Mapped mesh for SHSS approach and reference points.

For an external applied pressure $\Delta\sigma_{nom} = 1MPa$, the results of the tension at the reference points for hot spot type *a* are:

$$\Delta\sigma_{xx,0.4t} = 3.17274MPa \quad (5.43)$$

$$\Delta\sigma_{xx,1.0t} = 3.09208MPa \quad (5.44)$$

$$\Delta\sigma_{11,0.4t} = 3.17424MPa \quad (5.45)$$

$$\Delta\sigma_{11,1.0t} = 3.09396MPa \quad (5.46)$$

The structural hot-spot stress type *a* is detected with the equation (1.2):

$$\Delta SHSS_{LSE,xx} = 1,67 \cdot \sigma_{xx,0.4t} - 0,67 \cdot \sigma_{xx,1.0t} = 1,67 \cdot 3.17274 - 0,67 \cdot 3.09208 = 3.2268MPa \quad (5.47)$$

$$\Delta SHSS_{LSE,11} = 1,67 \cdot \sigma_{11,0.4t} - 0,67 \cdot \sigma_{11,1.0t} = 1,67 \cdot 3.17424 - 0,67 \cdot 3.09396 = 3.2280MPa \quad (5.48)$$

For an external applied pressure $\Delta\sigma_{nom} = 1MPa$, the results of the tension at the reference points for hot spot type *b* are:

$$\Delta\sigma_{xx,4mm} = 3.12408MPa \quad (5.49)$$

$$\Delta\sigma_{xx,8mm} = 3.05216MPa \quad (5.50)$$

$$\Delta\sigma_{xx,12mm} = 2.9612MPa \quad (5.51)$$

$$\Delta\sigma_{11,4mm} = 3.12599MPa \quad (5.52)$$

$$\Delta\sigma_{11,8mm} = 3.05398MPa \quad (5.53)$$

$$\Delta\sigma_{11,12mm} = 2.96265MPa \quad (5.54)$$

The structural hot-spot stress type *b* is detected with the following:

$$\Delta SHSS_{LSE} = 3 \cdot \Delta\sigma_{xx,4mm} - 3 \cdot \Delta\sigma_{xx,8mm} + \Delta\sigma_{xx,12mm} \quad (5.55)$$

$$\Delta SHSS_{LSE,xx} = 3 \cdot \Delta \sigma_{xx,4mm} - 3 \cdot \Delta \sigma_{xx,8mm} + \Delta \sigma_{xx,12mm} = 3 \cdot 0.98176 - 3 \cdot 0.99855 + 1.00006 = 0.9497 \quad (5.56)$$

$$\Delta SHSS_{LSE,11} = 3 \cdot \Delta \sigma_{11,4mm} - 3 \cdot \Delta \sigma_{11,8mm} + \Delta \sigma_{11,12mm} = 3 \cdot 0.98176 - 3 \cdot 0.99855 + 1.00006 = 0.9497 \quad (5.57)$$

The results of the all ideal model with angular misalignment are reported in the Appendix F.3.

Peak Stress Method (PSM) for ideal model with angular misalignment with sharp V-notch

The fatigue assessment for this model is performed by the application of the PSM approach for 2D structure with the adoption of four-node linear elements. The element PLANE 182 is chosen from the Ansys®APDL library with *Simple Enhanced Strain* as Key Option 1 and *Plane Strain* as Key Option 3. The model is characterised by a root with an initial opening length equal to 0.1 mm.

The weld toe is subjected to pure mode I because it is characterised by a V-notch opening angle 2α equal to 135° . On the other hand, the root is characterised by a V-notch opening angle equal to 0° , so it is subjected to mode I and also mode II.

Under mode I and mode II, the PSM requirements are defined in the following table:

Element type	Mesh algorithm	Mode I			
		$(a/d)_{min}$	2α	Mesh Pattern $2\alpha < 90^\circ$	Mesh Pattern $2\alpha > 90^\circ$
Plane 182 KeyOpt:Simple Enhanced Strain + Plane Strain	Free	3	$0^\circ < 2\alpha < 135^\circ$	Four adjacent elements share the same node	Two adjacent elements share the same node
Mode II					
Plane 182 KeyOpt:Simple Enhanced Strain + Plane Strain	Free	14	$0^\circ < 2\alpha < 135^\circ$	Four adjacent elements share the same node	Four adjacent elements share the same node up to $2\alpha = 102.5^\circ$

Table 5.14: Requirements for PSM.

The mode I PSM calibration constant is equal to $K_{FE}^* = 1.38 \pm 3\%$, instead for mode II, the calibration constant is equal to $K_{FE}^{**} = 3.38 \pm 3\%$.

The size of the element is obtained with the following procedure:

1. From literature the ratio $(a/d)_{min}$ is determined. In this case there are 2 ratio: the first one for mode I and the second for mode II. The highest ratio is chosen;
2. The value of a is the reference dimension for selecting the maximal FE sizes d for PSM application and is defined as the half of the thickness t ;
3. Subsequently, the minimum element size is defined as follow:

$$d_{min} = \frac{a}{14} = \frac{6}{14} = 0.214mm \quad (5.58)$$

4. The chosen dimension of elements is 0.2mm.

The λ_1 , e_1 , λ_2 and e_2 values are depended on the V-notch opening angle 2α , that is 135° for the weld toe and 0° for the root:

2α [°]	λ_1 (Mode I)	e_1 (Mode I)	λ_2 (Mode II)	e_2 (Mode II)
135°	0.674	0.117	/	/
0°	0.5	0.133	0.5	0.341

Table 5.15: Value of $\lambda_1, e_1, \lambda_2$ and e_2 in function of the opening angle 2α .

The corrective stress factors for mode I and II are calculated with the equation (2.24) for the weld toe and root. The results are reported in the *Table 5.16*.

2α [°]	f_{w1}	f_{w2}
135°	0.627	/
0°	0.633	2.473

Table 5.16: Values of the corrective stress factors f_{w1} and f_{w2} in function of the opening angle 2α .

Finally, the mesh can be laid on the model and the results is displayed on the *Figure 5.45*:

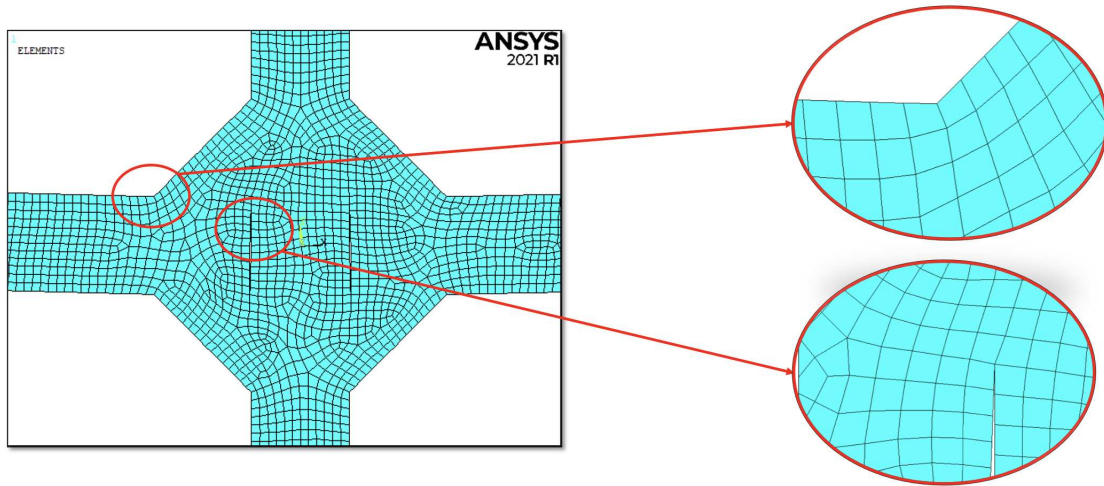


Figure 5.45: Mesh conformation with global element size $d = 0.2mm$.

After the application of load and constraint, the system can be solved:

Solution → *Solve* → *Current LS*

The results of the first principal stress is plotted in the *Figure 5.46*:

Two local reference systems (*Figure 5.47*) are created on the nodes that represent the weld toe and the apex of the root. The *WorkPlane* is rotated by an angle equal to 112.5° for the toe and by an angle equal to 90° for the root. The procedure for the creation of the local reference systems is the same as described in the paragraph 3.1.2.

Thanks to the creation of the local reference system, the tension $\Delta\sigma_{yy}$ can be extracted:

$$\Delta\sigma_{yy, weldtoe} = 7.7474MPa \quad (5.59)$$

$$\Delta\sigma_{yy, root} = 3.5517MPa \quad (5.60)$$

$$\Delta\tau_{xy, root} = 0.02118MPa \quad (5.61)$$

The equivalent peak stresses are calculated by the formula (2.23):

$$\Delta\sigma_{eq, peak, toe} = f_{w1} \cdot \sigma_{\theta\theta, \theta=0, peak} = 4.854MPa \quad (5.62)$$

$$\Delta\sigma_{eq, peak, root} = \sqrt{f_{w1}^2 \cdot \sigma_{\theta\theta, \theta=0, peak}^2 + f_{w2}^2 \cdot \tau_{r\theta, \theta=0, peak}^2} = 2.249MPa \quad (5.63)$$

The results of the all ideal model with angular misalignment are reported in the Appendix F.3.

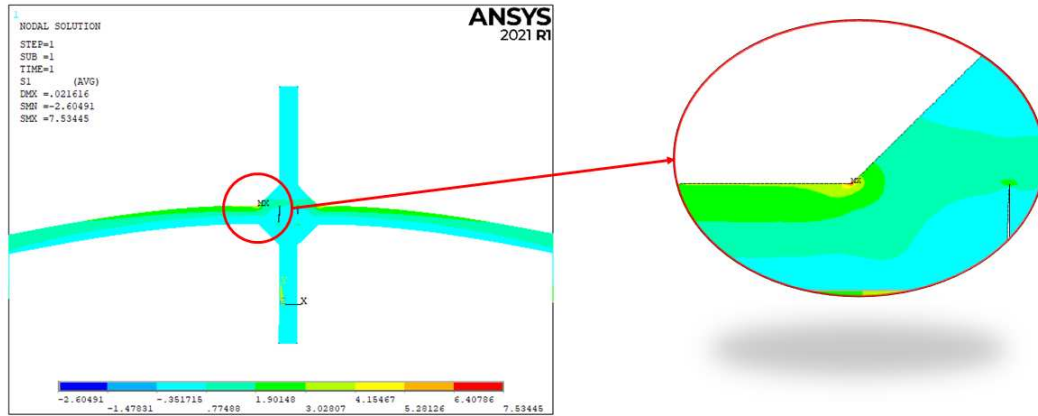


Figure 5.46: Plot of 1st principal stress for an external applied nominal stress range of 1MPa.

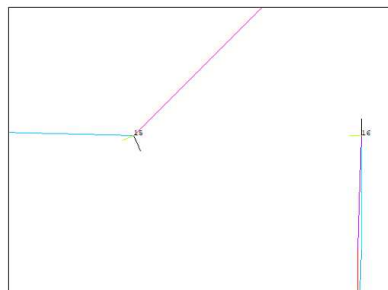


Figure 5.47: Local reference system at the weld toe and root.

Peak Stress Method (PSM) for ideal model with angular misalignment with HFMI groove

The fatigue assessment for this model is performed by the application of Peak Stress Method in combination with the SED approach with the adoption of four-node linear elements, considering only the weld toe. First of all, the dimensions of the HFMI groove are taken from the reference [47] and are reported in the following table:

depth [mm]	ρ_{HFMI} [mm]	width [mm]	2α [°]
0.3	3.31	4.649	135

Table 5.17: Dimension of HFMI groove.

The element PLANE 182 is chosen from the Ansys®APDL library with *Simple Enhanced Strain* as Key Option 1 and *Plane Strain* as Key Option 3.

The SED approach for blunt notches is based on the creation of a structural volume at the radiused weld toe, that can be rigidly rotated (*Figure 4.20*) to included the whole maximum principal stress, which is related to the highest strain energy density.

The first step is to determinate the inclination angle Φ with respect to the blunt notch bisector of the most stressed area that is indicated in red in Ansys®APDL.

To define the inclination angle, the model is meshed with a global element size equal to 0.5 mm and subsequently, two refinements with depth equal to 5 (see *Figure 5.48* for the refine options) are applied to the arc that represents the groove due to HFMI treatment (*Figure 5.49*) with the following commands:

Preprocessor → *Meshing* → *Modify Mesh* → *Refine At* → *Lines*



Figure 5.48: Options for the refinement.

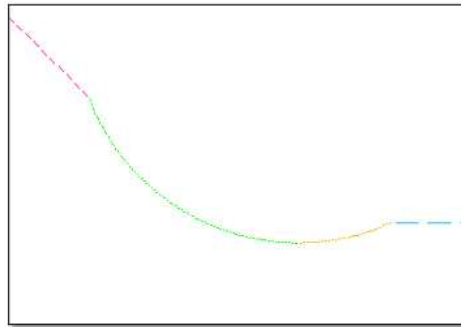


Figure 5.49: Arc that represents the HFMI groove where the refinements are applied.

The meshed model is displayed on the following figure:

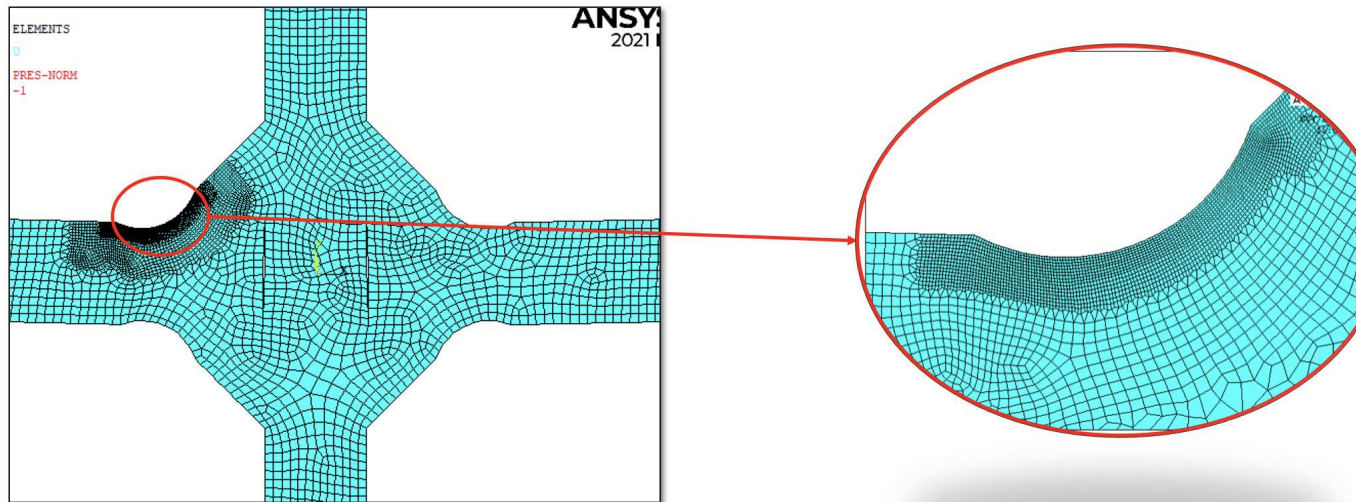


Figure 5.50: Mesh of the model to define the inclination angle.

The model is subjected to an external nominal stress $\Delta\sigma_{nom} = 1MPa$ applied on the main plate. Once the model is properly meshed, loaded and constraint, the system can be solve:

Solution→*Solve*→*Current LS*

The highest stress is not located exactly around the blunt notch bisector, so it is matter of quantifying the grades of rotation. The value of the angle is reported in the following equation and represents a clockwise rotation about the global z-axis:

$$\Phi = 18.2605^\circ \tag{5.64}$$

The circular sector is created according to equations (4.5) and (4.6):

$$q = \frac{2\pi - 2\alpha}{\pi} = 2 - \frac{135}{180} = 1.2582 \tag{5.65}$$

$$r_0 = \frac{q-1}{q} \cdot \rho_{HFMI} = \frac{1.25-1}{1.25} \cdot 3.31 = 0.6793\text{mm} \quad (5.66)$$

$$R_0 + r_0 = 0.28 + 0.6793 = 0.9593\text{mm} \quad (5.67)$$

Subsequently, the control volume to calculate the averaged Strain Energy Density (SED) is created. The result is reported in the following figure:



Figure 5.51: Illustration of the control Area to calculate the SED.

To create the mesh of the model, the following procedure is executed:

1. The element inside the structural volume are characterised by a *global element size* equal to 0.01mm with a *free-mesh* algorithm;

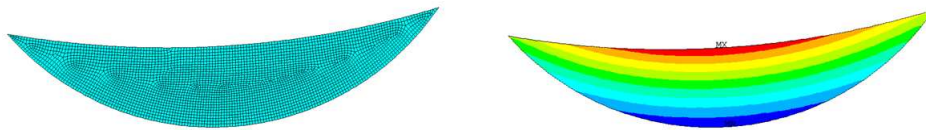


Figure 5.52: On the left, the mesh of the structural volume with global element size of 0.01. On the right, the proof that the highest stress is contained inside the volume.

2. The other volume is meshed with a *global element size* equal to 0.1 mm with a *free-mesh* algorithm.

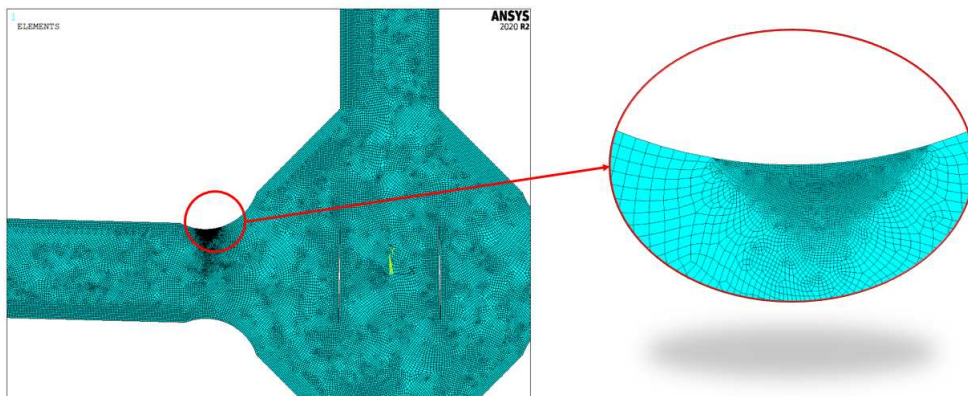


Figure 5.53: Mesh of the all structure.

Once the model is properly meshed, loaded and constraint, the system can be solved:

Solution→*Solve*→*Current LS*

The averaged Strain Energy Density is defined as the energy contained inside the structural volume. The same procedure described in the paragraph 4.2.2 is applied to detect the SED value.

The result of SED for the weld toe when the specimen is subjected to a nominal stress of 1 MPa is:

$$SENE = 1.45997 \cdot 10^{-5} MJ \quad (5.68)$$

$$VOLU = 0.298236 mm^3 \quad (5.69)$$

$$SED = \frac{SENE}{VOLU} = \frac{1.45997 \cdot 10^{-5}}{0.298236} = 4.8954 \cdot 10^{-5} \frac{MJ}{m^3} \quad (5.70)$$

From the SED, the equivalent peak stress is obtained with the following formula:

$$\Delta\sigma_{eq,peak} = \sqrt{\frac{2 \cdot E \cdot SED}{1 - \nu^2}} = \sqrt{\frac{2 \cdot 206000 \cdot 4.8954 \cdot 10^{-5}}{1 - 0.3^2}} = 4.7078 MPa \quad (5.71)$$

Subsequently, the equivalent peak stress at the weld root is detected with the same procedure used for the ideal model with angular misalignment with sharp V-notch. Thus, the results are:

$$\Delta\sigma_{yy,root} = 3.719 MPa \quad (5.72)$$

$$\Delta\tau_{xy,root} = 0.01747 MPa \quad (5.73)$$

The equivalent peak stresses are calculated by the formula (2.23):

$$\Delta\sigma_{eq,peak,root} = \sqrt{f_{w1}^2 \cdot \sigma_{\theta\theta,\theta=0,peak}^2 + f_{w2}^2 \cdot \tau_{r\theta,\theta=0,peak}^2} = 2.354 MPa \quad (5.74)$$

The results of the all ideal model with angular misalignment are reported in the Appendix F.3.

5.2.5 Definition of several ratio to understand the misalignment effect

After the FE analysis of the ideal model with and without angular misalignment, different ratios are defined to detect the misalignment effect and to understand the advantages that came from the HFMI post-welded treatment. These ratios are expressed in terms of equivalent peak stress, hot-spot stress and effective notch stress.

The ratios are:

1. The first factor is the ratio between the maximum equivalent peak stress between the root and the weld toe in the ideal model with angular misalignment and the maximum equivalent peak stress between the root and the weld toe in the ideal model without angular misalignment:

$$Factor_1 = \frac{\Delta\sigma_{max,eq,peak,between-root-and-toe-with-Misalignment}}{\Delta\sigma_{max,eq,peak,between-root-and-toe-without-Misalignment}} \quad (5.75)$$

The results are reported in the following table:

Name of .txt file	$\Delta\sigma_{max,eq,peak,between-root}$ <i>and-toe-with-Misalignment</i> [MPa]	$\Delta\sigma_{max,eq,peak,between-root}$ <i>and-toe-without-Misalignment</i> [MPa]	<i>Factor</i> ₁
355-WH-2	4.708	2.028	2.322
355-WH-3	4.434	1.831	2.422
355-WH-4	4.216	2.080	2.027
355-WH-5	4.122	2.027	2.033
355-WH-8	3.793	1.821	2.082
355-WH-11	3.732	1.971	1.894
355-WH-14	4.569	1.932	2.365
355-WH-16	4.013	1.964	2.044
355-WH-17	3.950	1.964	2.011
355-WH-18	4.043	1.817	2.225
355-WH-20	3.836	1.974	1.944
355-WH-21	3.858	1.974	1.955
355-WH-22	3.801	1.792	2.121

Table 5.18: Results of factor 1.

2. The second factor is the ratio between the effective notch stress, calculated with the elements PLANE 182, at the weld toe in the ideal model with angular misalignment and the effective notch stress, calculated with the elements PLANE 182, at the weld toe in the ideal model without angular misalignment:

$$Factor_2 = \frac{\Delta\sigma_{11,max,toe-with-Misalignment,PLANE182}}{\Delta\sigma_{11,max,toe-without-Misalignment,PLANE182}} \quad (5.76)$$

The results are reported in the following table:

Name of .txt file	$\Delta\sigma_{11,max,toe-with-Misalignment,}$ <i>PLANE182</i> [MPa]	$\Delta\sigma_{11,max,toe-without-Misalignment,}$ <i>PLANE182</i> [MPa]	<i>Factor</i> ₂
355-WH-2	6.476	2.778	2.331
355-WH-3	6.000	2.576	2.329
355-WH-4	5.975	2.840	2.104
355-WH-5	5.776	2.777	2.080
355-WH-8	5.239	2.576	2.034
355-WH-11	5.236	2.664	1.966
355-WH-14	6.209	2.642	2.350
355-WH-16	5.561	2.653	2.096
355-WH-17	5.495	2.653	2.071
355-WH-18	5.462	2.538	2.152
355-WH-20	5.393	2.719	1.984
355-WH-21	5.427	2.719	1.996
355-WH-22	5.216	2.538	2.055

Table 5.19: Results of factor 2.

3. The third factor is the ratio between the effective notch stress, calculated with the elements PLANE 183, at the weld toe in the ideal model with angular misalignment and the effective notch stress, calculated with the elements PLANE 183, at the weld toe in the ideal model without angular misalignment:

$$Factor_3 = \frac{\Delta\sigma_{11,max,toewithMisalignment,PLANE183}}{\Delta\sigma_{11,max,toewithoutMisalignment,PLANE183}} \quad (5.77)$$

The results are reported in the following table:

Name of .txt file	$\Delta\sigma_{11,max,toe-with-Misalignment,}$	$\Delta\sigma_{11,max,toe-without-Misalignment,}$	<i>Factor</i> ₃
	PLANE183 [MPa]	PLANE182 [MPa]	
355-WH-2	6.456	2.762	2.338
355-WH-3	5.979	2.564	2.332
355-WH-4	5.953	2.826	2.106
355-WH-5	5.755	2.761	2.085
355-WH-8	5.224	2.565	2.037
355-WH-11	5.221	2.650	1.970
355-WH-14	6.190	2.629	2.355
355-WH-16	5.542	2.640	2.099
355-WH-17	5.475	2.640	2.074
355-WH-18	5.447	2.527	2.155
355-WH-20	5.373	2.703	1.988
355-WH-21	5.409	2.703	2.001
355-WH-22	5.193	2.527	2.055

Table 5.20: Results of factor 3.

4. The fourth factor is the ratio between the hot-spot stress type *a* of the ideal model with angular misalignment and the hot-spot stress type *a* of the ideal model without angular misalignment:

$$Factor_4 = \frac{SHSS_{LSE,withMisalignment,typea}}{SHSS_{LSE,withoutMisalignment,typea}} \quad (5.78)$$

The results are reported in the following table:

Name of .txt file	$SHSS_{LSE,with-Misalignment,type-A}$	$SHSS_{LSE,without-Misalignment,type-A}$	<i>Factor</i> ₄
	[MPa]	[MPa]	
355-WH-2	3.227	0.994	3.245
355-WH-3	3.064	0.992	3.088
355-WH-4	2.892	0.990	2.920
355-WH-5	2.814	0.994	2.829
355-WH-8	2.614	0.992	2.635
355-WH-11	2.562	0.993	2.580
355-WH-14	3.149	0.993	3.171
355-WH-16	2.759	0.993	2.778
355-WH-17	2.720	0.993	2.739
355-WH-18	2.769	0.992	2.793
355-WH-20	2.622	0.994	2.639
355-WH-21	2.644	0.994	2.660
355-WH-22	2.620	0.992	2.642

Table 5.21: Results of factor 4.

5. The fifth factor is the ratio between the maximum first principal stress at the weld toe of the model obtained from the cloud of point and the effective notch stress, calculated with the elements PLANE 182, at the weld toe in the ideal model without angular misalignment:

$$Factor_4 = \frac{\Delta\sigma_{11,max,toe,from-cloud-point-with-Misalignment}}{\Delta\sigma_{11,max,toe-without-Misalignment,PLANE182}} \quad (5.79)$$

The results are reported in the following table:

Name of .txt file	$\Delta\sigma_{11,max,from-cloud-point}$ with-Misalignment [MPa]	$\Delta\sigma_{11,max,from-cloud-point}$ without-Misalignment,PLANE182 [MPa]	Factor ₅
355-WH-2	5.7937	2.778	2.086
355-WH-3	5.7993	2.576	2.251
355-WH-4	5.8974	2.840	2.077
355-WH-5	4.5343	2.777	1.633
355-WH-8	4.9200	2.576	1.910
355-WH-11	4.8354	2.664	1.815
355-WH-14	5.6188	2.642	2.127
355-WH-16	5.4915	2.653	2.070
355-WH-17	5.0055	2.653	1.887
355-WH-18	5.0221	2.538	1.979
355-WH-20	4.6786	2.719	1.721
355-WH-21	4.5449	2.719	1.672
355-WH-22	4.7214	2.538	1.860

Table 5.22: Results of factor 5.

6. The sixth factor is the ratio between the equivalent peak stress at the weld toe in the ideal model with angular misalignment and with sharp V-notch, and the equivalent peak stress at the weld toe in the ideal model with angular misalignment and with the HFMI groove:

$$Factor_4 = \frac{\Delta\sigma_{11,max,toe,fromcloudpointwithMisalignment}}{\Delta\sigma_{11,max,toewithoutMisalignment,PLANE182}} \quad (5.80)$$

The results are reported in the following table:

Name of .txt file	$\Delta\sigma_{eq,peak,toe-with-Misalignment}$ sharp-V-notch [MPa]	$\Delta\sigma_{eq,peak,toe-with-Misalignment}$ HFMI-groove [MPa]	Factor ₆
355-WH-2	4.854	4.708	1.031
355-WH-3	4.573	4.434	1.031
355-WH-4	4.512	4.216	1.070
355-WH-5	4.321	4.122	1.048
355-WH-8	3.963	3.793	1.045
355-WH-11	3.940	3.732	1.056
355-WH-14	4.672	4.569	1.023
355-WH-16	4.174	4.013	1.040
355-WH-17	4.124	3.950	1.044
355-WH-18	4.145	4.043	1.025
355-WH-20	4.017	3.836	1.047
355-WH-21	4.041	3.858	1.047
355-WH-22	3.913	3.801	1.029

Table 5.23: Results of factor 6.

5.2.6 Definition of k_{mis} factor for the detection of misalignment effect

After the definition of the different ratios, the aim is to obtain a k_{mis} factor to detect the effect of the axial e and angular misalignment α .

The procedure to define the expression of the k_{mis} factor consists to hypothesize some expression of the factor that consider the misalignment effect. These expression will be function of the axial and angular misalignment and the thickness t . Furthermore, these formula will be characterised by two constants β and γ that will be systematically changed to determine which values would result in minimum standard deviation σ_y for the used data.

The procedure to obtain the correct definition of the k_{mis} factor is characterised by the following steps:

1. Firstly, the experimental data used for the evaluation of k_{mis} factor are multiplied for a stress intensity factors calculated for each specimen from FE analysis. These factors are obtained from the preliminary analysis (see paragraph 5.2.2, in this thesis it is called actual model), from the application of the Effective Notch Stress method and PSM approach on the ideal model with angular misalignment (see paragraph 5.2.4). Subsequently, these values are multiplied also for the k_{mis} factor that consider the misalignment effect:

$$\sigma_{max,mis} = \sigma_{max} \cdot K_{s,actual/ENS/PSM} \cdot k_{mis} \quad (5.81)$$

2. The angular misalignment is converted in axial misalignment with the following formula:

$$e_{new} = \frac{l}{2} \cdot \tan(\alpha_{tot}) \quad (5.82)$$

where l is the total length of the sample and α_{tot} is the sum of the right and left angular misalignment. The results are reported in the following table:

Name of .txt file	σ_{max} [MPa]	σ_{min} [MPa]	$\Delta\sigma$ [MPa]	N_f [cycles]	t [mm]	α_{tot} [°]	e [mm]
355-WH-2	258.33	-116.67	375.00	2 799 750	6	2.641	13.837
355-WH-3	258.33	-116.67	375.00	3 387 000	6	2.452	12.846
355-WH-5	233.33	-100.00	333.33	3 410 280	6	2.137	11.194
355-WH-8	200.00	-83.33	283.33	8 750 324	6	1.896	9.932
355-WH-14	175.00	-75.00	250.00	6 673 500	6	2.538	13.296
355-WH-16	175.00	-75.00	250.00	7 085 250	6	2.068	10.833
355-WH-17	200.00	-83.33	283.33	4 420 500	6	2.034	10.653
355-WH-18	233.33	-100.00	333.33	3 607 500	6	2.102	11.014
355-WH-20	233.33	-100.00	333.33	3 261 000	6	1.931	10.113
355-WH-21	200.00	-83.33	283.33	4 446 750	6	1.965	10.293
355-WH-22	258.33	-116.67	375.00	2 341 500	6	1.948	10.203

Table 5.24: Results of axial misalignment from angular misalignment with the application of equation (5.82).

3. The expressions use for the detection of k_{mis} factor are the following:

$$k_{mis} = \gamma \cdot \left(1 + \beta \cdot \frac{e_{new}}{t} \right) \quad (5.83)$$

$$k_{mis} = \gamma \cdot \left(1 - \beta \cdot \frac{e_{new}}{t} \right) \quad (5.84)$$

$$k_{mis} = \frac{\gamma}{1 + \beta \cdot \frac{e_{new}}{t}} \quad (5.85)$$

$$k_{mis} = \gamma^{1 - \beta \cdot \frac{e_{new}}{t}} \quad (5.86)$$

$$k_{mis} = \gamma^{1 + \beta \cdot \frac{e_{new}}{t}} \quad (5.87)$$

$$k_{mis} = \gamma^{\frac{1}{1 - \beta \cdot \frac{e_{new}}{t}}} \quad (5.88)$$

$$k_{mis} = \gamma^{\frac{1}{1 + \beta \cdot \frac{e_{new}}{t}}} \quad (5.89)$$

$$k_{mis} = \gamma^{\beta \cdot \frac{e_{new}}{t}} \quad (5.90)$$

4. The two constants β and γ are systematically changed to determine which values would result in a minimum standard deviation σ_y for the data. The range of variation for both is between 0.1 and 10 with step-size equal to 0.05;
5. For each expression of the k_{mis} factor, the minimum standard deviation σ_y , the corresponding T_σ and slope B are extracted. The results are reported in the following subsection and two statistical analysis are conducted: the first one with a free slope; the second with a fixed slope equal to 5, that is the typical value of the design curve for the HFMI joints. The analysis is done through a MatLab code that is reported in the Appendix E.4

Results of statistical analysis with stress intensity factor from the actual model

The results of statistical analysis with the stress intensity factor from the actual model with a free slope are reported in the following table:

σ_y	β	γ	Formula of k_{mis}	T_σ	B (slope)
0.16662	0.1	0.7	$\gamma \cdot \left(1 + \beta \cdot \frac{e_{new}}{t} \right)$	7.7736	1.0892
0.15834	0.2	1.05	$\gamma \cdot \left(1 - \beta \cdot \frac{e_{new}}{t} \right)$	3.4863	1.6997
0.1587	0.8	1.8	$\frac{\gamma}{1 + \beta \cdot \frac{e_{new}}{t}}$	3.5805	1.668
0.15849	0.6	1.7	$\gamma^{1 - \beta \cdot \frac{e_{new}}{t}}$	3.5351	1.6826
0.15849	6.2	0.95	$\gamma^{1 + \beta \cdot \frac{e_{new}}{t}}$	3.5357	1.6824
0.12523	0.15	0.6	$\frac{1}{\gamma^{1 - \beta \cdot \frac{e_{new}}{t}}}$	4.3444	1.1429
0.15884	0.4	10	$\frac{1}{\gamma^{1 + \beta \cdot \frac{e_{new}}{t}}}$	3.6463	1.646
0.15849	6.2	0.95	$\gamma^{\beta \cdot \frac{e_{new}}{t}}$	3.5357	1.6824

Table 5.25: Results of statistical analysis with free slope and the stress intensity factor obtained from actual model.

As the Table 5.25 shows, the following formula is characterised by the minimum σ_y standard deviation

$$k_{mis} = \gamma^{1 - \beta \cdot \frac{e_{new}}{t}} \tag{5.91}$$

with $\beta = 0.15$ and $\gamma = 0.6$.

Subsequently, the different couples of β and γ values are plotted on 3D graph in function of the standard deviation σ_y . The graph is reported in the following figure:

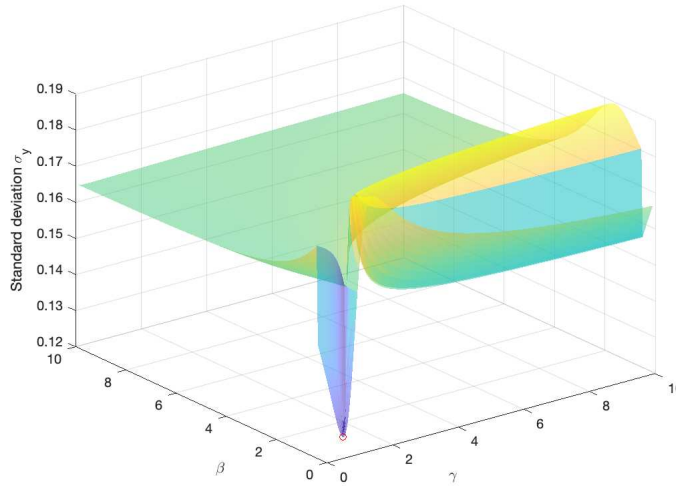


Figure 5.54: 3D surface where on the x and y axes are plotted the values of β and γ , along the z-axis is plotted the standard deviation σ_y . The red dot define the minimum value of the standard deviation.

As Figure 5.54 shows, the minimum standard deviation is obtained for β and γ values between 0.05 and 1. For this reason, another statistical analysis is done with a decrease of the definition interval of the two constant and also with a reduction of the step size, as Figure 5.55 shows.

```
gamma=[0.05:0.001:1]';
beta=[0.05:0.001:1]';
```

Figure 5.55: Definition of the two constants in MatLab.

The results are:

- $\sigma_y = 0.12523$;
- $\beta = 0.221$;
- $\gamma = 0.653$;
- $T_\sigma = 4.3027$;
- $m = 1.1505$;

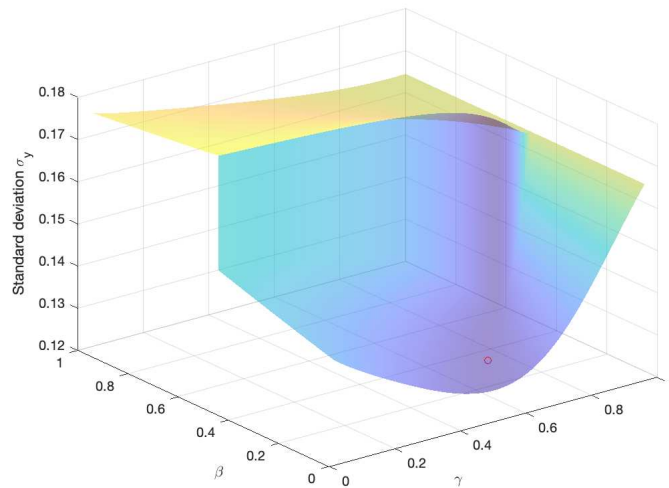


Figure 5.56: 3D surface where on the x and y axes are plotted the values of β and γ , along the z-axis is plotted the standard deviation σ_y . The red dot define the minimum value of the standard deviation.

The fatigue design curve for $\beta = 0.221$ and $\gamma = 0.653$ with a free slope is represented in the following figure:

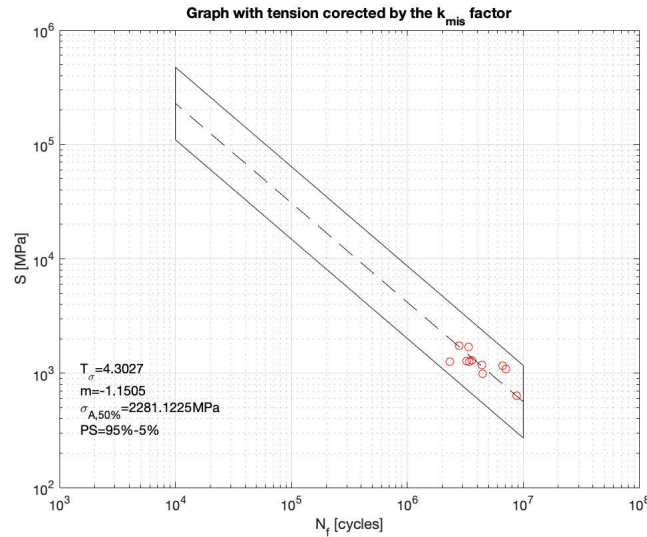


Figure 5.57: Fatigue design curve for $\beta = 0.221$ and $\gamma = 0.653$.

Subsequently, the same procedure is applied in the case of fixed slope $m = 5$. The results of statistical analysis with the stress intensity factor from the actual model with a fixed slope are reported in the following table:

σ_y	β	γ	Formula of k_{mis}	T_σ	B (slope)
0.36503	0.1	5.35	$\gamma \cdot \left(1 + \beta \cdot \frac{e_{new}}{t} \right)$	2.661	5
0.25609	0.25	2.15	$\gamma \cdot \left(1 - \beta \cdot \frac{e_{new}}{t} \right)$	1.987	5
0.25608	2.0	6.65	$\frac{\gamma}{1 + \beta \cdot \frac{e_{new}}{t}}$	1.9869	5
0.25427	0.25	5.25	$\gamma^{1 - \beta \cdot \frac{e_{new}}{t}}$	1.9773	5
0.25427	2.25	0.85	$\gamma^{1 + \beta \cdot \frac{e_{new}}{t}}$	1.9773	5
0.25033	0.35	0.9	$\gamma^{\frac{1}{1 - \beta \cdot \frac{e_{new}}{t}}}$	1.9565	5
0.2637	0.5	10	$\gamma^{\frac{1}{1 + \beta \cdot \frac{e_{new}}{t}}}$	2.0279	5
0.25427	2.55	0.85	$\gamma^{\beta \cdot \frac{e_{new}}{t}}$	1.9773	5

Table 5.26: Results of statistical analysis with fixed slope and the stress intensity factor obtained from actual model.

As the Table 5.26 shows, the following formula is characterised by the minimum σ_y standard deviation

$$k_{mis} = \gamma^{\frac{1}{1 - \beta \cdot \frac{e_{new}}{t}}} \quad (5.92)$$

with $\beta = 0.35$ and $\gamma = 0.9$.

Subsequently, the different couples of β and γ values are plotted on 3D graph in function of the standard deviation σ_y . The graph is reported in the following figure:

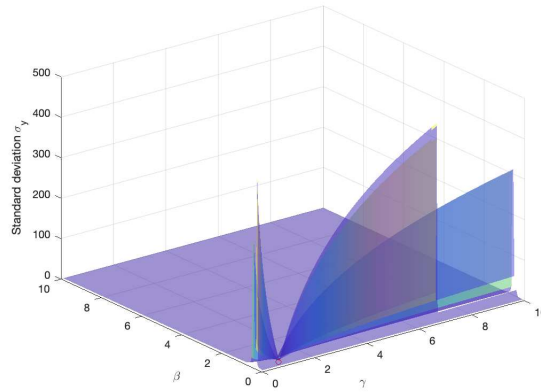


Figure 5.58: 3D surface where on the x and y axes are plotted the values of β and γ , along the z-axis is plotted the standard deviation σ_y . The red dot define the minimum value of the standard deviation.

As Figure 5.58 shows, the minimum standard deviation is obtained for β and γ values between 0.05 and 1 for β and for γ . For this reason, another statistical analysis is done with a decrease of the definition interval of the two constant and also with a reduction of the step size, as Figure 5.59 shows.

```
gamma=[0.05:0.001:1]';
beta=[0.05:0.001:1]';
```

Figure 5.59: Definition of the two constants in MatLab.

The results are:

- $\sigma_y = 0.25018$;
- $\beta = 0.345$;
- $\gamma = 0.895$;
- $T_\sigma = 1.9557$;
- $m = 5$;

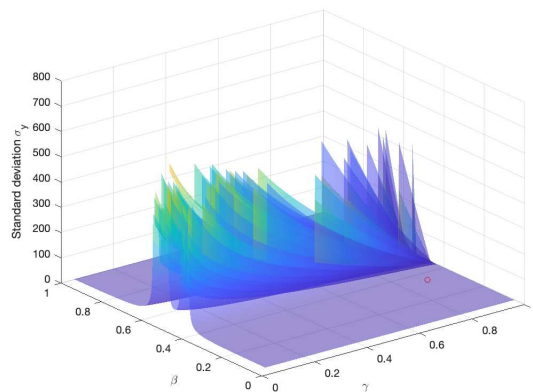


Figure 5.60: 3D surface where on the x and y axes are plotted the values of β and γ , along the z-axis is plotted the standard deviation σ_y . The red dot define the minimum value of the standard deviation.

The fatigue design curve for $\beta = 0.345$ and $\gamma = 0.895$ with a free slope is represented in the following figure:

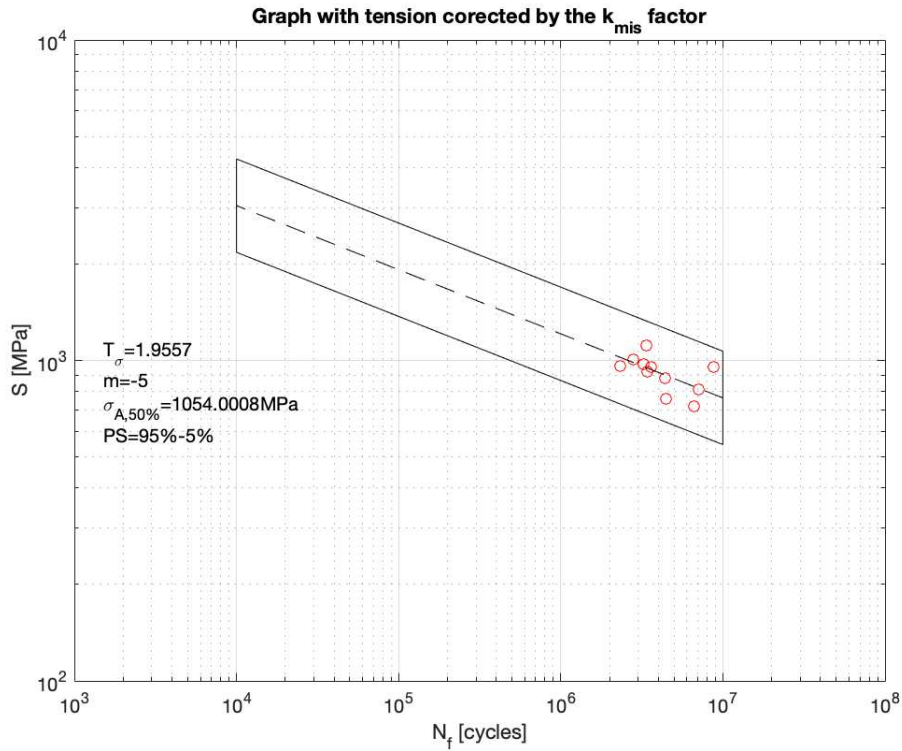


Figure 5.61: Fatigue design curve for $\beta = 0.345$ and $\gamma = 0.895$.

Results of statistical analysis with stress intensity factor from ENS approach

The results of statistical analysis with the stress intensity factor from the application of the ENS approach on the ideal model with angular misalignment with a free slope are reported in the following table:

σ_y	β	γ	Formula of k_{mis}	T_σ	B (slope)
0.12094	0.1	0.8	$\gamma \cdot \left(1 + \beta \cdot \frac{e_{new}}{t} \right)$	2.5171	1.7564
0.089685	0.2	9.1	$\gamma \cdot \left(1 - \beta \cdot \frac{e_{new}}{t} \right)$	1.608	2.5313
0.090314	0.75	4.35	$\frac{\gamma}{1 + \beta \cdot \frac{e_{new}}{t}}$	1.6218	2.504
0.08984	0.75	1.5	$\gamma^{1 - \beta \cdot \frac{e_{new}}{t}}$	1.6152	2.5118
0.08984	0.75	1.5	$\gamma^{1 + \beta \cdot \frac{e_{new}}{t}}$	2.0618	2.5112
0.088659	0.3	0.85	$\gamma^{1 - \beta \cdot \frac{e_{new}}{t}}$	1.5972	2.5383
0.090607	0.4	10	$\gamma^{1 + \beta \cdot \frac{e_{new}}{t}}$	1.6285	2.4909
0.08984	0.85	0.7	$\gamma^\beta \cdot \frac{e_{new}}{t}$	1.6154	2.5112

Table 5.27: Results of statistical analysis with free slope and the stress intensity factor obtained from the application of ENS approach on the ideal model with angular misalignment.

As the Table 5.27 shows, the following formula is characterised by the minimum σ_y standard deviation

$$k_{mis} = \gamma^{1 - \beta \cdot \frac{e_{new}}{t}} \tag{5.93}$$

with $\beta = 0.3$ and $\gamma = 0.85$.

Subsequently, the different couples of β and γ values are plotted on 3D graph in function of the standard deviation σ_y . The graph is reported in the following figure:

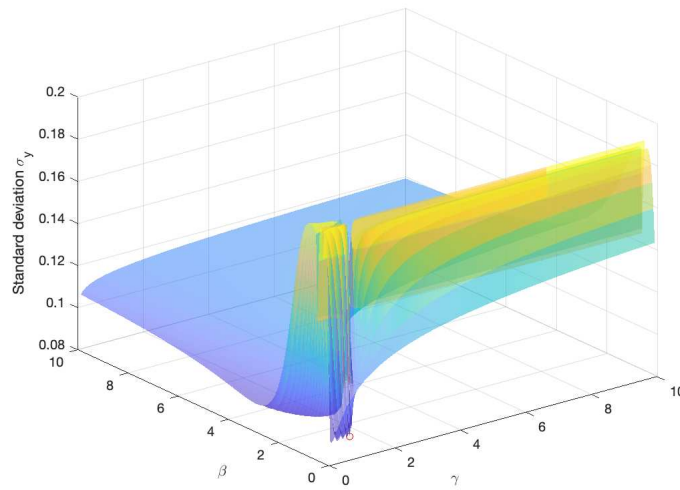


Figure 5.62: 3D surface where on the x and y axes are plotted the values of β and γ , along the z -axis is plotted the standard deviation σ_y . The red dot define the minimum value of the standard deviation.

As *Figure 5.62* shows, the minimum standard deviation is obtained for β and γ values between 0.05 and 1 for β and for γ . For this reason, another statistical analysis is done with a decrease of the definition interval of the two constant and also with a reduction of the step size, as *Figure 5.63* shows.

```
gamma=[0.05:0.001:1]';
beta=[0.05:0.001:1]';
```

Figure 5.63: Definition of the two constants in MatLab.

The results are:

- $\sigma_y = 0.067973$;
- $\beta = 0.599$;
- $\gamma = 0.998$;
- $T_\sigma = 1.6768$;
- $m = 1.7628$;

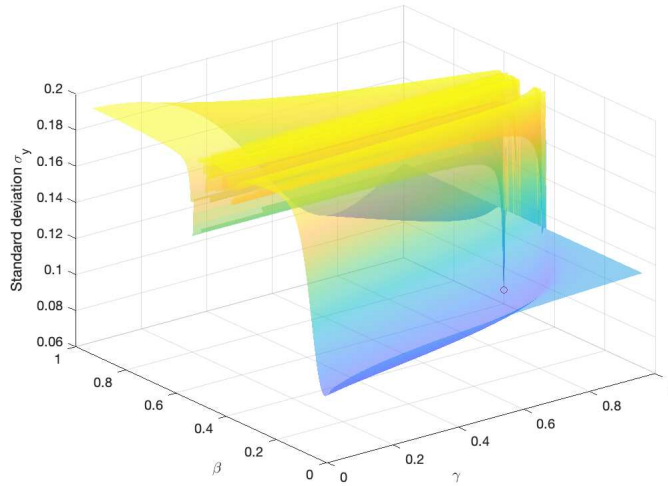


Figure 5.64: 3D surface where on the x and y axes are plotted the values of β and γ , along the z-axis is plotted the standard deviation σ_y . The red dot define the minimum value of the standard deviation.

The fatigue design curve for $\beta = 0.599$ and $\gamma = 0.998$ with a free slope is represented in the following figure:

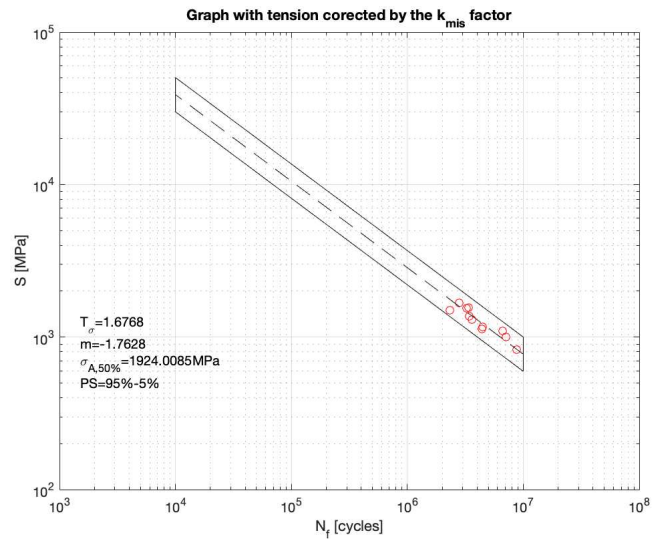


Figure 5.65: Fatigue design curve for $\beta = 0.599$ and $\gamma = 0.998$.

Subsequently, the same procedure is applied in the case of fixed slope $m = 5$. The results of statistical analysis with the stress intensity factor from the application of ENS on the ideal model with angular misalignment with a fixed slope are reported in the following table:

σ_y	β	γ	Formula of k_{mis}	T_σ	B (slope)
0.29553	0.1	7.55	$\gamma \cdot \left(1 + \beta \cdot \frac{e_{new}}{t}\right)$	2.1086	5
0.18597	0.2	6.45	$\gamma \cdot \left(1 - \beta \cdot \frac{e_{new}}{t}\right)$	1.6464	5
0.18764	1.1	8.2	$\frac{\gamma}{1 + \beta \cdot \frac{e_{new}}{t}}$	1.6538	5
0.18651	0.75	1.6	$\gamma^{1 - \beta \cdot \frac{e_{new}}{t}}$	1.6488	5
0.18651	6.85	0.95	$\gamma^{1 + \beta \cdot \frac{e_{new}}{t}}$	1.6488	5
0.18415	0.25	0.7	$\gamma^{\frac{1}{1 - \beta \cdot \frac{e_{new}}{t}}}$	1.6384	5
0.19047	0.5	10	$\gamma^{\frac{1}{1 + \beta \cdot \frac{e_{new}}{t}}}$	1.6664	5
0.18651	6.85	0.9	$\gamma^{\beta \cdot \frac{e_{new}}{t}}$	1.6464	5

Table 5.28: Results of statistical analysis with fixed slope and the stress intensity factor obtained from the application of ENS approach on the ideal model with angular misalignment.

As the Table 5.28 shows, the following formula is characterised by the minimum σ_y standard deviation

$$k_{mis} = \gamma^{\frac{1}{1 - \beta \cdot \frac{e_{new}}{t}}} \tag{5.94}$$

with $\beta = 0.25$ and $\gamma = 0.7$.

Subsequently, the different couples of β and γ values are plotted on 3D graph in function of the standard deviation σ_y . The graph is reported in the following figure:

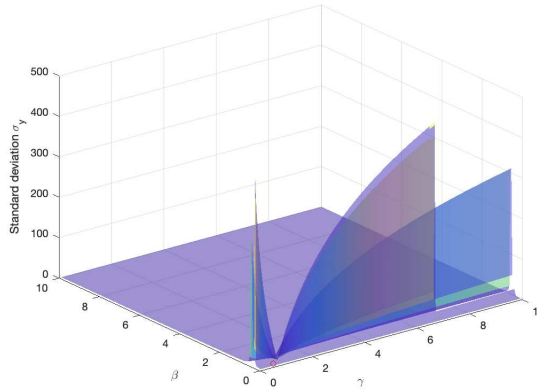


Figure 5.66: 3D surface where on the x and y axes are plotted the values of β and γ , along the z-axis is plotted the standard deviation σ_y . The red dot define the minimum value of the standard deviation.

As Figure 5.66 shows, the minimum standard deviation is obtained for β and γ values between 0.05 and 1 for β and for γ . For this reason, another statistical analysis is done with a decrease of the definition interval of the two constant and also with a reduction of the step size, as Figure 5.67 shows.

```
gamma=[0.05:0.001:1]';
beta=[0.05:0.001:1]';
```

Figure 5.67: Definition of the two constants in MatLab.

The results are:

- $\sigma_y = 0.18181$;
- $\beta = 0.391$;
- $\gamma = 0.966$;

- $T_\sigma = 1.6282$;
- $m = 5$;

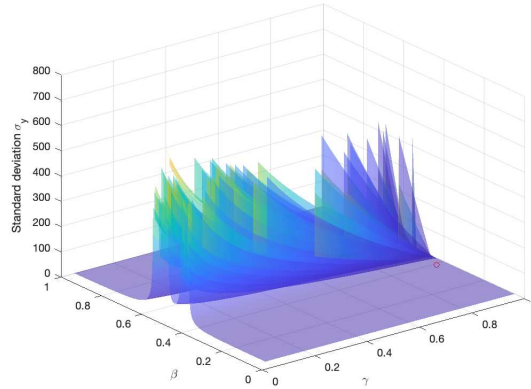


Figure 5.68: 3D surface where on the x and y axes are plotted the values of β and γ , along the z-axis is plotted the standard deviation σ_y . The red dot define the minimum value of the standard deviation.

The fatigue design curve for $\beta = 0.391$ and $\gamma = 0.966$ with a free slope is represented in the following figure:

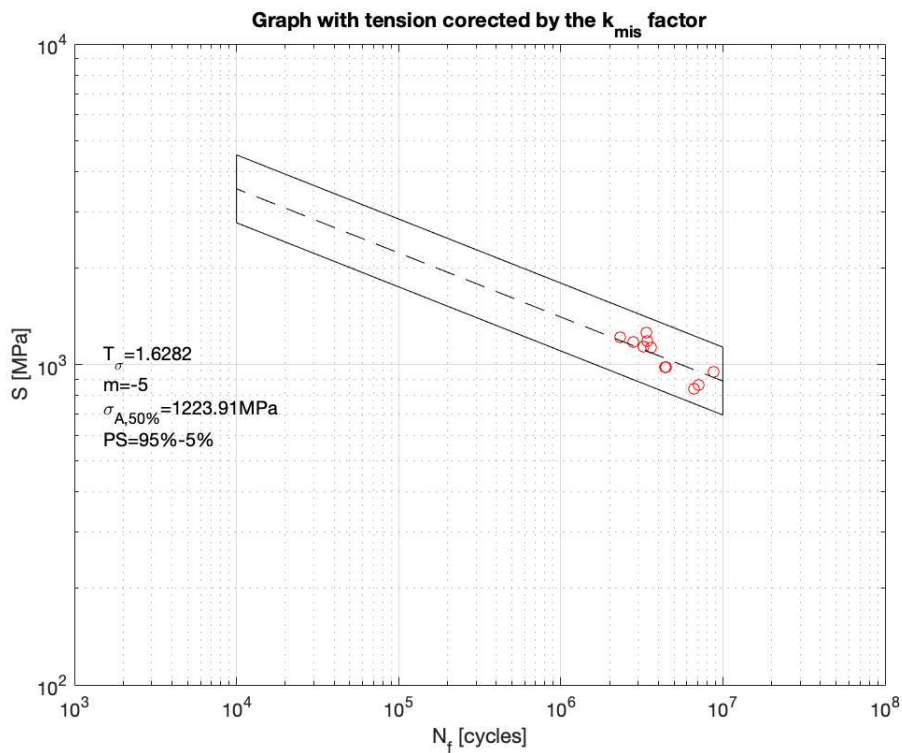


Figure 5.69: Fatigue design curve for $\beta = 0.391$ and $\gamma = 0.966$.

Results of statistical analysis with stress intensity factor from PSM approach

The results of statistical analysis with the stress intensity factor from the application of the PSM approach on the ideal model with angular misalignment with a free slope are reported in the following table:

σ_y	β	γ	Formula of k_{mis}	T_σ	B (slope)
0.12554	0.1	1.5	$\gamma \cdot \left(1 + \beta \cdot \frac{e_{new}}{t}\right)$	2.7576	1.6591
0.092684	0.2	4.7	$\gamma \cdot \left(1 - \beta \cdot \frac{e_{new}}{t}\right)$	1.652	2.4752
0.093498	0.95	7.15	$\frac{\gamma}{1 + \beta \cdot \frac{e_{new}}{t}}$	1.6638	2.4619
0.093014	6.9	1.05	$\gamma^{1 - \beta \cdot \frac{e_{new}}{t}}$	1.6558	2.4725
0.093014	3.2	0.9	$\gamma^{1 + \beta \cdot \frac{e_{new}}{t}}$	1.6557	2.4728
0.092359	0.25	0.7	$\frac{1}{\gamma^{1 - \beta \cdot \frac{e_{new}}{t}}}$	1.6419	2.4971
0.094309	0.45	10	$\frac{1}{\gamma^{1 + \beta \cdot \frac{e_{new}}{t}}}$	1.6843	2.4251
0.093014	3.2	0.9	$\gamma^{\beta \cdot \frac{e_{new}}{t}}$	1.6557	2.4728

Table 5.29: Results of statistical analysis with free slope and the stress intensity factor obtained from the application of PSM approach on the ideal model with angular misalignment.

As the Table 5.29 shows, the following formula is characterised by the minimum σ_y standard deviation

$$k_{mis} = \gamma^{\frac{1}{1 - \beta \cdot \frac{e_{new}}{t}}} \tag{5.95}$$

with $\beta = 0.25$ and $\gamma = 0.7$.

Subsequently, the different couples of β and γ values are plotted on 3D graph in function of the standard deviation σ_y . The graph is reported in the following figure:

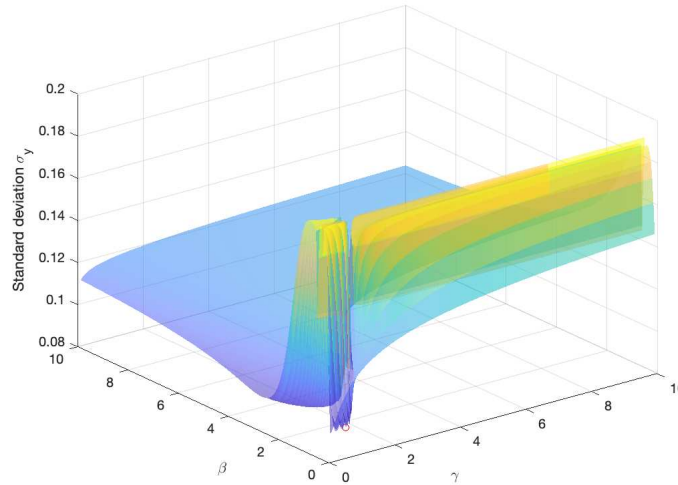


Figure 5.70: 3D surface where on the x and y axes are plotted the values of β and γ , along the z-axis is plotted the standard deviation σ_y . The red dot define the minimum value of the standard deviation.

As Figure 5.70 shows, the minimum standard deviation is obtained for β and γ values between 0.05 and 1 for β and for γ . For this reason, another statistical analysis is done with a decrease of the definition interval of the two constant and also with a reduction of the step size, as Figure 5.71 shows.

```
gamma=[0.05:0.001:1]';
beta=[0.05:0.001:1]';
```

Figure 5.71: Definition of the two constants in MatLab.

The results are:

- $\sigma_y = 0.071122$;
- $\beta = 0.599$;
- $\gamma = 0.998$;
- $T_\sigma = 1.7322$;
- $m = 1.7354$;

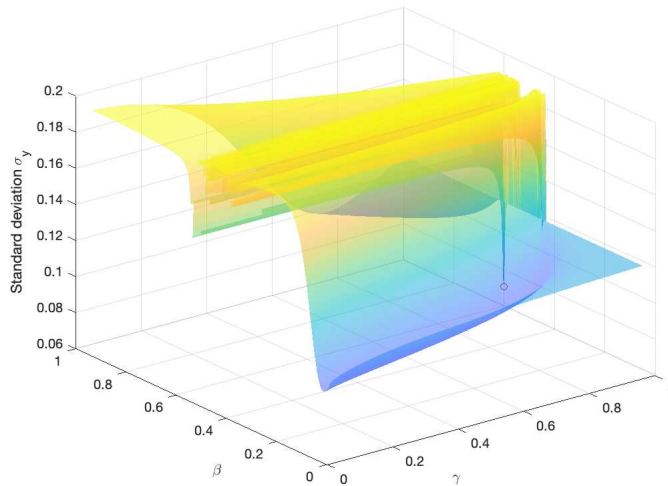


Figure 5.72: 3D surface where on the x and y axes are plotted the values of β and γ , along the z -axis is plotted the standard deviation σ_y . The red dot define the minimum value of the standard deviation.

The fatigue design curve for $\beta = 0.599$ and $\gamma = 0.998$ with a free slope is represented in the following figure:

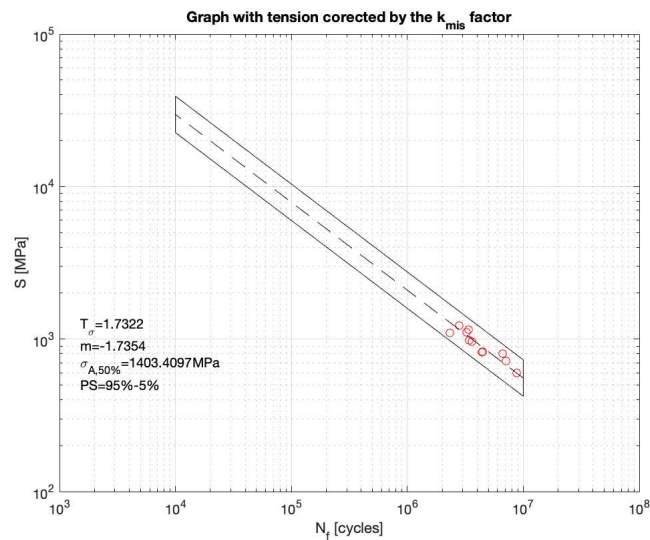


Figure 5.73: Fatigue design curve for $\beta = 0.599$ and $\gamma = 0.998$.

Subsequently, the same procedure is applied in the case of fixed slope $m = 5$. The results of statistical analysis with the stress intensity factor from the ideal model with angular misalignment with a fixed slope are reported in the following table:

σ_y	β	γ	Formula of k_{mis}	T_σ	B (slope)
0.31242	0.1	9.65	$\gamma \cdot \left(1 + \beta \cdot \frac{e_{new}}{t}\right)$	2.3109	5
0.19249	0.2	6.5	$\gamma \cdot \left(1 - \beta \cdot \frac{e_{new}}{t}\right)$	1.6755	5
0.1922	1.55	9.5	$\frac{\gamma}{1 + \beta \cdot \frac{e_{new}}{t}}$	1.6742	5
0.19102	0.2	6.9	$\gamma^{1 - \beta \cdot \frac{e_{new}}{t}}$	1.6689	5
0.19103	0.2	6.9	$\gamma^{1 + \beta \cdot \frac{e_{new}}{t}}$	1.6689	5
0.18948	0.3	0.8	$\gamma^{1 - \beta \cdot \frac{1}{e_{new}}}$	1.662	5
0,1984	0.5	10	$\gamma^{1 + \beta \cdot \frac{1}{e_{new}}}$	1.7022	5
0,19103	7.55	0.95	$\gamma^{\beta \cdot \frac{e_{new}}{t}}$	1.6689	5

Table 5.30: Results of statistical analysis with fixed slope and the stress intensity factor obtained from the application of PSM on the ideal model with angular misalignment.

As the Table 5.30 shows, the following formula is characterised by the minimum σ_y standard deviation

$$k_{mis} = \gamma^{\frac{1}{1 - \beta \cdot \frac{e_{new}}{t}}} \tag{5.96}$$

with $\beta = 0.3$ and $\gamma = 0.8$.

Subsequently, the different couples of β and γ values are plotted on 3D graph in function of the standard deviation σ_y . The graph is reported in the following figure:

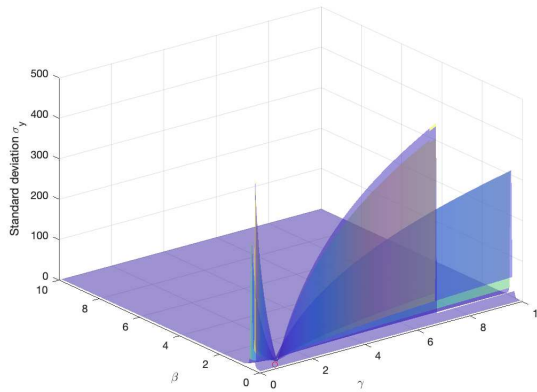


Figure 5.74: 3D surface where on the x and y axes are plotted the values of β and γ , along the z-axis is plotted the standard deviation σ_y . The red dot define the minimum value of the standard deviation.

As Figure 5.74 shows, the minimum standard deviation is obtained for β and γ values between 0.05 and 1 for β and for γ . For this reason, another statistical analysis is done with a decrease of the definition interval of the two constant and also with a reduction of the step size, as Figure 5.75 shows.

```
gamma=[0.05:0.001:1]';
beta=[0.05:0.001:1]';
```

Figure 5.75: Definition of the two constants in MatLab.

The results are:

- $\sigma_y = 0.18845$;
- $\beta = 0.338$;
- $\gamma = 0.891$;

- $T_\sigma = 1.6574$;
- $m = 5$;

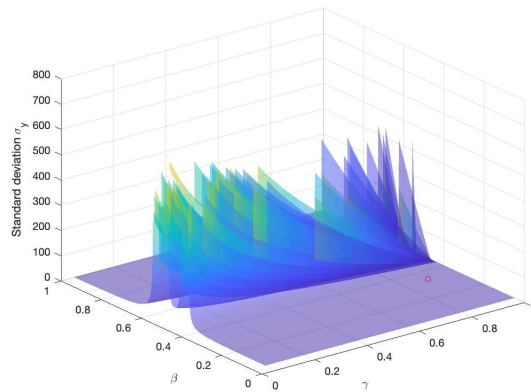


Figure 5.76: 3D surface where on the x and y axes are plotted the values of β and γ , along the z-axis is plotted the standard deviation σ_y . The red dot define the minimum value of the standard deviation.

The fatigue design curve for $\beta = 0.338$ and $\gamma = 0.891$ with a free slope is represented in the following figure:

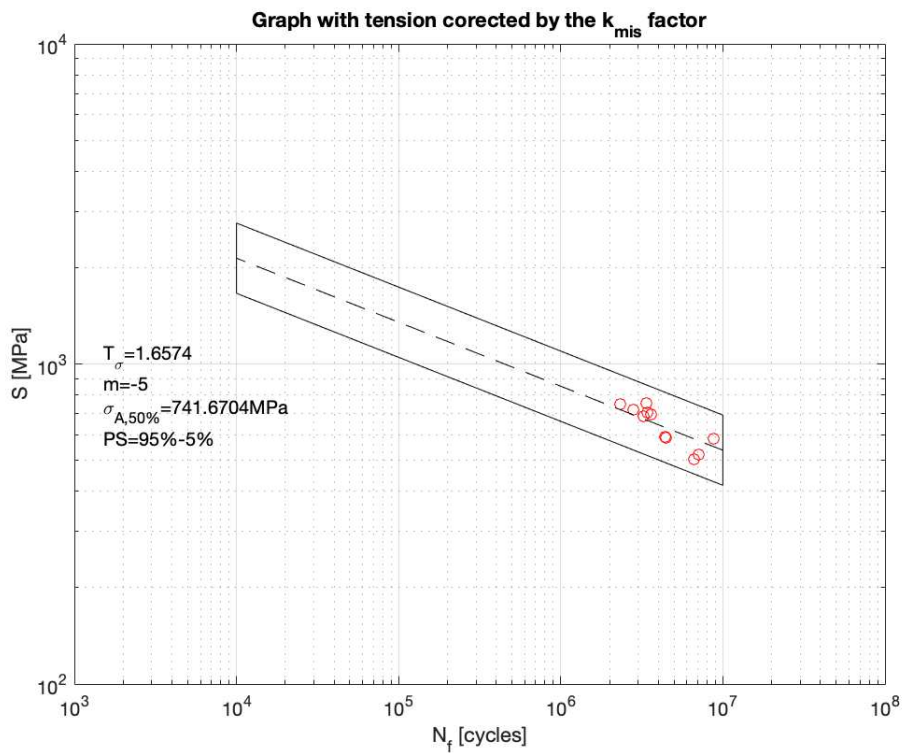


Figure 5.77: Fatigue design curve for $\beta = 0.338$ and $\gamma = 0.891$.

5.2.7 Definition of k_{mis} factor for the detection of misalignment effect for joint subjected to CAL condition

In a review of published experimental data on fatigue strength of welded joint characterised by angular or axial misalignment, subjected to Constant Amplitude Loading (CAL), 16 publications containing fatigue data for welded steel joints are analysed and studied. The objective is to define a k_{mis} factor to detect the misalignment effect on the fatigue strength of welded joint in CAL condition. The procedure is the same of that described in the paragraphs 5.2.4 and 5.2.6.

The experimental data are summarized in the following table:

Ref.	Steel type	f_y [MPa]	Stress ratio R	Plate Thickness [mm]	N° of data	Type of Joints
[49]	S1100	≥ 1100	0.1	6	20	Butt Joints
[50]	S1100	≥ 1100	0.1	8	8	Cruciform joints
[51]	BS 4369 Grade 43A	347	0	12.5	41	Cruciform joints partial pen. and fillet welds
[52]	S690	690	0.1	5	27	T-joints
[53]	DH-36	355	-1	5	57	Cruciform Joints
[54]	RAEX S275	287	0	12	11	Butt Joints
[55]	Optim 1100QC	1100	0.05 /0.1 /0.57	6	20	Butt Joints
[56]	15G ₂ ANb	370	0.5/-1	8	41	Cruciform Joints
[57]	Fe510 D1	455	0	8	8	Butt Joints
[58]	ASTM A36	250	0	12	42	Butt Joints
[59]	RAEX S275	287	0	12	32	Butt Joints
[60]	S960 MC	960	0.1/0.2	8	4	T-joints
[61]	HW-50 HW-70	580 820	0.1	20	22	Butt Joints
[62]	A36	250	0	12.5 and 15.9	19	Butt Joints
[63]	BS4260 Grade 43A	275	0	12.5	22	Butt Joints
[64]	Damex 355 MC Damex 550 MC Weldax 960	355 550 960	0	12 3 3	72	Cruciform Joints

Table 5.31: Experimental constant amplitude axial fatigue data for welded joints.

Initially, each set of experimental data is subjected to a FE analysis to obtain the stress intensity factor of each joint. Indeed, the Peak Stress Method (PSM) and Effective Notch Stress (ENS) approach are applied to detect the stress intensity factor.

In the next section, the application of these two methods are described for only one type of cruciform joint [50] and one for butt joint [54].

The cruciform joints are a non-load-carrying cruciform joints made of S1100 ultra-high-strength steels plates with the base and adjoined plate thickness of $t_0 = t_1 = 8\text{mm}$, respectively. The following figure shows the shape and the principal dimensions of the sample:

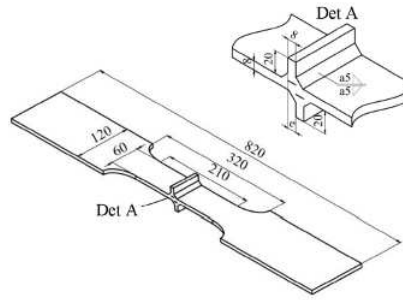


Figure 5.78: Geometry and principal dimension of the sample [50].

The boundary condition of the samples in the FE environment are displayed on the following figure:

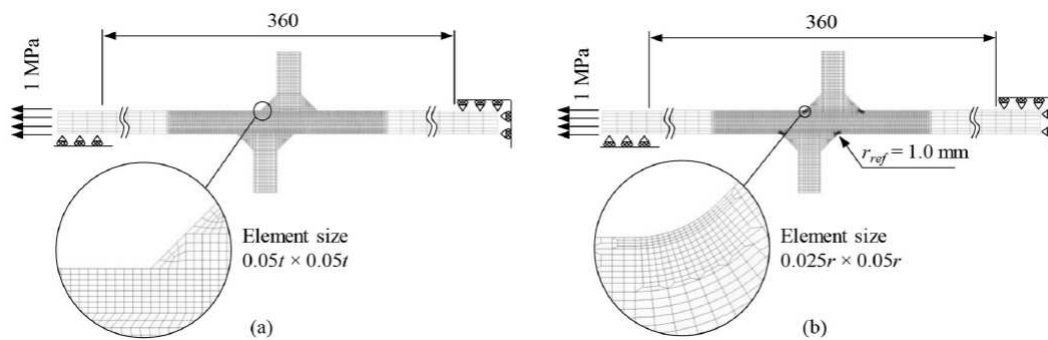


Figure 5.79: Boundary condition of the sample in the FE environment [50].

The butt joints are made of RAEX S275 low strength stress as base material. The following figure shows the shape and principal dimensions of the sample:

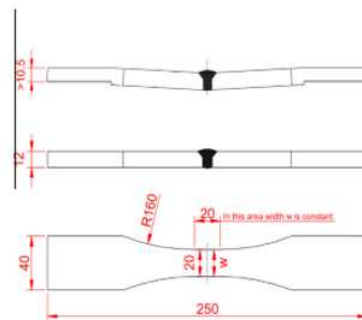


Figure 5.80: Geometry and principal dimension of the sample [54].

The boundary condition of the samples in the FE environment are displayed on the following figure:

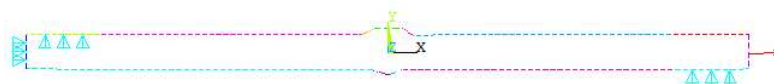


Figure 5.81: Boundary condition of the sample in the FE environment.

PSM approach for cruciform joint from [50]

The fatigue assessment for this model is performed by the application of the PSM approach for 2D structure with the adoption of four-node linear elements. The element PLANE 182 is chosen from the Ansys®APDL library with *Simple Enhanced Strain* as Key Option 1 and *Plane Strain* as Key Option 3. The model is characterised by a root with an initial opening length equal to 0.1 mm.

The weld toe is subjected to pure mode I because it is characterised by a V-notch opening angle 2α equal to 135° . The mode II at the root is neglected because is lower than the mode I. Under mode I, the PSM requirements are defined in the following table:

Element type	Mesh algorithm	Mode I			
		$(a/d)_{min}$	2α	Mesh Pattern $2\alpha < 90^\circ$	Mesh Pattern $2\alpha > 90^\circ$
Plane 182 KeyOpt:Simple Enhanced Strain + Plane Strain	Free	3	$0^\circ < 2\alpha < 135^\circ$	Four adjacent elements share the same node	Two adjacent elements share the same node

Table 5.32: Requirements for PSM.

The mode I PSM calibration constant is equal to $K_{FE}^* = 1.38 \pm 3\%$. The size of the element is obtained with the following procedure:

1. From literature the ratio $(a/d)_{min}$ is determined according to the *Table 5.32*. In this case the ratio for mode I is chosen and it is equal to 3;
2. The value of a is the reference dimension for selecting the maximal FE sizes d for PSM application and is defined as the half of the thickness t ;
3. Subsequently, the minimum element size is defined as follow:

$$d_{min} = \frac{a}{3} = \frac{4}{3} = 1.33mm \tag{5.97}$$

4. The chosen dimension of elements is 1mm.

The λ_1 and e_1 values are depended on the V-notch opening angle 2α , that is 135° for the weld toe:

2α [°]	λ_1 (Mode I)	e_1 (Mode I)
135°	0.674	0.117

Table 5.33: Value of λ_1 and e_1 in function of the opening angle 2α .

The corrective stress factors for mode I and II are calculated with the equation (2.24) for the weld toe and root. The results are reported in the *Table 5.11*.

2α [°]	f_{w1}
135°	1.0597

Table 5.34: Values of the corrective stress factor f_{w1} in function of the opening angle 2α .

Finally, the mesh can be laid on the model and the results is displayed on the *Figure 5.82*:

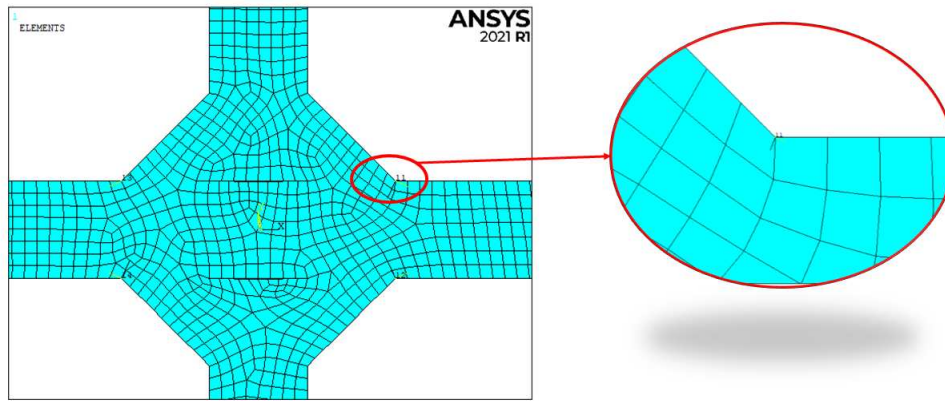


Figure 5.82: Mesh conformation with global element size $d = 1\text{mm}$.

After the application of load and constraint, the system can be solved:

Solution → *Solve* → *Current LS*

The results of the first principal stress is plotted in the *Figure 5.83*:

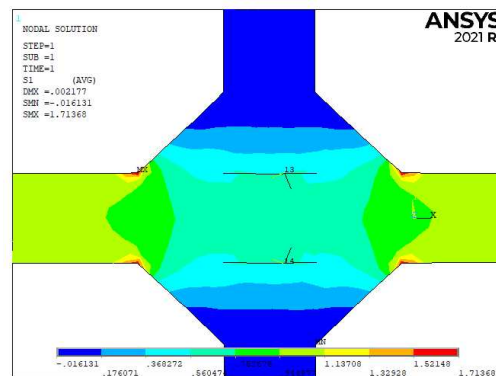


Figure 5.83: Plot of 1st principal stress for an external applied nominal stress range of 1MPa.

Local reference systems (*Figure 5.84*) are created on the nodes that represent the weld toe. The *WorkPlane* is rotated by an angle equal to 112.5° for the toe. The procedure for the creation of the local reference systems is the same as described in the paragraph 3.1.2.

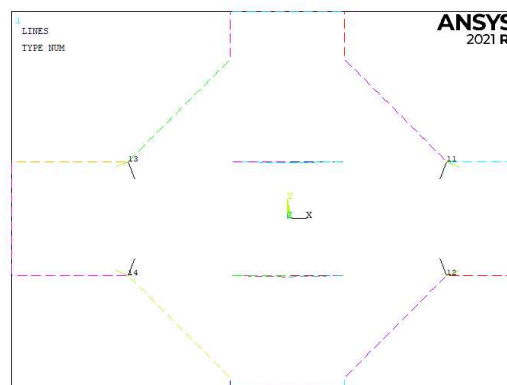


Figure 5.84: Local reference system at the weld toe and root.

Thanks to the creation of the local reference system, the tension $\Delta\sigma_{yy}$ can be extracted and the equivalent peak stresses can be calculated by the formula (2.23). The results of the all ideal model with angular misalignment are reported in the Appendix G.2.

ENS approach for cruciform joint from [50]

The fatigue assessment for this model is performed by the application of the Effective Notch Stress approach. The analysis is characterised by the using of 4-node linear element PLANE 182 with *Simple Enhanced Strain* as Key Option 1 and *Plane Strain* as Key Option 3.

To apply this approach, the *IIW Recommendations for Fatigue Assessment by Notch Stress Analysis for welded Structures* [2] is followed and the same rules of ideal model (see paragraph 5.2.3) are followed. For the worst case and practical applications, the actual radius ρ is assumed equal to zero. Thus, the ENS approach for fatigue assessment is reduced to $\rho_f = 1\text{mm}$ at weld toe or root.

To define the global element size of the model, the same rules described in the paragraph 5.2.3, are followed in this case.

For the analysis with the element PLANE 182, the global element size is equal to 0.1 mm, according to the IIW Recommendations [2]. To obtain the correct number of elements along the roots and the weld toe, two refinements are applied with depth of two elements. The mesh of the model is displayed on the following figure:

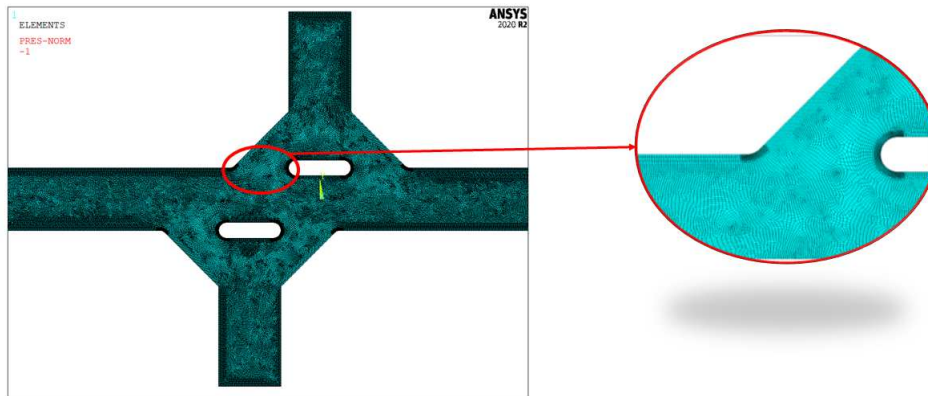


Figure 5.85: Mesh of the model with element PLANE 182.

Once the model is properly meshed, loaded and constraint, the system can be solved:

Solution → *Solve* → *Current LS*

The results of the first principal stress can be observed in the *Figure 5.86*, for an external applied pressure equal to 1 MPa:

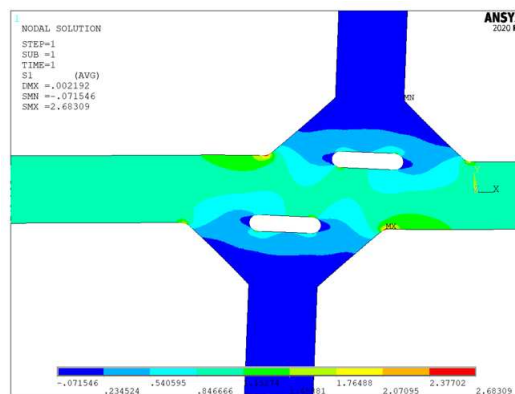


Figure 5.86: Plot of the first principal stress of ideal model with angular misalignment with element PLANE 182.

The results of the all ideal model with angular misalignment are reported in the Appendix G.2.

PSM approach for Butt joint from [54]

The fatigue assessment for this model is performed by the application of the PSM approach for 2D structure with the adoption of four-node linear elements. The element PLANE 182 is chosen from the Ansys®APDL library with *Simple Enhanced Strain* as Key Option 1 and *Plane Strain* as Key Option 3. The model is characterised by a root with an initial opening length equal to 0.1 mm.

The application of the PSM approach for the butt welded joints is described by Meneghetti, Campagnolo and Berto in [48]. The actual geometry of the weld bead is approximated in the FE models with a trapezoidal shape, defined as a function of the bead height h , width w and inclination angle 2α derived from the original papers. In this case the dimensions of the weld bead are:

h_{toe} [mm]	w_{toe} [mm]	$2\alpha_{toe}$ [°]	h_{root} [mm]	w_{root} [mm]	$2\alpha_{root}$ [°]
2.2	18.0	29	1.4	10	18

Table 5.35: Dimension weld bead.

The weld toe is subjected to pure mode I because it is characterised by a V-notch opening angle 2α equal to 150° . The mode II at the root is neglected because is lower than the mode I.

Under mode I, the PSM requirements are defined in the following table:

Element type	Mesh algorithm	Mode I			
		$(a/d)_{min}$	2α	Mesh Pattern $2\alpha < 90^\circ$	Mesh Pattern $2\alpha > 90^\circ$
Plane 182 KeyOpt:Simple Enhanced Strain + Plane Strain	Free	3	$0^\circ < 2\alpha < 135^\circ$	Four adjacent elements share the same node	Two adjacent elements share the same node

Table 5.36: Requirements for PSM.

The mode I PSM calibration constant is equal to $K_{FE}^* = 1.6682 \pm 3\%$. The size of the element is obtained with the following procedure:

1. From literature the ratio $(a/d)_{min}$ is determined according to the *Table 5.36*. In this case the ratio for mode I is chosen and it is equal to 3;
2. The value of a is the reference dimension for selecting the maximal FE sizes d for PSM application and is defined as the half of the thickness t ;
3. Subsequently, the minimum element size is defined as follow:

$$d_{min} = \frac{a}{3} = \frac{4}{3} = 1.33mm \tag{5.98}$$

4. The chosen dimension of elements is 0.5mm.

The λ_1 and e_1 values are depended on the V-notch opening angle 2α , that is 150° for the weld toe:

2α [°]	λ_1 (Mode I)	e_1 (Mode I)
150°	0.752	0.10304

Table 5.37: Value of λ_1 and e_1 in function of the opening angle 2α .

The corrective stress factors for mode I and II are calculated with the equation (2.24) for the weld toe and root. The results are reported in the *Table 5.38*.

2α [°]	f_{w1}
150°	0.9166

Table 5.38: Values of the corrective stress factor f_{w1} in function of the opening angle 2α .

Finally, the mesh can be laid on the model and the results is displayed on the *Figure 5.87*:

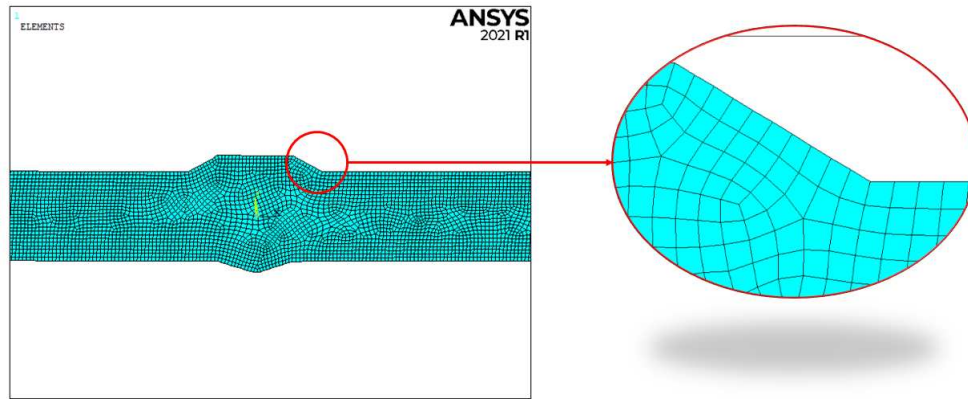


Figure 5.87: Mesh conformation with global element size $d = 0.5\text{mm}$.

After the application of load and constraint, the system can be solved:

Solution → *Solve* → *Current LS*

The results of the first principal stress is plotted in the *Figure 5.88*:

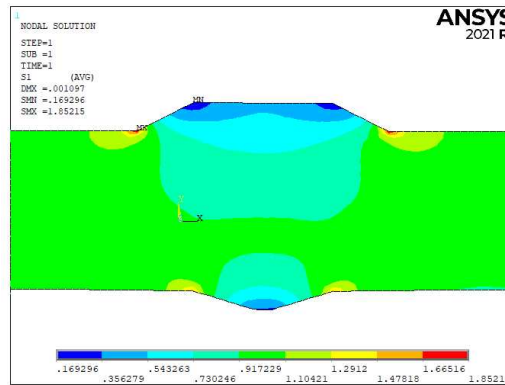


Figure 5.88: Plot of 1st principal stress for an external applied nominal stress range of 1MPa.

The maximum first principal stress $\Delta\sigma_{11,max}$ can be extracted and the equivalent peak stresses can be calculated by the formula (2.23).

The results of the all ideal model with angular misalignment are reported in the Appendix G.6.

ENS approach for Butt joint from [54]

The fatigue assessment for this model is performed by the application of the Effective Notch Stress approach. The analysis is characterised by the using of 4-node linear element PLANE 182 with *Simple Enhanced Strain* as Key Option 1 and *Plane Strain* as Key Option 3.

To apply this approach, the *IIW Recommendations for Fatigue Assessment by Notch Stress Analysis for welded Structures* [2] is followed and the same rules of ideal model (see paragraph 5.2.3) are followed . For the worst case and practical applications, the actual radius ρ is assumed equal to zero. Thus, the ENS approach for fatigue assessment is reduced to $\rho_f = 1\text{mm}$ at weld toe or root.

To define the global element size of the model, the same rules described in the paragraph 5.2.3,are followed in

this case.

For the analysis with the element PLANE 182, the global element size is equal to 0.1 mm, according to the IIW Recommendations [2]. To obtain the correct number of elements along the roots and the weld toe, two refinements are applied with depth of two elements. The mesh of the model is displayed on the following figure:

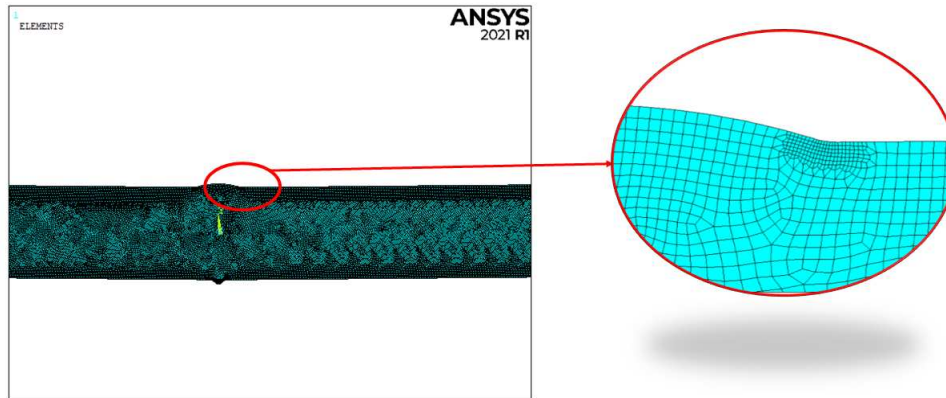


Figure 5.89: Mesh of the model with element PLANE 182.

Once the model is properly meshed, loaded and constraint, the system can be solved:

Solution → *Solve* → *Current LS*

The results of the first principal stress can be observed in the Figure 5.90, for an external applied pressure equal to 1 MPa:

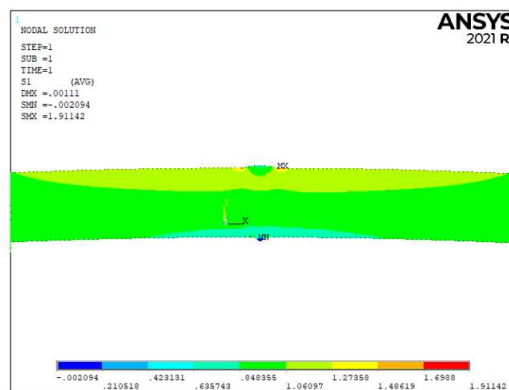


Figure 5.90: Plot of the first principal stress of ideal model with angular misalignment with element PLANE 182.

The results of the all ideal model with angular misalignment are reported in the Appendix G.6.

5.2.8 Definition of k_{mis} factor for the detection of misalignment effect in CAL condition

Initially, a statistical analysis is done without considering the misalignment factor k_{mis} . Thus, the used data are only the nominal stress and the relative fatigue life. Two different types of statistical analysis are done: the first one with a free slope; the second with a fixed slope equal to 3, typical slope value for the as-welded joints.

The results of the statistical analysis for the data used for the detection of k_{mis} when the Effective Notch Stress (ENS) method is applied to obtain the stress intensity factor are:

1. Free slope:

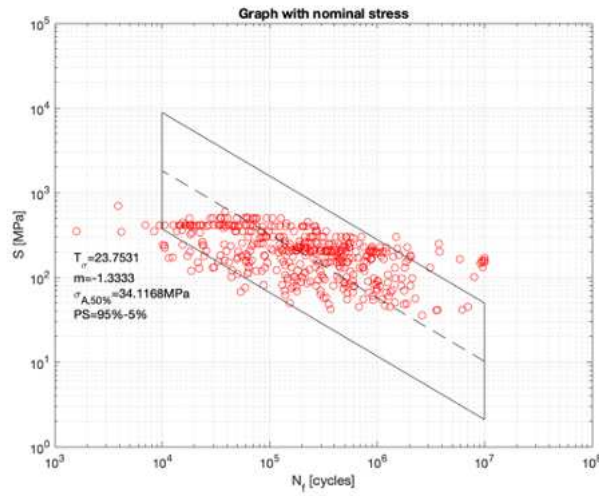


Figure 5.91: Fatigue design curve considering only the nominal stress and the relative fatigue life with free slope.

where:

- $\sigma_y = 0.5575$;
- $T_\sigma = 23.7531$;
- $m = 1.3333$.

2. Fixed slope:

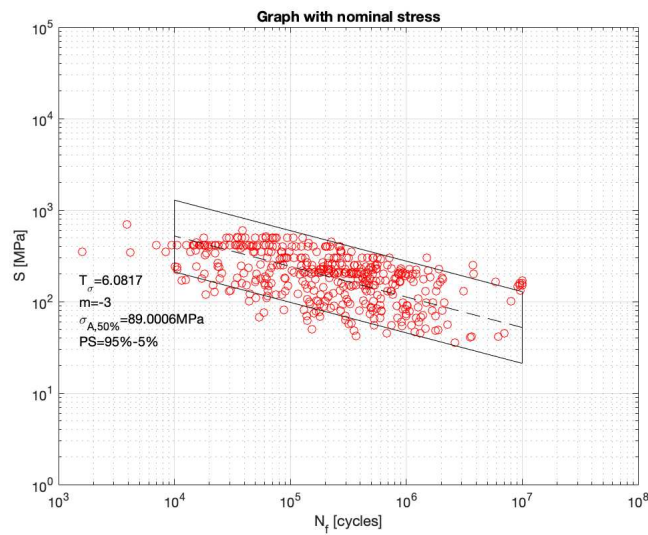


Figure 5.92: Fatigue design curve considering only the nominal stress and the relative fatigue life with fixed slope.

where:

- $\sigma_y = 0.7149$;
- $T_\sigma = 6.0817$;
- $m = 3$.

The results of the statistical analysis for the data used for the detection of k_{mis} when the Peak Stress Method (PSM) is applied to obtain the stress intensity factor are:

1. Free slope:

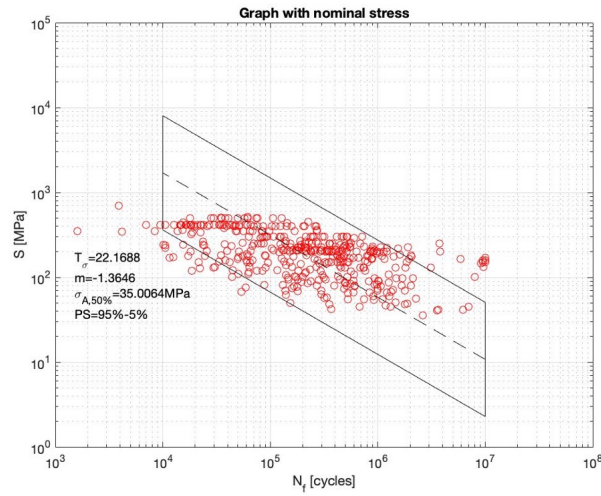


Figure 5.93: Fatigue design curve considering only the nominal stress and the relative fatigue life with free slope.

where:

- $\sigma_y = 0.5582$;
- $T_\sigma = 22.1688$;
- $m = 1.3646$.

2. Fixed slope:

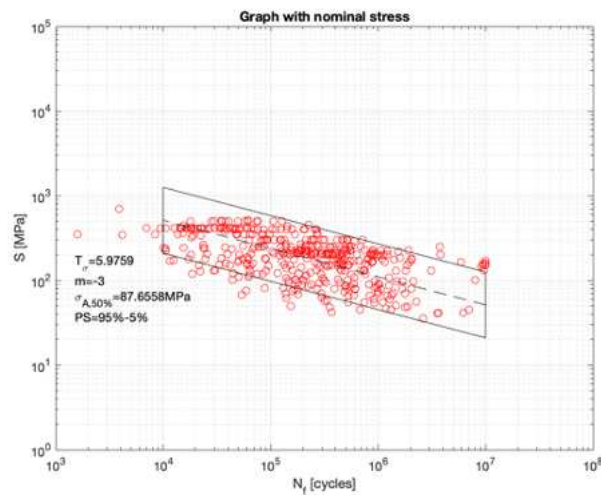


Figure 5.94: Fatigue design curve considering only the nominal stress and the relative fatigue life with fixed slope.

where:

- $\sigma_y = 0.7080$;
- $T_\sigma = 5.9759$;
- $m = 3$.

The procedure to define the expression of the k_{mis} factor in CAL condition is the same as that described in the paragraph 5.2.6 for VAL condition.

The steps of the procedure to obtain the correct definition of the k_{mis} factor are:

1. Firstly, the experimental data used for the evaluation of k_{mis} factor are multiplied for a stress intensity factors calculated for each specimen from FE analysis. These factors are obtained from the application of the Effective Notch Stress method and PSM approach on the ideal model with angular misalignment (see paragraph 5.2.7). Subsequently, these values are multiplied also for the k_{mis} factor that consider the misalignment effect:

$$\sigma_{max,mis} = \sigma_{max} \cdot K_{s,ENS/PSM} \cdot k_{mis} \quad (5.99)$$

2. There are two different types of misalignment:

- Axial misalignment e ;
- Angular misalignment α .

The angular misalignment is converted in axial misalignment with the following formula:

$$e_{tot} = \frac{l}{2} \cdot \tan(\alpha_{tot}) \quad (5.100)$$

where l is the total length of the sample. Thus, the total misalignment is defined as following:

$$e_{new} = e + \frac{l}{2} \cdot \tan(\alpha_{tot}) \quad (5.101)$$

The results of each joints are reported in the Appendix G.

3. The expressions use for the detection of k_{mis} factor are the following:

$$k_{mis} = \gamma \cdot \left(1 + \beta \cdot \frac{e_{tot}}{t} \right) \quad (5.102)$$

$$k_{mis} = \gamma \cdot \left(1 - \beta \cdot \frac{e_{tot}}{t} \right) \quad (5.103)$$

$$k_{mis} = \frac{\gamma}{1 + \beta \cdot \frac{e_{tot}}{t}} \quad (5.104)$$

$$k_{mis} = \gamma^{1 - \beta \cdot \frac{e_{tot}}{t}} \quad (5.105)$$

$$k_{mis} = \gamma^{1 + \beta \cdot \frac{e_{tot}}{t}} \quad (5.106)$$

$$k_{mis} = \gamma^{\frac{1}{1 - \beta \cdot \frac{e_{tot}}{t}}} \quad (5.107)$$

$$k_{mis} = \gamma^{\frac{1}{1 + \beta \cdot \frac{e_{tot}}{t}}} \quad (5.108)$$

$$k_{mis} = \gamma^{\beta \cdot \frac{e_{tot}}{t}} \quad (5.109)$$

4. The two constants β and γ are systematically changed to determine which values would result in a minimum standard deviation σ_y for the data. The range of variation for both is between 0.1 and 10 with step-size equal to 0.05;
5. For each expression of the k_{mis} factor, the minimum standard deviation σ_y , the corresponding T_σ and slope B are extracted. The results are reported in the following subsection and two statistical analysis are conducted: the first one with a free slope; the second with a fixed slope equal to 3, that is the typical value of the slope of the design curve for the as-welded joints. The analysis is done through a MatLab code that is the same as that used in the paragraph 5.2.6.

Results of statistical analysis with stress intensity factor from ENS approach

The results of statistical analysis with the stress intensity factor from the application of the ENS approach on FE model with misalignment with a free slope are reported in the following table:

σ_y	β	γ	Formula of k_{mis}	T_σ	B (slope)
0.38635	0.1	2.9	$\gamma \cdot \left(1 + \beta \cdot \frac{e_{tot}}{t}\right)$	3.5409	2.3148
0.37434	0.15	1.05	$\gamma \cdot \left(1 - \beta \cdot \frac{e_{tot}}{t}\right)$	3.1607	2.4642
0.37359	0.2	5.3	$\frac{\gamma}{1 + \beta \cdot \frac{e_{tot}}{t}}$	3.1374	2.4752
0.374	0.1	5.3	$\gamma^{1 - \beta \cdot \frac{e_{tot}}{t}}$	3.1525	2.4675
0.374	3.25	0.95	$\gamma^{1 + \beta \cdot \frac{e_{tot}}{t}}$	3.1521	2.4678
0.37444	0.1	0.25	$\gamma^{\frac{1}{1 - \beta \cdot \frac{e_{tot}}{t}}}$	3.1665	2.461
0.36617	1.35	1.25	$\gamma^{\frac{1}{1 + \beta \cdot \frac{e_{tot}}{t}}}$	3.0532	2.4852
0.374	3.25	0.95	$\gamma^{\beta \cdot \frac{e_{tot}}{t}}$	3.1521	2.4678

Table 5.39: Results of statistical analysis with free slope and the stress intensity factor obtained from the application of ENS approach on FE model with misalignment.

As the Table 5.39 shows, the following formula is characterised by the minimum σ_y standard deviation

$$k_{mis} = \gamma^{\frac{1}{1 + \beta \cdot \frac{e_{tot}}{t}}} \tag{5.110}$$

with $\beta = 1.35$ and $\gamma = 1.25$.

Subsequently, the different couples of β and γ values are plotted on 3D graph in function of the standard deviation σ_y . The graph is reported in the following figure:

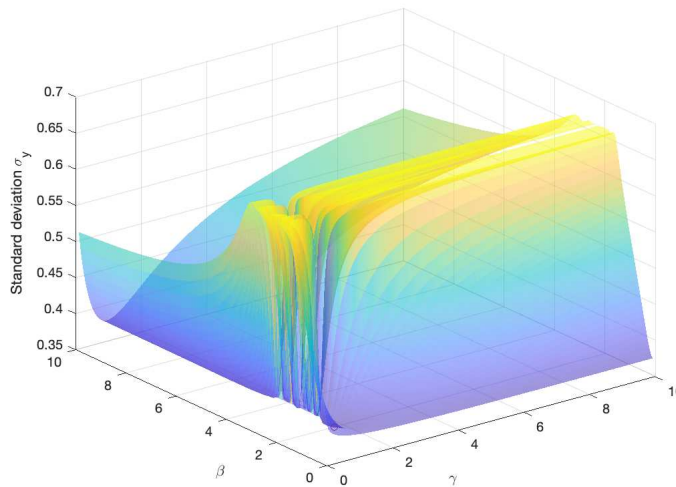


Figure 5.95: 3D surface where on the x and y axes are plotted the values of β and γ , along the z-axis is plotted the standard deviation σ_y . The red dot define the minimum value of the standard deviation.

As Figure 5.95 shows, the minimum standard deviation is obtained for β and γ values between 1 and 2 for β and γ . For this reason, another statistical analysis is done with a decrease of the definition interval of the two constant and also with a reduction of the step size, as Figure 5.96 shows.

```
beta=[1:0.001:2]';
gamma=[1:0.001:2]';
```

Figure 5.96: Definition of the two constants in MatLab.

The results are:

- $\sigma_y = 0.36615$;
- $\beta = 1.342$;
- $\gamma = 1.266$;
- $T_\sigma = 3.0504$;
- $m = 2.4871$;

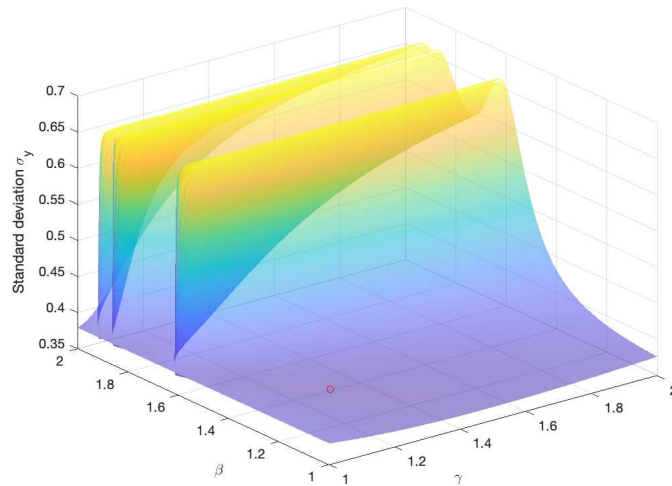


Figure 5.97: 3D surface where on the x and y axes are plotted the values of β and γ , along the z-axis is plotted the standard deviation σ_y . The red dot define the minimum value of the standard deviation.

The fatigue design curve for $\beta = 1.342$ and $\gamma = 1.266$ with a free slope is represented in the following figure:

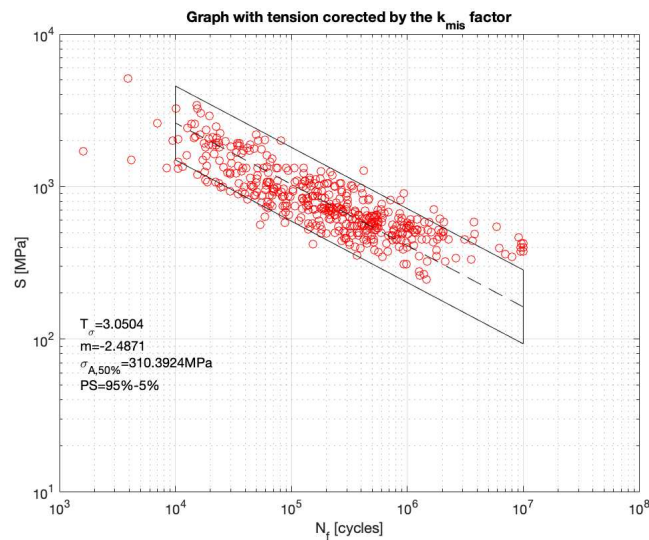


Figure 5.98: Fatigue design curve for $\beta = 1.342$ and $\gamma = 1.266$.

Subsequently, the same procedure is applied in the case of fixed slope $m = 3$. The results of statistical analysis with the stress intensity factor from the actual model with a fixed slope are reported in the following table:

σ_y	β	γ	Formula of k_{mis}	T_σ	B (slope)
0.41791	0.1	1.35	$\gamma \cdot \left(1 + \beta \cdot \frac{\epsilon_{tot}}{t}\right)$	2.8728	3
0.39276	0.15	2.8	$\gamma \cdot \left(1 - \beta \cdot \frac{\epsilon_{tot}}{t}\right)$	2.696	3
0.39069	0.25	2.45	$\frac{\gamma}{1 + \beta \cdot \frac{\epsilon_{tot}}{t}}$	2.682	3
0.39165	0.1	8.05	$\gamma^{1 - \beta \cdot \frac{\epsilon_{tot}}{t}}$	2.6885	3
0.39165	0.15	0.25	$\gamma^{1 + \beta \cdot \frac{\epsilon_{tot}}{t}}$	2.6885	3
0.39258	0.1	0.15	$\gamma^{\frac{1}{1 - \beta \cdot \frac{\epsilon_{tot}}{t}}}$	2.6948	3
0.38288	1.2	1.4	$\gamma^{\frac{1}{1 + \beta \cdot \frac{\epsilon_{tot}}{t}}}$	2.6296	3
0.39165	0.15	0.25	$\gamma^{\beta \cdot \frac{\epsilon_{tot}}{t}}$	2.6885	3

Table 5.40: Results of statistical analysis with fixed slope and the stress intensity factor obtained from the application of ENS approach on the FE model with misalignment.

As the Table 5.40 shows, the following formula is characterised by the minimum σ_y standard deviation

$$k_{mis} = \gamma^{\frac{1}{1 + \beta \cdot \frac{\epsilon_{tot}}{t}}} \tag{5.111}$$

with $\beta = 1.2$ and $\gamma = 1.4$.

Subsequently, the different couples of β and γ values are plotted on 3D graph in function of the standard deviation σ_y . The graph is reported in the following figure:

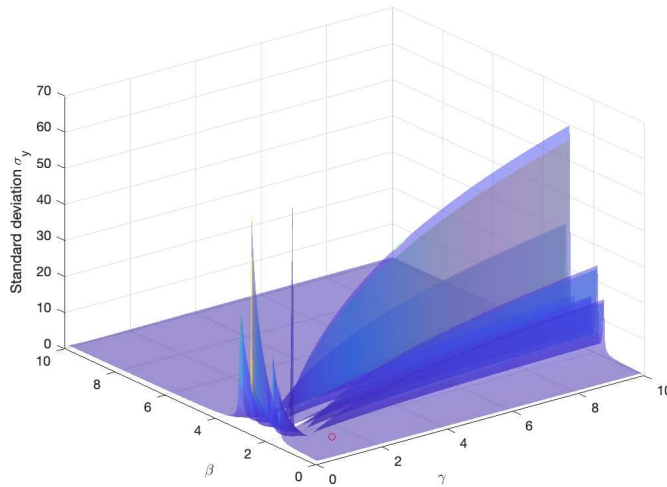


Figure 5.99: 3D surface where on the x and y axes are plotted the values of β and γ , along the z-axis is plotted the standard deviation σ_y . The red dot define the minimum value of the standard deviation.

As Figure 5.99 shows, the minimum standard deviation is obtained for β and γ values between 1 and 2 for β and γ . For this reason, another statistical analysis is done with a decrease of the definition interval of the two constant and also with a reduction of the step size, as Figure 5.100 shows.

```
beta=[1:0.001:2]';
gamma=[1:0.001:2]';
```

Figure 5.100: Definition of the two constants in MatLab.

The results are:

- $\sigma_y = 0.38286$;

- $\beta = 1.224$;
- $\gamma = 1.374$;
- $T_\sigma = 2.6295$;
- $m = 3$;

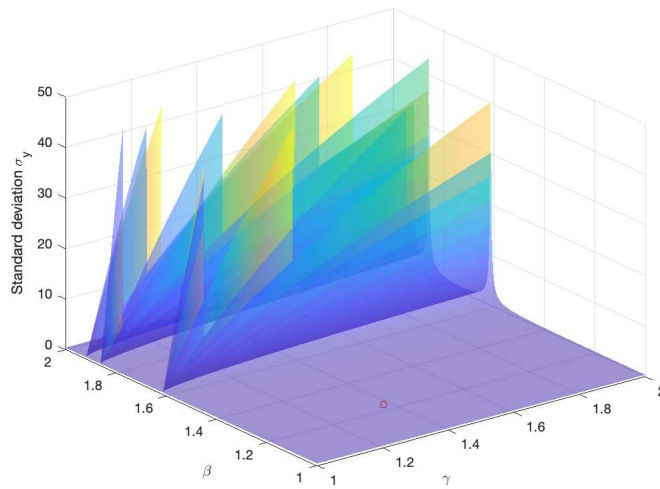


Figure 5.101: 3D surface where on the x and y axes are plotted the values of β and γ , along the z-axis is plotted the standard deviation σ_y . The red dot define the minimum value of the standard deviation.

The fatigue design curve for $\beta = 1.224$ and $\gamma = 1.374$ with a fixed slope is represented in the following figure:

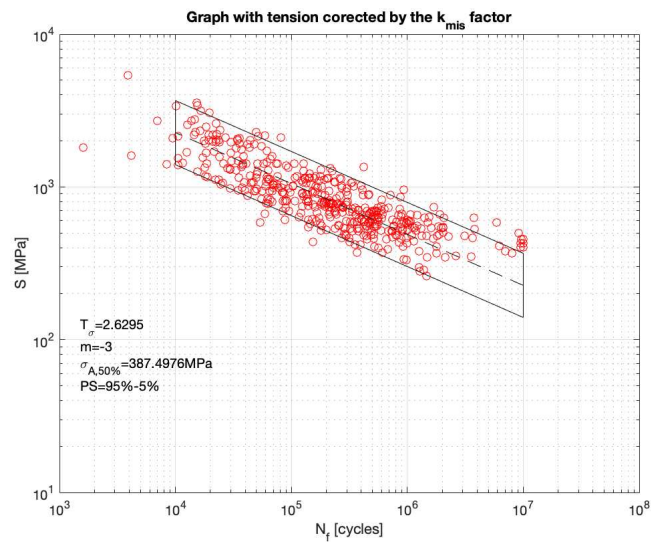


Figure 5.102: Fatigue design curve for $\beta = 1.224$ and $\gamma = 1.374$.

Results of statistical analysis with stress intensity factor from PSM approach

The results of statistical analysis with the stress intensity factor from the application of the PSM approach on the FE model with misalignment with a free slope are reported in the following table:

σ_y	β	γ	Formula of k_{mis}	T_σ	B (slope)
0.37426	0.1	9.2	$\gamma \cdot \left(1 + \beta \cdot \frac{e_{tot}}{t} \right)$	3.1611	2.4635
0.37266	0.1	5.9	$\gamma \cdot \left(1 - \beta \cdot \frac{e_{tot}}{t} \right)$	3.0394	2.5395
0.37238	0.1	9.85	$\frac{\gamma}{1 + \beta \cdot \frac{e_{tot}}{t}}$	3.0388	2.5381
0.37152	0.3	1.1	$\gamma^{1 - \beta \cdot \frac{e_{tot}}{t}}$	3.054	2.5208
0.37152	0.1	0.75	$\gamma^{1 + \beta \cdot \frac{e_{tot}}{t}}$	3.05387	2.5209
0.37138	0.6	0.95	$\frac{1}{\gamma^{1 - \beta \cdot \frac{e_{tot}}{t}}}$	3.0015	2.5597
0.37153	0.1	1.35	$\frac{1}{\gamma^{1 + \beta \cdot \frac{e_{tot}}{t}}}$	3.0549	2.5203
0.37152	0.1	0.75	$\gamma^{\beta \cdot \frac{e_{tot}}{t}}$	3.054	2.5209

Table 5.41: Results of statistical analysis with free slope and the stress intensity factor obtained from the application of PSM approach on the FE model with misalignment.

As the Table 5.41 shows, the following formula is characterised by the minimum σ_y standard deviation

$$k_{mis} = \gamma^{1 - \beta \cdot \frac{e_{tot}}{t}} \tag{5.112}$$

with $\beta = 0.6$ and $\gamma = 0.95$.

Subsequently, the different couples of β and γ values are plotted on 3D graph in function of the standard deviation σ_y . The graph is reported in the following figure:

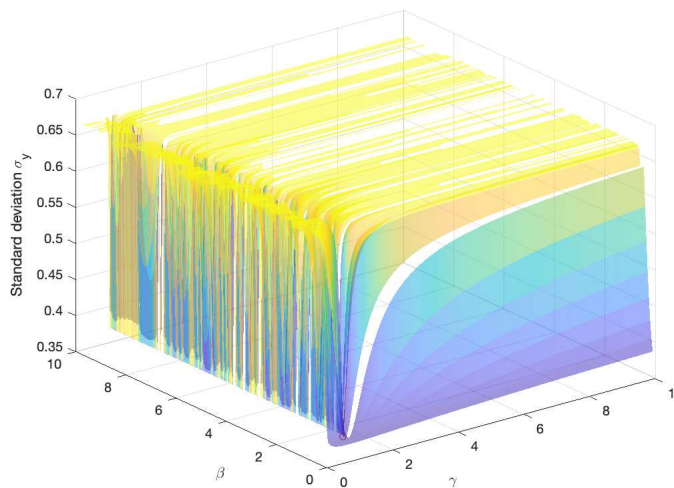


Figure 5.103: 3D surface where on the x and y axes are plotted the values of β and γ , along the z-axis is plotted the standard deviation σ_y . The red dot define the minimum value of the standard deviation.

As Figure 5.103 shows, the minimum standard deviation is obtained for β and γ values between 0.05 and 1 for β and γ . For this reason, another statistical analysis is done with a decrease of the definition interval of the two constant and also with a reduction of the step size, as Figure 5.104 shows.

```
beta=[0.05:0.001:1]';
gamma=[0.05:0.001:1]';
```

Figure 5.104: Definition of the two constants in MatLab.

The results are:

- $\sigma_y = 0.36985$;
- $\beta = 0.659$;
- $\gamma = 0.996$;
- $T_\sigma = 3.0143$;
- $m = 2.5394$;

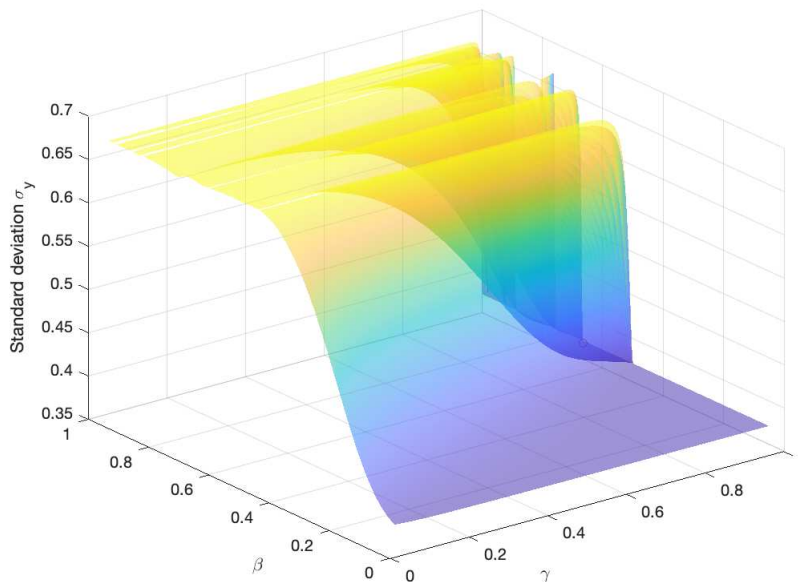


Figure 5.105: 3D surface where on the x and y axes are plotted the values of β and γ , along the z-axis is plotted the standard deviation σ_y . The red dot define the minimum value of the standard deviation.

The fatigue design curve for $\beta = 0.659$ and $\gamma = 0.996$ with a free slope is represented in the following figure:

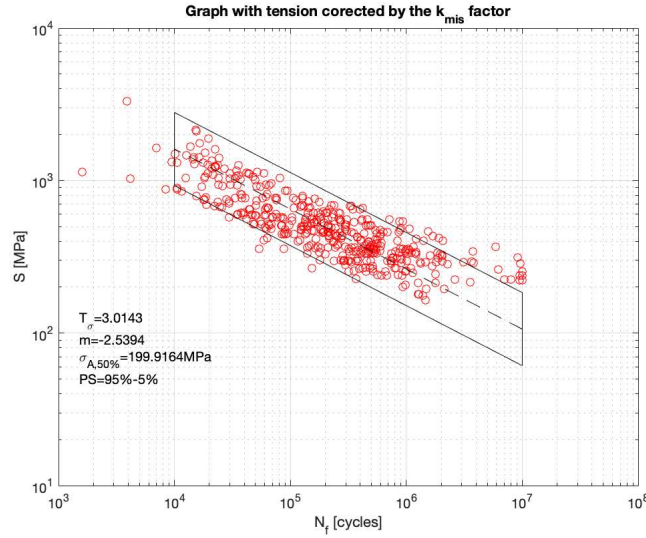


Figure 5.106: Fatigue design curve for $\beta = 0.659$ and $\gamma = 0.996$.

Subsequently, the same procedure is applied in the case of fixed slope $m = 3$. The results of statistical analysis with the stress intensity factor from the actual model with a fixed slope are reported in the following table:

σ_y	β	γ	Formula of k_{mis}	T_σ	B (slope)
0.39303	0.1	1	$\gamma \cdot \left(1 + \beta \cdot \frac{e_{tot}}{t}\right)$	2.6979	3
0.38587	0.1	6.7	$\gamma \cdot \left(1 - \beta \cdot \frac{e_{tot}}{t}\right)$	2.6495	3
0.3857	0.1	7.45	$\frac{\gamma}{1 + \beta \cdot \frac{e_{tot}}{t}}$	2.6484	3
0.3857	0.4	1.2	$\gamma^{1 - \beta \cdot \frac{e_{tot}}{t}}$	2.6475	3
0.38557	0.45	0.85	$\gamma^{1 + \beta \cdot \frac{e_{tot}}{t}}$	2.6475	3
0.38336	0.6	0.95	$\gamma^{\frac{1}{1 - \beta \cdot \frac{e_{tot}}{t}}}$	2.6328	3
0.38558	0.1	2.25	$\gamma^{\frac{1}{1 + \beta \cdot \frac{e_{tot}}{t}}}$	2.6554	3
0.38557	0.45	0.85	$\gamma^{\beta \cdot \frac{e_{tot}}{t}}$	2.6475	3

Table 5.42: Results of statistical analysis with fixed slope and the stress intensity factor obtained from the application of PSM on the FE model with misalignment.

As the Table 5.42 shows, the following formula is characterised by the minimum σ_y standard deviation

$$k_{mis} = \gamma^{\frac{1}{1 - \beta \cdot \frac{e_{tot}}{t}}} \tag{5.113}$$

with $\beta = 0.6$ and $\gamma = 0.95$.

Subsequently, the different couples of β and γ values are plotted on 3D graph in function of the standard deviation σ_y . The graph is reported in the following figure:

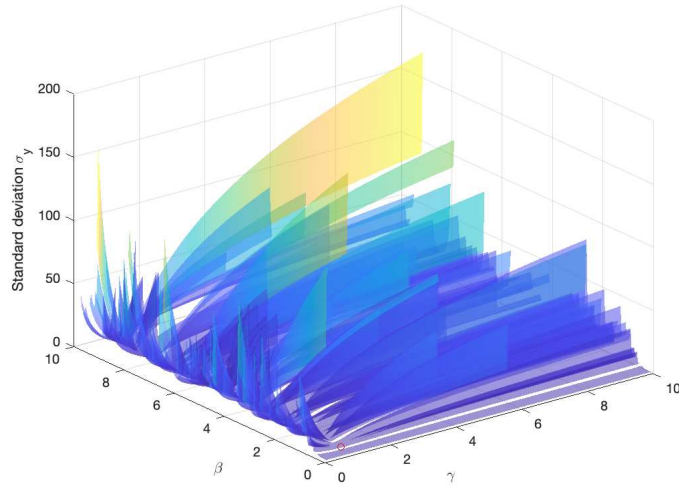


Figure 5.107: 3D surface where on the x and y axes are plotted the values of β and γ , along the z -axis is plotted the standard deviation σ_y . The red dot define the minimum value of the standard deviation.

As Figure 5.107 shows, the minimum standard deviation is obtained for β and γ values between 0.05 and 1 for β and γ . For this reason, another statistical analysis is done with a decrease of the definition interval of the two constant and also with a reduction of the step size, as Figure 5.108 shows.

```
beta=[0.05:0.001:1]';
gamma=[0.05:0.001:1]';
```

Figure 5.108: Definition of the two constants in MatLab.

The results are:

- $\sigma_y = 0.38267$;
- $\beta = 0.630$;
- $\gamma = 0.975$;
- $T_\sigma = 2.6282$;
- $m = 3$;

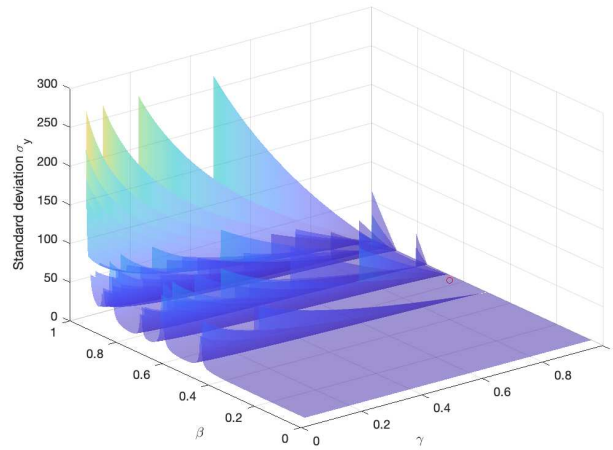


Figure 5.109: 3D surface where on the x and y axes are plotted the values of β and γ , along the z-axis is plotted the standard deviation σ_y . The red dot define the minimum value of the standard deviation.

The fatigue design curve for $\beta = 0.630$ and $\gamma = 0.975$ with a fixed slope is represented in the following figure:

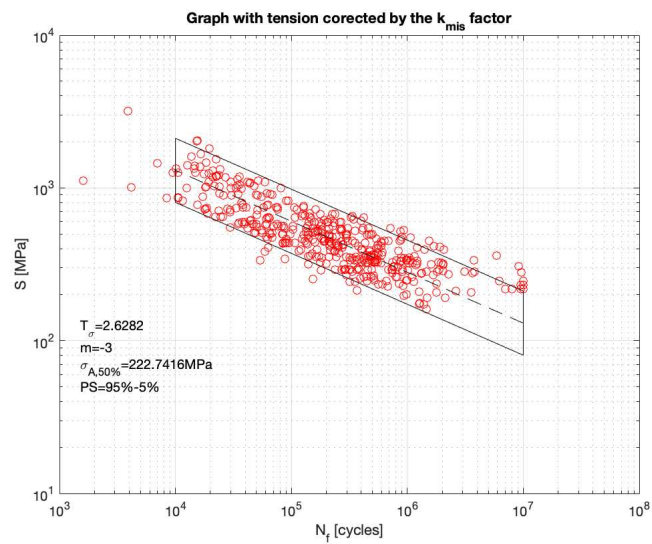


Figure 5.110: Fatigue design curve for $\beta = 0.630$ and $\gamma = 0.975$.

Comparison of the results

The results of the statistical analysis with the k_{mis} factor are compared with the initially results of the statistical analysis of the nominal stress and the relative fatigue life. These comparisons are reported in the following table:

ENS (Free slope)

<i>Without k_{mis}</i>		<i>With k_{mis}</i>		$\Delta\%$
T_σ	23.7531	T_σ	3.0504	-87.16%
σ_y	0.5575	σ_y	0.36615	-34.32%

Table 5.43: Comparison of the ENS results with free slope.

$$k_{mis} = \gamma^{\frac{1}{1+\beta \cdot \frac{e_{tot}}{T}}} \tag{5.114}$$

where:

- $\beta = 1.342$;
- $\gamma = 1.266$.

ENS (Fixed slope $m=3$)

<i>Without k_{mis}</i>		<i>With k_{mis}</i>		$\Delta\%$
T_σ	6.0817	T_σ	2.6295	-56.76%
σ_y	0.7149	σ_y	0.38286	-46.45%

Table 5.44: Comparison of the ENS results with fixed slope.

$$k_{mis} = \gamma^{\frac{1}{1+\beta \cdot \frac{e_{tot}}{T}}} \tag{5.115}$$

where:

- $\beta = 1.224$;
- $\gamma = 1.374$.

PSM (Free slope)

<i>Without k_{mis}</i>		<i>With k_{mis}</i>		$\Delta\%$
T_σ	22.1688	T_σ	3.0143	-86.40%
σ_y	0.5582	σ_y	0.36985	-33.74%

Table 5.45: Comparison of the PSM results with free slope.

$$k_{mis} = \gamma^{\frac{1}{1-\beta \cdot \frac{e_{tot}}{T}}} \tag{5.116}$$

where:

- $\beta = 0.659$;
- $\gamma = 0.996$.

PSM (Fixed slope $m=3$)				
Without k_{mis}		With k_{mis}		$\Delta\%$
T_σ	5.9759	T_σ	2.6282	-56.02%
σ_y	0.7080	σ_y	0.38267	-45.95%

Table 5.46: Comparison of the PSM results with fixed slope.

$$k_{mis} = \gamma^{1-\beta \cdot \frac{\sigma}{T}} \tag{5.117}$$

where:

- $\beta = 0.630$;
- $\gamma = 0.975$.

As the tables show, the consideration of the k_{mis} factor decreases the value of the standard deviation and the width of the scatter band. Furthermore, the expression of k_{mis} factor when the stress intensity factor obtained by the application of the ENS approach is the same for the free and fixed slope, with the value of two constant β and γ that are roughly the same. The same consideration can be done for the k_{mis} factor when the stress intensity factor obtained by the application of the PSM approach. In the next figures, the design fatigue curve are reported and the reader are able to recognize the different set of data.

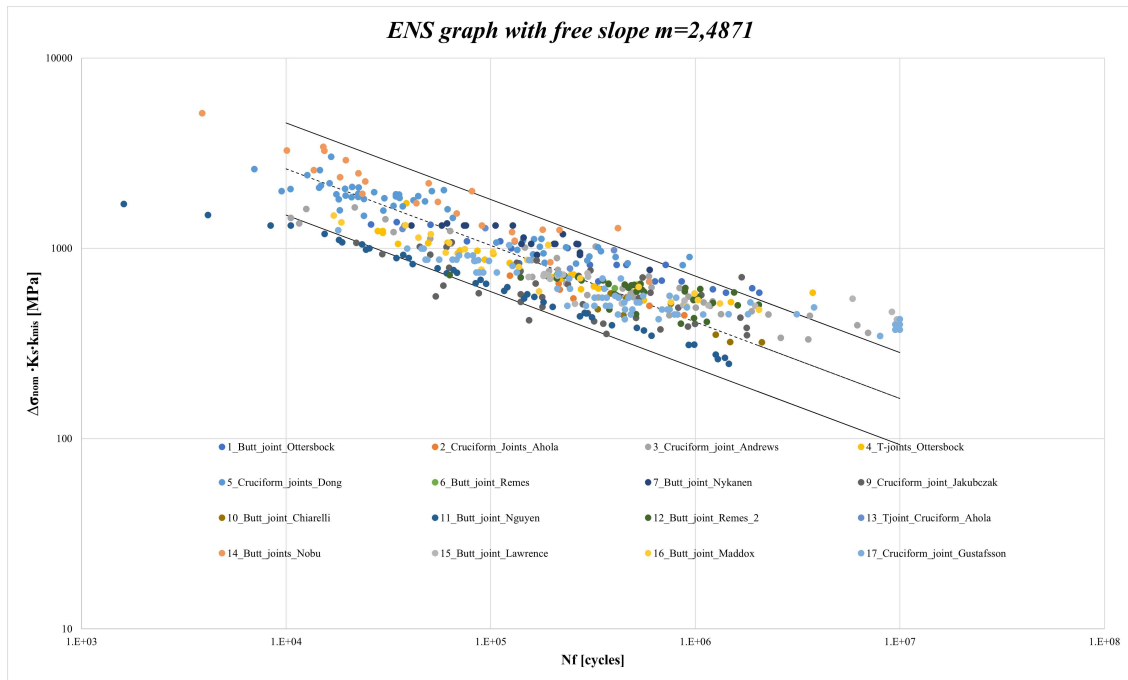


Figure 5.111: ENS Fatigue design curve for $\beta = 1.342$ and $\gamma = 1.266$ with free slope.

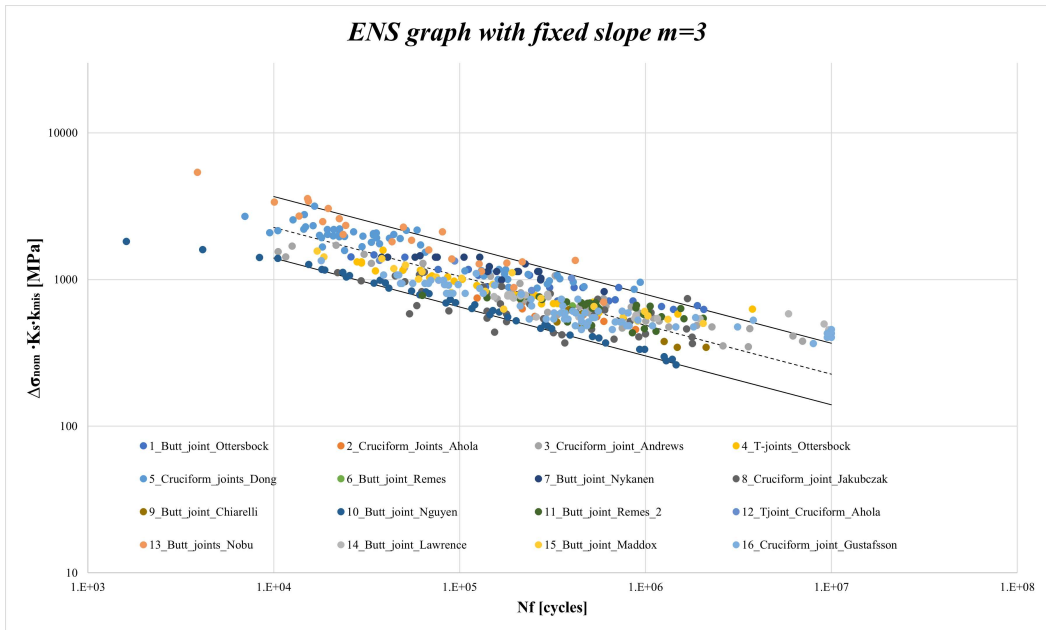


Figure 5.112: ENS Fatigue design curve for $\beta = 1.224$ and $\gamma = 1.374$ with fixed slope.

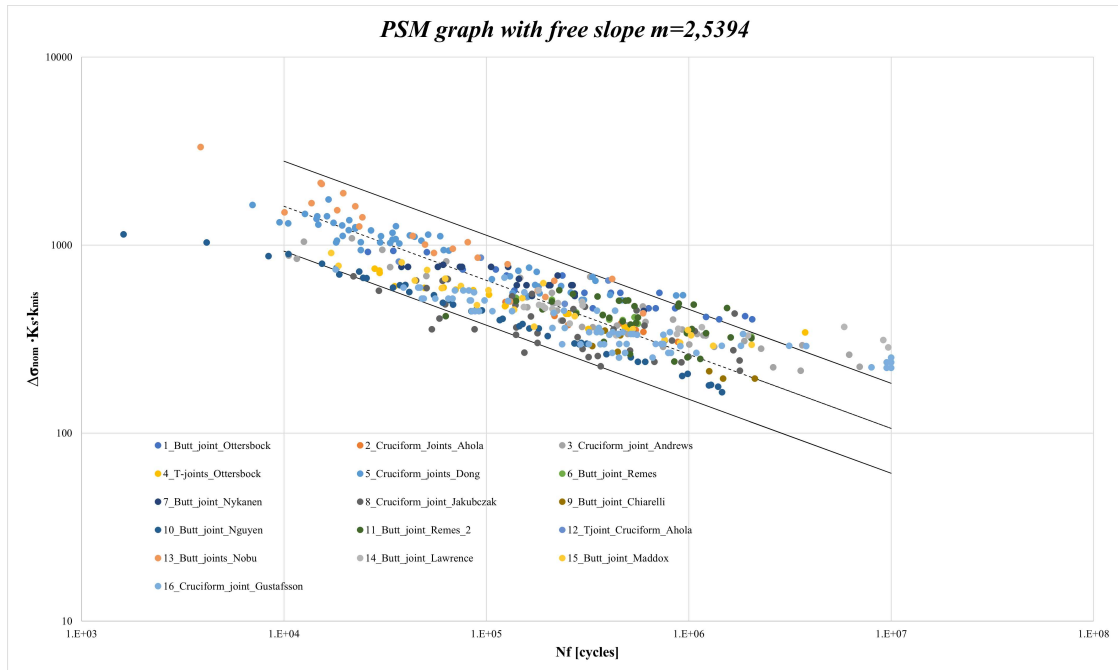


Figure 5.113: PSM Fatigue design curve for $\beta = 0.659$ and $\gamma = 0.996$ with free slope.

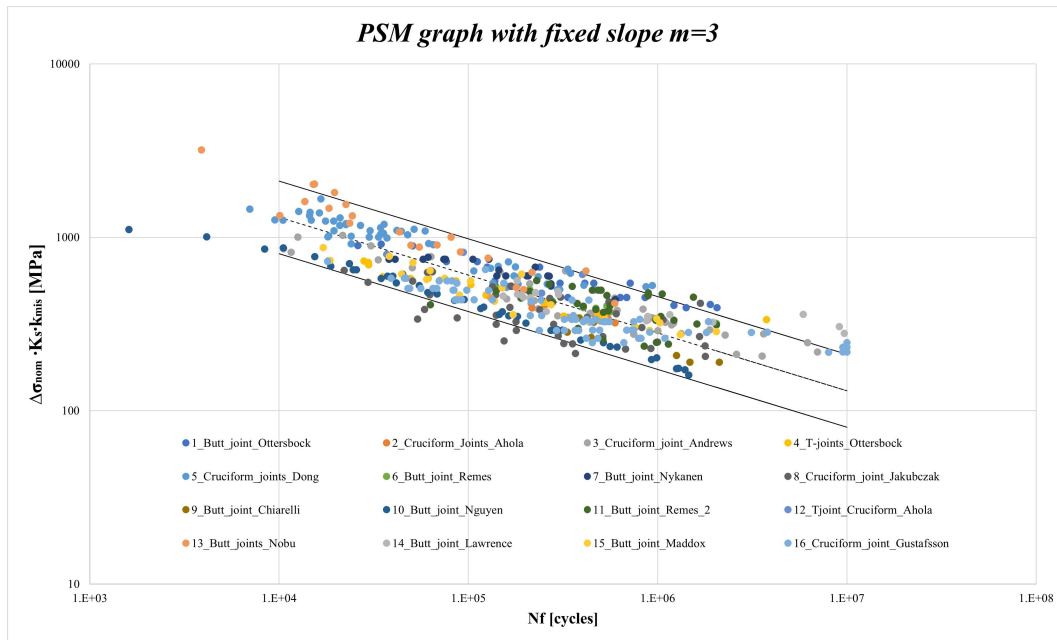


Figure 5.114: PSM Fatigue design curve for $\beta = 0.630$ and $\gamma = 0.975$ with fixed slope.

Chapter 6

Testing program and comparison of results

The objective of this chapter is to describe the experimental procedure that is applied to assess the effect of the misalignment on the cruciform joint and T-joint, subjected to an axial load and previously studied by Elena Pullin [66] and Daniele Berto [65] in 2019 . The experimental results are reported in this chapter. First, a briefly introduction on the tests and loading condition will be given. Then, a comparison between the experimental results, theoretical results obtained from Chapter 5 and the results obtained from IIW recommendations [1] will be made.

6.1 Experimental instrumentation

In this paragraph will be described the experimental instrumentation, used during the tests and also the instrumentation to acquire the data during the tests.

6.1.1 Geometry of the tested specimens

The specimens that are used in these tests, are two:

1. A cruciform load-carrying fillet welded joints under axial load (*Figure 6.1*) with a thickness t equal to 10 mm and width w equal to 40 mm;
2. A T nlc fillet-welded joints under axial load (*Figure 6.2*) with a thickness t equal to 10 mm and width w equal to 40 mm.

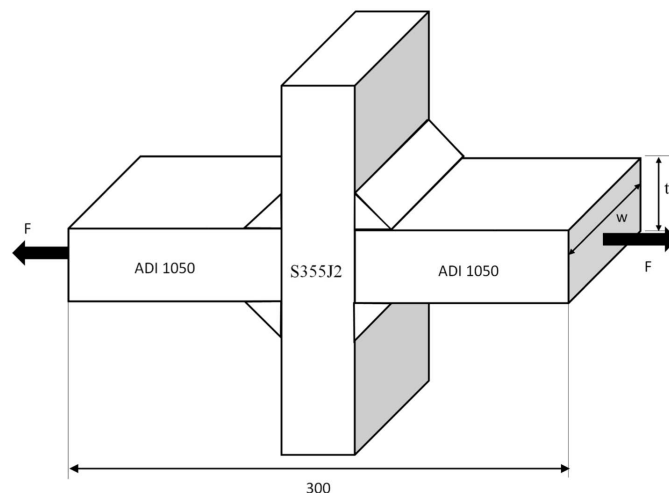


Figure 6.1: Geometry of the cruciform load-carrying fillet welded joints under axial load [66].

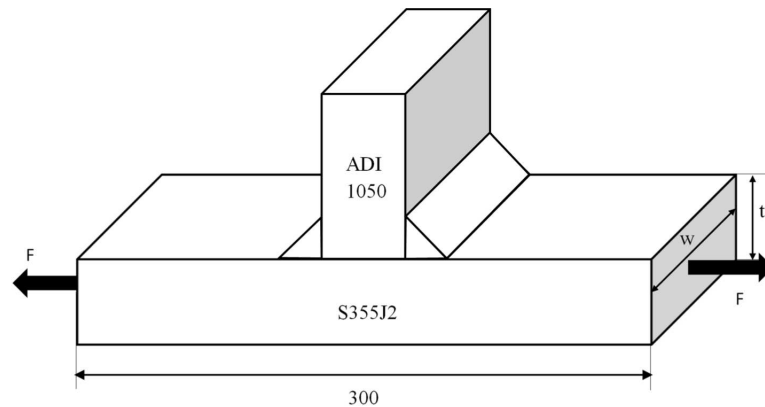


Figure 6.2: Geometry of the T nlc fillet welded joints under axial load [66].

These joint are the same as those analysed by Pullin and Berto in 2019 [66] [65]. The specimens are made of two different material:

1. ADI 1050, that is characterised by the following mechanical properties:

Material model	Yield strength f_y [MPa]	Elongation [%]	Young modulus [MPa]
ADI 1050	1050	6	168000

Table 6.1: Information about mechanical properties from ISO 17804.

2. S355J2, that is characterised by the following mechanical properties:

Material model	Yield strength f_y [MPa]	Elongation [%]	Young modulus [MPa]
S355J2	355	22	206000

Table 6.2: Information about mechanical properties.

These specimens are characterised by angular and axial misalignment. Berto and Pullin [65] [66] measured the misalignments for these specimens (the procedure is described in the paragraph 6.2) and the results are reported in the following table:

Specimen	Angular Misalignment α [°]	Axial Misalignment e [mm]
Cruciform Joint	0.243	1.353
T-joint	0.96	0

Table 6.3: Value of the angular and axial misalignment.

6.1.2 Strain gauge E.R.M.

The foil strain gauge is able to convert an input signal (linear variation of the length) into a electric output signal. The strain gauge is a device used to measure the local relative displacement between two points of

the samples, subjected to dynamic or static load. The foil strain gauge is typically uniaxial, thus it is able to measure the strain along only one direction.

The strain gauge is made up by the following elements:

- A *grid* that is made of metallic material and it is characterised by a electric resistance R that is defined as follows:

$$R = \rho \cdot \frac{l}{A} \quad (6.1)$$

where

- A is the section of the wire that made up the grid;
 - l is the total length of the rectified grid;
 - ρ is the resistivity of the grid material. In this case the grid is made of constantan (a copper–nickel alloy).
- *Polyimide Carrier* that is glued on the surface of the object under examination and gives the electrical insulation. This elements transmit the strain of the object to the grid;
 - An *adhesive* to transmit the strain to the carrier;
 - A *protection* because the grid is sensitive to the work environment. In this case the protection is silicon SG250.

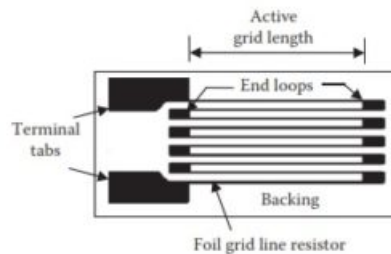


Figure 6.3: Scheme of the structure of the strain gauge.

In the following table are reported the all characteristics of the used strain gauge:

Producer	KYOWA Strain Gauge
Type	KFG-3-120-C1-11L3M3R
Gauge Factor	$2.11 \pm 1.0\%$
Gage Length	3 mm
Gage Resistance(24°.50%RH)	$120.0 \pm 0.8\Omega$
Adoptable Thermal Expansion	11.7 PPM/°C (for Steel)
Temperature Coefficient of Gage Factor	$+0.008\%/^{\circ}\text{C}$
Applicable Gage Cement	CC-33A, EP-34B

Table 6.4: Characteristic of the used strain gauge.



Figure 6.4: The used strain gauge attached to the welded joint.

Strain Gauge principle

The principle of the strain gauge is based on the changing of its electric resistance R due to the strain of the grid. Indeed, the resistance is proportional to the length l and material resistivity ρ , inversely proportional to conductor's cross section A as the equation (6.1) shows. If the surface where the strain gauge is glued, is subjected by a deformation due to the application of the load, the resistance variation is related to the variation of the three terms L , ρ and A :

$$\frac{\Delta R}{R} = \frac{\Delta \rho}{\rho} + \frac{\Delta l}{l} + \frac{\Delta A}{A} \quad (6.2)$$

The conductor follows the Elasticity rules, so the $\frac{\Delta l}{l}$ represents the strain of the conductor in longitudinal direction and $\frac{\Delta A}{A}$ is the variation of the cross section of the conductor:

$$\varepsilon = \frac{\sigma}{E} \quad (6.3)$$

$$\varepsilon_t = -\nu \cdot \varepsilon_l \quad (6.4)$$

$$\frac{\Delta A}{A} = -2 \cdot \nu \cdot \varepsilon_l \quad (6.5)$$

$$\frac{\Delta l}{l} = \varepsilon_l \quad (6.6)$$

Where;

- ε_t is the deformation in transversal direction of the conductor;
- E is Young modulus;
- ν is the coefficient of Poisson.

Substituting the equations (6.5) and (6.6) in the (6.2), the result is:

$$\frac{\Delta R}{R} = \frac{\Delta \rho}{\rho} + (1 + 2 \cdot \nu) \cdot \varepsilon_l \quad (6.7)$$

From the last equation, the variation of the resistance R depends on the longitudinal deformation and on the variation of the resistivity.

One of the most important metrological characteristics of the strain gauge is the *gauge factor*, that is defined as follows:

$$K = \frac{\Delta R/R}{\Delta l/l} = \frac{\Delta R/R}{\varepsilon_l} = 1 + 2 \cdot \nu + \frac{\Delta \rho/\rho}{\varepsilon_l} \quad (6.8)$$

The gauge factor is defined experimentally from the producer of the strain gauge and in this case is equal to $2.11 \pm 1.0\%$.

Normally, one strain gauge is not sufficient to obtain an accurate measurement because the variation of the resistance in output are too small to read it correctly. For this reason, the output signal is amplified thanks to the use of Wheatstone bridge control units, where instead of using the four resistance, one or more strain gauge are inserted. One example is displayed on the following figure:

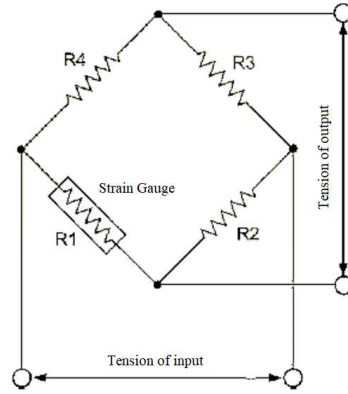


Figure 6.5: Example of 1/4 of Wheatstone bridge configuration.

In the case of full bridge (4 strain gauge inside the Wheatstone bridge configuration), the output potential difference U is defined as follows:

$$U = \frac{V}{4} \cdot \left(\frac{\Delta R_1}{R_1} - \frac{\Delta R_2}{R_2} + \frac{\Delta R_3}{R_3} - \frac{\Delta R_4}{R_4} \right) = V \cdot \frac{K}{4} \cdot (\varepsilon_1 - \varepsilon_2 + \varepsilon_3 - \varepsilon_4) = V \cdot \frac{k}{4} \cdot \varepsilon_{tot} \quad (6.9)$$

Where V is the input tension of the bridge. The equation (6.9) defined the relation between the measured deformation from the four strain gauge and the potential difference measured in the configuration. The most common Wheatstone bridge configuration are:

- Full bridge configuration with 4 strain gauge;
- Half bridge configuration with 2 strain gauge and 2 resistance;
- Quarter bridge configuration with 1 strain gauge and 3 resistance.

In this thesis, the quarter bridge configuration is used to measure the strain of the welded joint and the following equation is valid:

$$U = V \cdot \frac{K}{4} \cdot \varepsilon_1 \quad (6.10)$$

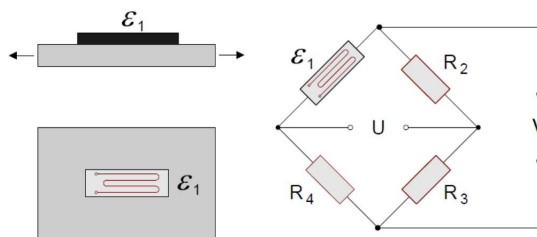


Figure 6.6: Quarter bridge configuration.

6.1.3 Strain gauge control unit IMC

The acquisition of the output signal of the strain gauge is done by a strain gauge control unit IMC-CRONOS PL2 (Figure 6.7). After the definition of the type of Wheatstone bridge and the gauge factor K of the strain gauge, the control unit gives the value of the strain along the direction of the grid. This value is visible thanks the using of a personal computer that is also an data store during the acquisition.



Figure 6.7: On the left there is an image of the strain gauge control unit IMC. On the right, there is an image of the system for the acquisition (personal compute, strain gauge control unit and relative cables).

The functioning of the acquisition system is explained on the *Figure 6.8*, where the all elements are illustrated.

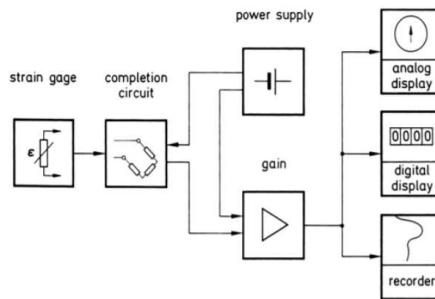


Figure 6.8: Scheme of the acquisition system of the strain during the test.

The strain gauge control unit IMC is able to acquire signal until 50 kHz of frequency and it is characterised by eight analogical channel and four digital channel. A Wheatstone bridge can be connected for each analogical channel.

6.1.4 Connectors

The connection between the cables of the strain gauge and the strain gauge control unit is executed by the connectors. Each connector is able to host two channel for the acquisition. After connecting the cable of strain gauge with the right Wheatstone bridge configuration, the connectors are closed and fixed through two screws to the control units inputs. In this way, the strain gauge control units are able to send the input signal of the bridge and at the same time to transmit the output signal to the personal computer, defined in $\mu\epsilon$. In the *Figure 6.9* is displayed a scheme of the possible connection of the connector. In based on how the strain gauge cables are connected in the connector, the configuration can be a quarter or half bridge.

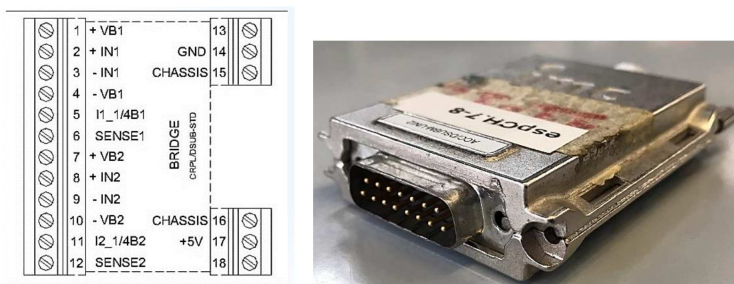


Figure 6.9: On the left there is a scheme of the inside of the connector. On the right, there is an image of a connector.

6.1.5 Multimeter

The multimeter is a instrument used to control the following things:

- The right functioning of the strain gauge cables;
- The right connection of the strain gauge cables;
- To verify that there is not a contact between the grid of strain gauge and the surface of the samples.

The multimeter is characterized by two elements that are put in contact with the cables of the strain gauge to verify the electrical resistance.



Figure 6.10: Multimeter used to control the strain gauge cables.

6.1.6 Schenck Hydropuls®PSA machine

The machine used for the test is a *Schenck Hydropuls®PSA*, an axial testing machine, that is characterised by the following features:

<i>Characteristics</i>	
Force capacity	100 kN
Actuator dynamic stroke	100 mm
Max vertical test space	550 mm
Grips depth	50 mm
<i>Specimen Testing</i>	
Specimen type	flat and round
Thickness	0 mm to 15 mm
Diameter	6 mm to 17 mm

Table 6.5: Characteristic *Schenck Hydropuls®PSA*.

The test machine is displayed on the following figure:

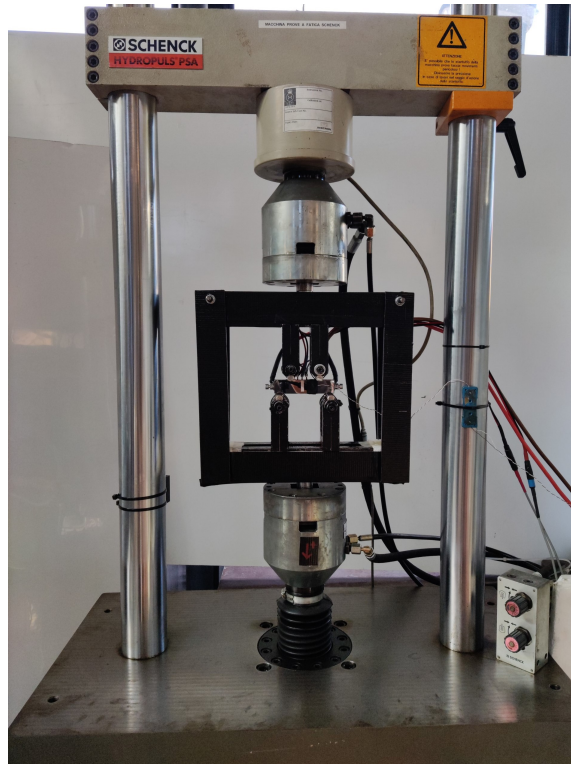


Figure 6.11: Schenck Hydropuls®PSA, an axial testing machine in the laboratory of Materials Characterization of the University of Padua.

6.2 Misalignment measurement method

The method used for the measure of the welded joint misalignment is described in this paragraph. As described in the *Chapter 5*, misalignment can influence the fatigue life of the specimens. When the welded joints are clamped by the machine, they tend to straighten due to the action of the clamps of the axial testing machine. This leads to undesired displacements of the welded joints extremities and a secondary bending moment is introduced.

This effect increases the degree of stress and strain concentration near the weld bead, which deteriorates the fatigue properties of the welded joints. For this reason the misalignment effect has to be considered.

As described in the paragraph 5.1, there are two types of misalignment:

1. *Axial misalignment* consists in an eccentricity between the axes of the two plates from the ideal condition (perfectly parallel), as *Figure 6.12a* shows;
2. *Angular misalignment* consists in the angle between the axes of the two plates when they have the origin at the same point, as *Figure 6.12b* shows;

The specimens usually present both of them simultaneously (*Figure 6.12c*).

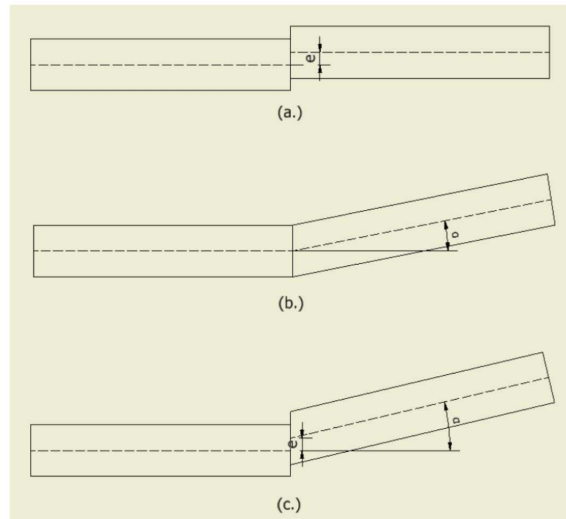


Figure 6.12: Misalignment of welded specimen: a) axial misalignment, b) angular misalignment, c) combined misalignment [66].

6.2.1 Description of measurement method

In this paragraph the measurement method is described and a numerical-controlled milling machine with a touch probe is used to measure both of the misalignment. The procedure is characterised by the following steps:

1. The first step is characterised by the clamping of the specimen on the work plane of the machine, as *Figure 6.13* shows. It is advisable to constrain the welded joint on the steel side because its surface is more regular than the one of the ADI side.



Figure 6.13: Welded joint clamped on the work plane of the machine [66].

2. Subsequently, the touch probe has to be placed at the middle point of the joint width to measure the all points on the longitudinal plane.

3. When the touch probe is on the edge of the specimen, the X-axis is set to zero, as *Figure 6.14* shows.

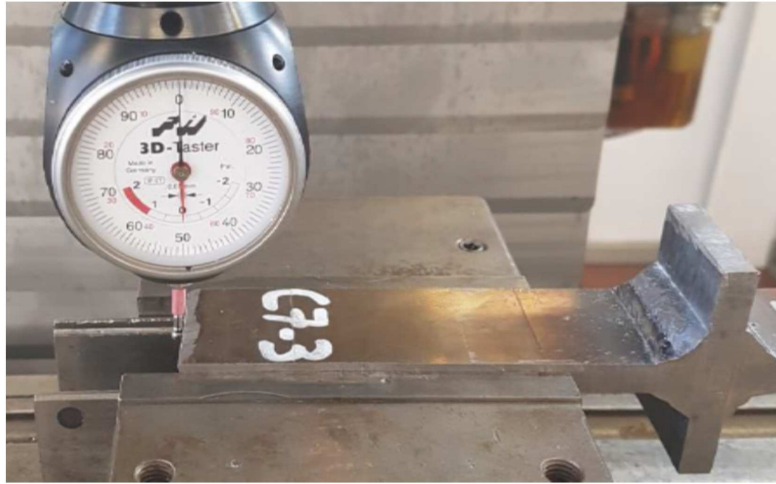


Figure 6.14: *Reset of the X-axis at the edge of the welded joint [66].*

4. The touch probe is moved to $x = 2\text{mm}$ and the all coordinates are reseted. Indeed, the X and Z axes will change, while the Y axis is kept constant at the middle-point (*Figure 6.15*).



Figure 6.15: *Set of the reference point O for the measurement [66].*

5. The x and z coordinates of the point A are measured. A is the point just before the weld toe on the S355J2 side. In the case of cruciform joint, one should pay attention to avoid hurting the fillet with the head of the touch probe (*Figure 6.16*).

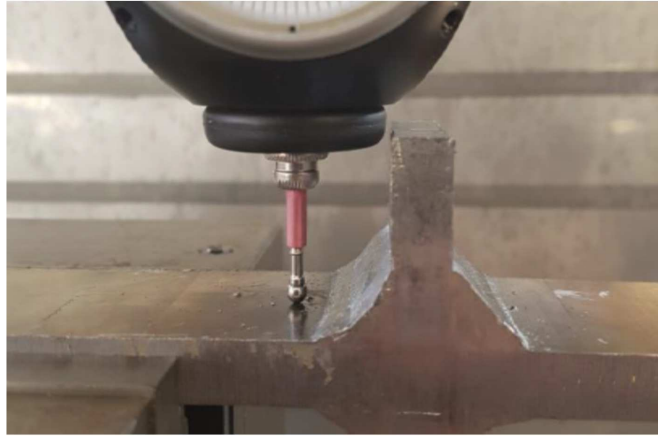


Figure 6.16: *The measurement of the coordinated of point A, before the weld toe on the steel side [66].*

6. The x and z coordinates of the point A' are measured. A' is the point just beyond the weld toe on the ADI side (Figure 6.17).

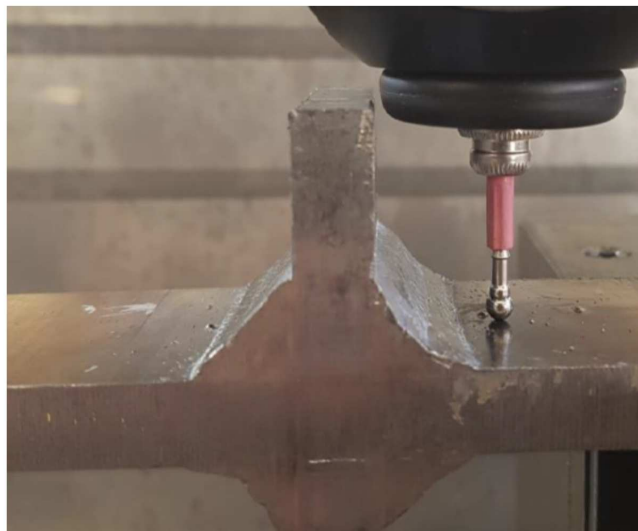


Figure 6.17: *The measurement of the coordinated of point A', beyond the weld toe on the ADI side [66].*

7. The x and z coordinates of the point O' are measured. O' is the point at the end of the specimen on the ADI side (Figure 6.18).

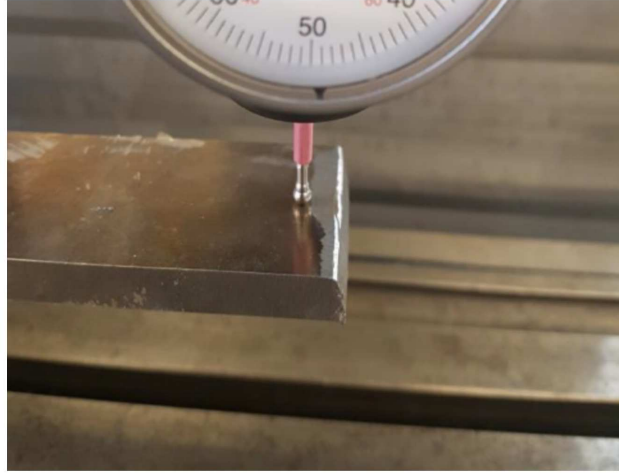


Figure 6.18: The measurement of the coordinated of point O' , at the end of the specimen on the ADI side [66].

8. The specimen are rotated of 180° and the same points are measured on the lower surface.
9. The misalignment are calculated with the following equation and procedure with reference to *Figure 6.19*:

- (a) The axial misalignment is calculated as the difference between the z-coordinates of the points before and beyond the weld toe. To increase the accuracy of the measurement, the average value is calculated from the ones obtained on the upper and lower surface of the specimen:

$$e = Z_A - Z_{A'} \quad (6.11)$$

- (b) Obtaining the coordinates of the four points on the surface, the total misalignment ΔZ is calculated as follows:

$$\Delta Z = Z_{O'} + l \cdot \beta_{S355J2} \quad (6.12)$$

where:

- l is the total length of the specimen;
- L_{S355J2} is the length of the steel plate;
- β_{S355J2} is the angle between the specimen and the work plane defined as:

$$\beta_{S355J2} = \arctan\left(\frac{Z_A - Z_O}{L_{S355J2}}\right) \quad (6.13)$$

- (c) e_1 is the misalignment due to the angular component α and it is obtained by the subtraction of e from ΔZ :

$$e_1 = \Delta Z - e \quad (6.14)$$

- (d) After that, the angular misalignment can be calculated in radiant:

$$\alpha = \tan\left(\frac{e_1}{l_{ADI}}\right) \quad (6.15)$$

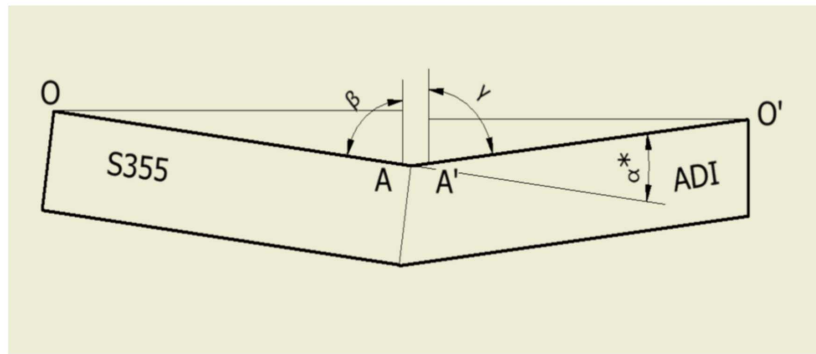


Figure 6.19: Parameters for the calculation of the misalignment [66].

The results are reported in the following table:

Specimen	Angular Misalignment α [°]	Axial Misalignment e [mm]
Cruciform Joint	0.243	1.353
T-joint	0.96	0

Table 6.6: Value of the angular and axial misalignment.

6.3 Experimental procedure

The first step of the experimental procedure is to define the number of strain gauge for each samples. In according to Berto and Pullin [65] [66], the cruciform joints is characterised by 4 strain gauges to study the bending on all four surface of the joint (Figure 6.20); the T-Joints is characterised by 8 strain gauges to study the bending on all four surface of the joint but only the 4 strain gauges closer to the weld toe are used (the strain gauges called CH3, CH7, CH6, CH2 in the Figure 6.21).

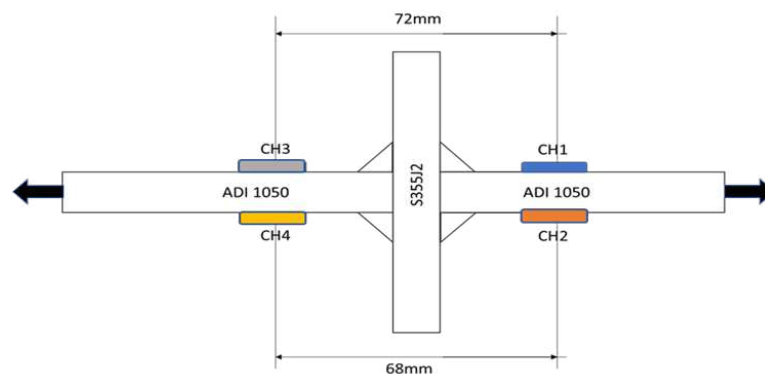


Figure 6.20: Disposition of the strain gauges in the cruciform joint.

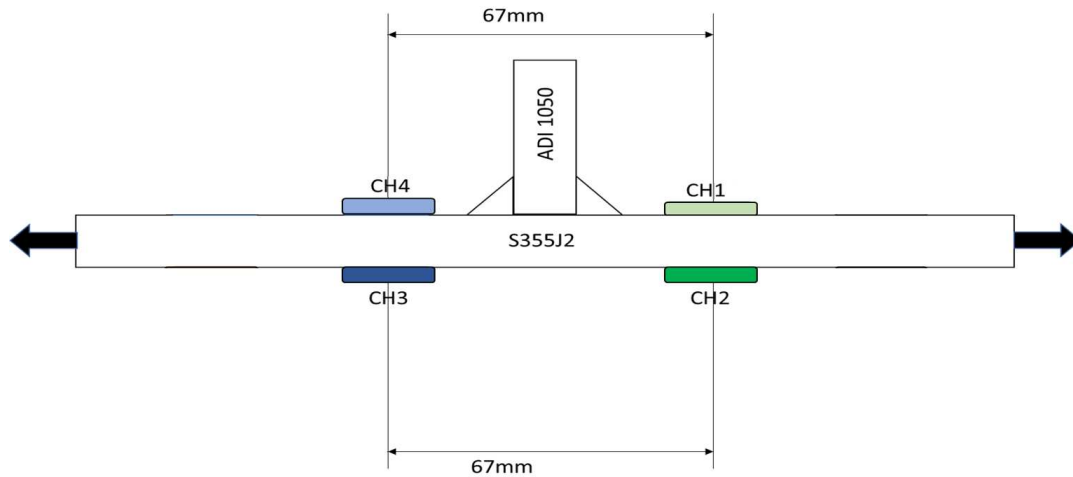


Figure 6.21: Disposition of the strain gauges in the T-joint.

The all strain gauges are already glued because they are used for the thesis work of Berto and Pullin. The subsequent steps are described in the following sections.

6.3.1 Verification of the functioning of the strain gauge cables with multimeter

Before the test of the samples, the right functioning of the strain gauges have to be verify to guarantee the correct acquisition of the data. This operation is done thanks to the using of the multimeter that allows to measure the electric resistance of a metallic object. As *Figure 6.10* shows, the initial value of the resistance that will be measured, has to be imposed. The nominal value of the resistance is 120Ω , so the knob is turned of 180° to obtain a range of 200Ω . Subsequently, the resistance is measured. The strain gauges are characterised by three different cables: 1 red cable and 2 white cables. To measure correctly the resistance of the strain gauge, one pointer of the multimeter is placed on the red cable; the other pointer is placed on the one of white cable. The value of the resistance on the display of the multimeter has to be higher than 120Ω . After that, the same procedure is repeated for the two white cables. The difference of the two measurement has to be equal to 120Ω .

6.3.2 Connection between strain gauges, connectors and strain gauge control unit IMC

After the verification of the functioning of the all strain gauges, the next step is the connection of the strain gauges cables inside the connectors. In this case, the quarter bridge configuration is chosen because thanks to its simplicity, this configuration is the most used one for the strain measurement.

A quarter bridge configuration gives in output a signal that is characterised by a contribute due to the bending. Indeed, the aim of this experimental experience is to quantify the bending contribute due to the misalignment of the welded joint, so this configuration is the best one to achieve the objective.

A quarter bridge configuration defines that a channel is dedicated for each strain gauge; the sample is characterised by four strain gauges, so four independent acquisition channels are necessary. Each connectors hosts two channel, two connectors are necessary to complete the connection between the strain gauges and the control unit. In the following figure are displayed an examples of connection between the strain gauge and connector with a quarter bridge configuration.

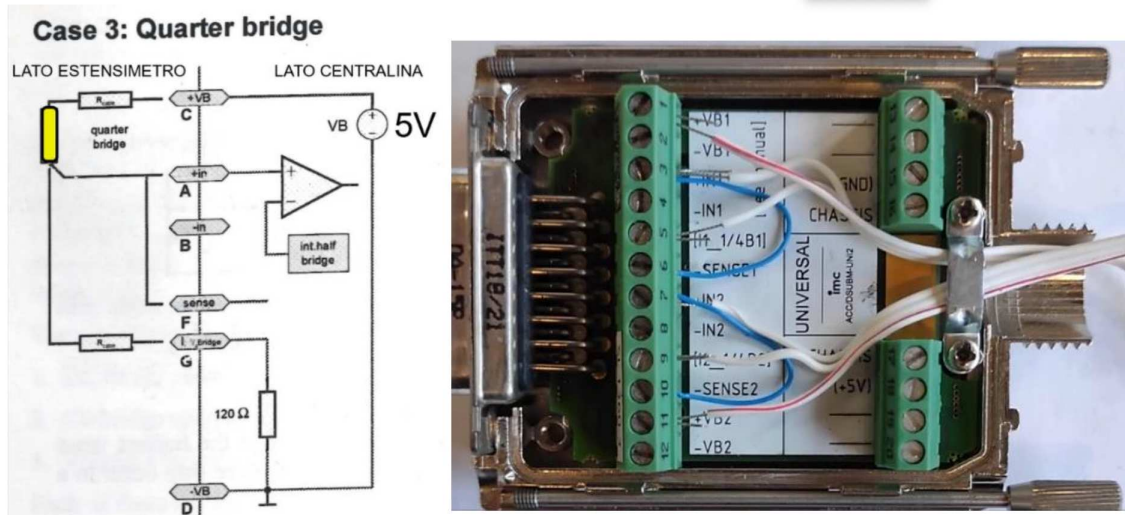


Figure 6.22: On the left, an image that represents a scheme of the connection of the cables to obtain a quarter bridge configuration for a strain gauge with three wires. On the right, a right connection of the cables.

The supply voltage of the connector is equal to 5 Volt. The red cable of the strain gauge has to be connected in $+VB$. One of the two white cables has to be inserted in the quarter bridge input (entrance number 5) to close the Wheatstone bridge circuit with a resistance equal to the initial one of the strain gauge (120 Ohm). Subsequently, the last white cable is connected to $+IN$ (entrance number 3) to allow the reading of the bridge imbalance. The last step is to connect the blue cables with a short circuit between the two terminals $+IN$ and $SENSE$.

This procedure is repeated for the second acquisition channel, using the terminals from 7 to 12. Subsequently, the connector is closed and the same procedure is repeated for the other connector.

The two connectors are connected to two input of the strain gauge control unit, as *Figure 6.23* shows. The connection is characterised by 4 strain gauges, so 4 quarter bridge configuration.



Figure 6.23: Connection between the two connectors en the strain gauge control unit.

6.3.3 Configuration of the software *IMC Devices*

In this paragraph is described the principal step for the configuration of the acquisition system. After turning on the computer, the program *IMC devices V2.6* is opened and the *New Experiment* is selected. Before starting the test, three steps have to be executed:

1. Configuration of the channel;
2. Data save settings;
3. Clearing of the channels, initialization and starting of the acquisition.

Configuration of the channel

To open the window for the channel configuration, the following commands are used:

Menu → *Settings* → *Configuration* → *Base*

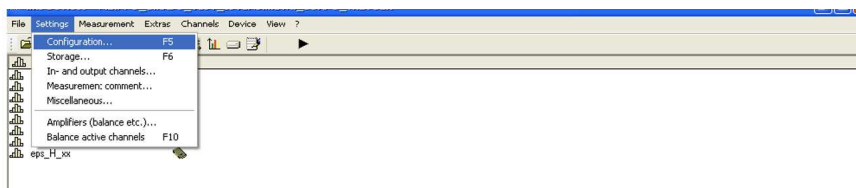


Figure 6.24: Window of IMC devices and commands for the configuration of the new set-up.

Subsequently, the channel of interest are selected and the section *Status* is imposed to *Active*. After that, the duration of acquisition is imposed equal to *Undefined* with a *Sampling* equal to 100 ms. In this case, the channel 1, 2, 3 and 4 are activated.

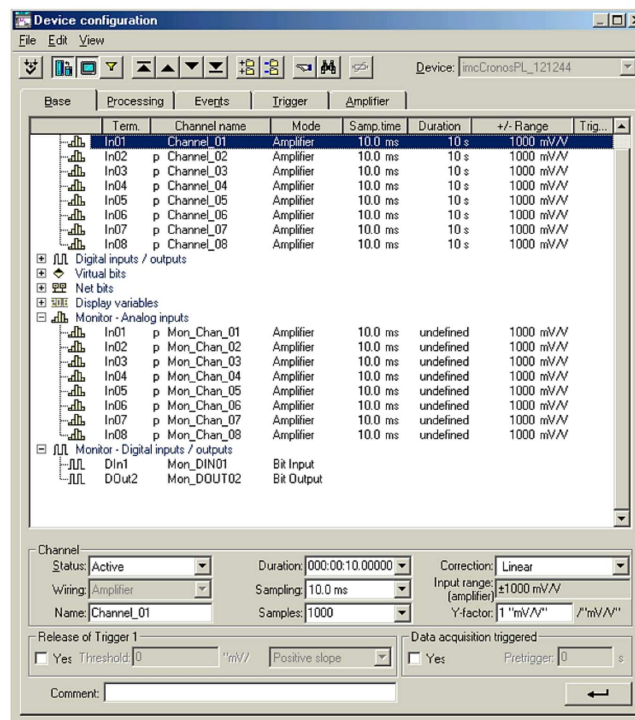


Figure 6.25: Window of Base for the configuration of the channels.

After that, the section *Amplifiers* is selected and the window *Strain Gauge* is opened for the selection of the quarter bridge configuration (Figure 6.26). After the definition of the bridge configuration, the value of the resistance has to be verified because it has to be equal to 120Ω (nominal value of the strain gauge). After that, the value of the Gauge factor *K* is inserted equal to 2.11 and the *Supply Voltage* has to be equal to 5V. The input

range is selected equal to $\pm 1900 \mu\text{eps}$ and it represents the maximum value of the strain that can be measured during the acquisition. This value derives from initial hypothesis. After these steps, the *Device Configuration* window is closed.



Figure 6.26: Amplifier section, Strain Gage window.

Data save settings

For the saving data, the following commands are applied:

Setting → *Storage* → *Selection of Drive*

Clearing of the channels, initialization and starting of the acquisition

Before the starting of the acquisition, the channels have to be activated to acquire the data. This operation is done with the following commands:

Device → *Connect*

After that, from *Settings* → *Amplifier*, the clearing of the channels is done. The meaning of this operation is that the initial strain is imposed equal to zero because during the previous steps the strain gauges can be read some deformation, with this offset, the deformation before the test are neglected. After the selection of the all channels, the *Bridge* is clicked to balance the bridge.

To see on the computer display the trend of the strain, *Show curve* is clicked. After that the acquisition can be started.

6.3.4 Mounting of the specimen in the machine

After the turning on the machine, the *Schenck* will be in *Displacement control* with interlock inserted.

Initially, only one extremities of the specimen is fixed because the deformation *out of the machine* (the deformation of the specimens when the specimen is not fixed with the both extremities) has to be measured. For this reason, the superior clamp is opened and it is distanced sufficiently to allow the insertion of the sample inside the inferior clamp. Before the tightening of the wedges, the specimen has to be aligned with the principal plate in the frontal plane. Indeed, during the the insertion of the sample, a bracket and bubble are used to verify the verticality. During these operations, the cable of the strain gauges must not be pulled o pitched.

After these verifications, the superior clamp can be closed (*Figure 6.27*) and the deformation on the computer display will be roughly equal to zero because the bridges was cleared just after the closed of superior clamp and also the sample is not subjected to bending or axial force .



Figure 6.27: Specimen inside the machine with closed clamp.

Subsequently, the inferior clamp is closed and the machine applies a force equal to 3.5 kN due to the dynamics of the clamping. To defined a force equal to zero, the command of the machine is changed from *Displacement control* to *Force control* and the value of 0 kN is manually inserted to re-establish the condition with external force equal to zero. This is the first applied static load. Indeed, the imposition of the external force equal to zero doesn't mean null bending moment acting on the specimen. Indeed, the welded joint is hyperstatically constrained at the two extremities and it is subjected by a bending stress. For this reason, the output signal of the strain gauge unit control are not neglected and the value of the strains measured by the strain gauges demonstrate the typical trend of bending stress. This is a confirm that the principal plate of the joint is characterised by a misalignment.

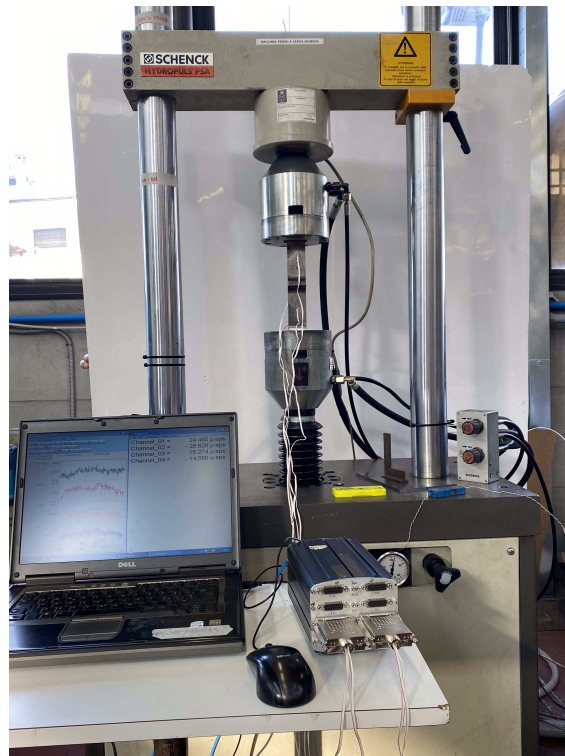


Figure 6.28: Image of the cruciform joint clamped hyperstatically inside the machine. As show the figure, the output strain are equal to $\pm 25\mu\epsilon$ s for the superior part and equal to $\pm 15\mu\epsilon$ s for the inferior part.

6.3.5 Manual application of the static load

To study the variation of the bending stress due to the misalignment of the welded joint, the specimen is subjected to different static load.

The yield strength of the ADI is equal to 1050 MPa and 355 MPa for the S355J2. For this reason the maximum applied load is 125 MPa. This value is lower than the S355J2 yield strength and it is chosen this value because if a higher load is applied, the joint will be slid out of the clamping.

The section of the both specimens is equal to 400mm^2 , so maximum applied force is:

$$F = \sigma_{max} \cdot A = 125 \cdot 400 = 50\text{kN} \quad (6.16)$$

The loads are applied as a loading ramp ascending descending from 0 kN to 50 kN with an increment equal to 5 kN, as the following graph shows:

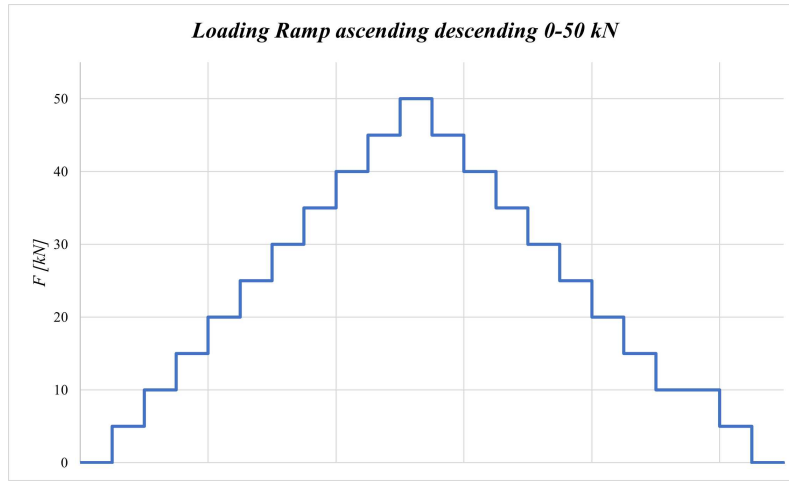


Figure 6.29: Loading ramp ascending descending 0kN-50kN-0kN of static load, manually applied to the cruciform and T-joint.

The null value of the force is the condition of 0 kN applied from the test machine when the both extremities of the specimen are clamped. Before the application of the subsequent load, the output signal has to be stabilized. The loading ramp is applied 3 times for each specimen because during the elaboration of the data, the value of the strain will be the average value of the all acquisition.

At the end of each loading ramp, the machine has to be placed in *Displacement control*, one of the two clamps are opened and the deformation *out of the machine* is acquired. After that, the acquisition is stopped and the clearing of the channels is repeated and the system is ready for a new acquisition.

6.3.6 Elaboration of the results

This step is characterised by the analysis of the strain that the strain gauge control unit has measured during the test. As *Figure 6.30* shows, the section A-A the total strain state measured can be divided in two contributes:

1. The first is a membrane contribution due to the tensile load;
2. The second is a bending contribution due to the misalignment of the welded joint and the clamping system.

The deformation due to each contribution are calculated with the following formulas:

$$\epsilon_{membr,sup}[\mu eps] = \frac{\epsilon_{CH1} + \epsilon_{CH2}}{2} \rightarrow \sigma_{membr,sup}[MPa] = E \cdot \epsilon_{membr,sup} \cdot 10^{-6} \quad (6.17)$$

$$\epsilon_{membr,inf}[\mu eps] = \frac{\epsilon_{CH3} + \epsilon_{CH4}}{2} \rightarrow \sigma_{membr,inf}[MPa] = E \cdot \epsilon_{membr,inf} \cdot 10^{-6} \quad (6.18)$$

$$\epsilon_{bend,sup}[\mu eps] = \epsilon_{max,CH1-CH2} - \epsilon_{membr,sup} \rightarrow \sigma_{bend,sup}[MPa] = E \cdot \epsilon_{bend,sup} \cdot 10^{-6} \quad (6.19)$$

$$\epsilon_{bend,inf}[\mu eps] = \epsilon_{max,CH3-CH4} - \epsilon_{membr,inf} \rightarrow \sigma_{bend,inf}[MPa] = E \cdot \epsilon_{bend,inf} \cdot 10^{-6} \quad (6.20)$$

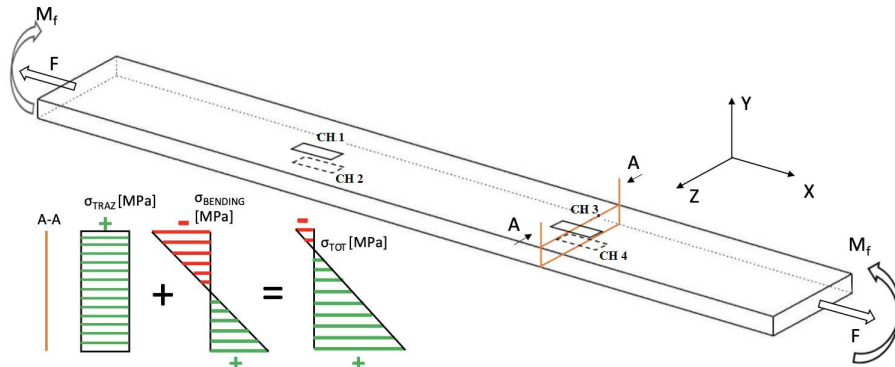


Figure 6.30: Scheme of the loaded plate and real solicitations acting on it. The bending moment acts along the z-axis and it induces a bending stress on the loaded plate. This stress adds up to the tensile stress, that is uniform along the all surface. The bending stress is characterised by the classic butterfly's trend. The superimposition of these two trends gives a new stress state that change the quantity of the fiber in compression and in traction.

The numerical results of the two specimen for each ramp are reported in the Appendix H with the definition of the relative error between the membrane stress and the theoretical stress. For each ramp loading, a graph is reported with the membrane and bending stress for the cruciform and T-joint and a comparison between the the experimental data obtained from the test and the results of the previous work has been done.

Results of cruciform joint

In *Figure 6.31* the membrane and bending stress are reported in function of the applied load. The real applied load is not equal to the ideal load due to an imprecision of the machine, as reported in the Appendix H.

The area between the two curves (first curve represents the phase of ascending load; the second one represents the phase of descending load) shows a hysteretic phenomenon that it decreases with the application of the subsequent loading ramps. Indeed the first ramp that was applied, is not really the first because Berto and Pullin during their work thesis have applied other ramp loading condition. For this reason the value of the hysteretic area is roughly null. As the *Table H.4* shows, the relative error between the membrane stress and the theoretical one is included between 0.67%, obtained in the superior part of the welded joint, and 10.06%, obtained in the inferior part of the welded joint.

As the graph in *Figure 6.31* shows, the bending stress increases in linear way for the both parts of the specimen. Furthermore, for an external force equal to 0 kN, the sample is subjected to a bending stress.

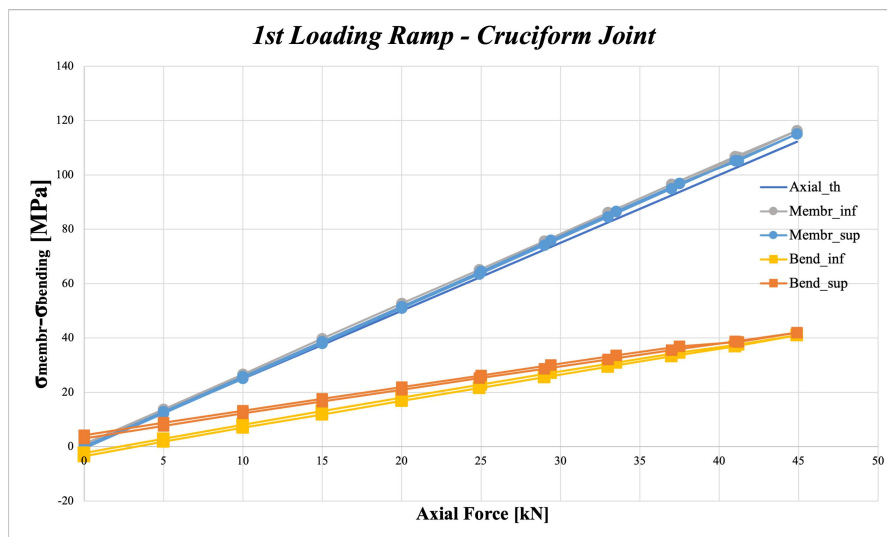


Figure 6.31: Distribution of the membrane and bending stress obtained in the cruciform joint for the application of the 1st loading ramp. In the graph, the theoretical stress are represented for a comparison with the measured membrane stress.

In *Figure 6.32* the membrane and bending stress are reported in function of the applied load for the 2nd loading ramp. The real applied load is not equal to the ideal load due to an imprecision of the machine, as reported in the Appendix H.

The difference between the theoretical stress line and the membrane stress line are lower than the case of the 1st loading ramp. Indeed as the *Table H.5* shows, the relative error between the membrane stress and the theoretical one is included between -0.19% , obtained in the superior part of the welded joint, and 8.72% , obtained in the inferior part of the welded joint.

As the graph in *Figure 6.32* shows, the bending stress increases in linear way for the both parts of the specimen. Furthermore as before, for an external force equal to 0 kN, the sample is subjected to a bending stress.

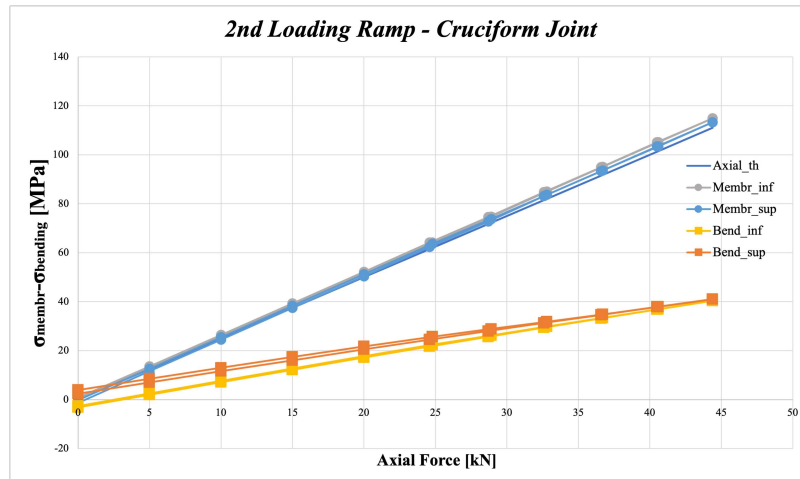


Figure 6.32: Distribution of the membrane and bending stress obtained in the cruciform joint for the application of the 2nd loading ramp. In the graph, the theoretical stress are represented for a comparison with the measured membrane stress.

In *Figure 6.33* the membrane and bending stress are reported in function of the applied load for the 3rd loading ramp. The real applied load is not equal to the ideal load due to an imprecision of the machine, as reported in the Appendix H.

The difference between the theoretical stress line and the membrane stress line are roughly equal to the case of 1st loading ramp. Indeed as the *Table H.6* shows, the relative error between the membrane stress and the theoretical one is included between -0.81% , obtained in the superior part of the welded joint, and 11.66% , obtained in the inferior part of the welded joint.

As the graph in *Figure 6.33* shows, the bending stress increases in linear way for the both parts of the specimen. Furthermore as before, for an external force equal to 0 kN, the sample is subjected to a bending stress.

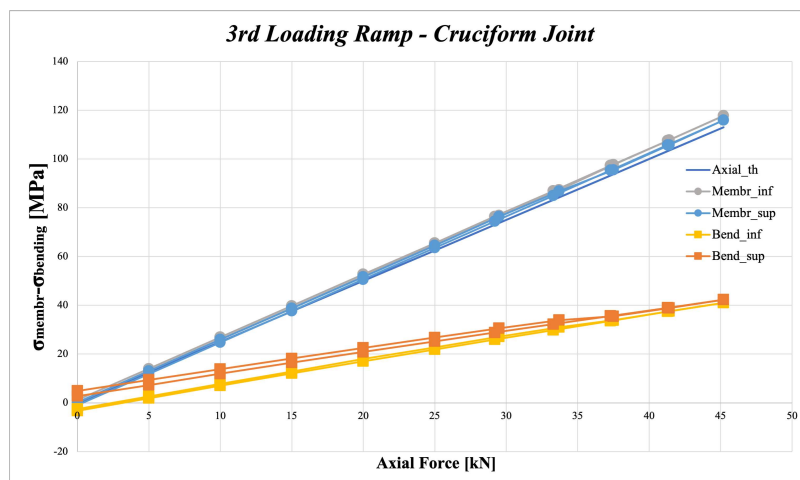


Figure 6.33: Distribution of the membrane and bending stress obtained in the cruciform joint for the application of the 3rd loading ramp. In the graph, the theoretical stress are represented for a comparison with the measured membrane stress.

The obtained results are in accordance with the results of Berto [65]. The comparison is done only for applied loads equal to 10, 20 and 30 kN because in this work has been applied a different loading ramp. Indeed, Berto has applied a ramp from 0 kN to 100 kN with a step size equal to 10 kN.

Another important difference between the tests is that in this thesis the axial testing machine used is a *Schenck Hydropuls®PSA*, instead Berto has used *MFL SYSTEME*. The comparison between the results is not done for applied force equal to 40 kN and 50 kN because, as described before, in this case the Schenck machine are not able to apply exactly the desired load, unlike the *MFL SYSTEME*. The comparison is done in terms of membrane stress and it is reported in the following table:

F_{real} [kN]	$F_{Pullin-Berto}$ [kN]	$\sigma_{membr,inf,avg}$ [MPa]	$\sigma_{membr,sup,avg}$ [MPa]	$\sigma_{membr,inf,Pul-Ber}$ [MPa]	$\sigma_{membr,sup,Pul-Ber}$ [MPa]	$\Delta_{inf}\%$	$\Delta_{sup}\%$
10	10	25.933	25.727	25.872	26.334	0.23	-2.30
20	20	51.695	51.470	52.416	53.004	-1.38	-2.89
29.27	30	75.773	75.347	79.044	79.212	-4.14	-4.88

Table 6.7: Comparison of the results for the cruciform joint.

Results of T-joint

In Figure 6.34 the membrane and bending stress are reported in function of the applied load. The real applied load is not equal to the ideal load due to an imprecision of the machine, as reported in the Appendix H.

The area between the two curves (first curve represents the phase of ascending load; the second one represents the phase of descending load) shows a hysteric phenomenon that it decreases with the application of the subsequent loading ramps. Indeed the first ramp that was applied, is not really the first because Berto and Pullin during their work thesis have applied other ramp loading condition. For this reason the value of the hysteric area is roughly null. As the Table H.10 shows, the relative error between the membrane stress and the theoretical one is included between 0.17%, obtained in the superior part of the welded joint, and 6.12%, obtained in the inferior part of the welded joint.

As the graph in Figure 6.34 shows, the bending stress can be consider roughly constant. Furthermore, for an external force equal to 0 kN, the sample is subjected to a bending stress.

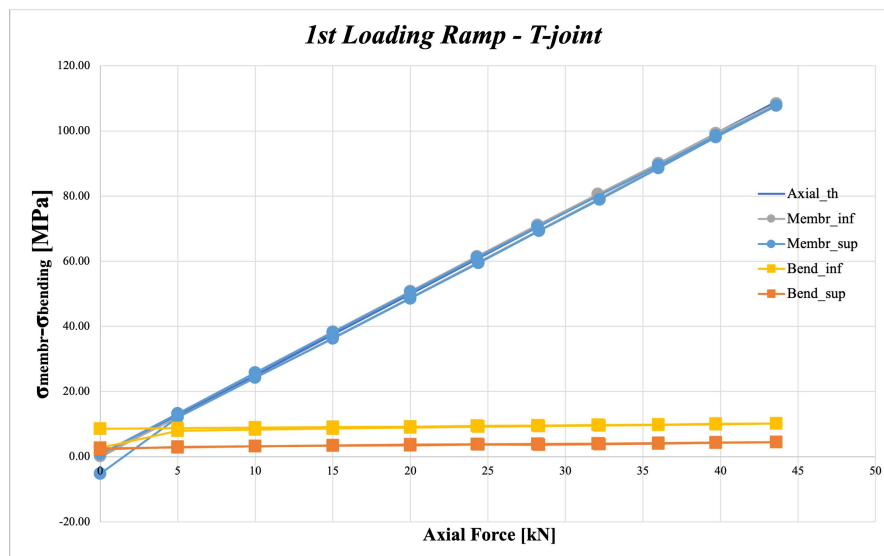


Figure 6.34: Distribution of the membrane and bending stress obtained in the T-joint for the application of the 1st loading ramp. In the graph, the theoretical stress are represented for a comparison with the measured membrane stress.

In Figure 6.35 the membrane and bending stress are reported in function of the applied load for the 2nd loading ramp. The real applied load is not equal to the ideal load due to an imprecision of the machine, as reported in the Appendix H.

The difference between the theoretical stress line and the membrane stress line are lower than the case of the 1st loading ramp. Indeed as the Table H.11 shows, the relative error between the membrane stress and

the theoretical one is included between 0.15%, obtained in the inferior part of the welded joint, and 4.01%, obtained in the superior part of the welded joint.

As the graph in *Figure 6.35* shows, the bending stress can be consider roughly constant. Furthermore as before, for an external force equal to 0 kN, the sample is subjected to a bending stress.

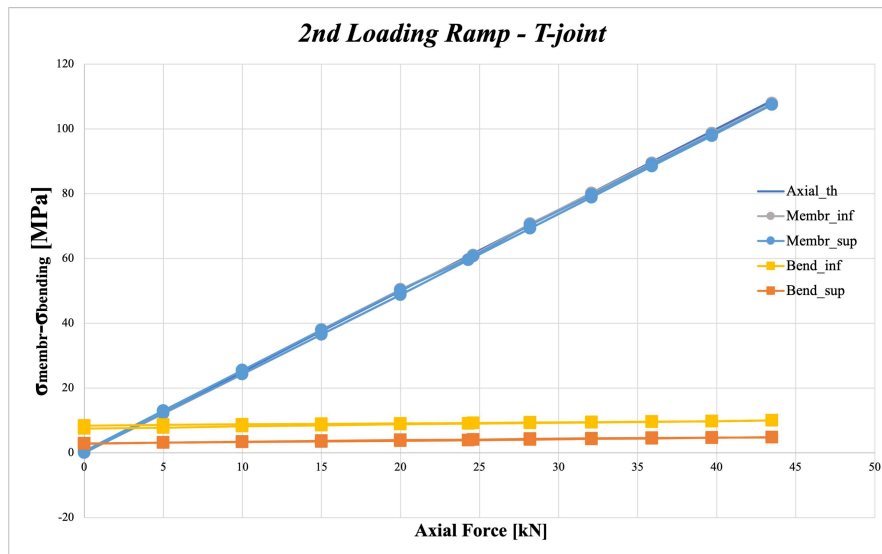


Figure 6.35: Distribution of the membrane and bending stress obtained in the T-joint for the application of the 2nd loading ramp. In the graph, the theoretical stress are represented for a comparison with the measured membrane stress.

In *Figure 6.36* the membrane and bending stress are reported in function of the applied load for the 3rd loading ramp. The real applied load is not equal to the ideal load due to an imprecision of the machine, as reported in the Appendix H.

The difference between the theoretical stress line and the membrane stress line are roughly equal to the case of 1st loading ramp. Indeed as the *Table H.12* shows, the relative error between the membrane stress and the theoretical one is included between -0.81% , obtained in the superior part of the welded joint, and 11.66% , obtained in the inferior part of the welded joint.

As the graph in *Figure 6.36* shows, the bending stress can be consider roughly constant. Furthermore as before, for an external force equal to 0 kN, the sample is subjected to a bending stress.

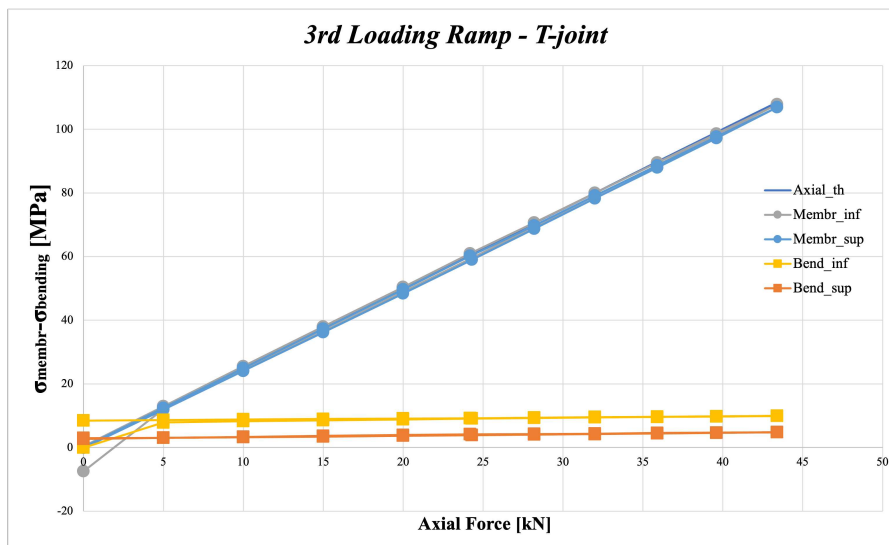


Figure 6.36: Distribution of the membrane and bending stress obtained in the T-joint for the application of the 3rd loading ramp. In the graph, the theoretical stress are represented for a comparison with the measured membrane stress.

The obtained results are in according with the results of Berto [65]. The comparison is done only for applied loads equal to 10, 20 and 30 kN because in this work has been applied a different loading ramp. Indeed, Berto

has applied a ramp from 0 kN to 135 kN for the T-joint with a different step size.

Another important difference between the tests is that in this thesis the axial testing machine used is a *Schenck Hydropuls®PSA*, instead Berto has used *MFL SYSTEME*. The comparison between the results is not done for applied force equal to 40 kN and 50 kN because, as described before, in this case the Schenck machine are not able to apply exactly the desired load, unlike the *MFL SYSTEME*. The comparison is done in terms of membrane stress and it is reported in the following table:

F_{real} [kN]	$F_{Pullin-Berto}$ [kN]	$\sigma_{membr,inf,avg}$ [MPa]	$\sigma_{membr,sup,avg}$ [MPa]	$\sigma_{membr,inf,Pul-Ber}$ [MPa]	$\sigma_{membr,sup,Pul-Ber}$ [MPa]	$\Delta_{inf}\%$	$\Delta_{sup}\%$
10	10	24.263	24.210	25.441	24.102	-4.63	0.45
20	20	48.801	48.597	51.191	49.028	-4.67	-0.88
28.23	30	69.395	69.070	77.765	73.542	-10.76	-6.08

Table 6.8: Comparison of the results for the T-joint.

6.4 Detection of the misalignment effect

In this paragraph the factor k_{mis} , that considers the effect of misalignment, will be calculated in three different way:

1. The first k_{mis} is calculated by the using of the formula obtained in the paragraph 5.2.8. These formula are obtained by a statistical analysis with the minimization of the standard deviation value;
2. The second one is calculated from the formula obtained from the IIW guideline [1];
3. The third k_{mis} is obtained from experimental data.

6.4.1 Calculation of k_{mis} with obtained formula in paragraph 5.2.8

The value of k_{mis} for the cruciform and T-joint are calculated from the formulas obtained in the paragraph 5.2.8 in case of fixed and free slope. The expression are the following:

- Formula obtained from the consideration of stress intensity factor calculated by the application of the Effective Notch Stress method with a free slope:

$$k_{mis} = \gamma^{1+\beta \cdot \frac{a_{tot}}{r}} \quad (6.21)$$

where:

- $\beta = 1.342$;
- $\gamma = 1.266$.

- Formula obtained from the consideration of stress intensity factor calculated by the application of the Effective Notch Stress method with a fixed slope $m = 3$:

$$k_{mis} = \gamma^{1+\beta \cdot \frac{a_{tot}}{r}} \quad (6.22)$$

where:

- $\beta = 1.224$;
- $\gamma = 1.374$.

- Formula obtained from the consideration of stress intensity factor calculated by the application of the Peak Stress Method with a free slope:

$$k_{mis} = \gamma^{1-\beta \cdot \frac{a_{tot}}{r}} \quad (6.23)$$

where:

- $\beta = 0.659$;

– $\gamma = 0.996$.

- Formula obtained from the consideration of stress intensity factor calculated by the application of the Peak Stress Method with a fixed slope $m = 3$:

$$k_{mis} = \gamma^{\frac{1}{1-\beta \cdot \frac{e_{tot}}{l}}} \quad (6.24)$$

where:

– $\beta = 0.630$;

– $\gamma = 0.975$.

The welded joints, as described in the paragraph 6.2.1, are characterised by two different types of misalignment:

1. Axial misalignment e ;
2. Angular misalignment α ;

The angular misalignment α is converted in an equivalent axial misalignment with the following formula:

$$e_{new} = \frac{l}{2} \cdot \tan(\alpha) \quad (6.25)$$

where l is the total length of the sample. Thus the total misalignment of the welded joint is defined as follows:

$$e_{tot} = e + e_{new} = e + \frac{l}{2} \cdot \tan(\alpha) \quad (6.26)$$

The results are reported in the following tables:

Method	β	γ	Formula of k_{mis}	Slope	e [mm]	α [°]	l/2 [mm]	e_{tot} [mm]	t [mm]	k_{mis}
ENS	1.342	1.266	$\gamma^{\frac{1}{1+\beta \cdot \frac{e_{tot}}{l}}}$	Free	1.323	0.243	150	1.96	10	1.2053
ENS	1.224	1.274	$\gamma^{\frac{1}{1+\beta \cdot \frac{e_{tot}}{l}}}$	Fixed	1.323	0.243	150	1.96	10	1.2921
PSM	0.659	0.996	$\gamma^{\frac{1}{1-\beta \cdot \frac{e_{tot}}{l}}}$	Free	1.323	0.243	150	1.96	10	0.9954
PSM	0.630	0.975	$\gamma^{\frac{1}{1-\beta \cdot \frac{e_{tot}}{l}}}$	Fixed	1.323	0.243	150	1.96	10	0.9715

Table 6.9: Results of k_{mis} for the cruciform joint.

Method	β	γ	Formula of k_{mis}	Slope	e [mm]	α [°]	l/2 [mm]	e_{tot} [mm]	t [mm]	k_{mis}
ENS	1.342	1.266	$\gamma^{\frac{1}{1+\beta \cdot \frac{e_{tot}}{l}}}$	Free	0	0.96	150	2.51	10	1.1929
ENS	1.224	1.274	$\gamma^{\frac{1}{1+\beta \cdot \frac{e_{tot}}{l}}}$	Fixed	0	0.96	150	2.51	10	1.2750
PSM	0.659	0.996	$\gamma^{\frac{1}{1-\beta \cdot \frac{e_{tot}}{l}}}$	Free	0	0.96	150	2.51	10	0.9952
PSM	0.630	0.975	$\gamma^{\frac{1}{1-\beta \cdot \frac{e_{tot}}{l}}}$	Fixed	0	0.96	150	2.51	10	0.9704

Table 6.10: Results of k_{mis} for the T-joint.

6.4.2 Calculation of k_{mis} with formula from IIW guideline [1]

In this case the value of the k_{mis} factor is calculated using the formula obtained from the IIW recommendations [1].

The cruciform joint is characterised by an angular and axial misalignment, thus the following formula are used to consider the effect of the angular misalignment in a cruciform joint:

$$k_{mis,angular} = 1 + \lambda \cdot \alpha \cdot \frac{\left(\frac{l}{2}\right)^2}{t \cdot \frac{l}{2}} \quad (6.27)$$

where:

- λ is a constant that depends on the restraint and in this case is equal to 3;
- α is the angular misalignment of the cruciform joint expresses in radiant ($4.24 \cdot 10^{-3} rad$);
- l is the total length of the specimen (300 mm);
- t is the thickness of the specimen (10 mm).

If the values of the parameters are inserted in the equation (6.27) the results is:

$$k_{mis,angular} = 1 + \lambda \cdot \alpha \cdot \frac{\left(\frac{l}{2}\right)^2}{t \cdot l} = 1 + 3 \cdot 4.24 \cdot 10^{-3} \cdot \frac{\left(\frac{300}{2}\right)^2}{10 \cdot 300} = 1.0954 \quad (6.28)$$

The following formula are used to consider the effect of the axial misalignment in a cruciform joint:

$$k_{mis,axial} = 1 + \lambda \cdot \alpha \cdot \frac{e \cdot \frac{l}{2}}{t \cdot l} \quad (6.29)$$

where:

- λ is a constant that depends on the restraint and in this case is equal to 3;
- e is the axial misalignment of the cruciform joint expresses in millimetres (1.323 mm);
- l is the total length of the specimen (300 mm);
- t is the thickness of the specimen (10 mm).

If the values of the parameters are inserted in the equation (6.29) the results is:

$$k_{mis,axial} = 1 + \lambda \cdot \alpha \cdot \frac{e \cdot \frac{l}{2}}{t \cdot l} = 1 + 3 \cdot \frac{1.323 \cdot \frac{300}{2}}{10 \cdot 300} = 1.198 \quad (6.30)$$

To consider the effect of both misalignment, the following formula is used:

$$k_{mis,IIW} = 1 + (k_{mis,axial} - 1) + (k_{mis,angular} - 1) \quad (6.31)$$

If the values of the $k_{mis,angular}$ and $k_{mis,axial}$ are inserted in the equation (6.31) the results is:

$$k_{mis,IIW} = 1 + (k_{mis,axial} - 1) + (k_{mis,angular} - 1) = 1 + (1.198 - 1) + (1.0954 - 1) = 1.2939 \quad (6.32)$$

The T-joint is characterised by only an angular misalignment, so the k_{mis} factor is defined as follows:

$$k_{mis,angular} = 1 + \lambda \cdot \alpha \cdot \frac{\left(\frac{l}{2}\right)^2}{t \cdot l} \quad (6.33)$$

where:

- λ is a constant that depends on the restraint and in this case is equal to 3;
- α is the angular misalignment of the cruciform joint expresses in radiant (0.0168 rad);
- l is the total length of the specimen (300 mm);
- t is the thickness of the specimen (10 mm).

The equation (6.33) is valid for angular misalignment of cruciform joint. Due to the lack of a formula for T-joint, the equation is extended for this type of joint.

If the values of the parameters are inserted in the equation (6.33) the results is:

$$k_{mis,angular} = 1 + \lambda \cdot \alpha \cdot \frac{\left(\frac{l}{2}\right)^2}{t \cdot l} = 1 + 3 \cdot 0.0168 \cdot \frac{\left(\frac{300}{2}\right)^2}{10 \cdot 300} = 1.377 \quad (6.34)$$

The results are summarised in the following table:

Joint	e [mm]	α [rad]	l [mm]	t [mm]	$k_{mis,angular}$	$k_{mis,axial}$	$k_{mis,tot}$
Cruciform	1.323	$4.24 \cdot 10^{-3}$	300	10	1.0954	1.198	1.2939
T-joint	0	0.0168	300	10	1.377	1	1.377

Table 6.11: Summary of results of $k_{mis,IW}$.

6.4.3 Calculation of k_{mis} from experimental data

In this case the value of the k_{mis} factor is calculated from the experimental data obtained from the previous test. Firstly, the ratio between the σ_{bend} and σ_{membr} is calculated for each test and for each applied load. This ratio is called R in this thesis. Subsequently, the average value is calculated. The results are reported in the following table:

$F_{real,avg}$ [kN]	Test 1		Test 2		Test 3		Average value	
	R_{inf}	R_{sup}	R_{inf}	R_{sup}	R_{inf}	R_{sup}	$R_{inf,avg}$	$R_{sup,avg}$
5	0.2228	0.6812	0.1917	0.6759	0.1998	0.7200	0.2048	0.6924
10	0.3127	0.5125	0.2961	0.5091	0.2992	0.5318	0.3027	0.5178
15	0.3391	0.4549	0.3259	0.4533	0.3303	0.4683	0.3318	0.4588
20	0.3501	0.4247	0.3425	0.4233	0.3480	0.4367	0.3469	0.4283
24.93	0.3553	0.4066	0.3489	0.4039	0.3508	0.4150	0.3517	0.4085
29.27	0.3573	0.3952	0.3512	0.3909	0.3536	0.4009	0.3541	0.3957
33.33	0.3580	0.3880	0.3511	0.3798	0.3545	0.3908	0.3545	0.3862
37.23	0.3575	0.3812	0.3513	0.3721	0.3467	0.3713	0.3519	0.3749
41.07	0.3522	0.3663	0.3518	0.3666	0.3481	0.3673	0.3507	0.3667
44.83	0.3531	0.3647	0.3518	0.3621	0.3487	0.3645	0.3512	0.3637
40.93	0.3461	0.3688	0.3498	0.3661	0.3477	0.3686	0.3479	0.3678
36.97	0.3450	0.3737	0.3492	0.3711	0.3453	0.3732	0.3465	0.3727
32.97	0.3419	0.3801	0.3473	0.3767	0.3431	0.3796	0.3441	0.3788
28.96	0.3378	0.3873	0.3443	0.3844	0.3399	0.3868	0.3406	0.3862
24.83	0.3314	0.3975	0.3390	0.3929	0.3341	0.3964	0.3348	0.3956
20	0.3198	0.4120	0.3295	0.4072	0.3235	0.4119	0.3243	0.4104
15	0.2984	0.4365	0.3100	0.4293	0.3046	0.4364	0.3043	0.4341
10	0.2621	0.4862	0.2706	0.4738	0.2623	0.4809	0.2650	0.4803
5	0.1330	0.6257	0.1475	0.6095	0.1354	0.6114	0.1386	0.6155

Table 6.12: Results of ratio R for the cruciform joint.

$F_{real,avg}$ [kN]	Test 1		Test 2		Test 3		Average value	
	R_{inf}	R_{sup}	R_{inf}	R_{sup}	R_{inf}	R_{sup}	$R_{inf,avg}$	$R_{sup,avg}$
5	0.6522	0.2485	0.6413	0.2556	0.6482	0.2552	0.6472	0.2531
10	0.3429	0.1318	0.3368	0.1356	0.3394	0.1341	0.3397	0.1338
15	0.2366	0.0919	0.2322	0.0944	0.2339	0.0950	0.2342	0.0938
20	0.1827	0.0718	0.1802	0.0747	0.1809	0.0758	0.1813	0.0741
24.33	0.1535	0.0628	0.1510	0.0652	0.1521	0.0652	0.1522	0.0644
28.23	0.1344	0.0526	0.1326	0.0588	0.1338	0.0590	0.1336	0.0568
32.10	0.1204	0.0488	0.1186	0.0540	0.1192	0.0533	0.1194	0.0520
35.93	0.1095	0.0451	0.1074	0.0500	0.1081	0.0505	0.1083	0.0485
39.67	0.1005	0.0438	0.0988	0.0472	0.0992	0.0475	0.0995	0.0462
43.50	0.0936	0.0411	0.0921	0.0442	0.0921	0.0448	0.0926	0.0434
39.67	0.1016	0.0438	0.0985	0.0473	0.0990	0.0475	0.0997	0.0462
35.93	0.1096	0.0468	0.1072	0.0510	0.1077	0.0513	0.1082	0.0497
32.07	0.1205	0.0499	0.1179	0.0557	0.1189	0.0550	0.1191	0.0535
28.20	0.1343	0.0548	0.1319	0.0607	0.1322	0.0609	0.1328	0.0588
24.37	0.1533	0.0628	0.1505	0.0672	0.1509	0.0683	0.1516	0.0661
20	0.1817	0.0732	0.1793	0.0787	0.1807	0.0786	0.1806	0.0768
15	0.2376	0.0903	0.2340	0.0977	0.2357	0.0973	0.2358	0.0951
10	0.3453	0.1231	0.3439	0.1339	0.3452	0.1343	0.3448	0.1304
5	0.6600	0.2164	0.6640	0.2387	0.6691	0.2460	0.6644	0.2337

Table 6.13: Results of ratio R for the T-joint.

After that, the k_{mis} factor that considers the misalignment effect is defined as follows:

$$k_{mis} = \frac{\sigma_{membr,sup/inf} + \sigma_{bend,sup/inf}}{\sigma_{membr,sup/inf}} \quad (6.35)$$

If the values of the average stress are substituted inside the equation (6.35), the results are:

$F_{real,avg}$ [kN]	$\sigma_{membr,sup,avg}$ [MPa]	$\sigma_{membr,inf,avg}$ [MPa]	$\sigma_{bend,sup,avg}$ [MPa]	$\sigma_{bend,inf,avg}$ [MPa]	$k_{mis,exp,sup}$	$k_{mis,exp,inf}$
5	12.85	13.02	8.90	2.67	1.693	1.205
10	25.73	25.93	13.32	7.85	1.518	1.303
15	38.59	38.84	17.71	12.88	1.459	1.332
20	51.47	51.69	22.04	17.93	1.428	1.347
24.93	64.18	64.52	26.22	22.69	1.408	1.352
29.27	75.35	75.77	29.82	26.83	1.396	1.354
33.33	85.67	86.24	33.09	30.58	1.386	1.355
37.23	95.28	96.50	35.72	33.95	1.375	1.352
41.07	104.80	106.47	38.43	37.34	1.367	1.351
44.83	114.77	116.29	41.75	40.84	1.364	1.351
40.93	104.79	106.46	38.55	37.04	1.368	1.348
36.97	94.55	96.28	35.24	33.36	1.373	1.346
32.97	84.20	85.91	31.90	29.56	1.379	1.344
28.96	73.77	75.54	28.49	25.73	1.386	1.341
24.83	63.15	64.94	24.98	21.74	1.396	1.335
20	50.62	52.49	20.78	17.02	1.410	1.324
15	37.72	39.60	16.37	12.05	1.434	1.304
10	24.83	26.66	11.93	7.06	1.480	1.265
5	11.91	13.77	7.33	1.91	1.616	1.139

Table 6.14: Results of $k_{mis,exp}$ for the cruciform joint.

$F_{real,avg}$ [kN]	$\sigma_{membr,sup,avg}$ [MPa]	$\sigma_{membr,inf,avg}$ [MPa]	$\sigma_{bend,sup,avg}$ [MPa]	$\sigma_{bend,inf,avg}$ [MPa]	$k_{mis,exp,sup}$	$k_{mis,exp,inf}$
5	16.10	12.10	3.05	7.83	1.190	1.647
10	28.28	24.26	3.24	8.24	1.115	1.340
15	40.44	36.48	3.41	8.54	1.084	1.234
20	52.17	48.80	3.60	8.85	1.069	1.181
24.33	62.57	59.63	3.82	9.07	1.061	1.152
28.23	72.27	69.40	3.92	9.27	1.054	1.134
32.10	81.87	79.12	4.09	9.45	1.050	1.119
35.93	91.44	88.81	4.29	9.62	1.047	1.108
39.67	100.90	98.30	4.51	9.78	1.045	1.099
43.50	104.27	108.02	4.66	10.01	1.045	1.093
39.67	95.10	98.83	4.53	9.85	1.048	1.100
35.93	85.90	89.65	4.42	9.70	1.052	1.108
32.07	76.50	80.22	4.26	9.56	1.056	1.119
28.20	66.99	70.80	4.13	9.40	1.062	1.133
24.37	57.16	61.16	4.01	9.27	1.070	1.152
20	46.00	50.53	3.85	9.12	1.084	1.181
15	33.62	38.11	3.59	8.99	1.107	1.236
10	21.22	25.60	3.31	8.83	1.156	1.345
5	8.74	13.04	3.01	8.66	1.344	1.664

Table 6.15: Results of $k_{mis,exp}$ for the T-joint.

Subsequently, the average value of the $k_{mis,exp,inf/sup}$ is calculated and the results are reported in the following table:

Type of Joint	$k_{mis,exp,sup,avg}$	$k_{mis,exp,inf,avg}$
Cruciform	1.433	1.318
T-joint	1.091	1.218

Table 6.16: Results of $k_{mis,exp,avg}$ for cruciform and T-joint.

Chapter 7

Conclusions

The present work delved into the effect of the misalignment on the fatigue behaviour of welded joint, made of steel, in CAL (Constant Amplitude Loading) and in VAL (Variable Amplitude Loading) condition. In the case of CAL condition, as described in the *Chapter 5*, four new design curve are proposed for the Effective Notch Stress approach and Peak Stress Method to consider the misalignment effect through the definition of a factor k_{mis} , that is a function of the thickness and the misalignment of the joint. The scatter band of these curve are obtained through a statistical analysis with the objective to minimize the standard deviation and the ratio T_{σ} . This method has been applied with a imposed slope m equal to 3 (typical value of the fatigue design curve for welded joint in as-welded condition) and also for a free slope. These design curve are represented in the following figure with the relative definition of the factor k_{mis} :

$$k_{mis} = \gamma^{1+\beta \cdot \frac{t}{t_0}} \quad (7.1)$$

where:

- $\beta = 1.342$;
- $\gamma = 1.266$.

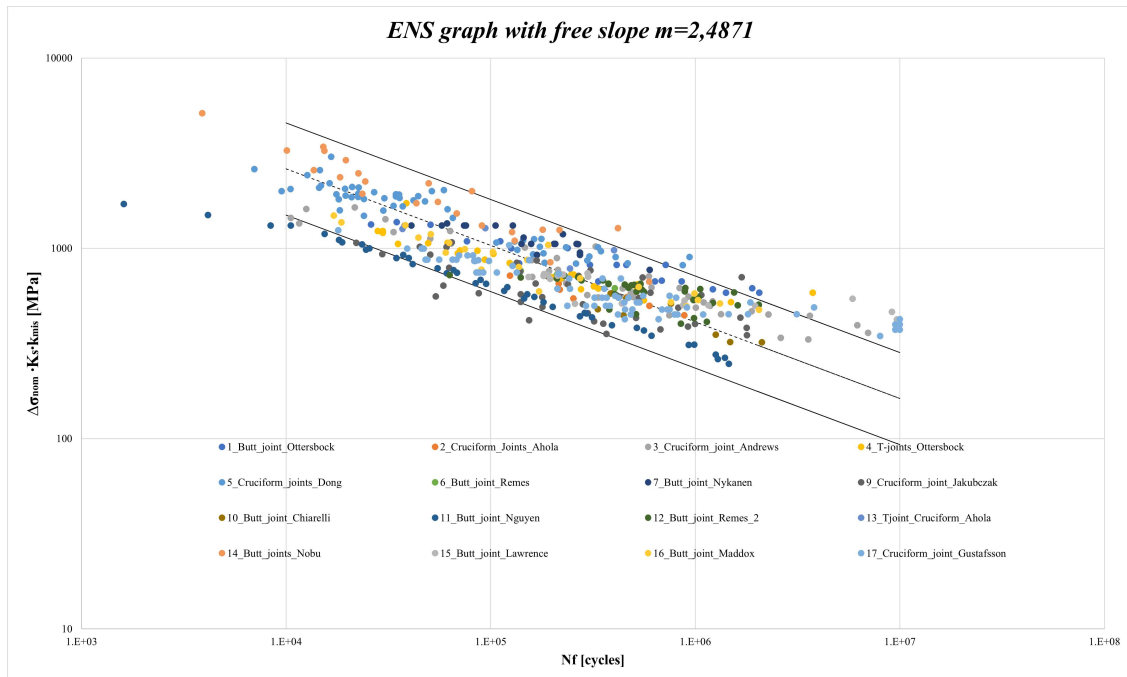


Figure 7.1: ENS Fatigue design curve for $\beta = 1.342$ and $\gamma = 1.266$ with free slope.

$$k_{mis} = \gamma^{1+\beta} \frac{1}{\sigma_{nom} \cdot K_S \cdot K_{mis}} \quad (7.2)$$

where:

- $\beta = 1.224$;
- $\gamma = 1.374$.

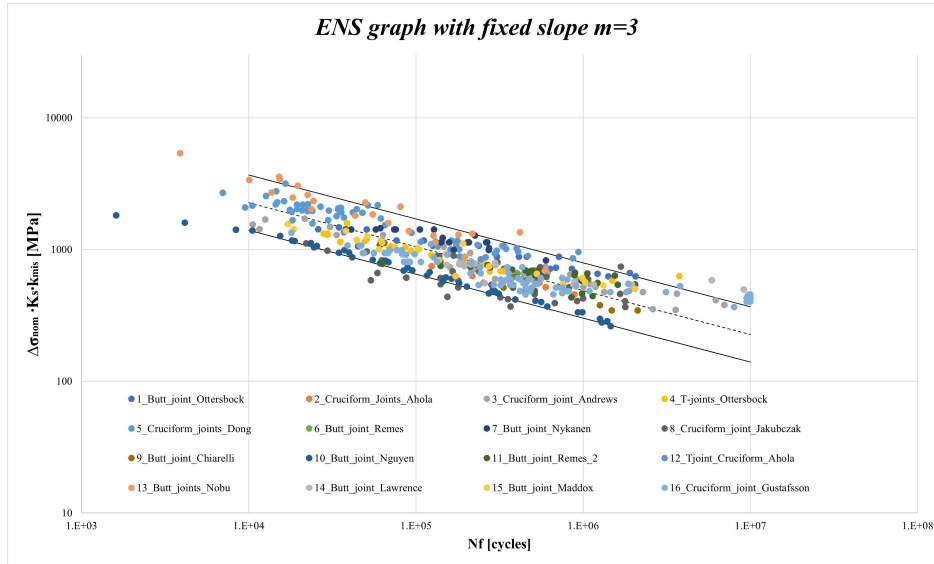


Figure 7.2: ENS Fatigue design curve for $\beta = 1.224$ and $\gamma = 1.374$ with fixed slope.

$$k_{mis} = \gamma^{1-\beta} \frac{1}{\sigma_{nom} \cdot K_S \cdot K_{mis}} \quad (7.3)$$

where:

- $\beta = 0.659$;
- $\gamma = 0.996$.

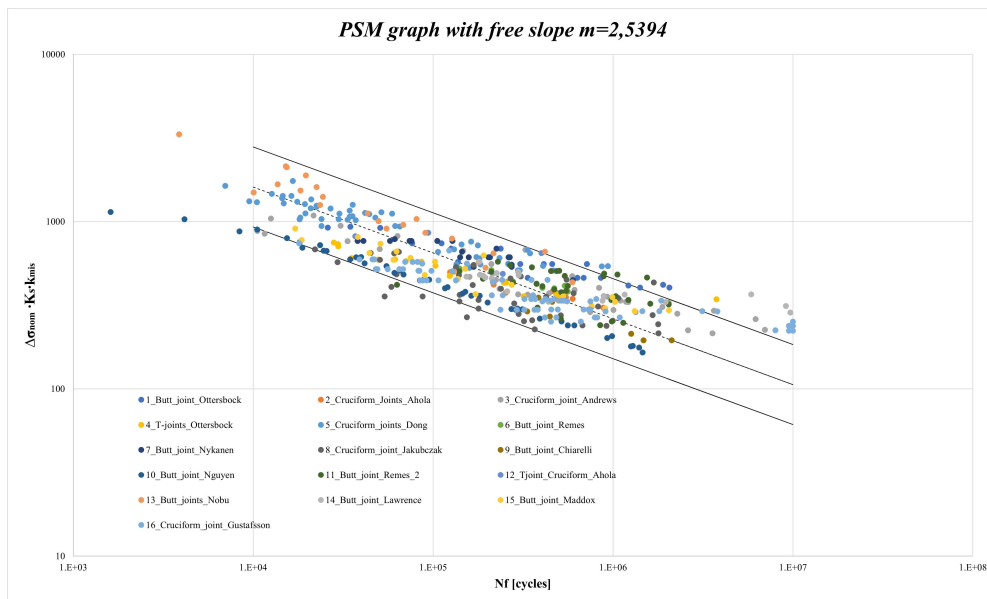


Figure 7.3: PSM Fatigue design curve for $\beta = 0.659$ and $\gamma = 0.996$ with free slope.

$$k_{mis} = \gamma^{1-\beta \cdot \frac{\epsilon_{tot}}{t}} \quad (7.4)$$

where:

- $\beta = 0.630$;
- $\gamma = 0.975$.

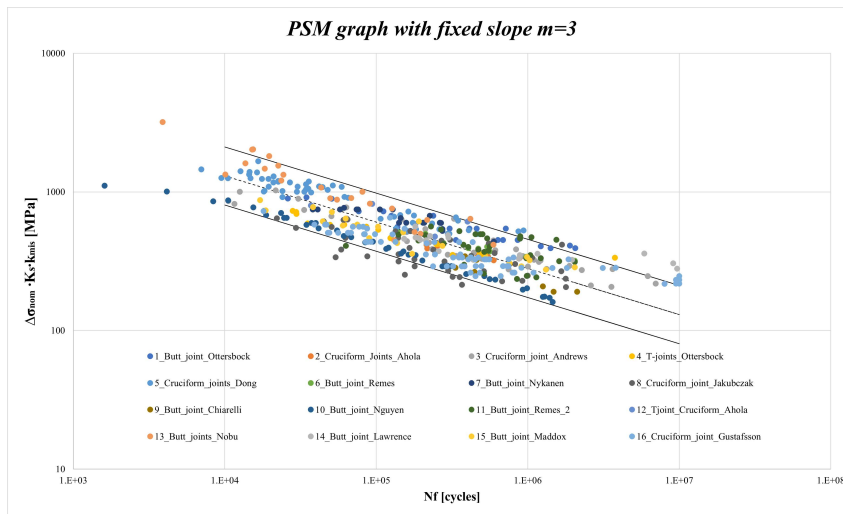


Figure 7.4: PSM Fatigue design curve for $\beta = 0.630$ and $\gamma = 0.975$ with fixed slope.

The expression of the k_{mis} are compared with the factor obtained from experimental results and from IIW guideline [1] in the *Chapter 6* for the welded joint analysed in the same chapter. The values of the k_{mis} factor are plotted in the following graph in terms of the applied force during the test and the results are summarised in the *Table 7.1*:

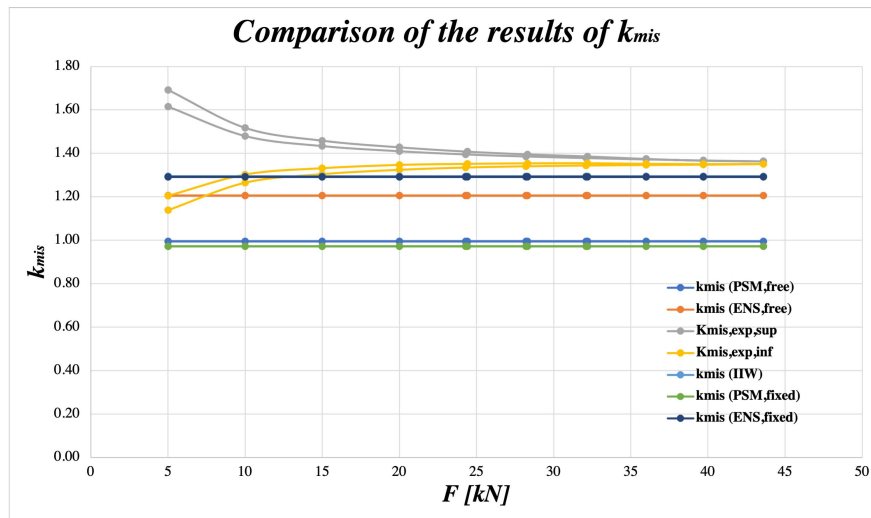


Figure 7.5: Comparison of the value of k_{mis} factor for the cruciform joint.

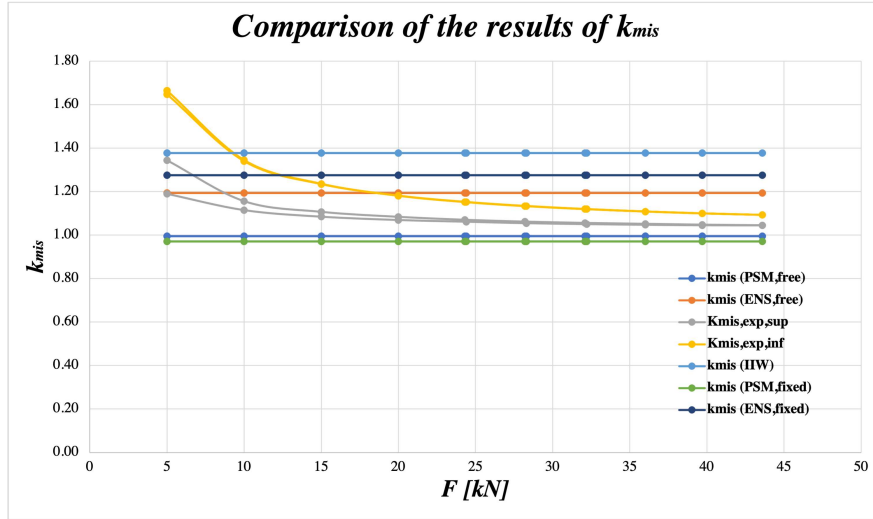


Figure 7.6: Comparison of the value of k_{mis} factor for the T-joint.

Cruciform Joint						
$k_{mis,PSM,free}$	$k_{mis,PSM,fixed}$	$k_{mis,ENS,free}$	$k_{mis,ENS,fixed}$	$k_{mis,IIW}$	$k_{mis,exp,inf,avg}$	$k_{mis,exp,sup,avg}$
0.9954	0.9715	1.2053	1.2921	1.2939	1.318	1.433
T-Joint						
0.9952	0.9704	1.1929	1.2750	1.377	1.218	1.091

Table 7.1: Results of k_{mis} for the cruciform and T-joint.

The relative errors between $k_{mis,ENS,fixed}$, $k_{mis,IIW}$, $k_{mis,exp,inf,avg}$ and $k_{mis,exp,sup,avg}$ are calculated for the cruciform joint:

$$\Delta\%_{ENS,fixed/IIW} = \frac{k_{mis,ENS,fixed} - k_{mis,IIW}}{k_{mis,IIW}} \cdot 100 = -0.139\% \quad (7.5)$$

$$\Delta\%_{ENS,free/exp,inf,avg} = \frac{k_{mis,ENS,free} - k_{mis,exp,inf,avg}}{k_{mis,exp,inf,avg}} \cdot 100 = -8.551\% \quad (7.6)$$

$$\Delta\%_{ENS,free/exp,sup,avg} = \frac{k_{mis,ENS,free} - k_{mis,exp,sup,avg}}{k_{mis,exp,sup,avg}} \cdot 100 = -15.890\% \quad (7.7)$$

$$\Delta\%_{ENS,fixed/exp,inf,avg} = \frac{k_{mis,ENS,fixed} - k_{mis,exp,inf,avg}}{k_{mis,exp,inf,avg}} \cdot 100 = -1.965\% \quad (7.8)$$

$$\Delta\%_{ENS,fixed/exp,sup,avg} = \frac{k_{mis,ENS,fixed} - k_{mis,exp,sup,avg}}{k_{mis,exp,sup,avg}} \cdot 100 = -9.833\% \quad (7.9)$$

The relative errors between $k_{mis,ENS,fixed}$, $k_{mis,IIW}$, $k_{mis,exp,inf,avg}$ and $k_{mis,exp,sup,avg}$ are calculated for the T-joint:

$$\Delta\%_{ENS,fixed/IIW} = \frac{k_{mis,ENS,fixed} - k_{mis,IIW}}{k_{mis,IIW}} \cdot 100 = -7.407\% \quad (7.10)$$

$$\Delta\%_{ENS,free/exp,inf,avg} = \frac{k_{mis,ENS,free} - k_{mis,exp,inf,avg}}{k_{mis,exp,inf,avg}} \cdot 100 = -2.061\% \quad (7.11)$$

$$\Delta\%_{ENS,free/exp,sup,avg} = \frac{k_{mis,ENS,free} - k_{mis,exp,sup,avg}}{k_{mis,exp,sup,avg}} \cdot 100 = -9.340\% \quad (7.12)$$

$$\Delta\%_{ENS,fixed/exp,inf,avg} = \frac{k_{mis,ENS,fixed} - k_{mis,exp,inf,avg}}{k_{mis,exp,inf,avg}} \cdot 100 = -4.680\% \quad (7.13)$$

$$\Delta\%_{ENS,fixed/exp,sup,avg} = \frac{k_{mis,ENS,fixed} - k_{mis,exp,sup,avg}}{k_{mis,exp,sup,avg}} \cdot 100 = -16.865\% \quad (7.14)$$

As the graphs shows, for the cruciform joint the experimental values of the k_{mis} are higher than both of k_{mis} obtained from the IIW guideline [1] and the proposed formulas. Instead, for the T-joints the values of the factor

proposed from IIW guideline [1] and the new formula of k_{mis} for ENS are higher than the experimental value. These consideration is in according with the initial hypothesis because the external load of the cruciform joint is applied on the plate made of ADI 1050 (so the Young modulus of the ADI 1050 is used for the calculation of the membrane and bending stress), instead of the T-joint where the load is applied on the steel plate(so the Young modulus of the steel is used for the calculation of the membrane and bending stress). Indeed, the proposed formula are valid for the welded joint made of steel with different mechanical properties.

Another important consideration is that the value of k_{mis} calculated with the formula proposed in this work for ENS method with fixed slope and with the formula of IIW guideline [1] are in according each other for the cruciform joint. In the case of the T-joint, the relative error between $k_{mis,ENS,fixed}$ and $k_{mis,IIW}$ are higher than the cruciform joint because the formula of the IIW guideline [1] is calibrated for the cruciform joint and not for T-joint.

The proposed expression of the k_{mis} factor in the case of the application of ENS approach, can substitute the expression defined in the IIW guideline [1] (equations (6.27) and (6.29)) for the fatigue behaviour assessment of steel welded joint in as-welded condition and subjected to an axial load.

In the case of VAL condition, as described in the *Chapter 5*, four new design curve are proposed for the Effective Notch Stress approach and Peak Stress Method to consider the misalignment effect through the definition of a factor k_{mis} , that is a function of the thickness and the misalignment of the joint. In this case, the welded joint analysed are characterised by a HFMI post welded treatment. The scatter band of these curve are obtained through a statistical analysis with the objective to minimize the standard deviation and the ratio T_σ . This method has been applied with a imposed slope m equal to 5 (typical value of the fatigue design curve for welded joint HFMI post-welded treatment) and also for a free slope. These design curve are represented in the following figure with the relative definition of the factor k_{mis} :

$$k_{mis} = \gamma^{1-\beta \frac{t}{t_0}} \quad (7.15)$$

where:

- $\beta = 0.599$;
- $\gamma = 0.998$.

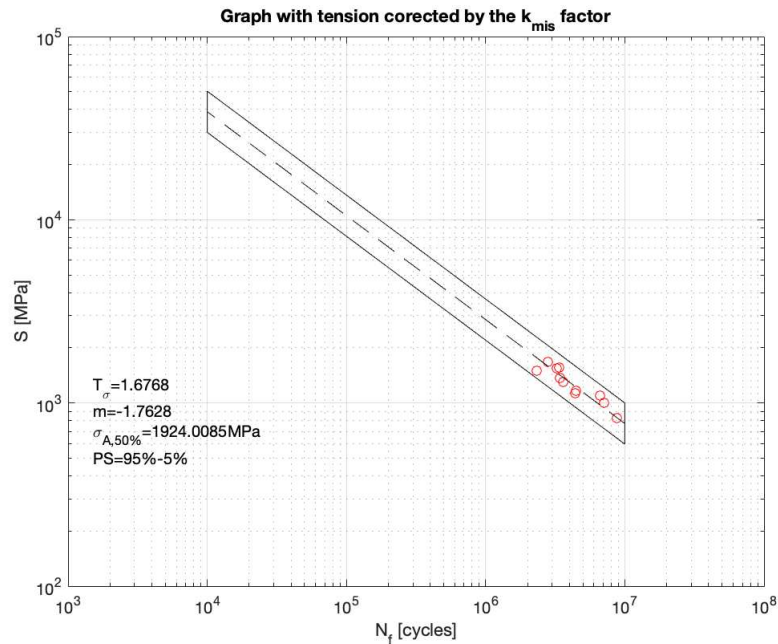


Figure 7.7: ENS Fatigue design curve for $\beta = 0.599$ and $\gamma = 0.998$ with free slope (VAL condition).

$$k_{mis} = \gamma^{1-\beta \cdot \frac{\sigma_{ref}}{S}} \quad (7.16)$$

where:

- $\beta = 0.391$;
- $\gamma = 0.966$.

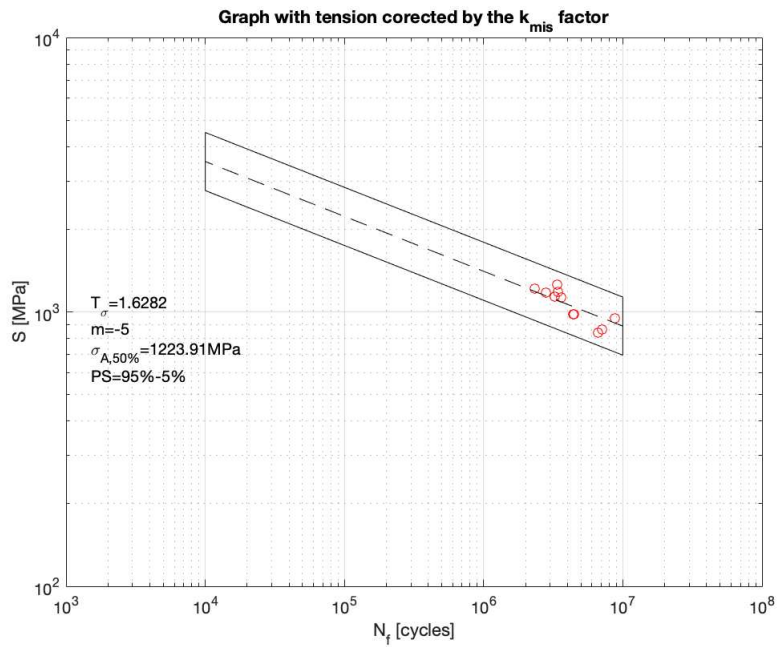


Figure 7.8: ENS Fatigue design curve for $\beta = 0.391$ and $\gamma = 0.966$ with fixed slope (VAL condition).

$$k_{mis} = \gamma^{1-\beta \cdot \frac{\sigma_{ref}}{S}} \quad (7.17)$$

where:

- $\beta = 0.599$;
- $\gamma = 0.998$.

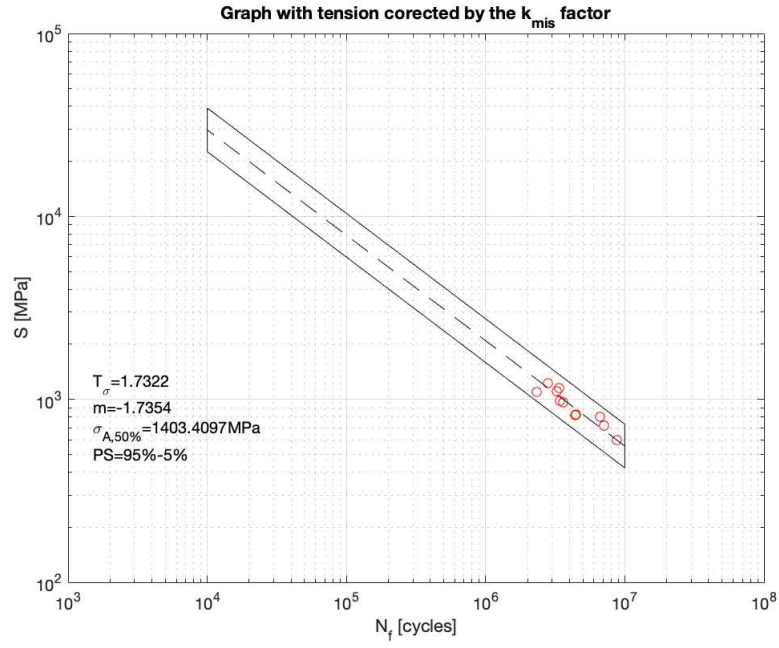


Figure 7.9: PSM Fatigue design curve for $\beta = 0.599$ and $\gamma = 0.998$ with free slope (VAL condition).

$$k_{mis} = \gamma^{1-\beta \cdot \frac{1}{T_{\sigma}}} \quad (7.18)$$

where:

- $\beta = 0.338$;
- $\gamma = 0.891$.

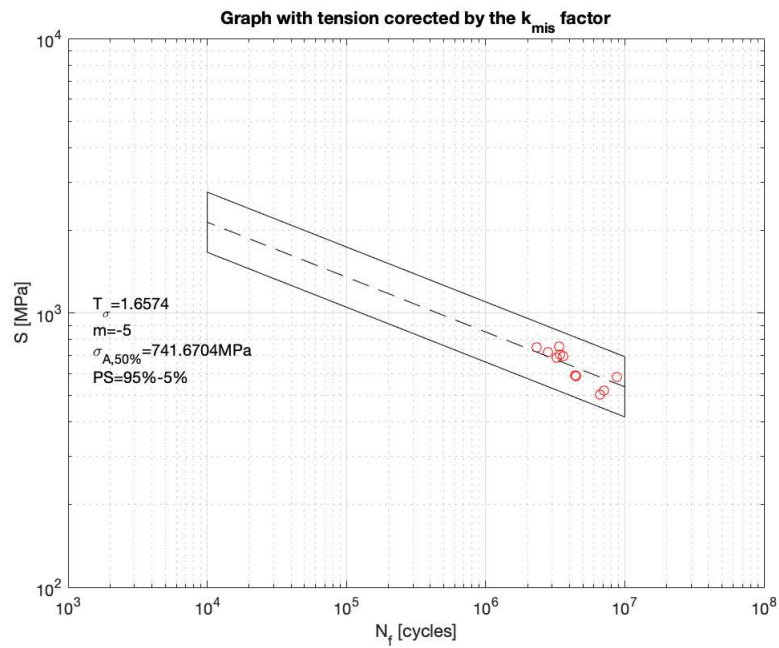


Figure 7.10: PSM Fatigue design curve for $\beta = 0.338$ and $\gamma = 0.891$ with fixed slope.

7.1 Future improvements

As further developments:

1. The FE analysis for the application of ENS and PSM approaches should be improved with the imposition of displacement to simulate the action of the clamps when the specimen is inserted in the test machine;
2. Experimental data collection of the misalignment joint in CAL condition should be performed at the University of Padua;
3. The procedure to detect the k_{mis} should be extended for HFMI welded joint in CAL condition;
4. To obtain a more accurate definition of the k_{mis} factor in VAL condition, the number of specimen should be increase;
5. The definition of the k_{mis} factor in VAL condition should be verify and compared with experimental results. Thus, the same experimental procedure executed for CAL condition should be applied.

Appendix A

Nodal stress $\Delta\sigma_{yy}$ and $\Delta\sigma_{11}$ and relative comparison

A.1 Brace side

$\Delta\sigma_{11}[MPa]$	$\Delta\sigma_{yy}[MPa]$	$\phi[^\circ]$	$\Delta\sigma_{yy,avg}[MPa]$	Rel. error yy-11 [%]
303.87	303.82	0	/	0.02
345.05	344.76	4.50	/	0.08
353.98	351.56	9.00	356.21	0.69
375.38	372.31	13.50	350.31	0.82
332.25	327.02	18.00	347.52	1.58
351.32	343.17	22.50	337.88	2.38
350.04	343.41	27.00	340.53	1.93
345.71	335.02	31.50	335.98	3.19
353.49	329.52	36.00	338.06	7.28
362.25	349.66	40.50	357.55	3.60
405.67	393.46	45.00	383.05	3.10
416.48	406.03	49.50	407.93	2.57
435.44	424.29	54.00	420.98	2.63
442.2	432.61	58.50	446.73	2.22
489.5	483.29	63.00	472.28	1.28
506.21	500.93	67.50	493.06	1.05
498.84	494.95	72.00	520.07	0.79
568.13	564.33	76.50	529.71	0.67
532.52	529.86	81.00	572.29	0.50
624.13	622.67	85.50	/	0.23
534.35	532.05	90.00	/	0.43

Table A.1: Nodal stress $\Delta\sigma_{yy}$ and $\Delta\sigma_{11}$ along the chord side and their relative error.

A.2 Chord side

$\Delta\sigma_{11}$ [MPa]	$\Delta\sigma_{yy}$ [MPa]	ϕ [°]	Rel. error [%]	$\Delta\sigma_{yy,avg}$ [MPa]
271.59	271.52	0.00	/	0.03
344.90	344.46	3.91	/	0.13
293.96	292.15	7.83	302.98	0.62
277.14	272.33	11.74	290.15	1.77
312.40	305.97	15.65	295.62	2.10
318.11	308.56	19.57	298.64	3.10
293.34	281.39	23.48	301.92	4.25
328.33	315.82	27.39	310.03	3.96
350.15	332.89	31.30	335.22	5.18
375.55	356.96	35.22	348.28	5.21
370.77	354.98	39.13	376.22	4.45
433.37	416.70	43.04	397.66	4.00
440.45	421.28	46.96	412.32	4.55
416.54	398.99	50.87	419.05	4.40
455.46	436.87	54.78	433.52	4.26
474.36	464.70	58.70	468.02	2.08
515.07	502.49	62.61	489.55	2.50
510.77	501.47	66.52	510.76	1.86
533.43	528.32	70.43	503.37	0.97
485.25	480.32	74.35	496.33	1.03
482.96	480.36	78.26	493.38	0.54
520.69	519.48	82.17	516.28	0.23
549.69	549.02	86.09	/	0.12
541.71	541.35	90.00	/	0.07

Table A.2: Nodal stress $\Delta\sigma_{yy}$ and $\Delta\sigma_{11}$ along the chord side and their relative error.

Appendix B

Nodal stress $\Delta\sigma_{11}$ and average peak stress value

B.1 Marquis 2010, longitudinal attachment FAT 71

Node	$\Delta\sigma_{11}$ [MPa]	$\overline{\Delta\sigma}_{yy,avg}$ [MPa]	$\overline{\Delta\sigma}_{11,peak}$
2	2.674	/	2.517
8	2.537	/	
6	2.420	2.517	
4	2.593	2.437	
1	2.294	2.449	
893	2.462	2.364	
891	2.331	2.357	
889	2.271	2.246	
887	2.126	2.150	
885	2.050	2.053	
883	1.984	1.972	
881	1.882	1.868	
879	1.737	1.752	
877	1.637	1.660	
875	1.605	1.549	
873	1.406	1.423	
871	1.257	1.278	
869	1.170	1.163	
867	1.060	1.072	
865	0.984	0.987	
863	0.918	/	
712	0.877	/	

Table B.1: Nodal stress $\Delta\sigma_{11}$ and averaged stress value along the weld toe.

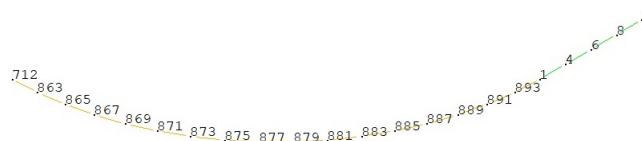


Figure B.1: Selected nodes along the weld toe.

B.2 Vanrostenberghe 2010, longitudinal attachment FAT 63

10 mm

Node	$\Delta\sigma_{11}$ [MPa]	$\overline{\Delta\sigma}_{yy,avg}$ [MPa]	$\overline{\Delta\sigma}_{11,peak}$
2	3.535	/	3.550
10	3.263	/	
8	4.004	3.462	
6	3.120	3.546	
4	3.514	3.341	
1	3.390	3.550	
879	3.747	3.480	
877	3.304	3.276	
875	2.777	2.851	
873	2.473	2.425	
871	2.024	2.081	
869	1.747	1.727	
867	1.411	/	
716	1.149	/	

Table B.2: Nodal stress $\Delta\sigma_{11}$ and averaged stress value along the weld toe.

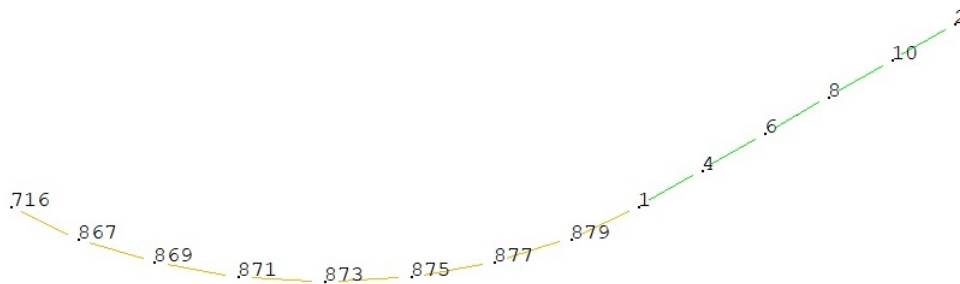


Figure B.2: Selected nodes along the weld toe.

20 mm

Node	$\Delta\sigma_{11}$ [MPa]	$\overline{\Delta\sigma}_{yy,avg}$ [MPa]	$\overline{\Delta\sigma}_{11,peak}$
2	4.112	/	3.778
20	3.537	/	
18	3.714	3.701	
16	3.850	3.778	
14	3.770	3.762	
12	3.667	3.659	
10	3.538	3.585	
8	3.548	3.585	
6	3.669	3.616	
4	3.632	3.668	
1	3.705	3.719	
895	3.819	3.716	
893	3.625	3.583	
891	3.304	3.363	
889	3.159	3.111	
887	2.869	2.974	
885	2.894	2.713	
883	2.376	2.428	
881	2.014	2.014	
879	1.654	1.684	
877	1.383	1.420	
875	1.222	/	
724	1.028	/	

Table B.3: Nodal stress $\Delta\sigma_{11}$ and averaged stress value along the weld toe.

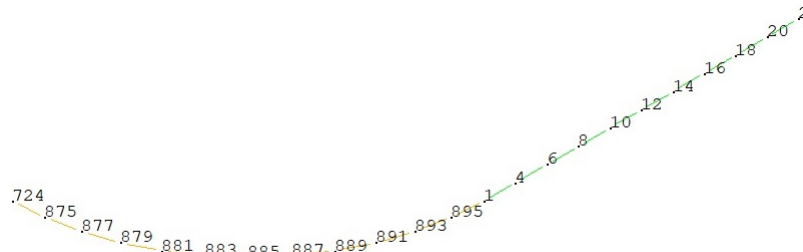


Figure B.3: Selected nodes along the weld toe.

Appendix C

Experimental results in As- welded condition

C.1 Marquis 2010, longitudinal stiffener FAT 71

Stress Ratio R	$\Delta\sigma_{nom}$ [MPa]	N_f [cycles]	$\Delta\sigma_{eq,peak,Tetra187}$ [MPa]	SED [MJ/mm ³]	SHSS _{LSE} [MPa]
-1	159.7	229 600	378.16	0.299	228.65
	158.9	265 500	376.27	0.296	227.50
	158.5	679 800	375.32	0.294	226.93
	149.5	402 100	354.01	0.262	214.04
	136.7	2 808 000	323.70	0.219	195.72
	116.8	564 900	276.58	0.160	167.23
	104.5	844 100	247.45	0.128	149.62
	100.5	6 403 000	237.98	0.118	143.89

Table C.1: Results of the 1st joint, Marquis 2010. The number barred represents the run-outs

C.2 Vanrostenberghe 2015, longitudinal stiffener FAT 63

10mm

Stress Ratio R	$\Delta\sigma_{nom}$ [MPa]	N_f [cycles]	$\Delta\sigma_{eq,peak,Tetra187}$ [MPa]	SED [MJ/mm ³]	SHSS _{LSE} [MPa]	$\Delta\sigma_{eq,peak,Brick185}$ [MPa]
0.1	50	10000000	0.059	168.641	70.183	167.196
	70	10000000	0.116	236.097	98.257	234.075
	90	3466968	0.191	303.554	126.330	300.953
	200	204202	0.944	674.563	280.733	668.784
	250	112546	1.475	843.204	350.917	835.981
	350	47716	2.891	1180.486	491.283	1170.373
	0.1	50	10000000	0.059	168.641	70.183
70		2333651	0.116	236.097	98.257	234.075
90		893070	0.191	303.554	126.330	300.953
200		88800	0.944	674.563	280.733	668.785
250		49800	1.475	843.204	350.917	835.981
300		33700	2.124	1011.845	421.100	1003.177

Table C.2: Results of the 1st joint, Vanrostenberghe 2015 10 mm. The number barred represents the run-outs

20mm

Stress Ratio R	$\Delta\sigma_{nom}$ [MPa]	N_f [cycles]	$\Delta\sigma_{eq,peak,Tetra187}$ [MPa]	SED [MJ/mm ³]	SHSS _{LSE} [MPa]	$\Delta\sigma_{eq,peak,Brick185}$ [MPa]
0.1	70	3600954	0.138	251.244	83.867	234.075
	90	1513276	0.228	323.028	107.829	300.953
	200	125887	1.126	717.839	239.620	668.784
	250	113433	1.760	897.299	299.525	835.981
	350	41521	3.449	1256.218	419.334	1170.373
0.5	70	10000000	0.138	251.244	83.867	234.075
	90	1612500	0.228	323.028	107.829	300.953
	125	828000	0.440	448.649	149.762	417.990
	200	136936	1.126	717.839	239.620	668.784
	250	85459	1.760	897.299	299.525	835.981
	300	49546	2.534	1076.759	359.429	1003.177

Table C.3: Results of the 1st joint, Vanrostenberghe 2015 20 mm. The number barred represents the run-outs

C.3 Yildirim 2020, transverse attachment FAT 80

Stress Ratio R	$\Delta\sigma_{nom}$ [MPa]	N_f [cycles]	$\Delta\sigma_{eq,peak,Plane182}$ [MPa]	SHSS _{LSE} [MPa]
0.1	153	827502	244.567	157.566
	190	334910	303.711	195.671
	153	837466	244.567	157.566
	190	383736	303.711	195.671
	117	11700000	187.022	120.492
	125	10052008	199.810	128.731
-0.43	190	608805	303.711	195.671
	243	201094	388.430	250.253
	153	1723400	244.567	157.566
	243	217785	388.430	250.253
	190	710346	303.711	195.671
	136	10122344	217.393	140.059

Table C.4: Results of the 3rd joint, Yildirim 2020. The number barred represents the run-outs

C.4 Okawa 2013, transverse attachment FAT 80

Stress Ratio R	$\Delta\sigma_{nom}$ [MPa]	N_f [cycles]	$\Delta\sigma_{eq,peak,Plane182}$ [MPa]	SHSS _{LSE} [MPa]
0.1	200	164000	434.833	213.217
	150	354000	326.125	159.913
	100	1320000	217.417	106.609
	80	5000000	173.933	85.287

Table C.5: Results of the 4th joint, Okawa 2013. The number barred represents the run-outs

C.5 Kuhulmann-Gunther 2009, transverse attachment FAT 80

Stress Ratio R	Material	$\Delta\sigma_{nom}$ [MPa]	N_f [cycles]	$\Delta\sigma_{eq,peak,Plane182}$ [MPa]	SHSS _{LSE} [MPa]
0.1	S355J2	300	67921	569.835	313.088
		300	64159	569.835	313.088
		170	574631	322.907	177.416
		170	456289	322.907	177.416
		125	1400261	237.431	130.453
		125	3712215	237.431	130.453
		225	185219	427.377	234.816
		225	168630	427.377	234.816
		125	1933751	237.431	130.453
0.1	S690QL	300	106797	569.835	313.088
		300	123652	569.835	313.088
		225	537534	427.377	234.816
		225	415746	427.377	234.816
		190	1028720	360.896	198.289
		190	575000	360.896	198.289
		190	1034355	360.896	198.289
		150	3517443	284.918	156.544
		150	1833757	284.918	156.544

Table C.6: Results of the 5th joint, Kuhlmann-Gunther 2009. The number barred represents the run-outs

Appendix D

Experimental results in HFMI-treated condition

D.1 Marquis 2010, longitudinal stiffener FAT 71

Stress Ratio R	$\Delta\sigma_{nom}$ [MPa]	N_f [cycles]	SED [MJ/mm ³]	$\Delta\sigma_{eq,peak,SED}$ [MPa]	SHSS _{LSE} [MPa]
-1	464	499 700	2.320	1024.805	664.321
	450	552 400	2.182	993.884	644.277
	446	208 600	2.143	985.050	638.550
	410	1 949 000	1.811	905.539	587.008
	337	964 800	1.224	744.309	482.492
	337	858 400	1.224	744.309	482.492
	317	447 500	1.083	700.136	453.857
	305	469 700	1.002	673.633	436.677
	257	2 907 000	0.712	567.618	367.954
	255	1 980 000	0.701	563.201	365.090

Table D.1: Results of the 1st joint in HFMI conditions, Marquis 2010.

D.2 Vanrostenberghe, longitudinal stiffener FAT 63

10mm

Material	Stress Ratio R	$\Delta\sigma_{nom}$ [MPa]	N_f [cycles]	SED [MJ/mm ³]	$\Delta\sigma_{eq,peak,SED}$ [MPa]	SHSS _{LSE} [MPa]
S700MC S690QL	0.1	90	10 000 000	0.112	225.418	126.330
		175	10 000 000	0.424	438.313	245.642
		90	6 000 000	0.112	225.418	126.330
		150	6 000 000	0.312	375.697	210.550
		90	2 000 000	0.112	225.418	126.330
		200	6 000 000	0.554	500.929	280.733
		225	10 000 000	0.701	563.545	315.825
		90	10 000 000	0.112	225.418	126.330
		200	10 000 000	0.554	500.929	280.733
		70	2 000 000	0.068	175.325	98.257
		90	2 000 000	0.112	225.418	126.330
		300	158 200	1.247	751.394	421.100
		150	2 031 700	0.312	375.697	210.550
		250	3 547 800	0.866	626.161	350.917
		350	101 200	1.697	876.626	491.283
		150	532 122	0.312	375.697	210.550
		350	187 828	1.697	876.626	491.283
		250	855 162	0.866	626.161	350.917
		350	82 506	1.697	876.626	491.283
		400	98 500	2.217	1001.858	561.467
250	317 200	0.866	626.161	350.917		
350	223 100	1.697	876.626	491.283		
225	18 010	0.701	563.545	315.825		
350	134 300	1.697	876.626	491.283		
S700MC	0.5	250	33 391	0.866	626.161	350.917
		200	84 895	0.554	500.929	280.733

Table D.2: Results of the 2nd joint, Vanrostenberghe 2015 in HFMI-treated condition. The number barred represents the run-outs.

20mm

Material	Stress Ratio R	$\Delta\sigma_{nom}$ [MPa]	N_f [cycles]	SED [MJ/mm ³]	$\Delta\sigma_{eq,peak,SED}$ [MPa]	SHSS _{LSE} [MPa]
S690QL	0.1	150	10 000 000	0.362	404.882	179.715
		250	10 000 000	1.006	674.803	299.525
		275	141 700	1.217	742.283	329.477
		200	480 200	0.644	539.842	239.620
		250	232 323	1.006	674.803	299.525
		350	80 830	1.971	944.724	419.334
		400	184 642	2.575	1079.685	359.429
		300	470 640	1.448	809.764	359.429
		350	123 655	1.971	944.724	419.334
S690QL	0.5	200	343 210	0.644	539.842	239.620
		125	1 019 256	0.251	337.402	149.762
		150	644 530	0.362	404.882	179.715
		275	56 926	1.217	742.283	329.477

Table D.3: Results of the 2nd joint in HFMI-treated condition, Vanrostenberghe 2015. The number barred represents the run-outs.

D.3 Yildirim 2020, transverse attachment FAT 80

Stress Ratio R	$\Delta\sigma_{nom}$ [MPa]	N_f [cycles]	SED [MJ/mm ³]	$\Delta\sigma_{eq,peak,SED}$ [MPa]	SHSS _{LSE} [MPa]
-0.43	242	798 406	0.344	450.038	249.223
	181	1 346 563	0.192	336.598	186.402
	242	433 673	0.344	450.038	249.223
	181	1 351 325	0.192	336.598	186.402
	181	1 695 096	0.192	336.598	186.402

Table D.4: Results of the 3rd joint in HFMI conditions, Yildirim 2020.

D.4 Okawa 2013, transverse attachment FAT 80

Stress Ratio R	$\Delta\sigma_{nom}$ [MPa]	N_f [cycles]	SED [MJ/mm ³]	$\Delta\sigma_{eq,peak,SED}$ [MPa]	SHSS _{LSE} [MPa]
-1	420	378 000	1.758	1017.268	447.756
	400	990 000	1.595	968.827	426.435
	380	2 295 000	1.439	920.386	405.113
0.1	250	5 000 000	0.623	605.517	266.522
	270	818 000	0.727	653.958	287.843
	260	1 067 000	0.674	629.738	277.183
	300	304 000	0.897	726.620	319.826
0.5	125	346 000	0.156	302.758	133.261
	175	346 000	0.305	423.862	186.565
	150	503 000	0.224	363.310	159.913
	135	3 450 000	0.182	326.979	143.922

Table D.5: Results of the 4th joint in HFMI conditions, Okawa 2013. The number barred represents the run-outs.

D.5 Kuhlmann-Gunther 2009, transverse attachment FAT 80

Material	Stress Ratio R	$\Delta\sigma_{nom}$ [MPa]	N_f [cycles]	SED [MJ/mm ³]	$\Delta\sigma_{eq,peak,SED}$ [MPa]	SHSS _{LSE} [MPa]
S355J2	0.1	300	1 426 998	0.752	665.414	313.088
		340	137 721	0.966	754.136	354.833
		340	116 159	0.966	754.136	354.833
		315	711 012	0.829	698.685	328.742
		315	298 866	0.829	698.685	328.742
		280	799 250	0.655	621.053	292.215
S690QL	0.1	340	768 457	0.9389	743.3803	354.8327
		340	478 283	0.9389	743.3803	354.8327
		315	759 450	0.8059	688.7200	328.7421
		315	1 270 270	0.8059	688.7200	328.7421
		400	193 512	1.2995	874.5651	417.4503
		400	228 100	1.2995	874.5651	417.4503
		280	2 119 665	0.6368	612.1956	292.2152

Table D.6: Results of the 5th joint in HFMI conditions, Kuhlmann-Gunther 2009.

D.6 Kuhlmann 2006, transverse attachment FAT 80

Material	Stress Ratio R	$\Delta\sigma_{nom}$ [MPa]	N_f [cycles]	SED [MJ/mm ³]	$\Delta\sigma_{eq,peak,SED}$ [MPa]	SHSS _{LSE} [MPa]
S355	0.1	306	108 489	0.666	625.881	321.751
		278	363 274	0.549	568.611	292.310
		253	455 624	0.455	517.477	266.023
		230	977 946	0.376	470.433	241.839
		261	349,432	0.484	533.839	274.435
		264	315 592	0.495	539.976	277.589
		217	1 146 656	0.335	443.844	228.170
		260	845 460	0.480	531.794	273.383
		320	89,949	0.728	654.516	336.472
		250	1 365 764	0.444	511.341	262.869
		294	200 637	0.614	601.336	309.133
S460	0.1	290	595 040	0.598	593.155	304.928
		320	174 924	0.728	654.516	336.472
		287	346 406	0.585	587.019	301.773
		250	992 769	0.444	511.341	262.869
		240	1 077822	0.409	490.887	252.354
		387	51 593	1.065	791.555	406.921
		294	221 726	0.614	601.336	309.133
		332	260 850	0.783	679.060	349.089
		356	162 744	0.901	728.149	374.325
		271	522 654	0.522	554.293	284.950

Table D.7: Results of the 6th joint in HFMI conditions, Kuhlmann 2006.

Appendix E

Matlab codes

E.1 MatLab code to build the model inside Ansys®APDL with the sampling

```
1  clc;
   clear all;
3  close all;

5  formatSpec = '%f_%f_%f';
   sizeA = [3 Inf];
7  data=importdata('355-WH-6.txt');%import cloud of points
   A=data;

9
11 for i=1:size(A,1)
    if A(i,1)==1
        A1(i,:)=A(i,:);
13    else
        A0(i,:)=A(i,:);
15
    end
17 end
   A0 = A0(~all(A0 == 0, 2),:);
19
   hold on
21 axis equal
   plot(A1(:,2),A1(:,3))
23 plot(A0(:,2),A0(:,3))

25 A1_camp=zeros(size(A1));
   A0_camp=zeros(size(A0));
27 n=10;% parameter for sampling

29 %Creation of matrix A1_camp
   for i=1:n:size(A1,1)
31     A1_camp(i,:)=A1(i,:);
   end
33 A1_camp = A1_camp(~all(A1_camp == 0, 2),:);
   plot(A1_camp(:,2),A1_camp(:,3),'r')
35
   %Creation of matrix A0_camp
37 for i=1:n:size(A0,1)
    A0_camp(i,:)=A0(i,:);
39 end

41 A0_camp = A0_camp(~all(A0_camp == 0, 2),:);
   plot(A0_camp(:,2),A0_camp(:,3),'r')
```

```

%Creation of matrix with the all coordinates after sampling
45 A_camp=[A1_camp;A0_camp];

47 %Opening of APDL file
fid=fopen('MAPDLi.txt','w');
49 fprintf(fid,'/CLEAR\n');

51 %Opening of Preprocessor
fprintf(fid,['/PREP7','\n']);
53
%Definition of element
55 fprintf(fid,'ET,1,PLANE182\n');
fprintf(fid,'KEYOPT,1,1,3\nKEYOPT,1,3,2\nKEYOPT,1,6,0\n');
57
%Definition of Material
59 E=206000;
ni=0.3;
61 fprintf(fid,['MPTEMP,,,,,,,,\nMPTEMP,1,0\nMPDATA,EX,1,,',num2str(E),'\n']);
fprintf(fid,['MPDATA,PRXY,1,,',num2str(ni),'\n']);
63

65 %Writing of keypoints
for i=1:size(A_camp)
67     fprintf(fid,['K,',num2str(i),',',num2str(A_camp(i,2)),',',num2str(A_camp(i,3)),',0','\n']);
end
69
%Interpolation to extend the joint
71
l=300;%length of the joint
73 L1=200;%length of constraint

75 %keypoint a x=-300 in top left
deltax= A1_camp(1,2)-A1_camp(2,2);
77 deltay= A1_camp(1,3)-A1_camp(2,3);
m=deltay/deltax;
79 xp=A1_camp(1,2);
yp=A1_camp(1,3);
81 y=@(x) m*(x-xp)+yp;
y1=y(-l);
83 fprintf(fid,['K,',num2str(i+1),',',num2str(-l),',',num2str(y1),',0','\n']);

85 %keypoint a x=-200 in top left
deltax=-l-A1_camp(1,2);
87 deltay=y1-A1_camp(1,3);
m=deltay/deltax;
89 xp=-l;
yp=y1;
91 y=@(x) m*(x-xp)+yp;
y5=y(-L1);
93 fprintf(fid,['K,',num2str(i+5),',',num2str(-L1),',',num2str(y5),',0','\n']);

95 %keypoint a x=-300 in bottom left
deltax= A0_camp(1,2)-A0_camp(2,2);
97 deltay= A0_camp(1,3)-A0_camp(2,3);
m=deltay/deltax;
99 xp=A0_camp(1,2);
yp=A0_camp(1,3);
101 y=@(x) m*(x-xp)+yp;
y2=y(-l);
103 fprintf(fid,['K,',num2str(i+2),',',num2str(-l),',',num2str(y2),',0','\n']);

105 %keypoint a x=-200 in bottom left
deltax=-l-A0_camp(1,2);

```

```

107 deltay=y2-A0_camp(1,3);
    m=deltay/deltax;
109 xp=-1;
    yp=y2;
111 y=@(x) m*(x-xp)+yp;
    y6=y(-L1);
113 fprintf(fid,['K',' ',num2str(i+6),' ',' ',num2str(-L1),' ',' ',num2str(y6),' ','0','\n']);

115 %keypoint a x=300 in top right
    deltax= A1_camp(end,2)-A1_camp(end-1,2);
117 deltay= A1_camp(end,3)-A1_camp(end-1,3);
    m=deltay/deltax;
119 xp=A1_camp(1,2);
    yp=A1_camp(1,3);
121 y=@(x) m*(x-xp)+yp;
    y3=y(1);
123 fprintf(fid,['K',' ',num2str(i+3),' ',' ',num2str(1),' ',' ',num2str(y3),' ','0','\n']);

125 %keypoint a x=200 in top right
    deltax=1-A1_camp(end,2);
127 deltay=y3-A1_camp(end,3);
    m=deltay/deltax;
129 xp=1;
    yp=y3;
131 y=@(x) m*(x-xp)+yp;
    y7=y(L1);
133 fprintf(fid,['K',' ',num2str(i+7),' ',' ',num2str(L1),' ',' ',num2str(y7),' ','0','\n']);

135
137 %keypoint a x=300 in bottom right
    deltax= A0_camp(end,2)-A0_camp(end-1,2);
    deltay= A0_camp(end,3)-A0_camp(end-1,3);
139 m=deltay/deltax;
    xp=A0_camp(1,2);
141 yp=A0_camp(1,3);
    y=@(x) m*(x-xp)+yp;
143 y4=y(1);
    fprintf(fid,['K',' ',num2str(i+4),' ',' ',num2str(1),' ',' ',num2str(y4),' ','0','\n']);
145
147 %keypoint a x=200 in top right
    deltax=1-A0_camp(end,2);
    deltay=y4-A0_camp(end,3);
149 m=deltay/deltax;
    xp=1;
151 yp=y4;
    y=@(x) m*(x-xp)+yp;
153 y8=y(L1);
    fprintf(fid,['K',' ',num2str(i+8),' ',' ',num2str(L1),' ',' ',num2str(y8),' ','0','\n']);
155

157 %Creation of the lines

159 for i=1:size(A_camp,1)-1
    if i==size(A1_camp,1)
161         i=i+1;
    end
163     fprintf(fid,['L',' ',num2str(i),' ',' ',num2str(i+1),' '\n']);

165 end

167 %Lines with the point that was created by interpolation
    fprintf(fid,['L',' ',' ',num2str(i+6),' ',' ','1','\n']);
169 fprintf(fid,['L',' ',' ',num2str(i+6),' ',' ',num2str(i+2),' '\n']);

```

```

fprintf(fid, ['L', ',', ',', num2str(size(A1_camp, 1)+1), ',', ',', num2str(i+7), '\n']);
171 fprintf(fid, ['L', ',', ',', num2str(i+7), ',', ',', num2str(i+3), '\n']);
fprintf(fid, ['L', ',', ',', num2str(size(A1_camp, 1)), ',', ',', num2str(i+8), '\n']);
173 fprintf(fid, ['L', ',', ',', num2str(i+8), ',', ',', num2str(i+4), '\n']);
fprintf(fid, ['L', ',', ',', num2str(size(A_camp, 1)), ',', ',', num2str(i+9), '\n']);
175 fprintf(fid, ['L', ',', ',', num2str(i+9), ',', ',', num2str(i+5), '\n']);

177 %Vertical Lines
fprintf(fid, ['L', ',', ',', num2str(i+2), ',', ',', num2str(i+3), '\n']);
179 fprintf(fid, ['L', ',', ',', num2str(i+4), ',', ',', num2str(i+5), '\n']);

181 %Creation of Area
fprintf(fid, ['FLST,2,', num2str(i+9), ',4\n']);
183
for i=1:size(A_camp,1)+8
185     fprintf(fid, ['FITEM,2,', num2str(i), '\n']);
end
187 fprintf(fid, 'AL,P51X\n');

189 %Creation of mesh
global_element_size=1;
191
fprintf(fid, ['ESIZE,', num2str(global_element_size), ',0,\n']);
193 fprintf(fid, 'MSHKEY,0\nCM,_Y,AREA\nASEL,,,,_4_\n');
fprintf(fid, 'CM,_Y1,AREA\nCHKMSH,' 'AREA' '\nCMSEL,S,_Y\n!* \n');
195 fprintf(fid, 'AMESH,_Y1\n!* \nCMDELE,_Y\nCMDELE,_Y1\nCMDELE,_Y2\n!* \n');

197 %Definition of constraint and Pressure
%Constraint
199 fprintf(fid, 'FLST,2,1,4,ORDE,1\n');
fprintf(fid, ['FITEM,2,', num2str(i-1), '\n']);
201 fprintf(fid, '!*\n/GO\nDL,P51X,_,UX,\nFLST,2,2,4,ORDE,2\n');
fprintf(fid, ['FITEM,2,', num2str(i-8), '\n', 'FITEM,2,', num2str(i-2), '!*\n']);
203 fprintf(fid, '/GO\nDL,P51X,_,UY,\nLPLOT\n');

205 %Pressure
p=-1;
207 fprintf(fid, 'FLST,2,1,4,ORDE,1\n');
fprintf(fid, ['FITEM,2,', num2str(i), '\n', '/GO\n!* \n']);
209 fprintf(fid, ['SFL,P51X,PRES,', num2str(p), '\n']);
fclose(fid);

```

E.2 MatLab code for the application of local approaches for ideal model

E.2.1 Code for application of ENS

```

clc;
2 clear all;
close all;

4
%Opening of APDL file
6 fid=fopen('ENS_model.txt','w');
fprintf(fid, '/CLEAR\n');

8
%% Opening of Preprocessor
10 fprintf(fid, ['/PREP7', '\n']);
%% Definition of element
12 % fprintf(fid, 'ET,1,PLANE182\n');
% fprintf(fid, 'KEYOPT,1,1,3\nKEYOPT,1,3,2\nKEYOPT,1,6,0\n');

14
% Definition of element PLANE 183

```

```

16 fprintf(fid,'ET,1,PLANE183\n');
17 fprintf(fid,'KEYOPT,1,1,0\nKEYOPT,1,3,2\nKEYOPT,1,6,0\n');
18
20 %% Definition of Material
21 E=206000;
22 ni=0.3;
23 fprintf(fid,['MPTEMP,,,,,,,,\nMPTEMP,1,0\nMPDATA,EX,1,,',num2str(E), ...
24 '\nMPDATA,PRXY,1,,',num2str(ni),'\n']);
25 %% Definition geometry parameters in mm
26 b=6;
27 t=6;
28 L=600;
29 z=6;
30 h=33;
31
32 r=1; % radius of root for ENS
33
34 %% Definition KP
35 %KP without root
36 fprintf(fid,'K,1,0,0,0\n');
37 fprintf(fid,['K,2,',num2str(L/2),',',0,0','\n']);
38 fprintf(fid,['K,3,',num2str(L/2),',',num2str(t/2),',',0','\n']);
39 fprintf(fid,['K,4,',num2str(b/2+z),',',num2str(t/2),',',0','\n']);
40 fprintf(fid,['K,5,',num2str(b/2),',',num2str(t/2+z),',',0','\n']);
41 fprintf(fid,['K,6,',num2str(b/2),',',num2str(t/2+z+h),',',0','\n']);
42 fprintf(fid,['K,7,0,',num2str(t/2+z+h),',',0','\n']);
43
44 %KP root for ENS
45 fprintf(fid,['K,8,',num2str(b/2-r),',',0,0','\n']);
46 fprintf(fid,['K,9,',num2str(b/2-r),',',num2str(t/2-r),',',0','\n']);
47 fprintf(fid,['K,10,',num2str(b/2),',',num2str(t/2),',',0','\n']);
48 fprintf(fid,['K,11,',num2str(b/2+r),',',num2str(t/2-r),',',0','\n']);
49 fprintf(fid,['K,12,',num2str(b/2),',',num2str(t/2-r),',',0','\n']); %center of arc
50 fprintf(fid,['K,13,',num2str(b/2+r),',',0,0','\n']);
51
52 %% Creation of lines
53
54 fprintf(fid,'L,1,8\n');
55 fprintf(fid,'L,8,9\n');
56 fprintf(fid,['LARC,9,10,12,',num2str(r),'\n']);
57 fprintf(fid,['LARC,10,11,12,',num2str(r),'\n']);
58 fprintf(fid,'L,11,13\n');
59 fprintf(fid,'L,13,2\n');
60 fprintf(fid,'L,2,3\n');
61 fprintf(fid,'L,3,4\n');
62 fprintf(fid,'L,4,5\n');
63 fprintf(fid,'L,5,6\n');
64 fprintf(fid,'L,6,7\n');
65 fprintf(fid,'L,7,1\n');
66 fprintf(fid,['LFILLT,8,9,',num2str(r),'\n']); %comando APDL per creazione fillet
67
68 n=13; %number of lines
69
70 %% Creation of Area
71 fprintf(fid,['FLST,2,',num2str(n),',',4\n']);
72 for i=1:n
73     fprintf(fid,['FITEM,2,',num2str(i),'\n']);
74 end
75 fprintf(fid,'AL,P51X\n');
76
77 %% Creation of mesh
78 m=4; %paratero che vale 6 per Plane182 e 4 per i Plane183

```

```

max_size=r/m;
80 realsize=num2str(max_size,3);
realsize2=realsize(1:3);
82 size=str2num(realsize2);
global_element_size=size;
84 %elements along fillet: >5 for PLANE182, >3 for PLANE183 weld toe
%elements along fillet: >40 for PLANE182, >24 for PLANE183 weld toe
86
fprintf(fid,['ESIZE',' ',num2str(global_element_size),' ',0,'\n']);
88 fprintf(fid,'MSHKEY,0\nCM,_Y,AREA\nASEL,_,_,_,_1\n');
fprintf(fid,'CM,_Y1,AREA\nCHKMSH, ' 'AREA' '\nCMSEL,S,_Y\n!* \n');
90 fprintf(fid,'AMESH,_Y1\n!* \nCMDELE,_Y\nCMDELE,_Y1\nCMDELE,_Y2\n!* \n');

92 %Refine at weld toe and root
fprintf(fid,'FLST,5,1,4,ORDE,1\nFITEM,5,13\n');
94 fprintf(fid,['CM,_Y,LINE\nLSEL,_,_,_,P51X\nCM,_Y1,LINE\nCMSEL,S,_Y' ...
'\nCMDELE,_Y\n!* \n!* \n']);
96 fprintf(fid,'LREF,_Y1,_,_,1,2,1,1\nCMDELE,_Y1\n!* \n');

98 fprintf(fid,'FLST,5,2,4,ORDE,2\nFITEM,5,3\nFITEM,5,-4\n');
fprintf(fid,['CM,_Y,LINE\nLSEL,_,_,_,P51X\nCM,_Y1,LINE\nCMSEL,S,_Y' ...
'\nCMDELE,_Y\n!* \n!* \n']);
100 fprintf(fid,'LREF,_Y1,_,_,1,2,1,1\nCMDELE,_Y1\n!* \n');
102
%% Definition of constraint and Pressure
104
%Constraint, symmetry boundary condition
106 fprintf(fid,'FLST,2,3,4,ORDE,3\n');
fprintf(fid,'FITEM,2,1\n');
108 fprintf(fid,'FITEM,2,6\n');
fprintf(fid,'FITEM,2,12\n');
110 fprintf(fid,'DL,P51X,_,SYMM\n');

112 %Pressure
p=-1;
114 fprintf(fid,'FLST,2,1,4,ORDE,1\n');
fprintf(fid,['FITEM,2,7\n','/GO\n!* \n']);
116 fprintf(fid,['SFL,P51X,PRES,',' ',num2str(p),' '\n']);

118 %% Solution
fprintf(fid,['SOLU\nSOLVE\n']);
120 fclose(fid);

```

E.2.2 Code for application of SHSS

```

clc;
2 clear all;
close all;
4
%Opening of APDL file
6 fid=fopen('HS_model.txt','w');
fprintf(fid,'/CLEAR\n');
8
%% Opening of Preprocessor
10 fprintf(fid,['/PREP7',' '\n']);
%% Definition of element
12 fprintf(fid,'ET,1,PLANE182\n');
fprintf(fid,'KEYOPT,1,1,3\nKEYOPT,1,3,2\nKEYOPT,1,6,0\n');
14
%% Definition of Material
16 E=206000;
ni=0.3;

```



```

18 fprintf(fid, ['MPTEMP,,,,,,,,,\nMPTEMP,1,0\nMPDATA,EX,1,,', num2str(E), ...
    '\nMPDATA,PRXY,1,,', num2str(ni), '\n']);
20 %% Definition geometry parameters in mm
    b=6;
22 t=6;
    L=600;
24 z=6;
    h=33;
26
    %% Definition KP
28 %KP without root
    fprintf(fid, 'K,1,0,0,0\n');
30 fprintf(fid, ['K,2,', num2str(L/2), ',,0,0', '\n']);
    fprintf(fid, ['K,3,', num2str(L/2), ',, ', num2str(t/2), ',,0', '\n']);
32 fprintf(fid, ['K,4,', num2str(b/2+z), ',, ', num2str(t/2), ',,0', '\n']);
    fprintf(fid, ['K,5,', num2str(b/2), ',, ', num2str(t/2+z), ',,0', '\n']);
34 fprintf(fid, ['K,6,', num2str(b/2), ',, ', num2str(t/2+z+h), ',,0', '\n']);
    fprintf(fid, ['K,7,0', ',, num2str(t/2+z+h), ',,0', '\n']);
36
    %% Creation of lines
38
    fprintf(fid, 'L,1,2\n');
40 fprintf(fid, 'L,2,3\n');
    fprintf(fid, 'L,3,4\n');
42 fprintf(fid, 'L,4,5\n');
    fprintf(fid, 'L,5,6\n');
44 fprintf(fid, 'L,6,7\n');
    fprintf(fid, 'L,7,1\n');
46 fprintf(fid, 'LANG,7,5,90,_,\n');
    fprintf(fid, 'LANG,1,5,90,_,\n');
48 fprintf(fid, 'LANG,11,4,90,_,\n');
    fprintf(fid, 'LANG,10,4,90,_,\n');
50 fprintf(fid, 'LANG,8,10,90,_,\n');
52
    %% Creation of areas
54 fprintf(fid, 'FLST,2,4,4\nFITEM,2,16\nFITEM,2,17\nFITEM,2,11\nFITEM,2,1\n');
    fprintf(fid, 'AL,P51X\n');
56 fprintf(fid, 'FLST,2,4,4\nFITEM,2,11\nFITEM,2,13\nFITEM,2,15\nFITEM,2,10\n');
    fprintf(fid, 'AL,P51X\n');
58 fprintf(fid, 'FLST,2,3,4\nFITEM,2,12\nFITEM,2,13\nFITEM,2,4\n');
    fprintf(fid, 'AL,P51X\n');
60 fprintf(fid, 'FLST,2,4,4\nFITEM,2,12\nFITEM,2,9\nFITEM,2,8\nFITEM,2,17\n');
    fprintf(fid, 'AL,P51X\n');
62 fprintf(fid, 'FLST,2,4,4\nFITEM,2,6\nFITEM,2,5\nFITEM,2,7\nFITEM,2,9\n');
    fprintf(fid, 'AL,P51X\n');
64 fprintf(fid, 'FLST,2,4,4\nFITEM,2,2\nFITEM,2,14\nFITEM,2,3\nFITEM,2,15\n');
    fprintf(fid, 'AL,P51X\n');
66
    %% Creation of mesh
68 d_max=0.4*t;
    global_element_size=d_max/6;
70 fprintf(fid, ['ESIZE,', num2str(global_element_size), ',,0,\n']);
    fprintf(fid, 'CM,_Y,AREA\nASEL,_,_,_,,3_\n');
72 fprintf(fid, 'CM,_Y1,AREA\nCHKMSH,' 'AREA' '\nCMSEL,S,_Y\n!* \n');
    fprintf(fid, ['MSHKEY,1\nAMESH,_Y1\nMSHKEY,1\n!* \nCMDELE,_Y\nCMDELE,_Y1' ...
74 '\nCMDELE,_Y2\n!* \n']);
    fprintf(fid, 'CM,_Y,AREA\nASEL,_,_,_,,6_\n');
76 fprintf(fid, 'CM,_Y1,AREA\nCHKMSH,' 'AREA' '\nCMSEL,S,_Y\n!* \n');
    fprintf(fid, ['MSHKEY,1\nAMESH,_Y1\nMSHKEY,1\n!* \nCMDELE,_Y\nCMDELE,_Y1' ...
78 '\nCMDELE,_Y2\n!* \n']);
    fprintf(fid, 'CM,_Y,AREA\nASEL,_,_,_,,2_\n');
80 fprintf(fid, 'CM,_Y1,AREA\nCHKMSH,' 'AREA' '\nCMSEL,S,_Y\n!* \n');

```

```

fprintf(fid, ['MSHKEY,1\nAMESH,_Y1\nMSHKEY,1\n!* \nCMDELE,_Y\nCMDELE,_Y1' ...
82 ' \nCMDELE,_Y2\n!* \n' ]);
fprintf(fid, 'CM,_Y,AREA\nASEL,_,_,_,,_____4_\n');
84 fprintf(fid, 'CM,_Y1,AREA\nCHKMSH, 'AREA' \nCMSEL,S,_Y\n!* \n');
fprintf(fid, ['MSHKEY,1\nAMESH,_Y1\nMSHKEY,1\n!* \nCMDELE,_Y\nCMDELE,_Y1' ...
86 ' \nCMDELE,_Y2\n!* \n' ]);
fprintf(fid, 'CM,_Y,AREA\nASEL,_,_,_,,_____1_\n');
88 fprintf(fid, 'CM,_Y1,AREA\nCHKMSH, 'AREA' \nCMSEL,S,_Y\n!* \n');
fprintf(fid, ['MSHKEY,1\nAMESH,_Y1\nMSHKEY,1\n!* \nCMDELE,_Y\nCMDELE,_Y1' ...
90 ' \nCMDELE,_Y2\n!* \n' ]);
fprintf(fid, 'CM,_Y,AREA\nASEL,_,_,_,,_____5_\n');
92 fprintf(fid, 'CM,_Y1,AREA\nCHKMSH, 'AREA' \nCMSEL,S,_Y\n!* \n');
fprintf(fid, ['MSHKEY,1\nAMESH,_Y1\nMSHKEY,1\n!* \nCMDELE,_Y\nCMDELE,_Y1' ...
94 ' \nCMDELE,_Y2\n!* \n' ]);
%% Definition of constraint and Pressure
96
%Constraint, symmetry boundary condition
98 fprintf(fid, 'FLST,2,6,4,ORDE,6\n');
fprintf(fid, 'FITEM,2,7\n');
100 fprintf(fid, 'FITEM,2,8\n');
fprintf(fid, 'FITEM,2,16\n');
102 fprintf(fid, 'FITEM,2,1\n');
fprintf(fid, 'FITEM,2,10\n');
104 fprintf(fid, 'FITEM,2,14\n');
fprintf(fid, 'DL,P51X,_,SYMM\n');
106
%Pressure
108 p=-1;
fprintf(fid, 'FLST,2,1,4,ORDE,1\n');
110 fprintf(fid, ['FITEM,2,2\n', '/GO\n!* \n' ]);
fprintf(fid, ['SFL,P51X,PRES, ', num2str(p), '\n' ]);
112
%% Solution
114 fprintf(fid, '/SOLU\nSOLVE\n');
116
%% Postprocessor
fprintf(fid, '/POST1\n');

```

E.2.3 Code for application of PSM (Sharp V-notch)

```

clc;
2 clear all;
close all;
4
%Opening of APDL file
6 fid=fopen('PSM_model.txt','w');
fprintf(fid, '/CLEAR\n');
8
%% Opening of Preprocessor
10 fprintf(fid, ['/PREP7', '\n' ]);
%% Definition of element
12 fprintf(fid, 'ET,1,PLANE182\n');
fprintf(fid, 'KEYOPT,1,1,3\nKEYOPT,1,3,2\nKEYOPT,1,6,0\n');
14
%% Definition of Material
16 E=206000;
ni=0.3;
18 fprintf(fid, ['MPTEMP,,,,,,,, \nMPTEMP,1,0\nMPDATA,EX,1,,', num2str(E), ...
' \nMPDATA,PRXY,1,,', num2str(ni), '\n' ]);
20 %% Definition geometry parameters in mm
b=6;
22 t=6;

```

```

L=600;
24 z=6;
h=33;
26 root_width=0.1;

28 %% Definition KP
%KP without root
30 fprintf(fid,'K,1,0,0,0\n');
fprintf(fid,['K,2,',num2str(L/2),'',0,0','\n']);
32 fprintf(fid,['K,3,',num2str(L/2),'',num2str(t/2),'',0','\n']);
fprintf(fid,['K,4,',num2str(b/2+z),'',num2str(t/2),'',0','\n']);
34 fprintf(fid,['K,5,',num2str(b/2),'',num2str(t/2+z),'',0','\n']);
fprintf(fid,['K,6,',num2str(b/2),'',num2str(t/2+z+h),'',0','\n']);
36 fprintf(fid,['K,7,0,',num2str(t/2+z+h),'',0','\n']);

38 %KP root for PSM
fprintf(fid,['K,8,',num2str(b/2),'',0,0','\n']);
40 fprintf(fid,['K,9,',num2str(b/2),'',num2str(t/2),'',0','\n']);
fprintf(fid,['K,10,',num2str(b/2+root_width),'',0,0','\n']);
42

%% Creation of lines
44
fprintf(fid,'L,1,8\n');
46 fprintf(fid,'L,8,9\n');
fprintf(fid,'L,9,10\n');
48 fprintf(fid,'L,10,2\n');
fprintf(fid,'L,2,3\n');
50 fprintf(fid,'L,3,4\n');
fprintf(fid,'L,4,5\n');
52 fprintf(fid,'L,5,6\n');
fprintf(fid,'L,6,7\n');
54 fprintf(fid,'L,7,1\n');
n=10; %number of lines

56

%% Creation of Area
58 fprintf(fid,['FLST,2,',num2str(n),'',4\n']);
for i=1:n
60     fprintf(fid,['FITEM,2,',num2str(i),'\n']);
end
62 fprintf(fid,'AL,P51X\n');
%% Creation of mesh
64 a=t/2; %dimensional parametr
ratio_min=3; %from literature PSM review A.Campagnolo
66 d_max=a/ratio_min; %maximum dimension of element

68 global_element_size=0.2;
fprintf(fid,['ESIZE,',num2str(global_element_size),'',0,\n']);
70 fprintf(fid,'MSHKEY,0\nCM,_Y,AREA\nASEL,_,_,_,_1\n');
fprintf(fid,'CM,_Y1,AREA\nCHKMSH,'AREA'\nCMSEL,S,_Y\n!*');
72 fprintf(fid,'AMESH,_Y1\n!*nCMDELE,_Y\nCMDELE,_Y1\nCMDELE,_Y2\n!*');
%% Definition of constraint and Pressure
74

%Constraint, symmetry boundary condition
76 fprintf(fid,'FLST,2,3,4,ORDE,3\n');
fprintf(fid,'FITEM,2,1\n');
78 fprintf(fid,'FITEM,2,4\n');
fprintf(fid,'FITEM,2,10\n');
80 fprintf(fid,'DL,P51X,_,SYMM\n');

82 %Pressure
p=-1;
84 fprintf(fid,'FLST,2,1,4,ORDE,1\n');
fprintf(fid,['FITEM,2,5\n','/GO\n!*']);

```

```

86 fprintf(fid, ['SFL,P51X,PRES,' , num2str(p), '\n']);
88 %% Creation of local reference system at weld toe tip and root
    alfa=112.5;
90 fprintf(fid, 'WPSTYLE,,,,,,,,,1\n');
    fprintf(fid, ['KWPAVE,4\nwprot,' , num2str(-alfa), '\n']);
92 fprintf(fid, 'CSWPLA,11,0,1,1,1,\n');
    fprintf(fid, 'WPCSYS,-1,0\n');
94 fprintf(fid, 'KWPAVE,9\nwprot,90\n');
    fprintf(fid, 'CSWPLA,12,0,1,1,\nWPSTYLE,,,,,,,,,0\n');
96
    %% Solution
98 fprintf(fid, '/SOLU\nSOLVE\n');
    fprintf(fid, '!*\n_/PSF,DEFA,_,1,0,1\n/PBF,DEFA,_,1_\n/PSYMB,CS,1_\n');
100 fprintf(fid, '/PSYMB,NDIR,0_\n/PSYMB,ESYS,0\n/PSYMB,ESYS,0_\n/PSYMB,ESYS,0_\n');
    fprintf(fid, ['/PSYMB,ESYS,0\n/PSYMB,LDIV,0\n_/PSYMB,LDIR,0\n/PSYMB,ADIR,0' ...
102 ' \n/PSYMB,ECON,0\n']);
    fprintf(fid, ['/PSYMB,XNODE,0\n/PSYMB,DOT,1\n/PSYMB,PCONV, \n/PSYMB,LAYR,0' ...
104 ' \n/PSYMB,FBCS,0\n']);
    fprintf(fid, '!*\n/PBC,ALL,_,1\n/REP\n!*'\n');
106 tic
    fclose(fid);
108 toc

```

E.2.4 Code for application of PSM (No sharp V-notch)

```

    clc;
    clear all;
    close all;
    delete('Tensioni_nodali.txt')
    delete('Coordinate_nodali.txt')
    clc
    %Opening of APDL file
    fid=fopen('PSM_model_HFMI_No_misalign.txt','w');
    fprintf(fid, '/CLEAR\n');
10
    %% Opening of Preprocessor
12 fprintf(fid, ['/PREP7','\n']);
    %% Definition of element
14 fprintf(fid, 'ET,1,PLANE182\n');
    fprintf(fid, 'KEYOPT,1,1,3\nKEYOPT,1,3,2\nKEYOPT,1,6,0\n');
16
    %% Definition of Material
18 E=206000;
    ni=0.3;
20 fprintf(fid, ['MPTEMP,,,,,,,,\nMPTEMP,1,0\nMPDATA,EX,1,,', num2str(E), ...
    '\nMPDATA,PRXY,1,,', num2str(ni), '\n']);
22 %% Definition geometry parameters in mm
    b=6;
24 t=6;
    L=600;
26 z=6;
    h=33;
28 root_width=0.1;

30 %% Definition KP
    %KP without root
32 fprintf(fid, 'K,1,0,0,0\n');
    fprintf(fid, ['K,2,', num2str(L/2), ',,0,0', '\n']);
34 fprintf(fid, ['K,3,', num2str(L/2), ',, num2str(t/2), ',,0', '\n']);
    fprintf(fid, ['K,4,', num2str(b/2+z), ',, num2str(t/2), ',,0', '\n']);
36 fprintf(fid, ['K,5,', num2str(b/2), ',, num2str(t/2+z), ',,0', '\n']);

```

```

fprintf(fid, ['K, 6, ', num2str(b/2), ', ', num2str(t/2+z+h), ', 0', '\n']);
38 fprintf(fid, ['K, 7, 0, ', num2str(t/2+z+h), ', 0', '\n']);

40 %KP root for PSM
fprintf(fid, ['K, 8, ', num2str(b/2), ', 0, 0', '\n']);
42 fprintf(fid, ['K, 9, ', num2str(b/2), ', ', num2str(t/2), ', 0', '\n']);
fprintf(fid, ['K, 10, ', num2str(b/2+root_width), ', 0, 0', '\n']);
44

%% Creation of lines
46
fprintf(fid, 'L, 1, 8\n');
48 fprintf(fid, 'L, 8, 9\n');
fprintf(fid, 'L, 9, 10\n');
50 fprintf(fid, 'L, 10, 2\n');
fprintf(fid, 'L, 2, 3\n');
52 fprintf(fid, 'L, 3, 4\n');
fprintf(fid, 'L, 4, 5\n');
54 fprintf(fid, 'L, 5, 6\n');
fprintf(fid, 'L, 6, 7\n');
56 fprintf(fid, 'L, 7, 1\n');
n=10; %number of lines

58

%% Creation of Area
60 fprintf(fid, ['FLST, 2, ', num2str(n), ', 4\n']);
for i=1:n
62     fprintf(fid, ['FITEM, 2, ', num2str(i), '\n']);
end
64 fprintf(fid, 'AL, P51X\n');
%% KP HFMI

66

%Dimension of the groove
68 rho=3.31; %standard deviation 1.25
depth=0.21+0.09; %standard deviation 0.09
70

%Groove
72 alfa=135/2;
alfa_rad=deg2rad(alfa);
74 xc=t/2+z+((rho-depth)/(tan(alfa_rad)));
yc=t/2+rho-depth;
76 fprintf(fid, 'NUMSTR, KP, 200\n');
fprintf(fid, ['K, ', num2str(xc), ', ', num2str(yc), ', 0', '\n']);
78 fprintf(fid, ['CYL4, ', num2str(xc), ', ', num2str(yc), ', ', num2str(rho), '\n']);

80 %% Creation of Area with HFMI groove
fprintf(fid, 'ASBA, 1, 2\n');
82

%% Creation of mesh
84

global_element_size=0.5;
86 fprintf(fid, ['ESIZE, ', num2str(global_element_size), ', 0, \n']);
fprintf(fid, 'MSHKEY, 0\nCM, _Y, AREA\nASEL, , , , 3\nCM, _Y1, AREA\n');
88 fprintf(fid, 'CHKMSH, ' 'AREA' '\nCMSEL, S, _Y\n!* \nAMESH, _Y1\n!* \nCMDELE, _Y\n');
fprintf(fid, 'CMDELE, _Y1\nCMDELE, _Y2\n!* \n');
90

%Refine mesh
92 fprintf(fid, ['FLST, 5, 2, 4, ORDE, 2\nFITEM, 5, 17\nFITEM, 5, -18\nCM, _Y, LINE' ...
    '\nLSEL, , , , P51X\n']);
94 fprintf(fid, 'CM, _Y1, LINE\nCMSEL, S, _Y\nCMDELE, _Y\n!* \n!* \n');
fprintf(fid, ['LREF, _Y1, , , 1, 5, 1, 1\nCMDELE, _Y1\n!* \nFLST, 5, 2, 4, ORDE, 2' ...
    '\nFITEM, 5, 17\nFITEM, 5, -18\n']);
96 fprintf(fid, ['CM, _Y, LINE\nLSEL, , , , P51X\nCM, _Y1, LINE\nCMSEL, S, _Y' ...
    '\nCMDELE, _Y\n!* \n!* \n']);
98 fprintf(fid, 'LREF, _Y1, , , 1, 5, 1, 1\nCMDELE, _Y1\n!* \n');

```

```

100 %% Definition of constraint and Pressure
102
103 %Constraint
104 fprintf(fid, ['FLST,2,3,4,ORDE,3\nFITEM,2,1\nFITEM,2,4\nFITEM,2,10' ...
105             '\nDL,P51X,_,SYMM\n']);
106
107 %Pressure
108 p=-1;
109 fprintf(fid, 'FLST,2,1,4,ORDE,1\nFITEM,2,5\nGO\n!* \n');
110 fprintf(fid, ['SFL,P51X,PRES,','num2str(p)',', \n']);
112 %% Solution
113 fprintf(fid, '/SOLU\nSOLVE\nFINISH\n');
114
115 %% Post processor
116
117 fprintf(fid, '/POST1\n!* \n');
118 fprintf(fid, 'FLST,5,2,4,ORDE,2\nFITEM,5,17\nFITEM,5,-18\nLSEL,S,_,_,P51X\n');
119 fprintf(fid, 'NSLL,S,1\n');
120
121 fprintf(fid, 'INRES,ALL\nFILE,','file','','rst','','.''\nSET, LAST\nSET, FIRST\nAVPRIN,0,_, \n');
122 fprintf(fid, 'ETABLE,_,S,1\n/OUTPUT,Tensioni_nodali,txt\nPRNSOL,_,_PRIN\n/OUT\n');
124 %macro for nodal coordinates
125 fprintf(fid, '/INPUT,export_nodal_coords,mac\n');
126 tic
127     ! run_ansys.bat
128 toc
130 %Opening of txt file called tensioni nodali and writing matrix nodal stress
132 file_tensioni=fopen('Tensioni_nodali.txt','r');
133 tensioni_nodali_11=txt2mat(file_tensioni);
134 fclose(file_tensioni);
135 %Researching of node with max principal stress
136 ten_max=max(tensioni_nodali_11(:,2));
137 index_nodo=find(tensioni_nodali_11(:,2)==ten_max);
138 nodo_ten_max=tensioni_nodali_11(index_nodo,1);
140 %Creation of txt file coordinate nodali and writing the matrix
142
143 file_coordinate=fopen('coordinate_nodali.txt','r');
144 coordinate_nodali_11=txt2mat_c(file_coordinate);
145 fclose(file_coordinate);
146 %Researching of node with max principal stress
147 nodo_max=find(coordinate_nodali_11(:,1)==nodo_ten_max(1,1));
148 coordinate_nodo_max=coordinate_nodali_11(nodo_max,:);
150 %Coordinates of the point with max principal stress on weld toe up-left
152
153 x1=coordinate_nodo_max(2);
154 y1=coordinate_nodo_max(3);
156
157 %% Calculation of inclination angle of structural volume
158
159 %Point A represents the coordinates of V-notch up-left
160 xA=t/2+z;
161 yA=t/2;
162

```

```

164 %Punto C represents the center of arc of HFMI groove
XC;
YC;
166
168 %Angular coefficient of the straight between A and C
% (Bisector)
m1=(yc-yA)/(xc-xA);
170
172 %Angular coefficient of the straight between C and 1 (point
%with max principal stress)
m2=(yc-y1)/(xc-x1);
174
176 %Inclination angle gamma
gamma_rad=atan(abs((m1-m2)/(1+m1*m2)));
178 gamma=rad2deg(gamma_rad);
%% Calculation of the center to create structural volume
180 %Geometrical parameters
alfa_2=2*alfa;
182 q=2-(alfa_2)/180;
r0=((q-1)/q)*rho;
184 R0=0.28;
R_SED=R0+r0;
186
188 %Inclination Angle of the straight between C and 1
psi=atan2((yc-y1),(xc-x1));
190
192 %Calculation of x2 and y2 coordinates of the center of the arc
%of structural volume for SED
% (Method 1)
x2=x1+r0*cos(psi);
194 y2=y1+r0*sin(psi);
%Equation of straight from 1 to 2 and inverse formula of the distance
196 %between 2 points (Method 2)
198
eq_y2=@(x) m2*(x-x1)+y1;
200 eq_x2=@(x) (x-x1).^2+(eq_y2(x)-y1).^2-r0^2;
202
204 %Plot of eq_x2 to verify the position of the zero
plot(linspace(x1,x1-5),eq_x2(linspace(x1,x1-5)))
grid on
206 %Initial point
x0=10;
208 x2_2=fsolve(eq_x2,x0);
hold on
210 plot(x2_2,eq_x2(x2_2),'or')
y2_2=eq_y2(x2_2);
212 %Verification of the length of the segment
length_x2_y2=sqrt((x2-x1)^2+(y2-y1)^2)
214 length_x2_y2_2=sqrt((x2_2-x1)^2+(y2_2-y1)^2)
r0
216
%% Creation of KP center of arc and the relative arc
218 %Selection all, opening of preprocessor, clean mesh, creation new geometry
220 fprintf(fid,'ALLSEL,ALL\n_/PREP7\n');
fprintf(fid,'ACLEAR,_____3\n');
222 fprintf(fid,['FLST,2,2,8\nFITEM,2,',num2str(x2),',',num2str(y2),',0\n']);
fprintf(fid,['FITEM,2,',num2str(x2),',',num2str(y2-R_SED),',0\n']);
224 fprintf(fid,'CIRCLE,P51X\n');

```

```

226 %Division of the lines of structural volume
fprintf(fid,'FLST,2,2,4,ORDE,2\nFITEM,2,17\nFITEM,2,-18\nLCOMB,P51X,_,0\n');
228 %
fprintf(fid,'FLST,2,2,4,ORDE,2\nFITEM,2,6_\nFITEM,2,12\n');
230 fprintf(fid,'FLST,3,1,4,ORDE,1\nFITEM,3,17\nLSBL,P51X,P51X,_,_,KEEP\n');

232 %Deleting of the lines in excess

234 fprintf(fid,'FLST,2,4,4,ORDE,4\nFITEM,2,7\nFITEM,2,11\nFITEM,2,18\nFITEM,2,-19\n');
fprintf(fid,'LDELE,P51X,_,_,1\n');
236

238 %Division of principal area
fprintf(fid,'FLST,3,2,4,ORDE,2\nFITEM,3,13\nFITEM,3,-14\nASBL,3,P51X\n');
240

%% Mesh of area

242 %Mesh Area of structural volume
size_SED=0.01;
fprintf(fid,['ESIZE',' ,num2str(size_SED),' ,0,']);
246 fprintf(fid,'MSHKEY,0\nCM,_Y,AREA\nASEL,_,_,_,1\n');
fprintf(fid,'CM,_Y1,AREA\nCHKMSH, ' ' AREA' '\nCMSEL,S,_Y\n!* \nAMESH,_Y1\n!*');
248 fprintf(fid,'CMDELE,_Y\nCMDELE,_Y1\nCMDELE,_Y2\n!* \n');

250 %Mesh external area
size_ext=0.1;
252 fprintf(fid,['ESIZE',' ,num2str(size_ext),' ,0,']);
fprintf(fid,'MSHKEY,0\nCM,_Y,AREA\nASEL,_,_,_,2\n');
254 fprintf(fid,'CM,_Y1,AREA\nCHKMSH, ' ' AREA' '\nCMSEL,S,_Y\n!* \nAMESH,_Y1\n!*');
fprintf(fid,'CMDELE,_Y\nCMDELE,_Y1\nCMDELE,_Y2\n!* \n');
256

%% Constraint and loads
258 fprintf(fid,'LSCLEAR,ALL\n');

260 %Constraint
fprintf(fid,' FLST,2,3,4,ORDE,3\nFITEM,2,1\nFITEM,2,4\nFITEM,2,10\nDL,P51X,_,SYMM\n');
262

%Pressure
264 fprintf(fid,'FLST,2,1,4,ORDE,1\nFITEM,2,5\n/GO\n!* \n');
fprintf(fid,['SFL,P51X,PRES, ' ,num2str(p),' , \n']);
266

%% Resolution of the model

268 fprintf(fid,'/SOLU\nSOLVE\n');
270

%% Post Process
272 fprintf(fid,'/POST1\n!* \n');

274 %Selection of structural area and attached elements
fprintf(fid,'ASEL,S,_,_,1\nESLA,S\n/AUTO,1\n/REP,FAST\n');
276

%Creation of Element Table SENE e VOLU
278 fprintf(fid,'AVPRIN,0,_, \nETABLE,_,SENE,\n!* \nAVPRIN,0,_, \nETABLE,_,VOLU,\n!* \n');
data=[r0 gamma ]
280

fclose(fid);

```

E.3 MatLab code for the application of local approaches for ideal model with misalignment

E.3.1 Code for application of ENS

```

1  clc;
2  clear all;
3  close all;

5  %Opening of APDL file
   fid=fopen('ENS_model_misalignment.txt','w');
7  fprintf(fid,'/CLEAR\n');

9  %% Opening of Preprocessor
   fprintf(fid,['/PREP7','\n']);
11 %% Definition of element
   % fprintf(fid,'ET,1,PLANE183\n');
13 % fprintf(fid,'KEYOPT,1,1,0\nKEYOPT,1,3,2\nKEYOPT,1,6,0\n');
   fprintf(fid,'ET,1,PLANE182\n');
15 fprintf(fid,'KEYOPT,1,1,3\nKEYOPT,1,3,2\nKEYOPT,1,6,0\n');

17 %% Definition of Material
   E=206000;
19 ni=0.3;
   fprintf(fid,['MPTEMP,,,,,,,,\nMPTEMP,1,0\nMPDATA,EX,1,,',num2str(E), ...
21   '\nMPDATA,PRXY,1,,',num2str(ni),'\n']);
   %% Definition geometry parameters in mm
23 %for i=[300 350 400 450 500 550 600]
   b=6;
25 t=6;
   L=600;
27 z=6;
   h=33;
29 root_width=0.1;
   alfa_dx=deg2rad(1.16);
31 alfa_sx=deg2rad(1.48);
   g=L/2-b/2-z;
33 v=100; %length for constraint
   r=1; % radius of root for ENS
35

   %% Definition KP
37 %External KP
   fprintf(fid,['K,1,',num2str(b/2),',',num2str(t/2+z+h),',',0','\n']);
39 fprintf(fid,['K,2,',num2str(b/2),',',num2str(t/2+z),',',0','\n']);
   fprintf(fid,['K,3,',num2str(b/2+z),',',num2str(t/2),',',0','\n']);
41 fprintf(fid,['K,4,',num2str(L/2),',',num2str(t/2+g*tan(alfa_dx)), ...
   ',0','\n']);
43 fprintf(fid,['K,5,',num2str(L/2),',',num2str(t/2+g*tan(alfa_dx)-t), ...
   ',0','\n']);
45 fprintf(fid,['K,6,',num2str(L/2-v),',',num2str(t/2+(g-v)*tan(alfa_dx)-t), ...
   ',0','\n']);
47 fprintf(fid,['K,7,',num2str(b/2+z),',',num2str(-t/2),',',0','\n']);
   fprintf(fid,['K,8,',num2str(b/2),',',num2str(-(t/2+z)),',',0','\n']);
49 fprintf(fid,['K,9,',num2str(b/2),',',num2str(-(t/2+z+h)),',',0','\n']);
   fprintf(fid,['K,10,',num2str(-b/2),',',num2str(-(t/2+z+h)),',',0','\n']);
51 fprintf(fid,['K,11,',num2str(-b/2),',',num2str(-(t/2+z)),',',0','\n']);
   fprintf(fid,['K,12,',num2str(-(b/2+z)),',',num2str(-t/2),',',0','\n']);
53 fprintf(fid,['K,13,',num2str(-L/2),',',num2str(t/2+g*tan(alfa_sx)-t), ...
   ',0','\n']);
55 fprintf(fid,['K,14,',num2str(-L/2),',',num2str(t/2+g*tan(alfa_sx)), ...
   ',0','\n']);
57 fprintf(fid,['K,15,',num2str(-(L/2-v)),',',num2str(t/2+(g-v)*tan(alfa_sx)), ...
   ',0','\n']);

```

```

59 fprintf(fid, ['K,16,', num2str(-(b/2+z)), ', ', num2str(t/2), ', 0', '\n']);
fprintf(fid, ['K,17,', num2str(-b/2), ', ', num2str(t/2+z), ', 0', '\n']);
61 fprintf(fid, ['K,18,', num2str(-b/2), ', ', num2str(t/2+z+h), ', 0', '\n']);

63 %KP for the root

65 fprintf(fid, ['K,19,', num2str(b/2-r), ', ', num2str(t/2-r), ', 0', '\n']);
fprintf(fid, ['K,20,', num2str(b/2), ', ', num2str(t/2), ', 0', '\n']);
67 fprintf(fid, ['K,21,', num2str(b/2), ', ', num2str(t/2-r), ', 0', '\n']); %center of arc
fprintf(fid, ['K,22,', num2str(b/2+r), ', ', num2str(t/2-r), ', 0', '\n']);
69
fprintf(fid, ['K,23,', num2str(b/2-r), ', ', num2str(-(t/2-r)), ', 0', '\n']);
71 fprintf(fid, ['K,24,', num2str(b/2), ', ', num2str(-t/2), ', 0', '\n']);
fprintf(fid, ['K,25,', num2str(b/2), ', ', num2str(-(t/2-r)), ', 0', '\n']); %center of arc
73 fprintf(fid, ['K,26,', num2str(b/2+r), ', ', num2str(-(t/2-r)), ', 0', '\n']);

75
fprintf(fid, ['K,27,', num2str(-(b/2-r)), ', ', num2str(t/2-r), ', 0', '\n']);
77 fprintf(fid, ['K,28,', num2str(-b/2), ', ', num2str(t/2), ', 0', '\n']);
fprintf(fid, ['K,29,', num2str(-b/2), ', ', num2str(t/2-r), ', 0', '\n']); %center of arc
79 fprintf(fid, ['K,30,', num2str(-(b/2+r)), ', ', num2str(t/2-r), ', 0', '\n']);

81 fprintf(fid, ['K,31,', num2str(-(b/2-r)), ', ', num2str(-(t/2-r)), ', 0', '\n']);
fprintf(fid, ['K,32,', num2str(-b/2), ', ', num2str(-t/2), ', 0', '\n']);
83 fprintf(fid, ['K,33,', num2str(-b/2), ', ', num2str(-(t/2-r)), ', 0', '\n']); %center of arc
fprintf(fid, ['K,34,', num2str(-(b/2+r)), ', ', num2str(-(t/2-r)), ', 0', '\n']);
85

87
%% Creation of lines
89
fprintf(fid, 'L,1,2\n');
91 fprintf(fid, 'L,2,3\n');
fprintf(fid, 'L,3,4\n');
93 fprintf(fid, 'L,4,5\n');
fprintf(fid, 'L,5,6\n');
95 fprintf(fid, 'L,6,7\n');
fprintf(fid, 'L,7,8\n');
97 fprintf(fid, 'L,8,9\n');
fprintf(fid, 'L,9,10\n');
99 fprintf(fid, 'L,10,11\n');
fprintf(fid, 'L,11,12\n');
101 fprintf(fid, 'L,12,13\n');
fprintf(fid, 'L,13,14\n');
103 fprintf(fid, 'L,14,15\n');
fprintf(fid, 'L,15,16\n');
105 fprintf(fid, 'L,16,17\n');
fprintf(fid, 'L,17,18\n');
107 fprintf(fid, 'L,18,1\n');
n=18;
109
%root lines
111 fprintf(fid, ['LARC,19,20,21,', num2str(r), '\n']);
fprintf(fid, ['LARC,20,22,21,', num2str(r), '\n']);
113 fprintf(fid, ['LARC,23,24,25,', num2str(r), '\n']);
fprintf(fid, ['LARC,24,26,25,', num2str(r), '\n']);
115 fprintf(fid, 'L,19,23\n');
fprintf(fid, 'L,22,26\n');
117
fprintf(fid, ['LARC,27,28,29,', num2str(r), '\n']);
119 fprintf(fid, ['LARC,28,30,29,', num2str(r), '\n']);
fprintf(fid, ['LARC,31,32,33,', num2str(r), '\n']);
121 fprintf(fid, ['LARC,32,34,33,', num2str(r), '\n']);

```

```

fprintf(fid,'L,27,31\n');
123 fprintf(fid,'L,30,34\n');
k=12;
125
fprintf(fid,['LFILLT,2,3,',num2str(r),' \n']); %comando APDL per creazione fillet
127 fprintf(fid,['LFILLT,6,7,',num2str(r),' \n']); %comando APDL per creazione fillet
fprintf(fid,['LFILLT,11,12,',num2str(r),' \n']); %comando APDL per creazione fillet
129 fprintf(fid,['LFILLT,15,16,',num2str(r),' \n']); %comando APDL per creazione fillet
m=4;
131 fprintf(fid,'LDIV,15,0.8668735095560043\n_');
fprintf(fid,'LDIV,6,0.8738266883278072\n_');
133 fprintf(fid,'LANG,3,44,90,_\n_');
fprintf(fid,'LANG,12,43,90,_\n_');
135

%% Creation of Area
fprintf(fid,'FLST,2,32,4\n');
139 fprintf(fid,['FITEM,2,35\nFITEM,2,34\nFITEM,2,16\nFITEM,2,17\nFITEM,2,18' ...
'\nFITEM,2,1\n']);
141 fprintf(fid,['FITEM,2,2\nFITEM,2,31\nFITEM,2,3\nFITEM,2,12\nFITEM,2,33' ...
'\nFITEM,2,11\n']);
143 fprintf(fid,['FITEM,2,10\nFITEM,2,9\nFITEM,2,8\nFITEM,2,7\nFITEM,2,32' ...
'\nFITEM,2,36\n']);
145 fprintf(fid,['FITEM,2,40\nFITEM,2,38\nFITEM,2,24\nFITEM,2,20\nFITEM,2,19' ...
'\nFITEM,2,23\n']);
147 fprintf(fid,['FITEM,2,21\nFITEM,2,22\nFITEM,2,29\nFITEM,2,25\nFITEM,2,26' ...
'\nFITEM,2,30\n']);
149 fprintf(fid,'FITEM,2,28\nFITEM,2,27\nAL,P51X\n');
fprintf(fid,'FLST,2,5,4\n');
151 fprintf(fid,['FITEM,2,14\nFITEM,2,13\nFITEM,2,39\nFITEM,2,15\nFITEM,2,40' ...
'\nAL,P51X\n']);
153 fprintf(fid,'FLST,2,5,4\n');
fprintf(fid,['FITEM,2,37\nFITEM,2,5\nFITEM,2,6\nFITEM,2,38\nFITEM,2,4' ...
'\nAL,P51X\n']);
155

%% Creation of mesh
m=6; %paratero che vale 6 per Plane182 e 4 per i Plane183
159 max_size=r/m;
realsize=num2str(max_size,3);
161 realsize2=realsize(1:3);
size=str2num(realsize2);
163 global_element_size=1;
%elements along fillet: >5 for PLANE182, >3 for PLANE183 weld toe
165 %elements along fillet: >40 for PLANE182, >24 for PLANE183 weld toe

167 fprintf(fid,['ESIZE,',num2str(global_element_size),' ,0,\n']);
fprintf(fid,'MSHKEY,0\nCM,_Y,AREA\nASEL,_,_,_,_1\n');
169 fprintf(fid,'CM,_Y1,AREA\nCHKMSH,' 'AREA' '\nCMSEL,S,_Y\n!* \n');
fprintf(fid,'AMESH,_Y1\n!* \nCMDELE,_Y\nCMDELE,_Y1\nCMDELE,_Y2\n!* \n');
171

%Refine at weld toe and root
173
fprintf(fid,'FLST,5,2,4,ORDE,2\nFITEM,5,4\nFITEM,5,13\n');
175 fprintf(fid,'CM,_Y,LINE_\nLSEL,_,_,_,P51X\nCM,_Y1,LINE\n');
fprintf(fid,'CMSEL,_,_Y\n!* \nLESIZE,_Y1,_,_,6,_,_,_,1\n!* \n_');
177

fprintf(fid,'FLST,5,2,4,ORDE,2\nFITEM,5,5\nFITEM,5,14\n');
179 fprintf(fid,'CM,_Y,LINE_\nLSEL,_,_,_,P51X\nCM,_Y1,LINE\n');
fprintf(fid,'CMSEL,_,_Y\n!* \nLESIZE,_Y1,_,_,100,_,_,_,1\n!* \n_');
181

fprintf(fid,'FLST,5,2,4,ORDE,2\nFITEM,5,37\nFITEM,5,39\n');
183 fprintf(fid,'CM,_Y,LINE_\nLSEL,_,_,_,P51X\nCM,_Y1,LINE\n');
fprintf(fid,'CMSEL,_,_Y\n!* \nLESIZE,_Y1,_,_,400,25,_,_,1\n!* \n_');

```

```

185 fprintf(fid,'FLST,5,2,4,ORDE,2\nFITEM,5,6\nFITEM,5,15\n');
187 fprintf(fid,'CM,_Y,LINE_\nLSEL,_,_,_,P51X\nCM,_Y1,LINE\n');
    fprintf(fid,'CMSEL,_,_Y\n!* \nLESIZE,_,_,_,250,1/20,_,_,_,1\n!* \n_');
189 fprintf(fid,'MSHKEY,0\nFLST,5,2,5,ORDE,2\nFITEM,5,2\nFITEM,5,-3\n_');
    fprintf(fid,'CM,_Y,AREA\nASEL,_,_,_,P51X\nCM,_Y1,AREA\nCHKMSH,' 'AREA' '\n');
191 fprintf(fid,['CMSEL,S,_,_Y\n!* \nAMESH,_,_Y1\n!* \nCMDELE,_,_Y\nCMDELE,_,_Y1' ...
    '\nCMDELE,_,_Y2\n!* \n']);

193
    %% Definition of constraint and Pressure
195
    %Constraint
197 fprintf(fid,'FLST,2,2,4,ORDE,2\n');
    fprintf(fid,'FITEM,2,5\n');
199 fprintf(fid,['FITEM,2,14\n','/GO\n!* \n']);
    fprintf(fid,'DL,P51X,_,UY,\n');

201
    fprintf(fid,'FLST,2,1,4,ORDE,1\n');
203 fprintf(fid,['FITEM,2,13\n','/GO\n!* \n']);
    fprintf(fid,'DL,P51X,_,UX,\n');

205
    %Pressure
207 p=-1;
    fprintf(fid,'FLST,2,1,4,ORDE,1\n');
209 fprintf(fid,['FITEM,2,4\n','/GO\n!* \n']);
    fprintf(fid,['SFL,P51X,PRES,' ,num2str(p),' \n']);

211
    %% Solution
213 fprintf(fid,'/SOLU\nSOLVE\n');
    fclose(fid);

```

E.3.2 Code for application of SHSS

```

1  clc;
    clear all;
3  close all;

5  %Opening of APDL file
    fid=fopen('HS_model_misalignment.txt','w');
7  fprintf(fid,'/CLEAR\n');

9  %% Opening of Preprocessor
    fprintf(fid,['/PREP7',' \n']);
11 %% Definition of element
    fprintf(fid,'ET,1,PLANE182\n');
13 fprintf(fid,'KEYOPT,1,1,3\nKEYOPT,1,3,2\nKEYOPT,1,6,0\n');

15 %% Definition of Material
    E=206000;
17 ni=0.3;
    fprintf(fid,['MPTEMP,,,,,,,,\nMPTEMP,1,0\nMPDATA,EX,1,,',' ,num2str(E), ...
19 '\nMPDATA,PRXY,1,,',' ,num2str(ni),' \n']);
    %% Definition geometry parameters in mm
21 b=6;
    t=6;
23 L=600;
    z=7;
25 h=33;
    alfa_dx=deg2rad(1.01);
27 alfa_sx=deg2rad(0.94);
    g=L/2-b/2-z;
29 v=100; %length for constraint

```

```

31 %% Definition KP
32 %%External KP
33 fprintf(fid, ['K,1,', num2str(b/2), ',', num2str(t/2+z+h), ',0', '\n']);
34 fprintf(fid, ['K,2,', num2str(b/2), ',', num2str(t/2+z), ',0', '\n']);
35 fprintf(fid, ['K,3,', num2str(b/2+z), ',', num2str(t/2), ',0', '\n']);
36 fprintf(fid, ['K,4,', num2str(L/2), ',', num2str(t/2+g*tan(alfa_dx)), ...
37     '0', '\n']);
38 fprintf(fid, ['K,5,', num2str(L/2), ',', num2str(t/2+g*tan(alfa_dx)-t), ...
39     '0', '\n']);
40 fprintf(fid, ['K,6,', num2str(L/2-v), ',', num2str(t/2+(g-v)*tan(alfa_dx)-t), ...
41     '0', '\n']);
42 fprintf(fid, ['K,7,', num2str(b/2+z), ',', num2str(-t/2), ',0', '\n']);
43 fprintf(fid, ['K,8,', num2str(b/2), ',', num2str(-(t/2+z)), ',0', '\n']);
44 fprintf(fid, ['K,9,', num2str(b/2), ',', num2str(-(t/2+z+h)), ',0', '\n']);
45 fprintf(fid, ['K,10,', num2str(-b/2), ',', num2str(-(t/2+z+h)), ',0', '\n']);
46 fprintf(fid, ['K,11,', num2str(-b/2), ',', num2str(-(t/2+z)), ',0', '\n']);
47 fprintf(fid, ['K,12,', num2str(-(b/2+z)), ',', num2str(-t/2), ',0', '\n']);
48 fprintf(fid, ['K,13,', num2str(-L/2), ',', num2str(t/2+g*tan(alfa_sx)-t), ...
49     '0', '\n']);
50 fprintf(fid, ['K,14,', num2str(-L/2), ',', num2str(t/2+g*tan(alfa_sx)), ...
51     '0', '\n']);
52 fprintf(fid, ['K,15,', num2str(-(L/2-v)), ',', num2str(t/2+(g-v)*tan(alfa_sx)), ...
53     '0', '\n']);
54 fprintf(fid, ['K,16,', num2str(-(b/2+z)), ',', num2str(t/2), ',0', '\n']);
55 fprintf(fid, ['K,17,', num2str(-b/2), ',', num2str(t/2+z), ',0', '\n']);
56 fprintf(fid, ['K,18,', num2str(-b/2), ',', num2str(t/2+z+h), ',0', '\n']);
57
58 %% Creation of lines
59
60 fprintf(fid, 'L,1,2\n');
61 fprintf(fid, 'L,2,3\n');
62 fprintf(fid, 'L,3,4\n');
63 fprintf(fid, 'L,4,5\n');
64 fprintf(fid, 'L,5,6\n');
65 fprintf(fid, 'L,6,7\n');
66 fprintf(fid, 'L,7,8\n');
67 fprintf(fid, 'L,8,9\n');
68 fprintf(fid, 'L,9,10\n');
69 fprintf(fid, 'L,10,11\n');
70 fprintf(fid, 'L,11,12\n');
71 fprintf(fid, 'L,12,13\n');
72 fprintf(fid, 'L,13,14\n');
73 fprintf(fid, 'L,14,15\n');
74 fprintf(fid, 'L,15,16\n');
75 fprintf(fid, 'L,16,17\n');
76 fprintf(fid, 'L,17,18\n');
77 fprintf(fid, 'L,18,1\n');
78
79 fprintf(fid, 'L,16,3\n');
80 fprintf(fid, 'L,12,7\n');
81 fprintf(fid, 'L,12,16\n');
82 fprintf(fid, 'L,7,3\n');
83 fprintf(fid, 'LANG,19,17,90, \n');
84 fprintf(fid, 'LANG,20,11,90, \n');
85 fprintf(fid, 'LANG,25,8,90, \n');
86 fprintf(fid, 'LANG,23,2,90, \n');
87 fprintf(fid, 'L,20,19\n');
88 fprintf(fid, 'L,21,22\n');
89 fprintf(fid, 'L,11,8\n');
90 fprintf(fid, 'L,17,2\n');
91 fprintf(fid, 'LANG,3,6,90, \n');
92 fprintf(fid, 'LANG,12,15,90, \n');

```

```

93 %% Creation of areas

95 fprintf(fid,'FLST,2,4,4\FITEM,2,21\FITEM,2,20\FITEM,2,31\FITEM,2,19\n');
95 fprintf(fid,'AL,P51X\n');
97 fprintf(fid,'FLST,2,4,4\FITEM,2,31\FITEM,2,23\FITEM,2,25\FITEM,2,32\n');
97 fprintf(fid,'AL,P51X\n');
99 fprintf(fid,'FLST,2,4,4\FITEM,2,32\FITEM,2,27\FITEM,2,29\FITEM,2,22\n');
99 fprintf(fid,'AL,P51X\n');
101 fprintf(fid,'FLST,2,3,4\FITEM,2,19\FITEM,2,16\FITEM,2,24\n');
101 fprintf(fid,'AL,P51X\n');
103 fprintf(fid,'FLST,2,4,4\FITEM,2,23\FITEM,2,24\FITEM,2,30\FITEM,2,34\n');
103 fprintf(fid,'AL,P51X\n');
105 fprintf(fid,'FLST,2,3,4\FITEM,2,30\FITEM,2,29\FITEM,2,2\n');
105 fprintf(fid,'AL,P51X\n');
107 fprintf(fid,'FLST,2,4,4\FITEM,2,34\FITEM,2,1\FITEM,2,17\FITEM,2,18\n');
107 fprintf(fid,'AL,P51X\n');
109 fprintf(fid,'FLST,2,3,4\FITEM,2,20\FITEM,2,26\FITEM,2,11\n');
109 fprintf(fid,'AL,P51X\n');
111 fprintf(fid,'FLST,2,4,4\FITEM,2,26\FITEM,2,25\FITEM,2,33\FITEM,2,28\n');
111 fprintf(fid,'AL,P51X\n');
113 fprintf(fid,'FLST,2,3,4\FITEM,2,27\FITEM,2,28\FITEM,2,7\n');
113 fprintf(fid,'AL,P51X\n');
115 fprintf(fid,'FLST,2,4,4\FITEM,2,33\FITEM,2,10\FITEM,2,8\FITEM,2,9\n');
115 fprintf(fid,'AL,P51X\n');
117 fprintf(fid,'FLST,2,4,4\FITEM,2,13\FITEM,2,37\FITEM,2,38\FITEM,2,14\n');
117 fprintf(fid,'AL,P51X\n');
119 fprintf(fid,'FLST,2,4,4\FITEM,2,15\FITEM,2,12\FITEM,2,38\FITEM,2,21\n');
119 fprintf(fid,'AL,P51X\n');
121 fprintf(fid,'FLST,2,4,4\FITEM,2,5\FITEM,2,4\FITEM,2,35\FITEM,2,36\n');
121 fprintf(fid,'AL,P51X\n');
123 fprintf(fid,'FLST,2,4,4\FITEM,2,3\FITEM,2,6\FITEM,2,22\FITEM,2,36\n');
123 fprintf(fid,'AL,P51X\n');
125
125 %% Creation of mesh
127 d_max=0.4*t;
127 global_element_size=d_max/6;
129 fprintf(fid,['ESIZE','num2str(global_element_size),'0,\n']);
129 fprintf(fid,'CM,_Y,AREA\nASEL,_,_,_,_12_\n');
131 fprintf(fid,'CM,_Y1,AREA\nCHKMSH,''AREA''\nCMSEL,S,_Y\n!* \n');
131 fprintf(fid,['MSHKEY,1\nAMESH,_Y1\nMSHKEY,1\n!* \nCMDELE,_Y\nCMDELE,_Y1' ...
133 '\nCMDELE,_Y2\n!* \n']);
133 fprintf(fid,'CM,_Y,AREA\nASEL,_,_,_,_13_\n');
135 fprintf(fid,'CM,_Y1,AREA\nCHKMSH,''AREA''\nCMSEL,S,_Y\n!* \n');
135 fprintf(fid,['MSHKEY,1\nAMESH,_Y1\nMSHKEY,1\n!* \nCMDELE,_Y\nCMDELE,_Y1' ...
137 '\nCMDELE,_Y2\n!* \n']);
137 fprintf(fid,'CM,_Y,AREA\nASEL,_,_,_,_15_\n');
139 fprintf(fid,'CM,_Y1,AREA\nCHKMSH,''AREA''\nCMSEL,S,_Y\n!* \n');
139 fprintf(fid,['MSHKEY,1\nAMESH,_Y1\nMSHKEY,1\n!* \nCMDELE,_Y\nCMDELE,_Y1' ...
141 '\nCMDELE,_Y2\n!* \n']);
141 fprintf(fid,'CM,_Y,AREA\nASEL,_,_,_,_14_\n');
143 fprintf(fid,'CM,_Y1,AREA\nCHKMSH,''AREA''\nCMSEL,S,_Y\n!* \n');
143 fprintf(fid,['MSHKEY,1\nAMESH,_Y1\nMSHKEY,1\n!* \nCMDELE,_Y\nCMDELE,_Y1' ...
145 '\nCMDELE,_Y2\n!* \n']);
145 fprintf(fid,'CM,_Y,AREA\nASEL,_,_,_,_4_\n');
147 fprintf(fid,'CM,_Y1,AREA\nCHKMSH,''AREA''\nCMSEL,S,_Y\n!* \n');
147 fprintf(fid,['MSHKEY,1\nAMESH,_Y1\nMSHKEY,1\n!* \nCMDELE,_Y\nCMDELE,_Y1' ...
149 '\nCMDELE,_Y2\n!* \n']);
149 fprintf(fid,'CM,_Y,AREA\nASEL,_,_,_,_1_\n');
151 fprintf(fid,'CM,_Y1,AREA\nCHKMSH,''AREA''\nCMSEL,S,_Y\n!* \n');
151 fprintf(fid,['MSHKEY,1\nAMESH,_Y1\nMSHKEY,1\n!* \nCMDELE,_Y\nCMDELE,_Y1' ...
153 '\nCMDELE,_Y2\n!* \n']);
153 fprintf(fid,'CM,_Y,AREA\nASEL,_,_,_,_8_\n');
155 fprintf(fid,'CM,_Y1,AREA\nCHKMSH,''AREA''\nCMSEL,S,_Y\n!* \n');

```


E.3.3 Code for application of PSM (Sharp V-notch)

```

clc;
2 clear all;
close all;
4
5 %Opening of APDL file
6 fid=fopen('PSM_model_misalignment.txt','w');
fprintf(fid,'/CLEAR\n');
8
9 %% Opening of Preprocessor
10 fprintf(fid,['/PREP7','\n']);
%% Definition of element
12 fprintf(fid,'ET,1,PLANE182\n');
fprintf(fid,'KEYOPT,1,1,3\nKEYOPT,1,3,2\nKEYOPT,1,6,0\n');
14
15 %% Definition of Material
16 E=206000;
ni=0.3;
18 fprintf(fid,['MPTEMP,,,,,,,,\nMPTEMP,1,0\nMPDATA,EX,1,,',num2str(E), ...
'\nMPDATA,PRXY,1,,',num2str(ni),'\n']);
20 %% Definition geometry parameters in mm
b=6;
22 t=6;
L=600;
24 z=7;
h=33;
26 root_width=0.1;
alfa_dx=deg2rad(1.01);
28 alfa_sx=deg2rad(0.94);
g=L/2-b/2-z;
30 v=100; %length for constraint
32 %% Definition KP
%External KP
34 fprintf(fid,['K,1,',num2str(b/2),',',num2str(t/2+z+h),',0','\n']);
fprintf(fid,['K,2,',num2str(b/2),',',num2str(t/2+z),',0','\n']);
36 fprintf(fid,['K,3,',num2str(b/2+z),',',num2str(t/2),',0','\n']);
fprintf(fid,['K,4,',num2str(L/2),',',num2str(t/2+g*tan(alfa_dx)), ...
38 '0','\n']);
fprintf(fid,['K,5,',num2str(L/2),',',num2str(t/2+g*tan(alfa_dx)-t), ...
40 '0','\n']);
fprintf(fid,['K,6,',num2str(L/2-v),',',num2str(t/2+(g-v)*tan(alfa_dx)-t), ...
42 '0','\n']);
fprintf(fid,['K,7,',num2str(b/2+z),',',num2str(-t/2),',0','\n']);
44 fprintf(fid,['K,8,',num2str(b/2),',',num2str(-(t/2+z)),',0','\n']);
fprintf(fid,['K,9,',num2str(b/2),',',num2str(-(t/2+z+h)),',0','\n']);
46 fprintf(fid,['K,10,',num2str(-b/2),',',num2str(-(t/2+z+h)),',0','\n']);
fprintf(fid,['K,11,',num2str(-b/2),',',num2str(-(t/2+z)),',0','\n']);
48 fprintf(fid,['K,12,',num2str(-(b/2+z)),',',num2str(-t/2),',0','\n']);
fprintf(fid,['K,13,',num2str(-L/2),',',num2str(t/2+g*tan(alfa_sx)-t), ...
50 '0','\n']);
fprintf(fid,['K,14,',num2str(-L/2),',',num2str(t/2+g*tan(alfa_sx)), ...
52 '0','\n']);
fprintf(fid,['K,15,',num2str(-(L/2-v)),',',num2str(t/2+(g-v)*tan(alfa_sx)), ...
54 '0','\n']);
fprintf(fid,['K,16,',num2str(-(b/2+z)),',',num2str(t/2),',0','\n']);
56 fprintf(fid,['K,17,',num2str(-b/2),',',num2str(t/2+z),',0','\n']);
fprintf(fid,['K,18,',num2str(-b/2),',',num2str(t/2+z+h),',0','\n']);
58
59 %KP for the root
60 fprintf(fid,['K,19,',num2str(b/2),',0,0','\n']);
fprintf(fid,['K,20,',num2str(b/2),',',num2str(t/2),',0','\n']);

```



```

62 fprintf(fid, ['K,21,' , num2str(b/2+root_width),',',0,0', '\n']);
63 fprintf(fid, ['K,22,' , num2str(b/2+root_width),',',', num2str(-t/2),',',0', '\n']);
64
65 fprintf(fid, ['K,23,' , num2str(-b/2),',',0,0', '\n']);
66 fprintf(fid, ['K,24,' , num2str(-b/2),',',', num2str(t/2),',',0', '\n']);
67 fprintf(fid, ['K,25,' , num2str(-(b/2+root_width)),',',0,0', '\n']);
68 fprintf(fid, ['K,26,' , num2str(-(b/2+root_width)),',',', num2str(-t/2),',',0', '\n']);
69
70 %% Creation of lines
71
72 fprintf(fid, 'L,1,2\n');
73 fprintf(fid, 'L,2,3\n');
74 fprintf(fid, 'L,3,4\n');
75 fprintf(fid, 'L,4,5\n');
76 fprintf(fid, 'L,5,6\n');
77 fprintf(fid, 'L,6,7\n');
78 fprintf(fid, 'L,7,8\n');
79 fprintf(fid, 'L,8,9\n');
80 fprintf(fid, 'L,9,10\n');
81 fprintf(fid, 'L,10,11\n');
82 fprintf(fid, 'L,11,12\n');
83 fprintf(fid, 'L,12,13\n');
84 fprintf(fid, 'L,13,14\n');
85 fprintf(fid, 'L,14,15\n');
86 fprintf(fid, 'L,15,16\n');
87 fprintf(fid, 'L,16,17\n');
88 fprintf(fid, 'L,17,18\n');
89 fprintf(fid, 'L,18,1\n');
90 n=18;
91
92 %Lines for root
93
94 fprintf(fid, 'L,19,20\n');
95 fprintf(fid, 'L,20,21\n');
96 fprintf(fid, 'L,21,22\n');
97 fprintf(fid, 'L,22,19\n');
98
99 fprintf(fid, 'L,23,24\n');
100 fprintf(fid, 'L,24,25\n');
101 fprintf(fid, 'L,25,26\n');
102 fprintf(fid, 'L,26,23\n');
103
104 %number of line for root
105 k=8;
106
107 %% Creation of Area
108 fprintf(fid, ['FLST,2,' , num2str(n+k),',',4\n']);
109 for i=1:(n+k)
110     fprintf(fid, ['FITEM,2,' , num2str(i), '\n']);
111 end
112 fprintf(fid, 'AL,P51X\n');
113
114 %% Creation of mesh
115 a=t/2; %dimensional parametr
116 ratio_min=3; %from literature PSM review A.Campagnolo
117 d_max=a/ratio_min; %maximum dimension of element
118
119 global_element_size=0.2;
120 fprintf(fid, ['ESIZE,' , num2str(global_element_size),',',0, '\n']);
121 fprintf(fid, 'MSHKEY,0\nCM,_Y,AREA\nASEL,1,1,1,1,1,1,1,1,1,1\n');
122 fprintf(fid, 'CM,_Y1,AREA\nCHKMSH, ' , AREA' '\nCMSEL,S,_Y\n!* \n');
123 fprintf(fid, 'AMESH,_Y1\n!* \nCMDELE,_Y\nCMDELE,_Y1\nCMDELE,_Y2\n!* \n');

```

```

126 %% Definition of constraint and Pressure

128 %Constraint
fprintf(fid,'FLST,2,2,4,ORDE,2\n');
130 fprintf(fid,'FITEM,2,5\n');
fprintf(fid,['FITEM,2,14\n','/GO\n!* \n']);
132 fprintf(fid,'DL,P51X,_,UY,\n');

134 fprintf(fid,'FLST,2,1,4,ORDE,1\n');
fprintf(fid,['FITEM,2,13\n','/GO\n!* \n']);
136 fprintf(fid,'DL,P51X,_,UX,\n');

138 %Pressure
140 p=-1;
fprintf(fid,'FLST,2,1,4,ORDE,1\n');
142 fprintf(fid,['FITEM,2,4\n','/GO\n!* \n']);
fprintf(fid,['SFL,P51X,PRES',' ,num2str(p),' \n']);
144

%% Creation of local reference system at weld toe tip and root
146 alfa=112.5;
fprintf(fid,'WPSTYLE,,,,,,,,1\n');
148 fprintf(fid,['KWPAVE,3\nwprot',' ,num2str(-alfa),' \n']);
fprintf(fid,'CSWPLA,11,0,1,1,\n');
150 fprintf(fid,'WPCSYS,-1,0\n');
fprintf(fid,'KWPAVE,20\nwprot,90\n');
152 fprintf(fid,'CSWPLA,12,0,1,1,\nWPSTYLE,,,,,,,,0\n');
fprintf(fid,'WPCSYS,-1,0\n');
154

fprintf(fid,'WPSTYLE,,,,,,,,1\n');
156 fprintf(fid,['KWPAVE,7\nwprot',' ,num2str(alfa),' \n']);
fprintf(fid,'wprot,0,180,0\n');
158 fprintf(fid,'CSWPLA,13,0,1,1,\n');
fprintf(fid,'WPCSYS,-1,0\n');
160 fprintf(fid,'KWPAVE,22\nwprot,-90\n');
fprintf(fid,'wprot,0,180,0\n');
162 fprintf(fid,'CSWPLA,14,0,1,1,\nWPSTYLE,,,,,,,,0\n');
fprintf(fid,'WPCSYS,-1,0\n');
164

fprintf(fid,'WPSTYLE,,,,,,,,1\n');
166 fprintf(fid,['KWPAVE,16\n_wprot',' ,num2str(alfa),' \n']);
fprintf(fid,'wprot,0,0,180\n');
168 fprintf(fid,'CSWPLA,15,0,1,1,\n');
fprintf(fid,'WPCSYS,-1,0\n');
170 fprintf(fid,'KWPAVE,24\nwprot,90\n');
fprintf(fid,'CSWPLA,16,0,1,1,\nWPSTYLE,,,,,,,,0\n');
172 fprintf(fid,'WPCSYS,-1,0\n');

174 fprintf(fid,'WPSTYLE,,,,,,,,1\n');
fprintf(fid,['KWPAVE,12\nwprot',' ,num2str(-alfa),' \n']);
176 fprintf(fid,'wprot,0,0,180\n');
fprintf(fid,'wprot,0,180,0\n');
178 fprintf(fid,'CSWPLA,17,0,1,1,\n');
fprintf(fid,'WPCSYS,-1,0\n');
180 fprintf(fid,'KWPAVE,26\nwprot,-90\n');
fprintf(fid,'wprot,0,180,0\n');
182 fprintf(fid,'CSWPLA,18,0,1,1,\nWPSTYLE,,,,,,,,0\n');

184 %% Solution
fprintf(fid,'/SOLU\nSOLVE\n');
186 fprintf(fid,['!* \n_/PSF,DEFA,_,1,0,1\n/PBF,DEFA,_,1_\n/PSYMB,CS,1_\n');
fprintf(fid,['/PSYMB,NDIR,0_\n/PSYMB,ESYS,0\n/PSYMB,ESYS,0_\n' ...

```

```

188     '\n/PSYMB,ESYS,0_\n');
fprintf(fid,['/PSYMB,ESYS,0\n/PSYMB,LDIV,0\n_/PSYMB,LDIR,0\n/PSYMB,ADIR,0' ...
190     '\n/PSYMB,ECON,0\n']);
fprintf(fid,['/PSYMB,XNODE,0\n/PSYMB,DOT,1\n/PSYMB,PCONV,\n/PSYMB,LAYR,0' ...
192     '\n/PSYMB,FBCS,0\n']);
fprintf(fid,['!\n/PBC,ALL,_,1\n/REP\n!* \n');
194
fclose(fid);

```

E.3.4 Code for application of PSM (No sharp V-notch)

```

1  clc;
   clear all;
3  close all;
   delete('Tensioni_nodali.txt')
5  delete('Coordinate_nodali.txt')
   clc
7  %Opening of APDL file
   fid=fopen('PSM_model_HFMI.txt','w');
9  fprintf(fid,'/CLEAR\n');

11 % Opening of Preprocessor
   fprintf(fid,['/PREP7','\n']);
13
   %% Definition of element
15 fprintf(fid,'ET,1,PLANE182\n');
   fprintf(fid,'KEYOPT,1,1,3\nKEYOPT,1,3,2\nKEYOPT,1,6,0\n');
17
   %% Definition of Material
19 E=206000;
   ni=0.3;
21 fprintf(fid,['MPTEMP,,,,,,,,\nMPTEMP,1,0\nMPDATA,EX,1,,',num2str(E), ...
   '\nMPDATA,PRXY,1,,',num2str(ni),' \n']);
23
   %% Definition geometry parameters in mm
25 b=6;
   t=6;
27 L=600;
   z=7;
29 h=33;
   root_width=0.1;
31 alfa_dx=deg2rad(1.01);
   alfa_sx=deg2rad(0.94);
33 g=L/2-b/2-z;
   v=100; %length for constraint
35
   %% Definition KP
37 %External KP
   fprintf(fid,['K,1,',num2str(b/2),',',num2str(t/2+z+h),',',0','\n']);
39 fprintf(fid,['K,2,',num2str(b/2),',',num2str(t/2+z),',',0','\n']);
   fprintf(fid,['K,3,',num2str(b/2+z),',',num2str(t/2),',',0','\n']);
41 fprintf(fid,['K,4,',num2str(L/2),',',num2str(t/2+g*tan(alfa_dx)),',',0','\n']);
   fprintf(fid,['K,5,',num2str(L/2),',',num2str(t/2+g*tan(alfa_dx)-t),',',0','\n']);
43 fprintf(fid,['K,6,',num2str(L/2-v),',',num2str(t/2+(g-v)*tan(alfa_dx)-t), ...
   '0','\n']);
45 fprintf(fid,['K,7,',num2str(b/2+z),',',num2str(-t/2),',',0','\n']);
   fprintf(fid,['K,8,',num2str(b/2),',',num2str(-t/2+z),',',0','\n']);
47 fprintf(fid,['K,9,',num2str(b/2),',',num2str(-t/2+z+h),',',0','\n']);
   fprintf(fid,['K,10,',num2str(-b/2),',',num2str(-t/2+z+h),',',0','\n']);
49 fprintf(fid,['K,11,',num2str(-b/2),',',num2str(-t/2+z),',',0','\n']);
   fprintf(fid,['K,12,',num2str(-b/2+z),',',num2str(-t/2),',',0','\n']);
51 fprintf(fid,['K,13,',num2str(-L/2),',',num2str(t/2+g*tan(alfa_sx)-t),',',0','\n']);

```

```

fprintf(fid, ['K,14,', num2str(-L/2), ', ', num2str(t/2+g*tan(alfa_sx)), '0', '\n']);
53 fprintf(fid, ['K,15,', num2str(-(L/2-v)), ', ', num2str(t/2+(g-v)*tan(alfa_sx)), ...
    '0', '\n']);
55 fprintf(fid, ['K,16,', num2str(-(b/2+z)), ', ', num2str(t/2), ', 0', '\n']);
fprintf(fid, ['K,17,', num2str(-b/2), ', ', num2str(t/2+z), ', 0', '\n']);
57 fprintf(fid, ['K,18,', num2str(-b/2), ', ', num2str(t/2+z+h), ', 0', '\n']);

59 %KP for the root
fprintf(fid, ['K,19,', num2str(b/2), ', 0,0', '\n']);
61 fprintf(fid, ['K,20,', num2str(b/2), ', ', num2str(t/2), ', 0', '\n']);
fprintf(fid, ['K,21,', num2str(b/2+root_width), ', 0,0', '\n']);
63 fprintf(fid, ['K,22,', num2str(b/2+root_width), ', ', num2str(-t/2), ', 0', '\n']);

65 fprintf(fid, ['K,23,', num2str(-b/2), ', 0,0', '\n']);
fprintf(fid, ['K,24,', num2str(-b/2), ', ', num2str(t/2), ', 0', '\n']);
67 fprintf(fid, ['K,25,', num2str(-(b/2+root_width)), ', 0,0', '\n']);
fprintf(fid, ['K,26,', num2str(-(b/2+root_width)), ', ', num2str(-t/2), ', 0', '\n']);

69
71 %% Creation of lines
fprintf(fid, 'L,1,2\n');
73 fprintf(fid, 'L,2,3\n');
fprintf(fid, 'L,3,4\n');
75 fprintf(fid, 'L,4,5\n');
fprintf(fid, 'L,5,6\n');
77 fprintf(fid, 'L,6,7\n');
fprintf(fid, 'L,7,8\n');
79 fprintf(fid, 'L,8,9\n');
fprintf(fid, 'L,9,10\n');
81 fprintf(fid, 'L,10,11\n');
fprintf(fid, 'L,11,12\n');
83 fprintf(fid, 'L,12,13\n');
fprintf(fid, 'L,13,14\n');
85 fprintf(fid, 'L,14,15\n');
fprintf(fid, 'L,15,16\n');
87 fprintf(fid, 'L,16,17\n');
fprintf(fid, 'L,17,18\n');
89 fprintf(fid, 'L,18,1\n');
n=18;

91
93 %Lines for root
fprintf(fid, 'L,19,20\n');
95 fprintf(fid, 'L,20,21\n');
fprintf(fid, 'L,21,22\n');
97 fprintf(fid, 'L,22,19\n');

99 fprintf(fid, 'L,23,24\n');
fprintf(fid, 'L,24,25\n');
101 fprintf(fid, 'L,25,26\n');
fprintf(fid, 'L,26,23\n');

103
105 %number of line for root
k=8;

107 %% Creation of Area
fprintf(fid, ['FLST,2,', num2str(n+k), ', 4\n']);
109 for i=1:(n+k)
    fprintf(fid, ['FITEM,2,', num2str(i), '\n']);
111 end
fprintf(fid, 'AL,P51X\n');

113
%% KP HFMI

```

```

115 %Dimension of the groove
117 rho=3.31;%standard deviation 1.25
    depth=0.21+0.09; %standard deviation 0.09
119
120 %Groove up-right
121
122 alfa=((135-rad2deg(alfa_dx))/2)+rad2deg(alfa_dx);
123 alfa_rad=deg2rad(alfa);
    xc=t/2+z+((rho-depth)/(tan(alfa_rad)));
125 yc=t/2+rho-depth;
fprintf(fid,'NUMSTR,KP,200\n');
127 fprintf(fid,['K,',',',num2str(xc),',',',',num2str(yc),',',',',0',',','\n']);
fprintf(fid,['CYL4,',',',num2str(xc),',',',',num2str(yc),',',',',num2str(rho),',',',','\n']);
129
130 %Groove up-left
131
132 beta=((135-rad2deg(alfa_sx))/2)+rad2deg(alfa_sx);
133 beta_rad=deg2rad(beta);
    xc1=t/2+z+((rho-depth)/(tan(beta_rad)));
135 yc1=t/2+rho-depth;
fprintf(fid,['K,',',',num2str(-xc1),',',',',num2str(yc1),',',',',0',',','\n']);
137 fprintf(fid,['CYL4,',',',num2str(-xc1),',',',',num2str(yc1),',',',',num2str(rho),',',',','\n']);
139 %Groove bottom-right
140
141 fprintf(fid,['K,',',',num2str(xc),',',',',num2str(-yc),',',',',0',',','\n']);
143 fprintf(fid,['CYL4,',',',num2str(xc),',',',',num2str(-yc),',',',',num2str(rho),',',',','\n']);
145 %Groove bottom-left
146
147 fprintf(fid,['K,',',',num2str(-xc1),',',',',num2str(-yc1),',',',',0',',','\n']);
fprintf(fid,['CYL4,',',',num2str(-xc1),',',',',num2str(-yc1),',',',',num2str(rho),',',',','\n']);
149
150 %% Creation of Area with HFMI groove
151 fprintf(fid,'FLST,3,4,5,ORDE,2\nFITEM,3,2\nFITEM,3,-5\nASBA,1,P51X\n');
153
154 %% Creation of mesh
155
156 global_element_size=0.5;
157 fprintf(fid,['ESIZE,',',',num2str(global_element_size),',',',',0',',','\n']);
fprintf(fid,'MSHKEY,0\nCM,_Y,AREA\nASEL,_,_,_,,6\n');
159 fprintf(fid,'CM,_Y1,AREA\nCHKMSH,'AREA'\nCMSEL,S,_Y\n!* \n');
fprintf(fid,'AMESH,_Y1\n!* \nCMDELE,_Y\nCMDELE,_Y1\nCMDELE,_Y2\n!* \n');
161
162 %Refine of mesh at the groove up-left
163
164 fprintf(fid,['FLST,5,2,4,ORDE,2\nFITEM,5,53\nFITEM,5,-54\nCM,_Y,LINE' ...
165     '\nLSEL,_,_,_,P51X\n']);
fprintf(fid,'CM,_Y1,LINE\nCMSEL,S,_Y\nCMDELE,_Y\n!* \n!* \n');
167 fprintf(fid,['LREF,_Y1,_,_,1,5,1,1\nCMDELE,_Y1\n!* \nFLST,5,2,4,ORDE,2' ...
    '\nFITEM,5,53\nFITEM,5,-54\n']);
169 fprintf(fid,['CM,_Y,LINE\nLSEL,_,_,_,P51X\nCM,_Y1,LINE\nCMSEL,S,_Y' ...
    '\nCMDELE,_Y\n!* \n!* \n']);
171 fprintf(fid,'LREF,_Y1,_,_,1,5,1,1\nCMDELE,_Y1\n!* \n');
173 %% Definition of constraint and Pressure
175
176 %Constraint
fprintf(fid,'FLST,2,2,4,ORDE,2\n');
177 fprintf(fid,'FITEM,2,5\n');

```

```

fprintf(fid, ['FITEM,2,14\n', '/GO\n!* \n']);
179 fprintf(fid, 'DL,P51X,_,UY, \n');

181 fprintf(fid, 'FLST,2,1,4,ORDE,1\n');
fprintf(fid, ['FITEM,2,13\n', '/GO\n!* \n']);
183 fprintf(fid, 'DL,P51X,_,UX, \n');

185
    %Pressure
187 p=-1;
fprintf(fid, 'FLST,2,1,4,ORDE,1\n');
189 fprintf(fid, ['FITEM,2,4\n', '/GO\n!* \n']);
fprintf(fid, ['SFL,P51X,PRES, ', num2str(p), ' \n']);
191

193
    %% Solution
195 fprintf(fid, '/SOLU\nSOLVE\nFINISH\n');
    %% Post processor
197
fprintf(fid, '/POST1\n!* \n');
199 fprintf(fid, 'FLST,5,2,4,ORDE,2\nFITEM,5,53\nFITEM,5,-54\nLSEL,S,_,_,P51X\n');
fprintf(fid, 'NSLL,S,1\n');
201

203 fprintf(fid, ['INRES,ALL\nFILE, ''file'', ''rst'', ''.''\nSET, LAST' ...
    '\nSET, FIRST\nAVPRIN,0,_, \n']);
205 fprintf(fid, ['ETABLE,_,S,1\n/OUTPUT,Tensioni_nodali,txt' ...
    '\nPRNSOL,_,S,_,PRIN\n/OUT\n']);
207

    %macro for nodal coordinates
209 fprintf(fid, '/INPUT,export_nodal_coords,mac\n');
tic
211 ! run_ansys.bat
toc
213

    %Opening of txt file tensioni nodali and writing of matrix tensioni nodali
215
    file_tensioni=fopen('Tensioni_nodali.txt','r');
217 tensioni_nodali_11=txt2mat(file_tensioni);
fclose(file_tensioni);
219 %Research of node with max principal stress
    ten_max=max(tensioni_nodali_11(:,2));
221 index_nodo=find(tensioni_nodali_11(:,2)==ten_max);
    nodo_ten_max=tensioni_nodali_11(index_nodo,1);
223

    %Creation of txt file coordinate nodali and creation of matrix
225 file_coordinate=fopen('coordinate_nodali.txt','r');
    coordinate_nodali_11=txt2mat_c(file_coordinate);
227 fclose(file_coordinate);
    %Researching of node with max principal stress
229 nodo_max=find(coordinate_nodali_11(:,1)==nodo_ten_max);
    coordinate_nodo_max=coordinate_nodali_11(nodo_max,:);
231 %Coordinates of the point with max principal stress at weld toe up-left
    x1=coordinate_nodo_max(2);
233 y1=coordinate_nodo_max(3);

235 %% Calculation of inclination angle for structural volume

237 %Point A represents the coordinates of the V-notch up-left
    xA=-(t/2+z);
239 yA=t/2;

```

```

241 %Point C represents the center of arc of the HFMI groove
    xc1_ul=-xc1;
243 yc1_ul=yc1;

245 %Angular coefficient of the straight between A and the center od the arc of HFMI groove
    m1=(yc1_ul-yA)/(xc1_ul-xA);
247
    %Angular coefficient of the straight between center of HFMI groove and 1
249 % (point with max prinicpal stress
    m2=(yc1_ul-y1)/(xc1_ul-x1);
251
    %Inclination angle gamma
253 gamma_rad=atan(abs((m1-m2)/(1+m1*m2)));
    gamma=rad2deg(gamma_rad);
255
    %% Calculation of the center to create structural volume
257 %Geometrical parameter
    delta=135-rad2deg(alfa_sx);
259 q=2-delta/180;
    r0=((q-1)/q)*rho;
261 R0=0.28;
    R_SED=R0+r0;
263
    %Inclination angle of straight from C to 1
265 psi=atan2((yc1_ul-y1),(xc1_ul-x1));

267 %Calculation of x2 e y2 coordinates of the arc center of structural volume for SED
    % (Method 1)
269 x2=x1+r0*cos(psi);
    y2=y1+r0*sin(psi);
271 %Equation of straight from 1 to 2 ed inverse formula of distance between 2 points
    % (Method 2)
273
    eq_y2=@(x) m2*(x-x1)+y1;
275 eq_x2=@(x) (x-x1).^2+(eq_y2(x)-y1).^2-r0^2;

277 %Plot of eq_x2 to verify the position of the zero
    plot(linspace(x1,x1-5),eq_x2(linspace(x1,x1-5)))
279 grid on
    %Initial point
281 x0=-11;
    x2_2=fsolve(eq_x2,x0);
283 hold on
    plot(x2_2,eq_x2(x2_2),'or')
285 y2_2=eq_y2(x2_2);
    %Verification of the length of the segment
287
    length_x2_y2=sqrt((x2-x1)^2+(y2-y1)^2)
289 length_x2_y2_2=sqrt((x2_2-x1)^2+(y2_2 -y1)^2)
    r0
291
    %% Creation of KP center of arc and the relative arc
293 %Selection all, opening of preprocessor, clean mesh, creation new geometry
    fprintf(fid,'ALLSEL,ALL\n_/PREP7\n');
295 fprintf(fid,'ACLEAR, _ _ _ _ _ _ _ _ 6\n');
    fprintf(fid,['FLST,2,2,8\nFITEM,2,' , num2str(x2) , ' , num2str(y2) , ' , 0\n']);
297 fprintf(fid,['FITEM,2,' , num2str(x2) , ' , num2str(y2-R_SED) , ' , 0\n']);
    fprintf(fid,'CIRCLE,P51X\n');
299
    %Division of the lines of structural volume
301 fprintf(fid,'FLST,2,2,4,ORDE,2\nFITEM,2,2\nFITEM,2,7\n');
    fprintf(fid,'FLST,3,2,4,ORDE,2\nFITEM,3,53\nFITEM,3,-54\n');
303 fprintf(fid,'LSBL,P51X,P51X, _ , _ , KEEP\n_ ');

```

```

305 %Deleting of the lines in excess
fprintf(fid,' FLST,2,4,4,ORDE,4\nFITEM,2,3\nFITEM,2,6\nFITEM,2,15\nFITEM,2,-16\n');
307 fprintf(fid,' LDELE,P51X,_,_,1\n');

309 %Division of principal area
fprintf(fid,' FLST,3,2,4,ORDE,2\nFITEM,3,11\nFITEM,3,-12\nASBL,6,P51X\n');
311

313 %% Mesh of areas
315 %Mesh Area of structural volume
size_SED=0.05;
fprintf(fid,['ESIZE',' ,num2str(size_SED),' ,0,']);
317 fprintf(fid,' MSHKEY,0\nCM,_Y,AREA\nASEL,_,_,_,1\n');
fprintf(fid,' CM,_Y1,AREA\nCHKMSH, ' ' AREA' '\nCMSEL,S,_Y\n!* \nAMESH,_Y1\n!*');
319 fprintf(fid,' CMDELE,_Y\nCMDELE,_Y1\nCMDELE,_Y2\n!* \n');

321 %Mesh external area
size_ext=1;
323 fprintf(fid,['ESIZE',' ,num2str(size_ext),' ,0,']);
fprintf(fid,' MSHKEY,0\nCM,_Y,AREA\nASEL,_,_,_,2\n');
325 fprintf(fid,' CM,_Y1,AREA\nCHKMSH, ' ' AREA' '\nCMSEL,S,_Y\n!* \nAMESH,_Y1\n!*');
fprintf(fid,' CMDELE,_Y\nCMDELE,_Y1\nCMDELE,_Y2\n!* \n');
327

329 %% Resolution of the model
fprintf(fid,' /SOLU\nSOLVE\n');
331

333 %% Post Process
fprintf(fid,' /POST1\n!* \n');

335 %Selection of structural area and attached elements
fprintf(fid,' ASEL,S,_,_,1\nESLA,S\n/AUTO,1\n/REP,FAST\n');
337

339 %Creation of Element Table SENE e VOLU
fprintf(fid,' AVPRIN,0,_,_,\nETABLE,_,SENE,\n!* \nAVPRIN,0,_,_,\nETABLE,_,VOLU,\n!* \n');
data=[rad2deg(alfa_sx) r0 gamma ]
341 fclose(fid);

```

E.4 MatLab code for the statistical analysis for the detection of misalignment factor

E.4.1 Free slope

```

1 clc
clear variables;
3 close all;

5 %% Reading of the data from excel file
S_max=xlsread('Data.xlsx','PSM','B:B');
7 N=xlsread('Data.xlsx','PSM','E:E');
t=xlsread('Data.xlsx','PSM','G:G'); %Thickness
9 e=xlsread('Data.xlsx','PSM','I:I'); %Misalignment
K_actual=xlsread('Data.xlsx','PSM','F:F'); %stress intensity Factor
11 % ideal with misalignment

13

15 %Definition of factors
gamma=[4.05:0.001:5]';
beta=[0.05:0.001:1]';
17

```



```

et=e./t;
19
  %Trasformation of tha number of cycle in logarithmic
21 N_log=log10(N);
  %Definizione della PS scelta e del livello di confidenza
23 prob_suv=95;
  liv_conf=95;
25 nu=length(S_max)-1;

27 %Definition of number of cycles
  Nmin=10000;
29 Nmax=10000000;
  Nlim=2000000;
31
  %% Calaculation of average value of the logarithmic data of number of cycles
33 N_avg_log=mean(N_log);

35 %% Calculation of Liebermann parameter
  %Creation of the matrix to define the Liebermann parameter (it summaries the
37 %confidence level and the PS

39 Confidenza=xlsread('Data.xlsx','Lieb','A:A');
  PS=xlsread('Data.xlsx','Lieb','B:B');
41 GDL=xlsread('Data.xlsx','Lieb','C:C');
  ps_valori=xlsread('Data.xlsx','Lieb','D:D');
43
  Lieb=[Confidenza PS GDL ps_valori];
45
  k=find(Lieb(:,1)==liv_conf & Lieb(:,2)==prob_suv & Lieb(:,3)==nu);
47 k_lieb=Lieb(k,4);

49 %% Beginning of iterative cycle

51 %Pre-location of the vectors
  S_max_new=zeros(length(S_max),length(beta),length(gamma));
53 S_max_new_log=zeros(length(S_max),length(beta),length(gamma));
  %sigma_y=zeros(length(gamma),length(beta));
55 %Tsigma=zeros(length(gamma),length(beta));
  %B=-5;
57 for i=1:length(gamma)
  for j=1:length(beta)
59   %k_mis(:,j,i)=gamma(i)*(1+beta(j).*et);
  k_mis(:,j,i)=abs(gamma(i)*(1-beta(j).*et));
61   %k_mis(:,j,i)=abs(gamma(i)./(1+beta(j).*et));
  %k_mis(:,j,i)=gamma(i).^(1-beta(j).*et);
63   %k_mis(:,j,i)=gamma(i).^(1+beta(j).*et);
  %k_mis(:,j,i)=gamma(i).^(1/(1-beta(j).*et));
65   %k_mis(:,j,i)=gamma(i).^(1/(1+beta(j).*et));
  %k_mis(:,j,i)=gamma(i).^(beta(j).*et);
67   S_max_new(:,j,i)=S_max.*K_actual.*k_mis(:,j,i);
  S_max_new_log(:,j,i)=log10(S_max_new(:,j,i));
69   %Calculation of the average value for the tension
  S_avg_new_log=mean(S_max_new_log(:,j,i));
71   %Calculation of the slope
  B(i,j)=sum((S_max_new_log(:,j,i)-S_avg_new_log).* ...
73   (N_log-N_avg_log))./sum((S_max_new_log(:,j,i)-S_avg_new_log).^2);
  %Calculation of intercept
75   A=N_avg_log-B(i,j)*S_avg_new_log;
  %Calculation of standard deviation
77   sigma_y(i,j)=sqrt((sum((N_log-(A+B(i,j).*S_max_new_log(:,j,i)).^2)) ...
  /(length(S_max)-2)));
79   sigma_S=sigma_y(i,j)/B(i,j);
  %Calculation of Tsigma

```

```

81     lim_inf=A-sigma_y(i,j)*k_lieb;
82     lim_sup=A+sigma_y(i,j)*k_lieb;
83     %Tension at N=2*10^6 for PS 5%,50%,95%
84     sigma_inf_95=10^(-lim_inf/B(i,j))*Nlim^(1/B(i,j));
85     sigma_sup_5=10^(-lim_sup/B(i,j))*Nlim^(1/B(i,j));
86     sigma_50=10^(-A/B(i,j))*Nlim^(1/B(i,j));
87     Tsigma(i,j)=sigma_sup_5/sigma_inf_95;
88     Tsigma2(i,j)=10^(-(2*sigma_y(i,j)*k_lieb)/B(i,j));
89
90     end
91 end

93 [sigma_y_min,loc]=min(sigma_y(:));
94 [ii,jj]=ind2sub(size(sigma_y),loc);
95 fprintf(['The minimum value of standard deviation is ', num2str(sigma_y_min), ...
96         ' for beta equal to ', num2str(beta(jj)), ' and gamma equal to ', num2str(gamma(ii)), '\n']);
97 fprintf(['The Tsigma associated to the minimum value of standard deviation is equal to ' ...
98         ' ', num2str(Tsigma2(ii,jj)), '\n']);
99 fprintf(['The slope associated to the minimum value of standard deviation is equal to ' ...
100         ' ', num2str(B(ii,jj)), '\n']);
101 gamma_ok=gamma(ii);
102 beta_ok=beta(jj);
103
104 [BETA,GAMMA]=meshgrid(beta,gamma);
105 s=surf(GAMMA,BETA,sigma_y,'FaceAlpha',0.5);
106 s.EdgeColor='none'
107 xlabel('\gamma');
108 ylabel('\beta');
109 zlabel('Standard deviation \sigma_y');
110 hold on
111 plot3(gamma_ok,beta_ok,sigma_y_min,'or','MarkerSize',5)

```

E.4.2 Fixed slope m=5

```

clc
2 clear variables;
3 close all;
4
5 %% Reading of the data from excel file
6 S_max=xlsread('Data.xlsx','PSM','B:B');
7 N=xlsread('Data.xlsx','PSM','E:E');
8 t=xlsread('Data.xlsx','PSM','G:G'); %Thickness
9 e=xlsread('Data.xlsx','PSM','I:I'); %Misalignment
10 K_actual=xlsread('Data.xlsx','PSM','F:F'); %stress intensity Factor
11 % ideal with misalignment
12
13
14 %Definition of factors
15 gamma=[6.05:0.001:7]';
16 beta=[0.05:0.001:1]';
17
18 et=e./t;
19
20 %Trasformation of the number of cycle in logarithmic
21 N_log=log10(N);
22
23 %Definizione della PS scelta e del livello di confidenza
24 prob_suv=95;
25 liv_conf=95;
26 nu=length(S_max)-1;
27
28 %Definition of number of cycles

```

```

Nmin=10000;
30 Nmax=10000000;
Nlim=2000000;
32
%% Calaculation of average value of the logarithmic data of number of cycles
34 N_avg_log=mean(N_log);

36 %% Calculation of Liebermann parameter
%Creation of the matrix to define the Liebermann parameter (it summaries the
38 %confidence level and the PS

40 Confidenza=xlsread('Data.xlsx','Lieb','A:A');
PS=xlsread('Data.xlsx','Lieb','B:B');
42 GDL=xlsread('Data.xlsx','Lieb','C:C');
ps_valori=xlsread('Data.xlsx','Lieb','D:D');
44
Lieb=[Confidenza PS GDL ps_valori];
46
k=find(Lieb(:,1)==liv_conf & Lieb(:,2)==prob_suv & Lieb(:,3)==nu);
48 k_lieb=Lieb(k,4);

50 %% Beginning of iterative cycle

52 %Pre-location of the vectors
S_max_new=zeros(length(S_max),length(beta),length(gamma));
54 S_max_new_log=zeros(length(S_max),length(beta),length(gamma));
%sigma_y=zeros(length(gamma),length(beta));
56 %Tsigma=zeros(length(gamma),length(beta));
B=-5;
58 for i=1:length(gamma)
    for j=1:length(beta)
60         %k_mis(:,j,i)=gamma(i)*(1+beta(j).*et);
        %k_mis(:,j,i)=abs(gamma(i)*(1-beta(j).*et));
62         %k_mis(:,j,i)=abs(gamma(i)./(1+beta(j).*et(:)));
        k_mis(:,j,i)=gamma(i).^(1-beta(j).*et);
64         %k_mis(:,j,i)=gamma(i).^(1+beta(j).*et);
        %k_mis(:,j,i)=gamma(i).^(1/(1-beta(j).*et));
66         %k_mis(:,j,i)=gamma(i).^(1/(1+beta(j).*et));
        %k_mis(:,j,i)=gamma(i).^(beta(j).*et);
68         S_max_new(:,j,i)=S_max.*K_actual.*k_mis(:,j,i);
        S_max_new_log(:,j,i)=log10(S_max_new(:,j,i));
70         %Calculation of the average value for the tension
        S_avg_new_log=mean(S_max_new_log(:,j,i));
72         %Calculation of intercept
        A=N_avg_log-B*S_avg_new_log;
74         %Calculation of standard deviation
        sigma_y(i,j)=sqrt((sum((N_log-(A+B.*S_max_new_log(:,j,i))).^2)/(length(S_max)-2));
76         sigma_S=sigma_y(i,j)/B;
        %Calculation of Tsigma
78         lim_inf=A-sigma_y(i,j)*k_lieb;
        lim_sup=A+sigma_y(i,j)*k_lieb;
80         %Tension at N=2*10^6 for PS 5%,50%,95%
        sigma_inf_95=10^(-lim_inf/B)*Nlim^(1/B);
82         sigma_sup_5=10^(-lim_sup/B)*Nlim^(1/B);
        sigma_50=10^(-A/B)*Nlim^(1/B);
84         Tsigma(i,j)=sigma_sup_5/sigma_inf_95;
        Tsigma2(i,j)=10^(-(2*sigma_y(i,j)*k_lieb)/B);
86
    end
88 end

90 [sigma_y_min,loc]=min(sigma_y(:));
[ii,jj]=ind2sub(size(sigma_y),loc);

```

```

92 fprintf(['The_minimum_value_of_standard_deviation_is_', num2str(sigma_y_min), ...
    '_for_beta_equal_to_', num2str(beta(jj)), '_and_gamma_equal_to_', num2str(gamma(ii)), '\n']);
94 fprintf(['The_Tsigma_associated_to_the_minimum_value_of_standard_deviation_is_equal_to' ...
    '_ ', num2str(Tsigma2(ii, jj)), '\n']);
96 gamma_ok=gamma(ii);
    beta_ok=beta(jj);
98
    [BETA, GAMMA]=meshgrid(beta, gamma);
100 s=surf(GAMMA, BETA, sigma_y, 'FaceAlpha', 0.5);
    s.EdgeColor='none'
102 xlabel('\gamma');
    ylabel('\beta');
104 zlabel('Standard_deviation_\sigma_y');
    hold on
106 plot3(gamma_ok, beta_ok, sigma_y_min, 'or', 'MarkerSize', 5)

```

Appendix F

Results of misalignment analysis

F.1 Dimension of HFMI groove

Ideal model

Name of .txt file	depth [mm]	ρ_{HFMI} [mm]	width [mm]	ϕ (Inclinationangle)[°]
355-WH-2	3.31	0.3	4.48	2.41
355-WH-3	3.31	0.3	4.48	4.46
355-WH-4	3.31	0.3	4.48	3.27
355-WH-5	3.31	0.3	4.48	2.41
355-WH-8	3.31	0.3	4.48	4.46
355-WH-11	3.31	0.3	4.48	1.02
355-WH-14	3.31	0.3	4.48	1.88
355-WH-16	3.31	0.3	4.48	1.02
355-WH-17	3.31	0.3	4.48	1.02
355-WH-18	3.31	0.3	4.48	5.32
355-WH-20	3.31	0.3	4.48	0.69
355-WH-21	3.31	0.3	4.48	0.69
355-WH-22	3.31	0.3	4.48	6.18

Table F.1: Dimension of HFMI groove.

Ideal model with angular misalignment

Name of .txt file	depth [mm]	ρ_{HFMI} [mm]	width [mm]	ϕ (Inclinationangle)[°]
355-WH-2	3.31	0.3	4.649	18.26
355-WH-3	3.31	0.3	4.642	18.29
355-WH-4	3.31	0.3	4.631	17.47
355-WH-5	3.31	0.3	4.625	17.5
355-WH-8	3.31	0.3	4.623	17.51
355-WH-11	3.31	0.3	4.605	17.6
355-WH-14	3.31	0.3	4.652	18.24
355-WH-16	3.31	0.3	4.628	17.49
355-WH-17	3.31	0.3	4.621	17.52
355-WH-18	3.31	0.3	4.622	18.39
355-WH-20	3.31	0.3	4.603	17.61
355-WH-21	3.31	0.3	4.596	17.64
355-WH-22	3.31	0.3	4.588	17.68

Table F.2: Dimension of HFMI groove.

F.2 Results of ideal model

ENS results

Name of .txt file	$\Delta\sigma_{11,max,toe,ENS183}$ [MPa]	$\Delta\sigma_{11,max,root,ENS183}$ [MPa]	$\Delta\sigma_{11,max,toe,ENS182}$ [MPa]	$\Delta\sigma_{11,max,root,ENS182}$ [MPa]
355-WH-2	2.762	3.032	2.778	3.046
355-WH-3	2.564	2.756	2.576	2.768
355-WH-4	2.826	3.111	2.84	3.124
355-WH-5	2.761	3.032	2.777	3.046
355-WH-8	2.565	2.756	2.576	2.768
355-WH-11	2.65	2.883	2.664	2.897
355-WH-14	2.629	2.853	2.642	2.866
355-WH-16	2.64	2.87	2.653	2.882
355-WH-17	2.64	2.87	2.653	2.882
355-WH-18	2.527	2.695	2.538	2.707
355-WH-20	2.703	2.958	2.719	2.971
355-WH-21	2.703	2.958	2.719	2.971
355-WH-22	2.527	2.695	2.538	2.706

Table F.3: ENS results of ideal model.

SHSS results

Name of .txt file	$SHSS_{LSE,typeA}$ [MPa]	$SHSS_{LSE,typeB}$ [MPa]
355-WH-2	0.994	0.950
355-WH-3	0.992	0.948
355-WH-4	0.990	0.950
355-WH-5	0.994	0.950
355-WH-8	0.992	0.948
355-WH-11	0.993	0.949
355-WH-14	0.993	0.948
355-WH-16	0.993	0.949
355-WH-17	0.993	0.949
355-WH-18	0.992	0.947
355-WH-20	0.994	0.949
355-WH-21	0.994	0.949
355-WH-22	0.950	0.947

Table F.4: SHSS results of ideal model.

PSM results of ideal model with sharp V-notch

Name of .txt file	$\sigma_{eq,peak,toe}$ [MPa]	$\sigma_{eq,peak,root}$ [MPa]
355-WH-2	1.946	1.945
355-WH-3	1.850	1.768
355-WH-4	1.977	1.994
355-WH-5	1.944	1.946
355-WH-8	1.851	1.771
355-WH-11	1.892	1.844
355-WH-14	1.878	1.834
355-WH-16	1.886	1.844
355-WH-17	1.886	1.844
355-WH-18	1.831	1.731
355-WH-20	1.917	1.898
355-WH-21	1.917	1.898
355-WH-22	1.831	1.731

Table F.5: PSM results of ideal model with sharp V-notch.

PSM results of ideal model with HFMI groove

Name of .txt file	$\sigma_{eq,peak,toe}$ [MPa]	$\sigma_{eq,peak,root}$ [MPa]
355-WH-2	1.685	2.028
355-WH-3	1.607	1.831
355-WH-4	1.699	2.08
355-WH-5	1.685	2.027
355-WH-8	1.607	1.821
355-WH-11	1.635	1.971
355-WH-14	1.630	1.932
355-WH-16	1.631	1.964
355-WH-17	1.631	1.964
355-WH-18	1.597	1.817
355-WH-20	1.652	1.974
355-WH-21	1.652	1.974
355-WH-22	1.596	1.792

Table F.6: PSM results of ideal model with HFMI groove.

F.3 Results of ideal model with misalignment

ENS results

Name of .txt file	$\Delta\sigma_{11,max,toe,ENS182}$ [MPa]	$\Delta\sigma_{11,max,root,ENS182}$ [MPa]	$\Delta\sigma_{11,max,toe,ENS183}$ [MPa]	$\Delta\sigma_{11,max,root,ENS183}$ [MPa]
355-WH-2	6.476	3.955	6.456	3.937
355-WH-3	6.000	3.445	5.979	3.428
355-WH-4	5.975	3.934	5.953	3.894
355-WH-5	5.776	3.776	5.755	3.758
355-WH-8	5.239	3.284	5.224	3.269
355-WH-11	5.236	3.455	5.221	3.442
355-WH-14	6.209	3.628	6.190	3.606
355-WH-16	5.561	3.506	5.542	3.491
355-WH-17	5.495	3.493	5.475	3.478
355-WH-18	5.462	3.253	5.447	3.238
355-WH-20	5.393	3.590	5.373	3.577
355-WH-21	5.427	3.604	5.409	3.590
355-WH-22	5.216	3.211	5.193	3.200

Table F.7: ENS results of ideal model with misalignment.

SHSS results

Name of .txt file	$SHSS_{LSE,typeA}$ [MPa]	$SHSS_{LSE,typeB}$ [MPa]
355-WH-2	3.227	3.177
355-WH-3	3.064	3.015
355-WH-4	2.892	2.844
355-WH-5	2.814	2.766
355-WH-8	2.614	2.568
355-WH-11	2.562	2.516
355-WH-14	3.149	3.100
355-WH-16	2.759	2.712
355-WH-17	2.720	2.673
355-WH-18	2.769	2.722
355-WH-20	2.622	2.575
355-WH-21	2.644	2.597
355-WH-22	2.620	2.573

Table F.8: SHSS results of ideal model with angular misalignment.

PSM results of ideal model with angular misalignment with sharp V-notch

Name of .txt file	$\sigma_{eq,peak,toe}$ [MPa]	$\sigma_{eq,peak,root}$ [MPa]
355-WH-2	4.854	2.249
355-WH-3	4.573	1.981
355-WH-4	4.512	2.243
355-WH-5	4.321	2.161
355-WH-8	3.963	1.900
355-WH-11	3.940	1.988
355-WH-14	4.672	2.063
355-WH-16	4.174	2.002
355-WH-17	4.124	2.010
355-WH-18	4.145	1.881
355-WH-20	4.017	2.056
355-WH-21	4.041	2.062
355-WH-22	3.913	1.854

Table F.9: PSM results of ideal model with angular misalignment with sharp V-notch.

PSM results of ideal model with angular misalignment with HFMI groove

Name of .txt file	$\sigma_{eq,peak,toe}$ [MPa]	$\sigma_{eq,peak,root}$ [MPa]
355-WH-2	4.708	2.354
355-WH-3	4.434	2.060
355-WH-4	4.216	2.357
355-WH-5	4.122	2.261
355-WH-8	3.793	1.951
355-WH-11	3.732	2.066
355-WH-14	4.569	2.161
355-WH-16	4.013	2.094
355-WH-17	3.950	2.099
355-WH-18	4.043	1.941
355-WH-20	3.836	2.141
355-WH-21	3.858	2.145
355-WH-22	3.801	1.913

Table F.10: PSM results of ideal model with angular misalignment with HFMI groove.

Appendix G

Results of analysis of joint in CAL condition

G.1 Results and Experimental data from [49]

t [mm]	e [mm]	e/t	e_{tot} [mm]	α [°]	e from α [mm]	$\Delta\sigma_{nom}$ [MPa]	N_f [cycles]	K_{PSM} [MPa]	K_{ENS} [MPa]
6	0.75	0.125	0	0	0.75	503.01	34656	1.864	2.22782
6	0.75	0.125	0	0	0.75	399.83	76468	1.864	2.22782
6	0.75	0.125	0	0	0.75	399.91	111382	1.864	2.22782
6	0.75	0.125	0	0	0.75	300.32	305213	1.864	2.22782
6	0.75	0.125	0	0	0.75	300.37	412357	1.864	2.22782
6	0.75	0.125	0	0	0.75	300.44	459685	1.864	2.22782
6	0.75	0.125	0	0	0.75	248.45	685737	1.864	2.22782
6	0.75	0.125	0	0	0.75	300.44	715870	1.864	2.22782
6	0.75	0.125	0	0	0.75	223.62	1218111	1.864	2.22782
6	0.75	0.125	0	0	0.75	225.93	1897191	1.864	2.22782
6	1.5	0.25	0	0	1.5	400.49	26017	2.306	2.79286
6	1.5	0.25	0	0	1.5	399.33	50771	2.306	2.79286
6	1.5	0.25	0	0	1.5	300.44	125851	2.306	2.79286
6	1.5	0.25	0	0	1.5	250.10	137685	2.306	2.79286
6	1.5	0.25	0	0	1.5	300.57	237529	2.306	2.79286
6	1.5	0.25	0	0	1.5	200.84	335883	2.306	2.79286
6	1.5	0.25	0	0	1.5	200.93	633937	2.306	2.79286
6	1.5	0.25	0	0	1.5	201.01	856480	2.306	2.79286
6	1.5	0.25	0	0	1.5	175.66	1412010	2.306	2.79286
6	1.5	0.25	0	0	1.5	175.67	2056716	2.306	2.79286

Table G.1: Experimental constant amplitude axial fatigue data for welded joints [49] and PSM and ENS results.

G.2 Results and Experimental data from [50]

t [mm]	e [mm]	e/t	e_{tot} [mm]	α [°]	e from α [mm]	$\Delta\sigma_{nom}$ [MPa]	N_f [cycles]	K_{PSM} [MPa]	K_{ENS} [MPa]
8	6	0.75	0	0	6.00	206	214769	2.123	2.81873
8	6	0.75	0	0	6.00	168	547795	2.123	2.81873
8	9	1.125	0	0	9.00	206	217244	2.074	2.68309
8	9	1.125	0	0	9.00	244	124297	2.074	2.68309
8	9	1.125	0	0	9.00	169	596207	2.074	2.68309
8	9	1.125	0	0	9.00	188	463560	2.074	2.68309
8	16	2	0	0	16.00	206	253715	1.799	2.48121
8	16	2	0	0	16.00	168	883148	1.799	2.48121

Table G.2: Experimental constant amplitude axial fatigue data for welded joints [50] and PSM and ENS results.

G.3 Results and Experimental data from [51]

t [mm]	e [mm]	e/t	e_{tot} [mm]	α [°]	e from α [mm]	$\Delta\sigma_{nom}$ [MPa]	N_f [cycles]	K_{PSM} [MPa]	K_{ENS} [MPa]
12.5	3.125	0.25	0	0	3.125	142.59	192516	3.243	4.45172
12.5	3.125	0.25	0	0	3.125	122.88	233970	3.243	4.45172
12.5	3.125	0.25	0	0	3.125	91.85	1004330	3.243	4.45172
12.5	6.25	0.5	0	0	6.25	114.44	212919	4.321	5.83969
12.5	6.25	0.5	0	0	6.25	87.22	493070	4.321	5.83969
12.5	6.25	0.5	0	0	6.25	82.82	926731	4.321	5.83969
12.5	6.25	0.5	0	0	6.25	66.9	1333205	4.321	5.83969
12.5	9.375	0.75	0	0	9.375	85.54	223484	5.289	7.21842
12.5	9.375	0.75	0	0	9.38	70	296799	5.289	7.21842
12.5	9.375	0.75	0	0	9.38	54.75	747473	5.289	7.21842
12.5	9.375	0.75	0	0	9.38	40.92	3569802	5.289	7.21842
12.5	12.5	1	0	0	12.50	74.2	159327	6.378	8.61132
12.5	12.5	1	0	0	12.50	58.03	335894	6.378	8.61132
12.5	12.5	1	0	0	12.50	49.05	1883456	6.378	8.61132
12.5	12.5	1	0	0	12.50	35.5	2613788	6.378	8.61132
12.5	12.5	1	0	0	12.50	41.45	6195096	6.378	8.61132
12.5	3.125	0.25	0	0	3.13	221.92	10546	3.984	5.46003
12.5	3.125	0.25	0	0	3.13	172.78	50566	3.984	5.46003
12.5	3.125	0.25	0	0	3.13	132.98	158660	3.984	5.46003
12.5	3.125	0.25	0	0	3.13	94.26	441328	3.984	5.46003
12.5	3.125	0.25	0	0	3.125	84.95	498642	3.984	5.46003
12.5	6.25	0.5	0	0	6.25	153.07	33457	5.024	6.911761
12.5	6.25	0.5	0	0	6.25	132.83	63934	5.024	6.911761
12.5	6.25	0.5	0	0	6.25	111.62	210834	5.024	6.911761
12.5	6.25	0.5	0	0	6.25	72.86	484413	5.024	6.911761
12.5	6.25	0.5	0	0	6.25	78.26	610690	5.024	6.911761
12.5	6.25	0.5	0	0	6.25	169.66	11576	5.024	6.911761
12.5	6.25	0.5	0	0	6.25	66.08	1215377	5.024	6.911761
12.5	6.25	0.5	0	0	6.25	56.41	2276374	5.024	6.911761
12.5	6.25	0.5	0	0	6.25	45.11	6997402	5.024	6.911761
12.5	9.375	0.75	0	0	9.375	171.55	12549	6.125	8.34399
12.5	9.375	0.75	0	0	9.375	66.05	836434	6.125	8.34399
12.5	9.375	0.75	0	0	9.375	55.44	1100322	6.125	8.34399
12.5	12.5	1	0	0	12.5	152.15	21673	7.237	9.74413
12.5	12.5	1	0	0	12.5	132	30590	7.237	9.74413
12.5	12.5	1	0	0	12.5	114.56	63374	7.237	9.74413
12.5	12.5	1	0	0	12.5	93.61	146796	7.237	9.74413
12.5	12.5	1	0	0	12.5	94.74	325959	7.237	9.74413
12.5	12.5	1	0	0	12.5	66.03	593349	7.237	9.74413
12.5	12.5	1	0	0	12.5	46.27	1182798	7.237	9.74413
12.5	12.5	1	0	0	12.5	41.07	3632513	7.237	9.74413

Table G.3: Experimental constant amplitude axial fatigue data for welded joints [51] and PSM and ENS results.

G.4 Results and Experimental data from [52]

t [mm]	e [mm]	e/t	e_{tot} [mm]	α [°]	e from α [mm]	$\Delta\sigma_{nom}$ [MPa]	N_f [cycles]	K_{PSM} [MPa]	K_{ENS} [MPa]
5	1.07	0.213	0	0	1.066	300	247930	1.445	2.019
5	1.19	0.238	0	0	1.189	500	29639	1.474	2.059
5	0.80	0.160	0	0	0.800	250	3753730	1.380	1.923
5	1.07	0.213	0	0	1.066	300	254183	1.445	2.019
5	1.09	0.217	0	0	1.087	400	70625	1.454	2.026
5	0.76	0.152	0	0	0.759	400	103163	1.371	1.920
5	1.03	0.205	0	0	1.025	500	29676	1.431	2.006
5	1.07	0.213	0	0	1.066	400	86119	1.445	2.019
5	1.21	0.242	0	0	1.210	500	28103	1.507	2.066
5	0.02	0.004	0	0	0.021	500	49513	1.189	1.683
5	-0.14	-0.029	0	0	-0.144	400	124270	1.194	1.630
5	-0.06	-0.012	0	0	-0.062	300	319375	1.200	1.656
5	-0.04	-0.008	0	0	-0.041	500	35196	1.214	1.663
5	-0.10	-0.021	0	0	-0.103	400	123710	1.189	1.643
5	-0.08	-0.016	0	0	-0.082	300	514187	1.200	1.649
5	0.12	0.025	0	0	0.123	300	523098	1.228	1.716
5	0.04	0.008	0	0	0.041	500	61503	1.194	1.690
5	-2.359	-0.472	0	0	-2.359	300	560492	/	0.933
5	-1.579	-0.316	0	0	-1.579	400	199715	/	1.169
5	-2.605	-0.521	0	0	-2.605	500	68931	/	0.859
5	-2.687	-0.537	0	0	-2.687	500	70962	/	0.835
5	-1.620	-0.324	0	0	-1.620	350	335610	/	1.157
5	-1.846	-0.369	0	0	-1.846	400	220275	/	1.088
5	-1.846	-0.369	0	0	-1.846	300	1493630	/	1.088
5	-2.174	-0.435	0	0	-2.174	500	93505	/	0.989
5	-2.174	-0.435	0	0	-2.174	350	275958	/	0.989
5	-3.097	-0.619	0	0	-3.097	600	38765	/	0.711

Table G.4: Experimental constant amplitude axial fatigue data for welded joints [52] and PSM and ENS results.

G.5 Results and Experimental data from [53]

t [mm]	e [mm]	e/t	e_{tot} [mm]	α [°]	e from α [mm]	$\Delta\sigma_{nom}$ [MPa]	N_f [cycles]	K_{PSM} [MPa]	K_{ENS} [MPa]
5	1	0.2	1.41	3.69	4.69	414	16600	4.272	6.596
5	0	0	0.65	1.70	1.70	414	18100	2.512	3.719
5	0.95	0.19	0.05	0.13	1.08	414	59100	2.711	4.076
5	0.65	0.13	0.72	1.89	2.54	414	22600	2.998	4.386
5	1.45	0.29	0.78	2.04	3.49	414	12700	3.562	5.190
5	0.65	0.13	2.27	5.95	6.60	414	7000	4.077	5.779
5	0.4	0.08	0.29	0.76	1.16	414	61600	2.287	3.239
5	0.95	0.19	1.71	4.48	5.43	207	177100	3.533	4.926
5	1	0.2	0.21	0.55	1.55	207	936200	2.632	3.6832
5	0.05	0.01	0.92	2.41	2.46	414	37119	2.480	3.477
5	1.05	0.21	0.99	2.59	3.64	414	10500	3.178	4.392
5	0.95	0.19	0.74	1.94	2.89	414	22512	2.980	4.091
5	0.6	0.12	1.72	4.50	5.10	414	17600	3.215	4.199
5	0.2	0.04	0.74	1.94	2.14	414	65300	2.269	3.004
5	0.35	0.07	1.24	3.25	3.60	207	261000	2.723	3.562
5	0.75	0.15	0.57	1.49	2.24	414	29892	2.505	3.296
5	1.4	0.28	1.13	2.96	4.36	414	9500	3.224	4.330
5	0.15	0.03	1.36	3.56	3.71	207	867700	2.627	3.504
5	1.55	0.31	1.56	4.09	5.64	207	143800	3.584	4.839
5	0.3	0.06	1.79	4.69	4.99	414	35800	3.076	4.014
5	1.55	0.31	0.69	1.81	3.36	414	22500	3.024	3.968
5	0.25	0.05	1.21	3.17	3.42	414	18300	2.574	3.380
5	1.55	0.31	0.91	2.38	3.93	207	345900	3.148	4.161
5	1.15	0.23	0.64	1.68	2.83	207	183300	2.697	3.541
5	1	0.2	0.19	0.50	1.50	414	24000	2.284	3.021

Table G.5: Experimental constant amplitude axial fatigue data for welded joints [53] and PSM and ENS results.

t [mm]	e [mm]	e/t	e_{tot} [mm]	α [°]	e from α [mm]	$\Delta\sigma_{nom}$ [MPa]	N_f [cycles]	K_{PSM} [MPa]	K_{ENS} [MPa]
10	0.6	0.06	0.46	1.20	1.80	414	14600	3.458	5.148
10	0	0	0.13	0.34	0.34	414	35600	2.613	3.6991
10	0.2	0.02	0.15	0.39	0.59	207	134700	2.697	3.810
10	0.4	0.04	0.12	0.31	0.71	414	51600	2.761	3.894
10	0.5	0.05	0.02	0.05	0.55	207	161000	2.585	3.602
10	0.1	0.01	0.26	0.68	0.78	207	303700	2.480	3.539
10	1.8	0.18	0.13	0.34	2.14	414	14800	3.117	4.291
10	0.6	0.06	1.74	4.56	5.16	414	16300	3.462	4.618
10	0.8	0.08	0.82	2.15	2.95	414	19400	3.093	4.195
10	0.3	0.03	1.92	5.03	5.33	207	131000	3.321	4.576
10	0.2	0.02	0.14	0.37	0.57	414	24000	2.517	3.521
10	0.4	0.4	1.78	4.66	8.66	414	21000	3.310	4.545
10	1.5	0.15	0.54	1.41	2.91	207	106600	3.194	4.375
10	0.5	0.05	0.18	0.47	0.97	414	44200	2.690	3.690
10	0.7	0.07	0.48	1.26	1.96	414	26900	2.906	3.953
10	0.2	0.02	0.5	1.31	1.51	414	34400	2.592	3.722
10	0.1	0.01	0.71	1.86	1.96	414	19500	2.713	3.790
10	0.9	0.09	0.6	1.57	2.47	207	174000	2.979	4.118
10	1.1	0.11	0.32	0.84	1.94	207	233700	2.940	4.058
10	0.4	0.04	0.26	0.68	1.08	414	47800	2.563	3.4745
10	0.3	0.03	1.98	5.19	5.49	414	14477	3.350	4.395
10	0	0	0.88	2.30	2.30	207	408200	2.633	3.630
10	1.1	0.11	0.36	0.94	2.04	414	34400	2.826	3.857
10	0.8	0.08	0.18	0.47	1.27	414	30200	2.707	3.616
10	0.1	0.01	0.36	0.94	1.04	207	296100	2.478	3.389
10	0.1	0.01	0.49	1.28	1.38	414	33500	2.490	3.306
10	0.1	0.01	0.78	2.04	2.14	207	467100	2.470	3.353
10	0.7	0.07	0.82	2.15	2.85	414	41900	2.731	3.644
10	1.1	0.11	0.78	2.04	3.14	414	20900	2.917	3.802
10	1.6	0.16	0.41	1.07	2.67	207	181300	2.924	3.819
10	0.4	0.04	2.22	5.81	6.21	207	335000	3.298	4.302
10	0.5	0.05	3.26	8.54	9.04	207	162800	3.702	4.857

Table G.6: Experimental constant amplitude axial fatigue data for welded joints [53] and PSM and ENS results.

G.6 Results and Experimental data from [54]

t [mm]	e [mm]	e/t	e_{tot} [mm]	α [°]	e from α [mm]	$\Delta\sigma_{nom}$ [MPa]	N_f [cycles]	K_{PSM} [MPa]	K_{ENS} [MPa]
12	0.25	0.021	0.51	1.11	1.363	199	1037495	1.800	2.275
12	0.29	0.024	0.46	1.00	1.294	181	2041188	1.808	2.280
12	0.32	0.027	0.39	0.85	1.171	224	471601	1.787	2.268
12	0.24	0.020	0.41	0.89	1.134	249	277963	1.766	2.229
12	0.17	0.014	0.36	0.79	0.955	201	979349	1.736	2.168
12	0.03	0.003	0.38	0.83	0.859	252	376019	1.698	2.093
12	0.07	0.006	1.63	3.56	3.627	269	140088	1.960	2.390
12	0.12	0.010	1.52	3.32	3.437	263	210665	1.959	2.322
12	0.17	0.014	1.35	2.95	3.116	247	539280	1.680	2.194
12	0.12	0.010	1.15	2.51	2.629	229	404503	1.764	2.247
12	0.02	0.002	1.01	2.20	2.224	253	560784	1.514	1.911

Table G.7: Experimental constant amplitude axial fatigue data for welded joints [54] and PSM and ENS results.

G.7 Results and Experimental data from [55]

t [mm]	e [mm]	e/t	e_{tot} [mm]	α [°]	e from α [mm]	$\Delta\sigma_{nom}$ [MPa]	N_f [cycles]	K_{PSM} [MPa]	K_{ENS} [MPa]
6	0.136	0.023	0.24	0.628	1	500	38016	1.5385	2.1552
6	0.136	0.023	0.24	0.628	1	500	57593	1.5385	2.1552
6	0.136	0.023	0.24	0.628	1	500	75725	1.5385	2.1552
6	0.136	0.023	0.24	0.628	1	400	141306	1.5385	2.1552
6	0.136	0.023	0.24	0.628	1	400	157878	1.5385	2.1552
6	0.136	0.023	0.24	0.628	1	399	267032	1.5385	2.1552
6	0.136	0.023	0.24	0.628	1	292	598080	1.5385	2.1552
6	0.136	0.023	0.24	0.628	1	500	40987	1.5385	2.1552
6	0.136	0.023	0.24	0.628	1	500	74000	1.5385	2.1552
6	0.136	0.023	0.24	0.628	1	500	105620	1.5385	2.1552
6	0.136	0.023	0.24	0.628	1	500	128174	1.5385	2.1552
6	0.136	0.0227	0.24	0.63	0.764	350	168112	1.5385	2.1552
6	0.136	0.0227	0.24	0.63	0.764	400	203678	1.5385	2.1552
6	0.136	0.0227	0.24	0.63	0.764	400	207136	1.5385	2.1552
6	0.136	0.0227	0.24	0.63	0.764	450	225330	1.5385	2.1552
6	0.136	0.0227	0.24	0.63	0.764	400	262538	1.5385	2.1552
6	0.136	0.0227	0.24	0.63	0.764	350	273018	1.5385	2.1552
6	0.136	0.0227	0.24	0.63	0.764	360	273227	1.5385	2.1552
6	0.136	0.0227	0.24	0.63	0.764	513	61200	1.5385	2.1552
6	0.136	0.0227	0.24	0.63	0.764	432	144580	1.5385	2.1552

Table G.8: Experimental constant amplitude axial fatigue data for welded joints [55] and PSM and ENS results.

G.8 Results and Experimental data from [56]

t [mm]	e [mm]	e/t	e_{tot} [mm]	α [°]	e from α [mm]	$\Delta\sigma_{nom}$ [MPa]	N_f [cycles]	K_{PSM} [MPa]	K_{ENS} [MPa]
8	3	0.375	0	0	3	105	140321	3.486	4.651
8	3	0.375	0	0	3	102	424464	3.486	4.651
8	3	0.375	0	0	3	93	282371	3.486	4.651
8	3	0.375	0	0	3	90	825675	3.486	4.651
8	3	0.375	0	0	3	79	1661524	3.486	4.651
8	3	0.375	0	0	3	79	513275	3.486	4.651
8	3	0.375	0	0	3	74	997801	3.486	4.651
8	3	0.375	0	0	3	70	1780947	3.486	4.651
8	6	0.75	0	0	6	81	87363	4.465	6.418
8	6	0.75	0	0	6	77	178685	4.465	6.418
8	6	0.75	0	0	6	68	178911	4.465	6.418
8	6	0.75	0	0	6	63	298391	4.465	6.418
8	6	0.75	0	0	6	57	319751	4.465	6.418
8	6	0.75	0	0	6	54	919445	4.465	6.418
8	6	0.75	0	0	6	48	1787957	4.465	6.418
8	8	1	0	0	8	76	58738	5.408	7.571
8	8	1	0	0	8	67	53806	5.408	7.571
8	8	1	0	0	8	62	140224	5.408	7.571
8	8	1	0	0	8	50	154168	5.408	7.571
8	8	1	0	0	8	48	354824	5.408	7.571
8	8	1	0	0	8	42	367356	5.408	7.571
8	8	1	0	0	8	45	675948	5.408	7.571
8	3	0.375	0	0	3	186	60837	3.486	4.651
8	3	0.375	0	0	3	154	133974	3.486	4.651
8	3	0.375	0	0	3	138	139252	3.486	4.651
8	3	0.375	0	0	3	132	269111	3.486	4.651
8	3	0.375	0	0	3	107	603725	3.486	4.651
8	6	0.75	0	0	6	98	1682973	4.465	6.418
8	6	0.75	0	0	6	79	1070233	4.465	6.418
8	6	0.75	0	0	6	90	238555	4.465	6.418
8	6	0.75	0	0	6	109	62598	4.465	6.418
8	6	0.75	0	0	6	106	307115	4.465	6.418
8	6	0.75	0	0	6	149	64545	4.465	6.418
8	6	0.75	0	0	6	129	29496	4.465	6.418
8	8	1	0	0	8	128	22032	5.408	7.571
8	8	1	0	0	8	110	50672	5.408	7.571
8	8	1	0	0	8	103	167911	5.408	7.571
8	8	1	0	0	8	84	552900	5.408	7.571
8	8	1	0	0	8	78	165906	5.408	7.571
8	8	1	0	0	8	65	530106	5.408	7.571
8	8	1	0	0	8	121	44973	5.408	7.571

Table G.9: Experimental constant amplitude axial fatigue data for welded joints [56] and PSM and ENS results.

G.9 Results and Experimental data from [57]

t [mm]	e [mm]	e/t	e_{tot} [mm]	α [°]	e from α [mm]	$\Delta\sigma_{nom}$ [MPa]	N_f [cycles]	K_{PSM} [MPa]	K_{ENS} [MPa]
8	1.2	0.15	0	0	1	176.68	385123	1.998	2.69184
8	1.2	0.15	0	0	1	146.11	333625	1.998	2.69184
8	1.2	0.15	0	0	1	135.94	445968	1.998	2.69184
8	1.2	0.15	0	0	1	166.51	459132	1.998	2.69184
8	1.2	0.15	0	0	1	156.21	759754	1.998	2.69184
8	1.2	0.15	0	0	1	107.20	1259943	1.998	2.69184
8	1.2	0.15	0	0	1	98.08	1479637	1.998	2.69184
8	1.2	0.15	0	0	1	98.05	2117314	1.998	2.69184

Table G.10: Experimental constant amplitude axial fatigue data for welded joints [57] and PSM and ENS results.

G.10 Results and Experimental data from [58]

t [mm]	e [mm]	e/t	e_{tot} [mm]	α [°]	e from α [mm]	$\Delta\sigma_{nom}$ [MPa]	N_f [cycles]	K_{PSM} [MPa]	K_{ENS} [MPa]
12	1.2	0.1	0	0	1.20	339.83	18777	2.060	2.569
12	1.2	0.1	0	0	1.20	235.26	68417	2.060	2.569
12	1.2	0.1	0	0	1.20	197.59	120479	2.060	2.569
12	1.2	0.1	0	0	1.20	175.81	163191	2.060	2.569
12	1.2	0.1	0	0	1.20	144.78	287447	2.060	2.569
12	1.2	0.1	0	0	1.20	116.95	560059	2.060	2.569
12	1.2	0.1	0	0	1.20	98.19	928456	2.060	2.569
12	1.2	0.1	0	0	1.20	87.37	1257607	2.060	2.569
12	2.4	0.2	0	0	2.40	348.36	8391	2.524	3.143
12	2.4	0.2	0	0	2.40	243.86	37387	2.524	3.143
12	2.4	0.2	0	0	2.40	202.80	65846	2.524	3.143
12	2.4	0.2	0	0	2.40	180.45	89189	2.524	3.143
12	2.4	0.2	0	0	2.40	151.52	150861	2.524	3.143
12	2.4	0.2	0	0	2.40	120.01	294013	2.524	3.143
12	2.4	0.2	0	0	2.40	100.79	517745	2.524	3.143
12	2.4	0.2	0	0	2.40	82.22	988543	2.524	3.143
12	2.4	0.2	0	0	2.40	70.34	1394716	2.524	3.143
12	3.6	0.3	0	0	3.6	343.48	4149	3.021	3.684
12	3.6	0.3	0	0	3.6	240.79	23537	3.021	3.684
12	3.6	0.3	0	0	3.6	204.19	39807	3.021	3.684
12	3.6	0.3	0	0	3.6	179.93	55022	3.021	3.684
12	3.6	0.3	0	0	3.6	149.61	94973	3.021	3.684
12	3.6	0.3	0	0	3.6	119.66	181382	3.021	3.684
12	3.6	0.3	0	0	3.6	99.50	313082	3.021	3.684
12	3.6	0.3	0	0	3.6	79.59	610086	3.021	3.684
12	3.6	0.3	0	0	3.6	60.03	1289507	3.021	3.684
12	4.8	0.4	0	0	4.8	348.35	1611	3.297	4.213
12	4.8	0.4	0	0	4.8	242.56	15422	3.297	4.213
12	4.8	0.4	0	0	4.8	203.65	25566	3.297	4.213
12	4.8	0.4	0	0	4.8	181.21	34630	3.297	4.213
12	4.8	0.4	0	0	4.8	150.70	60989	3.297	4.213
12	4.8	0.4	0	0	4.8	121.72	116463	3.297	4.213
12	4.8	0.4	0	0	4.8	100.22	201052	3.297	4.213
12	4.8	0.4	0	0	4.8	80.17	391780	3.297	4.213
12	4.8	0.4	0	0	4.8	50.28	1458411	3.297	4.213
12	6	0.5	0	0	6	201.23	18161	3.766	4.774
12	6	0.5	0	0	6	179.06	24599	3.766	4.774
12	6	0.5	0	0	6	150.35	41608	3.766	4.774
12	6	0.5	0	0	6	119.11	84421	3.766	4.774
12	6	0.5	0	0	6	99.04	145719	3.766	4.774
12	6	0.5	0	0	6	79.99	272716	3.766	4.774
12	6	0.5	0	0	6	239.62	10523	3.766	4.774

Table G.11: Experimental constant amplitude axial fatigue data for welded joints [58] and PSM and ENS results.

G.11 Results and Experimental data from [59]

t [mm]	e [mm]	e/t	e_{tot} [mm]	α [°]	e from α [mm]	$\Delta\sigma_{nom}$ [MPa]	N_f [cycles]	K_{PSM} [MPa]	K_{ENS} [MPa]
12	0.25	0.021	0.51	1.11	1.36	199	1037495	1.805	2.258
12	0.29	0.024	0.46	1.00	1.29	181	2041188	1.776	2.262
12	0.32	0.027	0.39	0.85	1.17	224	471601	1.763	2.252
12	0.24	0.020	0.41	0.89	1.13	249	277963	1.739	2.213
12	0.17	0.014	0.36	0.79	0.96	201	979349	1.701	2.152
12	0.14	0.012	0.4	0.87	1.01	269	189524	1.702	2.147
12	0.03	0.003	0.38	0.83	0.86	252	376019	1.693	2.074
12	0.02	0.002	0.43	0.94	0.96	200	1217355	1.706	2.089
12	0.13	0.011	0.38	0.83	0.96	224	516276	1.694	2.134
12	0.17	0.014	0.4	0.87	1.04	226	549004	1.713	2.168
12	0.25	0.021	0.38	0.83	1.08	184	1611693	1.763	2.207
12	0.31	0.008	0.38	0.83	1.14	201	513309	1.314	1.818
12	0.42	0.026	0.42	0.92	1.34	302	63011	1.392	1.951
12	0.3	0.035	0.48	1.05	1.35	190	984909	1.338	1.844
12	0.09	0.025	0.49	1.07	1.16	251	380053	1.222	1.544
12	0.19	0.008	0.2	0.44	0.63	201	849199	1.202	1.602
12	0.19	0.016	0.34	0.74	0.93	201	1138300	1.239	1.650
12	0.07	0.006	1.63	3.56	3.63	269	140088	1.885	2.211
12	0.12	0.010	1.52	3.32	3.44	263	210665	1.915	2.226
12	0.17	0.014	1.35	2.95	3.12	247	539280	1.928	2.216
12	0.12	0.010	1.15	2.51	2.63	229	404503	1.802	2.090
12	0.02	0.002	1.01	2.20	2.22	253	560784	1.639	1.936
12	0.43	0.036	0.42	0.92	1.35	252	354052	2.127	2.195
12	0.39	0.033	0.44	0.96	1.35	264	267320	2.088	2.178
12	0.43	0.036	0.35	0.76	1.19	242	451699	2.102	2.164
12	0.47	0.039	0.37	0.81	1.28	226	1057498	2.146	2.197
12	0.49	0.041	0.38	0.83	1.32	235	487091	2.166	2.214
12	0.51	0.043	0.36	0.79	1.30	218	888604	2.171	2.217
12	0.58	0.048	0.34	0.74	1.32	260	229253	2.223	2.250
12	0.47	0.039	0.34	0.74	1.21	239	502035	2.133	2.185
12	0.49	0.041	0.32	0.70	1.19	218	1546593	2.131	2.188
12	0.46	0.038	0.37	0.81	1.27	230	892600	2.137	2.191

Table G.12: Experimental constant amplitude axial fatigue data for welded joints [59] and PSM and ENS results.

G.12 Results and Experimental data from [60]

t [mm]	e [mm]	e/t	e_{tot} [mm]	α [°]	e from α [mm]	$\Delta\sigma_{nom}$ [MPa]	N_f [cycles]	K_{PSM} [MPa]	K_{ENS} [MPa]
8	0	0	1.15	6.60	6.60	299	94000	2.892	3.817
8	0	0	1.39	7.99	7.99	210	400000	3.119	4.214
8	0	0	0.33	1.88	1.88	378	37000	2.171	2.797
8	0	0	0.18	1.02	1.02	248	244000	1.975	2.581

Table G.13: Experimental constant amplitude axial fatigue data for welded joints [60] and PSM and ENS results.

G.13 Results and Experimental data from [61]

t [mm]	e [mm]	e/t	e_{tot} [mm]	α [°]	e from α [mm]	$\Delta\sigma_{nom}$ [MPa]	N_f [cycles]	K_{PSM} [MPa]	K_{ENS} [MPa]
20	10	0.5	0	0	10	288.56	80854	3.607	6.017
20	10	0.5	0	0	10	184.34	418307	3.607	6.017
20	15	0.75	0	0	15	698.07	3882	4.800	6.525
20	15	0.75	0	0	15	351.00	13677	4.800	6.525
20	15	0.75	0	0	15	321.69	18348	4.800	6.525
20	15	0.75	0	0	15	234.95	43322	4.800	6.525
20	15	0.75	0	0	15	165.92	127196	4.800	6.525
20	20	1.0	0	0	20	159.97	68262	6.040	8.611
20	20	1.0	0	0	20	88.62	195644	6.040	8.611
20	30	1.5	0	0	30	163.86	49755	8.705	12.405
20	30	1.5	0	0	30	93.50	179379	8.705	12.405
20	10	0.5	0	0	10	253.07	55076	3.607	6.017
20	10	0.5	0	0	10	180.29	216858	3.607	6.017
20	15	0.75	0	0	15	444.29	15369	4.800	6.525
20	15	0.75	0	0	15	396.14	19609	4.800	6.525
20	15	0.75	0	0	15	338.04	22527	4.800	6.525
20	15	0.75	0	0	15	263.91	23570	4.800	6.525
20	15	0.75	0	0	15	179.80	90653	4.800	6.525
20	15	0.75	0	0	15	90.99	594386	4.800	6.525
20	20	1.0	0	0	20	358.95	15175	6.040	8.611
20	20	1.0	0	0	20	235.80	24393	6.040	8.611
20	30	1.5	0	0	30	243.24	10081	8.705	12.405
20	30	1.5	0	0	30	243.24	10081	8.705	12.405

Table G.14: Experimental constant amplitude axial fatigue data for welded joints [61] and PSM and ENS results.

G.14 Results and Experimental data from [62]

t [mm]	e [mm]	e/t	e_{tot} [mm]	α [°]	e from α [mm]	$\Delta\sigma_{nom}$ [MPa]	N_f [cycles]	K_{PSM} [MPa]	K_{ENS} [MPa]
12.5	0	0	0.57	1.78	1.78	227.5	181000	2.540	2.585
12.5	0	0	0.31	0.96	0.96	227.5	195000	2.040	2.458
12.5	0	0	0.63	1.96	1.96	227.5	226000	2.170	2.634
12.5	0	0	0.77	2.38	2.38	227.5	297000	2.206	2.693
12.5	0	0	0.54	1.67	1.67	227.5	299000	2.113	2.553
12.5	0	0	0.71	2.20	2.20	165.5	887000	2.176	2.654
12.5	0	0	0.69	2.13	2.13	131	9680000	2.191	2.662
12.5	0	0	0.77	2.38	2.38	144.8	9130000	2.171	2.653
12.5	0	0	0.25	0.78	0.78	165.5	1960000	2.007	2.425
12.5	0	0	0.26	0.82	0.82	165.5	874000	2.044	2.448
12.5	0	0	0.25	0.78	0.78	165.5	1160000	2.224	2.439
15.9	0	0	0.92	2.85	2.85	227.5	212300	2.021	2.615
15.9	0	0	0.08	0.25	0.25	227.5	153000	2.069	2.468
15.9	0	0	0.09	0.28	0.28	227.5	213000	2.017	2.521
15.9	0	0	0.26	0.82	0.82	227.5	190000	2.097	2.556
15.9	0	0	0.33	1.03	1.03	227.5	182000	2.121	2.591
15.9	0	0	0.21	0.64	0.64	165.5	258000	2.320	2.475
15.9	0	0	0.46	1.42	1.42	165.5	5868000	2.228	2.656
15.9	0	0	0.09	0.28	0.28	165.5	438000	2.008	2.463

Table G.15: Experimental constant amplitude axial fatigue data for welded joints [62] and PSM and ENS results.

G.15 Results and Experimental data from [63]

t [mm]	e [mm]	e/t	e_{tot} [mm]	α [°]	e from α [mm]	$\Delta\sigma_{nom}$ [MPa]	N_f [cycles]	K_{PSM} [MPa]	K_{ENS} [MPa]
12.5	3.2	0.256	0	0	3.2	240	191100	2.630	3.645
12.5	3.2	0.256	0	0	3.2	220	102560	2.630	3.645
12.5	3.2	0.256	0	0	3.2	200	150700	2.630	3.645
12.5	3.2	0.256	0	0	3.2	160	273380	2.630	3.645
12.5	3.2	0.256	0	0	3.2	120	758960	2.630	3.645
12.5	6.3	0.504	0	0	6.3	200	51000	3.709	5.161
12.5	6.3	0.504	0	0	6.3	180	62650	3.709	5.161
12.5	6.3	0.504	0	0	6.3	160	60200	3.709	5.161
12.5	6.3	0.504	0	0	6.3	130	89900	3.709	5.161
12.5	6.3	0.504	0	0	6.3	100	172300	3.709	5.161
12.5	6.3	0.504	0	0	6.3	90	1028400	3.709	5.161
12.5	6.3	0.504	0	0	6.3	80	2045200	3.709	5.161
12.5	9.5	0.76	0	0	9.5	180	17100	5.090	7.350
12.5	9.5	0.76	0	0	9.5	160	38200	5.090	7.350
12.5	9.5	0.76	0	0	9.5	120	74800	5.090	7.350
12.5	9.5	0.76	0	0	9.5	70	990100	5.090	7.350
12.5	9.5	0.76	0	0	9.5	60	906500	5.090	7.350
12.5	12.5	1	0	0	12.5	120	18600	6.554	10.312
12.5	12.5	1	0	0	12.5	100	44300	6.554	10.312
12.5	12.5	1	0	0	12.5	70	137400	6.554	10.312
12.5	12.5	1	0	0	12.5	55	528300	6.554	10.312
12.5	12.5	1	0	0	12.5	45	1319000	6.554	10.312

Table G.16: Experimental constant amplitude axial fatigue data for welded joints [63] and PSM and ENS results.

G.16 Results and Experimental data from [64]

t [mm]	e [mm]	e/t	e_{tot} [mm]	α [°]	e from α [mm]	$\Delta\sigma_{nom}$ [MPa]	N_f [cycles]	K_{PSM} [MPa]	K_{ENS} [MPa]
12	0	0	0.29	1.13	1.13	150	351000	2.304	2.975
12	0	0	0.29	1.13	1.13	130	731000	2.304	2.975
12	0	0	0.29	1.13	1.13	130	687000	2.304	2.975
12	0	0	0.29	1.13	1.13	220	128000	2.304	2.975
12	0	0	0.29	1.13	1.13	130	748000	2.304	2.975
12	0	0	0.29	1.13	1.13	250	77000	2.304	2.975
12	0	0	0.29	1.13	1.13	150	421000	2.304	2.975
12	0	0	0.29	1.13	1.13	150	322000	2.304	2.975
12	0	0	0.29	1.13	1.13	130	454000	2.304	2.975
12	0	0	0.29	1.13	1.13	250	70000	2.304	2.975
12	0	0	0.29	1.13	1.13	150	369000	2.304	2.975
12	0	0	0.29	1.13	1.13	130	493000	2.304	2.975
12	0	0	0.29	1.13	1.13	150	806000	2.304	2.975
12	0	0	0.29	1.13	1.13	150	471000	2.304	2.975
12	0	0	0.29	1.13	1.13	250	82000	2.304	2.975
3	0	0	0.95	1.50	1.50	300	123000	2.256	3.008
3	0	0	0.95	1.50	1.50	150	450000	2.256	3.008
3	0	0	0.95	1.50	1.50	100	8000000	2.256	3.008
3	0	0	0.95	1.50	1.50	250	87000	2.256	3.008
3	0	0	0.95	1.50	1.50	130	1456000	2.256	3.008
3	0	0	0.95	1.50	1.50	130	1810000	2.256	3.008
3	0	0	0.95	1.50	1.50	130	3131000	2.256	3.008
3	0	0	0.95	1.50	1.50	200	242000	2.256	3.008
3	0	0	0.95	1.50	1.50	150	518000	2.256	3.008
3	0	0	0.95	1.50	1.50	150	533000	2.256	3.008
3	0	0	0.95	1.50	1.50	150	1856000	2.256	3.008
3	0	0	0.95	1.50	1.50	200	352000	2.256	3.008
3	0	0	0.95	1.50	1.50	200	433000	2.256	3.008
3	0	0	0.95	1.50	1.50	250	154000	2.256	3.008

Table G.17: Experimental constant amplitude axial fatigue data for welded joints [64] and PSM and ENS results.

t [mm]	e [mm]	e/t	e_{tot} [mm]	α [°]	e from α [mm]	$\Delta\sigma_{nom}$ [MPa]	N_f [cycles]	K_{PSM} [MPa]	K_{ENS} [MPa]
3	0	0	0.17	0.26	0.26	200	909000	1.456	1.983
3	0	0	0.17	0.26	0.26	200	3800000	1.456	1.983
3	0	0	0.17	0.26	0.26	300	215000	1.456	1.983
3	0	0	0.17	0.26	0.26	230	748000	1.456	1.983
3	0	0	0.17	0.26	0.26	230	405000	1.456	1.983
3	0	0	0.17	0.26	0.26	230	556000	1.456	1.983
3	0	0	0.17	0.26	0.26	350	98000	1.456	1.983
3	0	0	0.17	0.26	0.26	350	83000	1.456	1.983
3	0	0	0.17	0.26	0.26	350	84000	1.456	1.983
3	0	0	0.17	0.26	0.26	250	212000	1.456	1.983
3	0	0	0.17	0.26	0.26	250	244000	1.456	1.983
3	0	0	0.17	0.26	0.26	250	359000	1.456	1.983
3	0	0	0.21	0.33	0.33	200	382000	1.492	2.028
3	0	0	0.21	0.33	0.33	150	10000000	1.492	2.028
3	0	0	0.21	0.33	0.33	300	134000	1.492	2.028
3	0	0	0.21	0.33	0.33	180	817000	1.492	2.028
3	0	0	0.21	0.33	0.33	180	1091000	1.492	2.028
3	0	0	0.21	0.33	0.33	180	484000	1.492	2.028
3	0	0	0.21	0.33	0.33	350	48000	1.492	2.028
3	0	0	0.21	0.33	0.33	200	237000	1.492	2.028
3	0	0	0.21	0.33	0.33	300	88000	1.492	2.028
3	0	0	0.21	0.33	0.33	350	49000	1.492	2.028
3	0	0	0.21	0.33	0.33	150	9500000	1.492	2.028
3	0	0	0.21	0.33	0.33	350	65000	1.492	2.028
3	0	0	0.21	0.33	0.33	500	18000	1.492	2.028
3	0	0	0.21	0.33	0.33	200	292000	1.492	2.028
3	0	0	0.21	0.33	0.33	300	107000	1.492	2.028
3	0	0	0.21	0.33	0.33	300	92000	1.492	2.028
3	0	0	0.21	0.33	0.33	200	366000	1.492	2.028
3	0	0	0.21	0.33	0.33	300	85000	1.492	2.028
3	0	0	0.21	0.33	0.33	200	321000	1.492	2.028
3	0	0	0.21	0.33	0.33	180	793000	1.492	2.028
3	0	0	0.21	0.33	0.33	180	419000	1.492	2.028
3	0	0	0.21	0.33	0.33	350	56000	1.492	2.028
3	0	0	0.21	0.33	0.33	350	68000	1.492	2.028
3	0	0	0.21	0.33	0.33	160	10000000	1.492	2.028
3	0	0	0.21	0.33	0.33	400	39000	1.492	2.028
3	0	0	0.21	0.33	0.33	170	662000	1.492	2.028
3	0	0	0.21	0.33	0.33	160	9500000	1.492	2.028
3	0	0	0.21	0.33	0.33	400	46000	1.492	2.028
3	0	0	0.21	0.33	0.33	170	10000000	1.492	2.028
3	0	0	0.21	0.33	0.33	400	47000	1.492	2.028
3	0	0	0.21	0.33	0.33	170	452000	1.492	2.028

Table G.18: Experimental constant amplitude axial fatigue data for welded joints [64] and PSM and ENS results.

Appendix H

Experimental and elaboration results

H.1 Cruciform joint

H.1.1 Experimental data

Test 1

F [kN]	F_{real} [kN]	ϵ_{CH1} [μeps]	ϵ_{CH2} [μeps]	ϵ_{CH3} [μeps]	ϵ_{CH4} [μeps]
0 (out of machine)	0	4.1	1.4	5.0	0.3
0	0	25.9	-24.9	14.2	-12.9
5	5	129.3	24.5	59.8	94.1
10	10	232.4	74.9	105.6	201.8
15	15	334.8	125.4	152.2	308.4
20	20	437.1	176.5	199.6	414.7
25	25	539.8	227.7	247.4	520.1
30	29.4	630.8	273.5	290.5	613.4
35	33.5	715.0	315.3	330.4	698.9
40	37.5	796.0	356.6	370.3	782.4
45	41.2	855.9	397.0	410.9	857.6
50	44.9	935.1	435.3	447.7	936.4
45	41	857.1	395.2	415.3	854.8
40	37	776.3	353.9	376.4	772.9
35	33	694.7	312.0	337.4	687.9
30	28.99	612.0	270.3	298.3	602.6
25	24.9	528.4	227.8	259.4	516.4
20	20	428.1	178.3	213.1	413.6
15	15	325.3	127.6	166.1	307.3
10	10	222.6	77.0	116.9	200.0
5	5	118.6	27.3	71.0	92.8
0	0	14.6	-21.9	26.9	-14.6
0 (out of machine)	0	6.6	3.1	10.4	5.2

Table H.1: Experimental results of cruciform joint, Test 1.

Test 2

F [kN]	F_{real} [kN]	ϵ_{CH1} [μeps]	ϵ_{CH2} [μeps]	ϵ_{CH3} [μeps]	ϵ_{CH4} [μeps]
0 (out of machine)	0	0	0	0	0
0	0	21.9	-24.6	16.4	-14.5
5	5	125.7	24.3	62.6	92.3
10	10	228.7	74.4	108.5	199.8
15	15	331.8	124.8	155.9	306.7
20	20	434.1	175.9	202.3	413.0
25	24.8	531.4	225.7	248.9	515.6
30	28.9	610.8	267.5	288.2	600.3
35	32.8	687.0	308.8	328.1	683.1
40	36.7	764.0	349.6	367.0	764.5
45	40.6	841.7	390.1	405.5	845.7
50	44.4	918.5	430.2	443.4	924.7
45	40.5	841.1	390.3	406.9	844.8
40	36.6	761.4	349.3	367.9	762.8
35	32.6	681.0	308.4	329.3	679.7
30	28.7	599.8	266.7	290.9	596.3
25	24.6	517.1	225.4	252.3	511.1
20	20	421.5	177.6	208.1	412.7
15	15	318.4	127.1	161.3	306.2
10	10	215.2	76.8	114.8	200.0
5	5	110.8	26.9	69.0	92.8
0	0	6.9	-22.4	23.4	-14.4
0(out of machine)	0	2.5	1.2	3.9	3.9

Table H.2: Experimental results of cruciform joint, Test 2.

Test 3

F [kN]	F_{real} [kN]	ϵ_{CH1} [μeps]	ϵ_{CH2} [μeps]	ϵ_{CH3} [μeps]	ϵ_{CH4} [μeps]
0 (out of machine)	0	0	0	0	0
0	0	30.4	-28.1	16.1	-13.8
5	5	133.3	21.7	62.5	93.8
10	10	236.2	72.2	108.8	201.6
15	15	338.6	122.6	155.3	308.4
20	20	441.5	173.1	201.0	415.6
25	25	543.1	224.6	250.6	521.5
30	29.5	636.3	272.1	295.3	618.4
35	33.7	718.6	314.7	335.5	704.1
40	37.5	779.3	357.3	379.7	782.6
45	41.4	860.2	398.1	418.1	864.7
50	45.2	941.3	438.4	456.3	944.7
45	41.3	861.4	397.4	417.6	862.9
40	37.3	779.9	356.0	379.2	779.3
35	33.3	697.5	313.7	339.6	694.4
30	29.2	614.2	271.6	300.2	609.3
25	25	528.2	228.3	259.8	520.4
20	20	425.3	177.2	212.1	414.9
15	15	322.2	126.4	164.5	308.7
10	10	218.6	76.6	118.1	202.2
5	5	114.2	27.5	71.8	94.3
0	0	10.7	-21.6	26.6	-12.6
0 (out of machine)	0	2.8	2.2	8.3	5.9

Table H.3: Experimental results of cruciform joint, Test 3.

H.1.2 Elaboration results

Test 1

F_{real} [kN]	$\epsilon_{membr,inf}$ [μeps]	$\epsilon_{membr,sup}$ [μeps]	$\epsilon_{bend,inf}$ [μeps]	$\epsilon_{bend,sup}$ [μeps]	$\sigma_{membr,inf}$ [MPa]	$\sigma_{membr,sup}$ [MPa]	$\sigma_{bend,inf}$ [MPa]	$\sigma_{bend,sup}$ [MPa]	σ_{th} [MPa]	$\Delta\%_{inf}$	$\Delta\%_{sup}$
0 (o.m.)	2.67	2.71	-2.37	1.34	0.449	0.455	-0.398	0.226	0	/	/
0	0.65	0.53	-13.56	25.39	0.109	0.089	-2.278	4.265	0	/	/
5	76.97	76.88	17.15	52.37	12.931	12.916	2.881	8.798	12.50	3.45	3.33
10	153.71	153.62	48.07	78.73	25.824	25.808	8.075	13.227	25.00	3.30	3.23
15	230.32	230.12	78.11	104.69	38.693	38.660	13.122	17.587	37.50	3.18	3.09
20	307.14	306.83	107.54	130.32	51.600	51.547	18.066	21.893	50.00	3.20	3.09
25	383.78	383.76	136.36	156.04	64.474	64.472	22.908	26.215	62.50	3.16	3.16
29.4	451.95	452.12	161.49	178.66	75.928	75.956	27.130	30.014	73.50	3.30	3.34
33.5	514.61	515.13	184.25	199.86	86.455	86.542	30.954	33.577	83.75	3.23	3.33
37.5	576.35	576.31	206.06	219.71	96.826	96.820	34.619	36.910	93.75	3.28	3.27
41.2	634.22	626.43	223.34	229.46	106.548	105.240	37.521	38.549	103.00	3.45	2.17
44.9	692.08	685.21	244.36	249.87	116.270	115.115	41.053	41.978	112.25	3.58	2.55
41	635.04	626.16	219.79	230.93	106.686	105.195	36.924	38.796	102.50	4.08	2.63
37	574.66	565.15	198.25	211.20	96.542	94.944	33.305	35.482	92.50	4.37	2.64
33	512.65	503.39	175.29	191.36	86.124	84.569	29.449	32.148	82.50	4.39	2.51
28.99	450.48	441.15	152.15	170.84	75.681	74.113	25.561	28.701	72.48	4.42	2.26
24.9	387.89	378.14	128.53	150.30	65.166	63.528	21.594	25.250	62.25	4.68	2.05
20	313.36	303.22	100.22	124.92	52.645	50.940	16.837	20.987	50.00	5.29	1.88
15	236.69	226.44	70.62	98.83	39.764	38.042	11.864	16.604	37.50	6.04	1.45
10	158.48	149.80	41.54	72.83	26.625	25.167	6.979	12.235	25.00	6.50	0.67
5	1081.89	72.96	10.89	45.65	13.758	12.257	1.829	7.669	12.50	10.06	-1.95
0	6.16	-3.66	-20.72	18.26	1.035	-0.614	-3.480	3.068	0	/	/
0 (o.m.)	7.82	4.86	-2.62	1.73	1.314	554.074	-0.439	0.291	0	/	/

Table H.4: Elaborated results of cruciform joint, Test 1. The abbreviation o.m. means out of machine. In the case of the cruciform joint, the Young Modulus is equal to 168000 MPa, value of ADI 1050.

Where:

$$\sigma_{th} = F_{real} \cdot A \quad (H.1)$$

$$\Delta\%_{inf/sup} = \frac{\sigma_{membr,inf/sup} - \sigma_{th}}{\sigma_{th}} \cdot 100 \quad (H.2)$$

Test 2

F_{real} [kN]	$\epsilon_{membr,inf}$ [μeps]	$\epsilon_{membr,sup}$ [μeps]	$\epsilon_{bend,inf}$ [μeps]	$\epsilon_{bend,sup}$ [μeps]	$\sigma_{membr,inf}$ [MPa]	$\sigma_{membr,sup}$ [MPa]	$\sigma_{bend,inf}$ [MPa]	$\sigma_{bend,sup}$ [MPa]	σ_{th} [MPa]	$\Delta\%_{inf}$	$\Delta\%_{sup}$
0 (o.m.)	0	0	0	0	0	0	0	0	0	/	/
0	0.97	-1.35	-15.44	23.22	0.163	-0.227	-2.593	3.902	0	/	/
5	77.45	74.99	14.85	50.69	13.011	12.598	2.494	8.515	12.50	4.09	0.78
10	154.17	151.57	45.65	77.17	25.900	25.464	7.669	12.964	25.00	3.60	1.86
15	231.34	228.33	75.40	103.49	38.865	38.359	12.667	17.387	37.50	3.64	2.29
20	307.66	305.00	105.37	129.11	51.687	51.240	17.702	21.691	50.00	3.37	2.48
24.8	382.25	378.54	133.35	152.88	64.218	63.595	22.402	25.683	62.00	3.58	2.57
28.9	444.29	439.13	156.05	171.67	74.641	73.774	26.217	28.841	72.25	3.31	2.11
32.8	505.61	497.93	177.49	189.09	84.942	83.652	29.819	31.767	82.00	3.59	2.01
36.7	565.70	556.80	198.75	207.16	95.038	93.543	33.390	34.803	91.75	3.58	1.95
40.6	625.63	615.87	220.10	225.78	105.106	103.467	36.977	37.931	101.50	3.55	1.94
44.4	684.06	674.32	240.63	244.14	114.923	113.286	40.425	41.016	111.00	3.53	2.06
40.5	625.89	615.71	218.94	225.39	105.149	103.440	36.782	37.865	101.25	3.85	2.16
36.6	565.37	555.33	197.44	206.06	94.981	93.296	33.170	34.619	91.50	3.80	1.96
32.6	504.49	494.69	175.19	186.33	84.754	83.107	29.432	31.304	81.50	3.99	1.97
28.7	443.62	433.28	152.72	166.56	74.529	72.791	25.657	27.982	71.75	3.87	1.45
24.6	381.70	371.23	129.38	145.87	64.126	62.367	21.736	24.506	61.50	4.27	1.41
20	310.39	299.56	102.27	121.99	52.146	50.326	17.181	20.493	50.00	4.29	0.65
15	233.75	222.78	72.47	95.64	39.271	37.427	12.175	16.067	37.50	4.72	-0.19
10	157.43	146.02	42.59	69.19	26.448	24.531	7.156	11.623	25.00	5.79	-1.88
5	80.90	68.86	11.93	41.97	13.590	11.569	2.004	7.051	12.50	8.72	-7.45
0	4.46	-7.76	-18.90	14.64	0.748	-1.304	-3.175	2.459	0	/	/
0 (o.m.)	3.91	1.81	-0.02	0.65	0.657	0.303	-0.004	0.109	0	/	/

Table H.5: Elaborated results of cruciform joint, Test 2. The abbreviation o.m. means out of machine. In the case of the cruciform joint, the Young Modulus is equal to 168000 MPa, value of ADI 1050.

Where:

$$\sigma_{th} = F_{real} \cdot A \quad (H.3)$$

$$\Delta\%_{inf/sup} = \frac{\sigma_{membr,inf/sup} - \sigma_{th}}{\sigma_{th}} \cdot 100 \quad (H.4)$$

Test 3

F_{real} [kN]	$\epsilon_{membr,inf}$ [μeps]	$\epsilon_{membr,sup}$ [μeps]	$\epsilon_{bend,inf}$ [μeps]	$\epsilon_{bend,sup}$ [μeps]	$\sigma_{membr,inf}$ [MPa]	$\sigma_{membr,sup}$ [MPa]	$\sigma_{bend,inf}$ [MPa]	$\sigma_{bend,sup}$ [MPa]	σ_{th} [MPa]	$\Delta\%_{inf}$	$\Delta\%_{sup}$
0(o.m.)	0	0	0	0	0	0	0	0	0	/	/
0	1.13	1.17	-14.95	29.26	0.191	0.196	-2.512	4.916	0	/	/
5	78.14	77.52	15.61	55.81	13.128	13.023	2.623	9.376	12.50	5.02	4.18
10	155.21	154.22	46.44	82.02	26.075	25.909	7.801	13.779	25.00	4.30	3.64
15	231.87	230.61	76.58	108.00	38.954	38.742	12.865	18.143	37.50	3.88	3.31
20	308.32	307.28	107.28	134.19	51.797	51.623	18.023	22.544	50.00	3.59	3.25
25	386.04	383.86	135.43	159.28	64.855	64.488	22.752	26.759	62.50	3.77	3.18
29.5	456.84	454.22	161.54	182.11	76.749	76.309	27.138	30.594	73.75	4.07	3.47
33.7	519.80	516.68	184.27	201.94	87.326	86.803	30.958	33.926	84.25	3.65	3.03
37.5	581.15	568.31	201.49	211.02	97.633	95.475	33.851	35.452	93.75	4.14	1.84
41.4	641.39	629.13	223.29	231.07	107.753	105.693	37.513	38.820	103.50	4.11	2.12
45.2	700.49	689.88	244.24	251.45	117.683	115.901	41.032	42.243	113.00	4.14	2.57
41.3	640.22	629.37	222.63	232.01	107.557	105.733	37.402	38.977	103.25	4.17	2.41
37.3	579.26	567.91	200.02	211.95	97.316	95.409	33.604	35.608	93.25	4.36	2.32
33.3	517.01	505.56	177.37	191.91	86.857	84.935	29.797	32.241	83.25	4.33	2.02
29.2	454.77	442.91	154.56	171.33	76.401	74.409	25.966	28.784	73.00	4.66	1.93
25	390.06	378.26	130.31	149.95	65.530	63.547	21.891	25.192	62.50	4.85	1.68
20	313.50	301.24	101.42	124.08	52.669	50.608	17.039	20.845	50.00	5.34	1.22
15	236.61	224.29	72.07	97.88	39.751	37.680	12.107	16.444	37.50	6.00	0.48
10	160.15	147.60	42.00	70.98	26.905	24.797	7.057	11.924	25.00	7.62	-0.81
5	83.08	70.86	11.25	43.32	13.958	11.905	1.890	7.278	12.50	11.66	-4.76
0	7.00	-5.46	-19.61	16.18	1.176	-0.918	-3.295	2.718	0	/	/
0 (o.m.)	7.14	2.48	-1.19	0.28	1.199	0.416	-0.200	0.047	0	/	/

Table H.6: Elaborated results of cruciform joint, Test 3. The abbreviation o.m. means out of machine. In the case of the cruciform joint, the Young Modulus is equal to 168000 MPa, value of ADI 1050.

Where:

$$\sigma_{th} = F_{real} \cdot A \quad (H.5)$$

$$\Delta\%_{inf/sup} = \frac{\sigma_{membr,inf/sup} - \sigma_{th}}{\sigma_{th}} \cdot 100 \quad (H.6)$$

H.2 T-joint

H.2.1 Experimental data

Test 1

F [kN]	F_{real} [kN]	ϵ_{CH1} [μeps]	ϵ_{CH2} [μeps]	ϵ_{CH3} [μeps]	ϵ_{CH4} [μeps]
0 (out of machine)	0	0	0	0	0
0	0	14.1	-14.7	-36.0	37.4
5	5	73.2	44.1	20.5	97.3
10	10	133.1	102.1	77.6	158.6
15	15	192.4	160.0	134.9	218.6
20	20	252.7	218.9	193.6	280.1
25	24.4	306.8	270.6	245.5	334.5
30	28.3	354.0	318.6	292.1	382.8
35	32.2	401.7	364.4	338.5	431.1
40	36	449.3	410.5	384.7	479.3
45	39.7	496.9	455.1	430.7	526.9
50	43.6	544.5	501.5	476.8	575.3
45	39.7	499.4	457.5	432.9	530.9
40	36	454.4	413.8	389.1	484.9
35	32.1	408.1	369.4	344.0	438.3
30	28.2	361.6	324.0	298.9	391.6
25	24.3	315.5	278.2	252.7	344.2
20	20	263.1	227.2	201.8	291.4
15	15	201.7	168.3	141.9	230.3
10	10	140.5	109.7	82.0	168.6
5	5	78.3	50.5	21.9	106.9
0	0	16.1	-8.7	-38.2	44.8
0 (out of machine)	0	2.8	3.1	2.1	0.4

Table H.7: Experimental results of T-joint, Test 1.

Test 2

F [kN]	F_{real} [kN]	ϵ_{CH1} [μeps]	ϵ_{CH2} [μeps]	ϵ_{CH3} [μeps]	ϵ_{CH4} [μeps]
0 (out of machine)	0	0	0	0	0
0	0	13.4	-13.8	-36.0	36.5
5	5	74.6	44.2	21.0	96.0
10	10	134.2	102.1	77.9	157.0
15	15	194.2	160.7	136.0	218.2
20	20	254.7	219.3	193.9	279.2
25	24.3	307.8	270.1	245.5	332.8
30	28.2	355.9	316.4	292.1	381.3
35	32.1	403.4	362.1	338.4	429.4
40	35.9	450.7	407.8	384.5	477.0
45	39.7	497.3	452.5	429.6	523.7
50	43.5	544.5	498.4	475.6	572.1
45	39.7	499.3	454.2	431.7	526.0
40	35.9	454.7	410.6	387.8	480.9
35	32.1	408.5	365.4	343.1	434.8
30	28.2	362.0	320.6	297.8	388.2
25	24.6	314.3	274.7	251.6	340.8
20	20	262.7	224.4	200.8	288.6
15	15	201.6	165.7	141.4	227.8
10	10	140.2	107.1	81.1	166.2
5	5	78.2	48.0	21.1	104.5
0	0	16.3	-11.2	-39.0	42.5
0 (out of machine)	0	2.8	0.8	1.0	-0.6

Table H.8: Experimental results of T-joint, Test 2.

Test 3

F [kN]	F_{real} [kN]	ϵ_{CH1} [μeps]	ϵ_{CH2} [μeps]	ϵ_{CH3} [μeps]	ϵ_{CH4} [μeps]
0 (out of machine)	0	0	0	0	0
0	0	13.2	-15.1	-36.0	-36.4
5	5	72.3	42.9	20.7	96.9
10	10	132.4	101.1	77.8	157.8
15	15	192.5	159.1	135.8	218.8
20	20	252.7	217.1	194.3	280.1
25	24.3	305.0	267.7	245.2	333.2
30	28.2	353.0	313.7	291.4	381.4
35	32	400.3	359.7	337.8	429.2
40	35.9	448.3	405.2	384.0	477.1
45	39.6	494.4	449.5	429.0	523.4
50	43.4	542.0	495.5	475.0	571.4
45	39.6	496.4	451.4	431.1	525.9
40	35.9	451.9	407.8	387.5	481.0
35	32	405.2	363.0	342.0	434.3
30	28.2	358.9	317.7	297.5	388.1
25	24.2	312.0	272.1	251.3	340.6
20	20	260.1	222.1	200.4	288.8
15	15	198.7	163.5	140.9	227.8
10	10	137.1	104.6	81.1	166.7
5	5	75.2	45.5	20.8	104.7
0	0	13.5	-12.5	-39.1	43.1
0 (out of machine)	0	0.2	-1.3	0.3	0

Table H.9: Experimental results of T-joint, Test 3.

H.2.2 Elaboration results

Test 1

F_{real} [kN]	$\epsilon_{membr,inf}$ [μeps]	$\epsilon_{membr,sup}$ [μeps]	$\epsilon_{bend,inf}$ [μeps]	$\epsilon_{bend,sup}$ [μeps]	$\sigma_{membr,inf}$ [MPa]	$\sigma_{membr,sup}$ [MPa]	$\sigma_{bend,inf}$ [MPa]	$\sigma_{bend,sup}$ [MPa]	σ_{th} [MPa]	$\Delta\%_{inf}$	$\Delta\%_{sup}$
0 (o.m.)	0	0	0	0	0	0	0	0	0	0	0
0	0.71	-25.34	13.37	10.65	0.145	-5.220	2.753	2.193	35.18	/	/
5	58.89	58.67	38.41	14.58	12.131	12.085	7.912	3.003	12.50	-2.96	-3.32
10	118.06	117.63	40.49	15.51	24.321	24.233	8.341	3.194	25.00	-2.72	-3.07
15	176.76	176.21	41.82	16.20	36.413	36.299	8.615	3.337	37.50	-2.90	-3.20
20	236.88	235.83	43.27	16.92	48.797	48.580	8.913	3.486	50.00	-2.41	-2.84
24.4	290.00	288.73	44.50	18.12	59.740	59.478	9.168	3.733	61.00	-2.07	-2.49
28.3	337.48	336.33	45.35	17.70	69.521	69.285	9.342	3.647	70.75	-1.74	-2.07
32.2	384.81	383.05	46.34	18.69	79.270	78.908	9.547	3.850	80.50	-1.53	-1.98
36	431.98	429.89	47.28	19.38	88.988	88.557	9.740	3.993	90.00	-1.12	-1.60
39.7	478.78	475.99	48.11	20.86	98.628	98.053	9.911	4.298	99.25	-0.63	-1.21
43.6	526.05	522.99	49.26	21.51	108.365	107.736	10.147	4.431	109.00	-0.58	-1.16
39.7	481.89	478.43	48.96	20.94	99.270	98.556	10.086	4.314	99.25	0.02	-0.70
36	437.03	434.12	47.88	20.31	90.028	89.429	9.864	4.183	90.00	0.03	-0.63
32.1	391.19	388.74	47.15	19.38	80.586	80.080	9.714	3.993	80.25	0.42	-0.21
28.2	345.27	342.81	46.36	18.79	71.125	70.619	9.549	3.871	70.50	0.89	0.17
24.3	298.46	296.88	45.77	18.65	61.483	61.156	9.428	3.843	60.75	1.21	0.67
20	246.57	245.14	44.79	17.95	50.794	50.499	9.227	3.697	50.00	1.59	1.00
15	186.07	184.99	44.20	16.70	38.330	38.108	9.106	3.440	37.50	2.21	1.62
10	125.31	125.10	43.27	15.40	25.813	25.770	8.913	3.173	25.00	3.25	3.08
5	64.39	64.38	42.50	13.93	13.265	13.263	8.755	2.870	12.50	6.12	6.10
0	3.29	3.75	41.52	12.40	0.677	0.772	8.553	2.555	0	/	/
0 (o.m.)	1.24	2.96	-0.85	-0.19	0.255	0.610	-0.174	-0.038	0	/	/

Table H.10: Elaborated results of T-joint, Test 1. The abbreviation o.m. means out of machine. In the case of the cruciform joint, the Young Modulus is equal to 206000 MPa, value of S355J2.

Where:

$$\sigma_{th} = F_{real} \cdot A \quad (H.7)$$

$$\Delta\%_{inf/sup} = \frac{\sigma_{membr,inf/sup} - \sigma_{th}}{\sigma_{th}} \cdot 100 \quad (H.8)$$

Test 2

F_{real} [kN]	$\epsilon_{membr,inf}$ [μeps]	$\epsilon_{membr,sup}$ [μeps]	$\epsilon_{bend,inf}$ [μeps]	$\epsilon_{bend,sup}$ [μeps]	$\sigma_{membr,inf}$ [MPa]	$\sigma_{membr,sup}$ [MPa]	$\sigma_{bend,inf}$ [MPa]	$\sigma_{bend,sup}$ [MPa]	σ_{th} [MPa]	$\Delta\%_{inf}$	$\Delta\%_{sup}$
0 (o.m.)	0	0	0	0	0	0	0	0	0	/	/
0	0.22	-0.25	36.23	13.60	0.05	-0.051	7.463	2.801	0	/	/
5	58.52	59.41	37.53	15.18	12.05	12.238	7.730	3.127	12.50	-3.57	-2.10
10	117.46	118.14	39.56	16.01	24.20	24.338	8.150	3.299	25.00	-3.21	-2.65
15	177.10	177.44	41.11	16.76	36.48	36.552	8.469	3.452	37.50	-2.71	-2.53
20	236.58	236.98	42.64	17.70	48.73	48.818	8.784	3.647	50.00	-2.53	-2.36
24.3	289.16	288.96	43.66	18.84	59.57	59.526	8.994	3.881	60.75	-1.95	-2.02
28.2	336.70	336.16	44.64	19.78	69.36	69.249	9.196	4.074	70.50	-1.62	-1.44
32.1	383.88	382.76	45.51	20.67	79.08	78.848	9.375	4.257	80.00	-1.15	-1.48
35.9	430.77	429.22	46.25	21.47	88.74	88.418	9.528	4.422	89.75	-1.13	-1.48
39.7	476.65	474.92	47.10	22.41	98.19	97.834	9.702	4.617	99.00	-0.82	-1.18
43.5	523.87	521.49	48.26	23.06	107.92	107.426	9.942	4.751	108.50	-0.54	-0.99
39.7	478.86	476.77	47.15	22.53	98.64	98.216	9.714	4.641	99.0	-0.36	-0.79
35.9	434.32	432.62	46.56	22.07	89.47	89.119	9.592	4.546	89.75	-0.31	-0.70
32.1	388.94	386.97	45.87	21.55	80.12	79.716	9.449	4.438	80.00	0.15	-0.36
28.2	343.01	341.29	45.23	20.71	70.66	70.305	9.318	4.267	70.50	0.23	-0.28
24.6	296.19	294.48	44.58	19.78	61.02	60.663	9.184	4.074	60.50	0.85	0.27
20	244.71	243.56	43.88	19.17	50.41	50.174	9.039	3.949	50.00	0.82	0.35
15	184.60	183.61	43.20	17.94	38.03	37.825	8.898	3.695	37.50	1.41	0.87
10	123.64	123.61	42.53	16.55	25.47	25.463	8.760	3.409	25.00	1.88	1.85
5	62.81	63.11	41.70	15.07	12.94	13.001	8.591	3.104	12.50	3.51	4.01
0	1.74	2.56	40.73	13.72	0.36	0.528	8.391	2.826	0	/	/
0 (o.m.)	0.19	1.79	-0.79	0.98	0.04	0.369	-0.162	0.203	0	/	/

Table H.11: Elaborated results of cruciform joint, Test 2. The abbreviation o.m. means out of machine. In the case of the cruciform joint, the Young Modulus is equal to 206000 MPa, value of S355J2.

Where:

$$\sigma_{th} = F_{real} \cdot A \quad (H.9)$$

$$\Delta\%_{inf/sup} = \frac{\sigma_{membr,inf/sup} - \sigma_{th}}{\sigma_{th}} \cdot 100 \quad (H.10)$$

Test 3

F_{real} [kN]	$\epsilon_{membr,inf}$ [μeps]	$\epsilon_{membr,sup}$ [μeps]	$\epsilon_{bend,inf}$ [μeps]	$\epsilon_{bend,sup}$ [μeps]	$\sigma_{membr,inf}$ [MPa]	$\sigma_{membr,sup}$ [MPa]	$\sigma_{bend,inf}$ [MPa]	$\sigma_{bend,sup}$ [MPa]	σ_{th} [MPa]	$\Delta\%_{inf}$	$\Delta\%_{sup}$
0 (o.m.)	0	0	0	0	0	0	0	0	0	0	0
0	-36.22	-0.97	-0.21	14.14	-7.461	-0.201	-0.043	2.913	0	/	/
5	58.81	57.64	38.12	14.71	12.114	11.873	7.852	3.030	12.50	-3.09	-5.01
10	117.82	116.79	39.99	15.66	24.271	24.059	8.238	3.225	25.00	-2.92	-3.77
15	177.33	175.80	41.48	16.70	36.530	36.216	8.545	3.440	37.50	-2.59	-3.43
20	237.24	234.91	42.91	17.81	48.871	48.391	8.839	3.668	50.00	-2.26	-3.22
24.3	289.21	286.36	43.99	18.66	59.578	58.989	9.063	3.845	60.75	-1.93	-2.90
28.2	336.43	333.38	45.01	19.66	69.304	68.677	9.273	4.050	70.50	-1.70	-2.59
32	383.52	379.99	45.71	20.26	79.005	78.278	9.416	4.174	80.00	-1.24	-2.15
35.9	430.58	426.79	46.55	21.56	88.700	87.918	9.590	4.441	89.75	-1.17	-2.04
39.6	476.17	471.91	47.22	22.44	98.092	97.214	9.728	.622	99.00	-0.92	-1.80
43.4	523.19	518.73	48.18	23.22	107.777	106.859	9.926	4.784	108.50	-0.67	-1.51
39.6	478.51	473.92	47.39	22.49	98.573	97.627	9.761	4.634	99.00	-0.43	-1.39
35.9	434.27	429.82	46.77	22.07	89.460	88.542	9.635	4.546	89.75	-0.32	-1.35
32	388.12	384.12	46.16	21.11	79.952	79.129	9.509	4.348	80.00	-0.06	-1.09
28.2	342.79	338.31	45.31	20.61	70.615	69.692	9.335	4.245	70.50	0.16	-1.15
24.2	295.96	292.04	44.65	19.95	60.968	60.160	9.199	4.109	60.50	0.77	-0.56
20	244.57	241.10	44.20	18.95	50.382	49.667	9.106	3.905	50.00	0.76	-0.67
15	184.38	181.07	43.46	17.61	37.982	37.300	8.953	3.628	37.50	1.28	-0.53
10	123.88	120.86	42.77	16.23	25.520	24.898	8.810	3.344	25.00	2.08	-0.41
5	62.74	60.35	41.98	14.85	12.924	12.431	8.648	3.058	12.50	3.39	-0.55
0	2.00	0.50	41.11	12.97	0.412	0.103	8.469	2.672	0	/	/
0 (o.m.)	0.16	-0.51	-0.16	0.74	0.033	-0.105	-0.033	0.153	0	/	/

Table H.12: Elaborated results of cruciform joint, Test 3. The abbreviation o.m. means out of machine. In the case of the cruciform joint, the Young Modulus is equal to 206000 MPa, value of S355J2.

Where:

$$\sigma_{th} = F_{real} \cdot A \quad (H.11)$$

$$\Delta\%_{inf/sup} = \frac{\sigma_{membr,inf/sup} - \sigma_{th}}{\sigma_{th}} \cdot 100 \quad (H.12)$$

Bibliography

- [1] Hobbacher A.F., *IIW Collection Recommendations for Fatigue Design of Welded Joints and Components*, Singapore: Springer Singapore, 2nd edition 2016.
- [2] Fricke W., *IIW Recommendations for the Fatigue Assessment by Notch Stress Analysis for Welded Structures*, Hamburg University of Technology Ship Structural Design and Analysis, July 2010.
- [3] Marquis G., Barsoum Z., *IIW Collection IIW Recommendations for the HFMI Treatment For Improving the Fatigue Strength of Welded Joints*, Singapore: Springer Singapore, 2016.
- [4] Livieri P., Lazzarin P., *Fatigue strength of steel and aluminium welded joints based on generalised stress intensity factors and local strain energy value*, International Journal of Fracture, 133(3):247-276, 2005.
- [5] Meneghetti G., Lazzarin P., *Significance of the elastic peak stress evaluated by FE analyses at the point of singularity of sharp V-notched components*, Fatigue Fract. Eng. Mater. Struct., pages 95-106, 2007.
- [6] Lazzarin P., Tovo R., *A notch stress intensity factor approach to the stress analysis of welds*, Fatigue Fract. Eng. Mater. Struct., pages 1089-1104, 1998.
- [7] Meneghetti G., Campagnolo A., Avalle M., Castagnetti D., Colussi M., Corigliano P., De Agostinis M., Dragoni E., Fontanari V., Frendo F., Goglio L., Marannano G., Marulo G., Moroni F., Pantano A., Rebora A., Scattina A., Spaggiari A., Zuccarello B., *Rapid evaluation of notch stress intensity factors using the peak stress method: Comparison of commercial finite element codes for a range of mesh patterns*, Fatigue and Fracture of Engineering Materials and Structures, 41(5): pages 1044-1063, 2018.
- [8] Campagnolo A., Vormwald M., Shams E., Meneghetti G., *Multiaxial fatigue assessment of tube-tube steel joints with weld ends using the peak stress method*, International Journal of Fracture, 135, 2020.
- [9] Meneghetti G., Guzzella C., *The peak stress method to estimate the mode I notch stress intensity factor in welded joints using three-dimensional finite element models*, Engineerin Fracture Mechanics, 115:154-171, 2014.
- [10] Meneghetti G., Guzzella C., Atzori B., *The peak stress method combined with an 3D finite element models for fatigue assessment of toe and root cracking in steel welded joints subjected to axial or bending*, Fatigue Fract. Eng. Mater. Struct., 37:722-739, 2014.
- [11] Meneghetti G., Campagnolo A., *State-of-the-art review of peak stress method for fatigue strength assessment of welded joints*, International Journal of Fracture, 139 2020.
- [12] Ottersböck M., Leitner M., Stoschka M., Maurer W., *Analysis of fatigue notch effect due to axial misalignment for ultra high-strength steel butt joints*, Welding in the World, 63(3):851-865 2019.
- [13] Ahola A., Björk T., *Fatigue strength of misaligned non-load-carrying cruciform joints made of ultra-high-strength steel*, Journal of Constructional Steel Research, 175, 2020.
- [14] Liu X., Song W., Yan Z., Qiang W., Pan H., *Misalignment effect on stress concentration of thickness mismatched plate structures*, Procedia Structural Integrity, 2038-2045 2016.
- [15] Marquis G., Mikkola E., Yildirim H., Barsoum Z., *Fatigue strength improvement of steel structures by high-frequency mechanical impact: Proposed fatigue assessment guidelines*, Welding in the World, 57(6):803-822 2013.

- [16] Mikkola E., Remes H., Marquis G., *A finite element study on residual stress stability and fatigue damage in high-frequency mechanical impact (HFMI)-treated welded joint*, International Journal of Fatigue,94,16-29, 2017.
- [17] Yildirim H., Marquis G., *Fatigue strength improvement factors for high strength steel welded joints treated by high frequency mechanical impact*, International Journal of Fatigue,44,168-176, 2012.
- [18] Yildirim H., Remes H., Nussbaumer A., *Fatigue properties of as-welded and post-weld-treated high-strength steel joints: The influence of constant and variable amplitude loads*,International Journal of Fatigue, 138, 2020.
- [19] Fricke W., *Recent developments and future challenges in fatigue strength assessment of welded joints*, International Journal of Fatigue, 138, 2015.
- [20] Xiao Z., Yamada K., *A method of determining geometric stress for fatigue strength evaluation of steel welded joints*,International Journal of Fatigue, vol.26,pp. 1277-1293, 2004.
- [21] Gross R., Mendelson A., *Plane Elastostatic Analysis of V-Notched Plates*, Int. J. Fract. Mech., pages 267-276, 1972.
- [22] Nezhad H.,Ayre D.,Prevost R., *Development of damage tolerant aerospace composites using advanced interlaminar nanofiber*, School of aerospace, transport and manufacturing, page 16, 2017.
- [23] Meneghetti G., Campagnolo A., *Progettazione a fatica di componenti meccanici indeboliti da intagli a V a spigolo vivo- applicazione ai giunti saldati* Corso di Macchine 2, 2020/2021.
- [24] Meneghetti G., Campagnolo A., *Rapid estimation of notch stress intensity factors in 3D large-scale welded structures using the peak stress method*,MATEC Web Conf., page 165 2018.
- [25] Lazzarin P., Zambardi R., *A finite-volume-energy based approach to predict the static and fatigue behavior of components with sharp V-shaped notches*,International Journal of Fracture,112(3):275-298,Dec 2001.
- [26] Lazzarin P.,Sonsino C.M., Zambardi R., *A notch stress intensity approach to assess the multiaxial fatigue strength of welded tube-to-flange joints subjected to combined loadings*,Fatigue & Fracture of Engineering Materials & Structures, 27(2):127-140, Feb 2004.
- [27] Lazzarin P., Berto F., *Some expressions for the strain energy in a finite volume surrounding the root of blunt V-notches*, International Journal of Fracture, 135:161-185, 2005.
- [28] Meneghetti G., *The use of peak stresses for fatigue strength assessments of welded lap joints and cover plates with toe and root failures*,Engineering Fracture Mechanics, 89, 40-51, 2019.
- [29] Meneghetti G., *The peak stress method for fatigue strength assessment of tube-to-flange welded joints under torsion loading*, Welding in the World, 57(2):265-275, Feb 2013.
- [30] Campagnolo A., Roveda I., Meneghetti G., *The Peak Stress Method combined with 3D finite element models to assess the fatigue strength of complex welded structures*, Structural Integrity Procedia, 2019.
- [31] Lazzarin P., Livieri P., Berto F., Zappalorto M., *Local strain energy density and fatigue strength of welded joints under uniaxial and multiaxial*,Engineering Fracture Mechanics,75 1875-1889, 2008.
- [32] Meneghetti G., Campagnolo A., Visentin A., *Automated fatigue strength assessment of arc-welded structures according to the peak stress method*,Procedia Structural Integrity, 1062-1083, 2020.
- [33] Campagnolo A., Belluzzo F., Meneghetti G., Yildirim H., *Fatigue strength assessment of as-welded and HFMI treated welded joints according to structural and local approaches*, International Journal of Fatigue,2021.
- [34] Yildirim H.,Marquis G., Barsoum Z., *Fatigue assessment of high frequency mechanical impact (HFMI)-improved fillet welds by local approaches*, International Journal of Fatigue,52,57-67, 2013.
- [35] Yildirim H.,Marquis G., *Fatigue design of axially-loaded high frequency mechanical impact treated welds by the effective notch stress method*, Materials and Design,58,543-550, 2014.
- [36] Poutiainen I., Tanskanen P., Marquis G., *Finite element methods for structural hot spot stress determination - A comparison of procedures*,Int J Fatigue,26,1147-1157 2004.

- [37] Maddox S.J., *The Effect of Plate Thickness on the Fatigue Strength of Fillet Welded Joints*, Abington Publishing, Abington, Cambridge, 1987.
- [38] Gurney T.R., *The Fatigue Strength of Transverse Fillet Welded Joints*, Abington Publishing, Abington, Cambridge, 1991.
- [39] Gandhi P., Berge S., *Fatigue behavior of T-joints: square chords and circular braces*, J. Struct. Eng., 124:399-404, 1998.
- [40] Meneghetti G., Lazzarin P., *Significance of the elastic peak stress evaluated by FE analyses at the point of singularity of sharp V-notched components*, Fatigue Fract. Eng. Mater. Struct., pages 95-106, 2007.
- [41] Yildirim H., Marquis G., Sonsino C.M., *Lightweight design with welded high-frequency mechanical impact (HFMI) treated high-strength steel joints from S700 under constant and variable amplitude loadings*, International Journal of Fatigue, 91 (2016) 466–474.
- [42] FATWELDHSS, Technical report n°3 - 2013.
- [43] Okawa T., Shimanuki H., Funatsu Y., Nose T., Sumi Y., *Effect of preload and stress ratio on fatigue strength of welded joints improved by ultrasonic impact treatment*, Weld World (2013) 57:235–241.
- [44] Kuhlmann U., Gunther H., *Experimental investigations of the fatigue-enhancing effect of the PIT process (Experimentelle Untersuchungen zur ermüdungssteigernden Wirkung des PIT-Verfahrens)*, Versuchsbericht, Universität Stuttgart, Institut für Konstruktion und Entwurf, Sep 2009.
- [45] Pedersen M., Mouritsen O.Ø., Hansen M., Andersen J.G., Wenderby J., *Comparison of post weld treatment of high strength steel welded joints in medium cycle fatigue*, Weld World 2009; 54(7/8):208–17.
- [46] Yildirim H., Marquis G., *A Round Robin study of high frequency mechanical impact treated welded joints subjected to variable amplitude loading*, Welding in the World, vol. 57, nr. 3, pp. 437-447, 2013.
- [47] Yildirim H., Marquis G., *Notch stress analyses of high-frequency mechanical impact-improved welds by using $\rho_f = 1\text{mm}$ and $\rho_f = \rho + 1$ approaches*, Fatigue and Fracture of Engineering Materials and Structures, 561-569, 37(5), 2014.
- [48] Meneghetti G., Campagnolo A., Berto F., *Fatigue strength assessment of partial and full-penetration steel and aluminium butt-welded joints according to the peak stress method*, Fatigue and Fracture of Engineering Materials and Structures, (2015), 1419-1431, 38(12).
- [49] Ottersbock M., Leitner M., Stoschka M., Maurer W., *Analysis of fatigue notch effect due to axial misalignment for ultra high-strength steel butt joints*, Welding in the World, 815-865, 63(3), 2019.
- [50] Ahola A., Bjork T., *Fatigue strength of misaligned non-load-carrying cruciform joints made of ultra-high-strength steel*, Journal of Constructional Steel Research, 175, 2020.
- [51] Andrews R., *The effect of misalignment on the fatigue strength of welded cruciform joints*, Fatigue and Fracture of Engineering Materials and Structure, 755-768, 1996.
- [52] Ottersbock M., Leitner M., Stoschka M., *Impact of angular distortion on the fatigue performance of High-strength steel T-joints in as-welded and HFMI condition*, Metals, 8(5), 2018.
- [53] Xing S., Dong P., *An analytical SCF solution method for joint misalignments and application in fatigue test interpretation*, Marine Structures, 143-161, 50, 2016.
- [54] Remes H., *Strain-based approach to fatigue crack initiation and propagation in welded steel joints with arbitrary notch shape*, International Journal of Fatigue, 114-123, 52, 2013.
- [55] Nykanen T., Bjork, Laitinen R., *Fatigue strength prediction of ultra high strength steel butt-welded joints*, Fatigue and Fracture of Engineering Materials and Structures, 469-482, 36(6), 2013.
- [56] Jakubczak H., Glinka G., *Fatigue analysis of manufacturing defects in weldments*, International Journal of Fatigue, 51-57, 1986.
- [57] Chiarelli M., Lanciotti A., Sacchi M., *Fatigue resistance of MAG welded steel elements*, International Journal of Fatigue, 1099-1110, 1999.

- [58] Nguyen N.T., Wahab M., *The effect of undercut, misalignment and residual stresses on the fatigue behavior of butt welded joints*, Fatigue and Fracture of Engineering Materials and Structures, 769-718, 1996.
- [59] Remes H., Varsta P., *Statistics of weld geometry for laser-hybrid welded joints and its application within notch stress approach*, Welding in the World, Vol. 54, 2010.
- [60] Ahola A., Nykanen T., Bjork T., *Effect of loading type on the fatigue strength of asymmetric and symmetric transverse non-load carrying attachments*, Fatigue and Fracture of Engineering Materials and Structures, 670-682, 40(5), 2017.
- [61] Kunihiro I., Nobu I., *Fatigue strength of butt-welded joints angular distortion*, Fracture mechanics of ductile and tough materials and its application to energy related structures, 293-302, 1981.
- [62] Burk B.J., Lawrence F.V., *Influence of bending stresses on fatigue crack propagation life in butt joint welds*, Welding journal, 56(2),1977.
- [63] Wylde J.G, Maddox S.J., *Effect of misalignment on fatigue strength of transverse butt welded joints*, Proc. Mech. Eng., Conference Significance of Deviations from Design Shape, 37-51,1979.
- [64] Gustafsson M., *A study of thickness effect on fatigue in thin welded high strength steel joints*, Steel Research International, 873-881, 77(12),2006.
- [65] Berto D., *Definizione di metodi per la durabilità di giunzioni saldate ibride acciaio-ghisa sferoidale austemperata*, MA thesis, Università degli Studi di Padova, 2019.
- [66] Pullin E., *Development of local approaches for fatigue life prediction of Austempered Ductile Iron-to-Steel dissimilar joints*, MA thesis, Università degli Studi di Padova, 2019.
- [67] Belluzzo F., *Fatigue analysis of as-welded and HFMI-treated steel joints by local approaches*, MA thesis, Università degli Studi di Padova and Aarhus University, 2020.